



National Library
of Canada

Bibliothèque nationale
du Canada

Canadian Theses Service

Services des thèses canadiennes

Ottawa, Canada
K1A 0N4

CANADIAN THESES

THÈSES CANADIENNES

NOTICE

The quality of this microfiche is heavily dependent upon the quality of the original thesis submitted for microfilming. Every effort has been made to ensure the highest quality of reproduction possible.

If pages are missing, contact the university which granted the degree.

Some pages may have indistinct print especially if the original pages were typed with a poor typewriter ribbon or if the university sent us an inferior photocopy.

Previously copyrighted materials (journal articles, published tests, etc.) are not filmed.

Reproduction in full or in part of this film is governed by the Canadian Copyright Act, R.S.C. 1970, c. C-30.

**THIS DISSERTATION
HAS BEEN MICROFILMED
EXACTLY AS RECEIVED**

AVIS

La qualité de cette microfiche dépend grandement de la qualité de la thèse soumise au microfilmage. Nous avons tout fait pour assurer une qualité supérieure de reproduction.

S'il manque des pages, veuillez communiquer avec l'université qui a conféré le grade.

La qualité d'impression de certaines pages peut laisser à désirer, surtout si les pages originales ont été dactylographiées à l'aide d'un ruban usé ou si l'université nous a fait parvenir une photocopie de qualité inférieure.

Les documents qui font déjà l'objet d'un droit d'auteur (articles de revue, examens publiés, etc.) ne sont pas microfilmés.

La reproduction, même partielle, de ce microfilm est soumise à la Loi canadienne sur le droit d'auteur, SRC 1970, c. C-30.

**LA THÈSE A ÉTÉ
MICROFILMÉE TELLE QUE
NOUS L'AVONS REÇUE**

THE UNIVERSITY OF ALBERTA

A NUMERICAL STUDY OF SOME LINEAR AND NONLINEAR
ELASTODYNAMIC PROBLEMS

by

SHELLEY ANNE LORIMER

(C)

A THESIS

SUBMITTED TO THE FACULTY OF GRADUATE STUDIES AND RESEARCH
IN PARTIAL FULFILMENT OF THE REQUIREMENTS FOR THE DEGREE OF
DOCTOR OF PHILOSOPHY

DEPARTMENT OF MECHANICAL ENGINEERING

EDMONTON, ALBERTA

FALL 1986

Permission has been granted to the National Library of Canada to microfilm this thesis and to lend or sell copies of the film.

The author (copyright owner) has reserved other publication rights, and neither the thesis nor extensive extracts from it may be printed or otherwise reproduced without his/her written permission.

L'autorisation a été accordée à la Bibliothèque nationale du Canada de microfilmer cette thèse et de prêter ou de vendre des exemplaires du film.

L'auteur (titulaire du droit d'auteur) se réserve les autres droits de publication; ni la thèse ni de longs extraits de celle-ci ne doivent être imprimés ou autrement reproduits sans son autorisation écrite.

ISBN 0-315-32480-5

THE UNIVERSITY OF ALBERTA

RELEASE FORM

NAME OF AUTHOR SHELLEY ANNE LORIMER
TITLE OF THESIS A NUMERICAL STUDY OF SOME LINEAR AND NONLINEAR
 ELASTODYNAMIC PROBLEMS
DEGREE FOR WHICH THESIS WAS PRESENTED DOCTOR OF PHILOSOPHY
YEAR THIS DEGREE GRANTED FALL 1986

Permission is hereby granted to THE UNIVERSITY
OF ALBERTA LIBRARY to reproduce single copies of this
thesis and to lend or sell such copies for private,
scholarly or scientific research purposes only.

The author reserves other publication rights,
and neither the thesis nor extensive extracts from it
may be printed or otherwise reproduced without the
author's written permission.

(SIGNED) Shelley Lorimer

PERMANENT ADDRESS:

10436-32 Ave.
Edmonton, Alberta
T6J 4E8

DATED October 8 19 86

THE UNIVERSITY OF ALBERTA
FACULTY OF GRADUATE STUDIES AND RESEARCH

The undersigned certify that they have read, and recommend to the Faculty of Graduate Studies and Research for acceptance, a thesis entitled A NUMERICAL STUDY OF SOME LINEAR AND NONLINEAR ELASTODYNAMIC PROBLEMS submitted by SHELLEY ANNE LORIMER in partial fulfilment of the requirements for the degree of DOCTOR OF PHILOSOPHY.

[Handwritten signature]
SUPERVISOR

[Handwritten signature]

[Handwritten signature]

[Handwritten signature]

[Handwritten signature]

[Handwritten signature]

[Handwritten signature]

[Handwritten signature]

EXTERNAL EXAMINER

DATE July 11, 1986

THIS MANUSCRIPT IS DEDICATED TO
THE MOST IMPORTANT PEOPLE IN MY LIFE

JERRY and JESSICA

and

PETE, NORMA, MURRAY and SANDY BALASCAK

ABSTRACT

Some linear and nonlinear wave propagation problems in solids governed by hyperbolic systems of partial differential equations are solved using the MacCormack scheme. It is shown that the MacCormack scheme is a suitable method for the solution of boundary initial value problems governed by systems of the form

$$\frac{\partial U}{\partial t} + A(U) \frac{\partial U}{\partial x} + B(U) = 0$$

As a preliminary to application to wave propagation problems in solids, the MacCormack scheme is applied to several linear and nonlinear scalar equations. Stability of the MacCormack scheme applied to linear first order partial differential equations and a hyperbolic system of first order equations equivalent to the Klein Gordon equation is examined using the von Neumann method. The numerical results indicate that the term $B(U)$ in the governing equations can influence the stability of the MacCormack scheme.

The MacCormack scheme is, then, applied to various infinitesimal plane wave propagation problems in linear viscoelastic media. It is shown that the MacCormack scheme is a useful alternative to the Laplace transform technique, particularly for viscoelastic models with two relaxation times.

Finite amplitude wave propagation in incompressible hyperelastic solids is also investigated using the MacCormack scheme. Axial shear wave propagation and combined axial and torsional shear wave propagation in an axially symmetric unbounded hyperelastic solid are considered. The

governing equations are of the form (1), and no analytical solutions were found. The numerical scheme is useful in examining finite amplitude wave propagation problems which are difficult to solve in closed form. The numerical results obtained using a conservative difference scheme satisfy conservation of momentum and are consistent with mechanical energy considerations.

The MacCormack scheme is used to investigate finite amplitude wave propagation in a standard viscoelastic solid. The numerical results are compared to known analytical solutions. Conservation of momentum is satisfied even though a nonconservative difference scheme is used.

It is shown that the MacCormack scheme is extremely useful in obtaining solutions of boundary initial value problems governed by nonlinear hyperbolic systems of the form (1). These problems are dynamic problems of nonlinear elasticity and viscoelasticity. The numerical solutions demonstrate important wave propagation phenomena as well as being interesting applications of numerical analysis.

ACKNOWLEDGEMENTS

I would like to express my sincerest thanks to one of the finest supervisors, Dr. J.B. Haddow, who offered support and guidance throughout. I would also like to thank Dr. R.J. Tait for many helpful suggestions. There are numerous unseen contributions that go into completing a doctoral dissertation, and I would like to thank each and every person for any part they may have played in the completion of this work.

Special thanks is given to the Province of Alberta, Department of Mechanical Engineering and NSERC for providing funding, and Dianne Paine for her tremendous effort in word processing the manuscript.

Last, but not least, I would like to express my utmost gratitude and indebtedness to Jerry, Mom and Jessica for all the extra effort they have put in to complete this undertaking.

TABLE OF CONTENTS

		<u>PAGE</u>
CHAPTER 1	INTRODUCTION	
1.1	Importance of Wave Propagation in Solids	1
1.2	Numerical Solution of Wave Propagation Problems ..	3
1.3	Purpose of This Investigation	6
CHAPTER 2	NUMERICAL METHOD	
2.1	Selection of the MacCormack Scheme	8
2.2	Definition of Numerical Terms	12
2.3	Application of Boundary Conditions	14
2.4	Stability Analysis of the MacCormack Scheme Applied to Linear Systems of Equations	16
2.5	Application of the MacCormack Scheme to Scalar Equations	19
2.5.1	Problems Considered	19
2.5.2	Stability Criteria	20
2.5.3	Numerical Results	22
2.6	Application of the MacCormack Scheme to the Klein Gordon Equation	57
2.6.1	Problem Considered	57
2.6.2	Stability Criteria	60
2.6.3	Numerical Results	61
2.7	Concluding Remarks	73
CHAPTER 3	PLANE LINEAR VISCOELASTIC WAVE PROPAGATION	
3.1	Introduction of the Problem	74
3.2	Governing Equations	76

3.3	Wavefront Expansion	81
3.4	Implementation of the MacCormack Scheme	84
3.5	Momentum Considerations	88
3.6	Stability of the MacCormack Scheme for the Maxwell Model	88
3.7	Numerical Results	90
3.7.1	Maxwell Model ($\alpha_0 = 0, N = 1$)	90
3.7.2	Standard Model ($\alpha_0 > 0, N = 1$)	107
3.7.3	Viscoelastic Model with Two Relaxation Times (Extended Model), $N = 2$	120
CHAPTER 4	FINITE AMPLITUDE SHEAR WAVE PROPAGATION IN INCOMPRESSIBLE ISOTROPIC HYPERELASTIC SOLIDS	
4.1	Introduction of the Problems	135
4.2	Axial Shear Wave Propagation	137
4.2.1	Governing Equations	137
4.2.2	Formulation of the Problem	141
4.2.3	Implementation of the MacCormack Scheme	145
4.2.4	Momentum and Energy Considerations	149
4.2.5	Numerical Results	151
4.3	Plane Transverse Shear Wave Propagation	181
4.3.1	Governing Equations	181
4.3.2	Formulation of the Problem	184
4.3.3	Implementation of the MacCormack Scheme	187
4.3.4	Method of Characteristics	188
4.3.5	Momentum and Energy Considerations	191

	PAGE
4.3.6 Numerical Results	193
4.4 Combined Axial and Torsional Shear Wave Propagation	213
4.4.1 Governing Equations	213
4.4.2 Formulation of the Problem	216
4.4.3 Implementation of the MacCormack Scheme ...	223
4.4.4 Numerical Results	225
4.5 Concluding Remarks	246
CHAPTER 5 FINITE AMPLITUDE WAVE PROPAGATION IN A NONLINEAR VISCOELASTIC SOLID	
5.1 Introduction of the Problem	247
5.2 Governing Equations	249
5.3 Formulation of the Problem	253
5.4 Implementation of the MacCormack Scheme	254
5.5 Momentum Considerations	256
5.6 Numerical Results	256
5.7 Concluding Remarks	280
CHAPTER 6 CONCLUDING REMARKS	281
References	283
Appendix 1	286
Appendix 2	292
Appendix 3	299

LIST OF TABLES

<u>TABLE</u>	<u>DESCRIPTION</u>	<u>PAGE</u>
3.1	Nondimensional Momentum Calculations for a Maxwell Material subject to $\sigma(0,t) = \sigma_0 H(t)$, $\sigma_0 = 1$, and quiescent initial conditions, for $\nu = 0.999$.	106
3.2	Nondimensional Momentum Calculations for a Maxwell Material subject to $\sigma(0,t) = \sigma_0 \sin \pi t H(t) H(1-t)$, $\sigma_0 = 1$, and quiescent initial conditions, for $\nu = 0.999$.	106
4.1	Nondimensional Momentum Calculations for Axial Shear subject to $r(1,t) = r_0 H(t)$, with $r_0 = 1$, and quiescent unstressed initial conditions for $\gamma = 0$ and $\nu = 0.99$.	164
4.2	Nondimensional Momentum Calculations for Axial Shear subject to $r(1,t) = r_0 H(t)$, with $r_0 = 1$, and quiescent unstressed initial conditions for $\gamma = 0.1$ and $\nu = 0.99$.	164
4.3	Nondimensional Momentum and Energy Calculations for Axial Shear subject to $r(1,t) = r_0 \sin \pi t H(t) H(1-t)$, with $r_0 = 1$, and quiescent unstressed initial conditions for $\gamma = 0$ and $\nu = 0.99$.	171

TABLE

DESCRIPTION

PAGE

4.4	Nondimensional Momentum and Energy Calculations for Axial Shear subject to $\tau(1,t) = \tau_0 \sin \pi t H(t) H(1-t)$, with $\tau_0 = 1$, and quiescent unstressed initial conditions for $\gamma = 0.1$ and $\nu = 0.99$	171
4.5	Nondimensional Momentum Calculations for Axial Shear subject to $\tau(1,t) = \tau_0 H(t)$, with $\tau_0 = 1$, and quiescent unstressed initial conditions for $\gamma = 0$ and $\nu = 0.99$...	175
4.6	Nondimensional Momentum Calculations for Axial Shear subject to $\tau(1,t) = \tau_0 H(t)$, with $\tau_0 = 1$, and quiescent unstressed initial conditions for $\gamma = 0.1$ and $\nu = 0.99$...	175
4.7	Nondimensional Momentum Calculations for Axial Shear subject to $\tau(1,t) = \tau_0 \sin \pi t H(t) H(1-t)$, with $\tau_0 = 1$, and quiescent unstressed initial conditions for $\gamma = 0$ and $\nu = 0.99$	180
4.8	Nondimensional Momentum Calculations for Axial Shear subject to $\tau(1,t) = \tau_0 \sin \pi t H(t) H(1-t)$, with $\tau_0 = 1$, and quiescent unstressed initial conditions for $\gamma = 0.1$ and $\nu = 0.99$	180

TABLE

DESCRIPTION

PAGE

4.9	Normalized Momentum Calculations and Energy Calculations for Transverse Shear subject to $\tau(1,t) = \tau_0 \sin \pi t H(t)$ $H(1-t)$, with $\tau_0 = 1$, and quiescent unstressed initial conditions for $\gamma = 0.1$ and $\nu = 0.99$	208
4.10	Normalized Momentum Calculations and Energy Calculations for Transverse Shear subject to $\tau(1,t) = \tau_0 \sin \pi t H(t)$ $H(1-t)$, with $\tau_0 = 0.01$, and quiescent unstressed initial conditions and $\nu = 0.99$	208

LIST OF FIGURES

<u>FIGURE</u>	<u>DESCRIPTION</u>	<u>PAGE</u>
2.1	The MacCormack scheme applied to $u_t + u_x = 0$ subject to $u(x,0) = 0$, $u(0,t) = U_0 H(t)$, $U_0 = 1$, for $\nu = 1.0$, and $\Delta x = 0.01$.	23
2.2	The MacCormack scheme applied to $u_t + u_x = 0$ subject to $u(x,0) = 0$, $u(0,t) = U_0 H(t)$, $U_0 = 1$, for $\nu = 0.99$, $\Delta x = 0.01$.	24
2.3	The MacCormack scheme applied to $u_t + u_x = 0$ subject to $u(x,0) = 0$, $u(0,t) = U_0 H(t)$, $U_0 = 1$, for $\nu = 0.5$, and $\Delta x = 0.01$.	25
2.4	The MacCormack scheme applied to $u_t + u_x = 0$ subject to $u(x,0) = 0$, $u(0,t) = U_0 \sin \pi t H(t) H(1-t)$, $U_0 = 1$, for $\nu = 1.0$, and $\Delta x = 0.01$.	27
2.5	The MacCormack scheme applied to $u_t + u_x = 0$ subject to $u(x,0) = 0$, $u(0,t) = U_0 \sin \pi t H(t) H(1-t)$, $U_0 = 1$, for $\nu = 0.99$, and $\Delta x = 0.01$.	28

FIGURE

DESCRIPTION

PAGE

2.6	The MacCormack scheme applied to $u_t + u_x = 0$ subject to $u(x,0) = 0$, $u(0,t) = U_0 \sin \pi t H(t) H(1-t)$, $U_0 = 1$, for $\nu = 0.5$, and $\Delta x = 0.01$.	29
2.7	The MacCormack scheme applied to $u_t + u_x + u = 0$ subject to $u(x,0) = 0$, $u(0,t) = U_0 H(t)$, $U_0 = 1$, for $\nu = 1.0$, and $\Delta x = 0.01$.	31
2.8	The MacCormack scheme applied to $u_t + u_x + u = 0$ subject to $u(x,0) = 0$, $u(0,t) = U_0 H(t)$, $U_0 = 1$, for $\nu = 0.99$, and $\Delta x = 0.01$.	32
2.9	The MacCormack scheme applied to $u_t + u_x + u = 0$ subject to $u(x,0) = 0$, $u(0,t) = U_0 H(t)$, $U_0 = 1$, for $\nu = 0.5$, and $\Delta x = 0.01$.	33
2.10	The von Neumann stability analysis for the MacCormack finite difference scheme applied to $u_t + u_x + u = 0$ for $\Delta x = 0.01$ and $\Delta x = 0.025$.	34
2.11	The MacCormack scheme applied to $u_t + u_x + u = 0$ subject to $u(x,0) = 0$, $u(0,t) = U_0 H(t)$, $U_0 = 1$, for $\nu = 0.9975$, and $\Delta x = 0.01$.	36

FIGURE

DESCRIPTION

PAGE

- 2.12 The MacCormack scheme applied to $u_t + u_x + u = 0$ subject to $u(x,0) = 0$, $u(0,t) = U_0 H(t)$, $U_0 = 1$, for $\nu = 0.995$, and $\Delta x = 0.01$ 37
- 2.13 The MacCormack scheme applied to $u_t + u_x + u = 0$ subject to $u(x,0) = 0$, $u(0,t) = U_0 H(t)$, $U_0 = 1$, for $\nu = 0.9975$, and $\Delta x = 0.025$ 38
- 2.14 The MacCormack scheme applied to $u_t + u_x + u = 0$ subject to $u(x,0) = 0$, $u(0,t) = U_0 \sin \pi t H(t) H(1-t)$, $U_0 = 1$, for $\nu = 1.0$, and $\Delta x = 0.01$ 39
- 2.15 The MacCormack scheme applied to $u_t + u_x + u = 0$ subject to $u(x,0) = 0$, $u(0,t) = U_0 \sin \pi t H(t) H(1-t)$, $U_0 = 1$, for $\nu = 0.99$, and $\Delta x = 0.01$ 40
- 2.16 The MacCormack scheme applied to $u_t + u_x + u = 0$ subject to $u(x,0) = 0$, $u(0,t) = U_0 \sin \pi t H(t) H(1-t)$, $U_0 = 1$, for $\nu = 0.5$, and $\Delta x = 0.01$ 41
- 2.17 The MacCormack scheme applied to $u_t + uu_x = 0$ subject to $u(x,0) = 0$, $u(0,t) = U_0 H(t)$, $U_0 = 1$, for $\nu = 1.0$, and $\Delta x = 0.01$ 43

FIGURE

DESCRIPTION

PAGE

2.18 The MacCormack scheme applied to $u_t + uu_x = 0$ subject to $u(x,0) = 0$, $u(0,t) = U_0H(t)$, $U_0 = 1$, for $\nu = 0.99$, and $\Delta x = 0.01$ 44

2.19 The MacCormack scheme applied to $u_t + uu_x = 0$ subject to $u(x,0) = 0$, $u(0,t) = U_0H(t)$, $U_0 = 1$, for $\nu = 0.5$, and $\Delta x = 0.01$ 45

2.20 The MacCormack scheme applied to $u_t + uu_x = 0$ subject to $u(x,0) = 0$, $u(0,t) = U_0 \sin \pi t H(t) H(1-t)$, $U_0 = 1$, for $\nu = 1.0$, and $\Delta x = 0.01$ 46

2.21 The MacCormack scheme applied to $u_t + uu_x = 0$ subject to $u(x,0) = 0$, $u(0,t) = U_0 \sin \pi t H(t) H(1-t)$, $U_0 = 1$, for $\nu = 0.99$, and $\Delta x = 0.01$ 47

2.22 The MacCormack scheme applied to $u_t + uu_x = 0$ subject to $u(x,0) = 0$, $u(0,t) = U_0 \sin \pi t H(t) H(1-t)$, $U_0 = 1$, for $\nu = 0.5$, and $\Delta x = 0.01$ 48

2.23 The MacCormack scheme applied to $u_t + uu_x + u = 0$ subject to $u(x,0) = 0$, $u(0,t) = U_0H(t)$, $U_0 = 1$, for $\nu = 1.0$, and $\Delta x = 0.01$ 50

FIGURE**DESCRIPTION****PAGE**

- 2.24 The MacCormack scheme applied to $u_t + uu_x + u = 0$ subject to $u(x,0) = 0$, $u(0,t) = U_0 H(t)$, $U_0 = 1$, for $\nu = 0.99$, and $\Delta x = 0.01$ 51
- 2.25 The MacCormack scheme applied to $u_t + uu_x + u = 0$ subject to $u(x,0) = 0$, $u(0,t) = U_0 H(t)$, $U_0 = 1$, for $\nu = 0.5$, and $\Delta x = 0.01$ 52
- 2.26 The MacCormack scheme applied to $u_t + uu_x + u = 0$ subject to $u(x,0) = 0$, $u(0,t) = U_0 \sin \pi t H(t) H(1-t)$, $U_0 = 1$, for $\nu = 1.0$, and $\Delta x = 0.01$ 53
- 2.27 The MacCormack scheme applied to $u_t + uu_x + u = 0$ subject to $u(x,0) = 0$, $u(0,t) = U_0 \sin \pi t H(t) H(1-t)$, $U_0 = 1$, for $\nu = 0.99$, and $\Delta x = 0.01$ 54
- 2.28 The MacCormack scheme applied to $u_t + uu_x + u = 0$ subject to $u(x,0) = 0$, $u(0,t) = U_0 \sin \pi t H(t) H(1-t)$, $U_0 = 1$, for $\nu = 0.5$, and $\Delta x = 0.01$ 55
- 2.29 Effect of grid size on the numerical solution of $u_t + uu_x = 0$ subject to $u(x,0) = 0$, $u(0,t) = U_0 H(t)$, with $U_0 = 1$, for $\nu = 0.99$ using the MacCormack scheme. 56

FIGURE**DESCRIPTION****PAGE**

2.30	The von Neumann stability analysis for the MacCormack scheme applied to the Klein Gordon equation, for $\Delta x = 0.01$ and $\Delta x = 0.025$.	62
2.31	The MacCormack scheme applied to the Klein Gordon equation subject to $u(x,0) = 0$, $u(0,t) = U_0H(t)$, with $U_0 = 1$, for $\nu = 1.0$ and $\Delta x = 0.025$.	63
2.32	The MacCormack scheme applied to the Klein Gordon equation subject to $u(x,0) = 0$, $u(0,t) = U_0H(t)$, with $U_0 = 1$, for $\nu = 0.995$ and $\Delta x = 0.025$.	64
2.33	The MacCormack scheme applied to the Klein Gordon equation subject to $u(x,0) = 0$, $u(0,t) = U_0H(t)$, with $U_0 = 1$, for $\nu = 0.99$ and $\Delta x = 0.025$.	65
2.34	The MacCormack scheme applied to the Klein Gordon equation subject to $u(x,0) = 0$, $u(0,t) = U_0H(t)$, with $U_0 = 1$, for $\nu = 1.0$ and $\Delta x = 0.01$.	66
2.35	The MacCormack scheme applied to the Klein Gordon equation subject to $u(x,0) = 0$, $u(0,t) = U_0H(t)$, with $U_0 = 1$, for $\nu = 0.995$ and $\Delta x = 0.01$.	67

FIGURE

DESCRIPTION

PAGE

2.36 The MacCormack scheme applied to the Klein Gordon equation, subject to $u(x,0) = 0$, $u(0,t) = U_0H(t)$, with $U_0 = 1$, for $\nu = 0.99$ and $\Delta x = 0.01$ 68

2.37 The method of characteristics applied to the Klein Gordon equation, subject to $u(x,0) = 0$, $u(0,t) = U_0H(t)$, with $U_0 = 1$, for $\Delta x = 0.01$ 71

2.38 Comparison of numerical results obtained from the method of characteristics to those obtained from the MacCormack scheme for the Klein Gordon equation, subject to $u(x,0) = 0$, $u(0,t) = U_0 \sin \pi t H(t) H(1-t)$, with $U_0 = 1$ 72

3.1 Diagrammatic representation of Plane Wave Propagation in a semi-infinite viscoelastic medium. 79

3.2 Maxwell Model - Variation of nondimensional σ with nondimensional x for $v(0,t) = V_0H(t)$, with $V_0 = -1$, obtained using Laplace transforms (Christensen, 1982). 91

FIGURE	DESCRIPTION	PAGE
3.3	Maxwell Model - Comparison of the MacCormack solution to the Laplace transform solution (Christensen, 1982), for nondimensional σ versus nondimensional x for $v(0,t) = V_0 H(t)$, with $V_0 = -1$, and $\nu = 1.0$.	92
3.4	Maxwell Model - Comparison of the MacCormack solution to the Laplace transform solution (Christensen, 1982), for nondimensional σ versus nondimensional x for $v(0,t) = V_0 H(t)$, with $V_0 = -1$, and $\nu = 0.99$.	93
3.5	Maxwell Model - Comparison of the MacCormack solution to the Laplace transform solution (Christensen, 1982), for nondimensional σ versus nondimensional x for $v(0,t) = V_0 H(t)$, with $V_0 = -1$, and $\nu = 0.5$.	94
3.6	Maxwell Model - Variation of nondimensional σ with nondimensional x for $v(0,t) = V_0 H(t)$, with $V_0 = -1$, obtained using the MacCormack scheme with a wavefront expansion with $\nu = 0.5$.	96
3.7	The von Neumann stability analysis for the MacCormack scheme applied to the Maxwell Model for $\Delta x = 0.01$.	97

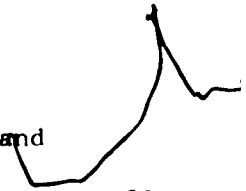
FIGURE

DESCRIPTION

PAGE

3.8 Maxwell Model - Variation of nondimensional σ with
nondimensional x for $\sigma(0,t) = \sigma_0 H(t)$, with $\sigma_0 = 1$ and
 $\nu = 1.0$, using the MacCormack scheme. 98

3.9 Maxwell Model - Variation of nondimensional σ with
nondimensional x for $\sigma(0,t) = \sigma_0 H(t)$, with $\sigma_0 = 1$ and
 $\nu = 0.999$ using the MacCormack scheme. 99



3.10 Maxwell Model - Variation of nondimensional σ with
nondimensional x for $\sigma(0,t) = \sigma_0 H(t)$, with $\sigma_0 = 1$ and
 $\nu = 0.9985$ using the MacCormack scheme. 100

3.11 Maxwell Model - Variation of nondimensional σ with
nondimensional x for $\sigma(0,t) = \sigma_0 H(t)$, with $\sigma_0 = 1$
and $\nu = 0.9990$, $\Delta x = 0.025$ using the MacCormack
scheme. 101

3.12 Maxwell Model - Variation of nondimensional σ with
nondimensional x for $\sigma(0,t) = \sigma_0 \sin \pi t H(t) H(1-t)$,
with $\sigma_0 = 1$ and $\nu = 1.0$ using the MacCormack
scheme. 103

FIGURE	DESCRIPTION	PAGE
3.13	Maxwell Model - Variation of nondimensional σ with nondimensional x for $\sigma(0,t) = \sigma_0 \sin \pi t H(t) H(1-t)$, with $\sigma_0 = 1$ and $\nu = 0.999$ using the MacCormack scheme.	104
3.14	Maxwell Model - Effect of grid size on numerical results obtained using the MacCormack scheme for nondimensional σ versus nondimensional x for $\sigma(0,t) = \sigma_0 H(t)$, with $\sigma_0 = 1$ and $\nu = 0.99$.	105
3.15	Standard Model $\alpha_0 = 1$ - Variation of nondimensional σ with nondimensional x for $\sigma(0,t) = \sigma_0 H(t)$, with $\sigma_0 = 1$ and $\nu = 1.0$ using the MacCormack scheme.	108
3.16	Standard Model $\alpha_0 = 0.9$ - Variation of nondimensional σ with nondimensional x for $\sigma(0,t) = \sigma_0 H(t)$, with $\sigma_0 = 1$ and $\nu = 1.0$ using the MacCormack scheme.	109
3.17	Standard Model $\alpha_0 = 0.1$ - Variation of nondimensional σ with nondimensional x for $\sigma(0,t) = \sigma_0 H(t)$, with $\sigma_0 = 1$ and $\nu = 1.0$ using the MacCormack scheme.	110

FIGURE**DESCRIPTION****PAGE**

3.18	Standard Model $\alpha_0 = 1.0$ - Variation of nondimensional σ with nondimensional x for $\sigma(0,t) = \sigma_0 \sin \pi t H(t) H(1-t)$, with $\sigma_0 = 1$ and $\nu = 1.0$ using the MacCormack scheme.	111
3.19	Standard Model $\alpha_0 = 0.9$ - Variation of nondimensional σ with nondimensional x for $\sigma(0,t) = \sigma_0 \sin \pi t H(t) H(1-t)$, with $\sigma_0 = 1$ and $\nu = 1.0$ using the MacCormack scheme.	112
3.20	Standard Model $\alpha_0 = 0.1$ - Variation of nondimensional σ with nondimensional x for $\sigma(0,t) = \sigma_0 \sin \pi t H(t) H(1-t)$, with $\sigma_0 = 1$ and $\nu = 1.0$ using the MacCormack scheme.	113
3.21	Standard Model $\alpha_0 = 0.9$ - Variation of nondimensional σ with nondimensional x for $\sigma(0,t) = \sigma_0 H(t)$, with $\sigma_0 = 1$ and $\nu = 1.0$ using the MacCormack scheme with a wavefront expansion.	115
3.22	Standard Model $\alpha_0 = 0.1$ - Variation of nondimensional σ with nondimensional x for $\sigma(0,t) = \sigma_0 H(t)$, with $\sigma_0 = 1$ and $\nu = 1.0$ using the MacCormack scheme with a wavefront expansion.	116

FIGURE

DESCRIPTION

PAGE

- 3.23 Standard Model $\alpha_0 = 1.0$ - Variation of nondimensional σ with nondimensional x for $\sigma(0,t) = \sigma_0 H(t)$, with $\sigma_0 = 1$ and $\nu = 0.5$ using the MacCormack scheme with a wavefront expansion. 117
- 3.24 Standard Model $\alpha_0 = 0.9$ - Variation of nondimensional σ with nondimensional x for $\sigma(0,t) = \sigma_0 H(t)$, with $\sigma_0 = 1$ and $\nu = 0.5$ using the MacCormack scheme with a wavefront expansion. 118
- 3.25 Standard Model $\alpha_0 = 0.1$ - Variation of nondimensional σ with nondimensional x for $\sigma(0,t) = \sigma_0 H(t)$, with $\sigma_0 = 1$ and $\nu = 0.5$ using the MacCormack scheme with a wavefront expansion. 119
- 3.26 Extended Model $\alpha_0 = 0.9$ - Variation of nondimensional σ with nondimensional x for $\sigma(0,t) = \sigma_0 H(t)$, with $\sigma_0 = 1$ and $\nu = 1.0$ using the MacCormack scheme. 121
- 3.27 Extended Model $\alpha_0 = 0.1$ - Variation of nondimensional σ with nondimensional x for $\sigma(0,t) = \sigma_0 H(t)$, with $\sigma_0 = 1$ and $\nu = 1.0$ using the MacCormack scheme. 122

FIGURE

DESCRIPTION

PAGE

3.28	Extended Model $\alpha_0 = 0.9$ - Variation of nondimensional σ with nondimensional x for $\sigma(0,t) = \sigma_0 H(t)$, with $\sigma_0 = 1$ and $\nu = 0.99$ using the MacCormack scheme. ...	123
3.29	Extended Model $\alpha_0 = 0.1$ - Variation of nondimensional σ with nondimensional x for $\sigma(0,t) = \sigma_0 H(t)$, with $\sigma_0 = 1$ and $\nu = 0.99$ using the MacCormack scheme. ...	124
3.30	Extended Model $\alpha_0 = 0.9$ - Variation of nondimensional σ with nondimensional x for $\sigma(0,t) = \sigma_0 \sin \pi t H(t) H(1-t)$, with $\sigma_0 = 1$ and $\nu = 0.99$ using the MacCormack scheme.	126
3.31	Extended Model $\alpha_0 = 0.1$ - Variation of nondimensional σ with nondimensional x for $\sigma(0,t) = \sigma_0 \sin \pi t H(t) H(1-t)$, with $\sigma_0 = 1$ and $\nu = 0.99$ using the MacCormack scheme.	127
3.32	A comparison of the Standard Model $\alpha_0 = 0.1$ to the Extended Model $\alpha_0 = 0.1$ for $\sigma(0,t) = \sigma_0 H(t)$, with $\sigma_0 = 1$ and $\nu = 0.99$ using the MacCormack scheme. ...	128

FIGURE

DESCRIPTION

PAGE

3.33 A comparison of the Standard Model $\alpha_0 = 0.1$ to the Extended Model $\alpha_0 = 0.1$, and $\tau_2/\tau_1 = 1$, for $\sigma(0,t) = \sigma_0 \sin \pi t H(t) H(1-t)$, with $\sigma_0 = 1$ and $\nu = 0.99$ using the MacCormack scheme. 129

3.34 Extended Model $\alpha_0 = 0.1$ - Variation of nondimensional σ with nondimensional x for $\sigma(0,t) = \sin \pi t$, with $\sigma_0 = 1$ and $\nu = 0.5$ using the MacCormack scheme with a wavefront expansion. 131

3.35 Extended Model $\alpha_0 = 0.9$ - Variation of nondimensional σ with nondimensional x for $\sigma(0,t) = \sigma_0 H(t)$, with $\sigma_0 = 1$ and $\nu = 0.5$ using the MacCormack scheme with a wavefront expansion. 132

3.36 Extended Model $\alpha_0 = 0.1$ - Variation of nondimensional σ with nondimensional x for $\sigma(0,t) = \sigma_0 H(t)$, with $\sigma_0 = 1$ and $\nu = 0.5$ using the MacCormack scheme with a wavefront expansion. 133

4.1 Diagrammatic representation of Axial Shear Wave Propagation in an Unbounded Isotropic Incompressible Hyperelastic solid. 142

FIGURE

DESCRIPTION

PAGE

4.2	Axial Shear - Variation of nondimensional τ with nondimensional r for $\gamma = 0$ subject to $\tau(1,t) = \tau_0 H(t)$, with $\tau_0 = 1$, using the MacCormack scheme, with $\nu = 1.0$	152
4.3	Axial Shear - Variation of nondimensional τ with nondimensional r for $\gamma = 0$ subject to $\tau(1,t) = \tau_0 H(t)$, with $\tau_0 = 1$, using the MacCormack scheme, with $\nu = 0.99$	153
4.4	Axial Shear - Variation of nondimensional τ with nondimensional r for $\gamma = 0$ subject to $\tau(1,t) = \tau_0 H(t)$, with $\tau_0 = 1$, using the MacCormack scheme, with $\nu = 0.5$	154
4.5	Axial Shear - Variation of nondimensional τ with nondimensional r for $\gamma = 0.1$ subject to $\tau(1,t) = \tau_0 H(t)$, with $\tau_0 = 1$, using the MacCormack scheme, with $\nu = 1.0$	155
4.6	Axial Shear - Variation of nondimensional τ with nondimensional r for $\gamma = 0.1$ subject to $\tau(1,t) = \tau_0 H(t)$, with $\tau_0 = 1$, using the MacCormack scheme, with $\nu = 0.99$	156

FIGURE

DESCRIPTION

PAGE

4.7	Axial Shear - Variation of nondimensional τ with nondimensional r for $\gamma = 0.1$ subject to $\tau(1,t) = \tau_0 H(t)$, with $\tau_0 = 1$, using the MacCormack scheme, with $\nu = 0.5$	157
4.8	Axial Shear - Effect of grid size on the variation of nondimensional τ with nondimensional r for $\gamma = 0$ using the MacCormack scheme with $\nu = 0.99$, for $\tau(1,t) = \tau_0 H(t)$, with $\tau_0 = 1$	159
4.9	Axial Shear - Effect of grid size on the variation of nondimensional τ with nondimensional r for $\gamma = 0.1$ using the MacCormack scheme with $\nu = 0.99$, for $\tau(1,t) = \tau_0 H(t)$, with $\tau_0 = 1$	160
4.10	Axial Shear - Variation of nondimensional τ with nondimensional r for $\gamma = 0$ subject to $\tau(1,t) = \tau_0 H(t)$, with $\tau_0 = 1$ using the MacCormack scheme with and without extrapolation with $\nu = 0.99$	161

FIGURE

DESCRIPTION

PAGE

4.11 Axial Shear - Variation of nondimensional τ with
nondimensional r for $\gamma = 0.1$ subject to
 $\tau(1,t) = \tau_0 H(t)$, with $\tau_0 = 1$ using the MacCormack
scheme with and without extrapolation with
 $\nu = 0.99$ 162

4.12 Axial Shear - A comparison of the numerical results
obtained for τ vs r with $\gamma = 0$ to those obtained
with $\gamma = 0.1$, subject to $\tau(1,t) = \tau_0 H(t)$, with
 $\tau_0 = 0.01$ using the MacCormack scheme with
 $\nu = 0.99$ 165

4.13 Axial Shear - Variation of nondimensional w with
nondimensional r for $\gamma = 0$ subject to
 $\tau(1,t) = \tau_0 H(t)$, with $\tau_0 = 1$ using the MacCormack
scheme with $\nu = 0.99$ 166

4.14 Axial Shear - Variation of nondimensional w with
nondimensional r for $\gamma = 0.1$ subject to
 $\tau(1,t) = \tau_0 H(t)$, with $\tau_0 = 1$ using the MacCormack
scheme with $\nu = 0.99$ 167

<u>FIGURE</u>	<u>DESCRIPTION</u>	<u>PAGE</u>
4.15	Axial Shear - Variation of nondimensional τ with nondimensional r for $\gamma = 0$ subject to $\tau(1,t) = \tau_0 \sin \pi t H(t) H(1-t)$, with $\tau_0 = 1$ using the MacCormack scheme with $\nu = 0.99$.	168
4.16	Axial Shear - Variation of nondimensional τ with nondimensional r for $\gamma = 0.1$ subject to $\tau(1,t) = \tau_0 \sin \pi t H(t) H(1-t)$, with $\tau_0 = 1$ using the MacCormack scheme with $\nu = 0.99$.	169
4.17	Axial Shear - Variation of nondimensional τ with nondimensional r for $\gamma = 0$ subject to $\tau(1,t) = \tau_0 H(t)$, with $\tau_0 = 1$ using the conservative and nonconservative MacCormack schemes with $\nu = 0.99$.	173
4.18	Axial Shear - Variation of nondimensional τ with nondimensional r for $\gamma = 0.1$ subject to $\tau(1,t) = \tau_0 H(t)$, with $\tau_0 = 1$ using the conservative and nonconservative MacCormack schemes with $\nu = 0.99$.	174

<u>FIGURE</u>	<u>DESCRIPTION</u>	<u>PAGE</u>
4.19	Axial Shear - Variation of nondimensional w with nondimensional r for $\gamma = 0$ subject to $\tau(1,t) = \tau_0 H(t)$, with $\tau_0 = 1$ using the conservative and nonconservative MacCormack schemes with $\nu = 0.99$.	176
4.20	Axial Shear - Variation of nondimensional w with nondimensional r for $\gamma = 0.1$ subject to $\tau(1,t) = \tau_0 H(t)$, with $\tau_0 = 1$ using the conservative and nonconservative MacCormack schemes with $\nu = 0.99$.	177
4.21	Axial Shear - Variation of nondimensional τ with nondimensional r for $\gamma = 0$ subject to $\tau(1,t) = \tau_0 \sin \pi t H(t) H(1-t)$, with $\tau_0 = 1$ using the conservative and nonconservative MacCormack schemes with $\nu = 0.99$.	178
4.22	Axial Shear - Variation of nondimensional τ with nondimensional r for $\gamma = 0.1$ subject to $\tau(1,t) = \tau_0 \sin \pi t H(t) H(1-t)$, with $\tau_0 = 1$ using the conservative and nonconservative MacCormack schemes with $\nu = 0.99$.	179

FIGURE

DESCRIPTION

PAGE

γ

4.23	Diagrammatic representation of Plane Transverse Shear Wave Propagation in an Unbounded Isotropic Incompressible Hyperelastic solid.	185
4.24	Diagrammatic representation of the method of characteristics applied to the transverse shear problem.	189
4.25	Transverse Shear - Variation of normalized τ with normalized X for $\gamma = 0$ subject to $\tau(0,t) = \tau_0 H(t)$, with $\tau_0 = 1$ using the MacCormack scheme with $\nu = 1.0$	194
4.26	Transverse Shear - Variation of normalized τ with normalized X for $\gamma = 0$ subject to $\tau(0,t) = \tau_0 H(t)$, with $\tau_0 = 1$ using the MacCormack scheme with $\nu = 0.99$	195
4.27	Transverse Shear - Variation of normalized τ with normalized X for $\gamma = 0$ subject to $\tau(0,t) = \tau_0 H(t)$, with $\tau_0 = 1$ using the MacCormack scheme with $\nu = 1.0$	196

<u>FIGURE</u>	<u>DESCRIPTION</u>	<u>PAGE</u>
4.28	Transverse Shear - Variation of normalized τ with normalized X for $\gamma = 0.1$ subject to $\tau(0,t) = \tau_0 H(t)$, with $\tau_0 = 1$ using the MacCormack scheme with $\nu = 1.0$.	197
4.29	Transverse Shear - Variation of normalized τ with normalized X for $\gamma = 0.1$ subject to $\tau(0,t) = \tau_0 H(t)$, with $\tau_0 = 1$ using the MacCormack scheme with $\nu = 0.99$.	198
4.30	Transverse Shear - Variation of normalized \dot{w} with normalized X for $\gamma = 0.1$ subject to $\tau(0,t) = \tau_0 H(t)$, with $\tau_0 = 1$ using the MacCormack scheme with $\nu = 1.0$.	200
4.31	Transverse Shear - Variation of normalized τ with X for $\gamma = 0$ subject to $\tau(0,t) = \tau_0 \sin \pi t H(t) H(1-t)$, with $\tau_0 = 1$ using the MacCormack scheme with $\nu = 1.0$.	201
4.32	Transverse Shear - Variation of normalized \dot{w} with normalized X for $\gamma = 0$ subject to $\tau(0,t) = \tau_0 \sin \pi t H(t) H(1-t)$, with $\tau_0 = 1$ using the MacCormack scheme with $\nu = 1.0$.	202

<u>FIGURE</u>	<u>DESCRIPTION</u>	<u>PAGE</u>
4.33	Transverse Shear - Variation of normalized τ with normalized X for $\gamma = 0.1$ subject to $\tau(0,t) = \tau_0 \sin \pi t H(t) H(1-t)$, with $\tau_0 = 1$ using the MacCormack scheme with $\nu = 1.0$.	203
4.34	Transverse Shear - Variation of normalized w with normalized X for $\gamma = 0.1$ subject to $\tau(0,t) = \tau_0 \sin \pi t H(t) H(1-t)$, with $\tau_0 = 1$ using the MacCormack scheme with $\nu = 1.0$.	204
4.35	Transverse Shear - Variation of normalized τ with normalized X for $\gamma = 0.1$ subject to $\tau(0,t) = \tau_0 \sin \pi t H(t) H(1-t)$, with $\tau_0 = 1$ using the MacCormack scheme with $\nu = 0.99$.	206
4.36	Transverse Shear - Variation of normalized τ with normalized X for $\gamma = 0.1$ subject to $\tau(0,t) = \tau_0 \sin \pi t H(t) H(1-t)$, with $\tau_0 = 1$ using the MacCormack scheme with $\nu = 0.99$.	207
4.37	Transverse Shear - A comparison of the numerical results obtained for τ vs X with $\gamma = 0$ to those obtained with $\gamma = 0.1$, subject to $\tau(0,t) = \tau_0 \sin \pi t H(t) H(1-t)$, with $\tau_0 = 0.01$ using the MacCormack scheme with $\nu = 0.99$.	210

<u>FIGURE</u>	<u>DESCRIPTION</u>	<u>PAGE</u>
4.38	Transverse Shear - Variation of normalized τ with normalized X for $\gamma = 0.1$ subject to $\tau(0,t) = \tau_0 H(t)$, with $\tau_0 = 1$ using the conservative and nonconservative MacCormack schemes with $\nu = 0.99$.	211
4.39	Transverse Shear - Variation of normalized τ with normalized X for $\gamma = 0.1$ subject to $\tau(0,t) = \tau_0 \sin \pi t H(t) H(1-t)$, with $\tau_0 = 1$ using the conservative and nonconservative MacCormack schemes with $\nu = 0.99$.	212
4.40	Transverse Shear - Variation of normalized τ with normalized X for $\gamma = 0$ subject to $\tau(0,t) = \tau_0 \sin \pi t H(t) H(1-t)$, with $\tau_0 = 1$ using the conservative and nonconservative MacCormack schemes with $\nu = 0.99$.	214
4.41	Diagrammatic representation of Combined Axial and Torsional Shear Wave Propagation in an Unbounded Isotropic Incompressible Hyperelastic Solid.	218
4.42	Combined Shear - Variation of nondimensional τ_{rz} with nondimensional r for $\gamma = 0$, for boundary condition (4.85), with $T_{11} = T_{12} = 0$ and $T_1 = T_2 = 1$, using the MacCormack scheme with $\nu = 1.0$.	226

FIGURE

DESCRIPTION

PAGE

- 4.43 Combined Shear - Variation of nondimensional $\tau_{r\theta}$ with nondimensional r for $\gamma = 0$, for boundary condition (4.85), with $T_{i1} = T_{i2} = 0$ and $T_1 = T_2 = 1$, using the MacCormack scheme with $\nu = 1.0$ 227
- 4.44 Combined Shear - Variation of nondimensional τ_{rz} with nondimensional r for $\gamma = 0.1$, for boundary condition (4.85), with $T_{i1} = T_{i2} = 0$ and $T_1 = T_2 = 1$, using the MacCormack scheme with $\nu = 1.0$ 228
- 4.45 Combined Shear - Variation of nondimensional $\tau_{r\theta}$ with nondimensional r for $\gamma = 0.1$, for boundary condition (4.85), with $T_{i1} = T_{i2} = 0$ and $T_1 = T_2 = 1$, using the MacCormack scheme with $\nu = 1.0$ 229
- 4.46 Combined Shear - Variation of nondimensional τ_{rz} with nondimensional r for $\gamma = 0$, for boundary condition (4.85), with $T_{i1} = T_{i2} = 0$ and $T_1 = T_2 = 1$, using the MacCormack scheme with $\nu = 0.99$ 230
- 4.47 Combined Shear - Variation of nondimensional $\tau_{r\theta}$ with nondimensional r for $\gamma = 0$, for boundary condition (4.85), with $T_{i1} = T_{i2} = 0$ and $T_1 = T_2 = 1$, using the MacCormack scheme with $\nu = 0.99$ 231

FIGURE

DESCRIPTION

PAGE

4.48 Combined Shear - Variation of nondimensional τ_{rz} with nondimensional r for $\gamma = 0.1$, for boundary condition (4.85), with $T_{11} = T_{12} = 0$ and $T_1 = T_2 = 1$, using the MacCormack scheme with $\nu = 0.99$ 232

4.49 Combined Shear - Variation of nondimensional $\tau_{r\theta}$ with nondimensional r for $\gamma = 0.1$, for boundary condition (4.85), with $T_{11} = T_{12} = 0$ and $T_1 = T_2 = 1$, using the MacCormack scheme with $\nu = 0.99$ 233

4.50 Combined Shear - Variation of nondimensional τ_{rz} with nondimensional r for $\gamma = 0$, for boundary condition (4.85), with $T_{11} = T_{12} = 0$ and $T_1 = T_2 = 1$, using the MacCormack scheme with and without extrapolation with $\nu = 0.99$ 235

4.51 Combined Shear - Variation of nondimensional $\tau_{r\theta}$ with nondimensional r for $\gamma = 0$, for boundary condition (4.85), with $T_{11} = T_{12} = 0$ and $T_1 = T_2 = 1$, using the MacCormack scheme with and without extrapolation with $\nu = 0.99$ 236

FIGURE

DESCRIPTION

PAGE

4.52 Combined Shear - Variation of nondimensional r_{rz} with nondimensional r for $\gamma = 0.1$, for boundary condition (4.85), with $T_{i1} = T_{i2} = 0$ and $T_1 = T_2 = 1$, using the MacCormack scheme with and without extrapolation with $\nu = 0.99$ 237

4.53 Combined Shear - Variation of nondimensional $r_{r\theta}$ with nondimensional r for $\gamma = 0.1$, for boundary condition (4.85), with $T_{i1} = T_{i2} = 0$ and $T_1 = T_2 = 1$, using the MacCormack scheme with and without extrapolation with $\nu = 0.99$ 238

4.54 Combined Shear - Variation of nondimensional r_{rz} with nondimensional r for $\gamma = 0.1$, for boundary condition (4.85), with $T_{i1} = T_{i2} = 0$ and $T_1 = T_2 = 1$ for combined shear and $T_1 = 1, T_2 = 0$ for axial shear, using the MacCormack scheme with extrapolation with $\nu = 0.99$ 239

4.55 Combined Shear - Variation of nondimensional $r_{r\theta}$ with nondimensional r for $\gamma = 0.1$, for boundary condition (4.85), with $T_{i1} = T_{i2} = 0$ and $T_1 = T_2 = 1$ for combined shear and $T_1 = 0, T_2 = 1$ for torsional shear, using the MacCormack scheme with extrapolation with $\nu = 0.99$ 240

FIGURE

DESCRIPTION

PAGE

4.56 Combined Shear - Variation of nondimensional τ_{rz} with nondimensional r for $\gamma = 0.1$, for boundary condition (4.86), with $T_1 = T_2 = 1$ for combined shear and $T_1 = 1, T_2 = 0$ for axial shear, using the MacCormack scheme with $\nu = 0.99$ 242

4.57 Combined Shear - Variation of nondimensional $\tau_{r\theta}$ with nondimensional r for $\gamma = 0.1$, for boundary condition (4.86), with $T_1 = T_2 = 1$ for combined shear and $T_1 = 0, T_2 = 1$ for torsional shear, using the MacCormack scheme with $\nu = 0.99$ 243

4.58 Combined Shear - Variation of nondimensional τ_{rz} and $\tau_{r\theta}$ with nondimensional r for $\gamma = 0$, for boundary condition (4.85), with $T_{i1} = T_{i2} = 0.5$ and $T_1 = T_2 = 0.5$, using the MacCormack scheme with $\nu = 0.99$ 244

4.59 Combined Shear - Variation of nondimensional τ_{rz} and $\tau_{r\theta}$ with nondimensional r for $\gamma = 0.1$, for boundary condition (4.85), with $T_{i1} = T_{i2} = 0.5$ and $T_1 = T_2 = 0.5$, using the MacCormack scheme with $\nu = 0.99$ 245

FIGURE

DESCRIPTION

PAGE

5.1 Diagrammatic representation of finite amplitude longitudinal stress wave propagation in semi-infinite incompressible isotropic standard viscoelastic rod. 250

5.2 Effect of Courant number on the variation of nondimensional S with nondimensional X for $m = 0.1$ and $S(0,t) = S_0H(t)$, with $S_0 = -1.0$, using the nonconservative MacCormack scheme with $\nu = 1.0$ 258

5.3 Variation of nondimensional S with nondimensional X for $m = 0.9$ and $S(0,t) = S_0H(t)$, with $S_0 = -0.16$, using the nonconservative MacCormack scheme with $\nu = 1.0$ 259

5.4 Variation of nondimensional S with nondimensional X for $m = 1.0$ and $S(0,t) = S_0H(t)$, with $S_0 = -0.16$, using the nonconservative MacCormack scheme with $\nu = 1.0$ 261

5.5 Variation of nondimensional S with nondimensional X for $m = 1.0$ and $S(0,t) = S_0H(t)$, with $S_0 = -0.16$, using the nonconservative MacCormack scheme with $\nu = 1.0$ 262

<u>FIGURE</u>	<u>DESCRIPTION</u>	<u>PAGE</u>
5.6	Variation of nondimensional S with nondimensional X for $m = 0.1$ and $S(0,t) = S_0 \sin \pi t H(t) H(1-t)$, with $S_0 = -0.16$, using the nonconservative MacCormack scheme with $\nu = 1.0$.	263
5.7	Variation of nondimensional S with nondimensional X for $m = 0.9$ and $S(0,t) = S_0 \sin \pi t H(t) H(1-t)$, with $S_0 = -0.16$, using the nonconservative MacCormack scheme with $\nu = 1.0$.	264
5.8	Variation of nondimensional S with nondimensional X for $m = 1.0$ and $S(0,t) = S_0 \sin \pi t H(t) H(1-t)$, with $S_0 = -0.16$, using the nonconservative MacCormack scheme with $\nu = 1.0$.	265
5.9	Variation of nondimensional S with nondimensional X for $m = 0.1$ and $S(0,t) = S_0 H(t)$, with $S_0 = 0.16$, using the nonconservative MacCormack scheme with $\nu = 1.0$.	266
5.10	Variation of nondimensional S with nondimensional X for $m = 0.9$ and $S(0,t) = S_0 H(t)$, with $S_0 = 0.16$, using the nonconservative MacCormack scheme with $\nu = 1.0$.	267

FIGURE

DESCRIPTION

PAGE

5.11 Variation of nondimensional S with nondimensional X
for $m = 1.0$ and $S(0,t) = S_0 H(t)$, with $S_0 = 0.16$,
using the nonconservative MacCormack scheme with
 $\nu = 1.0$ 268

5.12 Variation of nondimensional S with nondimensional X
for $m = 0.1$ and $S(0,t) = S_0 \sin \pi t H(t) H(1-t)$, with
 $S_0 = 0.16$, using the nonconservative MacCormack
scheme with $\nu = 1.0$ 270

5.13 Variation of nondimensional S with nondimensional X
for $m = 0.9$ and $S(0,t) = S_0 \sin \pi t H(t) H(1-t)$, with
 $S_0 = 0.16$, using the nonconservative MacCormack
scheme with $\nu = 1.0$ 271

5.14 Variation of nondimensional S with nondimensional X
for $m = 1.0$ and $S(0,t) = S_0 \sin \pi t H(t) H(1-t)$, with
 $S_0 = 0.16$, using the nonconservative MacCormack
scheme with $\nu = 1.0$ 272

5.15 Variation of nondimensional S with nondimensional X
for $m = 0.1$ and $S(0,t) = S_0 \sin \pi t H(t) H(1-t)$, with
 $S_0 = -1.0$, using the nonconservative MacCormack
scheme with $\nu = 1.0$ 273

<u>FIGURE</u>	<u>DESCRIPTION</u>	<u>PAGE</u>
5.16	Variation of nondimensional S with nondimensional X for $m = 0.9$ and $S(0,t) = S_0 \sin \pi t H(t) H(1-t)$, with $S_0 = -1.0$, using the nonconservative MacCormack scheme with $\nu = 1.0$	274
5.17	Variation of nondimensional S with nondimensional X for $m = 1.0$ and $S(0,t) = S_0 \sin \pi t H(t) H(1-t)$, with $S_0 = -1.0$, using the nonconservative MacCormack scheme with $\nu = 1.0$	275
5.18	Variation of nondimensional S with nondimensional X for $m = 0.1$ and $S(0,t) = S_0 \sin \pi t H(t) H(1-t)$, with $S_0 = 1.0$, using the nonconservative MacCormack scheme with $\nu = 1.0$	277
5.19	Variation of nondimensional S with nondimensional X for $m = 0.9$ and $S(0,t) = S_0 \sin \pi t H(t) H(1-t)$, with $S_0 = 1.0$, using the nonconservative MacCormack scheme with $\nu = 1.0$	278
5.20	Variation of nondimensional S with nondimensional X for $m = 1.0$ and $S(0,t) = S_0 \sin \pi t H(t) H(1-t)$, with $S_0 = 1.0$, using the nonconservative MacCormack scheme with $\nu = 1.0$	279

CHAPTER 1

INTRODUCTION

1.1 Importance of Wave Propagation in Solids

"The fascinating phenomena of wave propagation has always been central to the physical sciences and engineering" (Engelbrecht, 1983). In particular, "the propagation of mechanical disturbances in solids" (Achenbach, 1973) is of considerable interest, since "sudden loading as from an explosion or sudden displacement as in slip at a seismic fault in the earth causing an earthquake presents essentially dynamic problems" (Timoshenko and Goodier, 1951). This interest in wave propagation in solids has inevitably led to research into finite amplitude waves in nonlinear elasticity and nonlinear viscoelasticity.

Problems of wave propagation in solids are an important area in applied mechanics and there is considerable interest in solutions of these problems. Yet, there has been much less emphasis on numerical approaches to the solution of boundary initial value wave propagation problems in solids, particularly nonlinear problems, than for similar problems in fluid dynamics. The purpose of this research is to obtain numerical procedures which can be used in the solution of nonlinear hyperelastic and viscoelastic wave propagation problems, because of the inherent difficulty in obtaining closed form solutions. Some linear problems involving hyperelastic and viscoelastic solids are also considered..

There have been extensive studies on linear wave propagation in solids using analytical methods (Achenbach, 1973, Eringen, 1974). In particular, Achenbach demonstrates the usefulness of integral transform techniques, wavefront expansion techniques and the method of characteristics for the solution of boundary initial value infinitesimal amplitude wave propagation problems in elastic and viscoelastic solids. Achenbach also solved a problem of transient nonlinear wave finite amplitude wave propagation using a simple wave solution.

In this study, a distinction is made between linear and nonlinear wave propagation problems. Problems which give rise to a linear hyperbolic system of equations are classified as "linear", and problems which give rise to a quasi-linear (nonlinear) hyperbolic system of partial differential equations are classified as "nonlinear". The constitutive relationship determines whether elastic or viscoelastic materials are considered and the measure of the deformation distinguishes finite amplitude waves from infinitesimal amplitude waves. It is possible to have a linear finite amplitude wave propagation problem, if one considers dynamic shear of a Mooney-Rivlin hyperelastic solid.

The wave propagation problems considered, then, are boundary initial value problems governed by linear or quasi-linear hyperbolic systems of partial differential equations. Linear problems can be solved using integral transform techniques (Achenbach, 1973, Christensen, 1982), or the method of characteristics. For certain linear viscoelastic wave propagation problems, the Laplace transform technique results in complicated transforms, which may require numerical

inversion (Lee and Morrison, 1956), and the method of characteristics becomes unattractive for viscoelastic solids with more than one relaxation time. Nonlinear problems become even more difficult to solve, since Laplace transforms cannot be used and the method of characteristics is difficult to implement because shock paths do not, in general, coincide with characteristics (Haddow and Mioduchowski, 1975). Consequently, a suitable numerical technique, which is applicable to a variety of linear and nonlinear boundary initial value problems, is presented.

1.2 Numerical Solution of Wave Propagation Problems

There is extensive literature on the numerical solution of nonlinear hyperbolic equations (Anderson et al, 1984, Mitchell and Griffiths, 1980, Courant and Friedrichs, 1948), but the applications have been mainly to problems in gas dynamics and fluid dynamics. A numerical method is selected for application to wave propagation problems in solids in which the most important consideration is shock capturing. This is extremely important for the nonlinear problems. The numerical method proposed is a slight modification of the MacCormack scheme (MacCormack, 1969). It is well suited for application to boundary initial value problems and is a second order accurate finite difference scheme capable of predicting the position of shock fronts (Kutler, 1974).

There are some difficulties involved in the use of the MacCormack scheme, which become apparent as the method is applied to various

problems. Some of these difficulties are documented in the literature (Anderson et al, 1984, Kutler, 1974).

A major thrust of this study is the application of the MacCormack scheme to problems which are complicated by an additional term in the matrix representation of the system of equations. The numerical scheme was proposed originally for problems of two spatial dimensions and the application to one spatial dimension has been for systems of the form

$$\frac{\partial \underline{U}}{\partial t} + \underline{A}(\underline{U}) \frac{\partial \underline{U}}{\partial x} = \underline{0} \quad (1.1)$$

where \underline{U} is a column vector of the dependent variables, $\underline{A}(\underline{U})$ is a matrix function of \underline{U} and x and t are the spatial and temporal variables, respectively. The problems considered in this study are governed by systems of the form

$$\frac{\partial \underline{U}}{\partial t} + \underline{A}(\underline{U}) \frac{\partial \underline{U}}{\partial x} + \underline{B}(\underline{U}) = \underline{0} \quad (1.2)$$

except for transverse shear wave propagation in a hyperelastic solid which is governed by (1.1).

Some researchers have introduced source terms similar to $\underline{B}(\underline{U})$ in (1.2), but apparently have not presented any application of finite difference techniques such as the Lax-Wendroff and MacCormack schemes to the solution of boundary initial value problems governed by (1.2) (Kutler, 1974). It has been suggested that the term $\underline{B}(\underline{U})$ in (1.2) can affect the numerical stability of the solution (Mitchell, 1984). However, an in-depth assessment of the MacCormack scheme applied to

systems of equations (1.2) was not found. Consequently, the method is applied to various wave propagation problems and the solutions are assessed by various analytical and numerical means. As a result of the research, some conclusions are drawn regarding the application of the MacCormack scheme to the system of equations (1.2) based on the numerical results which are obtained and a stability analysis for some of the linear problems.

Before the MacCormack scheme is applied to the solution of wave propagation problems in solids, the difference scheme is analyzed in Chapter 2 using simple first order and second order wave equations. The numerical results are compared to results from known analytical solutions or solutions obtained using the method of characteristics, which is often used for the solution of problems governed by hyperbolic systems of equations. In addition, the effect of the term $\underline{B(U)}$ is examined in the simpler context of a scalar equation to determine some of the ramifications of an additional term in equation (1.2). A von Neumann stability analysis is used on the simpler first order linear equations with and without the term $\underline{B(U)}$, using the MacCormack scheme to determine the effect of the additional term. The analysis shows that the stability of the MacCormack scheme is affected by the additional term.

The application of the MacCormack scheme to the simpler first and second order equations indicates that the method is suitable for application to boundary initial value problems governed by (1.2), and the method is applied to the solution of various linear and nonlinear wave propagation problems in solids.

1.3 Purpose of This Investigation

The wave propagation problems considered are classified as:

- (a) linear viscoelastic infinitesimal amplitude wave propagation;
- (b) linear and nonlinear finite amplitude wave propagation in hyperelastic solids; and
- (c) nonlinear viscoelastic finite amplitude wave propagation.

Chapter 3 deals with solutions of infinitesimal amplitude wave propagation problems in viscoelastic media. The MacCormack scheme is applied to the solution of various boundary initial value problems governed by linear systems of equations (1.2), where A is a constant and $B(U)$ is a linear function of U . Numerical solutions are compared to exact solutions where possible, and conservation of momentum is examined. The MacCormack scheme is proposed as a useful alternative to Laplace transform solutions of linear problems.

Chapter 4 contains solutions of finite amplitude wave propagation problems in incompressible hyperelastic solids. The problems are governed by equations of the form (1.2). The hyperelastic solids considered give rise to linear or nonlinear systems of the form (1.2), depending on the strain energy function. The numerical solutions are compared with those from the method of characteristics where possible and conservation of momentum is examined. Mechanical energy is considered, particularly where evolution of shocks occur.

Chapter 5 deals with nonlinear finite amplitude wave propagation in a standard viscoelastic solid. Boundary initial value problems are solved using the MacCormack scheme. The numerical results are compared

with results obtained by Tait et al (1984), where possible. Further results are presented.

CHAPTER 2

NUMERICAL METHOD

2.1 Selection of The MacCormack Scheme

The MacCormack finite difference scheme was initially developed for the solution of a two dimensional hypervelocity impact cratering problem (MacCormack, 1969). The method was applied to the solution of a system of partial differential equations given in conservation form (Whitham, 1974) as

$$\frac{\partial U}{\partial t} + \frac{\partial F}{\partial x} + \frac{\partial G}{\partial y} = 0 \quad (2.1)$$

where \underline{U} is a column vector of the dependent variables, \underline{F} and \underline{G} are column vectors of the conservation variables, x and y are spatial variables and t is the temporal variable.

This scheme is often referred to as a two step variant of the Lax-Wendroff finite difference scheme (Mitchell and Griffiths, 1980 and Anderson et al, 1984). Both the Lax-Wendroff and MacCormack schemes are second order accurate shock capturing finite difference schemes based on a Taylor series expansion in time with the terms $O((\Delta t)^3)$ truncated.

The numerical scheme proposed by MacCormack for the solution of equation (2.1) is given by

$$\begin{aligned} \overline{U}_{-j,k}^{n+1} &= \overline{U}_{-j,k}^n - \frac{\Delta t}{\Delta x} (F_{-j+1,k}^n - F_{-j,k}^n) - \frac{\Delta t}{\Delta y} (G_{-j,k+1}^n - G_{-j,k}^n) \\ \overline{U}_{-j,k}^{n+1} &= \frac{1}{2} \left\{ \overline{U}_{-j,k}^n + \overline{U}_{-j,k}^{n+1} - \frac{\Delta t}{\Delta x} (\overline{F}_{-j,k}^{n+1} - \overline{F}_{-j-1,k}^{n+1}) - \frac{\Delta t}{\Delta y} (\overline{G}_{-j,k}^{n+1} - \overline{G}_{-j,k-1}^{n+1}) \right\} \end{aligned} \tag{2.2}$$

The subscripts refer to a spatial mesh of points (x_j, y_k) , with spacing Δx and Δy , and the superscripts refer to times $t = n\Delta t$ where Δt is the time increment. Equation (2.2)₁ is referred to as the predictor step and equation (2.2)₂ is referred to as the corrector step.

Since the central differencing is first order in each step in (2.2), the MacCormack scheme is more suitable than the Lax-Wendroff scheme for the solution of boundary initial value problems. Gottlieb and Turkel (1978) provide an excellent discussion on the application of boundary conditions using the MacCormack scheme. Anderson, et al (1984) also discuss some of the advantages in comparison to other finite difference schemes. Mitchell and Griffiths (1980) categorize the MacCormack scheme as suitable for application to nonlinear hyperbolic systems of partial differential equations. All the references cited in the last paragraph, the majority of which relate to fluid dynamics problems, recommend the use of the scheme for the solution of boundary initial value problems governed by nonlinear hyperbolic partial differential equations.

It appears that the MacCormack scheme has been applied predominantly to one dimensional systems of equations of the following form

$$\frac{\partial U}{\partial t} + A(U) \frac{\partial U}{\partial x} = 0 \tag{2.3}$$

where $\underline{A}(U)$ is a matrix function of \underline{U} , or the two dimensional analogue given by equation (2.1) (Mitchell and Griffiths, 1980, Anderson et al, 1984). There seems to be little information available on the application of this method to nonlinear hyperbolic systems of partial differential equations of the form

$$\frac{\partial \underline{U}}{\partial t} + \underline{A}(U) \frac{\partial \underline{U}}{\partial x} + \underline{B}(U) = \underline{C} \quad (2.4)$$

where $\underline{B}(U)$ is a vector function of \underline{U} , and possibly the spatial coordinate x .

Kutler (1974) and Richtmyer and Morton (1967), discuss various systems of equations with terms similar to $\underline{B}(U)$ in equation (2.4). However, no results are presented for specific applications.

The systems of equations considered in this study, which govern wave propagation in solids, are of the form given by equation (2.4), or the conservation form of equation (2.4) given by

$$\frac{\partial \underline{U}}{\partial t} + \frac{\partial \underline{Q}(U)}{\partial x} + \underline{B}(U) = \underline{0} \quad (2.5)$$

where \underline{Q} is a vector function of \underline{U} .

The MacCormack scheme, equation (2.2), is revised for application to equations (2.4) and (2.5). This modification, which incorporates the term $\underline{B}(U)$, is the version of the scheme used throughout this study.

¹ Whitham (1974) refers to systems of the form (2.4) as quasi-linear. The term nonlinear is used here to distinguish between equations (2.4) and the linear version given by equation (2.13).

The derivation of the modification is straightforward, and is based on a substitution of $\underline{B(U)}$ for $\partial G/\partial y$ in equation (2.1). A justification for this modification, using the linear version of equation (2.4), is presented in Appendix 1. The scheme is compared to the Lax-Wendroff scheme, and conclusions regarding their similarity are made.

The MacCormack scheme applied to equation (2.4) gives

$$\begin{aligned} \overline{U_{-j}^{n+1}} &= U_{-j}^n - \frac{\Delta t}{\Delta x} (A(U_{-j}^n)) (U_{-j+1}^n - U_{-j}^n) - \Delta t \underline{B(U_{-j}^n)} \\ U_{-j}^{n+1} &= \frac{1}{2} \left\{ U_{-j}^n + \overline{U_{-j}^{n+1}} - \frac{\Delta t}{\Delta x} (A(\overline{U_{-j}^{n+1}})) (\overline{U_{-j}^{n+1}} - \overline{U_{-j-1}^{n+1}}) - \Delta t \underline{B(\overline{U_{-j}^{n+1}})} \right\} \end{aligned} \quad (2.6)$$

and applied to equation (2.5) gives

$$\begin{aligned} \overline{U_{-j}^{n+1}} &= U_{-j}^n - \frac{\Delta t}{\Delta x} (Q(U_{-j+1}^n) - Q(U_{-j}^n)) - \Delta t \underline{B(U_{-j}^n)} \\ U_{-j}^{n+1} &= \frac{1}{2} \left\{ U_{-j}^n + \overline{U_{-j}^{n+1}} - \frac{\Delta t}{\Delta x} (Q(\overline{U_{-j}^{n+1}}) - Q(\overline{U_{-j-1}^{n+1}})) - \Delta t \underline{B(\overline{U_{-j}^{n+1}})} \right\} \end{aligned} \quad (2.7)$$

The same finite difference notation for subscripts and superscripts used by MacCormack is used here, except that the subscript k associated with Δy is no longer present, since only one spatial dimension is considered. The versions of the MacCormack scheme given by (2.6) and (2.7) are called forward backward (FB) difference schemes because the predictor step uses forward spatial differencing and the corrector step uses backward spatial differencing. Anderson et al (1984) suggest that the best resolution of discontinuities occurs when the difference in the predictor step is in the direction of the propagation of the discontinuity. Since the problems considered in this study involve

waves propagating in the positive spatial direction, the FB version is used.

The difference equations given by (2.6) are simplified if $\underline{A}(\underline{U})$ is a constant matrix \underline{A} . In addition, if $\underline{B}(\underline{U})$ is a linear function of \underline{U} , equation (2.4) reduces to a linear hyperbolic system of partial differential equations. The technique is applied later to linear hyperbolic systems of equations with the term $\underline{B}(\underline{U})$, for the solution of linear wave propagation problems in viscoelastic media.

2.2 Definition of Numerical Terms

Since the MacCormack scheme is a finite difference method, some knowledge of the fundamentals of finite difference schemes is necessary for the application of this technique. Anderson et al (1984), Roache (1982) and Mitchell and Griffiths (1980) provide a detailed account of finite difference schemes. A summary of some of the basic definitions used in discussing numerical solutions obtained using finite differences are presented.

(a) The Courant number ν is defined as $\nu = c\Delta t/\Delta x$ where c is the numerically greatest eigenvalue of $\underline{A}(\underline{U})$ for a given problem, and Δx and Δt are the spatial and temporal grid spacings respectively (Anderson et al, 1984).

(b) The modified equation is the partial differential equation that is actually solved numerically using the specified finite difference scheme. The modified equation can be used to examine stability of a finite difference scheme (Warming and Hyett, 1974).

(c) The truncation error is a measure of how well the solution of the partial differential equation satisfies the finite difference equations (Kutler, 1974).

(d) Accuracy is the order of the truncation error. The MacCormack scheme is second order accurate.

(e) If the solution of the difference equation approaches the solution of the partial differential equation, as the step size approaches zero, the finite difference scheme is convergent.

(f) Stability of a finite difference scheme is solely dependent on the difference scheme, and requires that the solution be bounded as the step size goes to zero. The stability analysis of the MacCormack scheme applied to various equations is examined in the Section 2.4.

(g) Numerical dispersion occurs as a result of phase errors in the numerical solution. Different Fourier components spread apart or disperse as the numerical solution proceeds and the phenomenon is referred to as numerical dispersion error. Numerical dispersion is a direct result of the odd order spatial derivative terms which appear in the modified equation. Second order accurate finite difference schemes are predominantly dispersive.

(h) Numerical dissipation is the damping of high frequency terms inherent to the finite difference scheme, and is present if there are even order spatial derivatives in the modified equation. First order accurate finite difference schemes such as Lax's first order scheme are predominantly dissipative.

(1) Numerical diffusion is the combined effect of numerical dispersion and numerical dissipation. This causes a discontinuity in the solution to be smeared out.

The above terms are very important in discussing the numerical results. It is important to note that the numerical solution is an approximation to the exact solution of the boundary initial value problem. Numerical phenomena such as dispersion or dissipation can affect the expected numerical results. The purpose of this chapter is to examine the MacCormack scheme with regard to stability, numerical dispersion and numerical dissipation.

2.3 Application of Boundary Conditions

Since boundary initial value problems are considered in this study, the numerical application of boundary conditions is important. Mitchell and Griffiths (1980) stress that boundary conditions are an added complication which can lead to instabilities in the numerical calculations. Stability analyses for systems of equations with boundary and initial value data are complicated. Therefore, in this study the stability of boundary conditions is not examined in detail. The boundary conditions are applied as proposed by Gottlieb and Turkel (1978), who have considered various types of boundary conditions for the MacCormack finite difference scheme and make recommendations.

Gottlieb and Turkel (1978) consider six groups of methods for the treatment of boundary conditions. From their analysis of stability and accuracy, they conclude that the difference operator in the MacCormack scheme should be reversed at a boundary. For a boundary condition

applied at the left edge ($x = 0$), the difference operator in the corrector step should be reversed, so that the MacCormack scheme uses forward forward (FF) differences at the left edge. The boundary condition at the left edge, U_0 , is obtained by replacing $(U_j - U_{j-1})$ with $(U_{j+1} - U_j)$ in equation (2.6)₂ and $(Q(U_j) - Q(U_{j-1}))$ with $(Q(U_{j+1}) - Q(U_j))$ in equation (2.7)₂. Assuming that $j = 0$ at the left edge, the boundary condition at the left edge for the MacCormack scheme is

$$\begin{aligned} \overline{U_{-0}^{n+1}} &= U_{-0}^n - \frac{\Delta t}{\Delta x} (A(U_{-0}^n)) (U_{-1}^n - U_{-0}^n) - \Delta t B(U_{-0}^n) \\ U_{-0}^{n+1} &= \frac{1}{2} \left\{ U_{-0}^n + \overline{U_{-0}^{n+1}} - \frac{\Delta t}{\Delta x} (A(\overline{U_{-0}^{n+1}})) (\overline{U_{-1}^{n+1}} - \overline{U_{-0}^{n+1}}) - \Delta t B(\overline{U_{-0}^{n+1}}) \right\} \end{aligned} \quad (2.8)$$

for the nonconservative scheme and

$$\begin{aligned} \overline{U_{-0}^{n+1}} &= U_{-0}^n - \frac{\Delta t}{\Delta x} (Q(U_{-1}^n) - Q(U_{-0}^n)) - \Delta t B(U_{-0}^n) \\ U_{-0}^{n+1} &= \frac{1}{2} \left\{ U_{-0}^n + \overline{U_{-0}^{n+1}} - \frac{\Delta t}{\Delta x} (Q(\overline{U_{-1}^{n+1}}) - Q(\overline{U_{-0}^{n+1}})) - \Delta t B(\overline{U_{-0}^{n+1}}) \right\} \end{aligned} \quad (2.9)$$

for the conservative scheme. It should be noted that the predictor steps, equations (2.8)₁, and (2.9)₁, are a direct consequence of the MacCormack scheme for $j = 0$ (see equations (2.6) and (2.7)). For the boundary condition at the left edge, only the corrector step is revised. Boundary conditions for the right edge can be obtained in a similar manner to those for the left edge, except that the differencing is reversed in the predictor step, to give backward backward (BB)

differences at the right edge. Assuming that $j = N$ at the right edge, the boundary conditions for U_N are given by

$$\overline{U_{-N}^{n+1}} = \overline{U_{-N}^n} - \frac{\Delta t}{\Delta x} (A(\overline{U_{-N}^n})) (\overline{U_{-N}^n} - \overline{U_{-N-1}^n}) - \Delta t B(\overline{U_{-N}^n}) \quad (2.10)$$

$$\overline{U_{-N}^{n+1}} = \frac{1}{2} \left\{ \overline{U_{-N}^n} + \overline{U_{-N}^{n+1}} - \frac{\Delta t}{\Delta x} (A(\overline{U_{-N}^{n+1}})) (\overline{U_{-N}^{n+1}} - \overline{U_{-N-1}^{n+1}}) - \Delta t B(\overline{U_{-N}^{n+1}}) \right\}$$

for the nonconservative scheme and

$$\overline{U_{-N}^{n+1}} = \overline{U_{-N}^n} - \frac{\Delta t}{\Delta x} (Q(\overline{U_{-N}^n}) - Q(\overline{U_{-N-1}^n})) - \Delta t B(\overline{U_{-N}^n}) \quad (2.11)$$

$$\overline{U_{-N}^{n+1}} = \frac{1}{2} \left\{ \overline{U_{-N}^n} + \overline{U_{-N}^{n+1}} - \frac{\Delta t}{\Delta x} (Q(\overline{U_{-N}^{n+1}}) - Q(\overline{U_{-N-1}^{n+1}})) - \Delta t B(\overline{U_{-N}^{n+1}}) \right\}$$

for the conservative scheme. In this case $(N + 1)$ is the number of grid points and N is the number of intervals in the finite difference grid. As this method of applying the boundary conditions is not applicable to one step methods, such as the Lax-Wendroff scheme, it demonstrates an important advantage of the MacCormack scheme. In some instances, when boundary conditions are specified as part of the problem, the difference methods for the boundaries may not be used. In particular this is true with scalar equations where there is only one dependent variable, which is specified at the boundary, and therefore does not require implementation of the Godunov boundary condition.

2.4 Stability Analysis of The MacCormack Scheme Applied to Linear Systems of Equations

Stability analyses of finite difference schemes are important, since some finite difference schemes are unconditionally unstable. A

stability analysis of the MacCormack scheme applied to equation (2.4) was not found, consequently, such an analysis is a part of this study.

Mitchell and Griffiths (1980) recommend the use of the von Neumann method to investigate stability for initial value problems governed by linear hyperbolic systems of equations. However, in this case, caution must be exercised in interpreting the results obtained from such a stability analysis for boundary initial value problems, because the von Neumann method does not include the effects of boundary conditions and is not always a sufficient condition for stability. There are some special cases, which will be discussed later, where the condition for stability using the von Neumann method is a necessary and sufficient stability condition for initial value problems. In general, for the boundary initial value problems considered, this is not the case.

Although the von Neumann method is not always a sufficient condition for stability for boundary initial value problems, it is a necessary condition, and if instability is indicated by the von Neumann method, the finite difference scheme is unstable. The von Neumann method is used to obtain a necessary condition for the stability of the MacCormack scheme applied to linear systems of hyperbolic equations of the form (2.4), where A is constant and $B(U)$ is a linear function of U . Stability analyses of nonlinear systems are not considered here, however, some of the results for linear systems can be extended to nonlinear systems (Anderson et al, 1984).

The von Neumann or Fourier analysis is based on the assumption that the error $\epsilon(x,t)$ in the numerical solution, due to roundoff errors, can be written as a series of the form

$$\underline{\epsilon}(x,t) = \sum_{m=0}^N \underline{B}_m e^{ik_m x} \quad (2.12)$$

where $\underline{\epsilon}$ is a vector of the error terms, \underline{B}_m is a column vector of the coefficients, and k_m is the wave number for a given m . A detailed explanation of the von Neumann analysis is given by Mitchell and Griffiths (1980) and Anderson et al (1984). A typical error term $\underline{\epsilon}(x,t) = \underline{B}_m e^{ik_m x}$ given in (2.12) is substituted into the linear version of equation (2.6), with \underline{A} constant and $\underline{B}(U) = \hat{\underline{B}}U$, a linear function of U (see Appendix 1). An amplification matrix \underline{G} is obtained as a result of this analysis. A necessary condition that must be satisfied if the numerical solution does not grow with time is $\lambda \leq 1$, where λ is the spectral radius of \underline{G} .

The amplification matrix for the MacCormack scheme applied to

$$\frac{\partial \underline{U}}{\partial t} + \underline{A} \frac{\partial \underline{U}}{\partial x} + \hat{\underline{B}} \underline{U} = 0 \quad (2.13)$$

is given as

$$\underline{G}(\Delta t, k) = \left\{ \left[\underline{I} - \Delta t \hat{\underline{B}} + \frac{(\Delta t)^2 \hat{\underline{B}}^2}{2} + \underline{A}^2 \left(\frac{\Delta t}{\Delta x} \right)^2 (\cos \beta - 1) + \frac{(\Delta t)^2}{2\Delta x} (\hat{\underline{B}}\underline{A} - \underline{A}\hat{\underline{B}})(\cos \beta - 1) \right] + i \left[\left(\frac{\Delta t}{\Delta x} \right)^2 \left[\frac{\hat{\underline{B}}\underline{A} + \underline{A}\hat{\underline{B}}}{2} \right] - \left(\frac{\Delta t}{\Delta x} \right)^2 \underline{A} \right] \sin \beta \right\} \quad (2.14)$$

where $\beta = k_m \Delta x$ (see Appendix 1).

A necessary condition for stability is that $\lambda \leq 1$. If \underline{G} is a normal matrix, then $\lambda \leq 1$ is a necessary and sufficient condition for stability of an initial value problem (Richtmyer and Morton, 1967). Equation (2.14) can be used to examine the stability of various systems of linear

equations or scalar equations by substituting the appropriate \hat{A} and \hat{B} terms.

2.5 Application of The MacCormack Scheme to Scalar Equations

2.5.1 Problems Considered

The MacCormack scheme given by equation (2.6) or (2.7), is applied to boundary initial value problems for each of the following normalized scalar equations

$$\frac{\partial u}{\partial t} + \frac{\partial u}{\partial x} = 0 \quad (2.15)$$

$$\frac{\partial u}{\partial t} + \frac{\partial u}{\partial x} + u = 0 \quad (2.16)$$

$$\frac{\partial u}{\partial t} + u \frac{\partial u}{\partial x} = 0 \quad (2.17)$$

$$\frac{\partial u}{\partial t} + u \frac{\partial u}{\partial x} + u = 0 \quad (2.18)$$

for the interval $0 \leq x < \infty$,

subject to quiescent initial conditions

$$u(x,0) = 0 \quad (2.19)$$

and boundary conditions

$$u(0,t) = U_0 H(t) \quad (2.20)$$

or

$$u(0,t) = U_0 \sin \pi t H(t) H(1-t) \quad (2.21)$$

where U_0 is a constant, and $H(t)$ is the Heaviside unit function, where $H(t) = 0$ for $t < 0$ and $H(t) = 1$ for $t > 0$.

These equations do not necessarily represent physical examples, but are used to examine numerical phenomena. For this reason, equations (2.15 - 2.18) are presented in normalized form. By considering a more general scalar equation

$$\frac{\partial u}{\partial t} + c \frac{\partial u}{\partial x} + \alpha u = 0 \quad (2.22)$$

where u , c , and α are constants, and making the substitution

$$\bar{t} = \alpha t \quad , \quad \bar{x} = \frac{\alpha x}{c} \quad (2.23)$$

equation (2.16), which is actually nondimensional, is obtained, where the superposed bars have been omitted. It is somewhat easier to consider nondimensional variables, so that the constants c and α are not part of the analysis of the numerical scheme. Equations (2.15), (2.17) and (2.18) are normalized in a similar manner, by suitably scaling the dependent and independent variables.

Equations (2.15 - 2.18), with the appropriate initial and boundary conditions, illustrate linear and nonlinear wave propagation with and without the term $B(U)$ appearing in equation (2.4). The numerical solutions of these equations demonstrate the numerical phenomena described in Section 2.2. Some of the boundary initial value problems that are solved numerically can also be solved in closed form using the method of characteristics (see Appendix 2). The numerical solutions are compared to the exact solutions where possible. The effects of Courant number and grid size are shown.

2.5.2 Stability Criteria

The stability of the MacCormack scheme applied to equations (2.15) and (2.16) can be examined using the scalar case of expression (2.14) for G obtained in Section 2.4. Since $u(0,t)$ is specified and the equation is scalar, the boundary condition is

exact in each case, and should not affect the stability of the numerical solution. For scalar equations the stability criteria is a necessary and sufficient condition for initial value problems and the scalar amplification factor G is considered rather than the matrix given by (2.14) (Richtmyer and Morton, 1967).

Application of the von Neumann analysis to equation (2.15) gives

$$G = \left\{ \left[1 + \left(\frac{\Delta t}{\Delta x}\right)^2 (\cos\beta - 1) \right] + \left[i \left(\frac{\Delta t}{\Delta x}\right)^2 \sin\beta \right] \right\} \quad (2.24)$$

and to equation (2.16) gives

$$G = \left\{ \left[1 - \Delta t + \frac{\Delta t^2}{2} + \left(\frac{\Delta t}{\Delta x}\right)^2 (\cos\beta - 1) \right] + i \left[\frac{\Delta t}{\Delta x} + \left(\frac{\Delta t}{\Delta x}\right)^2 \right] \sin\beta \right\} \quad (2.25)$$

Since the amplification matrices for the scalar equations are scalar quantities, i.e. complex numbers, the spectral radius λ is given by the modulus of G . By substituting $\nu = \Delta t/\Delta x$ for these problems, since $c = 1$, the spectral radius for the MacCormack scheme is

$$\lambda = \left(\left[1 + \nu^2 (\cos\beta - 1) \right]^2 - \nu^2 \sin^2\beta \right)^{1/2} \quad (2.26)$$

for equation (2.15) and,

$$\lambda = \left\{ \left[1 - \Delta t + \left(\frac{\Delta t}{2}\right)^2 + \nu^2 (\cos\beta - 1) \right]^2 + [\nu + \nu\Delta t]^2 \sin^2\beta \right\}^{1/2} \quad (2.27)$$

for equation (2.16).

The condition $\nu \leq 1$, for stability of the initial value problem, is satisfied for equation (2.15), however this is not true for equation (2.16). Equation (2.27) is more complicated than (2.26), since λ is not a function of ν alone, but is also a function of the grid spacing. The stability criteria for the MacCormack scheme applied to equation (2.16) is evaluated by plotting $(\lambda-1)$ against β for $0 \leq \beta \leq 2\pi$. The von Neumann stability criteria implies that, if $(\lambda-1) > 0$, for $\Delta x \neq 0$, the scheme is unstable, since the errors in the numerical solution grow with time. The results of the stability analysis for equation (2.16) are presented in the next section along with the numerical solutions obtained using the version of the MacCormack scheme equation given by (2.6).

It is interesting to note that the MacCormack scheme and the Lax-Wendroff method are identical for equations (2.15) and (2.16), and therefore the stability criteria are the same.

2.5.3 Numerical Results

In this section, the numerical solutions for the variation of u with x , at various times, have been obtained using the MacCormack scheme, unless otherwise specified. The results presented have the initial conditions (2.19). Figures 2.1 - 2.3 show the effect of Courant number on the solution obtained for equation (2.15) with the boundary condition (2.20), with $U_0 = 1$. The exact solution, obtained by the method of characteristics (see Appendix 2), is $u(x,t) = U_0 H(x - U_0 t)$, which describes a step discontinuity in the field variable u propagating unchanged in

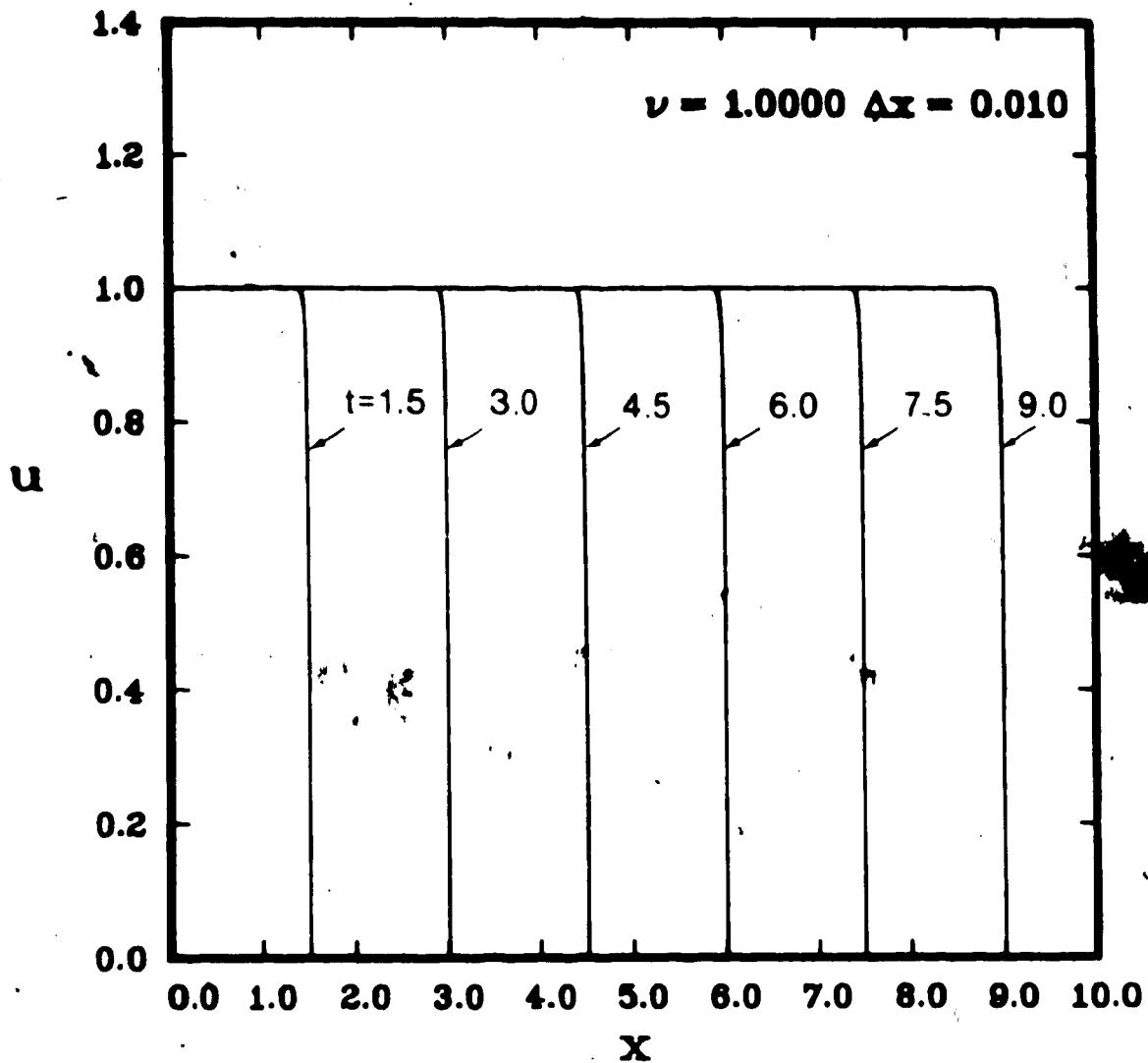


Fig. 2.1 The MacCormack scheme applied to $u_t + u_x = 0$ subject to $u(x,0) = 0$, $u(0,t) = U_0 H(t)$, $U_0 = 1$, for $\nu = 1.0$, and $\Delta x = 0.01$.

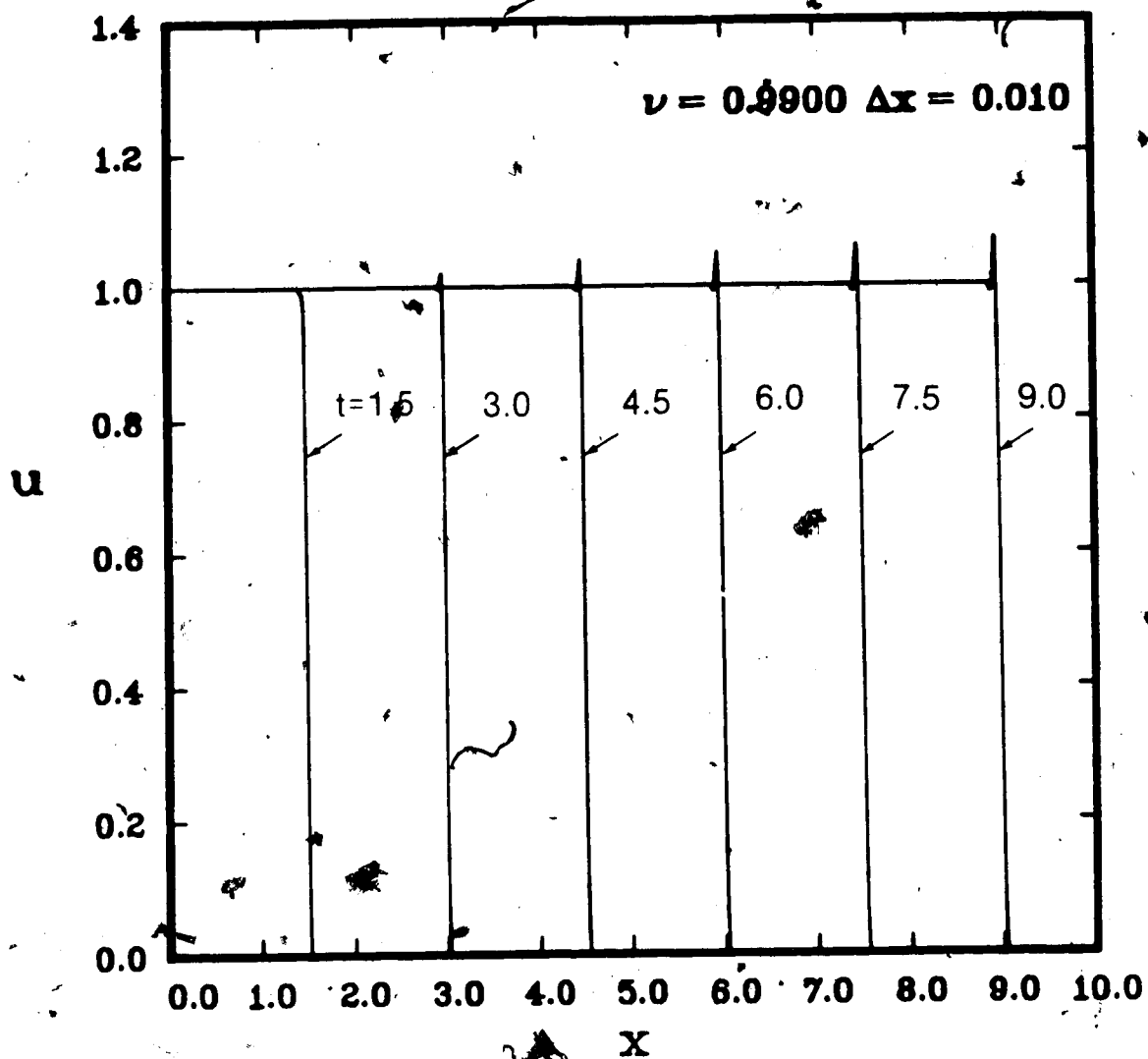


Fig. 2.2 The MacCormack scheme applied to $u_t + u_x = 0$ subject to $u(x,0) = 0$, $u(0,t) = U_0 H(t)$, $U_0 = 1$, for $\nu = 0.99$, and $\Delta x = 0.01$.

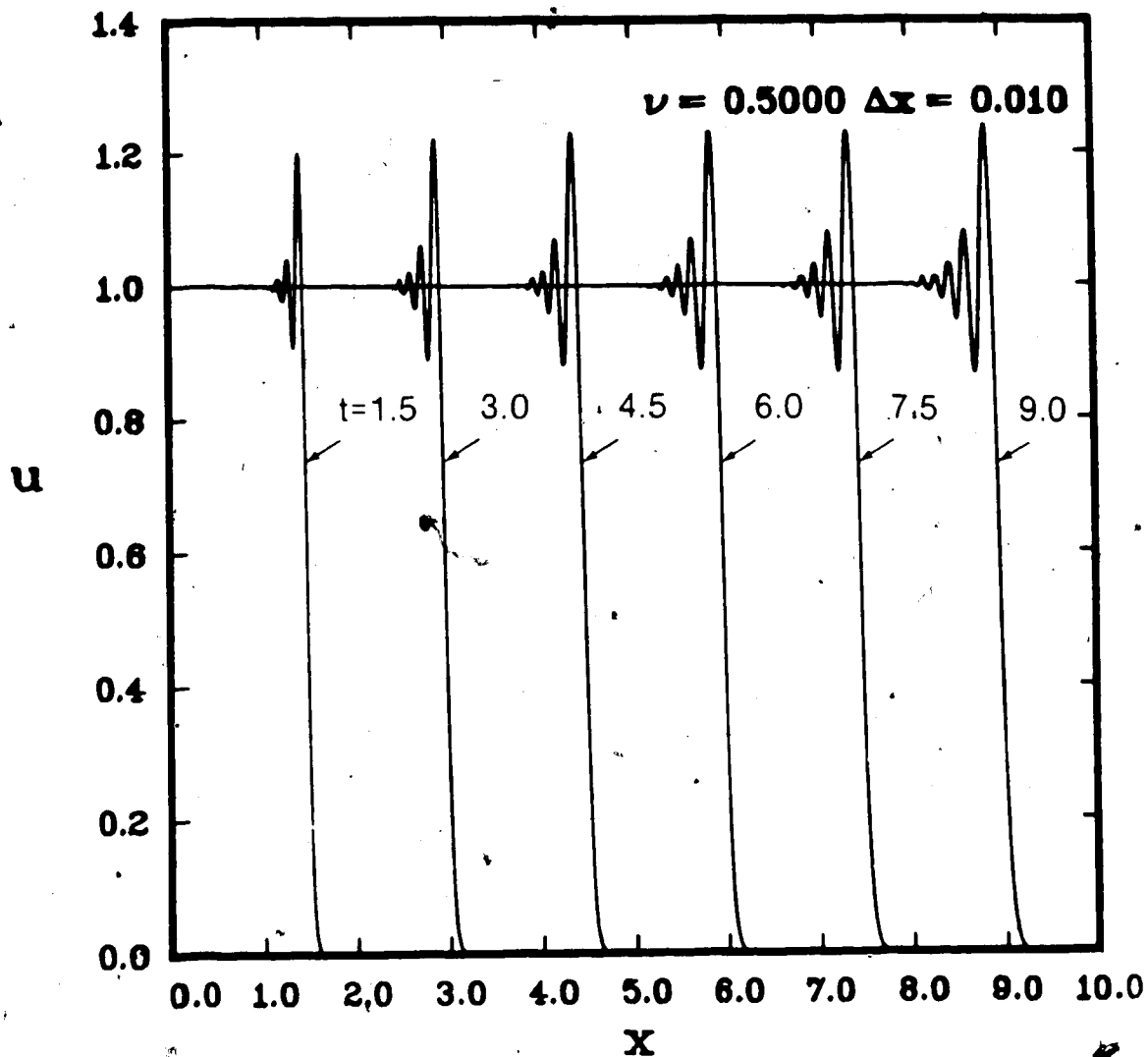


Fig. 2.3 The MacCormack scheme applied to $u_t + u_x = 0$ subject to $u(x,0) = 0$, $u(0,t) = U_0 H(t)$, $U_0 = 1$, for $\nu = 0.5$ and $\Delta x = 0.01$.

shape, in the positive x direction, with the wavefront located at $x = t$. The numerical results, presented for $\Delta x = 0.01$, for the various Courant numbers are, in general, in excellent agreement with the analytical solution except for numerical dispersion. Numerical dispersion appears as oscillations immediately behind the wavefront when $\nu = 0.99$ (Figure 2.2) and $\nu = 0.5$ (Figure 2.3). There is no numerical dispersion when $\nu = 1.0$ (Figure 2.1), which is consistent with results obtained by other authors (Anderson et al, 1984). There is no instability indicated by the results in Figure 2.1, which is also consistent with the von Neumann stability analysis of the finite difference scheme applied to equation (2.15). The stability condition given previously, $\nu \leq 1$, is the necessary and sufficient condition for stability of the initial value problem. Since the boundary condition is specified, there should be no boundary effects, and, therefore, the stability condition should directly apply to the boundary initial value solutions given in Figures 2.1 to 2.3.

Figures 2.4 - 2.6 show the effect of Courant number on the numerical solution of equation (2.15), with boundary condition (2.21), with $U_0 = 1$. The exact solution (see Appendix 2) is $u(x,t) = \sin\pi(t-x) H(t-x) H(1-(t-x))$, which describes a sine pulse of duration $t = 1$, propagating unchanged in shape in the positive x direction. The comments made regarding the step function are valid for the sine pulse, except that numerical dispersion is less severe for the sine pulse than for the step discontinuity, for a given Courant number. Mitchell and Griffiths (1980) confirm this

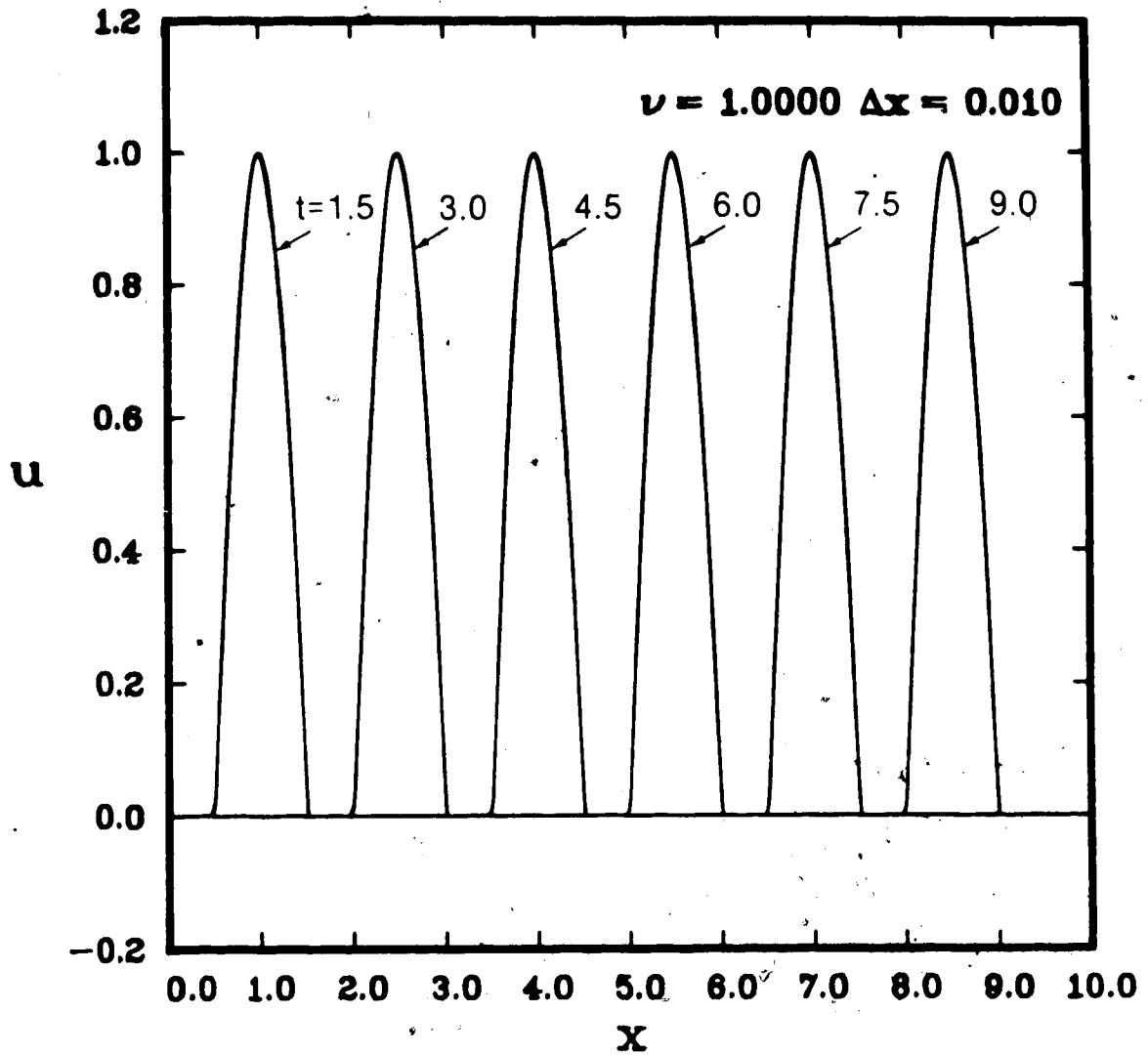


Fig. 2.4 The MacCormack scheme applied to $u_t + u_x = 0$ subject to $u(x,0) = 0$, $u(0,t) = U_0 \sin \pi t H(t) H(1-t)$, $U_0 = 1$ for $\nu = 1.0$ and $\Delta x = 0.01$.

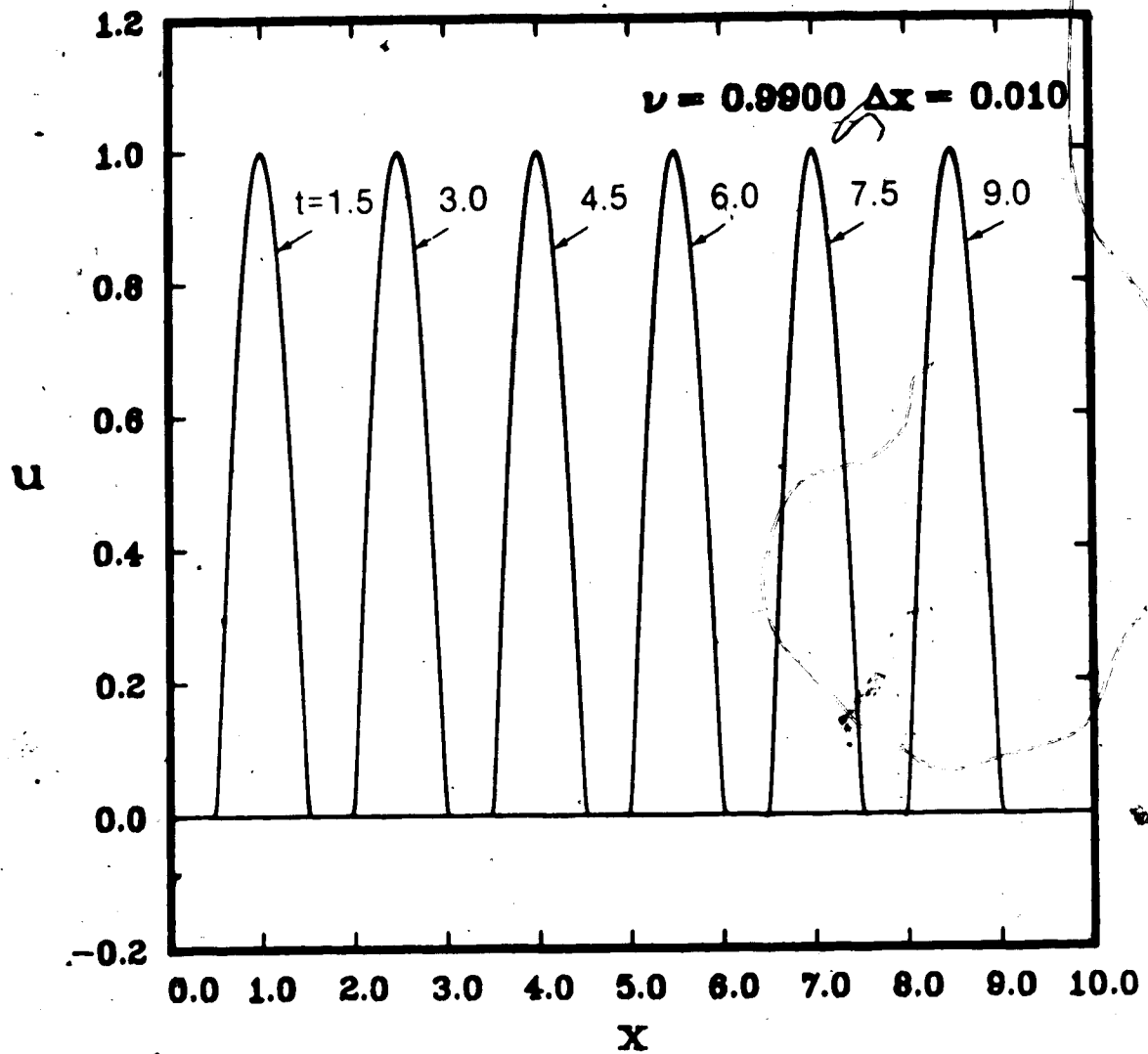


Fig. 2.5 The MacCormack scheme applied to $u_t + u_x = 0$ subject to $u(x,0) = 0$, $u(0,t) = U_0 \sin \pi t H(t) H(1-t)$, $U_0 = 1$, for $\nu = 0.99$ and $\Delta x = 0.01$.

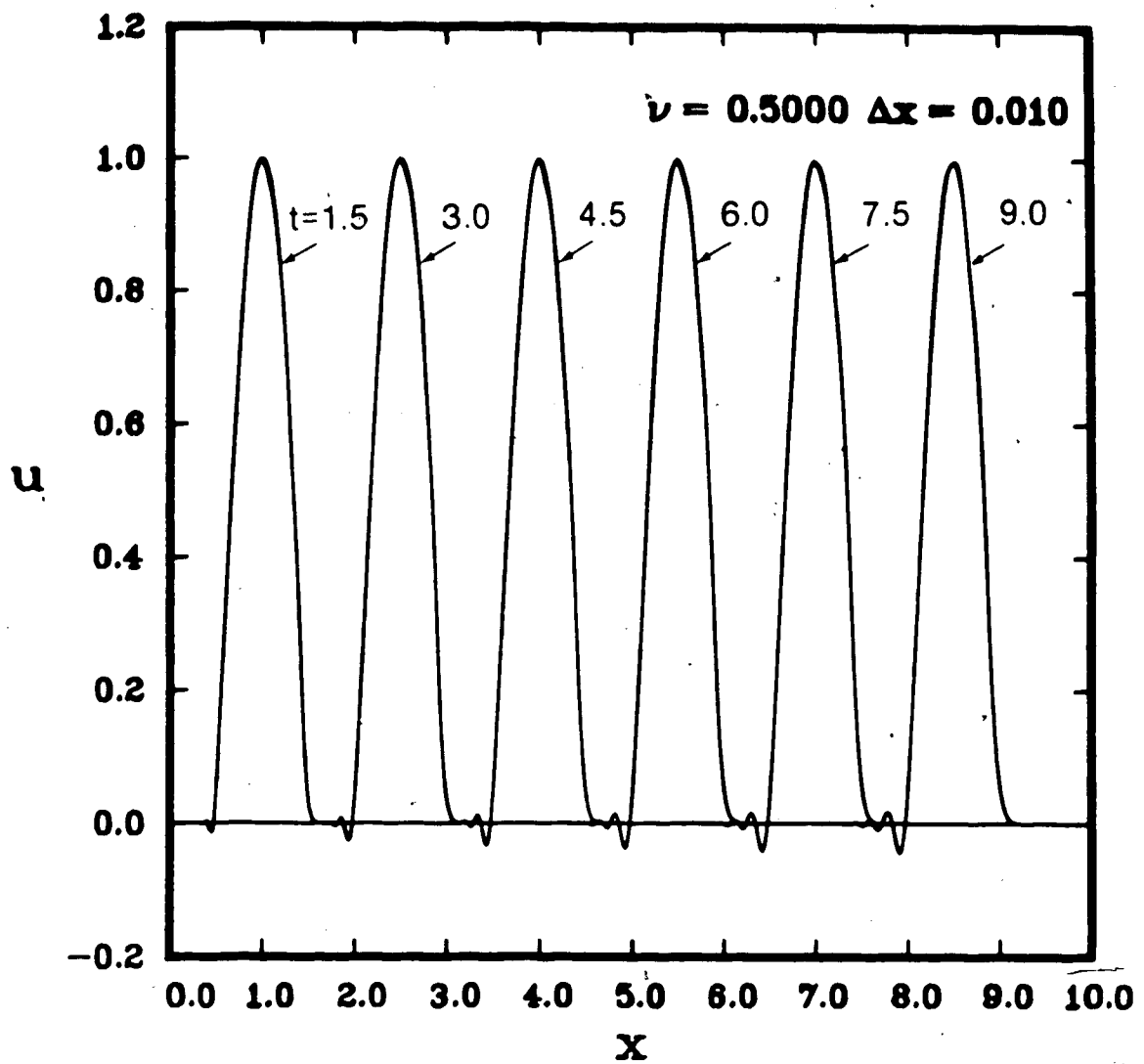


Fig. 2.6 The MacCormack scheme applied to $u_t + u_x = 0$ subject to $u(x,0) = u(0,t) = H(t)H(1-t)$, $U_0 = 1$, for $\nu = 0.5$, and $\Delta x = 0.01$

observation for initial value problems solved using the Lax-Wendroff technique. Since the Lax-Wendroff technique is equivalent to the MacCormack scheme for this problem, the comments made by Mitchell directly apply.

Figures 2.7 - 2.9 show the effect of Courant number on the numerical solution of equation (2.16), with boundary condition (2.20), with $U_0 = 1$. Numerical instability is indicated by the results presented in Figure 2.7, for $\nu = 1.0$, which does not appear in the results shown in Figure 2.1. This phenomena is extremely important, because it suggests that the additional term u in equation (2.16) affects the stability of the finite difference scheme. Numerical dispersion is also evident in Figures 2.8 and 2.9, with the same trends as were observed for equation (2.15). The exact solution corresponding to the numerical solution (see Appendix 2) is $u(x,t) = U_0 e^{-x} H(t-x)$. The numerical solution is in excellent agreement with the exact solution, except where instability or numerical dispersion is present.

Figures 2.10a and 2.10b show the results of the von Neumann stability analysis for the MacCormack scheme applied to equation (2.16). The quantity $(\lambda-1)$, is plotted against β for various Courant numbers and grid spacings of $\Delta x = 0.025$ and $\Delta x = 0.01$, respectively. The stability analysis indicates that the MacCormack scheme is unstable for $\nu = 1.0$ and $\Delta x = 0.01$. The numerical results (see Figure 2.7) are consistent with the stability analysis.

The stability analysis shows that the stability criterion is a function of the grid spacing. This can be seen directly from

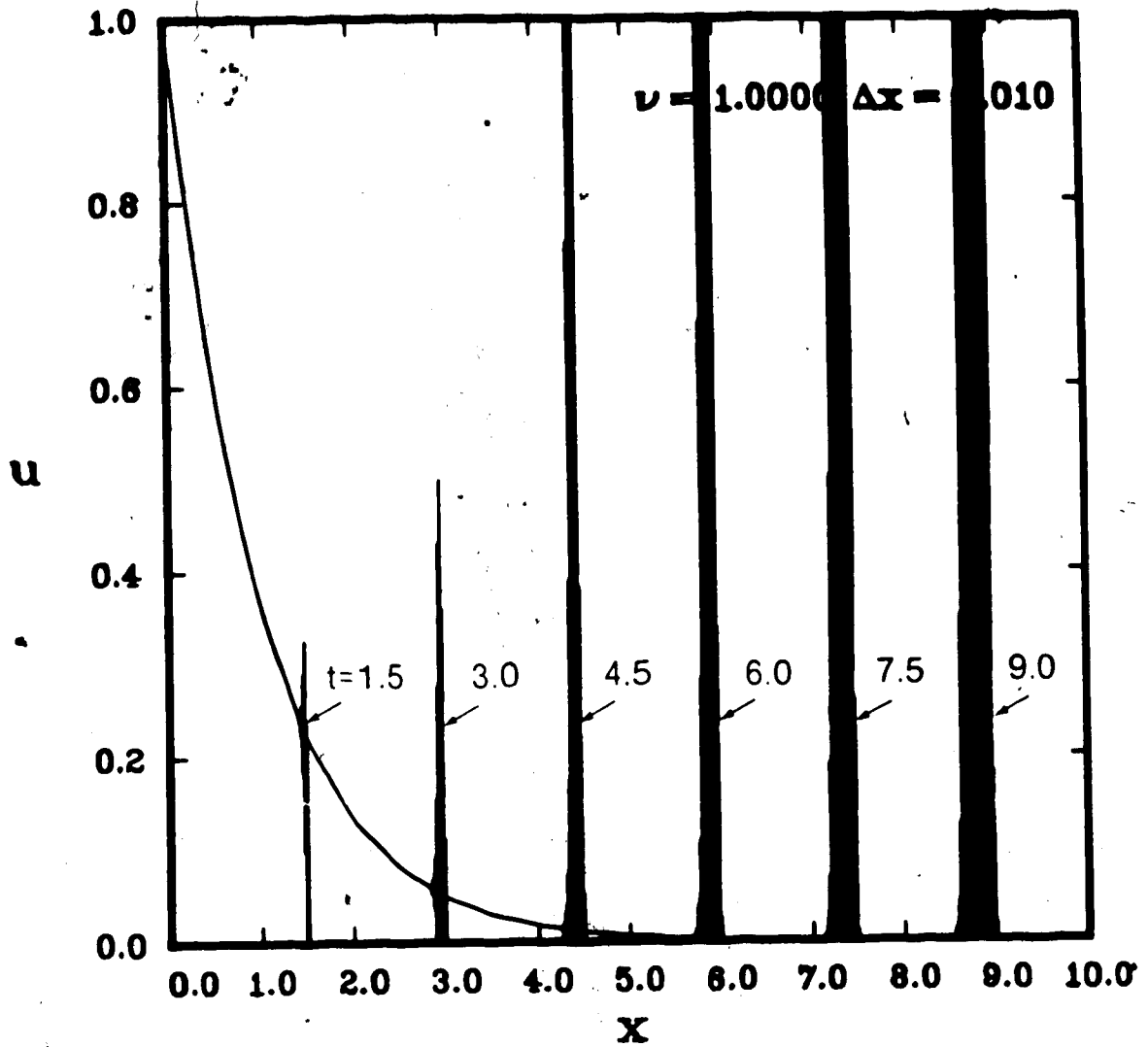


Fig. 2.7 The MacCormack scheme applied to $u_t + u_x + u = 0$ subject to $u(x,0) = 0$, $u(0,t) = U_0 H(t)$, $U_0 = 1$, for $\nu = 1.0$ and $\Delta x = 0.01$.

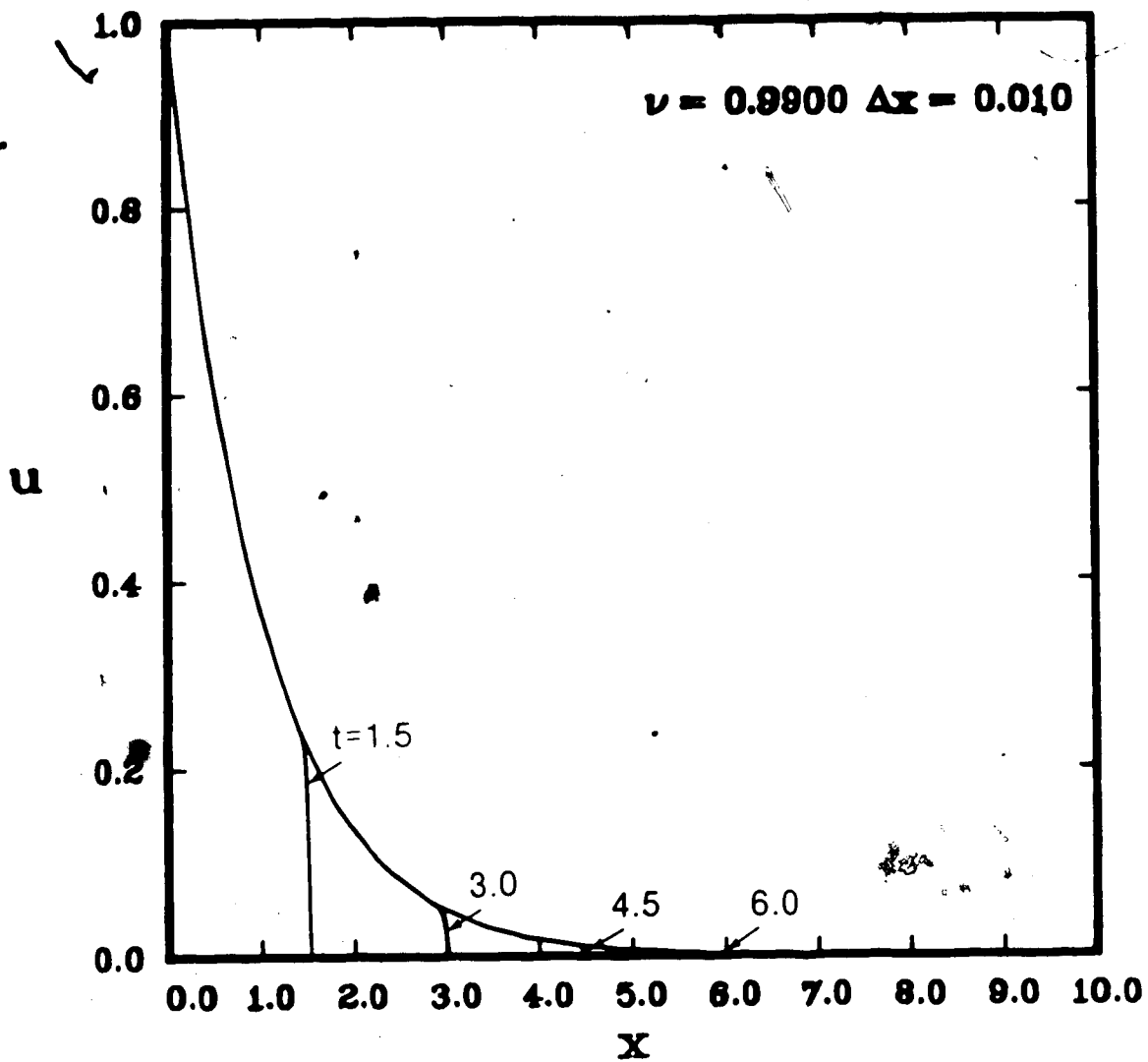


Fig. 2.8 The MacCormack scheme applied to $u_t + u_x + u = 0$ subject to $u(x,0) = 0$, $u(0,t) = U_0 H(t)$, $U_0 = 1$, for $\nu = 0.99$ and $\Delta x = 0.01$.

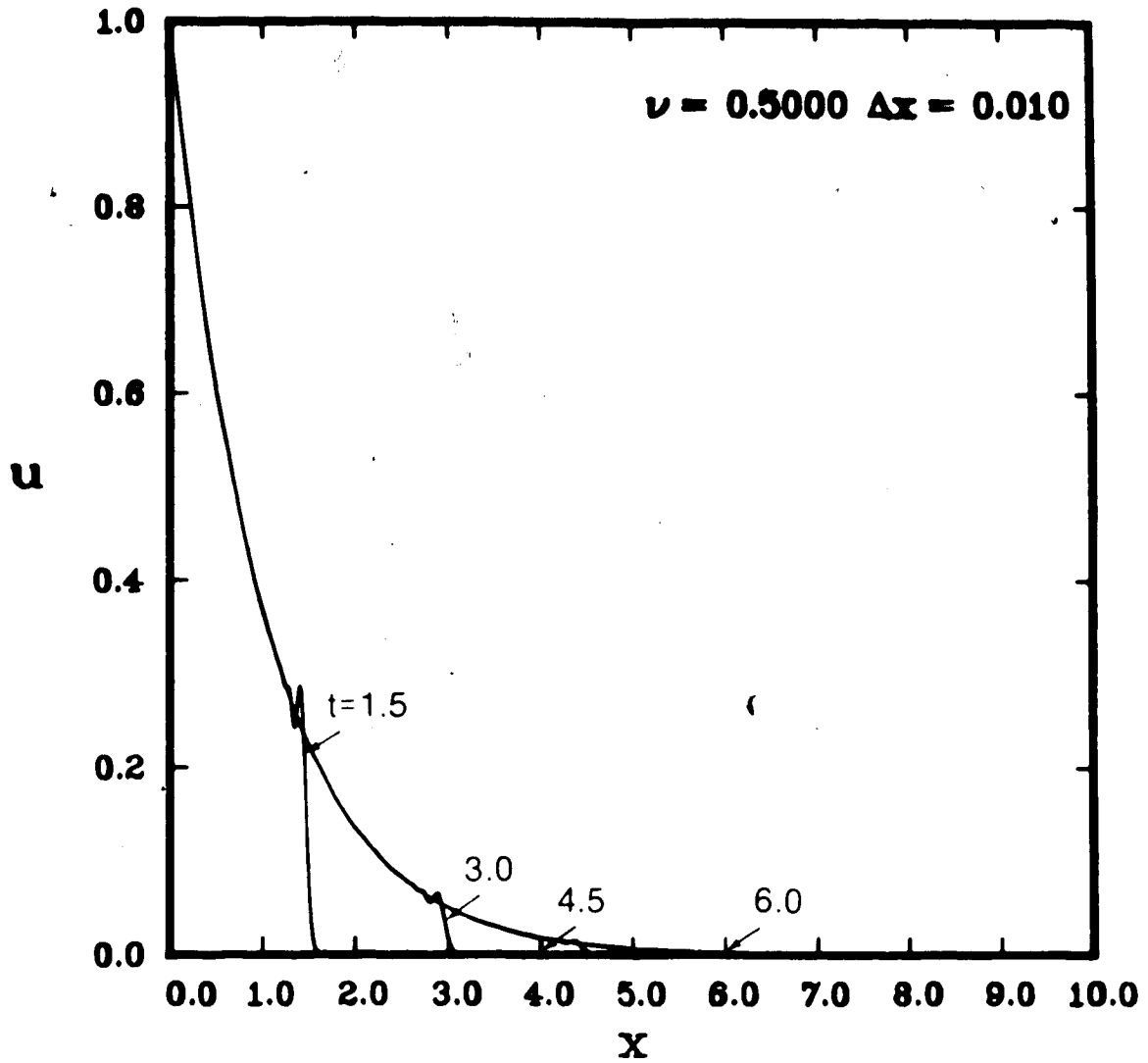


Fig. 2.9 The MacCormack scheme applied to $u_t + u_x + u = 0$ subject to $u(x,0) = 0$, $u(0,t) = U_0 H(t)$, $U_0 = 1$, for $\nu = 0.5$ and $\Delta x = 0.01$.

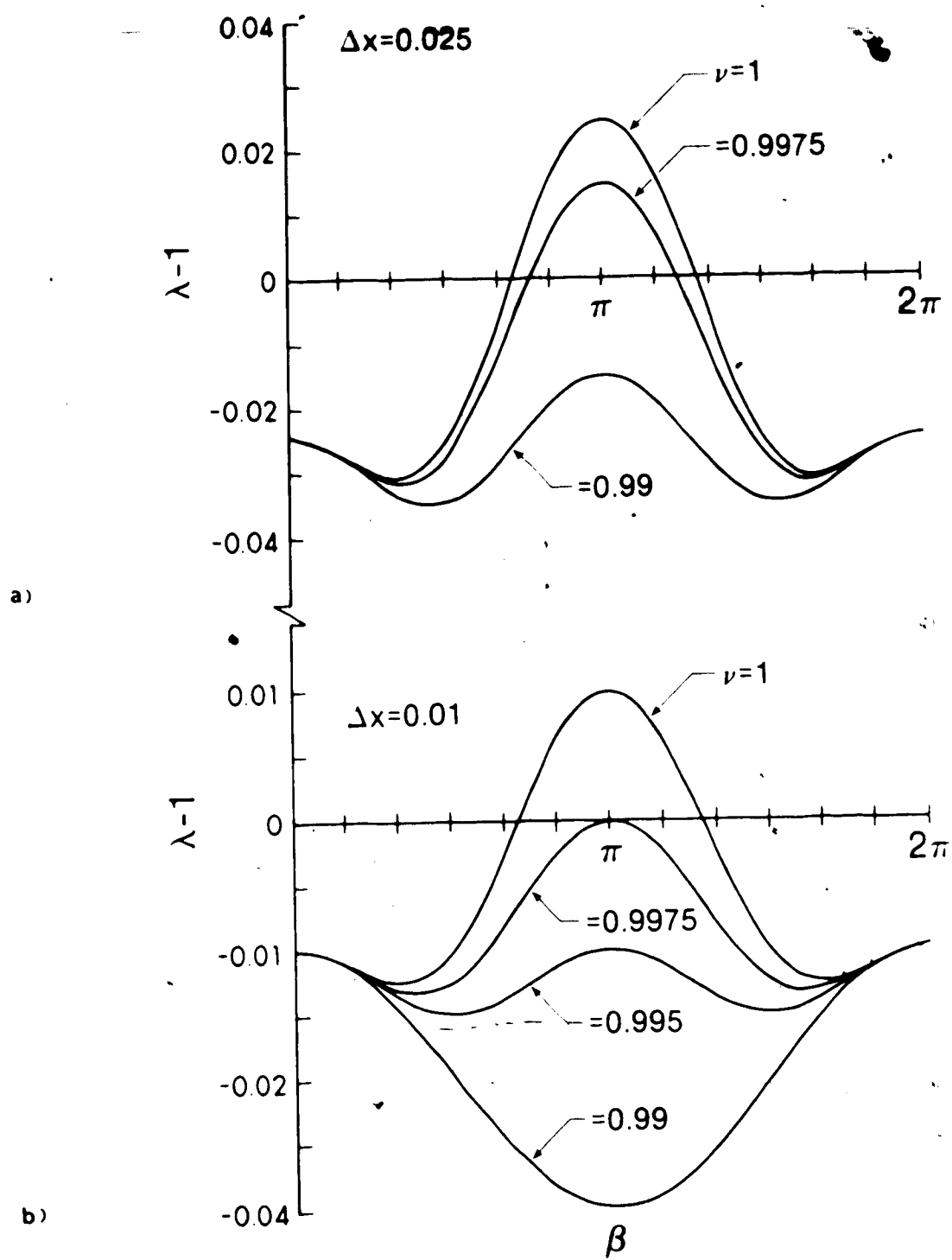


Fig. 2.10 von Neumann stability analysis for the MacCormack difference scheme applied to $u_t + u_x + u = 0$ for $\Delta x = 0.01$ and $\Delta x = 0.025$.

equation (2.27). This dependence of stability on grid spacing makes it difficult to obtain a simple stability criterion for the problem considered. A comparison of the graphs for $\Delta x = 0.01$ and $\Delta x = 0.025$ shows that the smaller grid size $\Delta x = 0.01$, is desirable for stability since the maximum Courant number for stability is closer to 1 than for $\Delta x = 0.025$.

Figures 2.11 and 2.12 show numerical solutions at various times for equation (2.16), for boundary condition (2.20), with $U_0 = 1$, for $\nu = 0.9975$ and 0.995 , respectively, with $\Delta x = 0.01$. Figure 2.13 shows similar solutions, for $\nu = 0.9975$, and $\Delta x = 0.025$. The stability analysis using the von Neumann method is consistent with these numerical results.

Figures 2.14 - 2.16 show the numerical solutions for equation (2.16), with boundary condition (2.21), with $U_0 = 1$. The exact solution (see Appendix 2) is $u(x,t) = U_0 e^{-x} \sin \pi(t-x) H(t-x) H(1-(t-x))$, which describes a sine pulse of duration $t = 1$ propagating in the positive x direction. The sine pulse changes shape due to the factor e^{-x} in the exact solution. The numerical solution is unstable for $\nu = 1.0$ (see Figure 2.14), similar to the step function, but the instability is less severe for the sine pulse for a given time than for the step function boundary condition (2.20). Numerical dispersion is evident in Figure 2.16 but less evident in Figure 2.15, since the solution attenuates rapidly. In some instances it can be difficult to distinguish between numerical dispersion and physical dispersion.

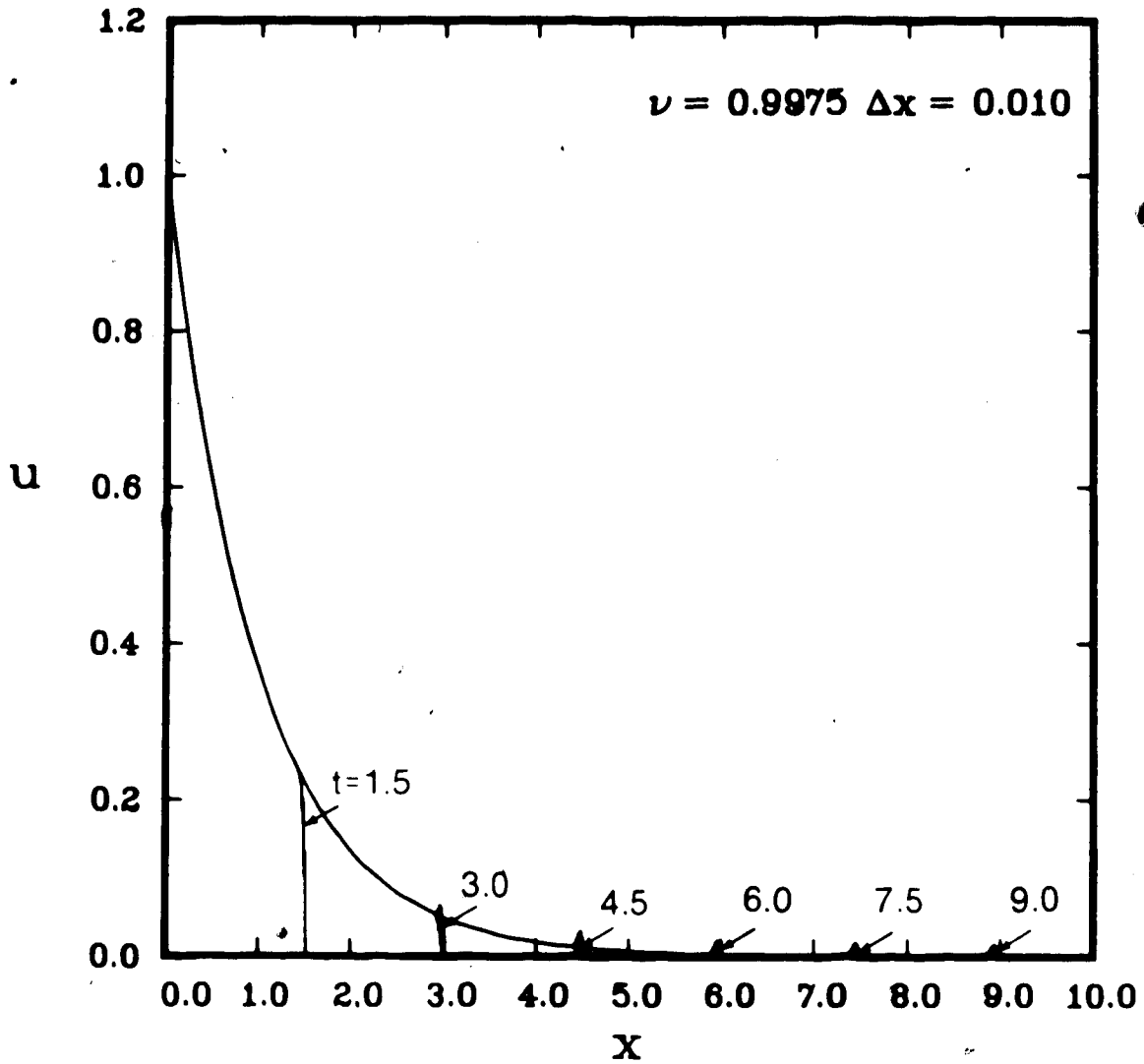


Fig. 2.11 The MacCormack scheme applied to $u_t + u_x + u = 0$ subject to $u(x,0) = 0$, $u(0,t) = U_0 H(t)$, $U_0 = 1$, for $\nu = 0.9975$ and $\Delta x = 0.01$.

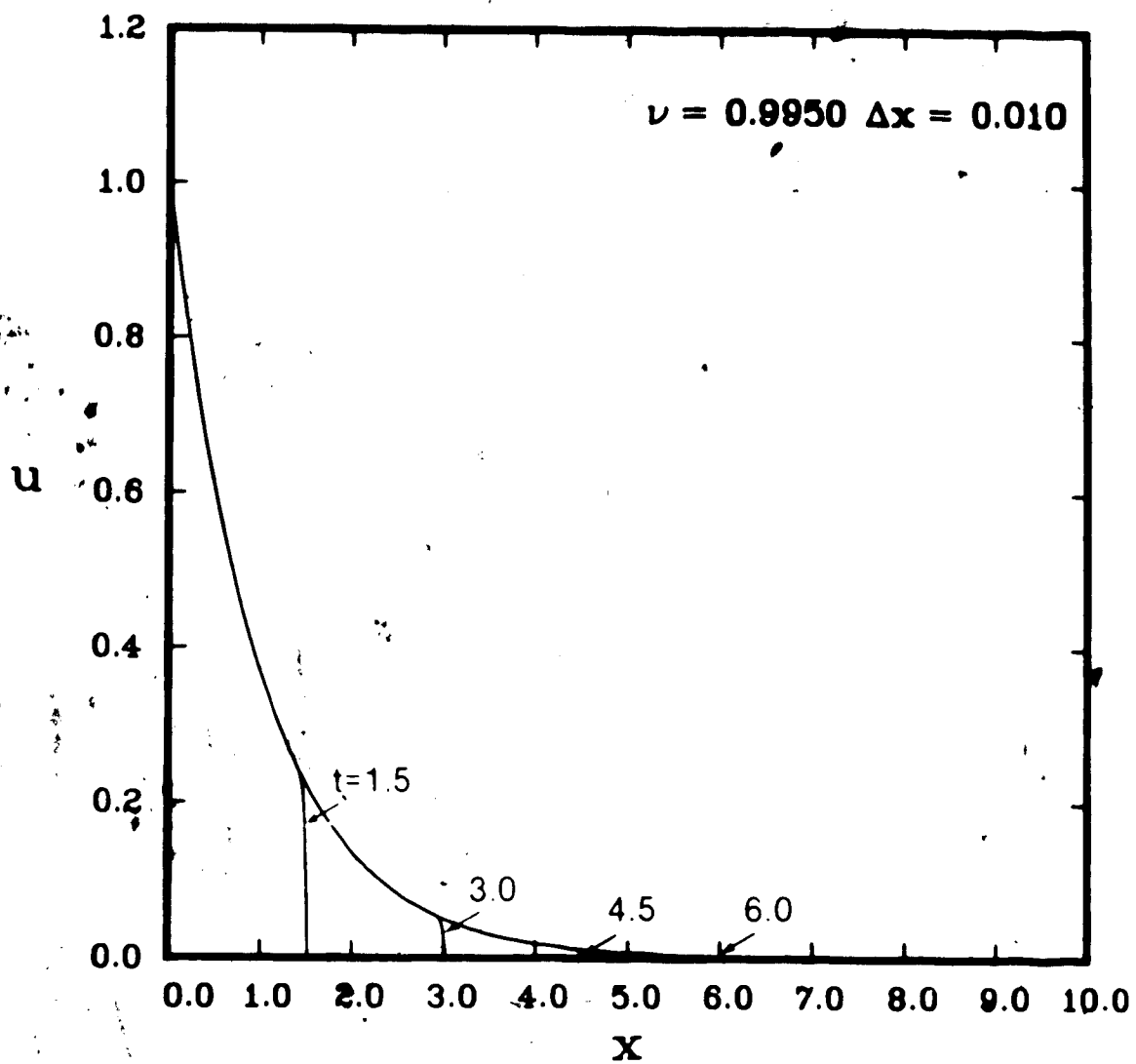


Fig. 2.12 The MacCormack scheme applied to $u_t + u_x + u = 0$ subject to $u(x, 0) = 0$, $u(0, t) = U_0 H(t)$, $U_0 = 1$, for $\nu = 0.995$ and $\Delta x = 0.01$.

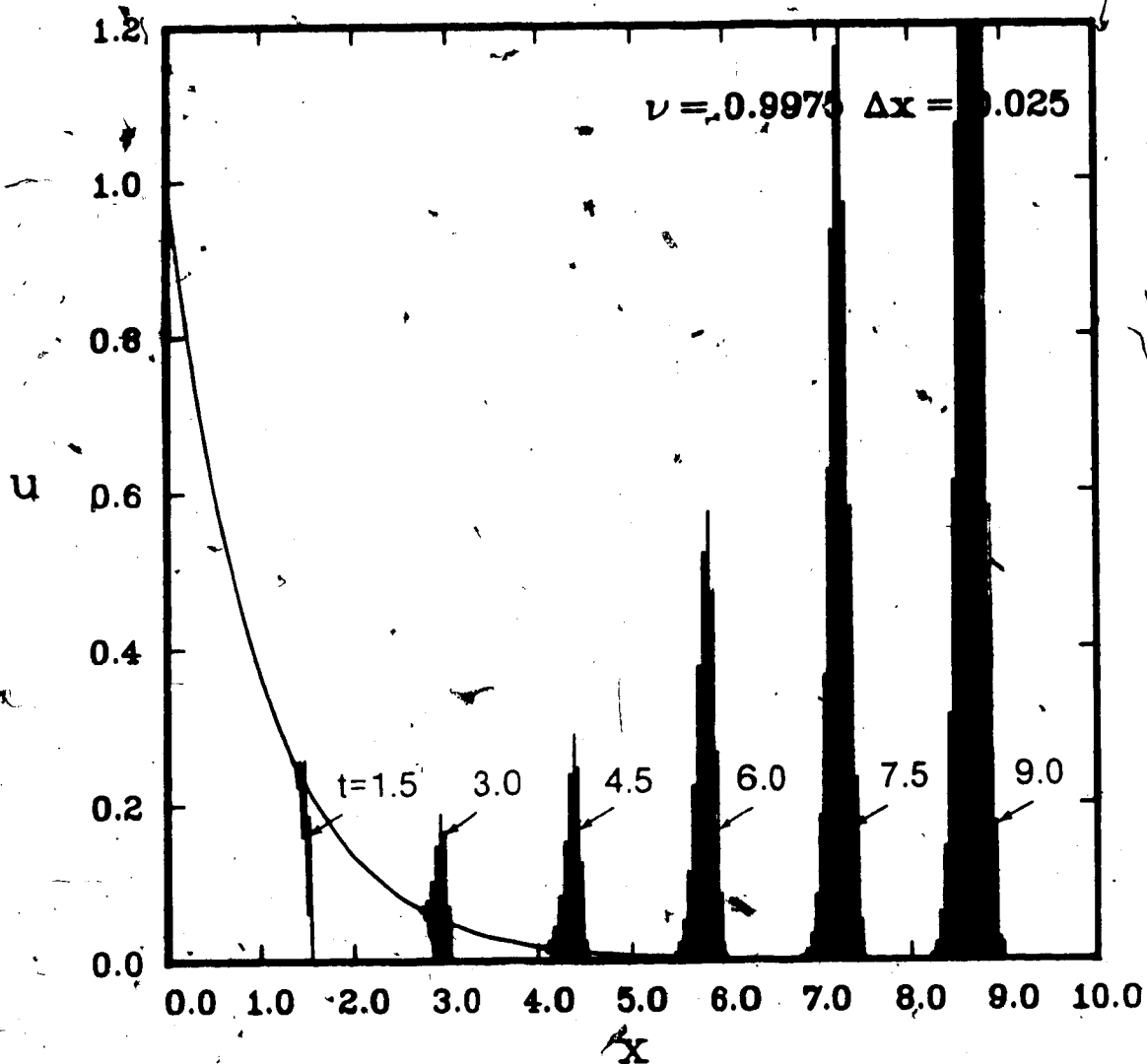


Fig. 2.13 The MacCormack scheme applied to $u_t + u_x + u = 0$ subject to $u(x,0) = 0$, $u(0,t) = U_0 H(t)$, $U_0 = 1$, for $\nu = 0.9975$ and $\Delta x = 0.025$.

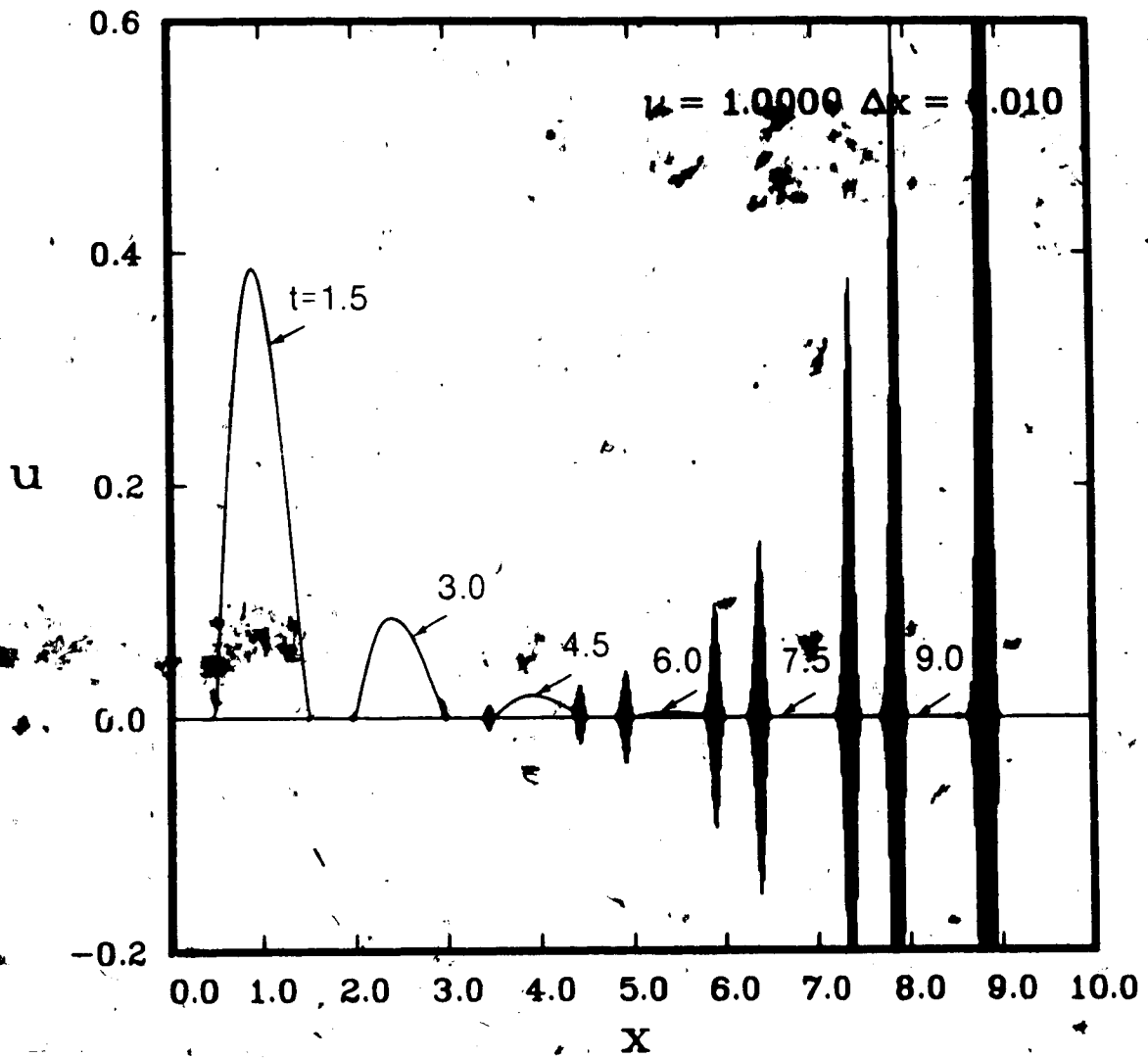


Fig. 2.14 The MacCormack scheme applied to $u_t + u_x + u^2 = 0$ subject to $u(x,0) = 0$, $u(0,t) = U_0 \sin \pi t \cdot H(t) \cdot H(1-t)$, $U_0 = 1$, for $\nu = 1.0$ and $\Delta x = 0.01$.

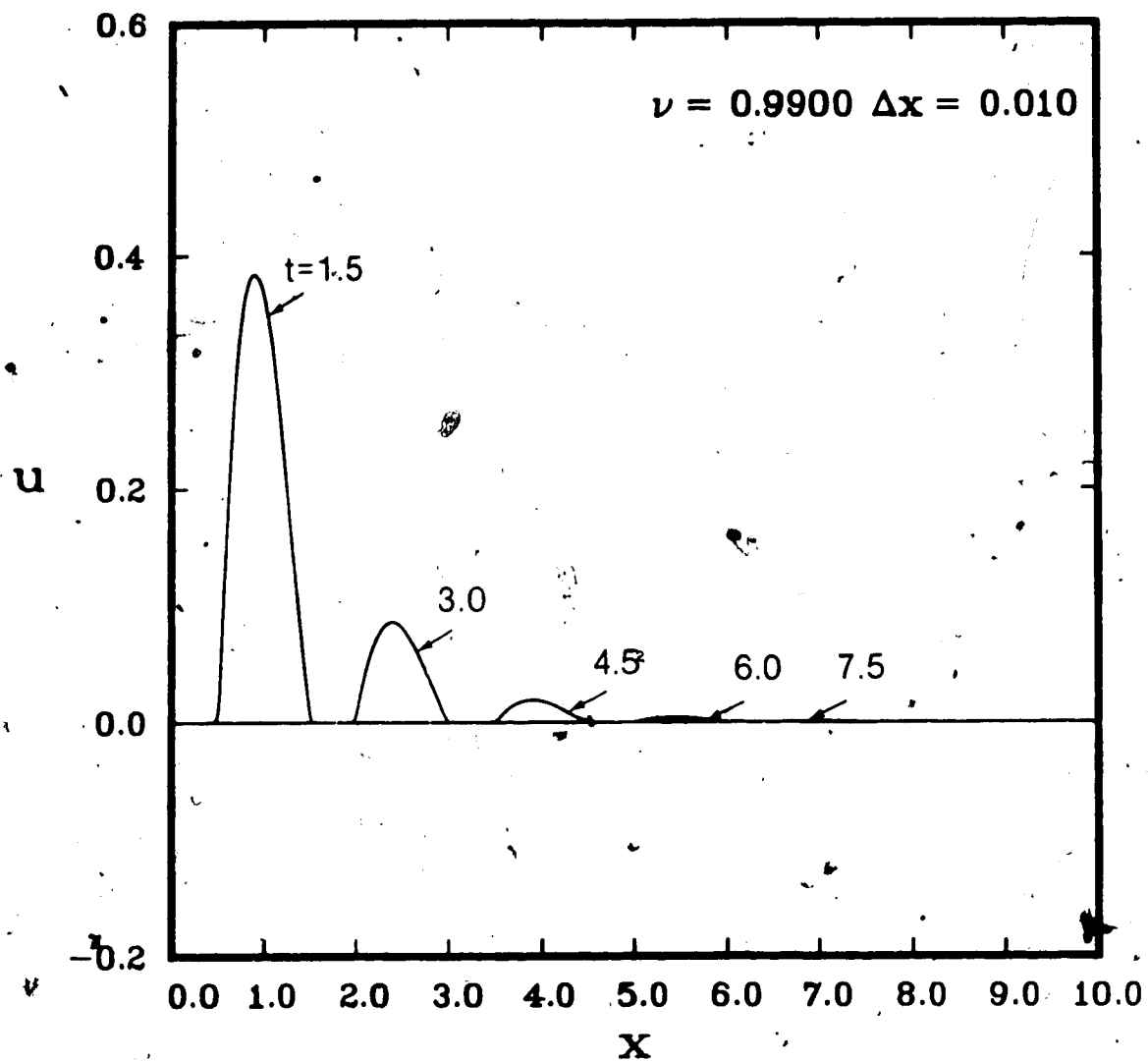


Fig. 2.15 The MacCormack scheme applied to $u_t + u_x + u = 0$, subject to $u(x, 0) = 0$, $u(0, t) = U_0 \sin \pi t \cdot H(t) H(1-t)$, $U_0 = 1$, for $\nu = 0.99$ and $\Delta x = 0.01$.

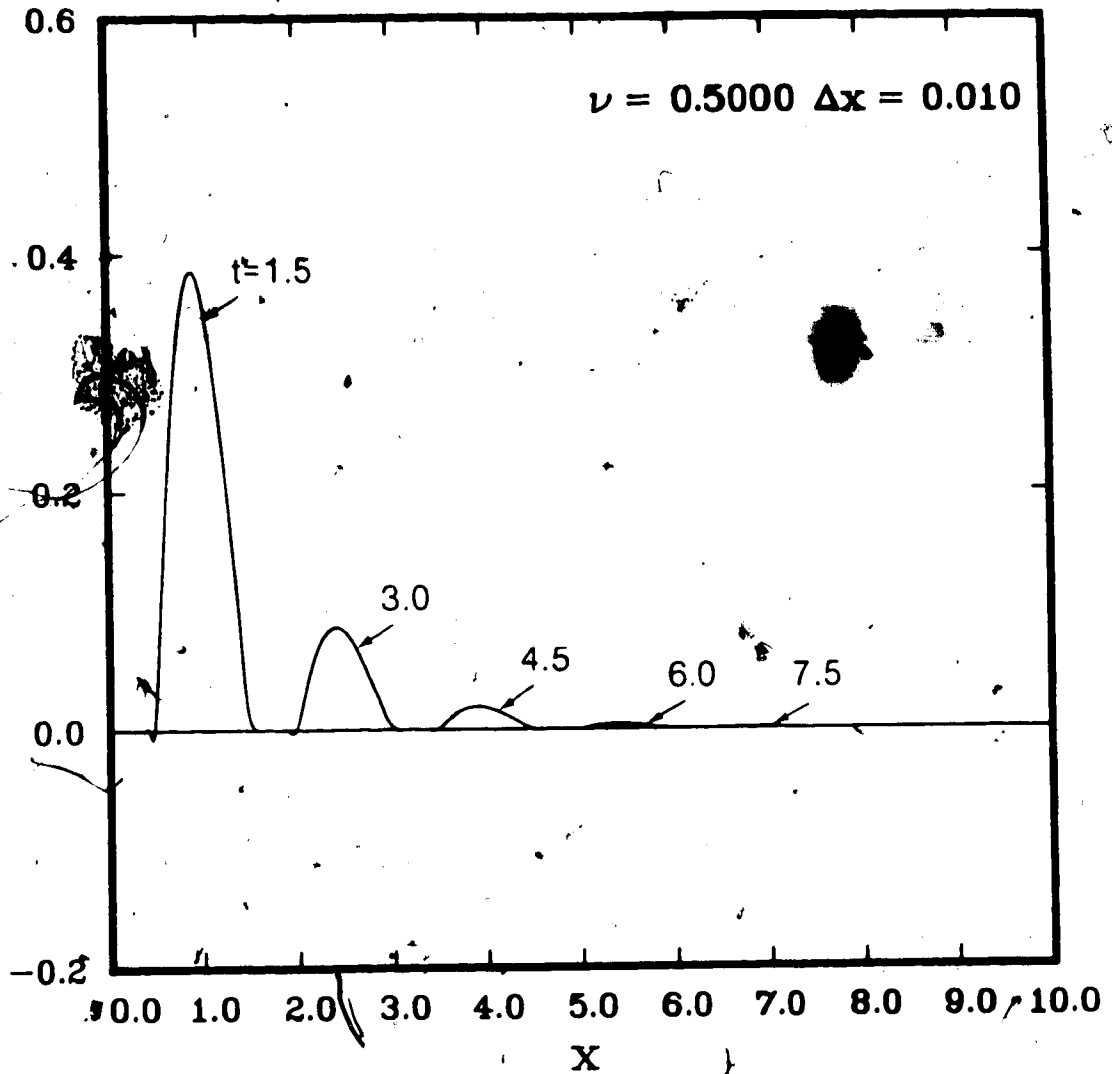


Fig. 2.16 The MacCormack scheme applied to $u_t + u_x + u = 0$ subject to $u(x,0) = 0$, $u(0,t) = U_0 \sin \pi t H(t) H(1-t)$, $U_0 = 1$, for $\nu = 0.5$ and $\Delta x = 0.01$.

The nonlinear versions of equations (2.15) and (2.16) are solved using the conservative MacCormack scheme (2.7). A value of $c = 1$ is used to determine the Courant number, rather than the wave speed u . This gives good results for $U_0 = 1$. Although the results from the von Neumann stability analyses for equations (2.15) and (2.16) do not directly apply, the numerical phenomena indicated by the numerical results for the linear scalar equations, are similar to those observed in the numerical solutions of the nonlinear scalar equations.

Figures 2.17 - 2.19 show the effect of Courant number on the numerical solutions of equation (2.17), for boundary condition (2.20), with $U_0 = 1$. The numerical solutions, at the times indicated, for $\nu = 1.0$ (see Figure 2.17), are stable but exhibit numerical dispersion for $\nu = 0.5$ (see Figure 2.19). There is much less dispersion in the solutions for $\nu = 0.99$, than for their linear counterparts (see Figure 2.2). The exact solution, obtained by the method of characteristics, indicates that a step discontinuity of magnitude U_0 must propagate with a shock speed $\dot{V} = (1/2)U_0$. The numerical solution is in good agreement with the exact solution. It should be noted, however, that the MacCormack scheme applied to equation (2.17) did not work for $U_0 = 0.01$. This behaviour is expected since u is associated with the wave speed, and as u becomes small, the wave speed tends to zero.

Figures 2.20 - 2.22 show the effect of Courant number on the numerical solution of equation (2.17), with boundary condition (2.21), with $U_0 = 1$. Since the boundary condition is a sine pulse

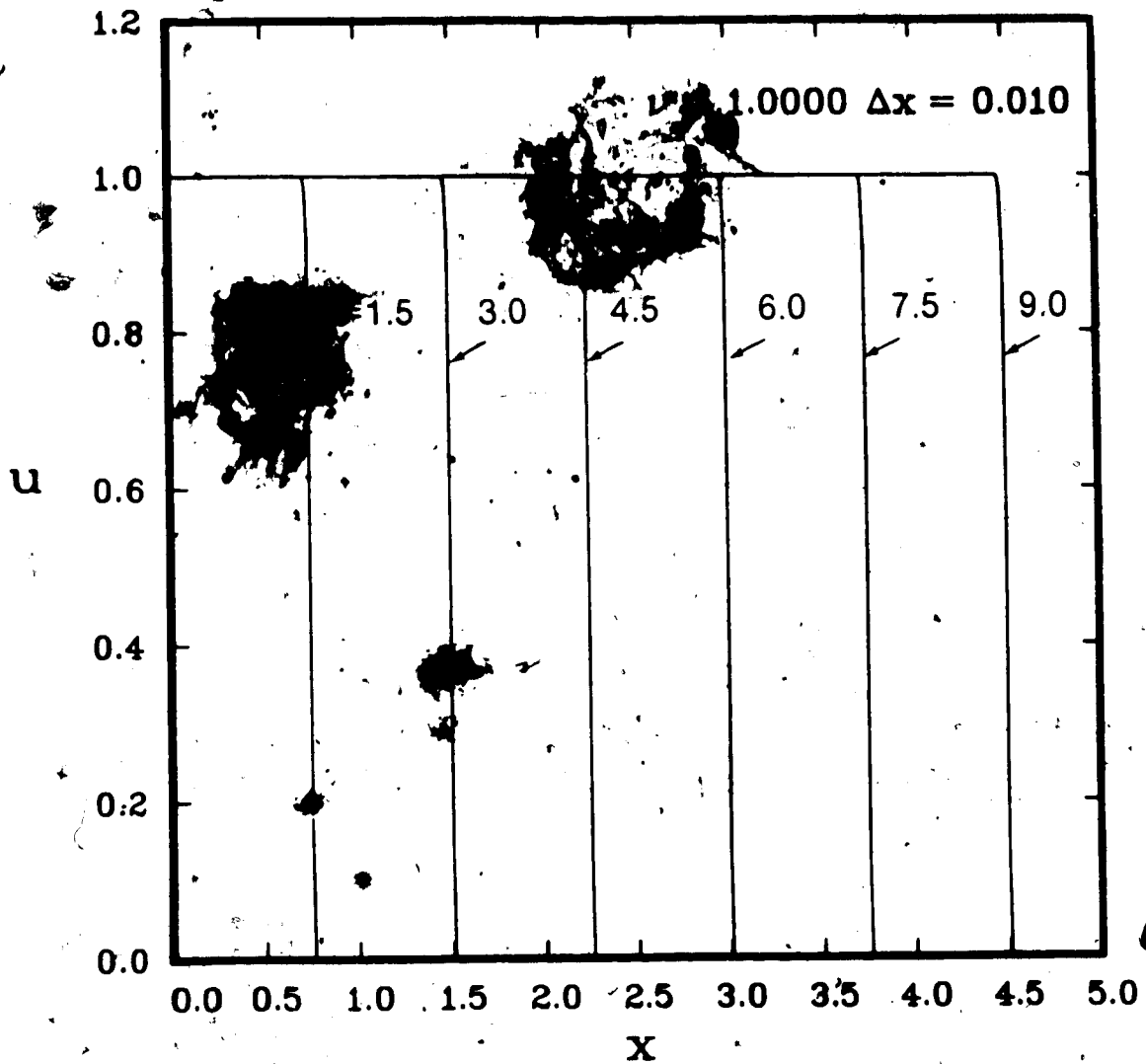


Fig. 2.17 The MacCormack scheme applied to $u_t + uu_x = 0$ subject to $u(x,0) = 0$, $u(0,t) = U_0 H(t)$, $U_0 = 1$, for $\nu = 1.0$ and $\Delta x = 0.01$.

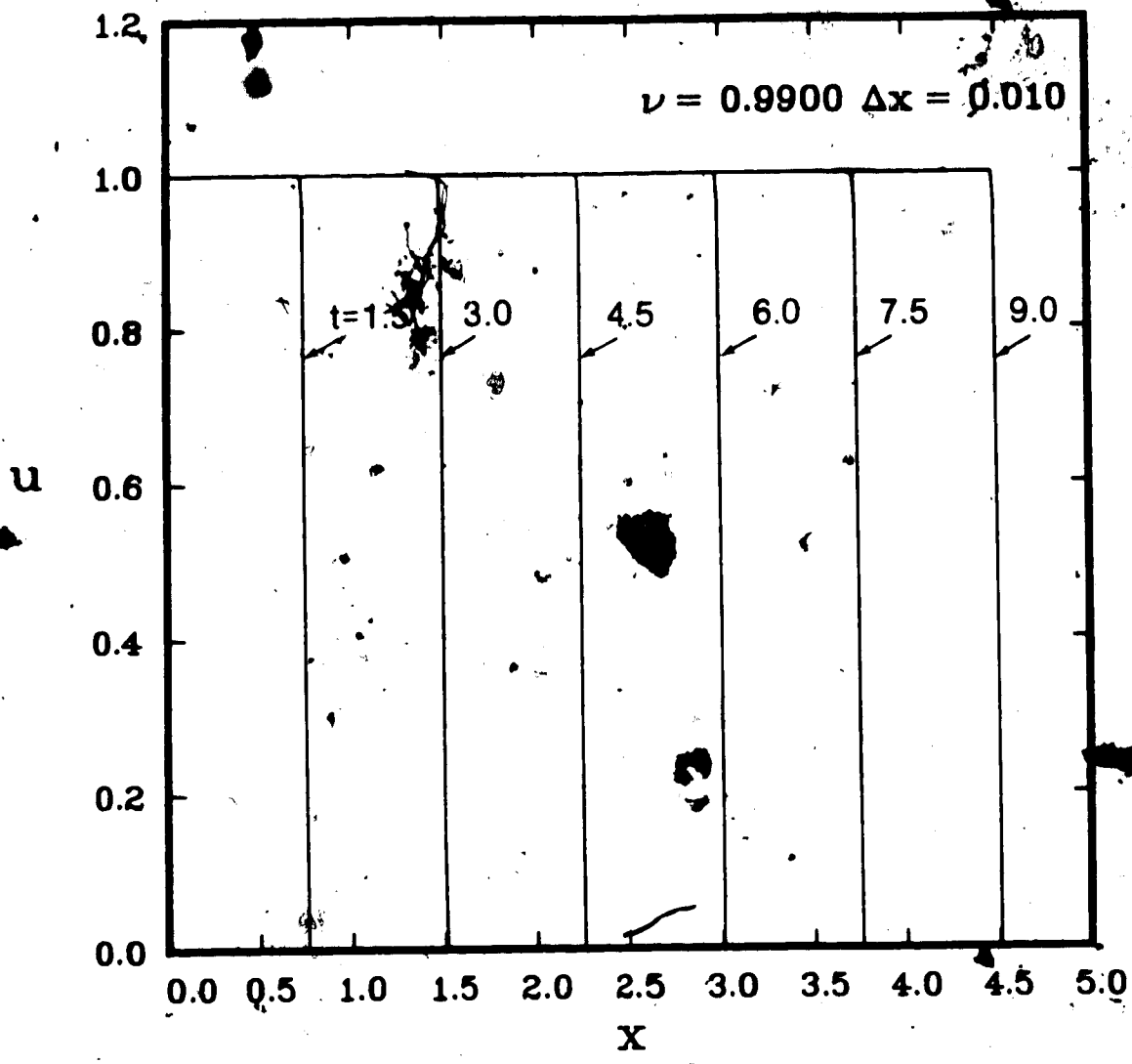


Fig. 2.18 The MacCormack scheme applied to $u_t + uu_x = 0$ subject to $u(x,0) = 0, u(0,t) = U_0 H(t), U_0 = 1$, for $\nu = 0.99$ and $\Delta x = 0.01$.

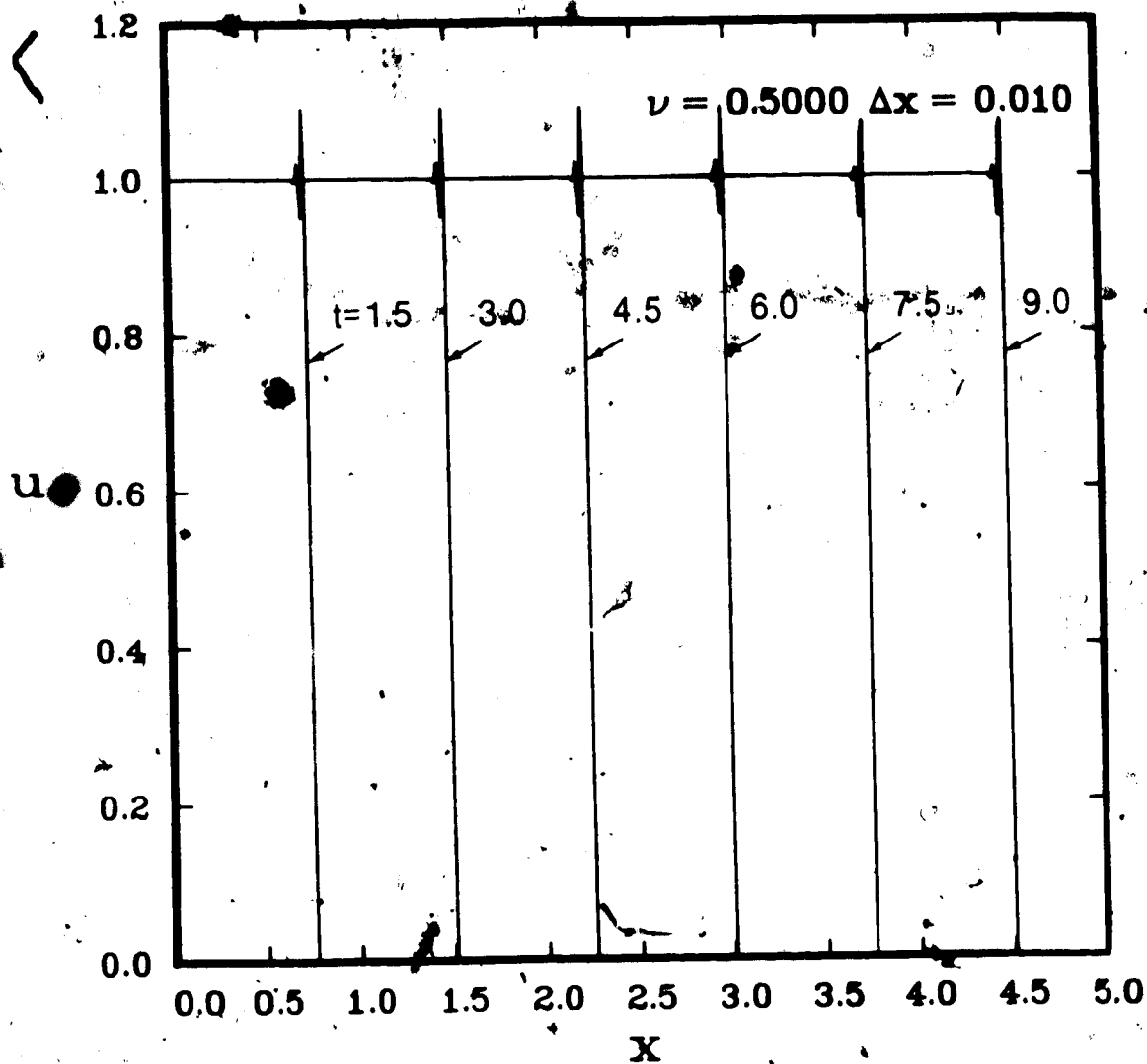


Fig. 2.19 The MacCormack scheme applied to $u_t + uu_x = 0$ subject to $u(x,0) = 0$, $u(0,t) = U_0 H(t)$, $U_0 = 1$, for $\nu = 0.5$ and $\Delta x = 0.01$.

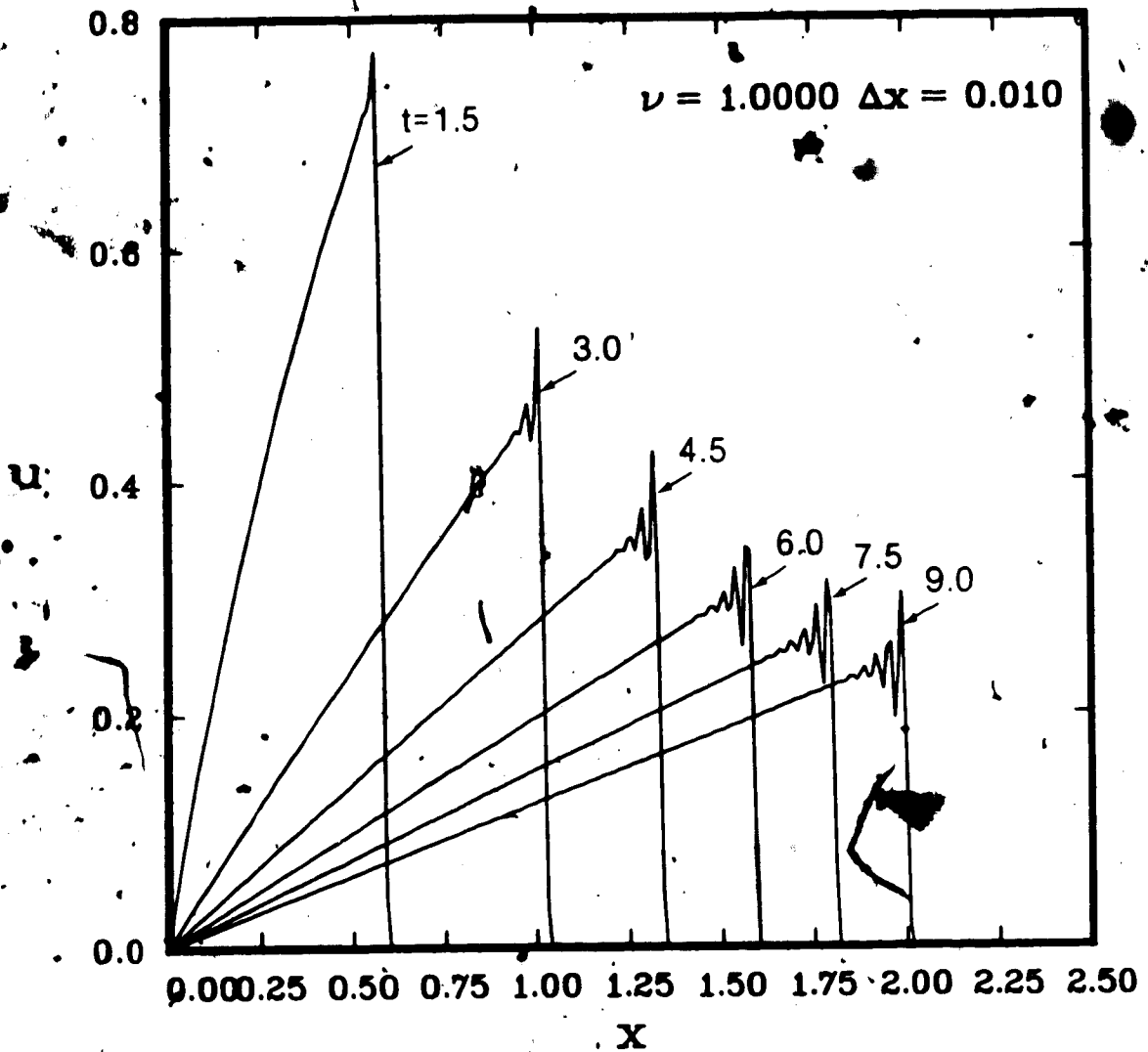


Fig. 2.20 The MacCormack scheme applied to $u_t + uu_x = 0$ subject to $u(x,0) = 0$, $u(0,t) = U_0 \sin \pi t H(t) H(1-t)$, $U_0 = 1$, for $\nu = 1.0$ and $\Delta x = 0.01$.

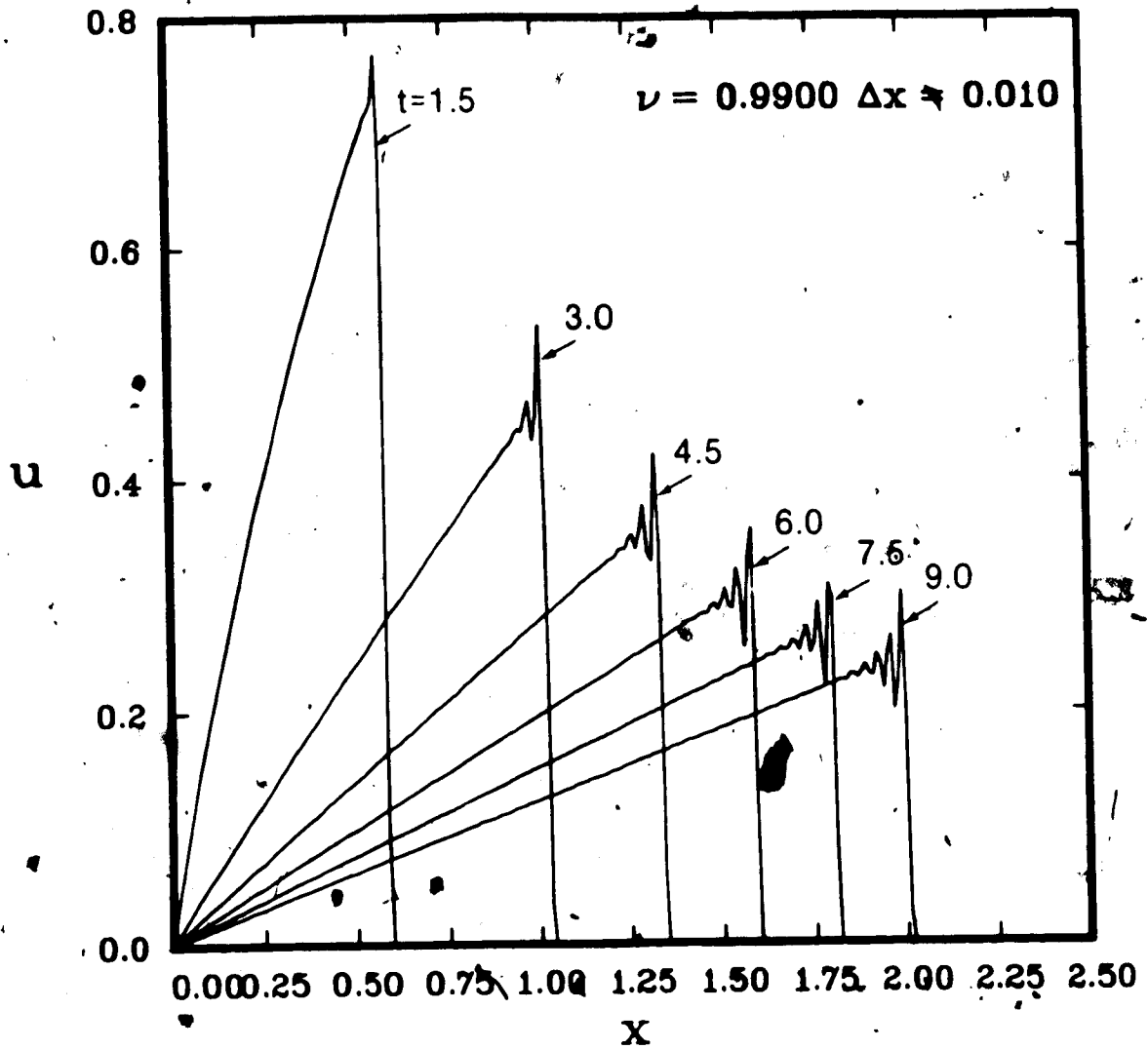


Fig. 2.21 The MacCormack scheme applied to $u_t + uu_x = 0$ subject to $u(x,0) = 0$, $u(0,t) = U_0 \sin \pi t H(t) H(1-t)$, $U_0 = 1$, for $\nu = 0.99$ and $\Delta x = 0.01$.

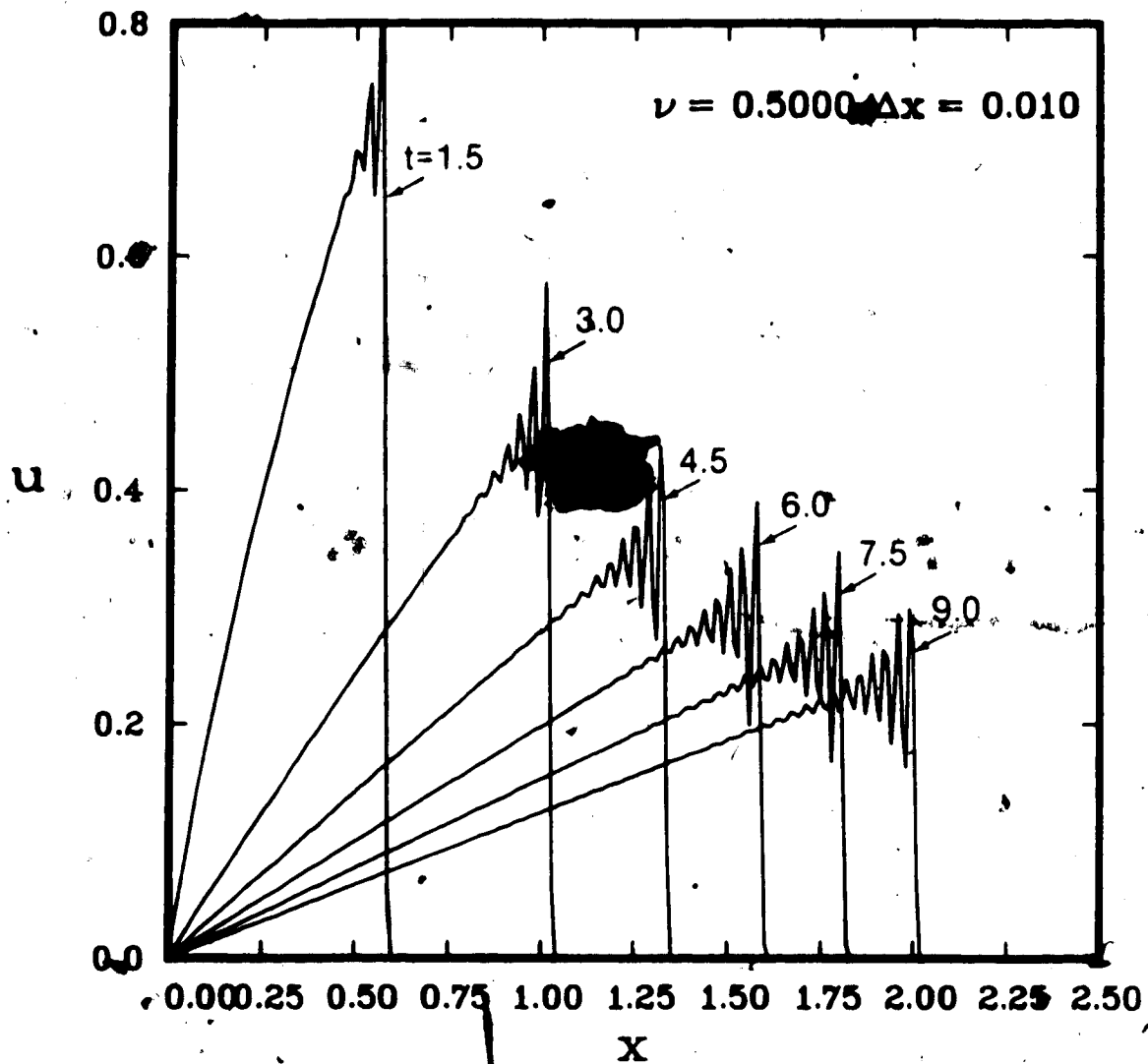


Fig. 2.22 The MacCormack scheme applied to $u_t + uu_x = 0$ subject to $u(x,0) = 0$, $u(0,t) = U_0 \sin t H(t) H(1-t)$, $U_0 = 1$, for $\nu = 0.5$ and $\Delta x = 0.01$.

of duration $t = 1$, it is evident from Figures 2.20 - 2.22 that the wave has broken, which is indicative of shock formation. There are oscillations behind the wavefront in each of the figures considered, and, the oscillations are most severe for $\nu = 0.5$ (see Figure 2.22).

The numerical solutions for equation (2.18), with boundary condition (2.20), with $U_0 = 1$ are shown for various Courant numbers in Figures 2.23 - 2.25. The numerical solution for $\nu = 1.0$ shows some numerical dispersion, but does not appear unstable for the times considered. The results are in excellent agreement with those obtained by the method of characteristics (see Appendix 2), which gives $u(x,t) = (1-x/U_0)H(1-e^{-(t/2)}-x)$. A comparison of Figure 2.23 to Figure 2.7, which is the linear counterpart, indicates that numerical instability in the solution to the linear equation (2.16) is not present in the solution to the nonlinear equation (2.18).

The numerical results for equation (2.18), for boundary condition (2.21), are shown in Figures 2.26 - 2.28 for various Courant numbers and times. There are severe oscillations in the numerical results in each figure, however, the oscillations are the worst for $\nu = 0.5$. There does not appear to be any instability for $\nu = 1.0$, which differs from the results obtained for the linear scalar equation (2.16).

Figure 2.29 shows the effect of grid size on the numerical solution of equation (2.17), with boundary condition (2.20), with $U_0 = 1$. There is very little difference between the solutions for $\Delta x = 0.02$ and $\Delta x = 0.01$, and therefore $\Delta x = 0.01$ was chosen as a

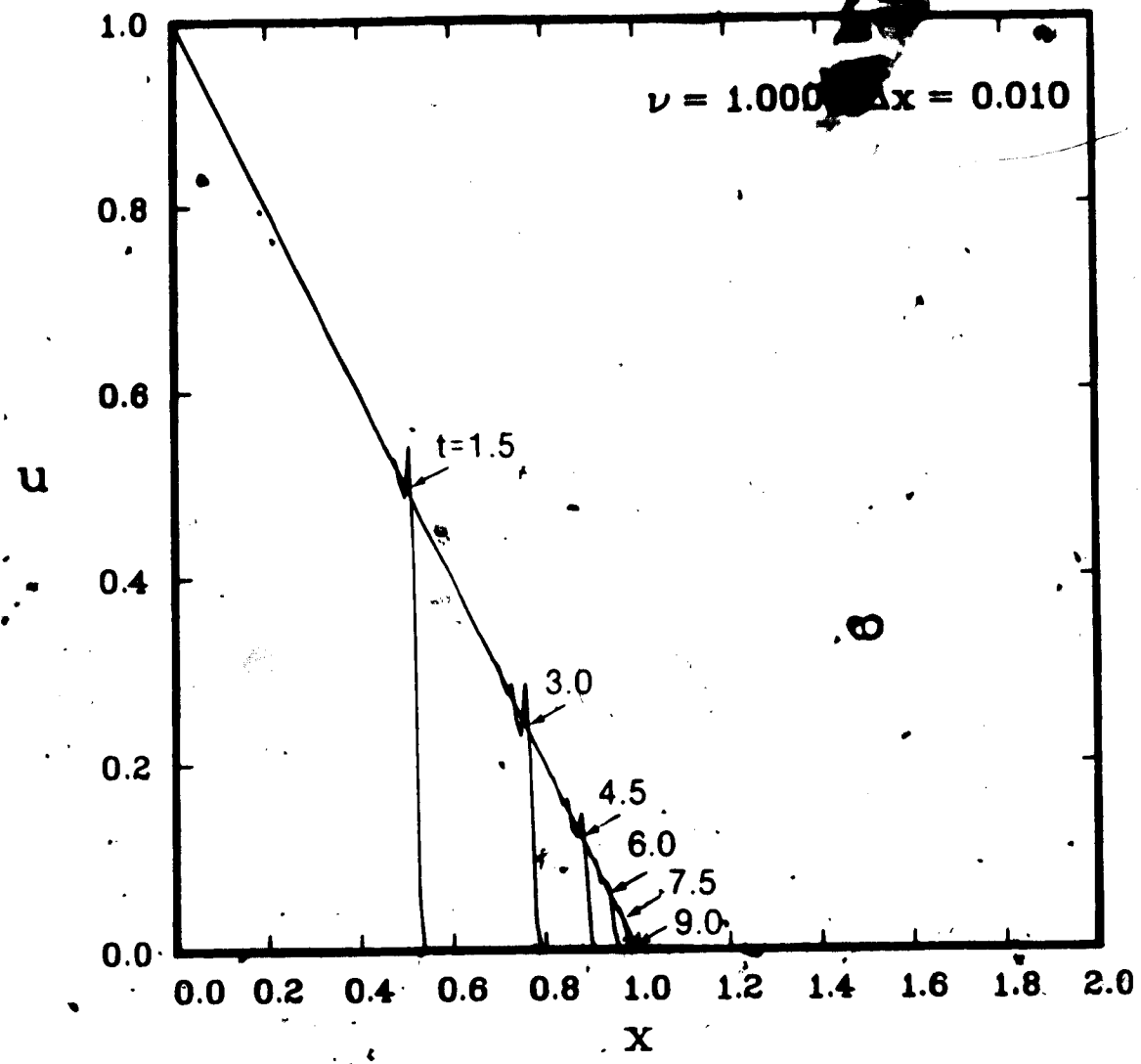


Fig. 2.23 The MacCormack scheme applied to $u_t + uu_x + u = 0$ subject to $u(x,0) = 0$, $u(0,t) = U_0 H(t)$, $U_0 = 1$, for $\nu = 1.0$ and $\Delta x = 0.01$.

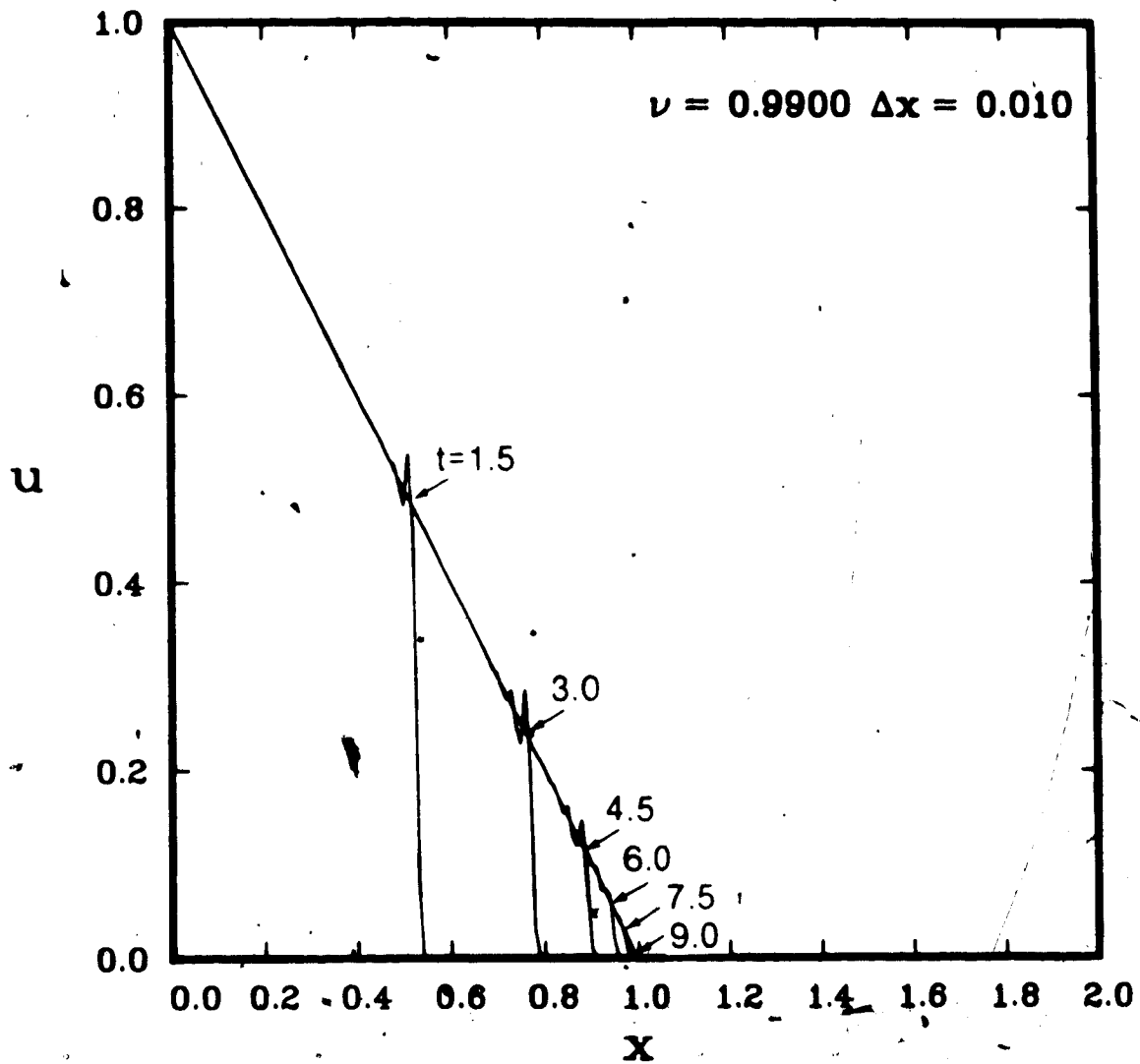


Fig. 2.24 The MacCormack scheme applied to $u_t + uu_x + \nu u = 0$ subject to $u(x,0) = 0$; $u(0,t) = U_0 H(t)$, $U_0 = 1$, for $\nu = 0.99$ and $\Delta x = 0.01$.

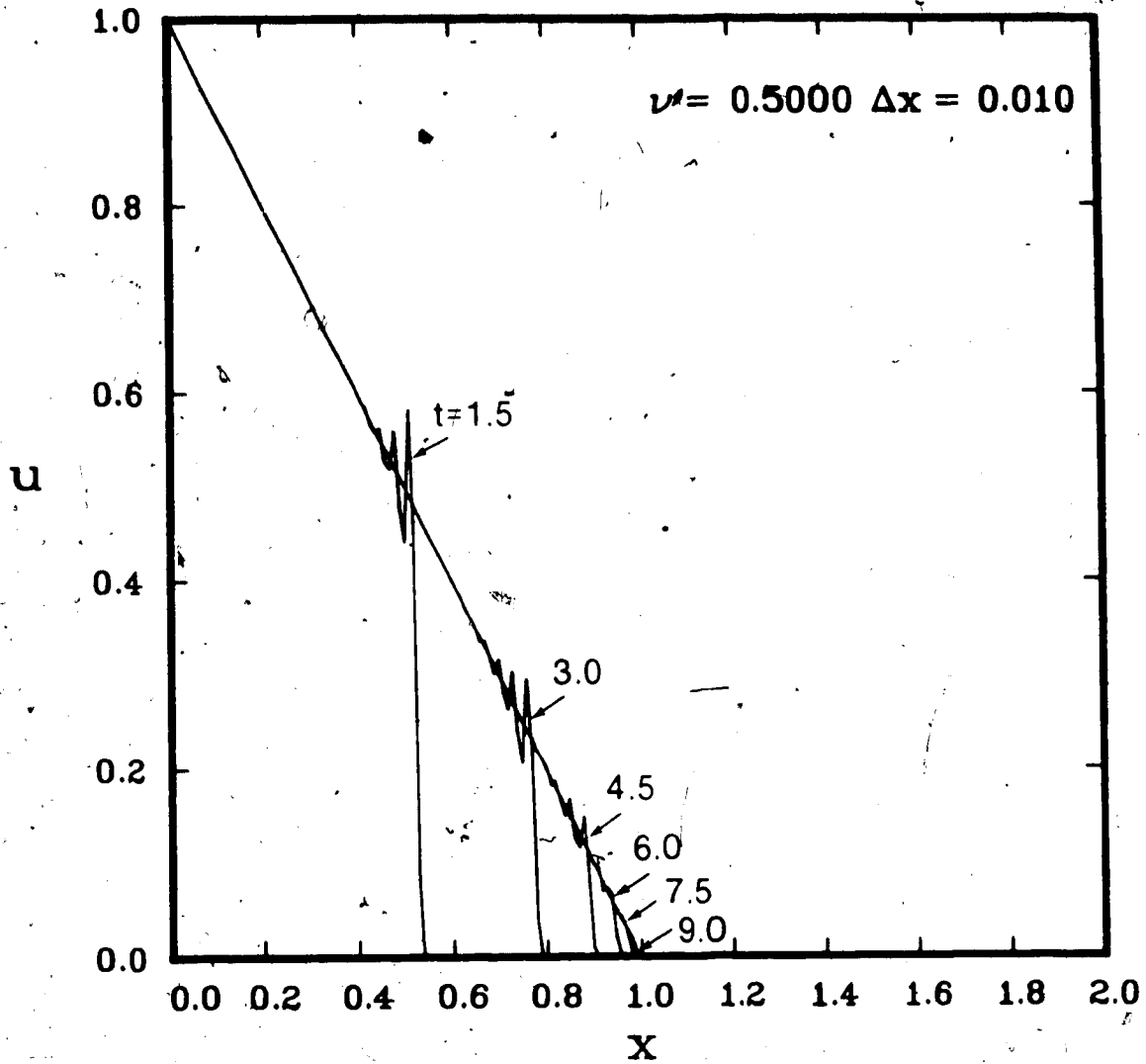


Fig. 2.25 The MacCormack scheme applied to $u_t + uu_x + u = 0$ subject to $u(x,0) = 0$, $u(0,t) = U_0 H(t)$, $U_0 = 1$, for $\nu = 0.5$ and $\Delta x = 0.01$.

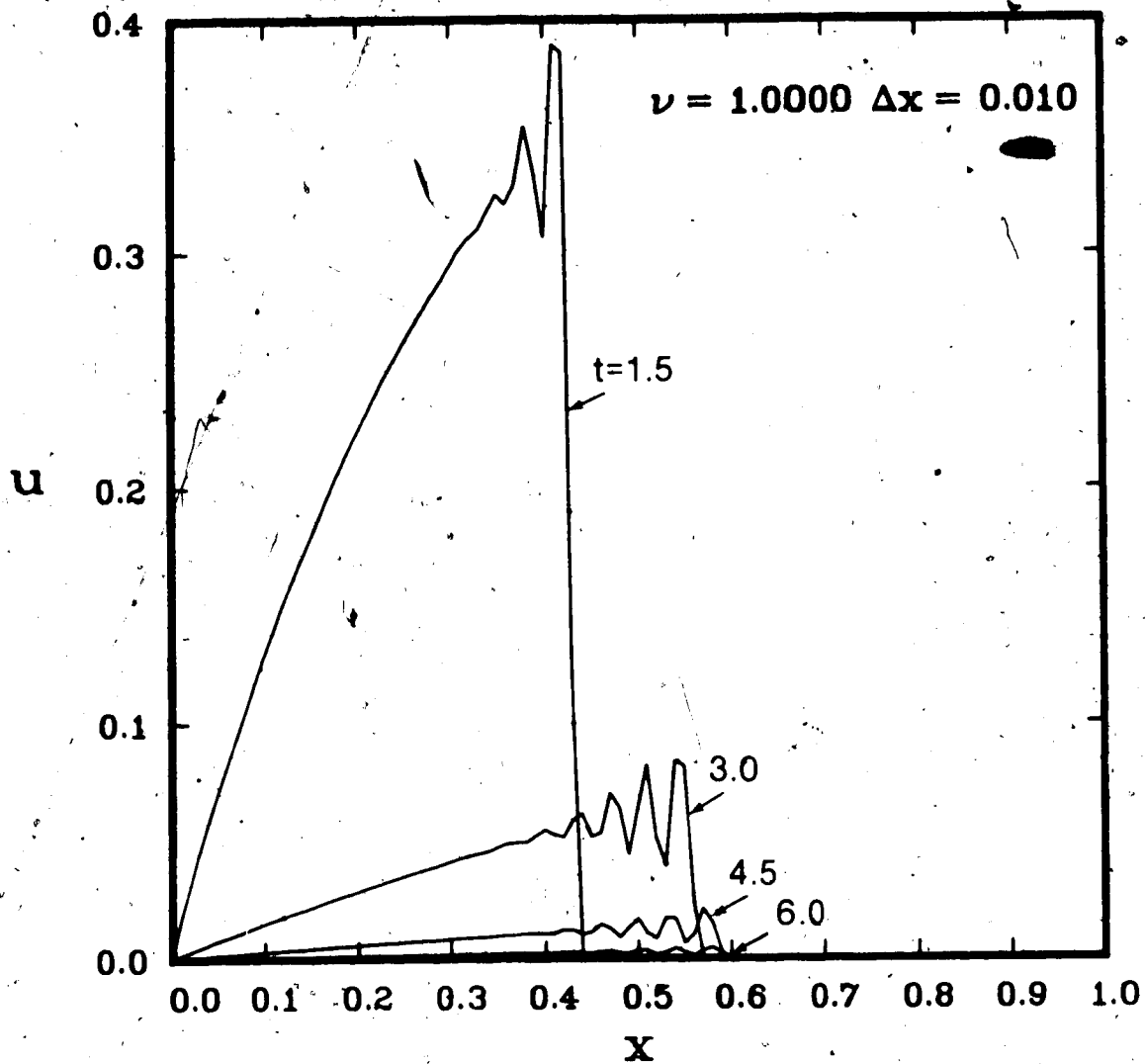


Fig. 2.26 The MacCormack scheme applied to $u_t + uu_x + u = 0$ subject to $u(x,0) = 0$, $u(0,t) = U_0 \sin \pi t H(t) H(1-t)$, $U_0 = 1$, for $\nu = 1.0$ and $\Delta x = 0.01$.

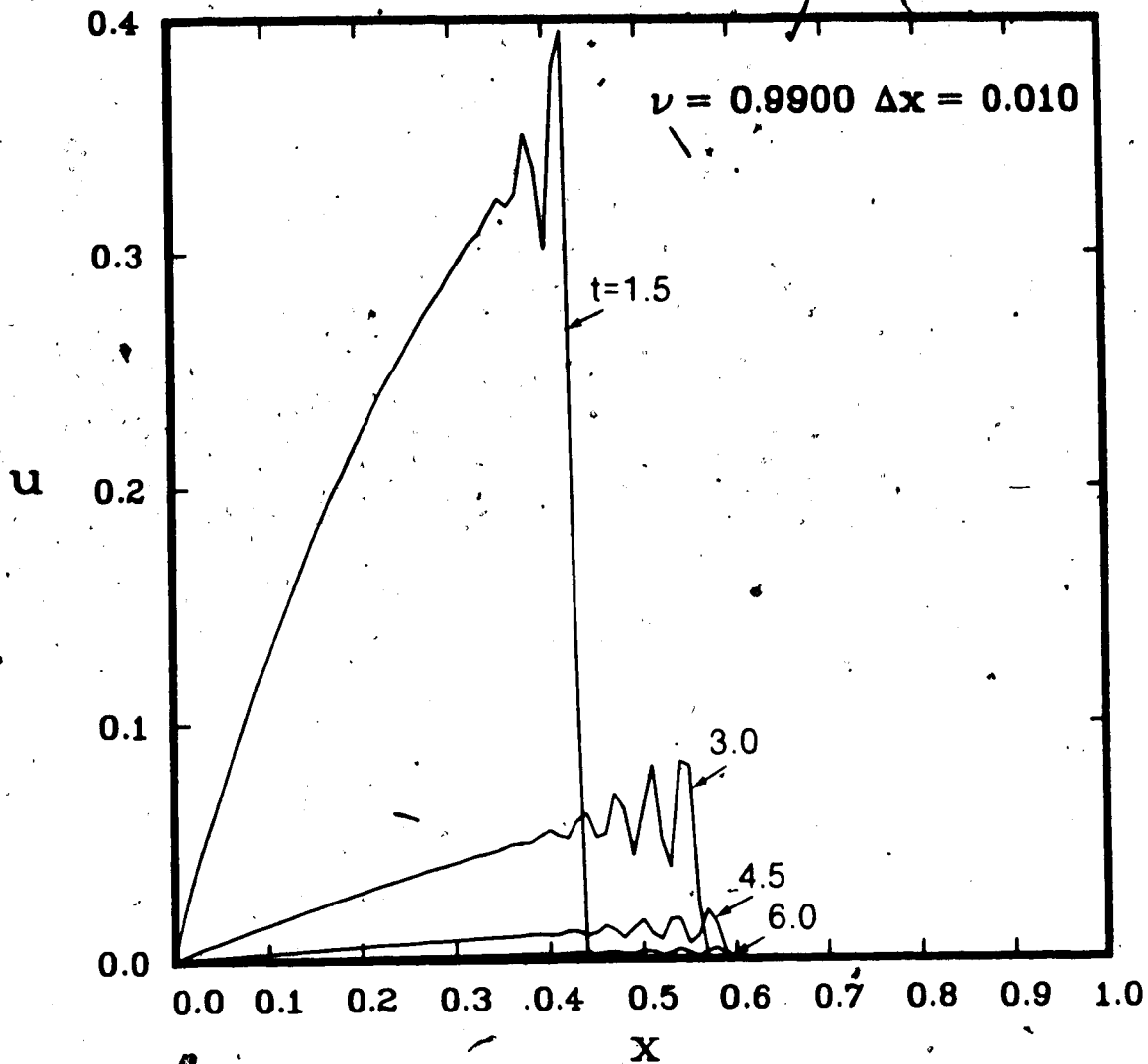


Fig. 2.27 The MacCormack scheme applied to $u_t + uu_x + u = 0$ subject to $u(x, 0) = 0$, $u(0, t) = U_0 \sin \pi t H(t) H(1-t)$, $U_0 = 1$, for $\nu = 0.99$ and $\Delta x = 0.01$.

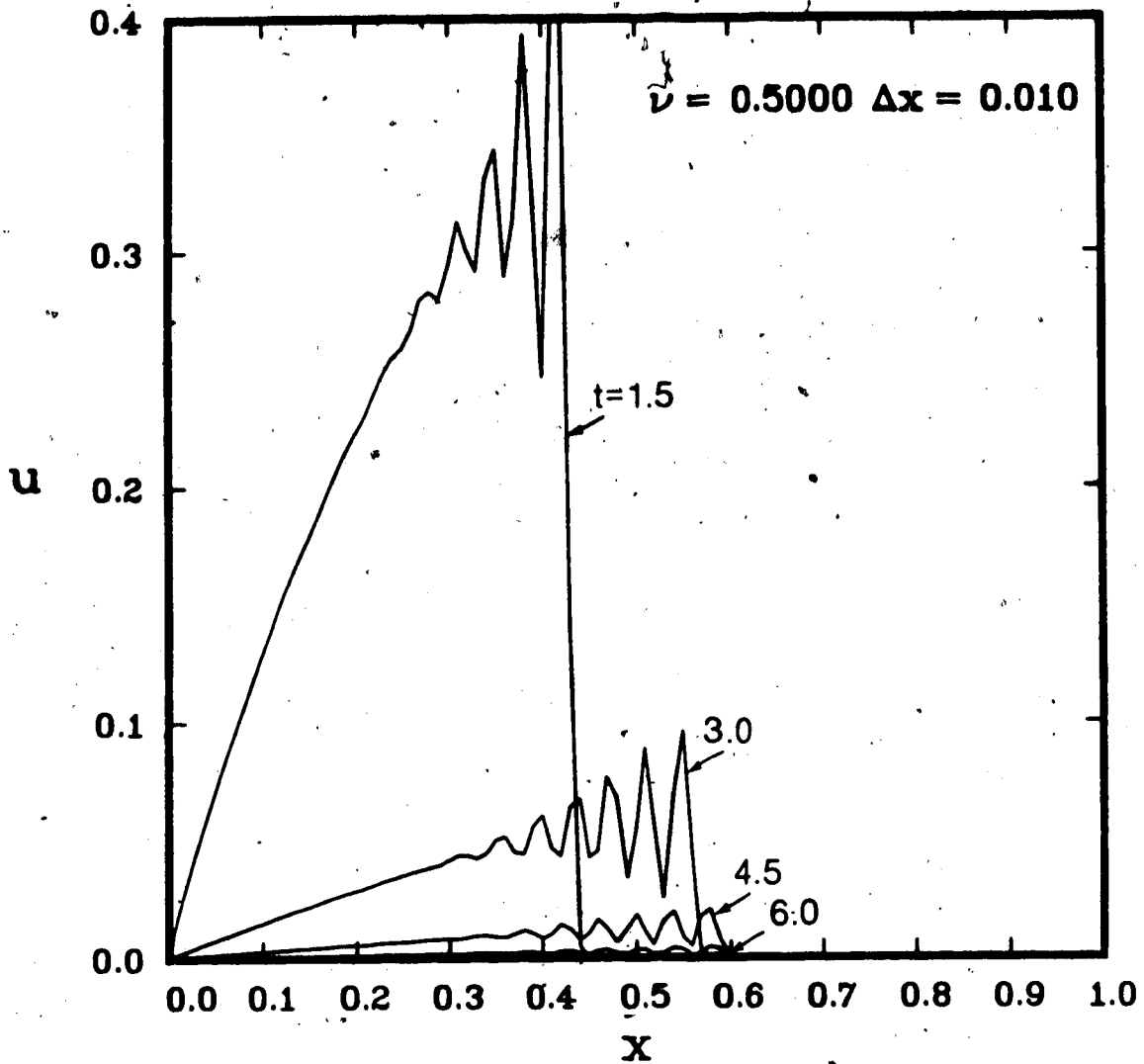


Fig. 2.28 The MacCormack scheme applied to $u_t + uu_x + \nu u = 0$ subject to $u(x, 0) = 0$, $u(0, t) = U_0 \sin \pi t H(t) H(1-t)$, $U_0 = 1$, for $\nu = 0.5$ and $\Delta x = 0.01$.

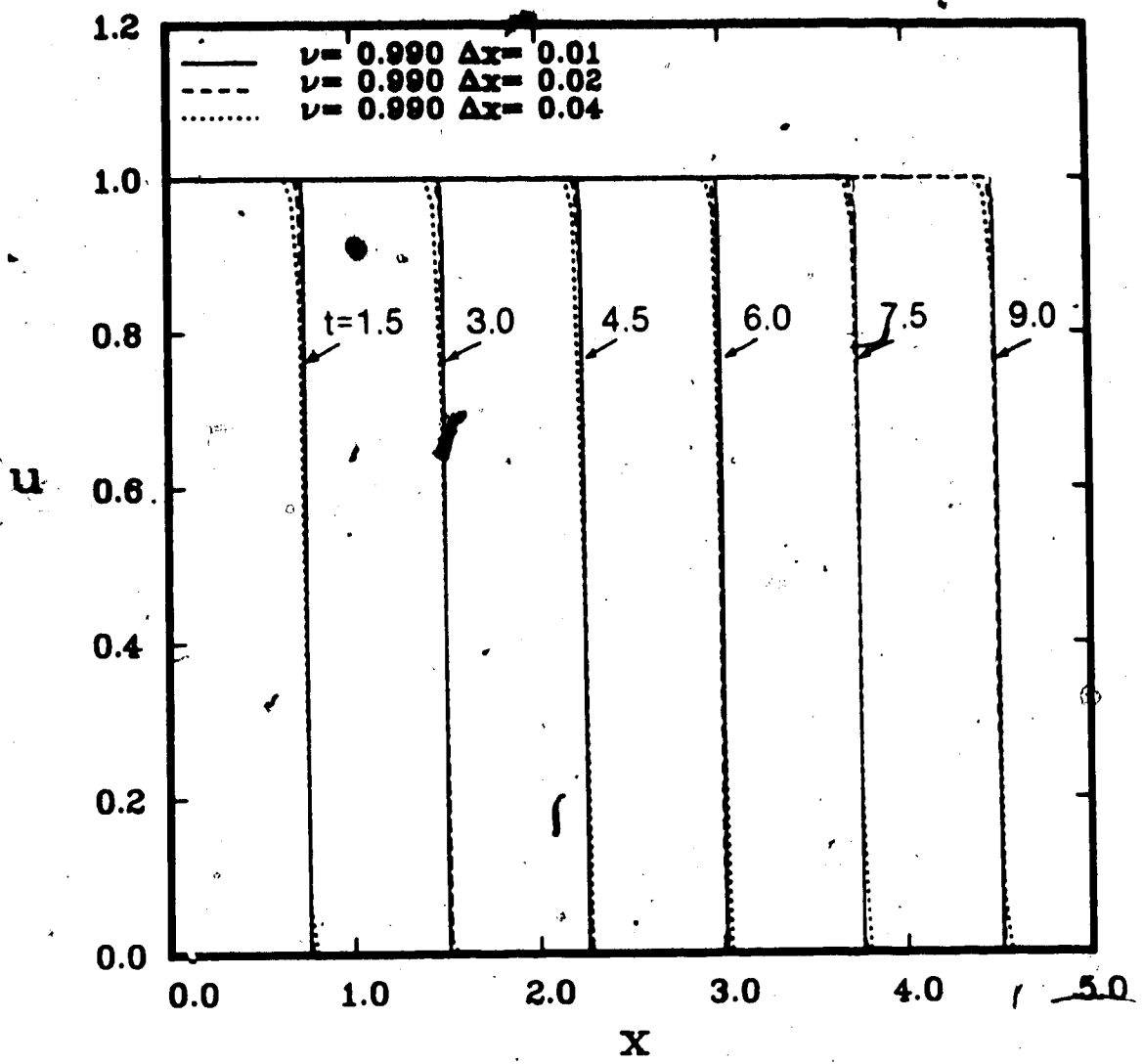


Fig. 2.29 Effect of grid size on the numerical solution of $u_t + uu_x = 0$ subject to $u(x,0) = 0$, $u(0,t) = U_0H(t)$, with $U_0 = 1$, for $\nu = 0.99$ using the MacCormack scheme.

suitable step size. The effect of grid size on the numerical solutions for equations (2.15), (2.16) and (2.18) for the various problems considered is similar to that presented in Figure 2.29.

2.6 Application of The MacCormack Scheme to the Klein Gordon Equation

2.6.1 Problem Considered

The previous section considers the application of the MacCormack scheme to scalar equations. The numerical results are useful in predicting the numerical phenomena associated with the application of the method. In this section, the application of the MacCormack scheme to a hyperbolic system of linear equations is considered, to examine the suitability of the method, and some of the inherent problems involved in solving boundary initial value problems governed by a system of partial differential equations.

The Klein Gordon equation is a second order linear partial differential equation,

$$\frac{\partial^2 u}{\partial t^2} - c^2 \frac{\partial^2 u}{\partial x^2} + \alpha^2 u = 0 \quad (2.28)$$

and the independent variables can be nondimensionalized using the nondimensionalization scheme

$$\bar{x} = \frac{\alpha x}{c}, \quad \bar{t} = \alpha t \quad (2.29)$$

to obtain

$$\frac{\partial^2 u}{\partial \bar{t}^2} - \frac{\partial^2 u}{\partial \bar{x}^2} + u = 0 \quad (2.30)$$

It is convenient to consider nondimensional independent variables with the superposed bars omitted, hereafter. Equation (2.30) can be put in the form of equation (2.13), by introducing

$$\varphi = \frac{\partial u}{\partial t} + \frac{\partial u}{\partial x} \quad (2.31)$$

to obtain a hyperbolic system of equations (Whitham, 1974),

$$\frac{\partial \varphi}{\partial t} - \frac{\partial \varphi}{\partial x} + u = 0 \quad (2.32)$$

$$\frac{\partial u}{\partial t} + \frac{\partial u}{\partial x} - \varphi = 0$$

which is of the form

$$\frac{\partial \underline{U}}{\partial t} + \underline{A} \frac{\partial \underline{U}}{\partial x} + \underline{\hat{B}} \underline{U} = \underline{0}$$

where

$$\underline{U} = \begin{bmatrix} \varphi \\ u \end{bmatrix}, \quad \underline{A} = \begin{bmatrix} -1 & 0 \\ 0 & 1 \end{bmatrix}, \quad \underline{\hat{B}} = \begin{bmatrix} 0 & 1 \\ -1 & 0 \end{bmatrix} \quad (2.33)$$

The eigenvalues of \underline{A} , given by (2.33), are ± 1 . Consequently, the Courant number is given by $\Delta t / \Delta x$. Numerical solutions of the system of equations (2.32), are obtained for boundary initial value problems for the interval $0 \leq x < \infty$, using the slightly modified MacCormack scheme given by equation (2.6), with $\underline{A}(\underline{U}) = \underline{A}$ and $\underline{B}(\underline{U}) = \underline{\hat{B}}$. Quiescent initial conditions

$$u(x,0) = 0, \quad \dot{u}(x,0) = 0 \quad (2.34)$$

are considered. The boundary condition $u(0,t)$ is specified but $\varphi(0,t)$ is not known a priori, and is obtained from a forward forward (FF) predictor corrector scheme, as discussed in Section 2.3, with φ_0^{n+1} obtained from equation (2.6)₁, and φ_0^{n+1} from

$$\varphi_0^{n+1} = \frac{1}{2} \left\{ \varphi_0^n + \varphi_0^{n+1} - \frac{1}{\Delta x} (\varphi_0^{n+1}) - \Delta t u_0^{n+1} \right\} \quad (2.35)$$

The modified MacCormack scheme is applied to the problem with quiescent initial conditions, and boundary conditions

$$u(0,t) = U_0 H(t) \quad (2.36)$$

or

$$u(0,t) = U_0 \sin \pi t H(t) H(1-t) \quad (2.37)$$

Results obtained from the method of characteristics (see Appendix 2) are compared with the results obtained using the MacCormack scheme. The method of characteristics is implemented numerically using finite differences. The relationships along the characteristics and the characteristic directions are given as

$$\frac{d\phi}{dt} + u = 0 \quad \text{on} \quad \frac{dx}{dt} = -1 \quad (2.38)$$

$$\frac{du}{dt} - \phi = 0 \quad \text{on} \quad \frac{dx}{dt} = +1$$

The specific details of this analysis are not included as part of this study. More information on the method of characteristics is given by Whitham (1974). Some of the boundary initial value problems considered are not necessarily physical examples, although the Klein Gordon equation governs certain physical phenomena. In

the context of this study, the Klein Gordon equation is used to examine numerical solutions of hyperbolic systems of equations obtained from the MacCormack scheme.

2.6.2 Stability Criteria

The von Neumann method of stability analysis, as outlined in Section 2.4, is used to investigate the stability of the MacCormack scheme applied to the system of equations (2.32). The amplification matrix for the finite difference scheme is

$$G = \begin{bmatrix} (L + iM) & -(\Delta t + P) \\ (\Delta t + P) & (L - iM) \end{bmatrix} \quad (2.39)$$

and its spectral radius is

$$\lambda = (L^2 + M^2 - P^2 + (\Delta t)^2)^{1/2} \quad (2.40)$$

where $L = (1 - ((\Delta t)^2/2) + \nu^2 (\cos\beta - 1))$, $M = (\nu \sin\beta)$, and $P = (\nu \Delta t (\cos\beta - 1))$ for $\nu = \Delta t/\Delta x$ and $\beta = k_m \Delta x$. If the stability for the Lax-Wendroff scheme, applied to equation (2.32), is considered, L and M are the same as above, but $P = 0$. The matrix G in (2.39) is a normal matrix only if $P = 0$. Hence, the stability analysis provides only a necessary condition for stability of initial value problems governed by (2.32).

For $\nu = 1.0$, the spectral radius given by (2.40) approaches 1 for all β as $\Delta x \rightarrow 0$, but for nonzero Δx , $\lambda > 1$ for all β in the neighbourhood of $\beta = 0$, and $\beta = 2\pi$, as indicated in Figure 2.30. This indicates that the slightly modified MacCormack scheme used in this study is unstable for $\nu = 1$, for the system of equations

(2.32). It follows from equation (2.40), that for $\Delta x \neq 0$, $\lambda > 1$ near $\beta = 0$ and $\beta = 2\pi$ as shown in Figure 2.30. This means that the finite difference scheme applied to the Klein Gordon equation is unstable. Figure 2.30 shows the relationships between $(\lambda-1)$ and β for $\nu = 0.99$ and 0.995 with $\Delta x = 0.01$ and $\Delta x = 0.025$. The positive values of $(\lambda-1)$, which indicate instability, are magnified as indicated. This stability analysis is useful in examining the numerical solutions of the boundary initial value problems governed by equation (2.32) which are solved using the slightly modified MacCormack scheme proposed in this chapter. Although the scheme is strictly unstable for all ν and $\Delta x \neq 0$, useful results are obtained with a suitable choice of these parameters.

2.6.3 Numerical Results

In this section, numerical solutions for the Klein Gordon equation are given for u versus nondimensional x and are presented for various nondimensional times t . The numerical results are obtained using the MacCormack scheme with the boundary conditions applied according to equation (2.35) unless otherwise specified. The results presented are for quiescent initial conditions as specified by equation (2.34). Figure 2.30 shows the results of the von Neumann stability analysis for the MacCormack scheme applied to the system of equations (2.32). The quantity $(\lambda-1)$ is plotted against β for various Courant numbers ($\nu = 0.99$ and $\nu = 0.995$) and grid spacings ($\Delta x = 0.025$, $\Delta x = 0.010$). The stability analysis indicates that the MacCormack scheme is unstable for the cases considered. Figures 2.31 - 2.36 show the numerical solutions for

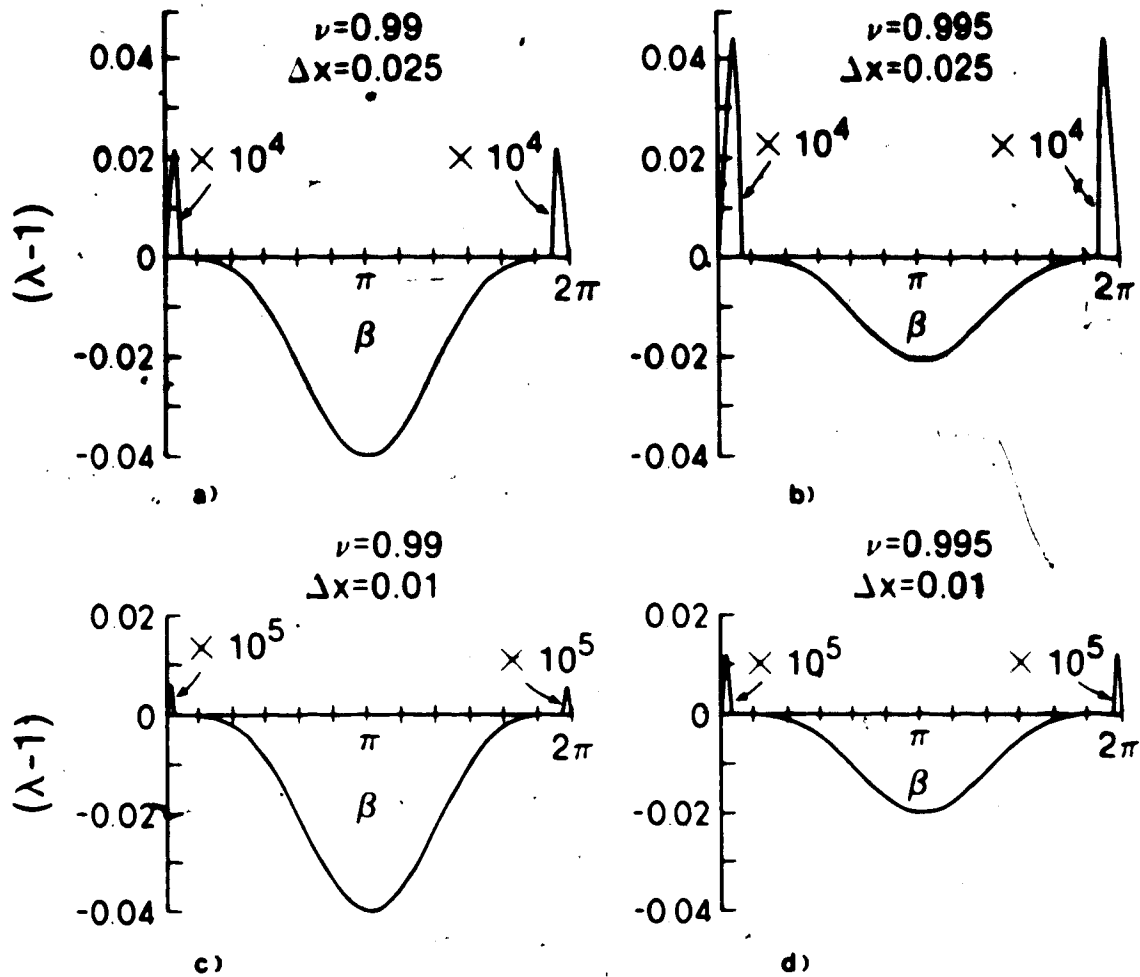


Fig. 2.30 The von Neumann stability analysis for the MacCormack scheme applied to the Klein Gordon equation, for $\Delta x = 0.01$ and $\Delta x = 0.025$.

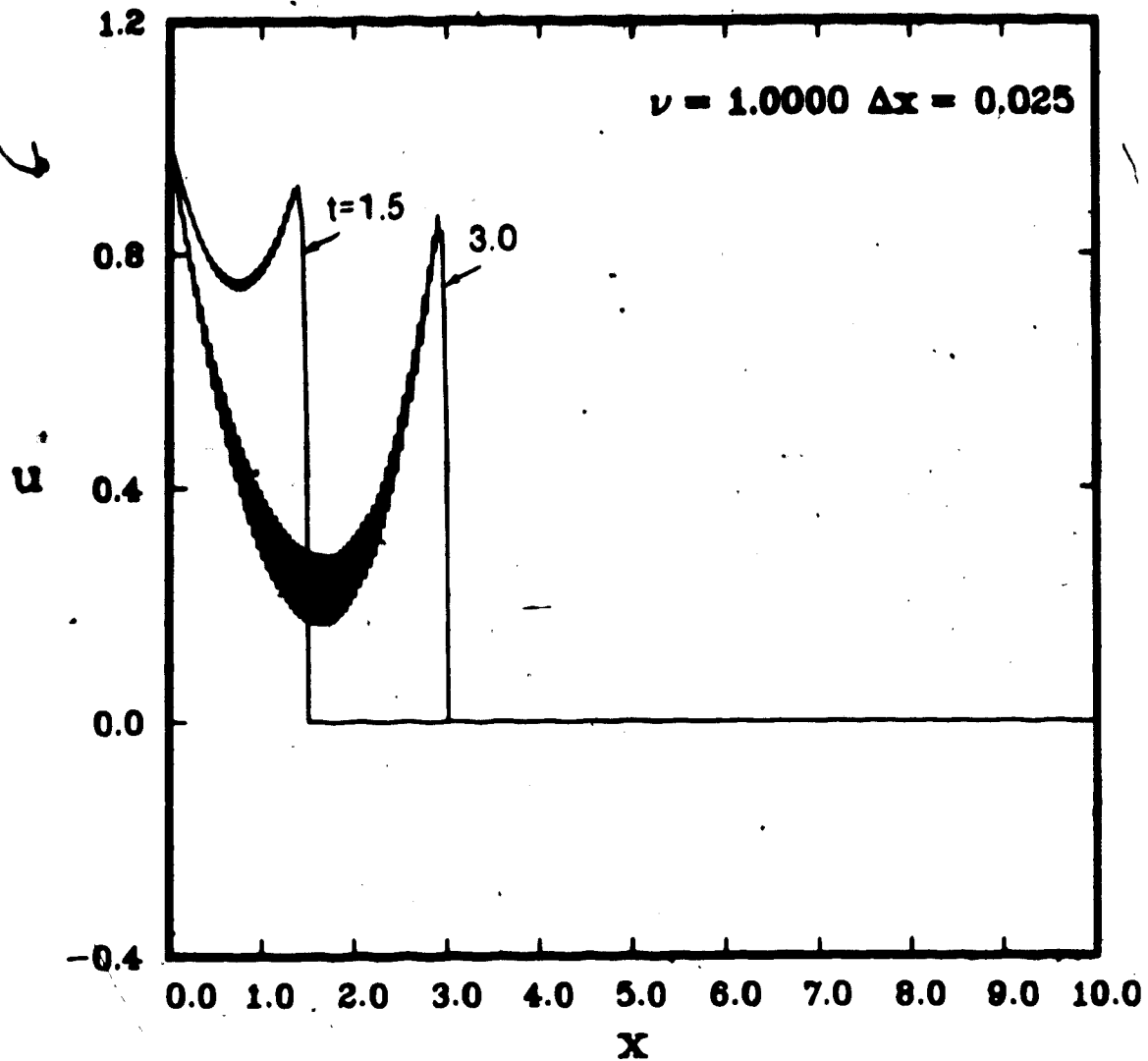


Fig. 2.31 The MacCormack scheme applied to the Klein Gordon equation subject to $u(x,0) = 0$, $u(0,t) = U_0 H(t)$, with $U_0 = 1$, for $\nu = 1.0$ and $\Delta x = 0.025$.

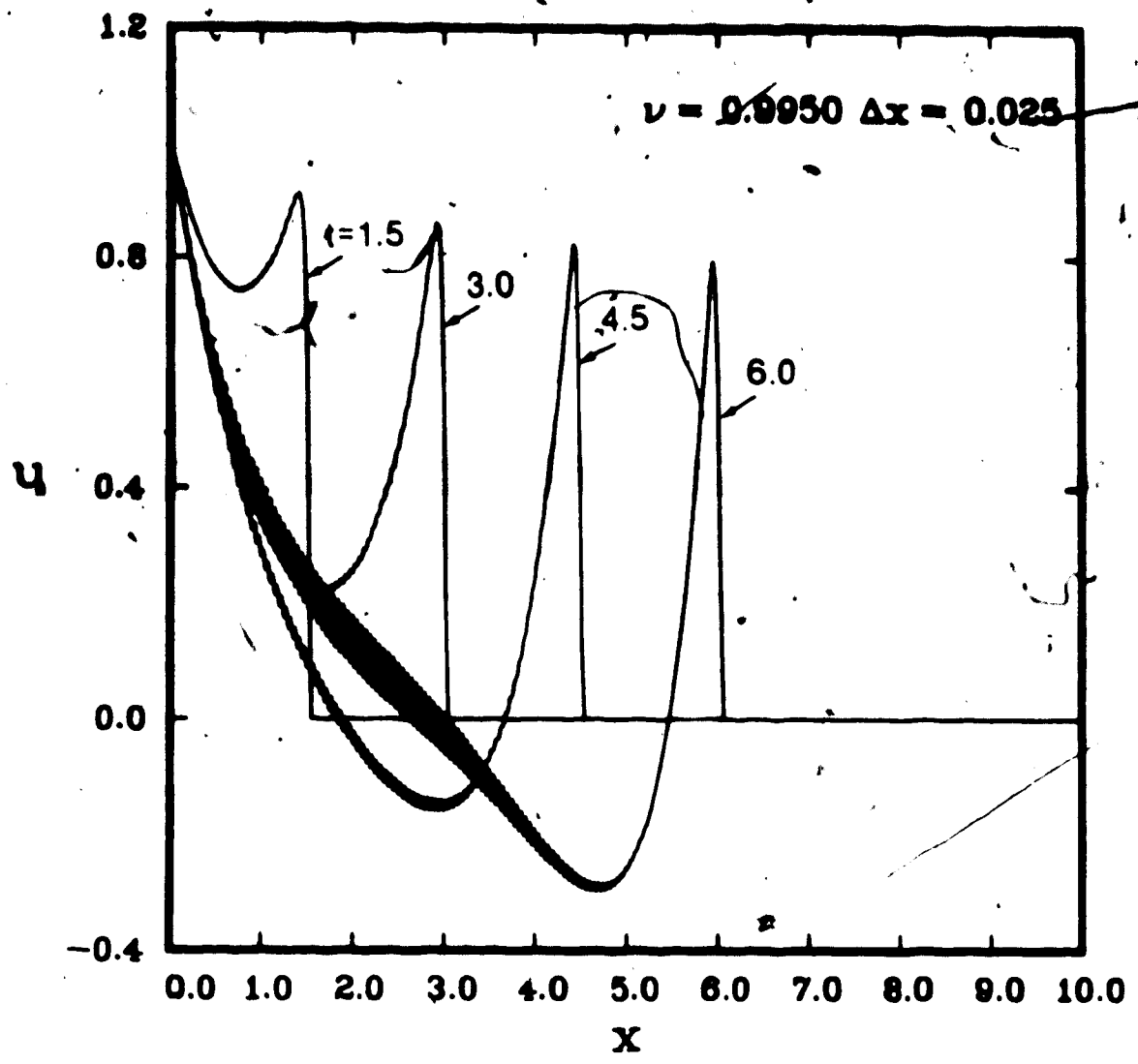


Fig. 2.32 The MacCormack scheme applied to the Klein Gordon equation subject to $u(x,0) = 0$, $u(0,t) = U_0 H(t)$, with $U_0 = 1$, for $\nu = 0.995$ and $\Delta x = 0.025$.

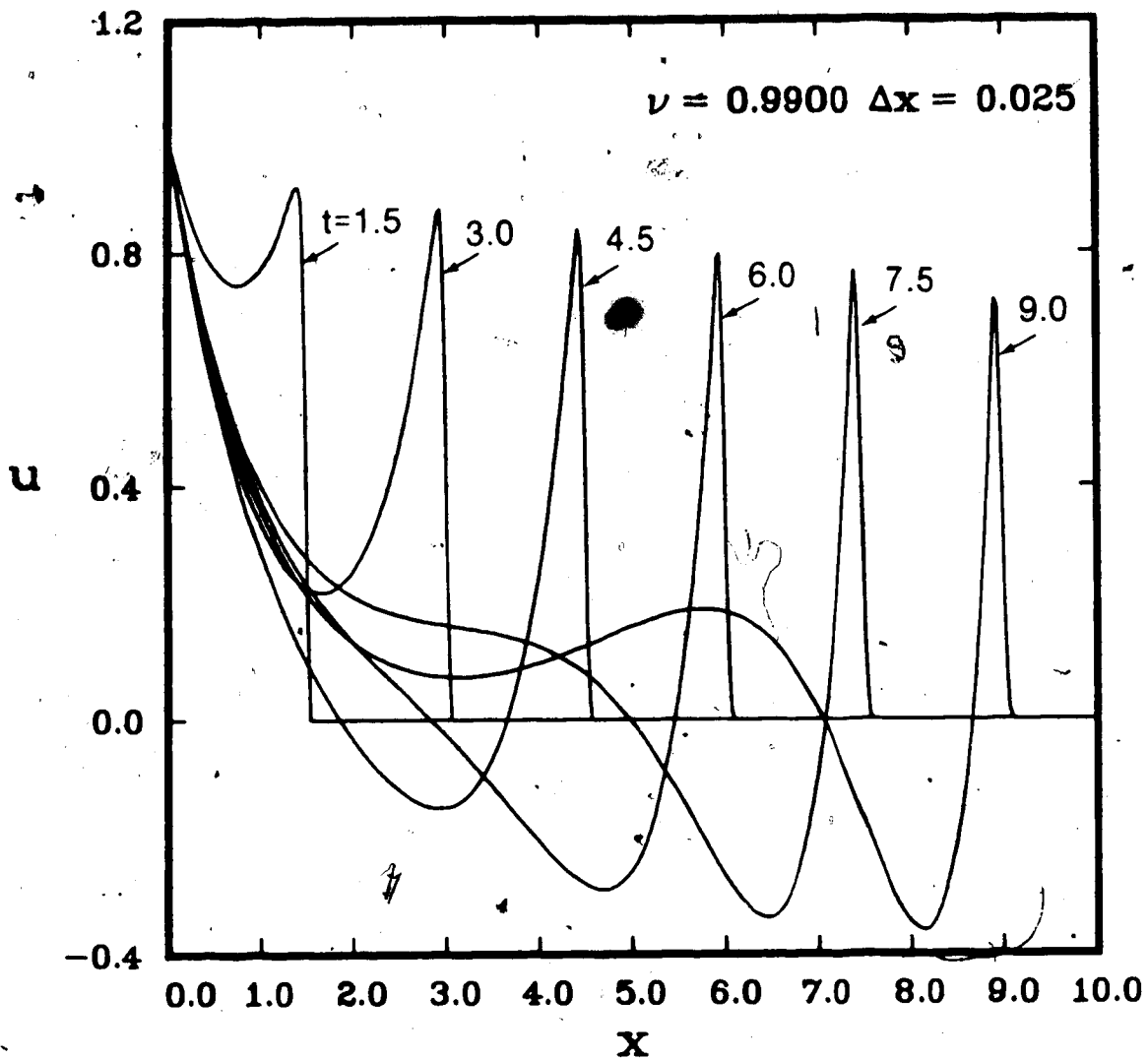


Fig. 2.33 The MacCormack scheme applied to the Klein-Gordon equation subject to $u(x,0) = 0$, $u(0,t) = U_0 H(t)$, with $U_0 = 1$, for $\nu = 0.99$ and $\Delta x = 0.025$.

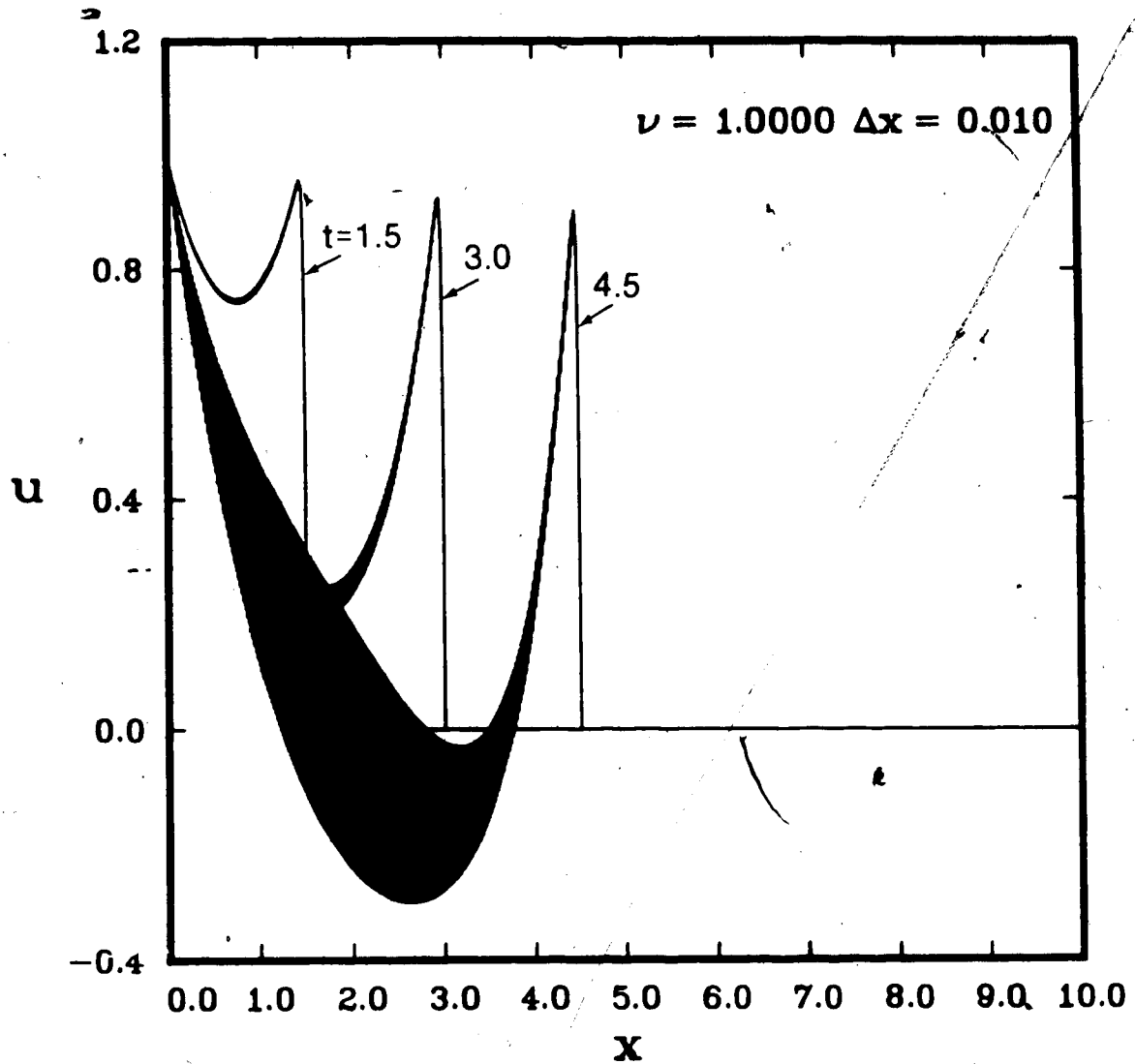


Fig. 2.34 The MacCormack scheme applied to the Klein Gordon equation subject to $u(x,0) = 0$, $u(0,t) = U_0 H(t)$, with $U_0 = 1$, for $\nu = 1.0$ and $\Delta x = 0.01$.

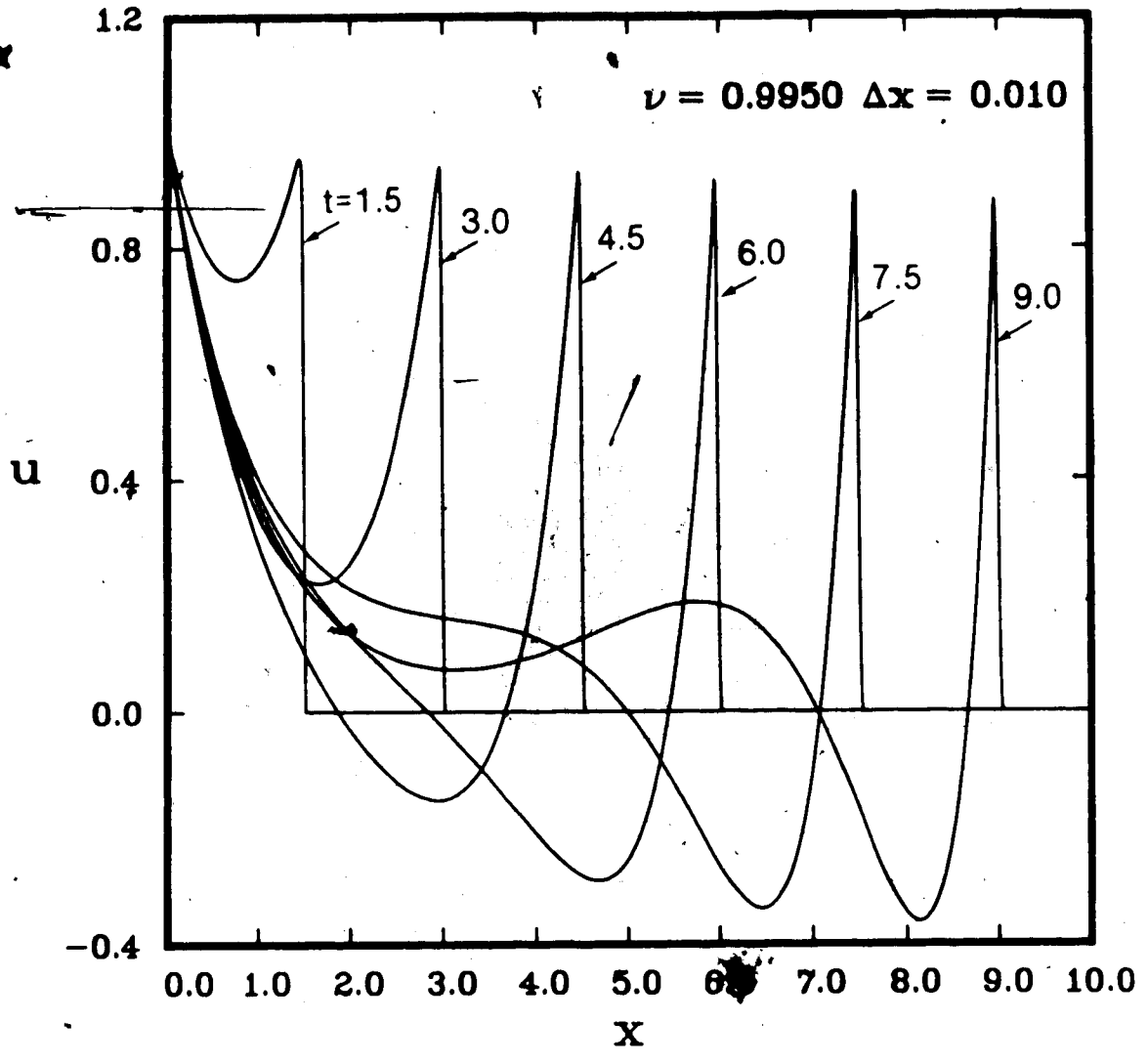


Fig. 2.35 The MacCormack scheme applied to the Klein Gordon equation subject to $u(x,0) = 0$, $u(0,t) = U_0 H(t)$, with $U_0 = 1$, for $\nu = 0.995$ and $\Delta x = 0.01$.

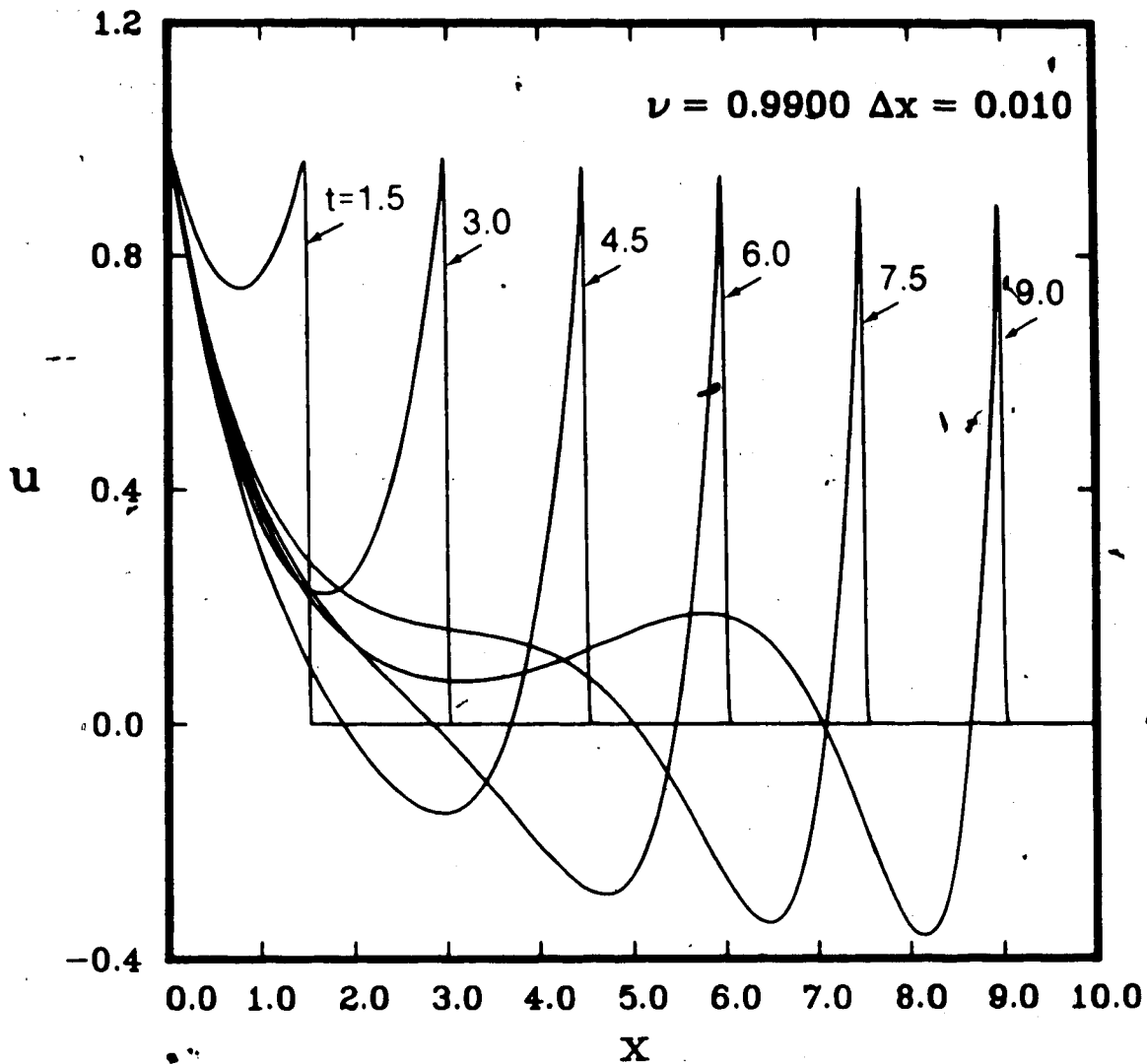


Fig. 2.36 The MacCormack scheme applied to the Klein Gordon equation subject to $u(x,0) = 0$, $u(0,t) = U_0 n(t)$, with $U_0 = 1$, for $\nu = 0.99$ and $\Delta x = 0.01$.

boundary condition (2.36), with $U_0 = 1$, for the grid spacings, $\Delta x = 0.025$ and $\Delta x = 0.01$, indicated in Figure 2.30. The numerical results in Figures 2.31 and 2.34 indicate that the solutions are unstable for $\nu = 1.0$, with $\Delta x = 0.025$ and $\Delta x = 0.010$, respectively. The numerical results confirm the results obtained from the stability analysis. The von Neumann analysis predicts instability for $\nu = 0.99$ and $\nu = 0.995$ for $\Delta x = 0.025$. Figures 2.32 and 2.33, which show the numerical solutions corresponding to the stability curves shown in Figures 2.30 b) and 2.30 a), respectively, indicate instability for $\nu = 0.995$ but not for $\nu = 0.990$, for the times indicated. Numerical results were also obtained for $\nu = 0.990$ to $\nu = 0.995$ in increments of 0.001. These results indicated a gradual transition to an unstable solution. Although the results in Figure 2.33 do not appear to be unstable, they may be unstable for larger times. For practical purposes, however, the solution is stable for $\nu = 0.990$ and $\Delta x = 0.025$. Figures 2.35 and 2.36 show the numerical solutions corresponding to the stability curves in Figures 2.30 d) and c), respectively. There is no instability indicated in the solutions shown in Figure 2.35 and 2.36. There is a gradual transition to an unstable solution with $\Delta x = 0.01$, similar to that observed with $\Delta x = 0.025$. The effect of grid size on stability is demonstrated by comparing the results in Figure 2.32 with those in Figure 2.35. The numerical solution obtained using $\Delta x = 0.025$ is more unstable for a given Courant number, than the results obtained for $\Delta x = 0.01$. Since it is desirable to have ν as close to 1.0 as possible, to minimize numerical dispersion, the

grid size $\Delta x = 0.01$ is more suitable than $\Delta x = 0.025$, in terms of stability. Figure 2.37 shows the numerical solution of the system of equations (2.32) with quiescent initial conditions and boundary condition (2.36), with $U_0 = 1$, using the method of characteristics. The numerical results obtained using the MacCormack scheme are in good agreement with the method of characteristics, except for the magnitude of the discontinuity at the wavefront. The position of the wavefront at $x = t$ is determined accurately in all of the figures, however, a comparison of Figure 2.36 to Figure 2.37, for $t = 9.0$, shows a significant difference in the magnitude of u at the wavefront. This might be attributed to numerical dispersion, which is typical of the MacCormack scheme. Figure 2.38 compares numerical results obtained using the MacCormack scheme ($\nu = 0.99$) with those obtained using the method of characteristics, for the solution of the Klein Gordon equation for boundary condition (2.37), with $U_0 = 1$. The results obtained from the MacCormack scheme are virtually identical to those obtained from the method of characteristics. The MacCormack scheme with $\nu = 1.0$ is unstable, although no results are presented. The degree of instability appears to be dependent on the type of boundary condition, i.e. instability is more severe for boundary condition (2.36) (discontinuity in the field variable) than for boundary condition (2.37) (discontinuity in the derivative of the field variable).

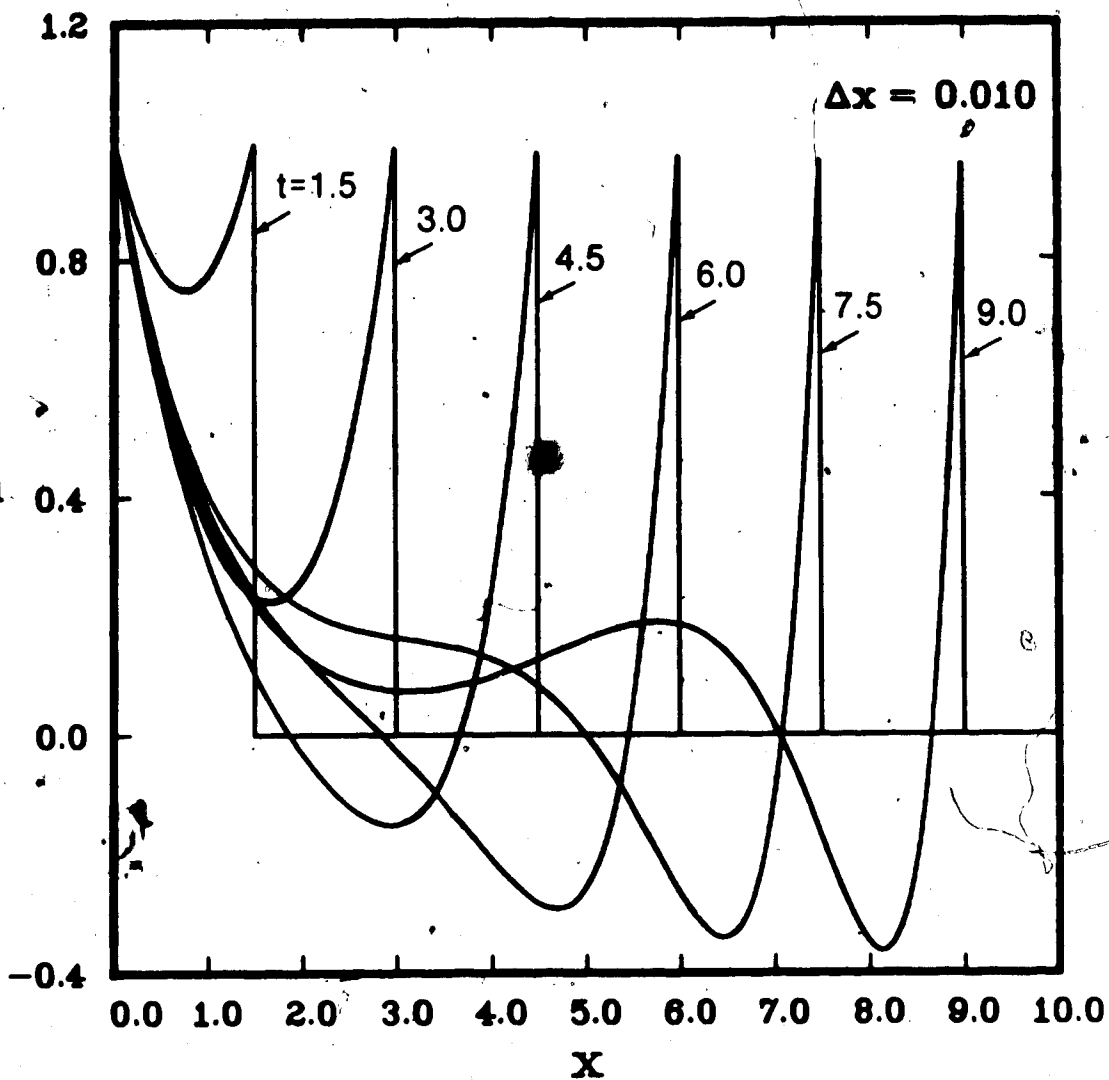


Fig. 2.37 The method of characteristics applied to the Klein Gordon equation subject to $u(x,0) = 0$, $u(0,t) = U_0 H(t)$, with $U_0 = 1$, for $\Delta x = 0.01$.

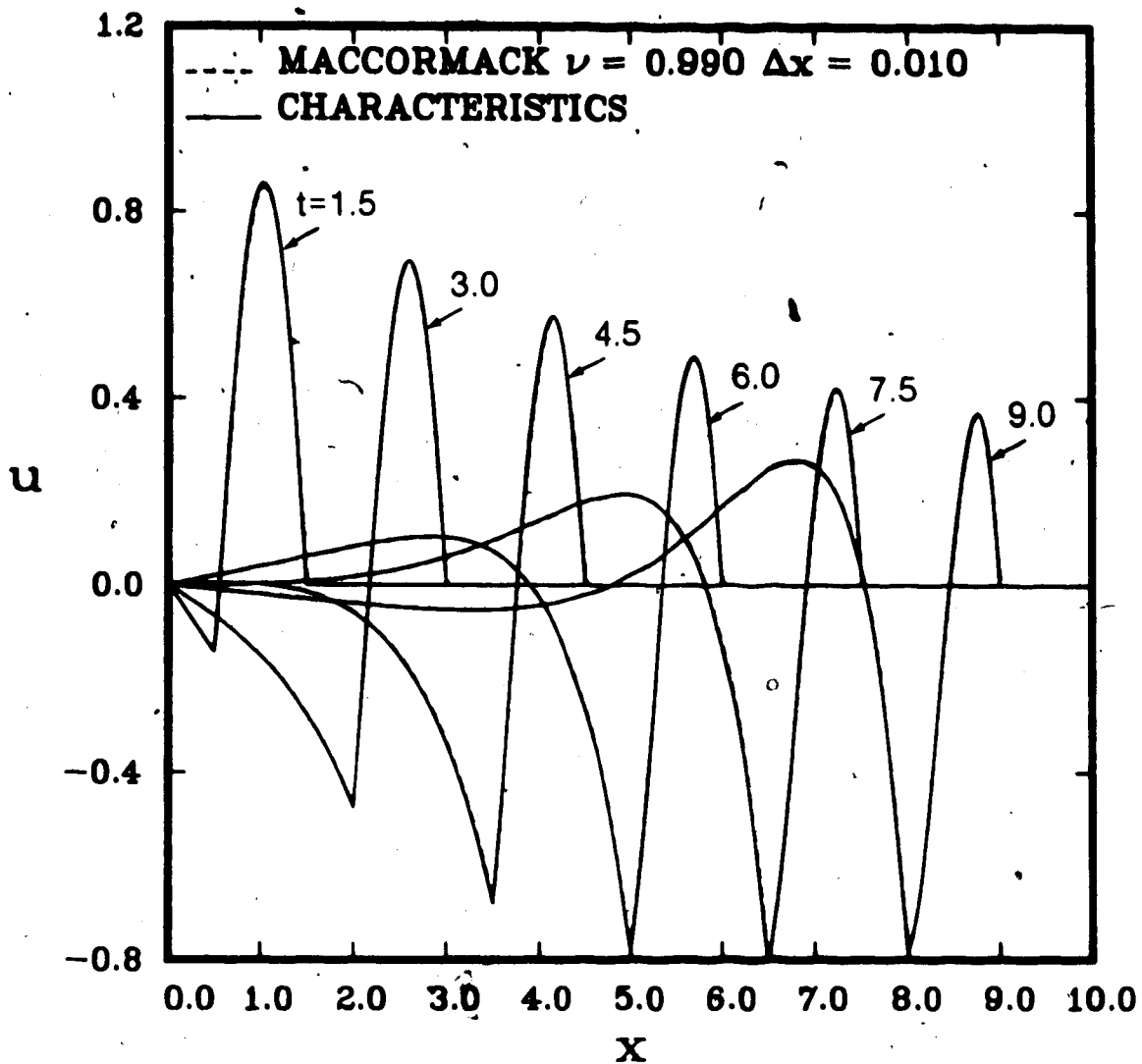


Fig. 2.38 Comparison of numerical results obtained from the method of characteristics to those obtained from the MacCormack scheme for the solution of the Klein Gordon equation subject to $u(x,0) = 0$, $u(0,t) = U_0 \sin \pi t H(t) H(1-t)$, with $U_0 = 1$.

2.7 Concluding Remarks

The results presented in this chapter indicate that the MacCormack scheme is a suitable method for the solution of boundary initial value problems governed by linear and nonlinear hyperbolic systems of equations provided Δx and ν are suitably chosen. The term $B(U)$ in (2.4) affects the stability of the MacCormack scheme, particularly for linear equations of the form (2.13). Although the additional term $B(U)$ causes instability in the numerical results for certain Courant numbers, it appears to dampen the oscillations, which appear as a result of numerical dispersion, as time increases.

CHAPTER 3

PLANE LINEAR VISCOELASTIC WAVE PROPAGATION

3.1 Introduction of the Problem

In this chapter, the MacCormack scheme introduced in Chapter 2 is used for the solution of plane linear viscoelastic wave propagation problems. A step function and a finite duration pulse application of spatially uniform stress at the surface of a viscoelastic half space are considered. This problem involves one spatial dimension and is governed by a linear hyperbolic system of partial differential equations expressed in matrix form by equation (2.4), where x and t are the spatial and temporal independent variables, respectively and \underline{U} is the column matrix of dependent variables. The problems considered are based on the assumption of a homogeneous and time translation invariant linear viscoelastic medium, so that the square matrix \underline{A} is constant and the column matrix $\underline{B}(\underline{U})$ is a linear function of \underline{U} , which does not depend on x and t .

Viscoelastic materials with relaxation moduli of the form

$$G(t) = E \left\{ \alpha_0 + \sum_{n=1}^N \alpha_n e^{-t/\tau_n} \right\} \quad (3.1)$$

are considered, where E is the appropriate impact modulus, $\alpha_n \geq 0$ for $(n = 0, 1, \dots, N)$, τ_n are the relaxation times and

$$\sum_{n=0}^N \alpha_n = 1$$

Equation (3.1) depends upon the assumption of a discrete relaxation spectrum, which may be regarded as an approximation to the integral form

$$G(t) = \alpha_0 E + \int_0^{\infty} F(\tau) e^{-t/\tau} d\tau \quad (3.2)$$

If $F(\tau)$ is replaced by a discrete approximation using the Dirac delta function, $\delta(t)$, so that $F(\tau) = \sum_{i=1}^N \alpha_i \delta(\tau - \tau_i)$, equation (3.1) is obtained. The discrete form of the relaxation function given by (3.1) is a more general specification of viscoelastic materials (Lockett, 1972).

For the special case when $N = 1$, the standard model, which is the simplest viscoelastic solid which exhibits an impact response, is obtained. When $\alpha_0 = 0$ and $N = 1$, the Maxwell model is obtained. In equation (2.4), the matrix A is a $((2N + 1) \times (2N + 1))$ matrix, and \underline{U} and $\underline{B}(\underline{U})$ are $((2N + 1) \times 1)$ matrices, if $\alpha_0 \neq 0$. When $\alpha_0 = 0$ and $N = 1$, a system of 2 equations is obtained rather than 3 equations when $\alpha_0 \neq 0$. The MacCormack scheme, modified to account for $\underline{B}(\underline{U}) \neq 0$, is applied to the governing equations with initial and boundary conditions specified. Stability and numerical dispersion are investigated. The numerical solution using the MacCormack scheme for wave propagation in a Maxwell material subject to a velocity boundary condition and quiescent initial conditions is compared to an exact solution obtained using Laplace transforms (Christensen, 1982). A further modification, incorporating results from a wavefront expansion, is introduced and numerical results with and without this modification are compared.

The main purpose of this chapter is to investigate the usefulness of the MacCormack scheme for linear systems with $\underline{B}(\underline{U}) \neq 0$, as a preliminary to application to nonlinear problems for which \underline{A} depends on \underline{U} and $\underline{B}(\underline{U})$ is a nonlinear function of \underline{U} . However, for linear viscoelastic wave propagation problems, the method is a useful alternative to the method of characteristics and to the Laplace transform method when numerical inversions of otherwise intractable transforms are required.

The method is outlined and numerical results are presented for $N = 1$, $N = 2$ and the special case of $\alpha_0 = 0$ with $N = 1$.

3.2 Governing Equations

The basic equations governing one dimensional plane wave propagation in viscoelastic materials are derived in detail in numerous texts (Flügge, 1974, Christensen, 1982, Pipkin, 1972, and Kolsky, 1963).

The governing system of partial differential equations for one dimensional plane wave propagation in a linear viscoelastic material (see Figure 3.1) consists of the equation of motion,

$$\frac{\partial v}{\partial t} - \frac{1}{\rho} \frac{\partial g}{\partial x} = 0 \quad (3.3)$$

the compatibility equation

$$\frac{\partial \epsilon}{\partial t} - \frac{\partial v}{\partial x} = 0 \quad (3.4)$$

and the constitutive equation,

$$\frac{\partial g}{\partial t} + \frac{g}{\tau_1} = q_2 \left(\frac{\partial \epsilon}{\partial t} + \frac{\alpha_0 \epsilon}{\tau_1} \right) \quad (3.5)$$

for $N = 1$ (Standard material), or

$$\frac{\partial \sigma}{\partial t} + \frac{\sigma}{r_1} - q_2 \frac{\partial \epsilon}{\partial t} \quad (3.6)$$

for $\alpha_0 = 0$, $N = 1$ (Maxwell material), or

$$\frac{\partial^2 \sigma}{\partial t^2} + p_1 \frac{\partial \sigma}{\partial t} + p_0 \sigma - q_2 \frac{\partial^2 \epsilon}{\partial t^2} + q_1 \frac{\partial \epsilon}{\partial t} + q_0 \epsilon \quad (3.7)$$

for $N = 2$, where v is the particle velocity, ρ is the density, ϵ is the strain, and $p_1 = (r_1 + r_2)/r_1 r_2$, $p_0 = (r_1 r_2)^{-1}$, $q_2 = E$, $q_1 = E[(\alpha_0 + \alpha_1)r_1 + (\alpha_0 + \alpha_2)r_2]/r_1 r_2$ and $q_0 = E\alpha_0/(r_1 r_2)$.

An equivalent hyperbolic system of first order partial differential equations expressible in the matrix form given by (2.4) consists of equation (3.3), equation (3.4) and

$$\frac{\partial \sigma}{\partial t} - E \frac{\partial v}{\partial x} + \frac{\sigma}{r_1} - \frac{E\alpha_0}{r_1} \epsilon = 0 \quad (3.8)$$

for $\alpha_0 = 0$ and $N = 1$;

$$\frac{\partial \sigma}{\partial t} - E \frac{\partial v}{\partial x} - \frac{\sigma}{r_1} = 0 \quad (3.9)$$

for $\alpha_0 = 0$, $N = 1$;

$$\frac{\partial \sigma}{\partial t} - E \frac{\partial v}{\partial x} + \frac{\sigma}{r_1} - \frac{E\alpha_0}{r_1} \epsilon = 0 \quad (3.10)$$

$$\frac{\partial v}{\partial t} - \frac{1}{\rho} \frac{\partial \sigma}{\partial x} = 0 \quad (3.11)$$

$$\frac{\partial \dot{\sigma}}{\partial t} - q_1 \frac{\partial v}{\partial x} - q_2 \frac{\partial \dot{v}}{\partial x} + p_1 \dot{\sigma} + p_0 \sigma - q_0 \epsilon = 0 \quad (3.12)$$

where $\dot{v} = \partial v / \partial t$ and $\dot{\sigma} = \partial \sigma / \partial t$, for $N = 2$.

The following nondimensionalization scheme is introduced

$$\bar{x} = \frac{x}{T} \left[\frac{\rho}{E} \right]^{1/2}, \quad \bar{t} = \frac{t}{T}, \quad \bar{r}_1 = \frac{r_1}{T}, \quad \bar{r}_2 = \frac{r_2}{T},$$

$$\bar{v} = v \left[\frac{\rho}{E} \right]^{1/2}, \quad \bar{\sigma} = \frac{\sigma}{E}, \quad \bar{\sigma} = \frac{\sigma T}{E},$$

$$\bar{q}_0 = q_0 \frac{T^2}{E}, \quad \bar{q}_1 = q_1 \frac{T}{E}, \quad \bar{q}_2 = \frac{q_2}{E} = 1.$$

(3.13)

$$\bar{p}_0 = p_0 T^2, \quad \bar{p}_1 = p_1 T,$$

where

$$T = \frac{\alpha_1 (r_1)^2 + \alpha_2 (r_2)^2}{\alpha_1 r_1 + \alpha_2 r_2}$$

is the mean relaxation time defined by Pipkin (1972). Not all of the variables in the nondimensionalization scheme (3.13) apply to the Maxwell and Standard models, since these two models have only one relaxation time r_1 . Henceforth, nondimensional quantities are used but the superposed bars are omitted.

The nondimensional governing equations can be put in the form of

$$\frac{\partial \underline{U}}{\partial t} + \underline{A} \frac{\partial \underline{U}}{\partial x} + \underline{B}(\underline{U}) = 0 \quad \text{with}$$

$$\underline{U} = \begin{bmatrix} v \\ \epsilon \\ \sigma \end{bmatrix}, \quad \underline{A} = \begin{bmatrix} 0 & 0 & -1 \\ -1 & 0 & 0 \\ -1 & 0 & 0 \end{bmatrix}, \quad \underline{B}(\underline{U}) = \begin{bmatrix} 0 \\ 0 \\ \sigma - \alpha_0 \epsilon \end{bmatrix} \quad (3.14)$$

for $N = 1$ and $\alpha_0 \neq 0$. For the special case when $\alpha_0 = 0$ and $N = 1$, the system of equations reduces to a second order system of equations given by

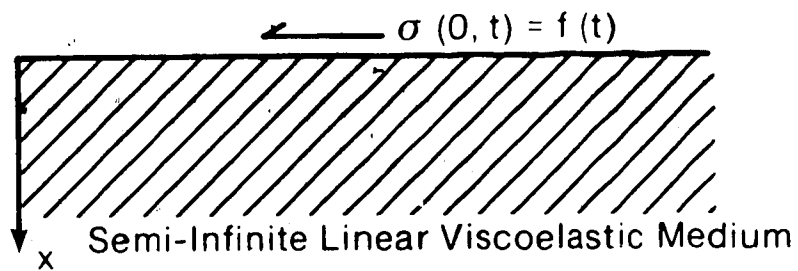


Fig. 3.1 Diagrammatic representation of Plane Wave Propagation in a semi-infinite viscoelastic medium.

$$\underline{U} = \begin{bmatrix} \sigma \\ \epsilon \\ v \end{bmatrix}, \quad \underline{A} = \begin{bmatrix} 0 & -1 \\ -1 & 0 \end{bmatrix}, \quad \underline{B}(\underline{U}) = \begin{bmatrix} \sigma \\ 0 \end{bmatrix} \quad (3.15)$$

For $N = 2$, the following system is obtained

$$\underline{U} = \begin{bmatrix} v \\ \epsilon \\ \sigma \\ \dot{v} \\ \dot{\sigma} \end{bmatrix}, \quad \underline{A} = \begin{bmatrix} 0 & 0 & -1 & 0 & 0 \\ -1 & 0 & 0 & 0 & 0 \\ 0 & 0 & 0 & 0 & 0 \\ 0 & 0 & 0 & 0 & 0 \\ -q_1 & 0 & 0 & -1 & 0 \end{bmatrix}, \quad \underline{B}(\underline{U}) = \begin{bmatrix} 0 \\ 0 \\ -\dot{\sigma} \\ 0 \\ p_1 \dot{\sigma} + p_0 \sigma - q_0 \epsilon \end{bmatrix} \quad (3.16)$$

In each case, \underline{A} has eigenvalues such that the nondimensional wave speed is 1. The third eigenvalue of $(3.16)_2$ is zero, and the remaining three eigenvalues of $(3.16)_2$ are zero.

Boundary initial value problems, for the interval $0 \leq x < \infty$, with quiescent initial conditions $\underline{U}(x,0) = \dot{\underline{U}}(x,0) = 0$ and the boundary condition,

$$\sigma(0,t) = \sigma_0 H(t) \quad (3.17)$$

where $H(t)$ is the unit step function, are considered (see Figure 3.1). The boundary condition (3.17) and the nondimensional creep functions

$$J(t) = \left\{ \frac{1 + e^{-\alpha_0 t}}{\alpha_0} \left[1 - \frac{1}{\alpha_0} \right] \right\}, \quad \text{for } N = 1, \alpha_0 > 0, \quad (3.18)$$

$$J(t) = (1 + t) \quad \text{for } N = 1, \alpha_0 = 0, \quad (3.19)$$

and

$$J(t) = (a_0 + a_1 e^{\lambda_1 t} + a_2 e^{\lambda_2 t}), \quad \text{for } N = 2, \quad (3.20)$$

give the strain

$$\epsilon(0,t) = \sigma_0 J(t) H(t) \quad (3.21)$$

The creep function given in equation (3.18) is not valid for the special case when $\alpha_0 = 0$. However, since ϵ is not a dependent variable in the system of equations (3.15), the creep function (3.19) is not explicitly used. In equation (3.20)

$$\lambda_1 = -\frac{1}{2} \left[q_1 + (q_1^2 - 4q_0)^{1/2} \right] \quad (3.22)$$

$$\lambda_2 = -\frac{1}{2} \left[q_1 - (q_1^2 - 4q_0)^{1/2} \right]$$

$$a_0 = \frac{p_0}{\lambda_1 \lambda_2} \quad a_1 = -\left[\frac{p_0 + (\lambda_1)^2 + p_1 \lambda_1}{\lambda_1 (\lambda_2 - \lambda_1)} \right] \quad a_2 = \left[\frac{p_0 + (\lambda_2)^2 + p_1 \lambda_2}{\lambda_2 (\lambda_2 - \lambda_1)} \right]$$

Boundary initial value problems for the interval $0 \leq x < \infty$, with quiescent initial conditions and the boundary condition

$$\sigma(0,t) = \sigma_0 \sin \pi t H(t) H(t^* - t) \quad (3.23)$$

which represents a sine pulse of finite duration, with $t^* = 1$, are also considered.

3.3 Wavefront Expansion

A useful technique, which can be incorporated into the the MacCormack scheme, for the solution of the linear viscoelastic wave propagation problems, is a wavefront expansion technique. Christensen (1982) uses this method to obtain the magnitude of a propagating discontinuity of stress in a viscoelastic rod. in terms of the

relaxation function. Achenbach and Reddy (1967) have obtained a solution similar to Christensen, which gives the solution at a fixed location. These solutions are valid near the wavefront, but do not give the entire solution of the problem. In this study, the wavefront expansion for a step function in stress is incorporated into the numerical procedure to obtain the entire solution for σ , ϵ and v . The procedure for incorporating the wavefront expansion into the numerical scheme is given in the next section. The wavefront expansion for a linear viscoelastic material is developed in this section.

The wavefront expansion in terms of the creep function $J(t)$, is obtained using a procedure similar to that of Christensen (1982) for the nondimensional boundary condition (3.17) and quiescent initial conditions.

The details of the wavefront expansion are given in Appendix 3. From the wavefront expansion, $\sigma|_{t=x}$, $\partial\sigma/\partial t|_{t=x}$, $\partial\sigma/\partial x|_{t=x}$ are obtained where σ , x , and t are the nondimensional variables in the governing equations obtained in Section 3.2. The wavefront expansion for boundary condition (3.17), with quiescent initial conditions gives the following expressions

$$\sigma \Big|_{t=x} = \sigma_0 \exp \left[\frac{J'(0)}{2J(0)} x \right]$$

$$\frac{\partial\sigma}{\partial t} \Big|_{t=x} = \sigma_0 \exp \left[\frac{-J'(0)}{2J(0)} x \right] \left\{ -\frac{J''(0)}{2J(0)} x + \frac{1}{2} \left[\frac{J'(0)}{2J(0)} \right]^2 x \right\} \quad (3.24)$$

$$\frac{\partial\sigma}{\partial x} \Big|_{t=x} = \sigma_0 \exp \left[\frac{-J'(0)}{2J(0)} x \right] \left\{ -\frac{J'(0)}{2J(0)} + \frac{J''(0)}{2J(0)} x - \frac{1}{2} \left[\frac{J'(0)}{2J(0)} \right]^2 x \right\}$$

where a prime denotes differentiation with respect to the argument

For the standard material, $N = 1$, the nondimensional creep function is given by equation (3.18). The derivatives $J'(t)$ and $J''(t)$ are given by

$$J'(t) = -\alpha_0 e^{-\alpha_0 t} \left[1 - \frac{1}{\alpha_0} \right]$$

$$J''(t) = \alpha_0^2 e^{-\alpha_0 t} \left[1 - \frac{1}{\alpha_0} \right] \quad (3.25)$$

Evaluating $J(0)$, $J'(0)$ and $J''(0)$ and substituting into equations (3.24), gives

$$\sigma \Big|_{t=x} = \sigma_0 \exp \left[- \frac{(1-\alpha_0)}{2} x \right] \quad (3.26)$$

$$\frac{\partial \sigma}{\partial t} \Big|_{t=x} = \sigma_0 \exp \left[- \frac{(1-\alpha_0)}{2} x \right] \left\{ -\frac{1}{2} (\alpha_0^2 - \alpha_0) x + \frac{1}{2} \left[\frac{1-\alpha_0}{2} \right]^2 x \right\}$$

$$\frac{\partial \sigma}{\partial x} \Big|_{t=x} = \sigma_0 \exp \left[- \frac{(1-\alpha_0)}{2} x \right] \left\{ -\frac{(1-\alpha_0)}{2} + \frac{1}{2} (\alpha_0^2 - \alpha_0) x - \left[\frac{1-\alpha_0}{2} \right]^2 x \right\}$$

A similar procedure can be used for the Maxwell model ($\alpha_0 = 0$, $N = 1$) and the model with two relaxation times, where $N = 2$. The procedure is straightforward, and the relationships for each model are not given.

The wavefront expansions given by equations (3.24) and (3.26) are valid only for the specified boundary condition. In other words, the relationships for σ , $\partial\sigma/\partial t$, and $\partial\sigma/\partial x$ must be evaluated for different boundary conditions. The wavefront expansion for boundary condition (3.23) is more complicated than that for boundary condition (3.17), and is not considered in this study. Because of the complexity in evaluating the wavefront expansion, the modification in the MacCormack

scheme, using the wavefront expansion, might be unattractive for certain problems. The wavefront expansion is used to illustrate elimination of numerical dispersion.

The exact solution given by Christensen (1982) for a Maxwell material subject to a velocity boundary condition $v(0,t) = V_0 H(t)$ is used to evaluate the numerical results obtained using the MacCormack scheme with and without a wavefront expansion. To incorporate the wavefront expansion into the MacCormack scheme, the wavefront expansion is evaluated for a velocity boundary condition for a Maxwell material using the same procedure outlined in Appendix 3. The expressions for the wavefront expansion for a Maxwell material subject to $v(0,t) = V_0 H(t)$ are given as

$$\sigma \Big|_{t=x} = -V_0 \exp \left\{ \frac{-x}{2} \right\} ,$$

$$\frac{\partial \sigma}{\partial x} \Big|_{t=x} = \frac{V_0}{\epsilon} x \exp \left\{ \frac{-x}{2} \right\} , \quad (3.28)$$

$$\frac{\partial \sigma}{\partial t} \Big|_{t=x} = -V_0 \exp \left\{ \frac{-x}{2} \right\} \left\{ \frac{-1}{2} + \frac{x}{\epsilon} \right\} ,$$

where all of the variables in equations (3.28) are nondimensional variables.

3.4 Implementation of the MacCormack Scheme

The predictor and corrector finite difference equations for the MacCormack scheme are given by equation (2.6). If $\underline{A}(U) = \underline{A}$, where \underline{A}

is a constant matrix, and $\underline{B}(\underline{U})$ is a linear function of \underline{U} , the difference equations are given by

$$\begin{aligned} \underline{U}_{-j}^{n+1} &= \underline{U}_{-j}^n - \frac{\Delta t}{\Delta x} \underline{A}(\underline{U}_{-j+1}^n - \underline{U}_{-j}^n) - \Delta t \underline{B}(\underline{U}_{-j}^n) \\ \underline{U}_{-j}^{n+1} &= \frac{1}{2} \left\{ \underline{U}_{-j}^n + \underline{U}_{-j}^{n+1} - \frac{\Delta t}{\Delta x} \underline{A}(\underline{U}_{-j}^{n+1} - \underline{U}_{-j-1}^{n+1}) - \Delta t \underline{B}(\underline{U}_{-j}^{n+1}) \right\}, \end{aligned} \quad (3.27)$$

where $\underline{U}_{-j}^n = \underline{U}(j\Delta x, n\Delta t)$ and $(\underline{B}(\underline{U}_{-j}^n)) = (0, 0, (\sigma - \alpha_0 \epsilon)_j^n)^T$ for

$N = 1$, $(\underline{B}(\underline{U}_{-j}^n)) = (\sigma_j^n, 0)^T$ for $\alpha_0 = 0$, $N = 1$ and $(\underline{B}(\underline{U}_{-j}^n)) =$

$(0, 0, -\sigma_j^n, 0, (p_1 \sigma + p_0 \sigma - q_0 \epsilon)_j^n)^T$, for $N = 2$.

Stability analyses of the MacCormack scheme with $\underline{B}(\underline{U}) = 0$, indicate that a necessary condition for stability is that $\nu \leq 1$ where ν is the Courant number defined previously as $\nu = c\Delta t/\Delta x$. In this case, $c = 1$, and $\nu = \Delta t/\Delta x$. So far, no stability analysis is available for the scheme when $\underline{B}(\underline{U}) \neq 0$. However, it was found in this study, that the MacCormack scheme is numerically unstable if $\nu = 1$. The stability analysis presented in Chapter 2, for the MacCormack scheme applied to linear hyperbolic systems of equations given by (2.13), is applied to the system of equations governing the Maxwell model. This analysis and results are presented in Section 3.6. Since the systems of equations governing the standard model and the model with two relaxation times result in (3×3) and (5×5) amplification matrices \underline{G} , respectively, stability of the MacCormack scheme, applied to these higher order systems, is not considered.

In order to apply the finite difference equations given by (3.27), $\sigma(0,t)$, $\epsilon(0,t)$ and $v(0,t)$ are required for $N = 1$ and, in addition, $\dot{\sigma}(0,t)$ and $\dot{v}(0,t)$ are required for $N = 2$. For the special case $\sigma_0 = 0$ and $N = 1$, only $\sigma(0,t)$ and $v(0,t)$ are required. Boundary condition (3.17) and $J(t)$ give $\sigma(0,t)$, $\epsilon(0,t)$ and $\dot{\sigma}(0,t)$ where required. The v_0^n are obtained from a forward forward (FF) difference predictor and corrector finite difference scheme, as described earlier (see Section 2.3), so that

$$\begin{aligned} \overline{v_0^{n+1}} &= v_0^n - \frac{\Delta t}{\Delta x} (-\sigma_1^n + \sigma_0^n) \\ v_0^{n+1} &= \frac{1}{2} \left\{ v_0^n + \overline{v_0^{n+1}} - \frac{\Delta t}{\Delta x} (-\sigma_1^{n+1} + \sigma_0^{n+1}) \right\} \end{aligned} \quad (3.29)$$

based on the nondimensional form of equation (3.3). For $N = 2$, the \dot{v}_0^n are then found from the predictor and corrector backward difference scheme,

$$\dot{v}_0^{n+1} = \frac{(v_0)^{n+1} - (v_0)^n}{\Delta t} \quad (3.30)$$

$$\dot{v}_0^{n+1} = 2\overline{\dot{v}_0^{n+1}} - \dot{v}_0^n$$

When the wavefront modification is not used, the initial values at $x = 0$, $t = 0$ are taken for boundary conditions with $\sigma_0 = 1$; $U_j = 0$ for $j \geq 2$ and $N = 1, 2$; $\sigma_0^n = 1$ for $n \geq 1$; $\sigma_0^1 = 0.5$, $\sigma_0^n = 1$ and $\dot{\sigma}_0^n = 0$ for $n \geq 2$, $\dot{\sigma}_0^1 = 1/\Delta t$ for $N = 2$.

An unmodified application of equation (3.27) to the problems considered, results in numerical dispersion and a smearing of the shock.

In order to eliminate these effects, the prior knowledge of the position of the wavefront and the discontinuity relations at the wavefront may be incorporated into the procedure.

The nondimensional form of the wavefront is $x = t$, for the linear problem considered, and the jumps in the field variables across the wavefront satisfy the nondimensional relations,

$$[\sigma] = [\epsilon] \quad , \quad [v] = -[\sigma] \quad (3.31)$$

since equations (3.3) and (3.4) are in conservation form. In equation (3.31) the square brackets $[\]$ indicate the jump in the quantity across the wavefront².

The first term in the wavefront expansion is given by equation (3.24)₁,

$$[\sigma] = e^{-\beta x} \quad (3.32)$$

where $\beta = \left\{ \frac{J'(0)}{2J(0)} \right\}$ and $[\sigma]$ denotes the jump in σ . Since the initial conditions are quiescent, $\underline{U} = 0$ just ahead of the wavefront, and the elements \underline{U} just behind the wavefront can be obtained from equations (3.31) and (3.32).

The modification, which incorporates the elements \underline{U} at the wavefront is now described. Suppose at the n^{th} time step the wavefront passes between the mesh points $(j\Delta x, n\Delta t)$, $((j+1)\Delta x, n\Delta t)$ or passes through $(j\Delta x, n\Delta t)$. Then the \underline{U}_s^n are obtained from the results at the $(n-1)^{\text{th}}$ step using equations (3.27), where $s < j$ if the wavefront passes

² In this context $[\]$ denote jump conditions. Elsewhere square $[\]$ brackets are used as brackets only. It should be clear where $[\]$ denote jumps in quantities.

through $(j\Delta x, n\Delta t)$, otherwise $s \leq j$. In both cases, fictitious values of the elements of U_{j+1}^n are obtained by extrapolation, using the wavefront values in order to apply equations (3.27) to the determination of U_j^{n+1} . An unmodified application of the scheme takes $U_{j+1}^n = 0$, since the presence of the wavefront is ignored. However, this results in numerical dispersion and smearing of the shock.

3.5 Momentum Considerations

Since momentum must be conserved for the problems considered, numerical evaluation of momentum provides a check on the numerical solution. The relationship for the nondimensional momentum is given by

$$\int_0^t \sigma(0, \eta) d\eta = \int_0^{x_f(t)} v dx, \quad (3.33)$$

where $x_f(t)$ is the position of the wavefront at time t . The right hand side of equation (3.33) is evaluated numerically using a Simpson's integration scheme. The left hand side is evaluated analytically by substituting the appropriate boundary condition, and integrating.

3.6 Stability of the MacCormack Scheme for the Maxwell Model

Since the governing equations (3.15) for the Maxwell model are linear and the system consists of two first order equations, the system can be put in the form (2.13) where \underline{A} is given by (3.15)₂ and $\hat{\underline{B}}$ is given

by
$$\hat{\underline{B}} = \begin{bmatrix} 1 & 0 \\ 0 & 0 \end{bmatrix}$$

The von Neumann stability analysis can be applied to examine the stability of the MacCormack scheme, by substituting the appropriate values for \underline{A} and \underline{B} into equation (2.14).

The amplification matrix for the MacCormack scheme applied to the Maxwell model is

$$\underline{G} = \begin{bmatrix} L & (-M + iN) \\ (M + iN) & P \end{bmatrix} \quad (3.34)$$

$$\text{where } L = \left\{ 1 - \Delta t + \frac{(\Delta t)^2}{2} + \nu^2 (\cos\beta - 1) \right\}, \quad N = \nu \left\{ \frac{1 - \Delta t}{2} \right\} \sin\beta$$

$P = (1 + \nu^2 (\cos\beta - 1))$ and $M = (\nu\Delta t (\cos\beta - 1))/2$ for the MacCormack scheme. The relation between $(\lambda - 1)$ and $\beta = k_m \Delta x$, where λ is the spectral radius is shown in Figure 3.7, for various Courant numbers.

The matrix given by (3.34) is not a normal matrix so that $\lambda \leq 1$ is a necessary but not sufficient condition for stability of an initial value problem. This condition is satisfied for $\nu \leq 0.9987$ when $\Delta x = 0.01$. These results will be discussed further in regard to the numerical results obtained using the MacCormack scheme. The investigation of stability for higher order linear systems becomes increasingly difficult, since the determination of the spectral radius is complicated with larger \underline{G} matrices. The spectral radius λ of the \underline{G} matrix can be evaluated numerically if a stability analysis is essential.

3.7 Numerical Results

The numerical results in this section have been obtained using the MacCormack scheme with a grid spacing of $\Delta x = 0.01$ unless otherwise specified. Numerical results are presented for nondimensional stress σ versus nondimensional distance x , at nondimensional times t . Only quiescent initial conditions $U(x,0) = 0$ are considered. The numerical results are divided into three sections, one for each of the viscoelastic models.

3.7.1 Maxwell Model ($\alpha_0 = 0, N = 1$)

Figure 3.2 shows the exact solution for the variation of σ with x obtained by Christensen (1982), for $v(0,t) = V_0 H(t)$. The exact solution, in terms of nondimensional variables, is

$$\sigma(x,t) = -V_0 e^{-t/2} I_0 \left\{ \left[\frac{t^2 - x^2}{2} \right]^{1/2} \right\} H(t-x), \quad (3.35)$$

where I_0 is the modified Bessel function of the first kind of order zero.

The wavefront occurs at $x = t$, and the magnitude of the stress at the wavefront can be found from the wavefront expansion for a Maxwell model. Figures 3.3 - 3.5 show the corresponding numerical solutions compared to the exact solution for the Maxwell model subject to $v(0,t) = V_0 H(t)$, with $V_0 = -1$. The numerical results are in good agreement with the exact solution except where numerical dispersion or numerical instability occur. Figure 3.3 indicates that the MacCormack scheme is unstable for the system of equations which govern the Maxwell viscoelastic material when

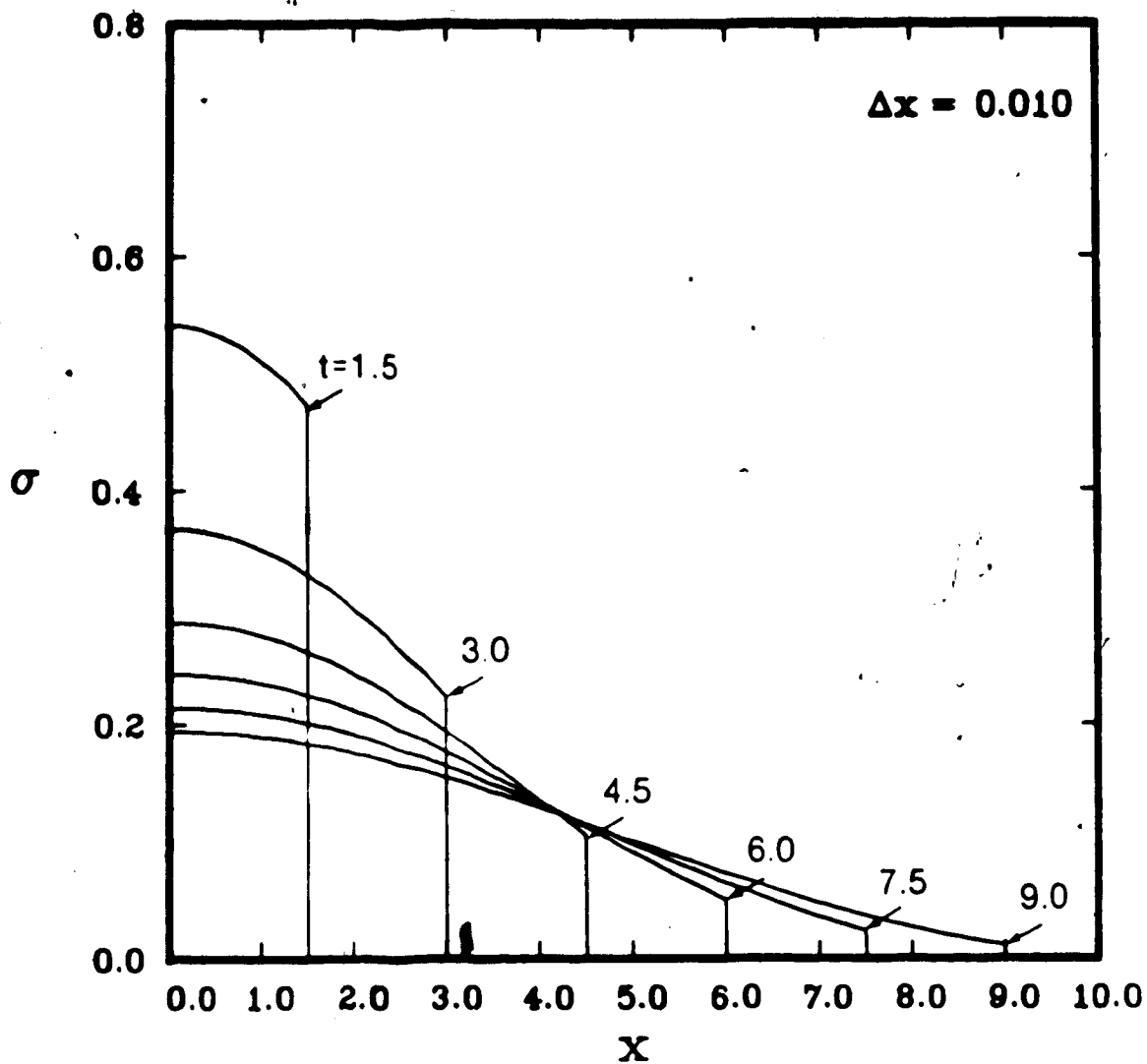


Fig. 3.2 Maxwell Model - Variation of nondimensional σ with nondimensional x for $v(0,t) = V_0 H(t)$, with $V_0 = -1$, obtained using Laplace transforms (Christensen, 1982).

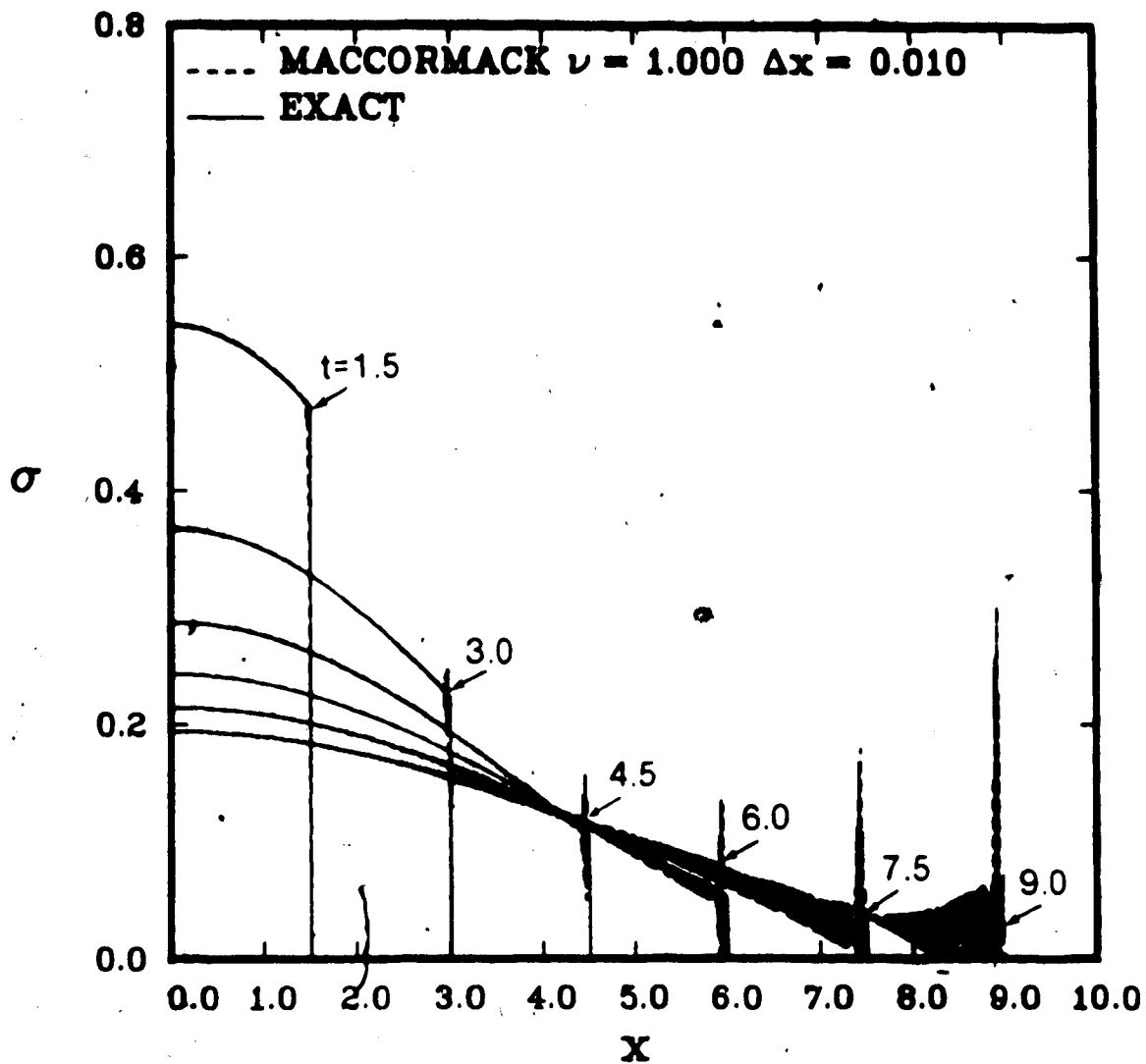


Fig. 3.3 Maxwell Model - Comparison of the MacCormack solution to the Laplace transform solution (Christensen, 1982), for nondimensional σ versus nondimensional x for $v(0,t) = V_0 H(t)$, with $V_0 = -1$, and $\nu = 1.0$.

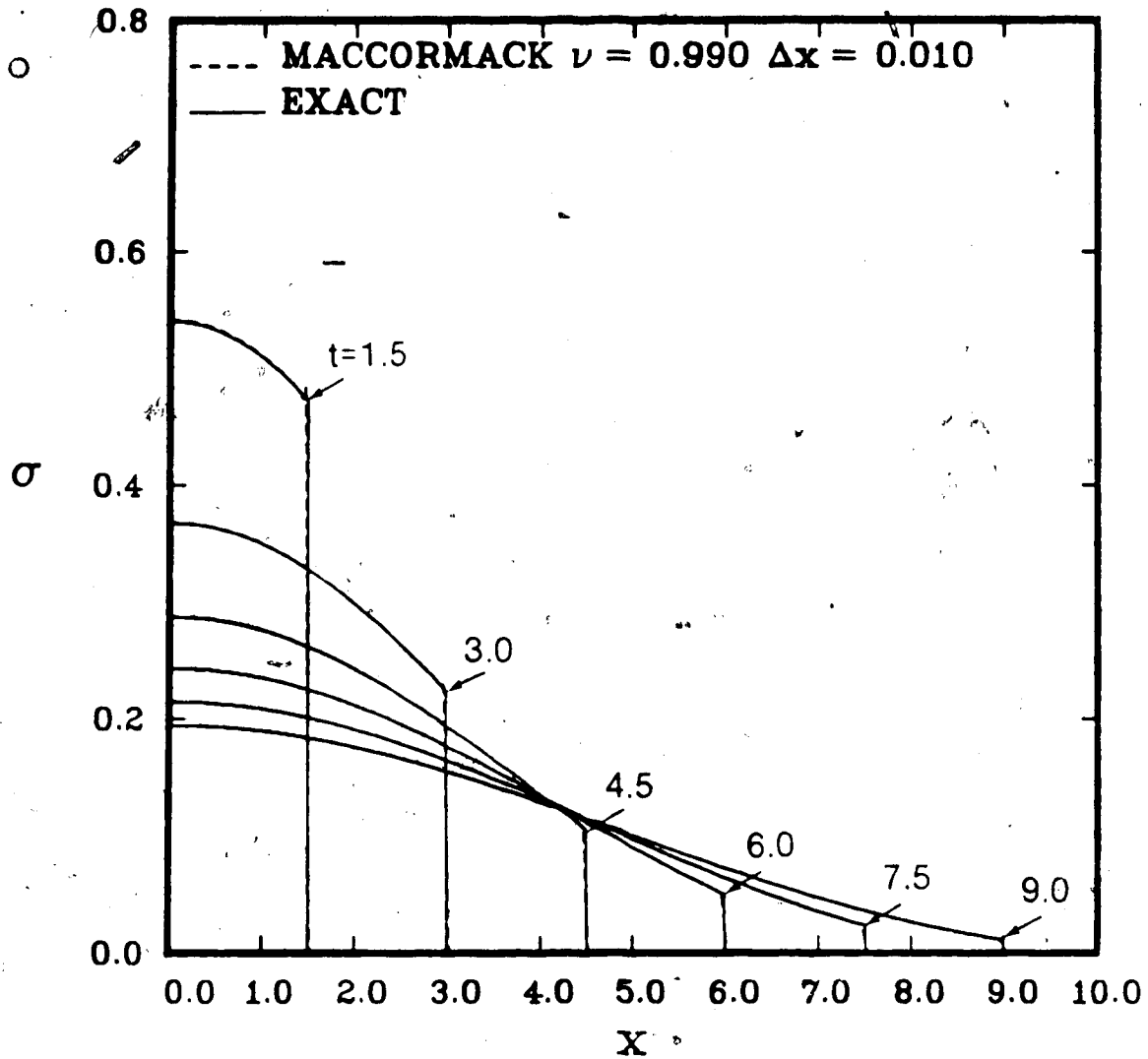


Fig. 3.4 Maxwell Model - Comparison of the MacCormack solution to the Laplace transform solution (Christensen, 1982), for nondimensional σ versus nondimensional x for $v(0,t) = V_0 H(t)$, with $V_0 = -1$, and $\nu = 0.99$.

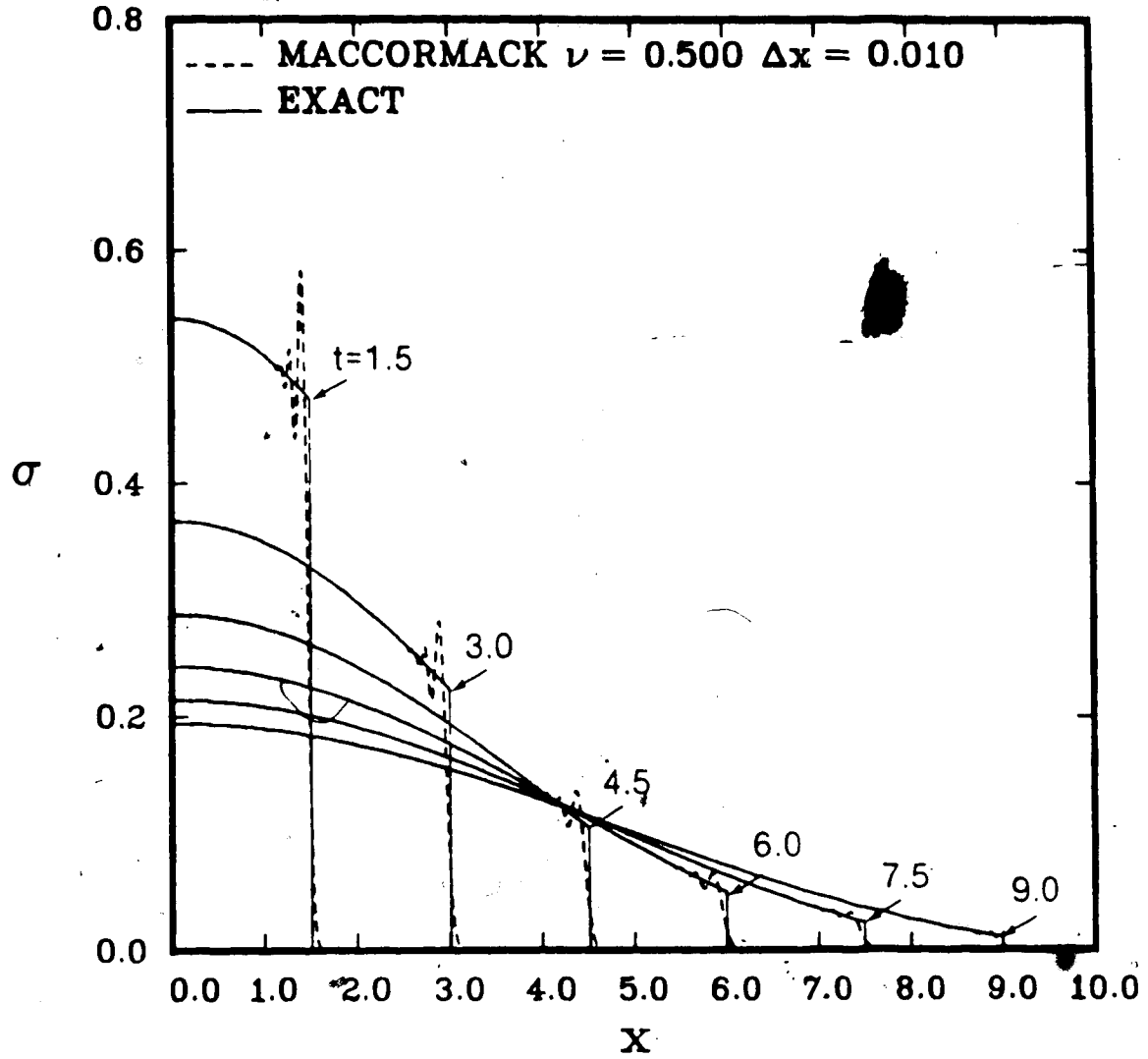


Fig. 3.5 Maxwell Model - Comparison of the MacCormack solution to the Laplace transform solution (Christensen, 1982), for nondimensional σ versus nondimensional x for $v(0,t) = V_0 H(t)$, with $V_0 = -1$, and $\nu = 0.5$.

$\nu = 1.0$. Figure 3.5 shows severe numerical dispersion for $\nu = 0.5$ but no instability.

Figure 3.6 shows numerical results obtained using the MacCormack scheme with a wavefront expansion for $v(0, t) = V_0 H(t)$, with $V_0 = -1$. The wavefront expansion technique is implemented for $\nu = 0.5$. It is evident from Figure 3.6 that the wavefront expansion modification eliminates dispersion such that the numerical solution is virtually identical to the exact solution (see Figure 3.2).

Figure 3.7 shows the results of the von Neumann stability analysis for the MacCormack scheme applied to the system of equations given by (3.15). The quantity $(\lambda-1)$ is plotted against β for various Courant numbers and a grid spacing of $\Delta x = 0.01$. The stability analysis indicates that the MacCormack scheme is unstable for $\nu = 1.0$. The numerical results presented in Figure 3.3 also confirm this instability.

Figures 3.8 - 3.10 show numerical results for boundary condition (3.17), with $\sigma_0 = 1$, for the Maxwell model, for Courant numbers $\nu = 1.0$, $\nu = 0.990$ and $\nu = 0.9985$, and $\Delta x = 0.01$ which correspond to the stability curves presented in Figure 3.7. The numerical results are consistent with the stability analysis. Figure 3.11 shows the numerical results for boundary condition (3.17), with $\sigma_0 = 1$, for $\Delta x = 0.025$. The results shown in Figures 3.9 - 3.11 indicate that the stability of the MacCormack scheme applied to the system of equations (3.15), is dependent on

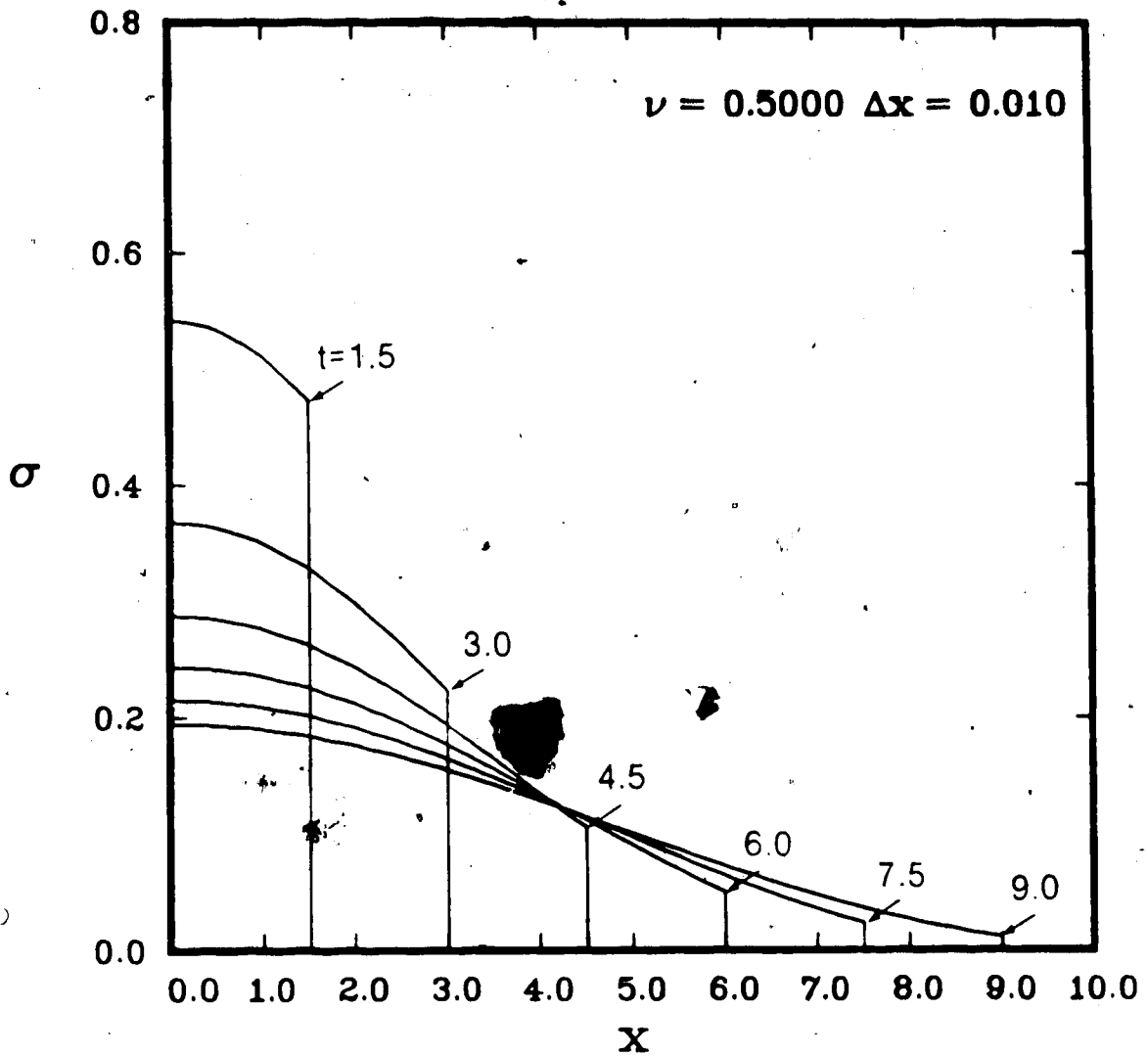


Fig. 3.6 Maxwell Model - Variation of nondimensional σ with nondimensional x for $v(0,t) = V_0 H(t)$, with $V_0 = -1$, obtained using the MacCormack scheme with a wavefront expansion with $\nu = 0.5$.

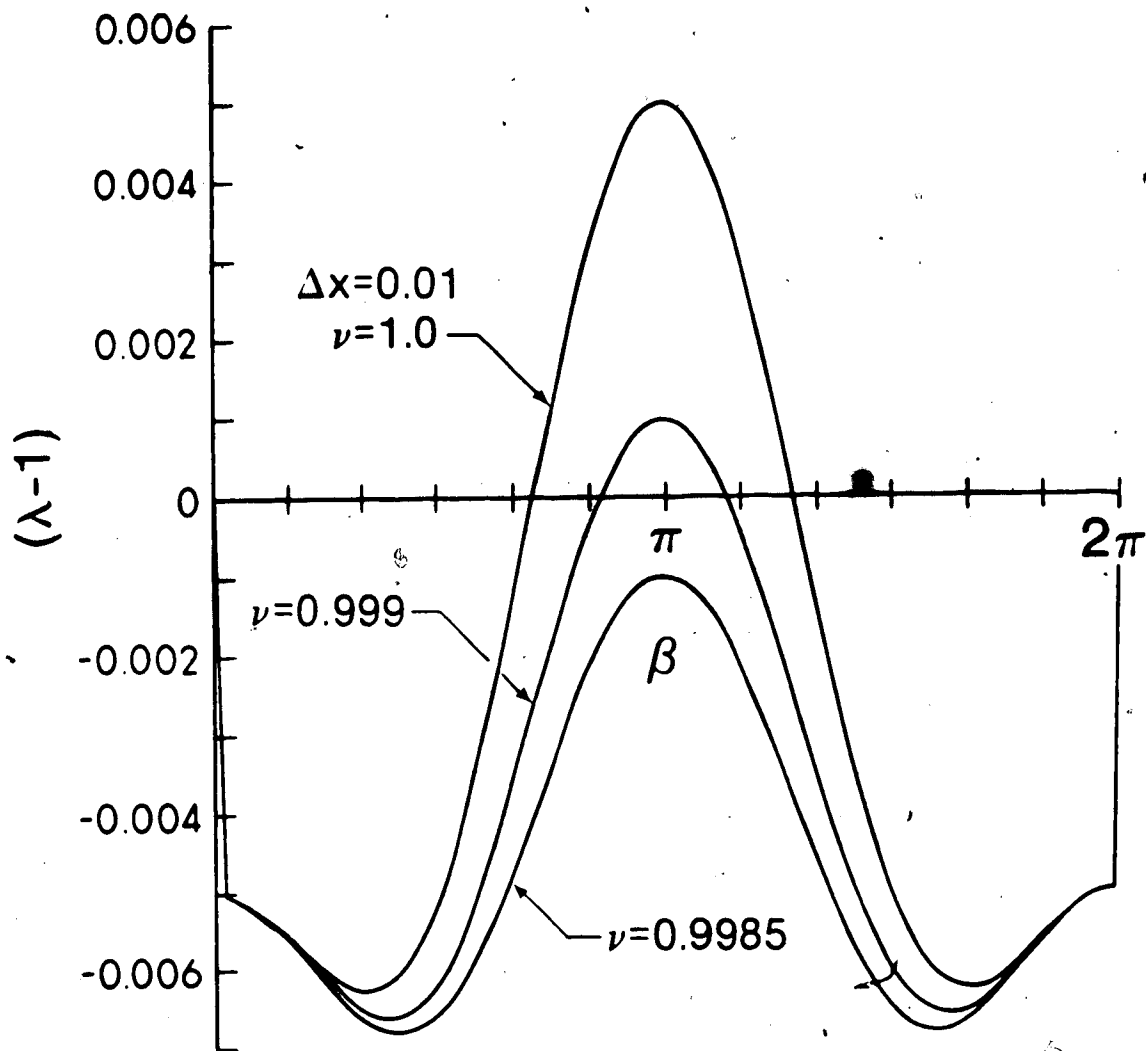


Fig. 3.7 The von Neumann stability analysis for the MacCormack scheme applied to the Maxwell Model for $\Delta x = 0.01$.

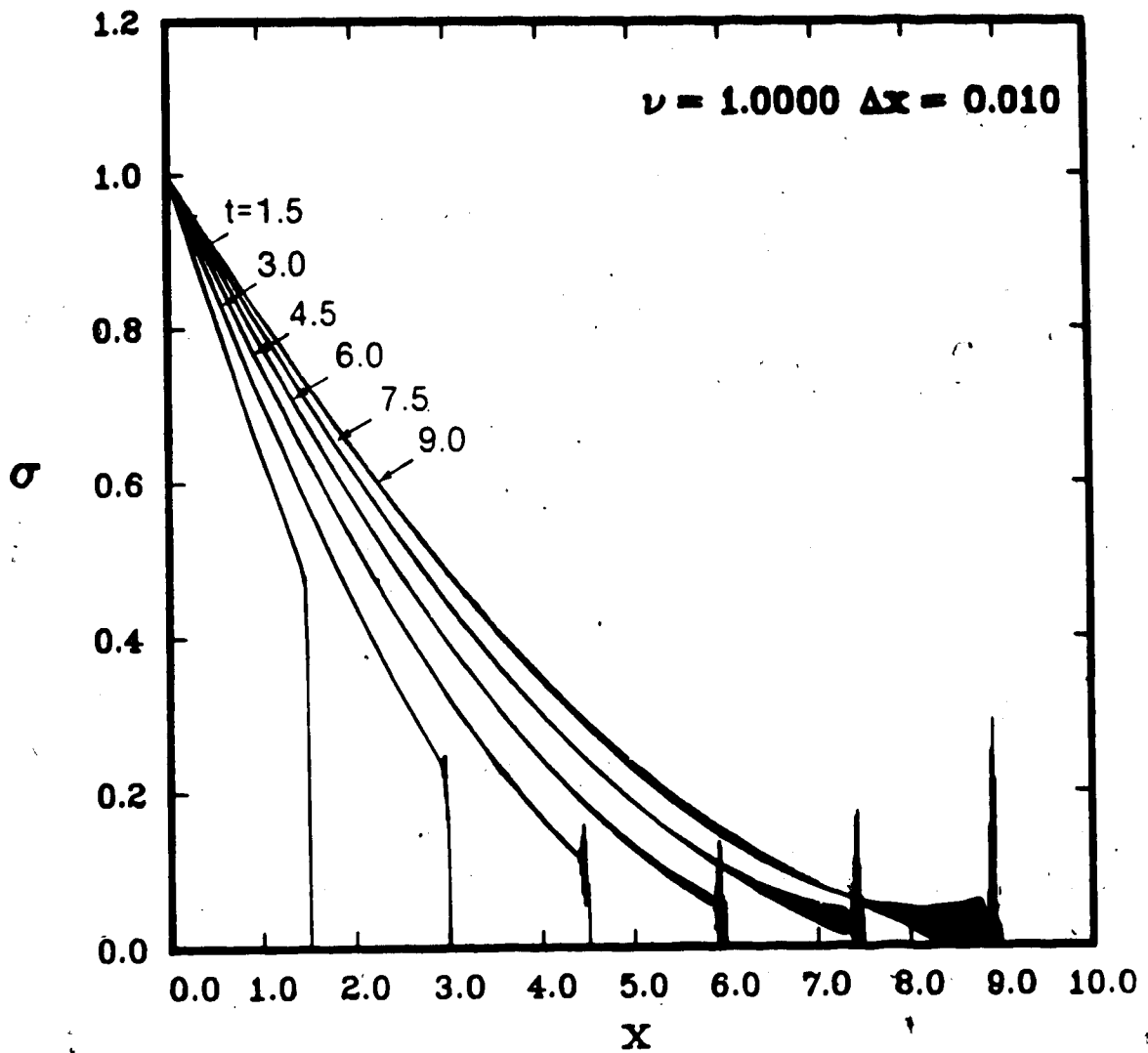


Fig. 3.8 Maxwell Model - Variation of nondimensional σ with nondimensional x for $\sigma(0,t) = \sigma_0 H(t)$, with $\sigma_0 = 1$ and $\nu = 1.0$, using the MacCormack scheme.

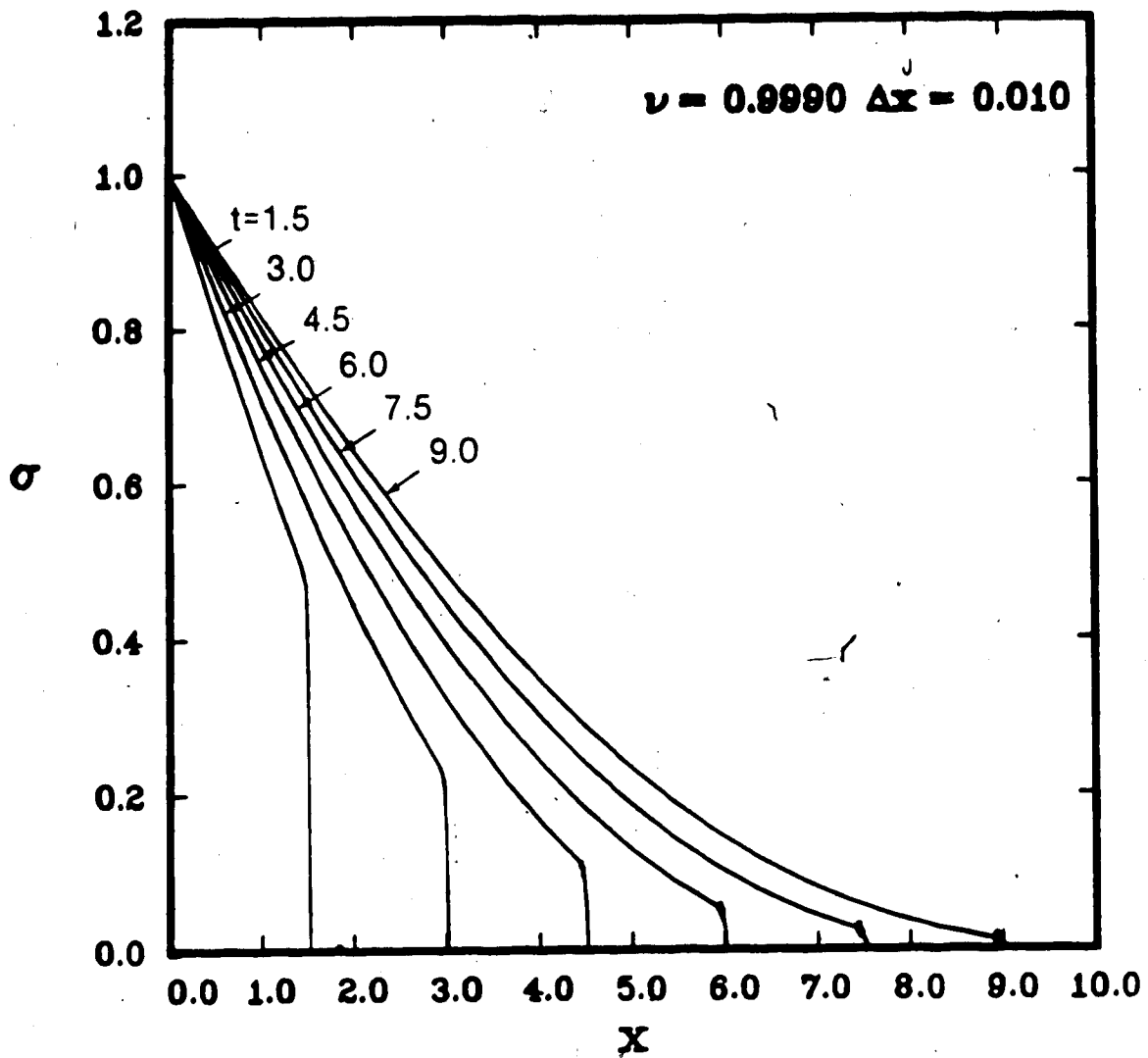


Fig. 3.9 Maxwell Model - Variation of nondimensional σ with nondimensional x for $\sigma(0,t) = \sigma_0 H(t)$, with $\sigma_0 = 1$ and $\nu = 0.999$ using the MacCormack scheme.

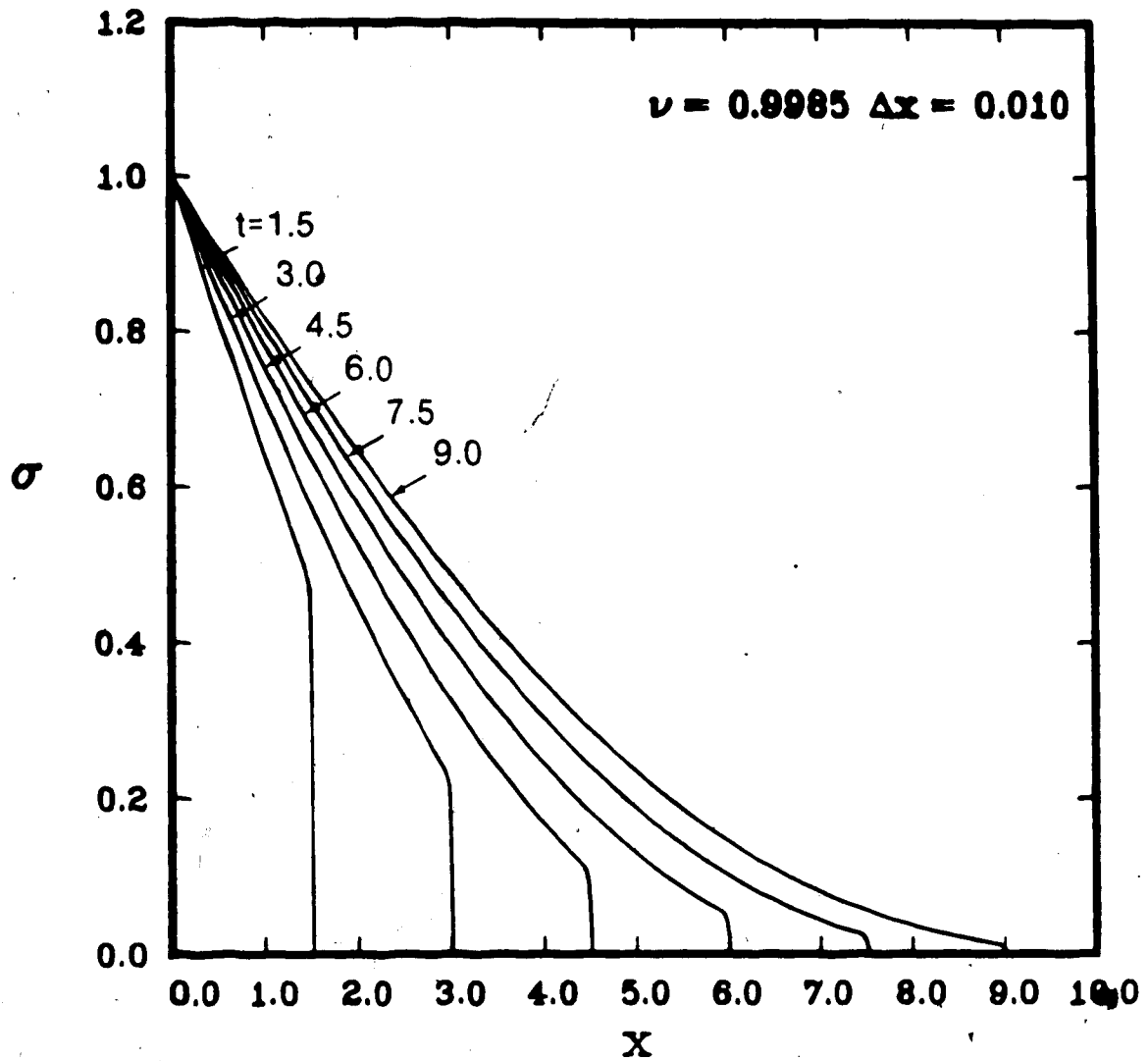


Fig. 3.10 Maxwell Model - Variation of nondimensional σ with nondimensional x for $\sigma(0,t) = \sigma_0 H(t)$, with $\sigma_0 = 1$ and $\nu = 0.9985$ using the MacCormack scheme.

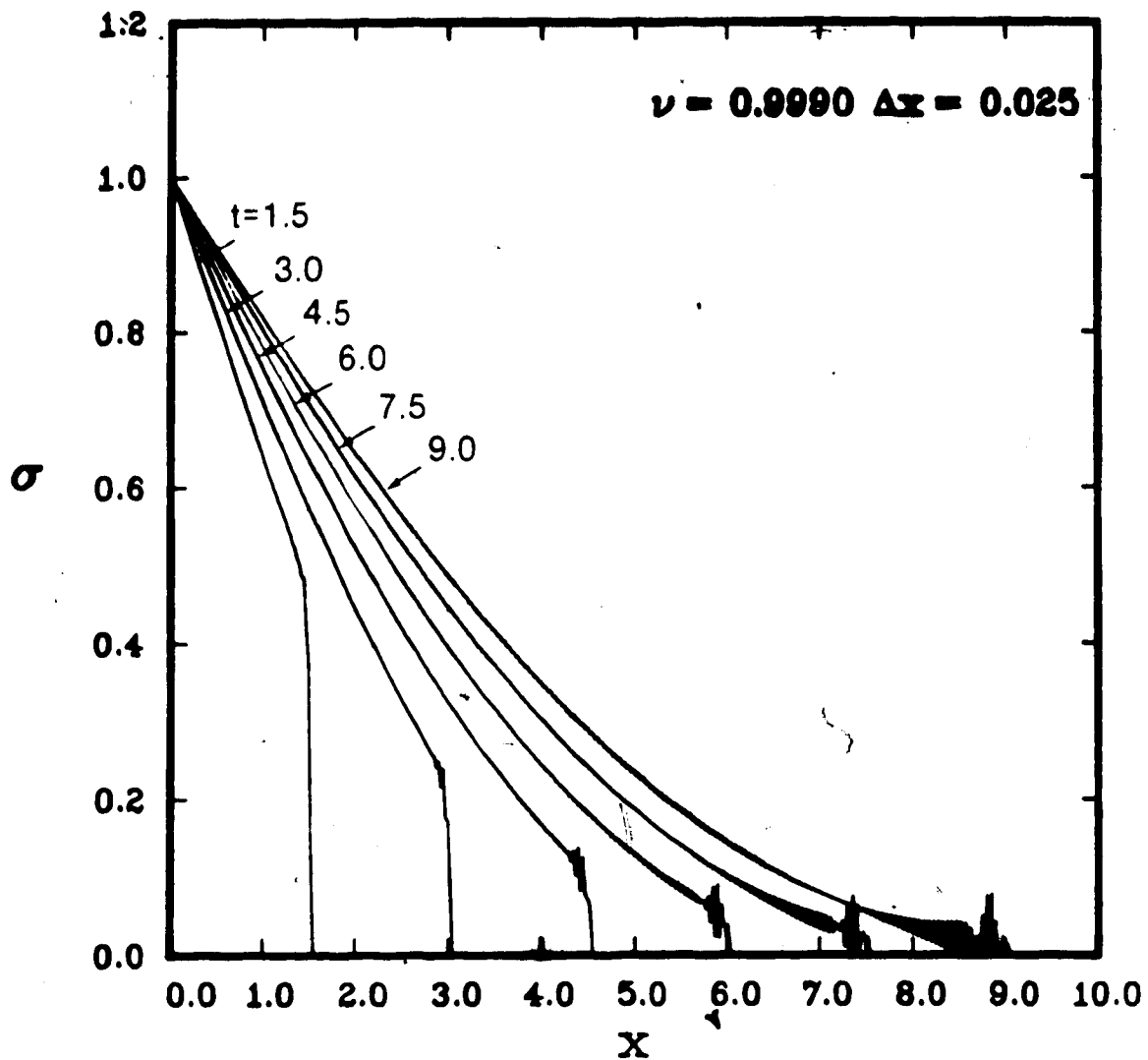


Fig. 3.11 Maxwell Model - Variation of nondimensional σ with nondimensional x for $\sigma(0,t) = \sigma_0 H(t)$, with $\sigma_0 = 1$ and $\nu = 0.9990$, $\Delta x = 0.025$ using the MacCormack scheme.

the grid size, since the numerical results show greater instability for $\Delta x = 0.025$ than for $\Delta x = 0.01$ for a given Courant number.

Figures 3.12 and 3.13 show the numerical results for boundary condition (3.23), with $\sigma_0 = 1$, for the Maxwell model, for Courant numbers $\nu = 1.0$ and $\nu = 0.99$, respectively. Figure 3.12 shows slowly growing instability at $t = 9$, however, the instability is less severe than for boundary condition (3.17) (see Figure 3.8).

Figure 3.14 shows the effect of grid size on the numerical solution for boundary condition (3.17), with $\sigma_0 = 1$. The coarse mesh size $\Delta x = 0.04$ indicates smearing of the shock front. There is almost no difference between $\Delta x = 0.02$ and $\Delta x = 0.01$, therefore, most of the numerical results are presented for $\Delta x = 0.01$.

All of the numerical results presented in this section satisfy conservation of momentum according to equation (3.33). The numerical dispersion present for small Courant numbers ($\nu = 0.5$) does not dramatically affect the momentum evaluated from the numerical results, but instability does affect momentum. Tables 3.1 and 3.2 illustrate typical momentum calculations for the Maxwell material for boundary condition (3.17) and (3.23), respectively with $\sigma_0 = 1$. Table 3.1 corresponds to Figure 3.9 and Table 3.2 corresponds to Figure 3.13. The wavefront, for all the numerical solutions presented, is located at $x = t$, which is in excellent agreement with theoretical predictions. Since $\Delta x = 0.01$ is a finite grid spacing for most of the results presented, the wavefront closely approximates a discontinuity.

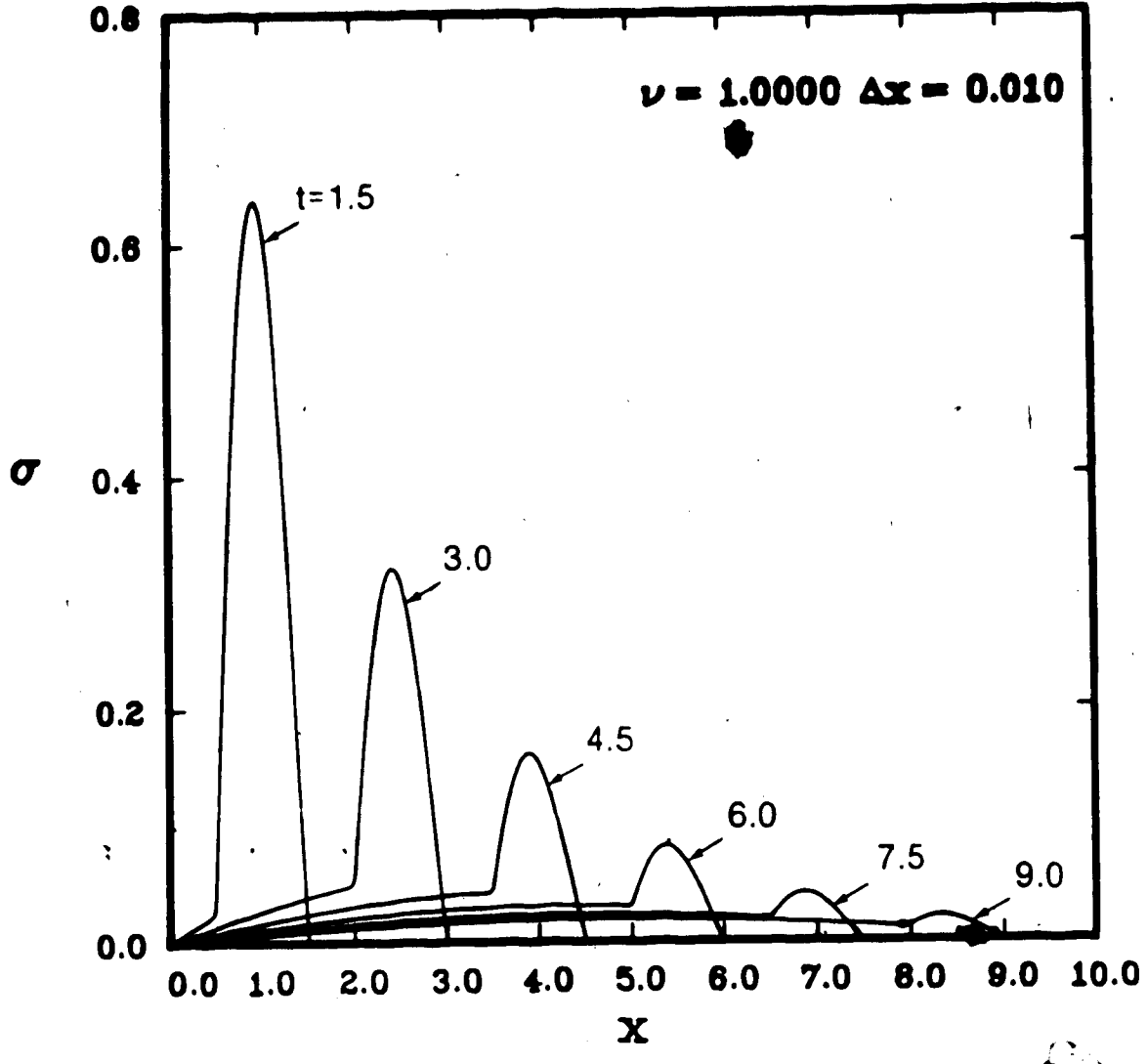


Fig. 3.12 Maxwell Model - Variation of nondimensional σ with nondimensional x for $\sigma(0,t) = \sigma_0 \sin \pi t H(t) H(1-t)$, with $\sigma_0 = 1$ and $\nu = 1.0$ using the MacCormack scheme.

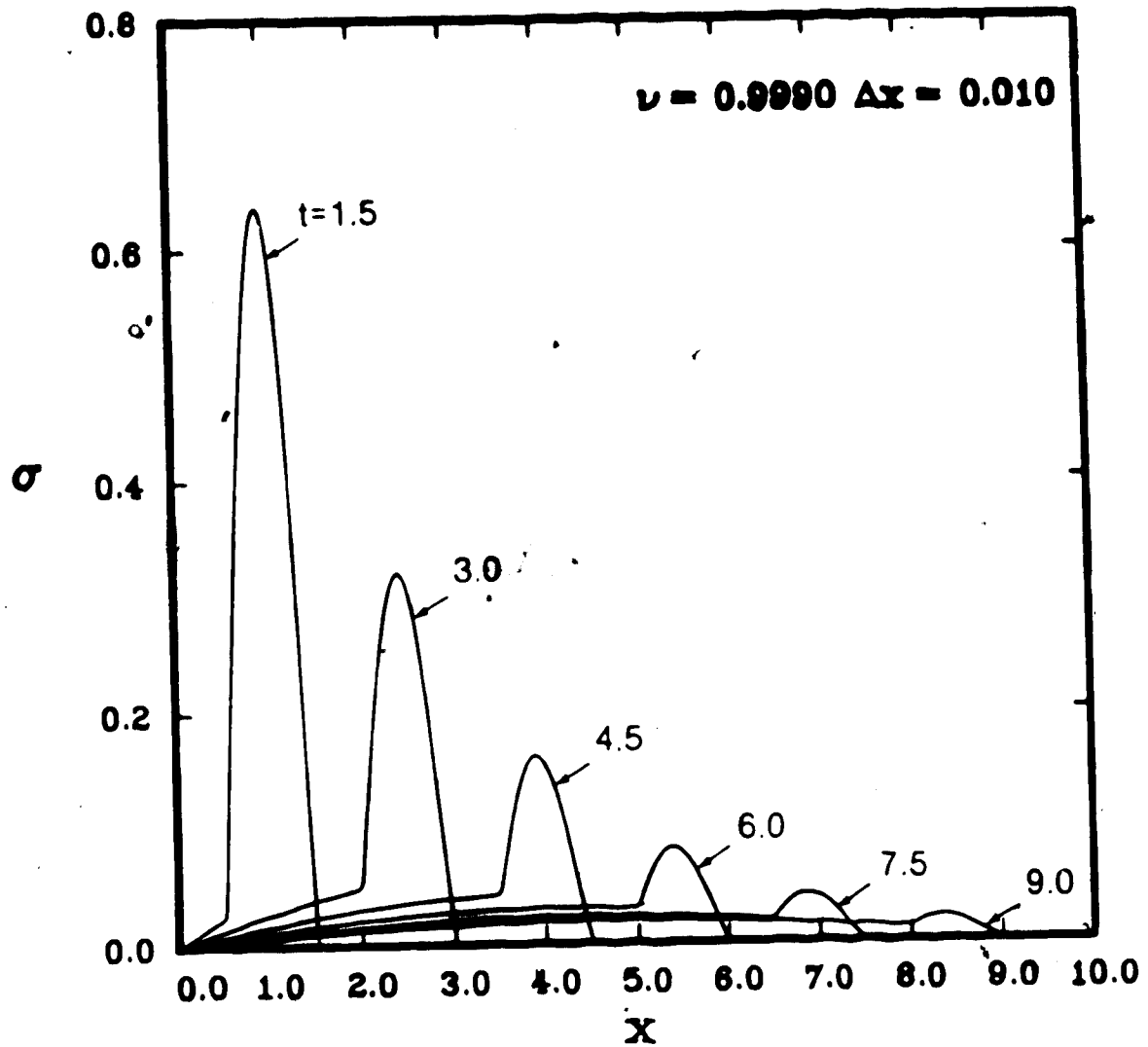


Fig. 3.13 Maxwell Model - Variation of nondimensional σ with nondimensional x for $\sigma(0,t) = \sigma_0 \sin \pi t H(t) H(1-t)$, with $\sigma_0 = 1$ and $\nu = 0.999$ using the MacCormack scheme.

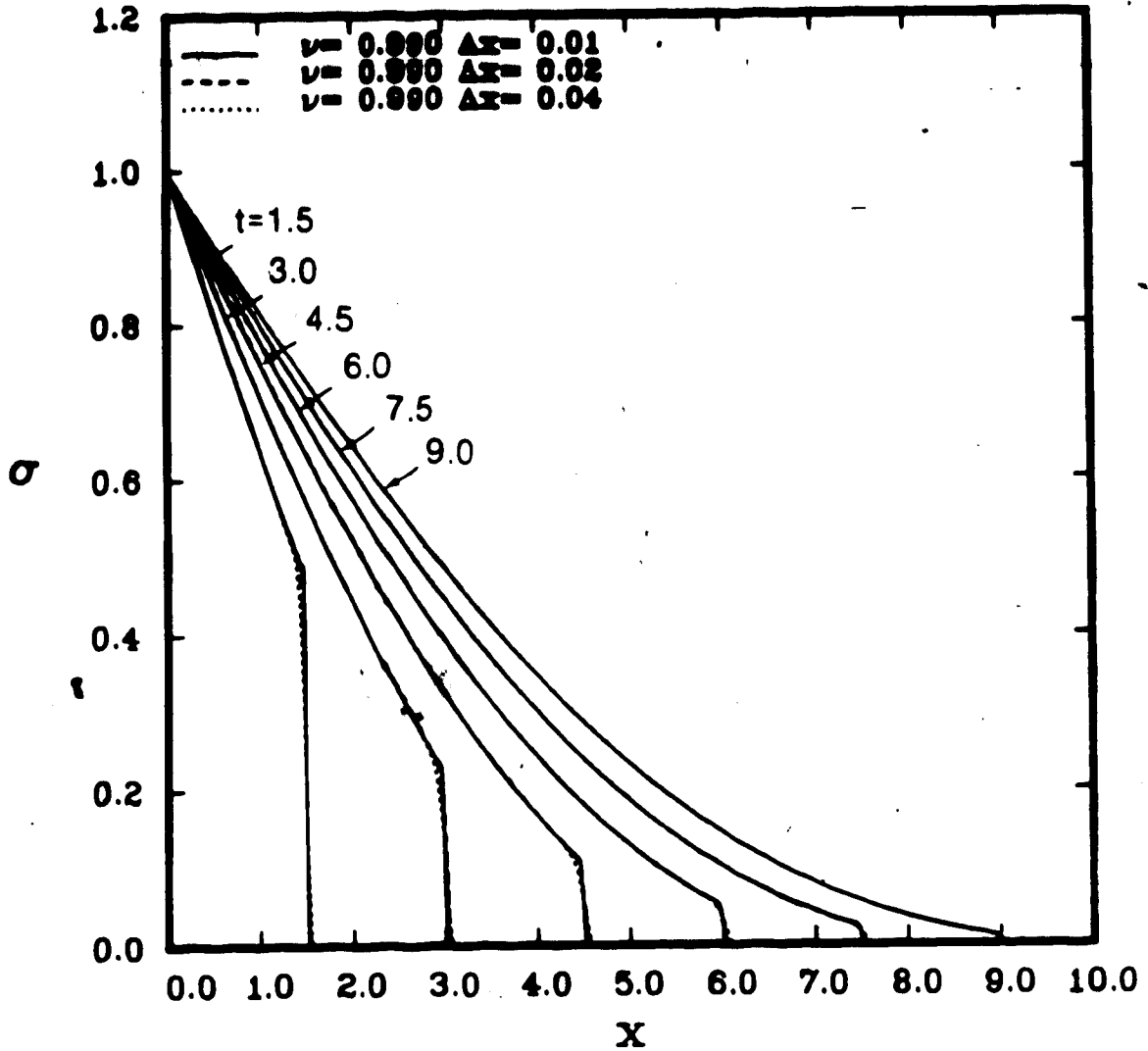


Fig. 3.14 Maxwell Model Effect of grid size on numerical results obtained using the MacCormack scheme for nondimensional σ versus nondimensional x for $\sigma(0,t) = \sigma_0 H(t)$, with $\sigma_0 = 1$ and $\nu = 0.99$.

Table 3.1 Nondimensional Momentum Calculations for a Maxwell Material subject to $\sigma(0,t) = -\sigma_0 H(t)$, $\sigma_0 = 1$, and quiescent initial conditions, for $\nu = 0.999$. (See Figure 3.9)

Nondimensional Time t	Exact Value of Momentum	Numerically Evaluated Momentum
1.5	-1.5	-1.497
3.0	-3.0	-2.994
4.5	-4.5	-4.490
6.0	-6.0	-5.987
7.5	-7.5	-7.484
9.0	-9.0	-8.981

Table 3.2 Nondimensional Momentum Calculations for a Maxwell Material subject to $\sigma(0,t) = \sigma_0 \sin t H(t) H(1-t)$, $\sigma_0 = 1$, and quiescent initial conditions for $\nu = 0.999$. (See Figure 3.13)

Nondimensional Time t	Exact Value of Momentum	Numerically Evaluated Momentum
1.5	-0.6366	-0.6356
3.0	-0.6366	-0.6358
4.5	-0.6366	-0.6359
6.0	-0.6366	-0.6359
7.5	-0.6366	-0.6359
9.0	-0.6366	-0.6359

3.7.2 Standard Model ($\alpha_0 > 0$, $N = 1$)

Figures 3.15 - 3.17 show the numerical results for boundary condition (3.17), with $\sigma_0 = 1$, for various values of α_0 . The values of α_0 illustrate varying degrees of viscoelasticity according to the relaxation function given by (3.1). A value of $\alpha_0 = 1$ corresponds to an elastic material, $\alpha_0 = 0.9$ corresponds to a material which is slightly viscoelastic and $\alpha_0 = 0.1$ corresponds to a very viscoelastic material. For the problems considered α_0 cannot be zero because the creep function is undefined when $\alpha_0 = 0$ is substituted in (3.18). The numerical results in Figure 3.15 with $\alpha_0 = 1$ show a discontinuity in stress of magnitude $\sigma = 1$ propagating in the positive x direction with the wavefront located at $x = t$. This is in complete agreement with the theory of infinitesimal elasticity, except for numerical dispersion which is present immediately behind the wavefront. Figures 3.16 and 3.17 show numerical results for $\alpha_0 = 0.9$ and $\alpha_0 = 0.1$, respectively. Numerical instability is evident in both figures, however, the wavefronts are located at $x = t$, as expected from theoretical considerations.

Figures 3.18 - 3.20 show the numerical results for boundary condition (3.23), with $\sigma_0 = 1$, for various values of α_0 . The numerical results in Figure 3.18 represent a stress pulse of magnitude $\sigma = 1$ propagating unchanged in shape in the positive x direction. The wavefront is at $x = t$. The results are in excellent agreement with expected results for an infinitesimal amplitude pulse propagating in a linear elastic medium. No

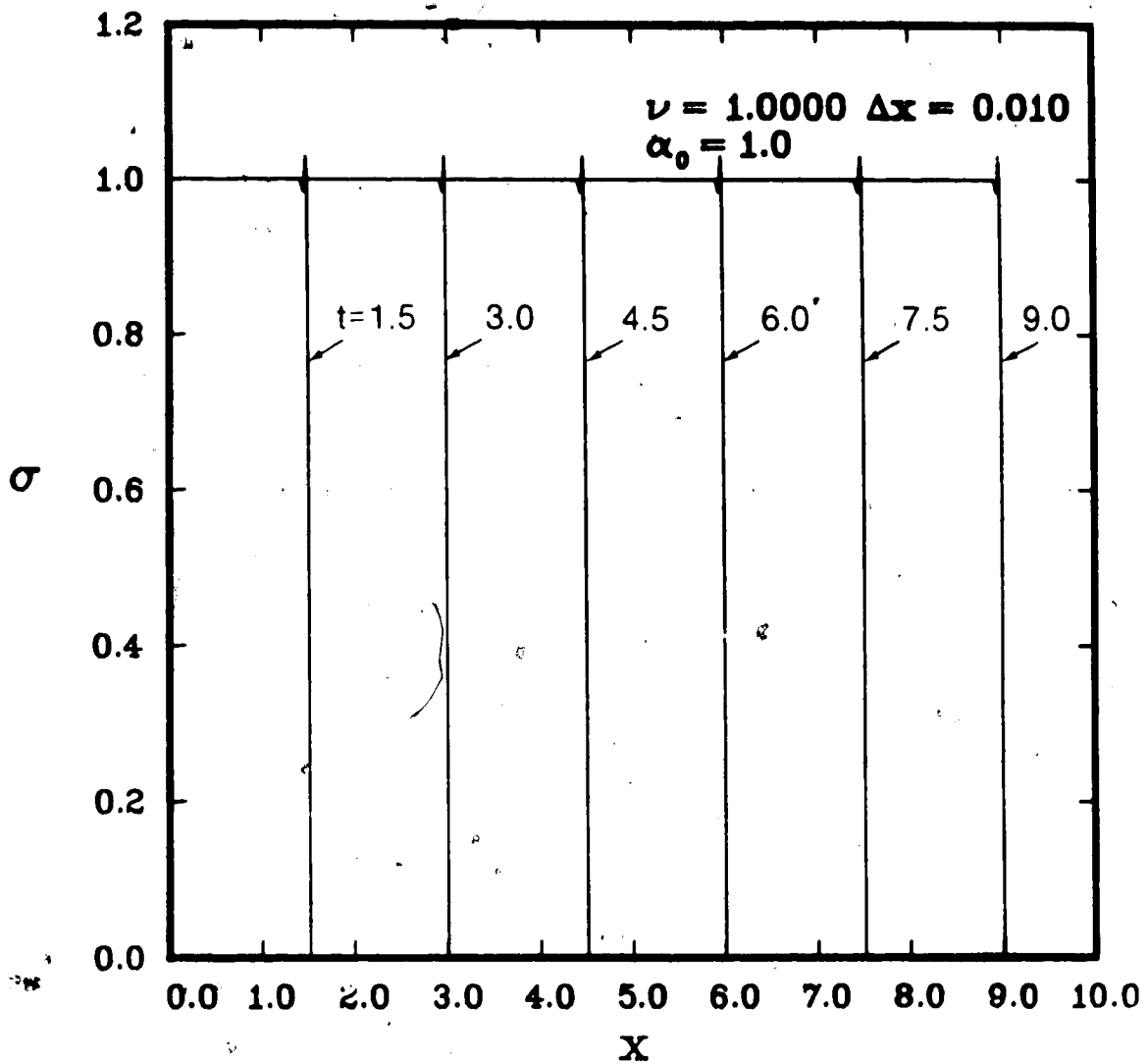


Fig. 3.15 Standard Model $\alpha_0 = 1$. - Variation of nondimensional σ with nondimensional x for $\sigma(0,t) = \sigma_0 H(t)$, with $\sigma_0 = 1$ and $\nu = 1.0$ using the MacCormack scheme.

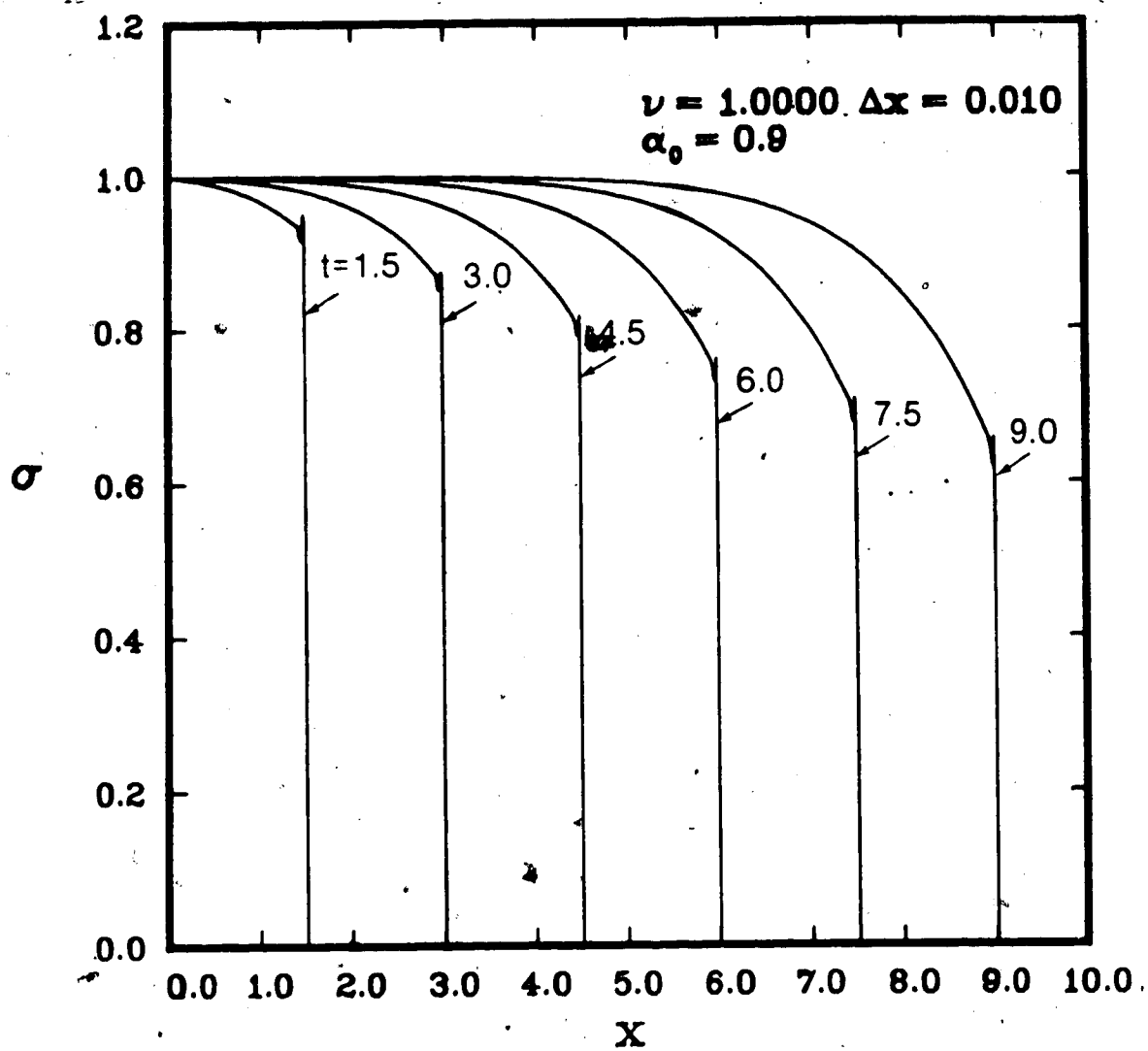


Fig. 3.16 Standard Model $\alpha_0 = 0.9$ - Variation of nondimensional σ with nondimensional x for $\sigma(0,t) = \sigma_0 H(t)$, with $\sigma_0 = 1$ and $\nu = 1.0$ using the MacCormack scheme.

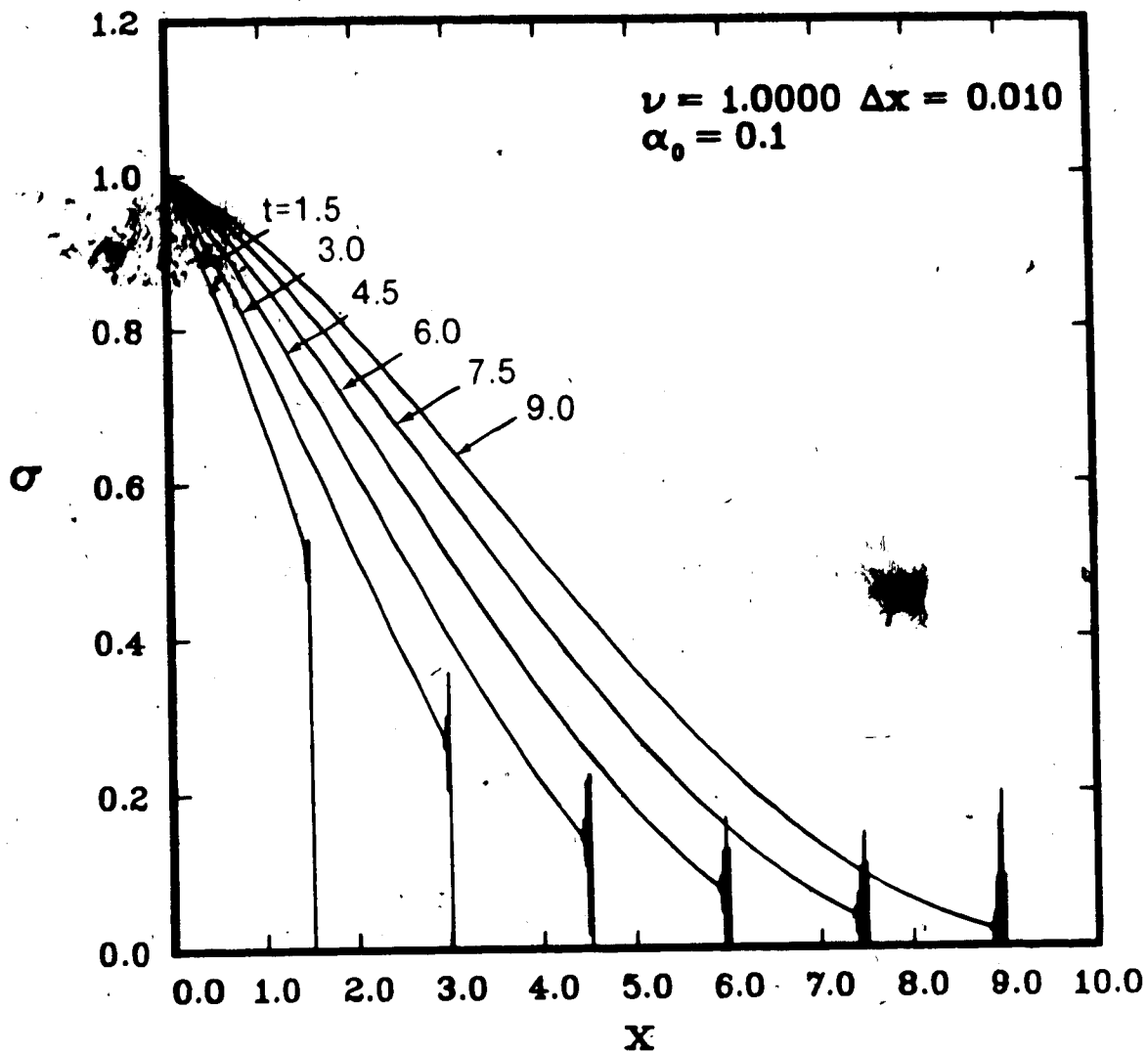


Fig. 3.17 Standard Model $\alpha_0 = 0.1$ - Variation of nondimensional σ with nondimensional x for $\sigma(0,t) = \sigma_0 H(t)$, with $\sigma_0 = 1$ and $\nu = 1.0$ using the MacCormack scheme.

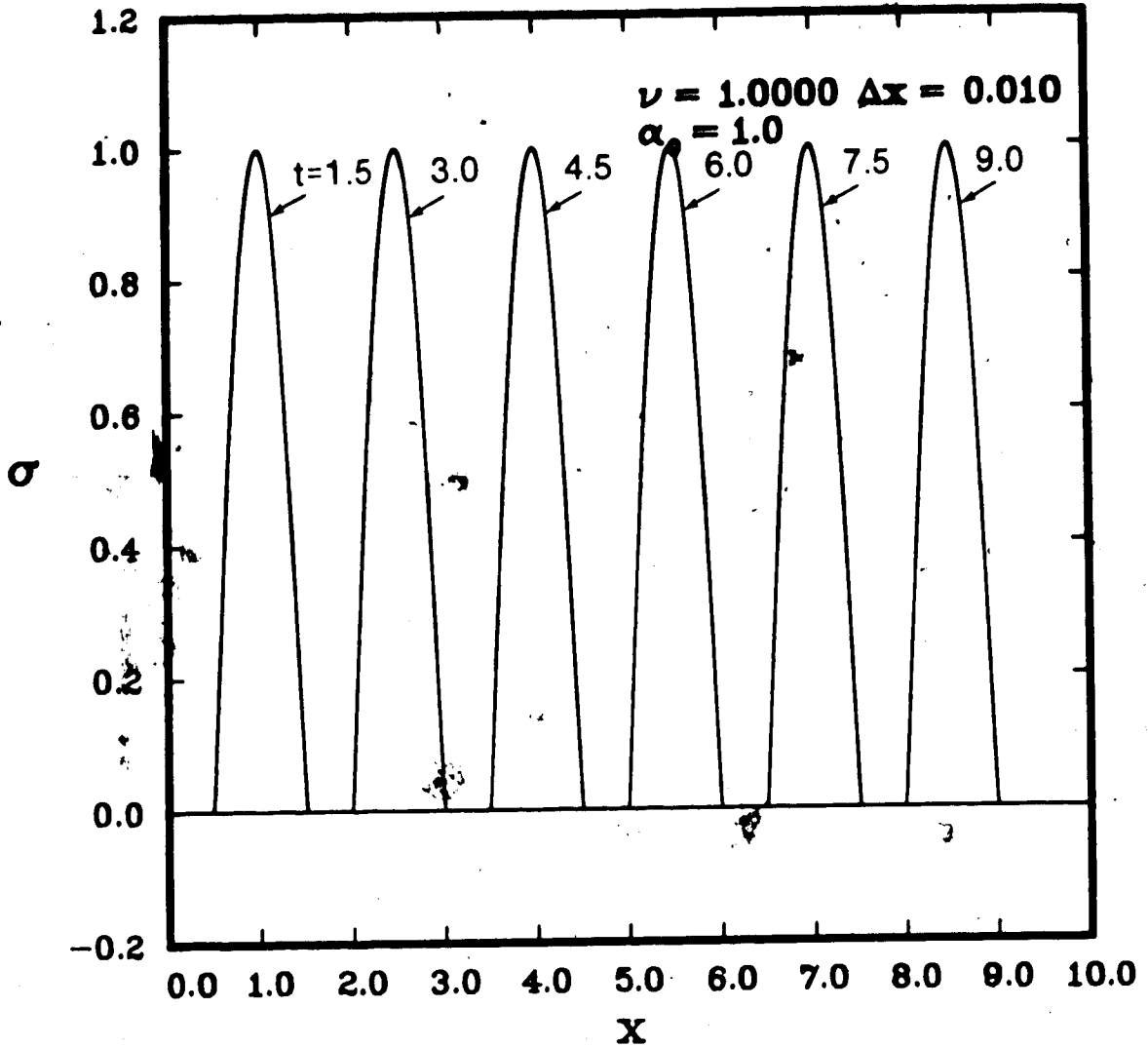


Fig. 3.13 Standard Model $\alpha_0 = 1.0$ - Variation of nondimensional σ with nondimensional x for $\sigma(0,t) = \sigma_0 \sin \pi t H(t) H(1-t)$, with $\sigma_0 = 1$ and $\nu = 1.0$ using the MacCormack scheme.

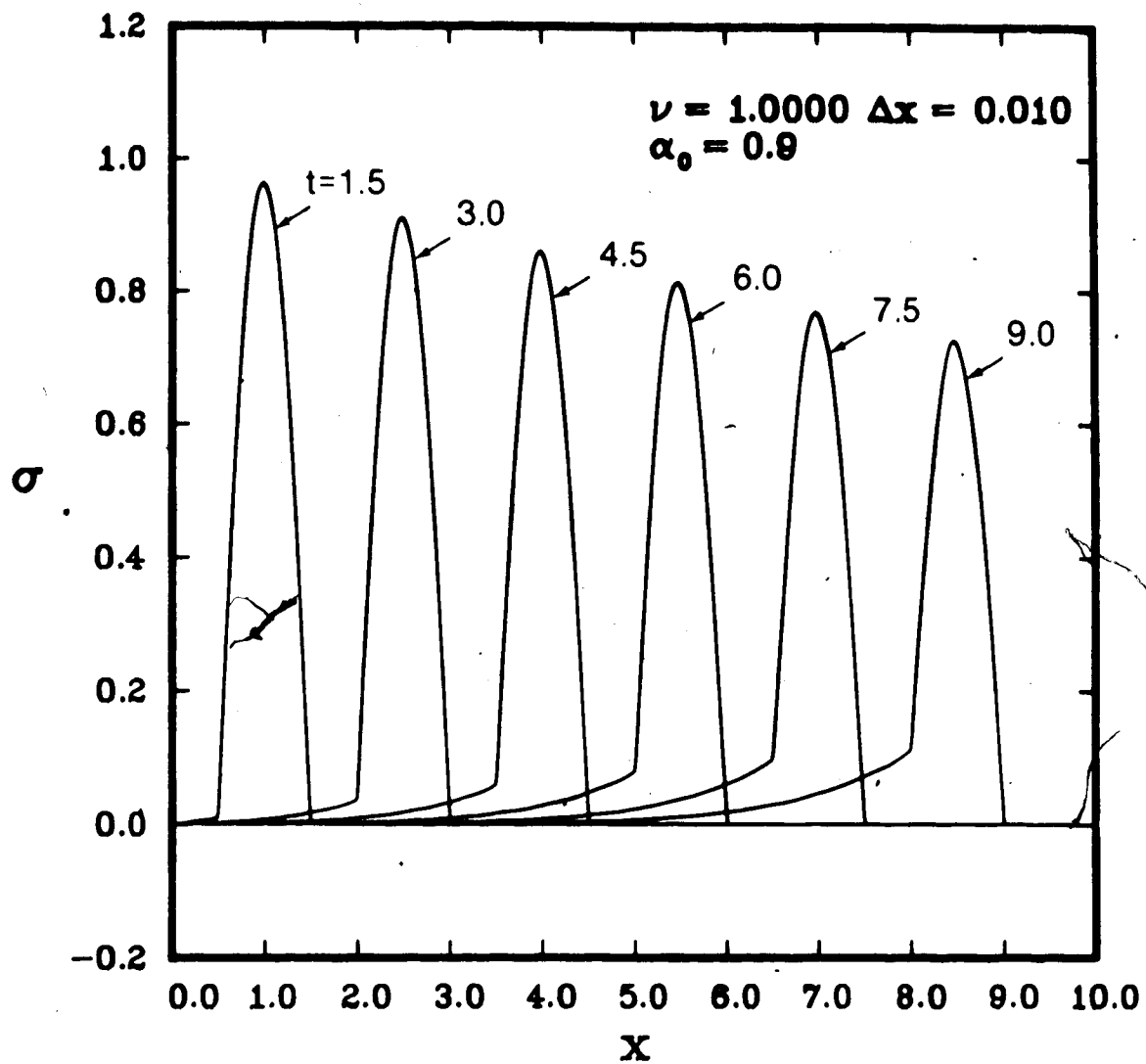


Fig. 3.19 Standard Model $\alpha_0 = 0.9$ - Variation of nondimensional σ with nondimensional x for $\sigma(0,t) = \sigma_0 \sin \pi t H(t) H(1-t)$, with $\sigma_0 = 1$ and $\nu = 1.0$ using the MacCormack scheme.

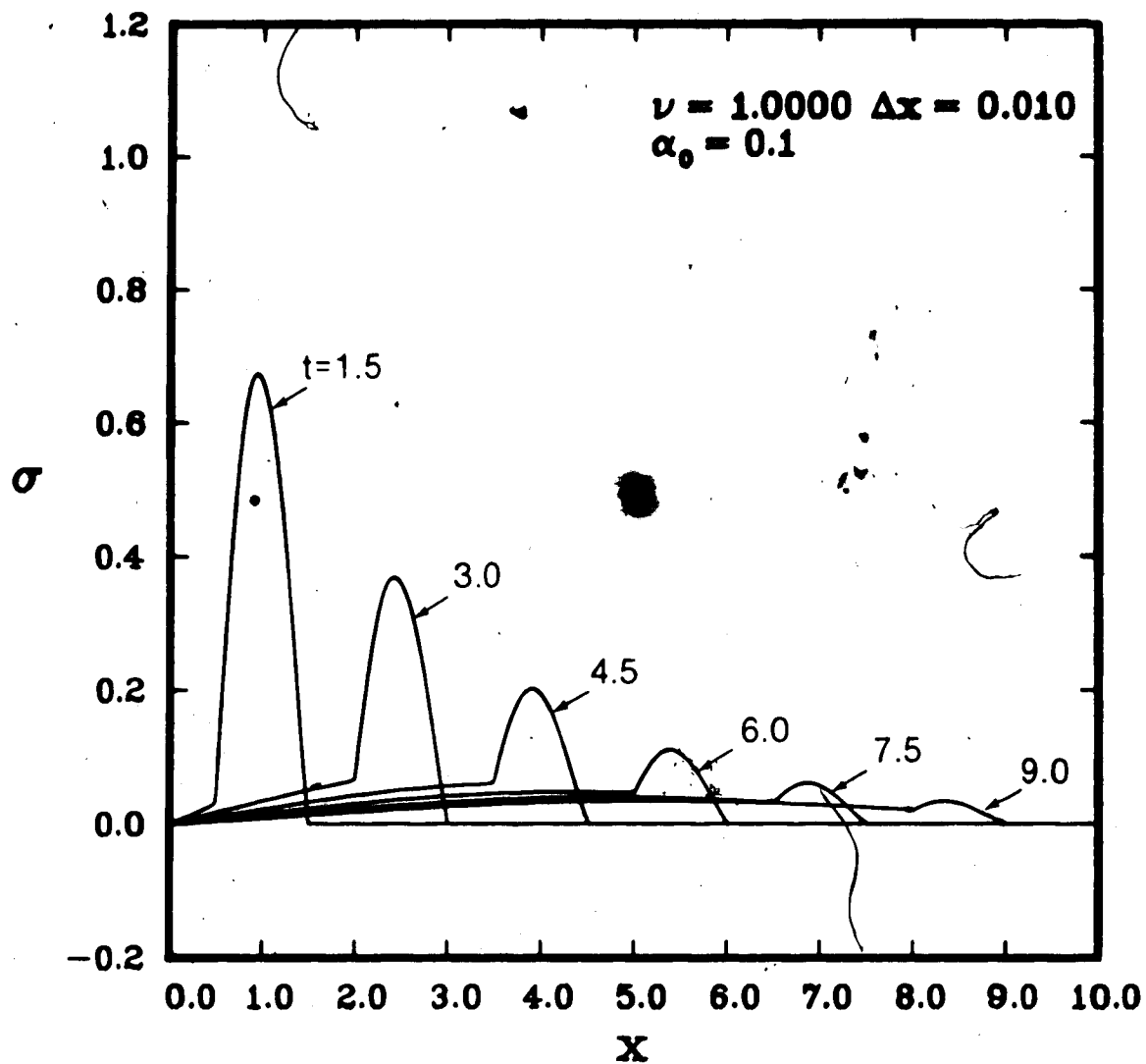


Fig. 3.20 Standard Model $\alpha_0 = 0.1$ - Variation of nondimensional σ with nondimensional x for $\sigma(0,t) = \sigma_0 \sin \pi t H(t) H(1-t)$, with $\sigma_0 = 1$ and $\nu = 1.0$ using the MacCormack scheme.

numerical dispersion is apparent. Figures 3.19 and 3.20 show numerical results for boundary condition (3.23), with $\sigma_0 = 1$, for $\alpha_0 = 0.9$ and $\alpha_0 = 0.1$. No analytical solutions were found to compare to these results. The Laplace transform technique described by Christensen (1982) for this boundary condition results in an extremely complicated inversion. The MacCormack scheme has a considerable advantage compared to the Laplace transform technique for this problem.

Figures 3.21 - 3.25 show the results obtained by incorporating the wavefront expansion into the MacCormack scheme for boundary condition (3.17), with $\sigma_0 = 1$. Figures 3.21 and 3.22 show the numerical results obtained with the wavefront expansion for $\nu = 1.0$, for $\alpha_0 = 0.9$ and $\alpha_0 = 0.1$, respectively. The modified numerical results do not show evidence of numerical dispersion but show some evidence of mild instability for $t = 9$ and $\alpha_0 = 0.1$ (see Figure 3.22). Figures 3.23 - 3.25 show similar numerical results obtained with the wavefront expansion for $\nu = 0.5$, for $\alpha_0 = 1.0$, $\alpha_0 = 0.9$ and $\alpha_0 = 0.1$, respectively. There is no evidence of numerical dispersion or numerical instability in any of these figures. The wavefront expansion modification influences the growth of numerical instability and eliminates numerical dispersion. However, the modification must be re-evaluated for different boundary conditions. The wavefront expansion technique has not been used for boundary condition (3.23).

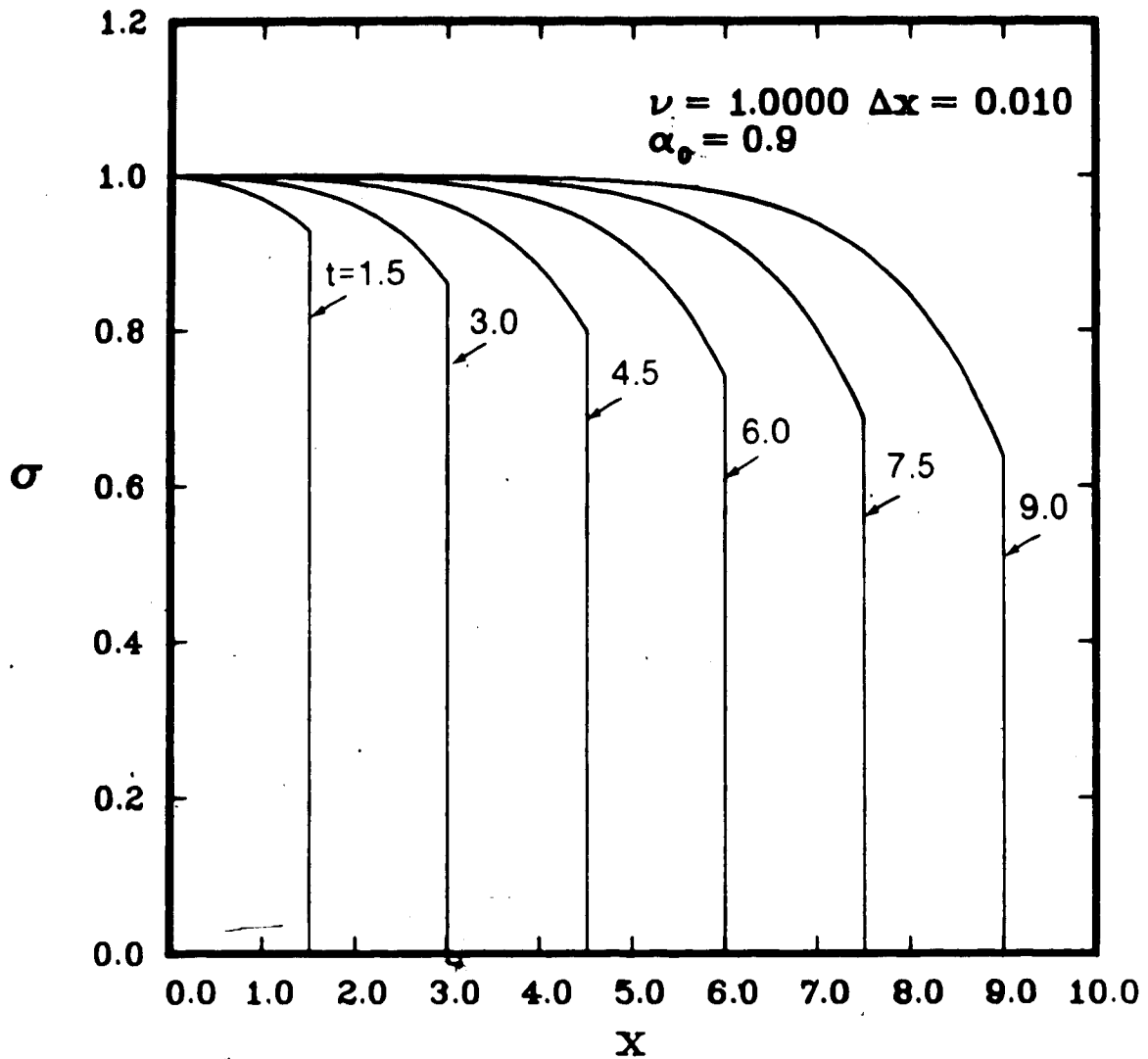


Fig. 3.21 Standard Model $\alpha_0 = 0.9$ - Variation of nondimensional σ with nondimensional x for $\sigma(0,t) = \sigma_0 H(t)$, with $\sigma_0 = 1$ and $\nu = 1.0$ using the MacCormack scheme with a wavefront expansion.

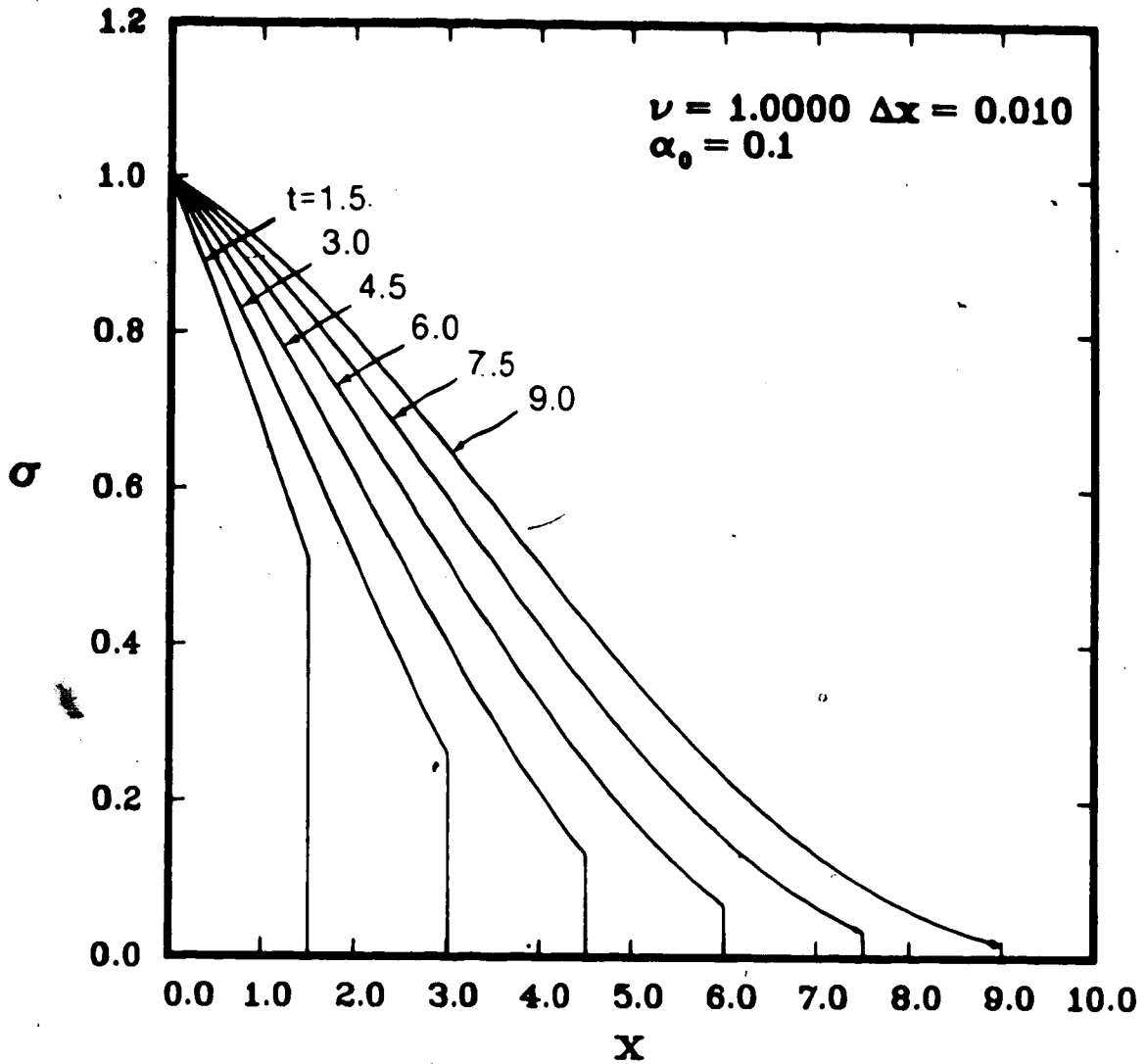


Fig. 3.22 Standard Model $\alpha_0 = 0.1$ - Variation of nondimensional σ with nondimensional x for $\sigma(0,t) = \sigma_0 H(t)$, with $\sigma_0 = 1$ and $\nu = 1.0$ using the MacCormack scheme with a wavefront expansion.

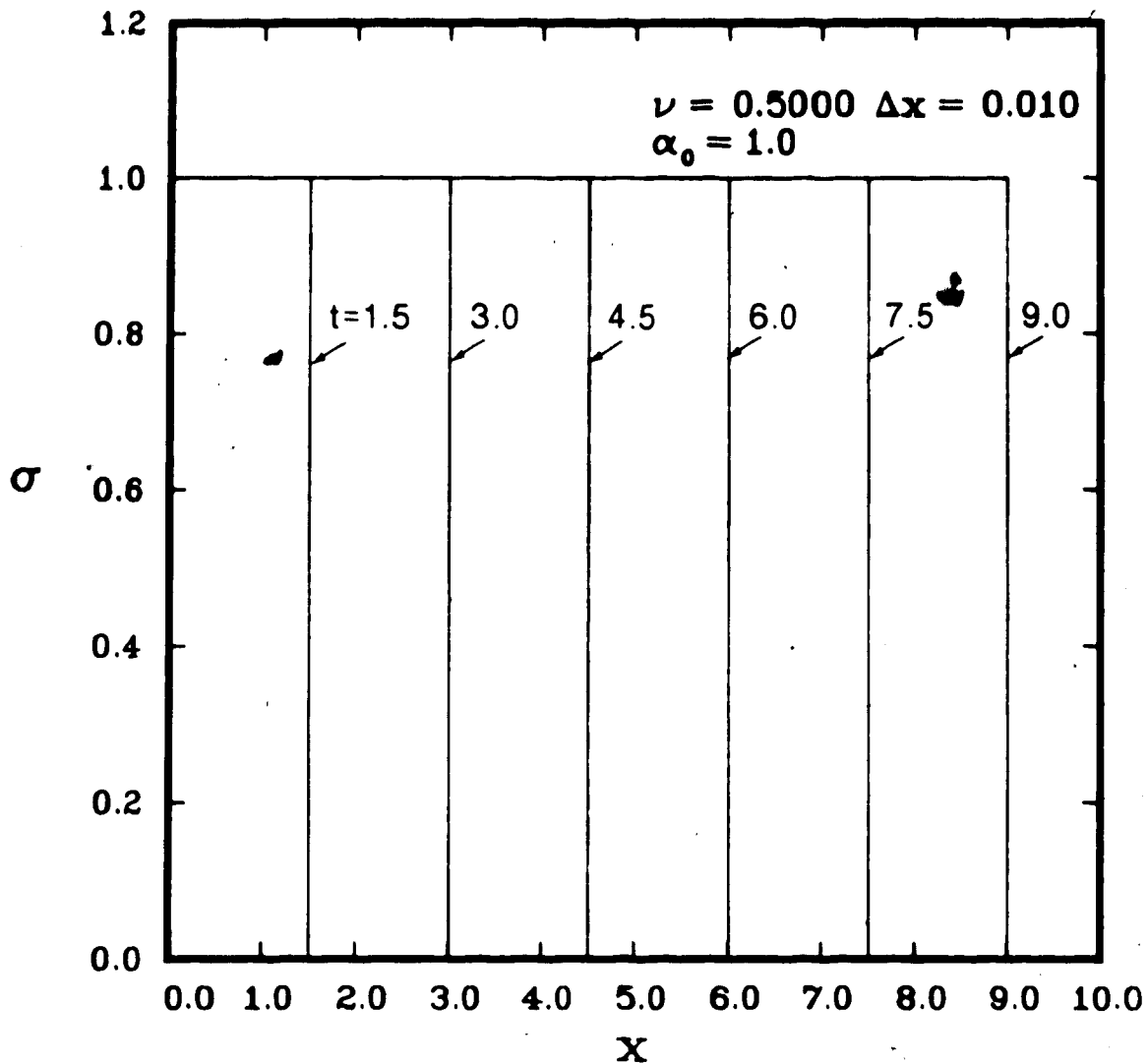


Fig. 3.23 Standard Model $\alpha_0 = 1.0$ - Variation of nondimensional σ with nondimensional x for $\sigma(0,t) = \sigma_0 H(t)$, with $\sigma_0 = 1$ and $\nu = 0.5$ using the MacCormack scheme with a wavefront expansion.

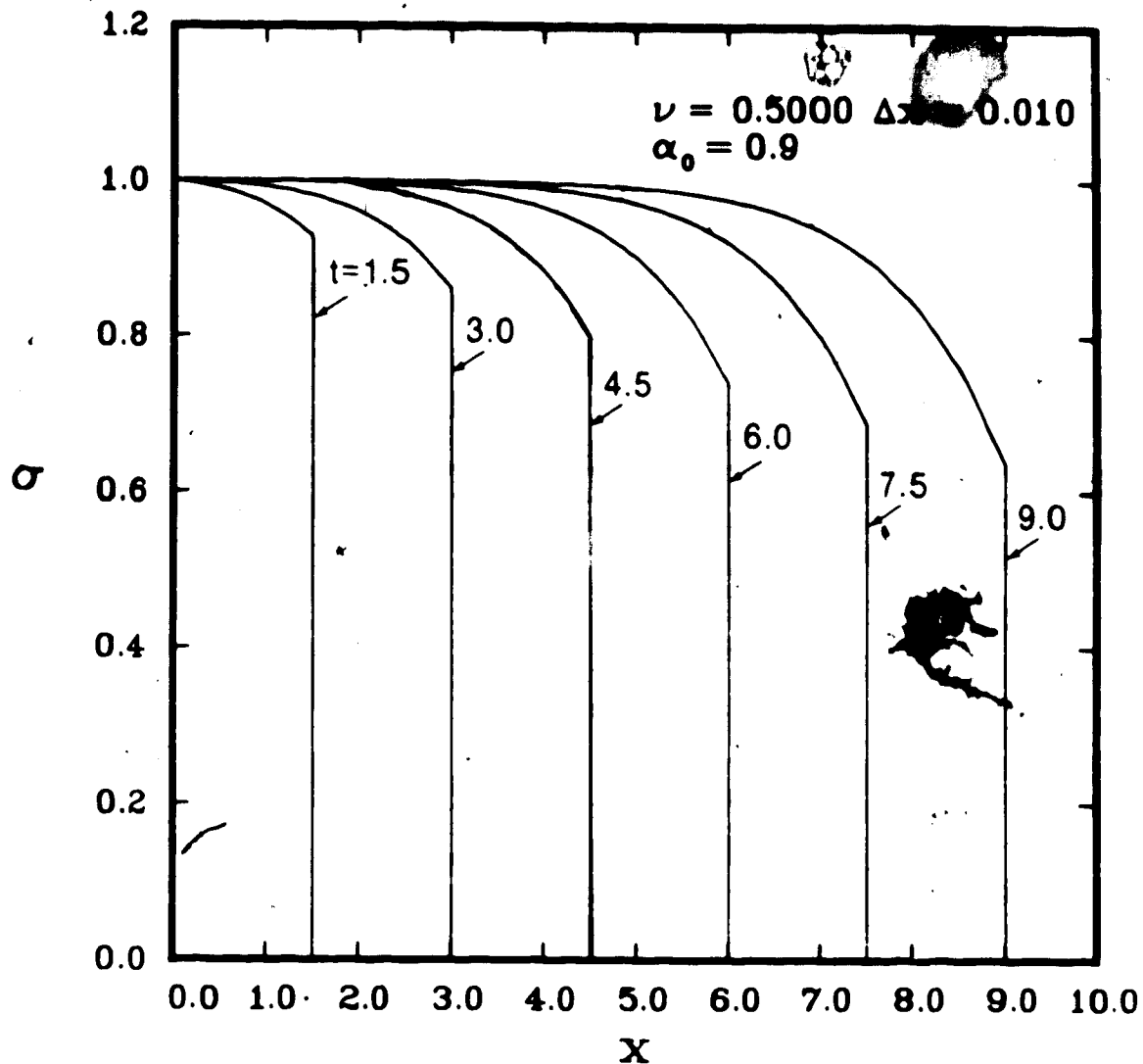


Fig. 3.24 Standard Model $\alpha_0 = 0.9$ - Variation of nondimensional σ with nondimensional x for $\sigma(0, t) = \sigma_0 H(t)$, with $\sigma_0 = 1$ and $\nu = 0.5$ using the MacCormack scheme with a wavefront expansion.

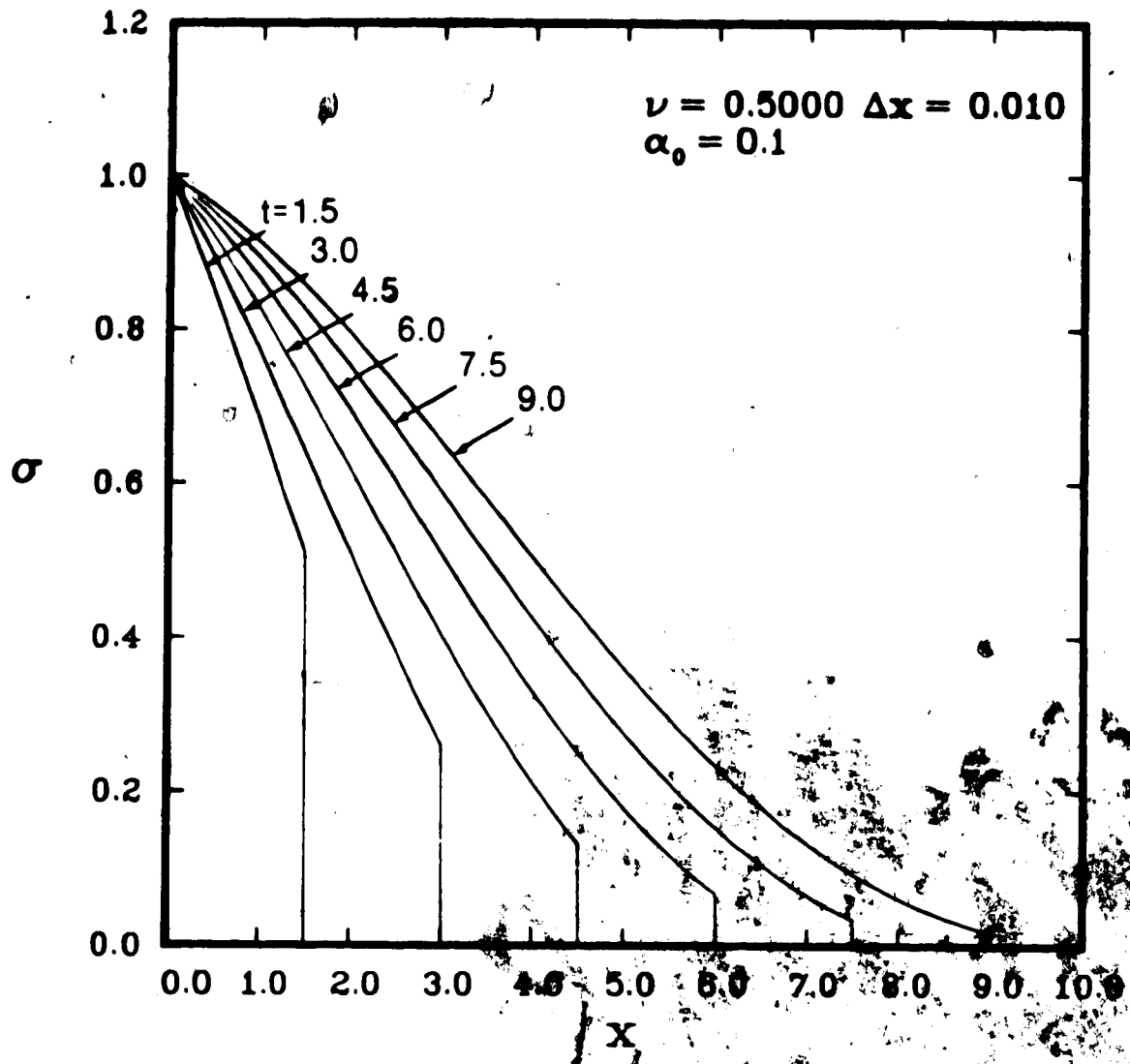


Fig. 3.25 Standard Model $\alpha_0 = 0.1$ - Variation of nondimensional σ with nondimensional x for $\sigma(0,t) = \sigma_0 H(t)$, with $\sigma_0 = 1$ and $\nu = 0.5$ using the MacCormack scheme with a wavefront expansion.

All of the numerical results in this section satisfy conservation of momentum according to equation (3.33) within acceptable numerical errors.

3.7.3 Viscoelastic Model with Two Relaxation Times (Extended Model), $N = 2$

Since the viscoelastic model with two relaxation times ($N = 2$), is a more general specification of viscoelastic materials, than the Maxwell or standard model, there are infinitely many more ways in which the parameters α_0 , α_1 , α_2 and r_2/r_1 , can be specified, so that $\sum_{n=0}^2 \alpha_n = 1$. In this study, two specific models are considered to demonstrate the numerical results

- (a) $\alpha_0 = 0.9$, $\alpha_1 = \alpha_2 = 0.05$, and $r_2/r_1 = 2.0$ and
- (b) $\alpha_0 = 0.1$, $\alpha_1 = \alpha_2 = 0.45$, and $r_2/r_1 = 2.0$.

These models are chosen so that a comparison can be made with standard model.

Figures 3.26 and 3.27 show numerical results obtained using the MacCormack scheme for boundary condition (3.17), with $\sigma_0 = 1$, for case (a) and case (b), respectively, for $\nu = 1.0$. The numerical results in Figure 3.26 show instability at the boundary, $x = 0$, which occurs for large times, $t > 6$, and numerical dispersion or instability behind the wavefront for all times. The numerical results in Figure 3.27 show severe instability at the wavefront for case (b).

Figures 3.28 and 3.29 show the numerical results for boundary condition (3.17), with $\sigma_0 = 1$, for case (a) and case (b) respectively, for $\nu = 0.99$. The results in Figure 3.28 show no

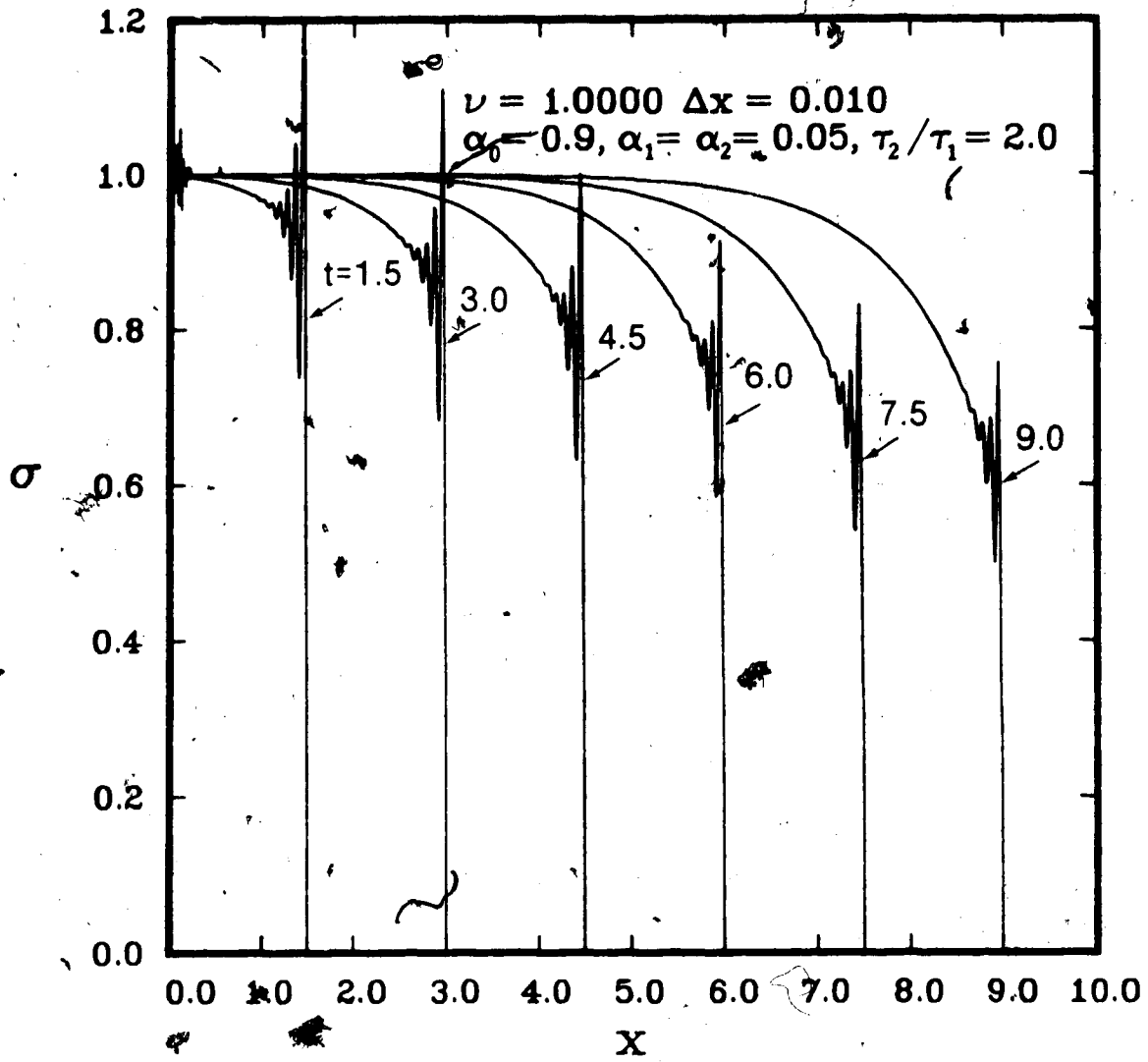


Fig. 3.26 Extended Model $\alpha_0 = 0.9$ - Variation of nondimensional σ with nondimensional x for $\sigma(x,t) = \sigma_0 H(t)$, with $\sigma_0 = 1$ and $\nu = 1.0$ using the MacCormack scheme.

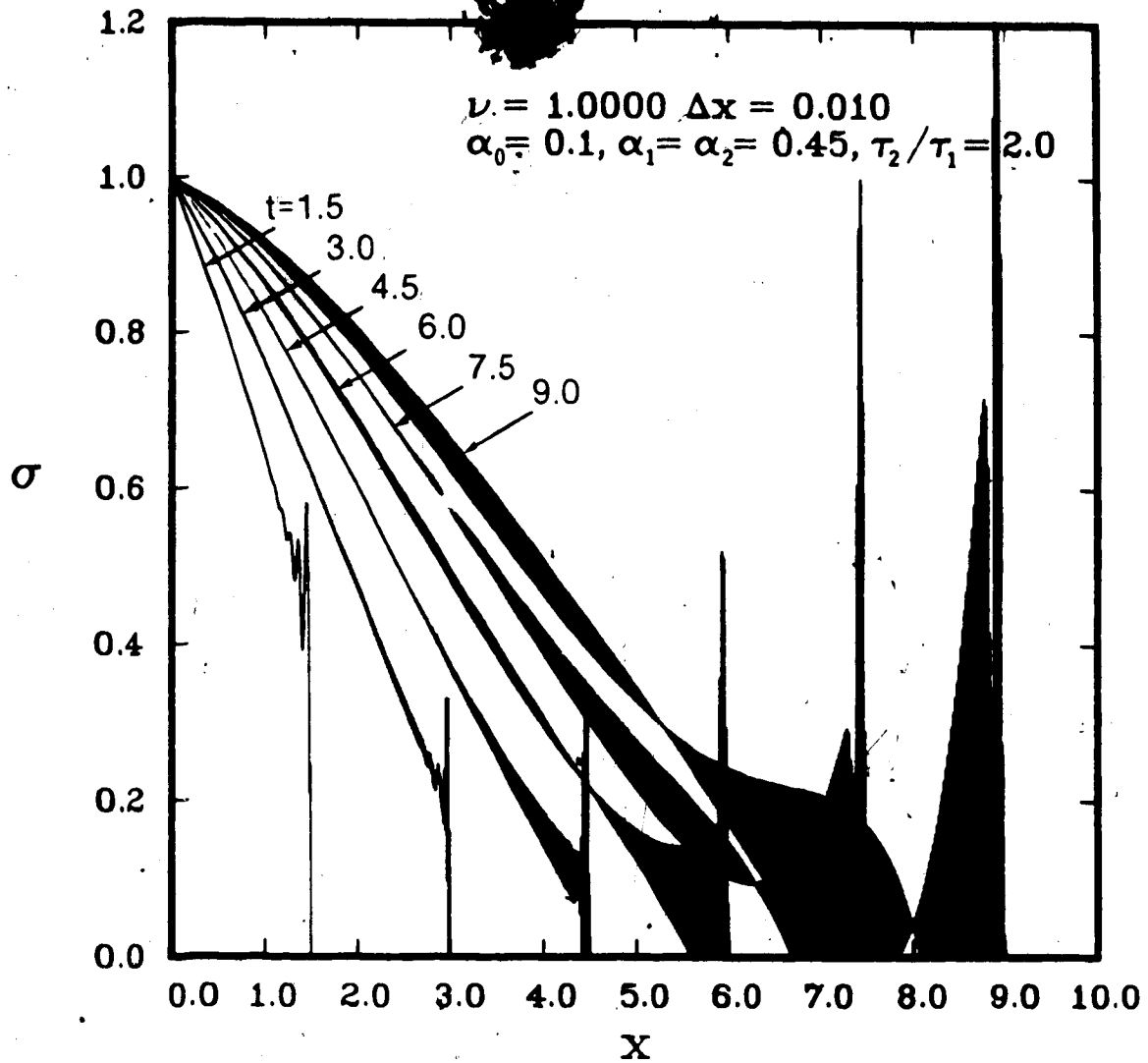


Fig. 3.27 Extended Model $\alpha_0 = 0.1$ - Variation of nondimensional σ with nondimensional x for $\sigma(0, t) = \sigma_0 H(t)$, with $\sigma_0 = 1$ and $\nu = 1.0$ using the MacCormack scheme.

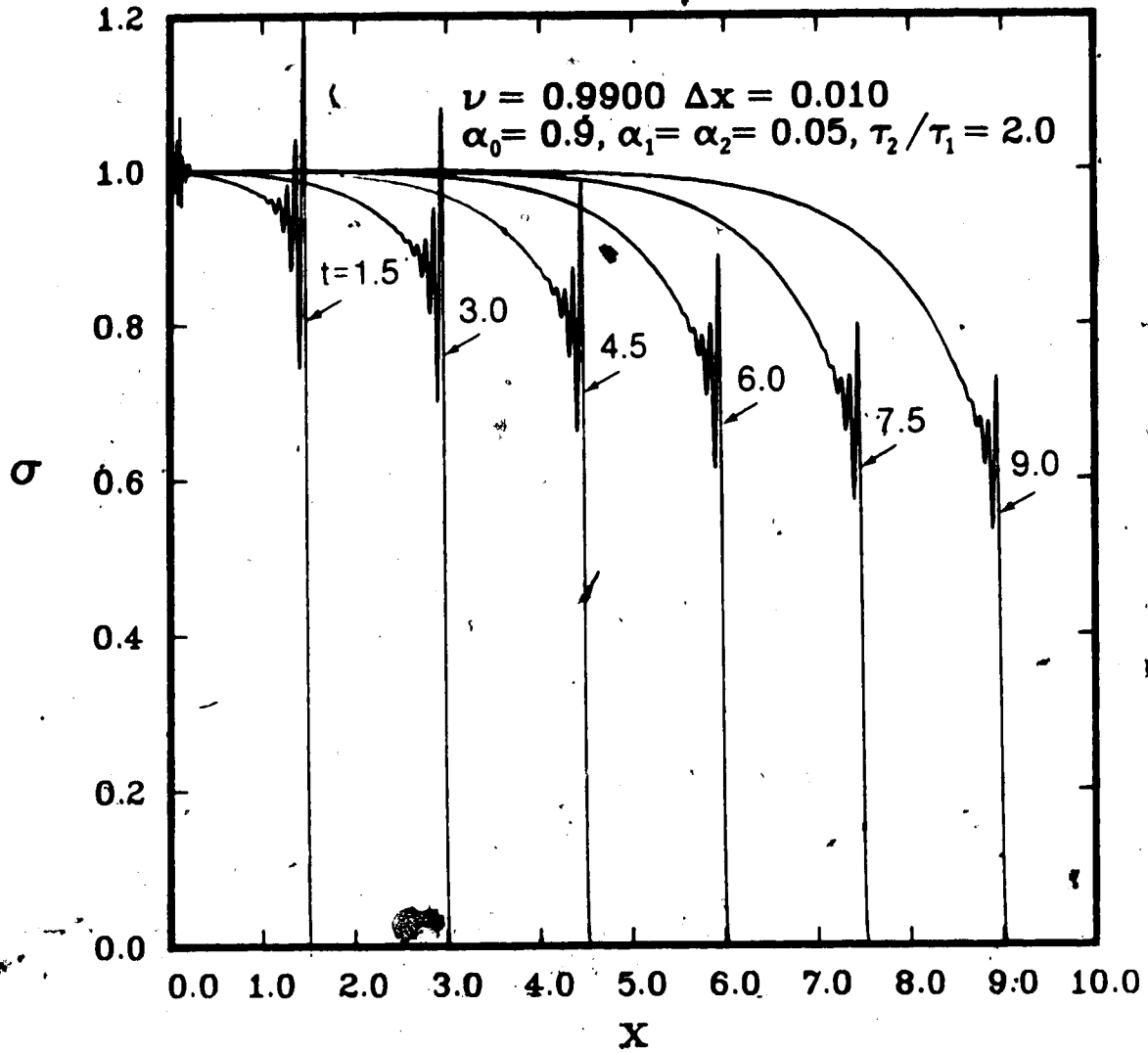


Fig. 3.28 Extended Model $\alpha_0 = 0.9$ - Variation of nondimensional σ with nondimensional x for $\sigma(0,t) = \sigma_0 H(t)$, with $\sigma_0 = 1$ and $\nu = 0.99$ using the MacCormack scheme.

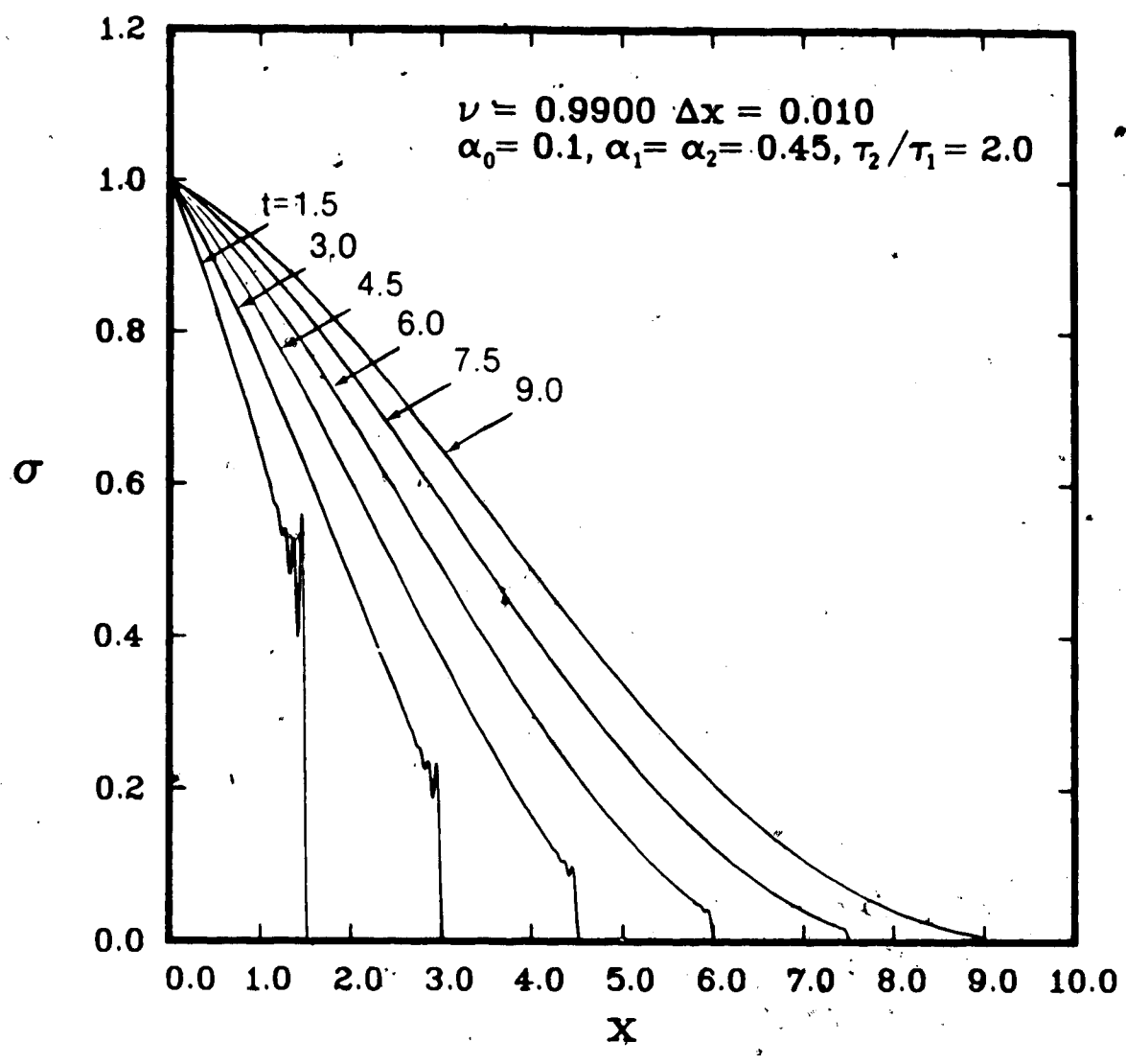


Fig. 3.29 Extended Model $\alpha_0 = 0.1$ - Variation of nondimensional σ with nondimensional x for $\sigma(0,t) = \sigma_0 H(t)$, with $\sigma_0 = 1$ and $\nu = 0.99$ using the MacCormack scheme.

improvement in the numerical solution in regard to instability at the boundary or at the wavefront, compared with $\nu = 1.0$ (see Figure 3.26). However, Figure 3.29 indicates that instability has been eliminated for $\nu = 0.99$ at the expense of numerical dispersion. The numerical dispersion in Figure 3.29 decreases with increasing time. This could be due to the presence of the $\underline{B(U)}$ term in the governing equations.

Figures 3.30 and 3.31 show numerical results for boundary condition (3.23), with $\sigma_0 = 1$, for case (a) and case (b), respectively, for $\nu = 0.99$. Figure 3.30 indicates severe instability at $x = 0$. Numerical evaluation of momentum for the numerical solutions presented in Figure 3.30 indicates that momentum is not conserved for $t > 6$. Figure 3.31 shows some instability at $x = 0$, however the instability is less severe than for case (a). The numerically evaluated momentum is approximately conserved for the times considered in Figure 3.31.

Figures 3.32 and 3.33 provide a comparison of the standard model and the viscoelastic model with two relaxation times, for boundary condition (3.17), with $\sigma_0 = 1$. In Figure 3.32, $\alpha_0 = 0.1$ for both models, but $\tau_2/\tau_1 = 2$ for the viscoelastic model with two relaxation times. There is a significant difference between the two sets of curves. This demonstrates the increased flexibility in using a viscoelastic model with two relaxation times. Figure 3.33 compares the standard model to the viscoelastic model with two relaxation times, for identical parameters, since $\alpha_0 = 0.1$,

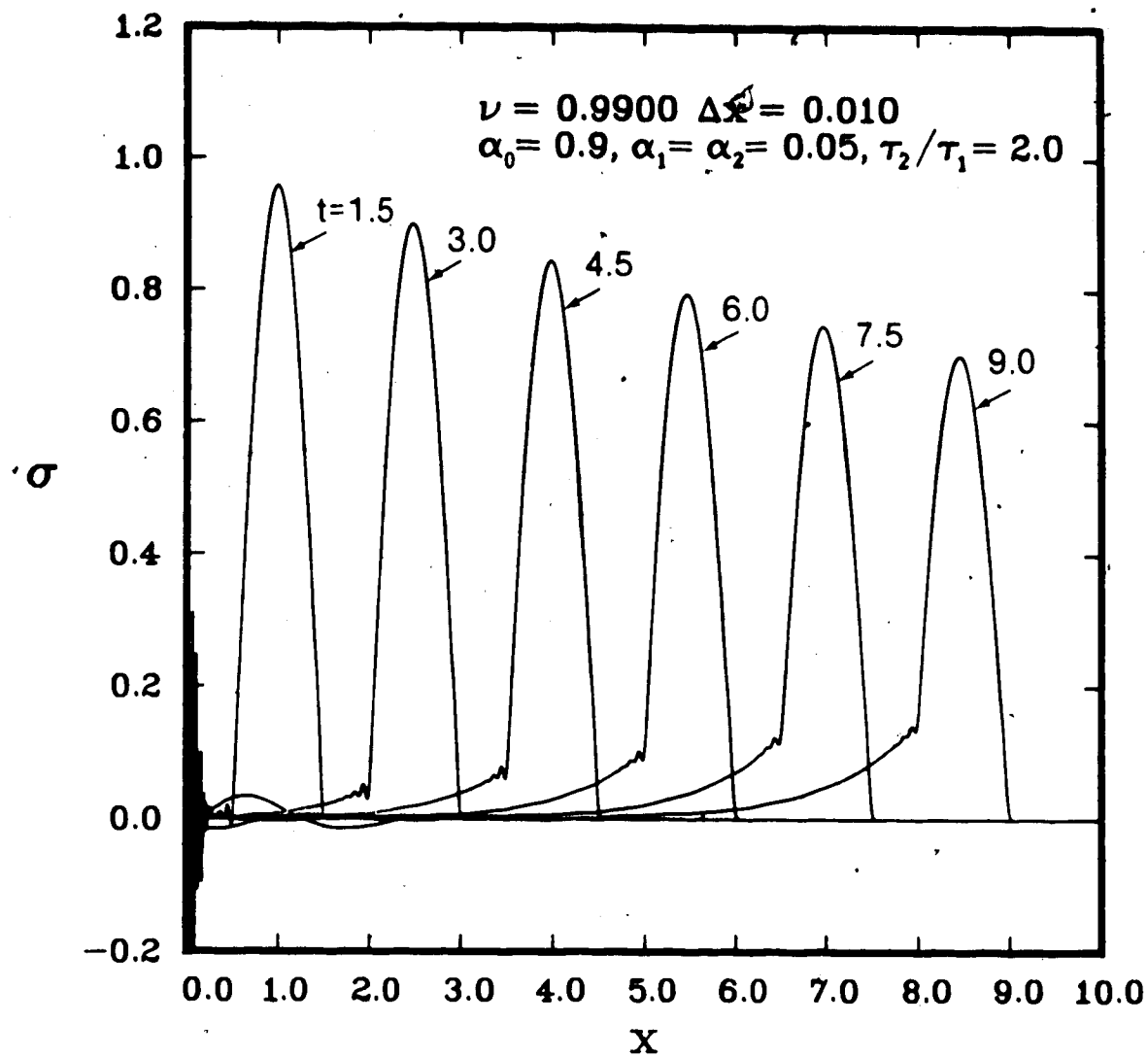


Fig. 3.30 Extended Model $\alpha_0 = 0.9$ - Variation of nondimensional σ with nondimensional x for $\sigma(0,t) = \sigma_0 \sin \pi t H(t) H(1-t)$, with $\sigma_0 = 1$ and $\nu = 0.99$ using the MacCormack scheme.

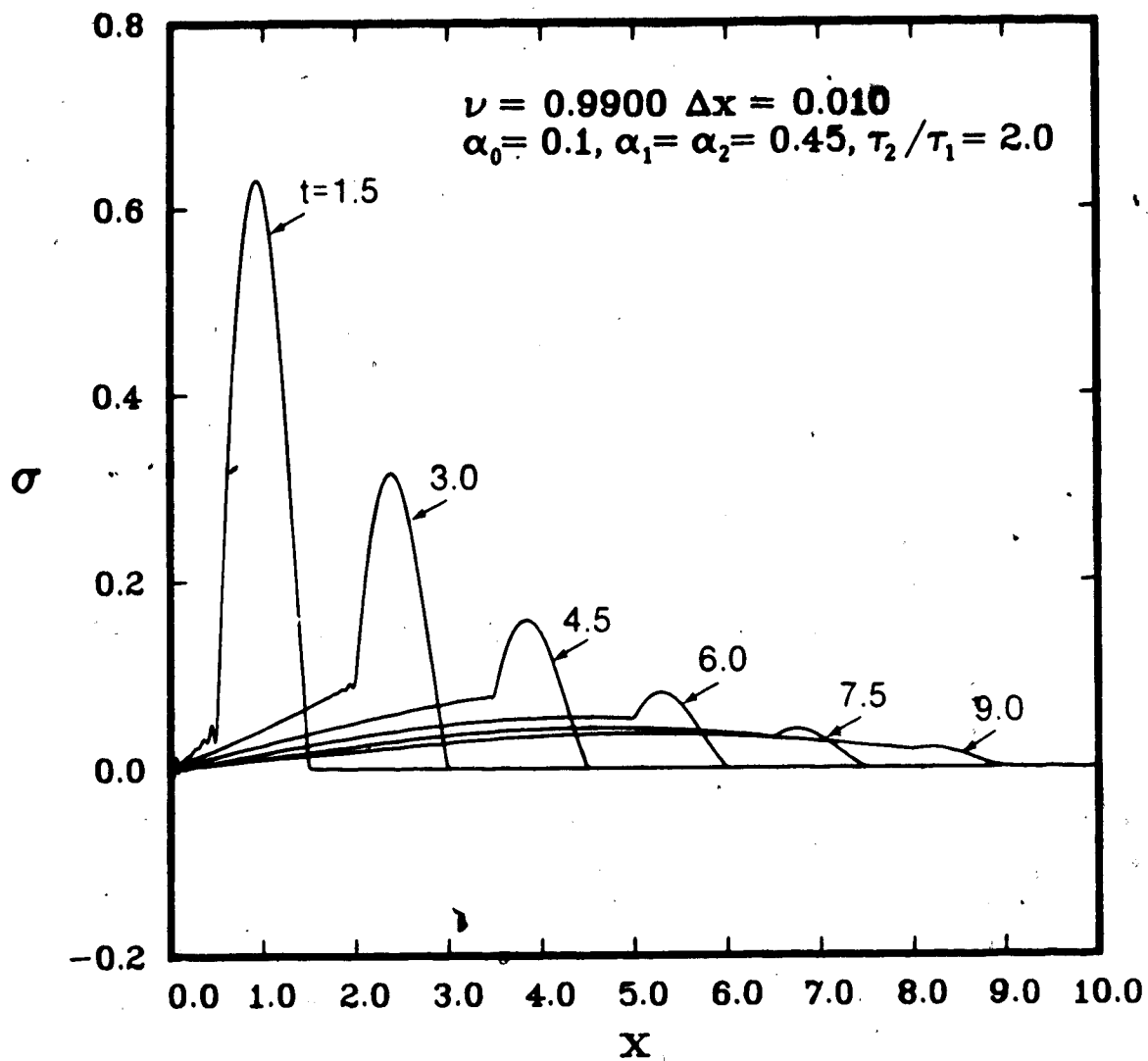


Fig. 3.31. Extended Model $\alpha_0 = 0.1$ - Variation of nondimensional σ with nondimensional x for $\sigma(0,t) = \sigma_0 \sin \pi t H(t) H(1-t)$, with $\sigma_0 = 1$ and $\nu = 0.99$ using the MacCormack

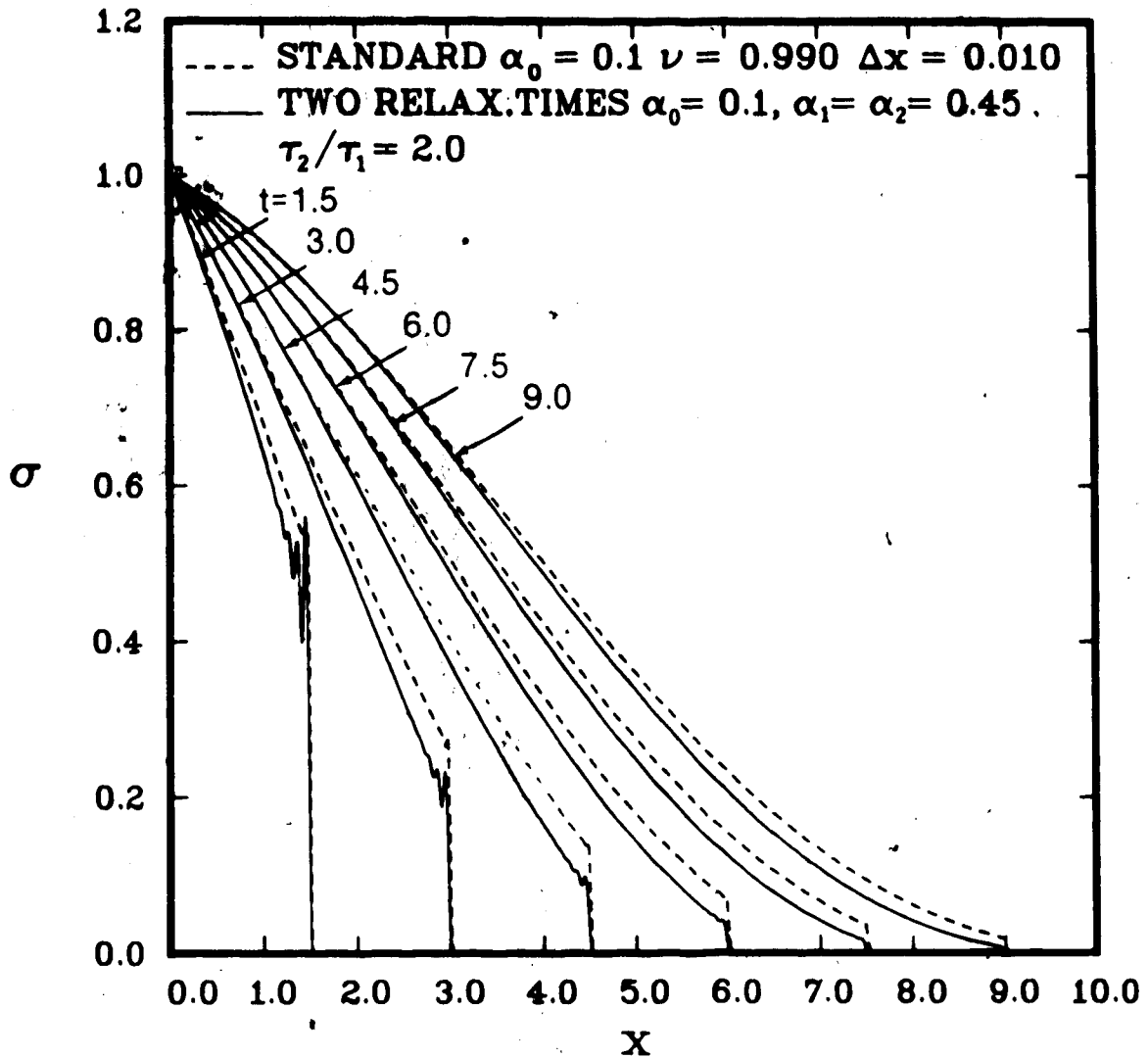


Fig. 3.32 A comparison of the Standard Model $\alpha_0 = 0.1$ to the Extended Model $\alpha_0 = 0.1$ for $\sigma(0, t) = \sigma_0 H(t)$, with $\sigma_0 = 1$ and $\nu = 0.99$ using the MacCormack scheme.

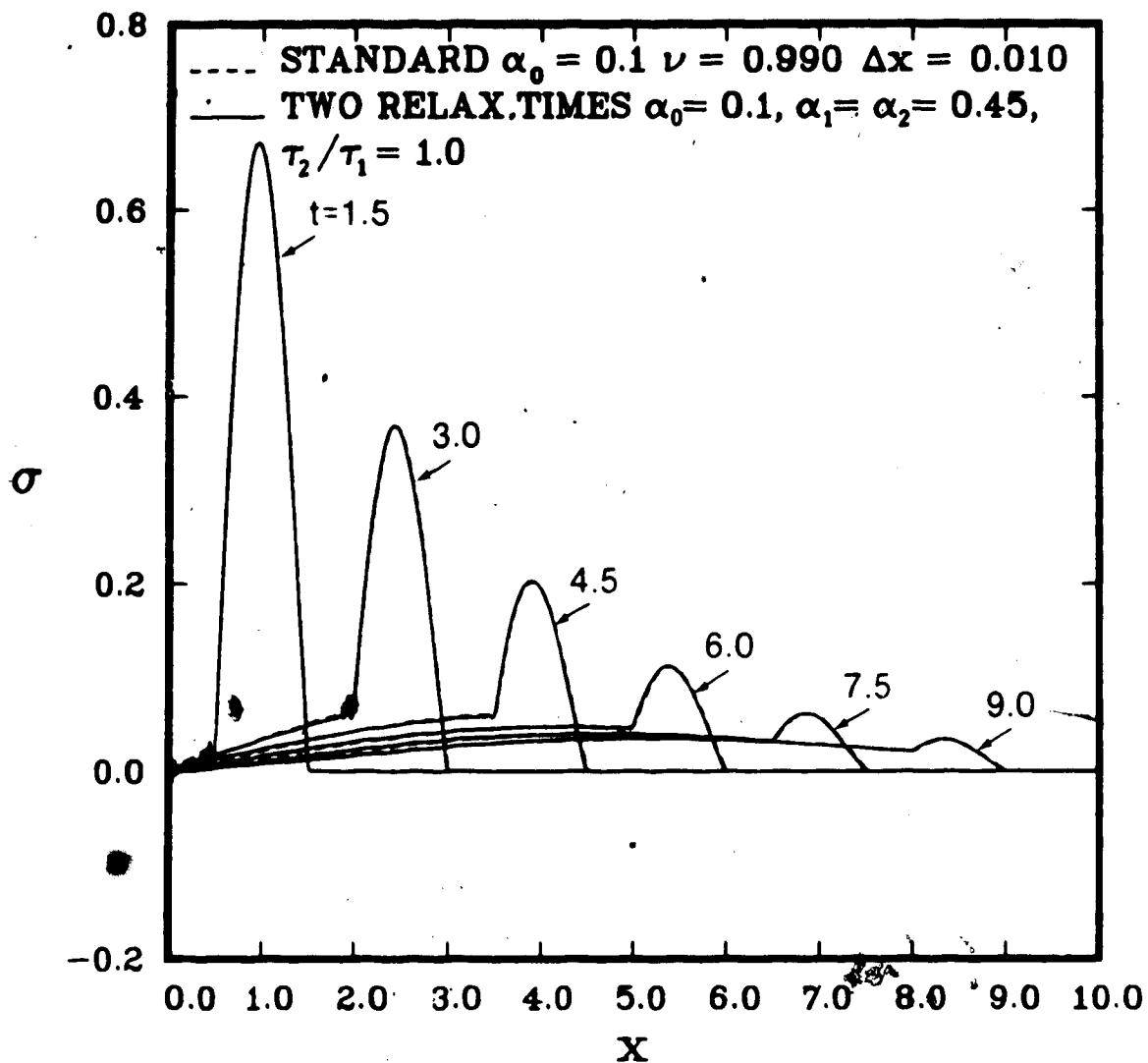


Fig. 3.33 A comparison of the Standard Model $\alpha_0 = 0.1$ to the Extended Model $\alpha_0 = 0.1$, and $\tau_2/\tau_1 = 1$, for $\sigma(0,t) = \sigma_0 \sin \pi t H(t)H(1-t)$, with $\sigma_0 = 1$ and $\nu = 0.99$ using the MacCormack scheme.

$\alpha_1 = \alpha_2 = 0.45$, and $\tau_2/\tau_1 = 1$ reduces to the standard model. The numerical results for the two different models are identical except for oscillations at $x = 0$, for the viscoelastic model with two relaxation times. This indicates that the results for $\tau_1 = \tau_2$ obtained from the system of 5 equations governing the more general viscoelastic model are identical to those obtained from the system of 3 equations that govern the standard model, except for the instability at the boundary. It is possible that the instability at the boundary is due to the variable \dot{v} , since $\dot{v}(0,t)$ is obtained using the Gottlieb boundary condition, which disregards the direct dependence on v . Several modifications of the boundary conditions were unsuccessfully attempted.

Figures 3.34 and 3.35 give numerical results obtained using the MacCormack scheme with a wavefront expansion for case (b) and case (a), respectively, for $\nu = 0.5$ and boundary condition (3.17). There is no numerical dispersion evident in the results in either figure. However, the instability at the boundary is still present. Figure 3.36 gives numerical results for $\alpha_0 = 0.1$, $\alpha_1 = 0.3$, $\alpha_2 = 0.6$ and $\tau_2/\tau_1 = 5$, obtained using the wavefront expansion modification. These results show how the parameters α_0 , α_1 , α_2 and τ_2/τ_1 can be varied to obtain numerical solutions for other viscoelastic models with two relaxation times.

All of the results presented in this section, except those in Figures 3.30 and 3.31, satisfy conservation of momentum according to equation (3.33). Except for numerical dispersion in some cases, and instability at the boundary, the numerical results

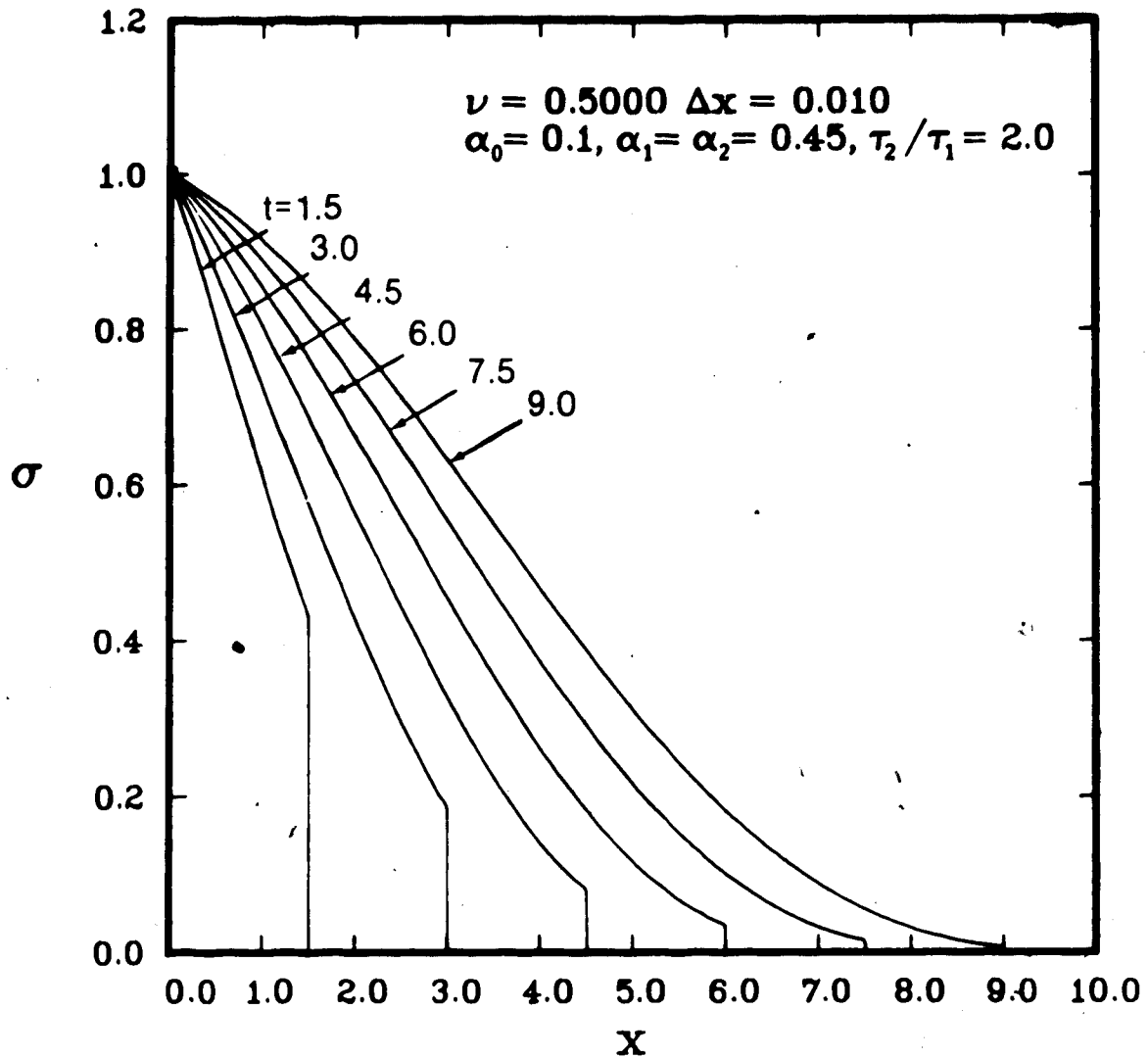


Fig. 3.34 Extended Model $\alpha_0 = 0.1$ - Variation of nondimensional σ with nondimensional x for $\sigma(0, t) = \sigma_0 H(t)$, with $\sigma_0 = 1$ and $\nu = 0.5$ using the MacCormack scheme with a wavefront expansion.

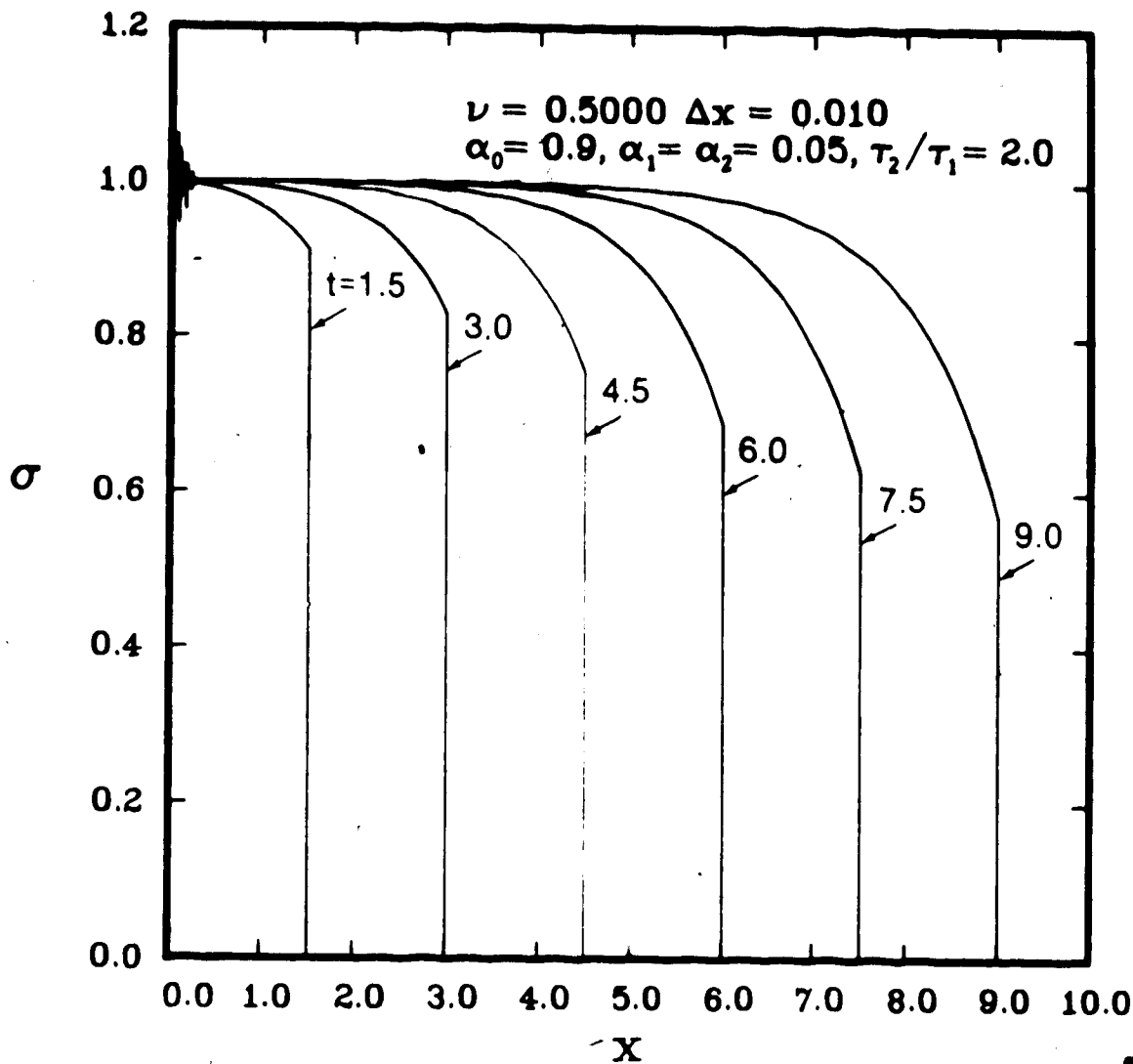


Fig. 3.35 Extended Model $\alpha_0 = 0.9$ - Variation of nondimensional σ with nondimensional x for $\sigma(0, t) = \sigma_0 H(t)$, with $\sigma_0 = 1$ and $\nu = 0.5$ using the MacCormack scheme with a wavefront expansion.

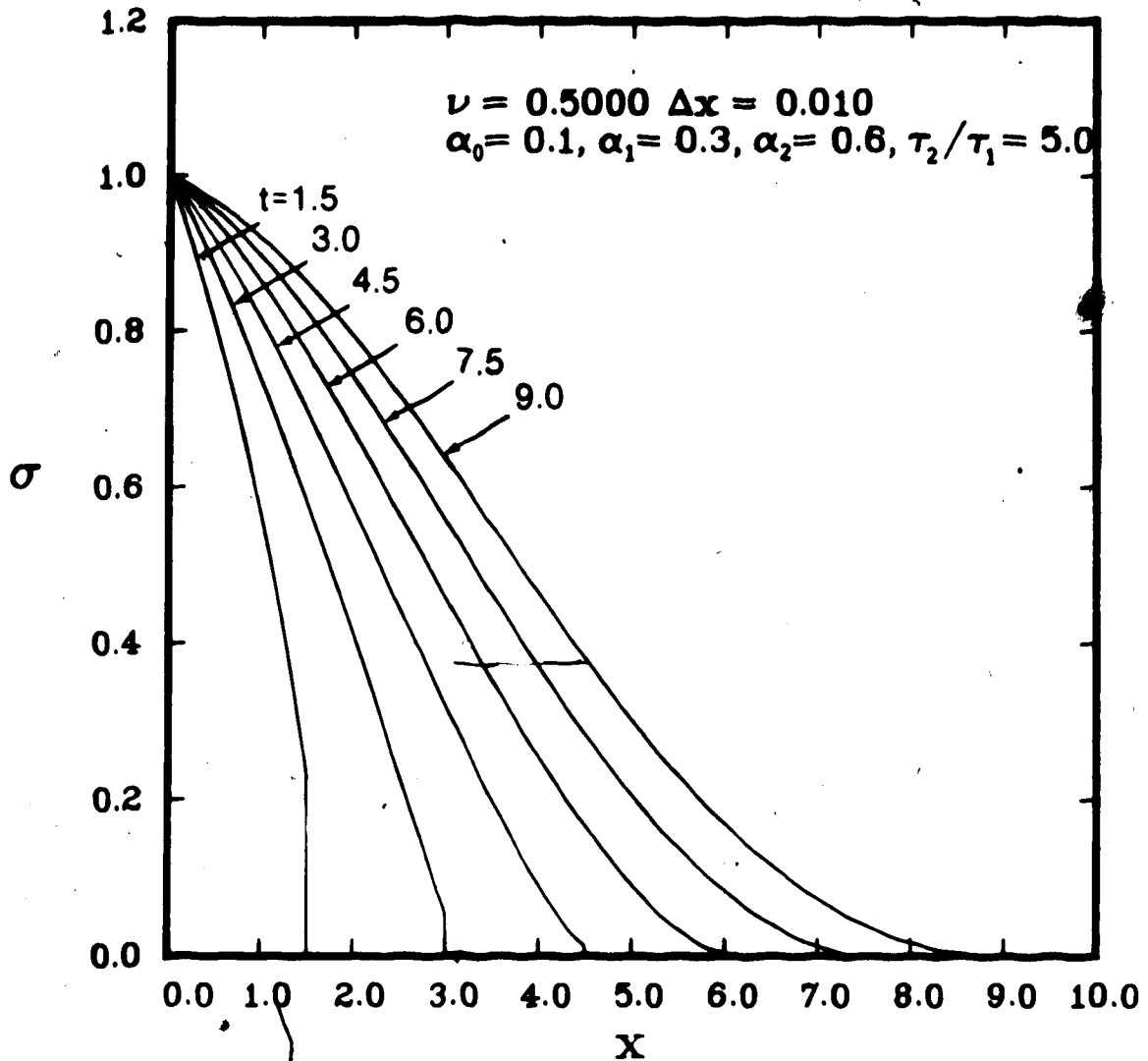


Fig. 3.36 Extended Model $\alpha_0 = 0.1$ - Variation of nondimensional σ with nondimensional x for $\sigma(0,t) = \sigma_0 H(t)$, with $\sigma_0 = 1$ and $\nu = 0.5$ using the MacCormack scheme with a wavefront expansion.

are in excellent agreement with theoretical considerations. The MacCormack scheme appears to be a viable method for solving wave propagation problems in viscoelastic materials whose relaxation function has the general form given by equation (3.1). For $N > 2$, the implementation of the MacCormack scheme is extremely complicated.

CHAPTER 4

FINITE AMPLITUDE, SHEAR WAVE PROPAGATION IN INCOMPRESSIBLE ISOTROPIC HYPERELASTIC SOLIDS

4.1 Introduction of the Problems

The propagation of infinitesimal amplitude axial shear waves in an isotropic elastic solid is governed by the linear wave equation

$$\frac{\partial^2 w}{\partial r^2} + \frac{1}{r} \frac{\partial w}{\partial r} = \frac{1}{c^2} \frac{\partial^2 w}{\partial t^2} \quad (4.1)$$

where w is the axial displacement, r is the radial coordinate, t is time and c is the wave speed. Boundary initial value problems governed by equation (4.1) can be solved by integral transform methods or the method of characteristics (Achenbach, 1973). Integral transform methods are not applicable to nonlinear problems of finite amplitude elastic wave propagation and the method of characteristics results in considerable computational difficulties, since shock paths do not, in general, coincide with characteristics. Consequently, the modified MacCormack scheme is used to obtain solutions to the nonlinear problems.

Finite amplitude axial shear wave propagation is governed by equation (4.1) for the Mooney-Rivlin and neo-Hookean materials, but for other incompressible hyperelastic models, equation (4.1) is replaced by a nonlinear partial differential equation. The Mooney-Rivlin and neo-Hookean materials are limiting cases of the more general materials

considered, so that the solution of the linear equation (4.1) can be used to check the validity of the numerical procedure.

Finite amplitude plane transverse shear wave propagation is also considered and the numerical results are compared with those obtained by the method of characteristics up to the time when the wave breaks. The breaking time is calculated from the characteristic method and is compared to the breaking time indicated by the numerical solution.

Conservation of momentum and mechanical energy dissipation are calculated for each problem considered for both axial and plane transverse shear wave propagation.

To demonstrate the applicability of the MacCormack scheme to more complicated problems, combined torsional and axial shear wave propagation in an incompressible isotropic hyperelastic solid are also considered. The deformation and stress fields for the combined infinitesimal torsional and axial shear of a linear elastic solid can be obtained from superposition by considering the torsional and axial shear separately, since the effects of torsion and axial shear are uncoupled. For finite deformation of a Mooney-Rivlin material, which is a special case of the strain energy function under consideration, the equations governing the propagation of finite amplitude axial and torsional waves are uncoupled and identical to those for classical linear infinitesimal elasticity. The major purpose of this section is to investigate the coupling that occurs when finite amplitude axial and torsional waves are simultaneously propagated in an incompressible hyperelastic material whose strain energy function is expressible as

power series (Ogden, 1984). The effects of prestress on the propagation of coupled finite amplitude waves are also examined.

4.2 Axial Shear Wave Propagation

4.2.1 Governing Equations

The governing equations for axial shear wave propagation are obtained from the theory of nonlinear elasticity. Treatments of the subject are given by Ogden (1984) and Spencer (1980). The materials considered are 'Green Elastic' or 'hyperelastic' materials and have a strain energy function which is expressible as a power series in terms of the basic invariants of the left Cauchy-Green tensor \underline{B} . A more detailed account of the theory which is presented is given by Ogden (1984).

Time dependent axial shear is defined by the deformation field

$$r = R, \theta = \theta, z = Z + w(R,t) \quad (4.2)$$

where (R, θ, Z) and (r, θ, z) are the cylindrical polar coordinates of a particle in the undeformed reference configuration and spatial configuration, respectively and $w(R,0) = 0$. The physical components of the deformation gradient tensor \underline{F} , and the left Cauchy-Green tensor $\underline{B} = \underline{F}\underline{F}^T$, where the superscript T denotes transpose, computed from equation (4.2) are

$$\underline{F} = \begin{bmatrix} 1 & 0 & 0 \\ 0 & 1 & 0 \\ w_R & 0 & 1 \end{bmatrix} \quad \underline{B} = \begin{bmatrix} 1 & 0 & w_R \\ 0 & 1 & 0 \\ w_R & 0 & 1+w_R^2 \end{bmatrix} \quad (4.3)$$

The basic invariants I_1 , I_2 and I_3 of \underline{B} are given by

$$I_1 = \text{tr} \underline{B}, \quad I_2 = \frac{1}{2}((\text{tr} \underline{B})^2 - \text{tr}(\underline{B}^2)), \quad I_3 = \det[\underline{B}]$$

and, for the specified deformation field are

$$I_1 = I_2 = 3 + w_R^2, \quad I_3 = 1 \quad (4.4)$$

where $w_R = \partial w / \partial R$ and from equation (4.2), it follows that $w_R = w_r = \partial w / \partial r$.

The Cauchy stress tensor $\underline{\sigma}$ for an isotropic incompressible hyperelastic solid is given by.

$$\underline{\sigma} = -p \underline{I} + 2 \frac{\partial W}{\partial I_1} \underline{B} - 2 \frac{\partial W}{\partial I_2} \underline{B}^{-1} \quad (4.5)$$

where $W(I_1, I_2)$ is the strain energy function and $-p$ is a hydrostatic stress which is not determined by the deformation (Spencer, 1980). It follows from equations (4.3), (4.4) and (4.5) that the nonzero components of Cauchy stress are

$$\sigma_r = -p + 2 \frac{\partial W}{\partial I_1} - 2(1 + w_r^2) \frac{\partial W}{\partial I_2} \quad (4.6)$$

$$\sigma_\theta = -p + 2 \frac{\partial W}{\partial I_1} - 2 \frac{\partial W}{\partial I_2} \quad (4.7)$$

$$\sigma_z = -p + 2(1 + w_r^2) \frac{\partial W}{\partial I_1} - 2 \frac{\partial W}{\partial I_2} \quad (4.8)$$

$$\tau_{rz} = 2 \left(\frac{\partial W}{\partial I_1} + \frac{\partial W}{\partial I_2} \right) w_r \quad (4.9)$$

with the usual notation for the physical components of Cauchy stress in cylindrical polar coordinates.

The nontrivial equations of motion for axial shear are

$$\frac{\partial \sigma_r}{\partial r} + \frac{\sigma_r - \sigma_\theta}{r} = 0 \quad (4.10)$$

$$\frac{\partial \tau_{rz}}{\partial r} + \frac{\tau_{rz}}{r} = \rho \ddot{w} \quad (4.11)$$

where a superposed dot denotes differentiation with respect to time, and p is taken as independent of θ and z . It follows from equations (4.4) and (4.9) that τ_{rz} is a function of w_r so that $w(r, t)$ can be obtained by solving equation (4.11), and the stress components σ_r , σ_θ and σ_z can then be obtained by substituting w_r in equations (4.6 - 4.8) and then solving equation (4.10) to obtain $p(r, t)$.

If the strain energy function for an incompressible isotropic hyperelastic solid is continually differentiable with respect to I_1 and I_2 , it can be expressed as a power series (Ogden, 1984)³,

$$W(I_1, I_2) = \sum_{p, q=0}^{\infty} C_{pq} (I_1 - 3)^p (I_2 - 3)^q \quad (4.12)$$

³ Holmes and Wilson, (1979) suggest that higher order strain energy functions are useful when the Mooney form is no longer adequate.

where C_{pq} are constants and $C_{00} = 0$. When C_{10} and C_{01} are the only nonzero C_{pq} , equation (4.12) gives the strain energy function for the Mooney-Rivlin material. Haines and Wilson (1979) have considered a strain energy function

$$W = C_{10}(I_1 - 3) + C_{01}(I_2 - 3) + C_{20}(I_1 - 3)^2 + C_{11}(I_1 - 3)(I_2 - 3) + C_{02}(I_2 - 3)^2 + C_{30}(I_1 - 3)^3 \quad (4.13)$$

and concluded, by comparing with experimental data, that the higher order strain energy function given by (4.13) is well represented for rubbers tested by Treloar (1958). The strain energy function given by (4.13) has an additional term $C_{30}(I_1 - 3)^3$, which has not been considered in this study. However, the general conclusion reached by Haines and Wilson is that higher order strain energy functions are useful, if the governing equations, which are more complicated as a result of the higher order terms, can be solved.

It may be deduced from equations (4.4) and (4.9) that, for strain energy functions of the form (4.12),

$$r_{rz} = \sum_{n=1}^{\infty} a_{2n-1} (w_r)^{2n-1} \quad (4.14)$$

where the a_{2n-1} are constants expressible in terms of the C_{pq} . If the series (4.14) is truncated so the maximum value of $(p+q) = N$, then

$$r_{rz} = \sum_{n=1}^N a_{2n-1} (w_r)^{2n-1} \quad (4.15)$$

For the Mooney-Rivlin material $N = 1$, so that the relation between τ_{rz} and w_r is linear.

The theory in this chapter is presented for $N = 2$, so that the strain energy function can be put in the form

$$W = \frac{\mu}{2} \left[\alpha(I_1 - 3) + (1 - \alpha)(I_2 - 3) + \gamma_1(I_1 - 3)^2 + \gamma_2(I_1 - 3)(I_2 - 3) + \gamma_3(I_2 - 3)^2 \right] \quad (4.16)$$

where μ is the modulus of rigidity for infinitesimal deformation from the ground state, and $0 \leq \alpha \leq 1$. It follows then that,⁴

$$\tau_{rz} = \mu \left[w_r + 2\gamma(w_r)^3 \right] \quad (4.17)$$

where $\gamma = \gamma_1 + \gamma_2 + \gamma_3$. Numerical results for the nonlinear problem are presented for $\gamma = 0.1$, which is realistic for certain elastomers (Treloar, 1958).

4.2.2 Formulation of the Problem

An axial, spatially uniform shearing stress is applied to the surface of a circular cylindrical cavity, of radius a (see Fig. 4.1), in an unbounded hyperelastic medium which is initially unstressed and at rest. The axis of the cavity coincides with the z axis of the cylindrical polar coordinate system. Two boundary

⁴ The symbol τ is used to denote shear stress. The shear stress being considered depends on the context of the problem.

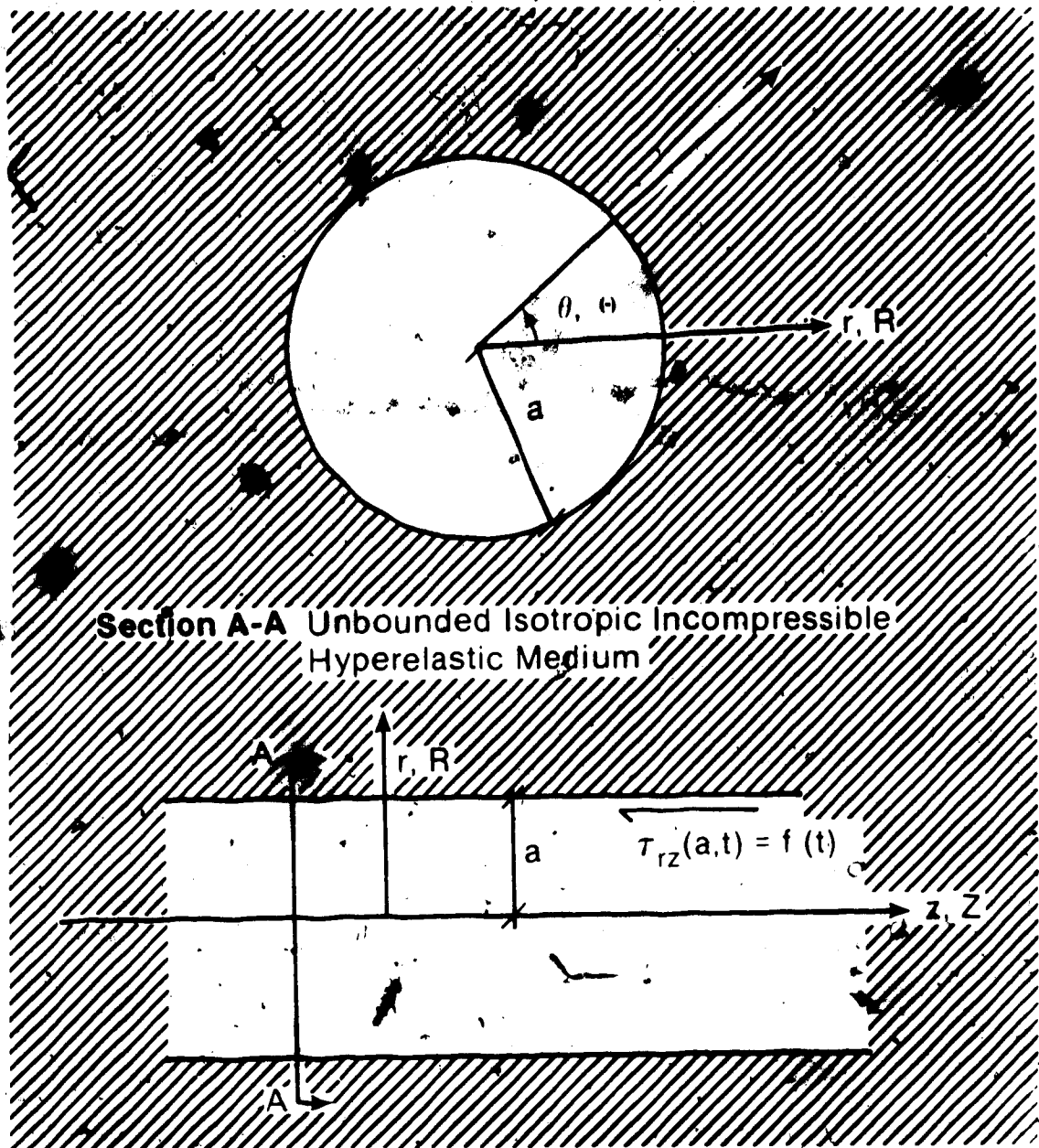


Fig 4.1 Diagrammatic representation of Axial Shear Wave Propagation in an Unbounded Isotropic Incompressible Hyperelastic Solid.

conditions are considered,

$$\tau_{rz}(a, t) = \tau_0 H(t),$$

or

$$\tau_{rz}(a, t) = \tau_0 \sin \frac{\pi t}{t^*} H(t) H(t^* - t),$$

(4.18)

and the initial conditions are

$$\tau_{rz}(r, 0) = 0, \quad w(r, 0) = 0,$$

(4.19)

where $H(t)$ is the unit step function and τ_0 and t^* are constants.

It is convenient to introduce the following nondimensionalization scheme,

$$\bar{\tau}_{rz} = \frac{\tau_{rz}}{\mu}, \quad (\bar{w}, \bar{r}) = \left(\frac{w, r}{a}\right), \quad \bar{t} = \left[\frac{\mu}{\rho}\right]^{1/2} \frac{t}{a}, \quad \bar{w} = w \left[\frac{\rho}{\mu}\right]^{1/2} \quad (4.20)$$

Henceforth, nondimensional variables are used but the superposed bars are omitted.

Substituting equation (4.17) into equation (4.11) and using the nondimensionalization scheme (4.20) gives

$$(1+6\gamma(w_r)^2) w_{rr} + \left\{ \frac{(1+2\gamma(w_r)^2)w_r}{r} \right\} - w = 0 \quad (4.21)$$

Equation (4.21) can be replaced by a hyperbolic system of first order partial differential equations

$$\frac{\partial w}{\partial t} - (1+6\gamma\epsilon^2) \frac{\partial \epsilon}{\partial r} - \frac{(1+2\gamma\epsilon^2)\epsilon}{r} = 0 \quad (4.22)$$

$$\frac{\partial \epsilon}{\partial t} - \frac{\partial \dot{w}}{\partial r} = 0 \quad (4.23)$$

where $\epsilon = w_r$. Equations (4.22) and (4.23) are of the form

$$\frac{\partial \underline{U}}{\partial t} + \underline{A}(\underline{U}) \frac{\partial \underline{U}}{\partial r} + \underline{B}(\underline{U}) = 0 \quad (4.24)$$

where

$$\underline{U} = \begin{bmatrix} \dot{w} \\ \epsilon \end{bmatrix}, \quad \underline{A}(\underline{U}) = \begin{bmatrix} 0 & -(1+6\gamma\epsilon^2) \\ -1 & 0 \end{bmatrix}, \quad \underline{B}(\underline{U}) = \begin{bmatrix} -(1+2\gamma\epsilon^2)\frac{\epsilon}{r} \\ 0 \end{bmatrix} \quad (4.25)$$

The eigenvalues of \underline{A} are the nondimensional wave speeds $\pm c$, where

$$c = (1+6\gamma\epsilon^2)^{1/2} \quad (4.26)$$

and the slopes of the two families of characteristics in the (r, t) plane are $dr/dt = \pm c$. Since results using the method of characteristics are not presented for this problem, the relationships along the characteristics are not given. In order to apply the numerical method, it is recommended that equation (4.22) be expressed in conservation form (Kutler, 1974),

$$\frac{\partial \dot{w}}{\partial t} - \frac{\partial}{\partial r} \left((1+2\gamma\epsilon^2) \frac{\epsilon}{r} \right) = 0 \quad (4.27)$$

Equation (4.23) is already in conservation form and the matrix form of equations (4.23) and (4.27) is

$$\frac{\partial \underline{U}}{\partial t} + \frac{\partial \underline{Q}(\underline{U})}{\partial r} + \underline{B}(\underline{U}) = 0 \quad (4.28)$$

where $\underline{Q} = (-(\epsilon + 2\gamma\epsilon^3), -\dot{w})^T$ and \underline{U} and $\underline{B}(\underline{U})$ are given by (4.25)₁ and (4.25)₃.

If a shock occurs, it follows from equations (4.23) and (4.27) that

$$[\dot{w}] = -V[\epsilon] \quad (4.29)$$

$$[\tau_{rz}] = [\epsilon + 2\gamma\epsilon^3] = -V[\dot{w}] \quad (4.30)$$

where V is the nondimensional shock speed and the square brackets $[]$ indicate the jump in the quantity.⁵ The shock speed V is then given by

$$V = \left\{ \frac{[\epsilon + 2\gamma\epsilon^3]}{[\epsilon]} \right\}^{1/2} \quad (4.31)$$

4.2.3 Implementation the MacCormack Scheme

The MacCormack finite difference scheme given by equation (2.6) for the nonconservation form of the equations and by equation (2.7) for the conservation form of the equations, is used to solve the systems of equations given in matrix form by equation (4.24) and equation (4.28), respectively. Both the nonconservation form and the conservation form of the systems of equations are considered using the numerical method to examine the effect of using a nonconservative finite difference scheme.

⁵ Square brackets denote jump conditions only when it is specified. Otherwise square brackets are used as enclosure brackets for mathematical expressions.

Application of the conservative version of the finite difference equations given by (2.7), gives the following predictor and corrector equations, respectively,

$$\overline{U}_{-j}^{n+1} = U_{-j}^n - \frac{\Delta t}{\Delta r} (Q(U_{-j+1}^n) - Q(U_{-j}^n)) - \Delta t B(U_{-j}^n) \quad (4.32)$$

$$U_{-j}^{n+1} = \frac{1}{2} \left\{ U_{-j}^n + \overline{U}_{-j}^{n+1} - \frac{\Delta t}{\Delta r} (Q(\overline{U}_{-j}^{n+1}) - Q(\overline{U}_{-j-1}^{n+1})) - \Delta t B(\overline{U}_{-j}^{n+1}) \right\}$$

The nonconservative version is given by

$$\overline{U}_{-j}^{n+1} = U_{-j}^n - \frac{\Delta t}{\Delta r} A(U_{-j}^n) (U_{-j+1}^n - U_{-j}^n) - \Delta t B(U_{-j}^n) \quad (4.33)$$

$$U_{-j}^{n+1} = \frac{1}{2} \left\{ U_{-j}^n + \overline{U}_{-j}^{n+1} - \frac{\Delta t}{\Delta r} A(\overline{U}_{-j}^{n+1}) (\overline{U}_{-j}^{n+1} - \overline{U}_{-j-1}^{n+1}) - \Delta t B(\overline{U}_{-j}^{n+1}) \right\}$$

In both cases,

$$U_{-j}^n = U(1 + j\Delta r, n\Delta t)$$

with the subscript and superscript notation (as indicated in Chapter 2).

The element $\epsilon(1, t)$ of $U(1, t)$ is obtained from the boundary condition (4.18) and the constitutive equation (4.17) so that ϵ_0^n is known for all n . In order to apply equations (4.32) or (4.33), w_0^n is also required for all n , and this is obtained by applying boundary conditions as discussed in Section 2.3 using forward forward (FF) differencing. For the conservative scheme,

$$\bar{w}_0^{n+1} = \bar{w}_0^n - \frac{\Delta t}{\Delta r} \left[(Q_1)_1^n - (Q_1)_0^n \right] - \Delta t (B_1)_0^n \quad (4.34)$$

$$\bar{w}_0^{n+1} = \frac{1}{2} \left\{ \bar{w}_0^n + \bar{w}_0^{n+1} - \frac{\Delta t}{\Delta r} \left((Q_1)_1^{n+1} - (Q_1)_0^{n+1} \right) - \Delta t (B_1)_0^{n+1} \right\} \quad (4.35)$$

where $Q_1 = -(\epsilon + 2\gamma\epsilon^2)$ and $B_1 = -(1 + 2\gamma\epsilon^2)\epsilon/r$ are the first elements of $\underline{Q}(U)$ and $\underline{B}(U)$, respectively. The boundary condition for the nonconservative scheme is given as

$$\bar{w}_0^{n+1} = \bar{w}_0^n - \frac{\Delta t}{\Delta r} (A_1)_0^n (\epsilon_1^n - \epsilon_0^n) - \Delta t (B_1)_0^n \quad (4.36)$$

$$\bar{w}_0^{n+1} = \frac{1}{2} \left\{ \bar{w}_0^n + \bar{w}_0^{n+1} - \frac{\Delta t}{\Delta r} (A_1)_1^{n+1} (\epsilon_1^{n+1} - \epsilon_0^{n+1}) - \Delta t (B_1)_0^{n+1} \right\} \quad (4.37)$$

where $A_1 = -(1 + 6\gamma\epsilon^2)$ and $B_1 = -(1 + 2\gamma\epsilon^2)\epsilon/r$.

This procedure for the application of boundary conditions, previously discussed in Section 2.3, was suggested by Gottlieb and Turkel (1978).

The stability analysis done in Section 2.4 shows that for linear hyperbolic systems of equations of the form (4.24) with $\underline{B}(U) = 0$, the MacCormack finite difference scheme is numerically stable if $\nu = 1$, where $\nu = c\Delta t/\Delta r$, is the Courant number for this difference scheme and c is the numerically greatest eigenvalue of \underline{A} . There is no analysis available at present regarding stability when $\underline{B}(U) \neq 0$, but numerical results obtained for the linear case, that is with $\gamma = 0$, indicate instability with $\nu = 1$. For the linear problem, $c = 1$ is constant, however when $\gamma \neq 0$, $c = (1 + 6\gamma\epsilon^2)^{1/2}$ so that for a constant Courant number, $\Delta t/\Delta r$

changes. Consequently, in the application of the scheme to the nonlinear problem, Δr is held constant and Δt is adjusted at each time step by assuming a constant value of $\nu < 1$ and taking c as the maximum of $(1+6\gamma c^2)^{1/2}$, obtained from the previous time step. This procedure was suggested by Hanagud and Abhyankar (1984), who considered a nonlinear finite amplitude wave propagation problem in a neo-Hookean material which resulted in a nonlinear hyperbolic system of equations with $B(U) = 0$.

Boundary condition $(4.18)_1$ results in a shock, initiated at $r = 1$, $t = 0$, which propagates radially outwards with speed V given by equation (4.31). For the linear problem, with $\gamma = 0$, $V = 1$ which is the same as the constant wave speed and the position of the shock front is trivially determined. When $\gamma \neq 0$, it follows from equation (4.31) and the initial conditions (4.19) that ϵ just behind the shock must be known in order to determine the shock speed. Consequently, the position of the shock is not known beforehand, but has to be determined as part of the solution. The solutions obtained from the application of equations (4.32) and (4.33) to the problem with $\gamma \neq 0$, and boundary condition $(4.18)_1$, locate the shock but the shock is smeared, that is, spread over several mesh intervals, and there is numerical dispersion behind the shock. In order to calculate the shock precisely for boundary condition $(4.18)_1$, the relationships between w and r and between ϵ and r for a given time t are extrapolated from the interval $[1, r^*]$, where r^* is chosen so that the dispersion occurs for $r > r^*$. The extrapolation is terminated when the jump conditions (4.29) and

(4.30) are satisfied. Since $\dot{w} - \epsilon = 0$ ahead of the shock, from (4.19), these conditions are equivalent to,

$$\dot{w}^2 - (1+2\gamma\epsilon^2) \epsilon^2 = 0 \quad (4.38)$$

4.2.4 Momentum and Energy Considerations

Since momentum must be conserved for the problems considered, numerical evaluation of momentum provides a check on the numerical solution. The nondimensional relation

$$\int_0^t \tau_{rz}(1, \eta) d\eta = \int_1^{r_f(t)} w r dr \quad (4.39)$$

where $r_f(t)$ is the position of the wavefront at time t , follows from conservation of momentum. The right hand side of equation (4.39) is evaluated numerically using a Simpson's integration scheme. The left hand side is evaluated analytically by substituting the appropriate boundary condition (4.18)₁ or (4.18)₂, and integrating. The exact values of nondimensional momentum, found from evaluating the left hand side of (4.39) for boundary conditions (4.18)₁ or (4.18)₂ with $\gamma = 0$ and $\gamma = 0.1$ are used to compare to those obtained from the numerical results and are presented in Tables 4.1 - 4.10.

Since momentum must be conserved, the numerical evaluation of momentum for each time step should be identical to the exact values found from the evaluation of the left hand side of (4.39).

For the axial shear problem, the mechanical energy is evaluated by considering the summation of the nondimensional strain and kinetic energies. The nondimensional mechanical energy for the problem considered is given by

$$E = \int_1^{r_f(t)} (\epsilon^2 + \gamma\epsilon^4) r \, dr + \int_1^{r_f(t)} (\dot{w})^2 r \, dr \quad (4.40)$$

When the boundary condition (4.18)₂ is considered for the nonlinear problem ($\gamma \neq 0$), the system is conservative until the wave breaks, and then mechanical energy is dissipated. Numerical evaluation of equation (4.40), using a Simpson's integration scheme, provides another check for the numerical solution. One would expect the numerical results to show dissipation of mechanical energy when the wave breaks (Haddow, 1985). It may also be shown that

$$2 \int_0^t v_{rz}(1, \eta) \dot{w}(1, \eta) d\eta = \int_1^{r_f(t)} \{(\epsilon^2 + \gamma\epsilon^4) + (\dot{w})^2\} r \, dr \quad (4.41)$$

must be satisfied until the wave breaks in the nonlinear problem and is always satisfied when $\gamma = 0$. If $t > 1$ for boundary condition (4.18)₂, with $t^* = 1$, the energy must be constant for the linear problem and constant until the wave breaks for the nonlinear problem. Results for the energy calculations are presented in Tables 4.3 and 4.4.

4.2.5 Numerical Results

The numerical results presented in this section have been obtained using the conservative version of the MacCormack scheme unless otherwise specified. Numerical results are presented for nondimensional values of stress $\tau = \tau_{rz}$ or velocity w , versus nondimensional distance r , at nondimensional times, t . Only quiescent unstressed initial conditions (4.19) are considered. In this case, τ and w correspond to nondimensional axial shear stress and axial particle velocity, respectively. Figures 4.2 - 4.4 show the effect of Courant number on the numerical solution τ vs r for boundary condition (4.18)₁, with $\tau_0 = 1$, for $\gamma = 0$, which is a linear problem. It should be noted that there is mild instability in the numerical results shown in Figure 4.2, for $\nu = 1.0$. This instability is not present for smaller ν , but numerical dispersion appears for $\nu = 0.99$, and $\nu = 0.5$. Since $\gamma = 0$, the nondimensional shock speed is $V = 1$, and the wavefront should be located at $r = t+1$. Excellent agreement is obtained with expected results for Figures 4.2 - 4.4, however, the smearing of the shock front, increases as ν decreases. This suggests that $\nu = 1.0$, to avoid instability, but that ν should be maintained as close to 1 as possible to minimize numerical dispersion. An appropriate value of ν is obtained using a trial and error approach.

Figures 4.5 - 4.7 show the effect of Courant number on the numerical solution τ vs r for boundary condition (4.18)₁, with $\tau_0 = 1$, for $\gamma = 0.1$, which is a nonlinear problem. Again, there seems to be some instability in the numerical results shown in

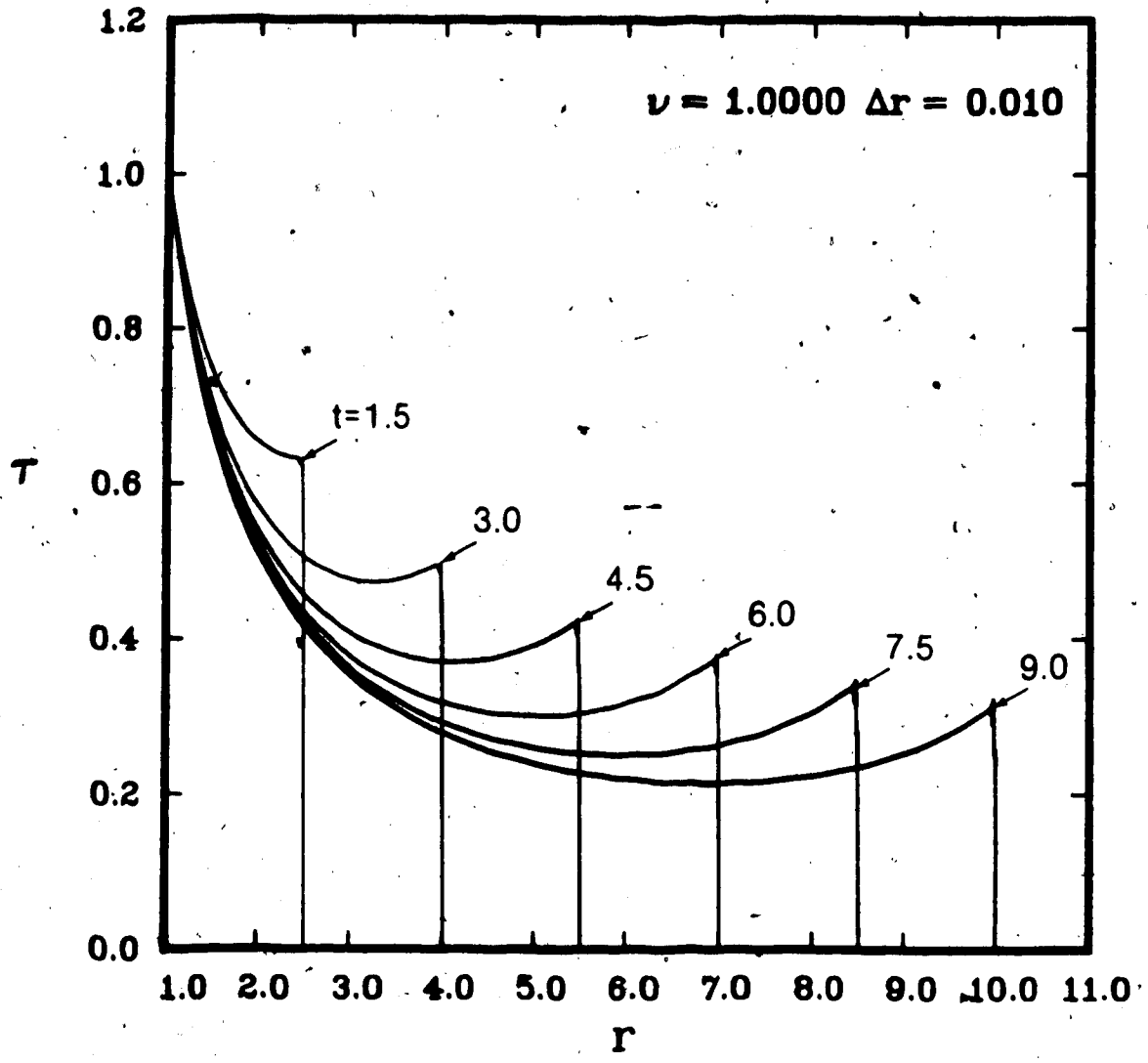


Fig. 4.2 Axial Shear - Variation of nondimensional τ with nondimensional r for $\gamma = 0$ subject to $\tau(1,t) = \tau_0 H(t)$, with $\tau_0 = 1$, using the MacCormack scheme, with $\nu = 1.0$.

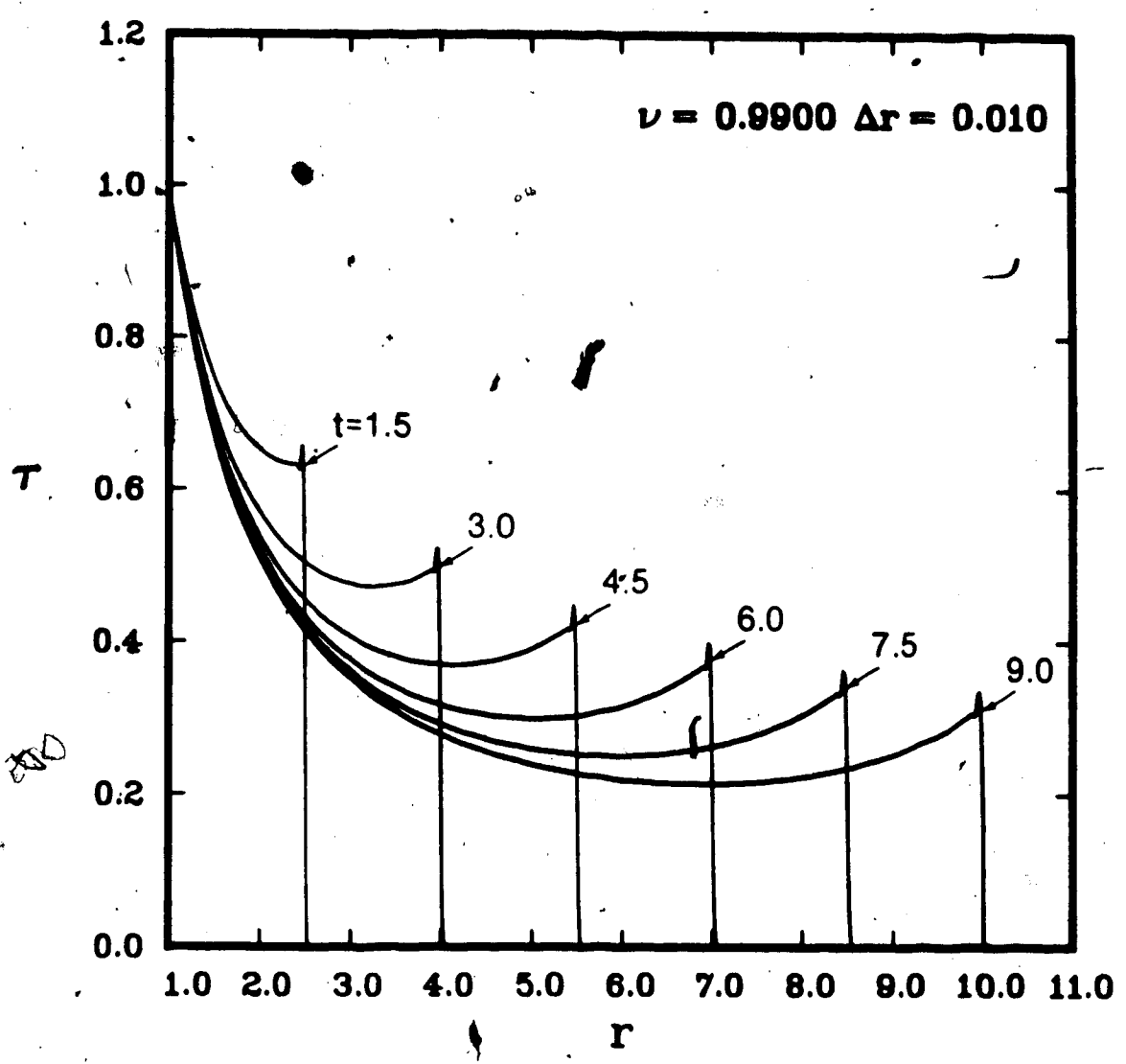


Fig. 4.3 Axial Shear - Variation of nondimensional T with nondimensional r for $\gamma = 0$ subject to $\tau(1,t) = \tau_0 H(t)$, with $\tau_0 = 1$, using the MacCormack scheme, with $\nu = 0.99$.

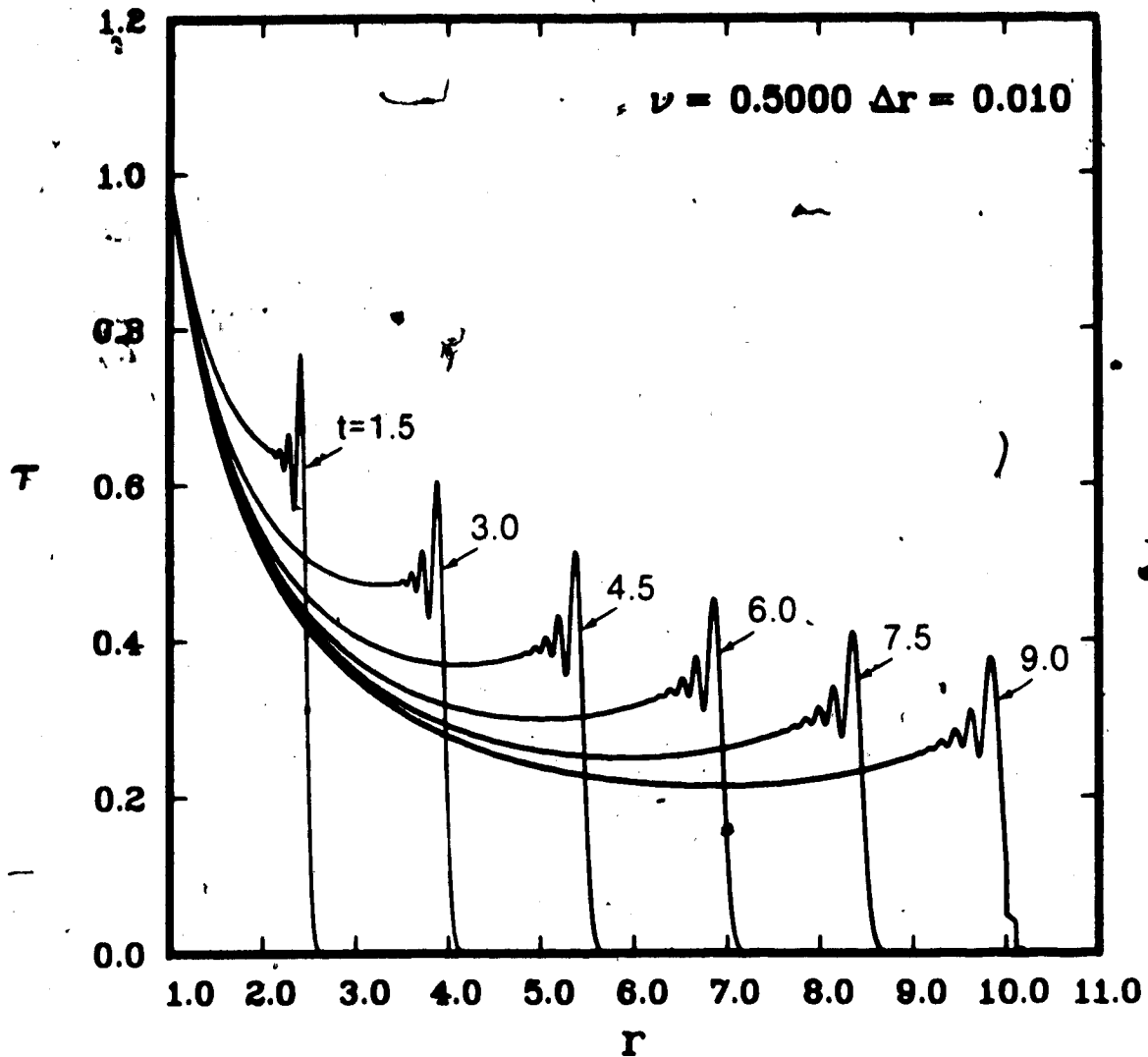


Fig. 4.4 Axial Shear. - Variation of nondimensional τ with nondimensional r for $\gamma = 0$ subject to $\tau(1,t) = \tau_0 H(t)$, with $\tau_0 = 1$, using the MacCormack scheme, with $\nu = 0.5$.

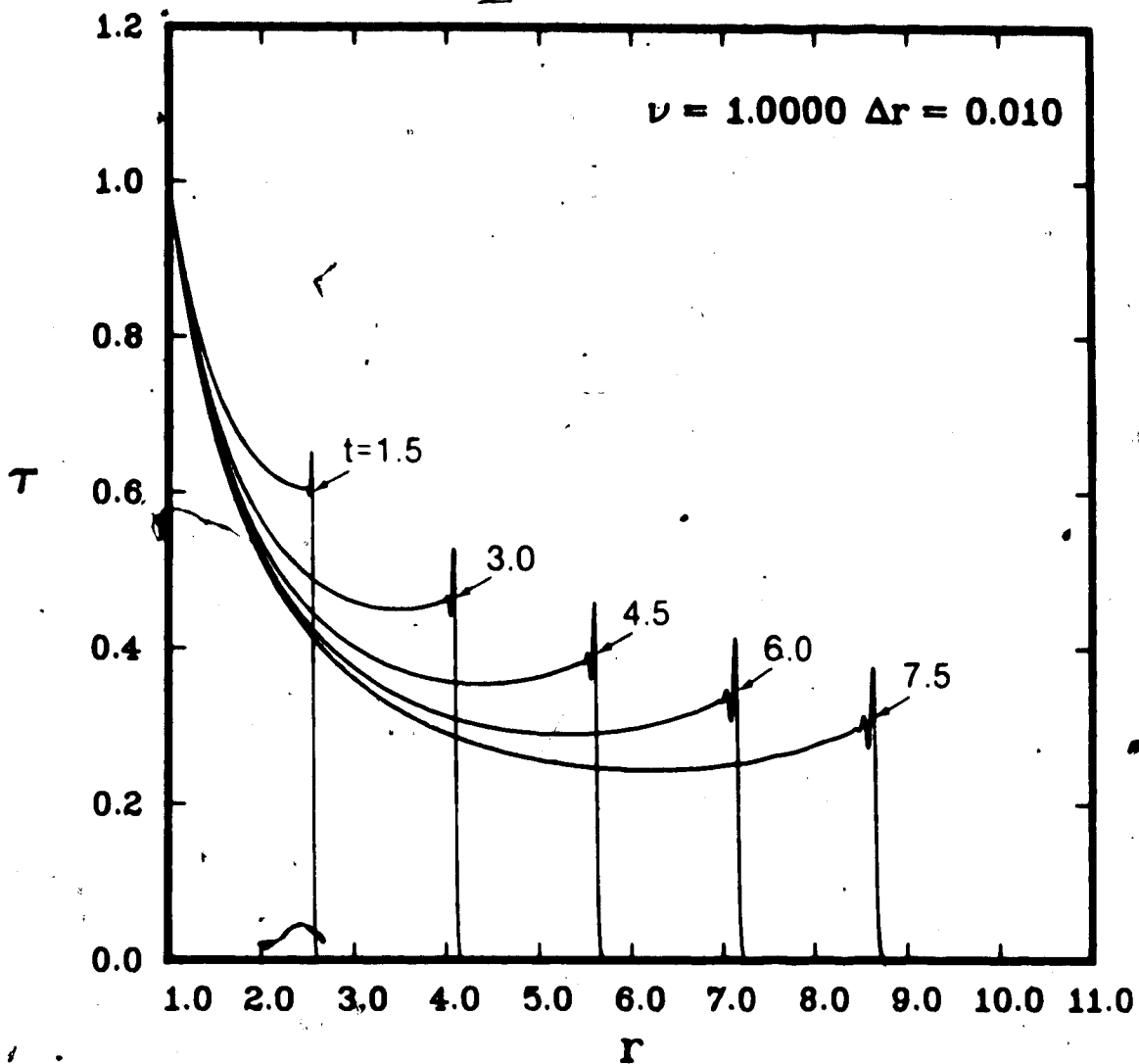


Fig. 4.5 Axial Shear - Variation of nondimensional τ with nondimensional r for $\gamma = 0.1$ subject to $\tau(1,t) = \tau_0 H(t)$, with $\tau_0 = 1$, using the MacCormack scheme, with $\nu = 1.0$.

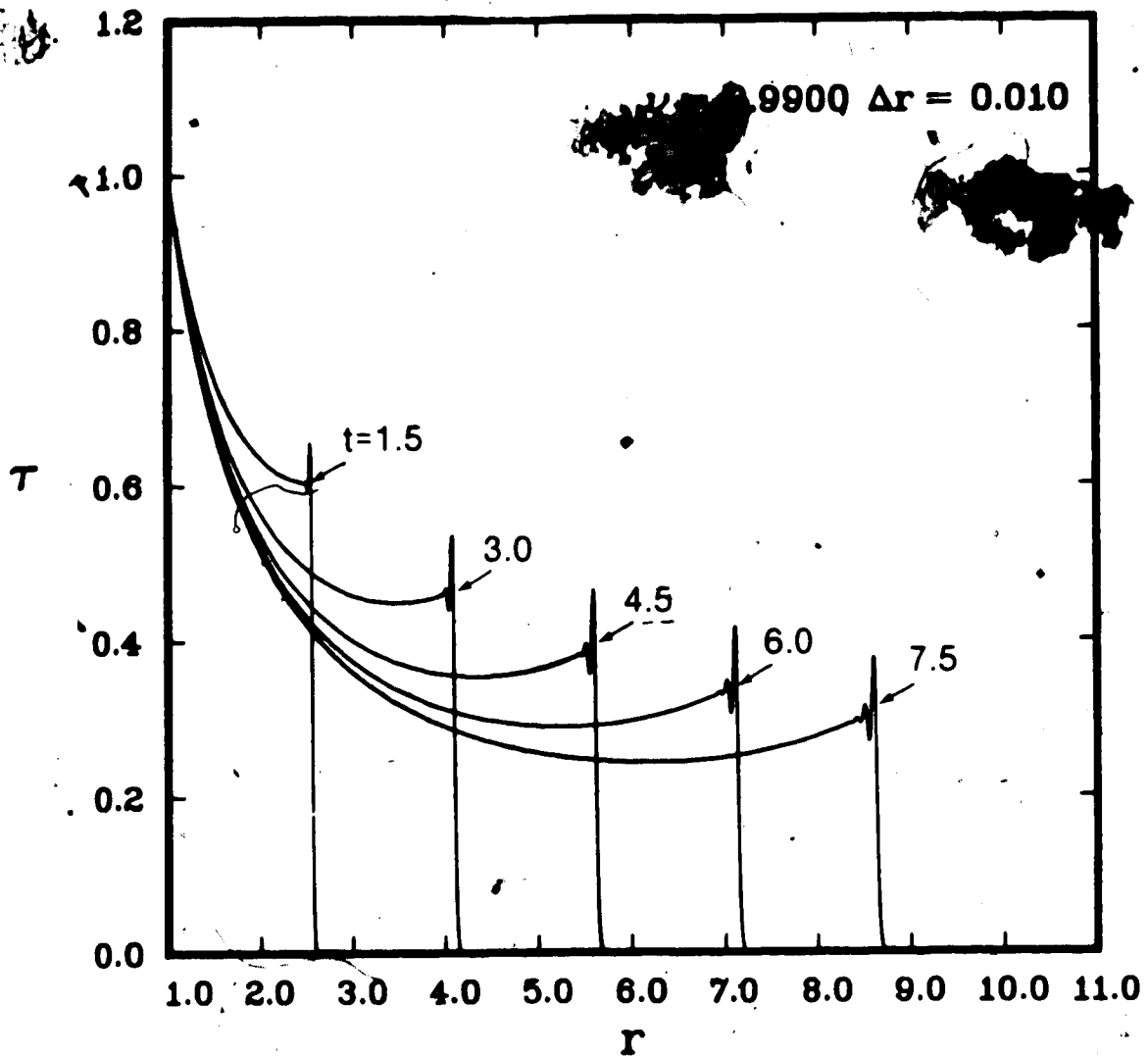


Fig. 4.6 Axial Shear - Variation of nondimensional τ with nondimensional r for $\gamma = 0.1$ subject to $\tau(1,t) = \tau_0 H(t)$, with $\tau_0 = 1$, using the MacCormack scheme, with $\nu = 0.99$.

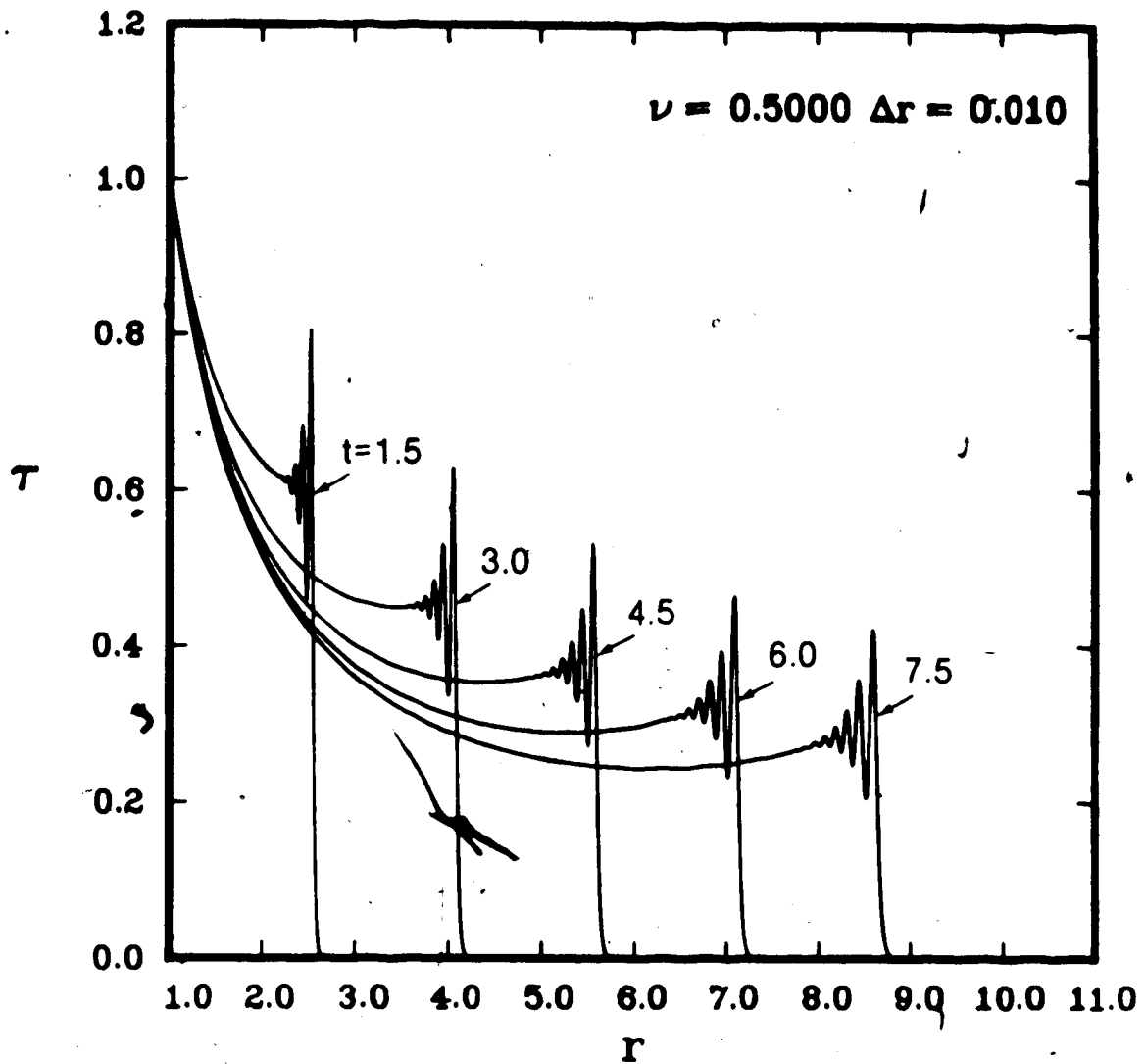


Fig. 4.7 Axial Shear - Variation of nondimensional τ with nondimensional r for $\gamma = 0.1$ subject to $\tau(1,t) = \tau_0 H(t)$, with $\tau_0 = 1$, using the MacCormack scheme, with $\nu = 0.5$.

Figure 4.5, as well as numerical dispersion. The numerical dispersion in the solutions presented in Figures 4.6 and 4.7 is more severe than for the linear counterparts (see Figures 4.3 and 4.4), for $\nu = 0.99$ and $\nu = 0.5$, respectively.

Figures 4.8 and 4.9 show the effect of grid size on the numerical solution for τ , for boundary condition (4.18)₁, with $r_0 = 1$, for $\gamma = 0$ and $\gamma = 0.1$, respectively, and a Courant number $\nu = 0.99$. A grid size of $\Delta r = 0.01$ is used hereafter, since the results give good resolution of shock fronts. Smaller grid sizes can be used, however, there is not much visible difference in the solution.

The remainder of the results presented in this section are for $\nu = 0.99$ and $\Delta r = 0.01$. There is no further discussion on the effects of Courant number or grid size on the MacCormack scheme for this solution. Most of the numerical phenomena described in Chapter 2 for the linear and nonlinear scalar equations have been summarized previously.

Since the Courant number is chosen to be $\nu < 1$ ($\nu = 0.99$) and $\Delta r = 0.01$, there is numerical dispersion present in the solutions (see Figures 4.3 and 4.6). Therefore, the extrapolation technique described in Section 4.2.3 is used to smooth the solutions. Figures 4.10 and 4.11 compare the numerical solutions for boundary condition (4.18)₁, with $r_0 = 1$, with and without the extrapolation technique for $\gamma = 0$ and $\gamma = 0.1$, respectively. The extrapolation technique eliminates numerical dispersion and ensures that the jump conditions (4.38) are satisfied. Momentum

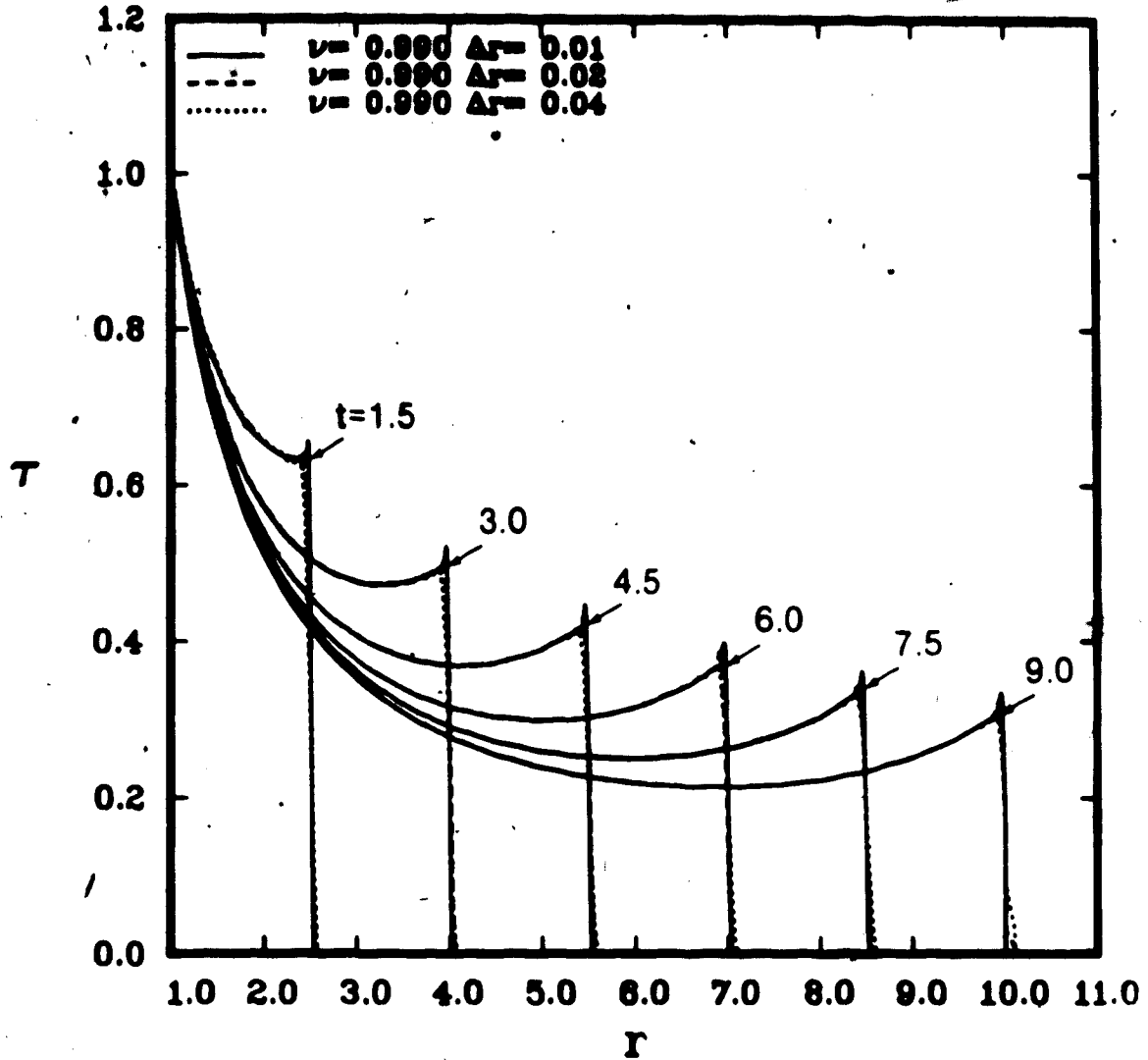


Fig. 4.8 Axial Shear - Effect of grid size on the variation of nondimensional τ with nondimensional r for $\gamma = 0$ using the MacCormack scheme with $\nu = 0.99$, for $\tau(1, t) = \tau_0 H(t)$, with $\tau_0 = 1$.

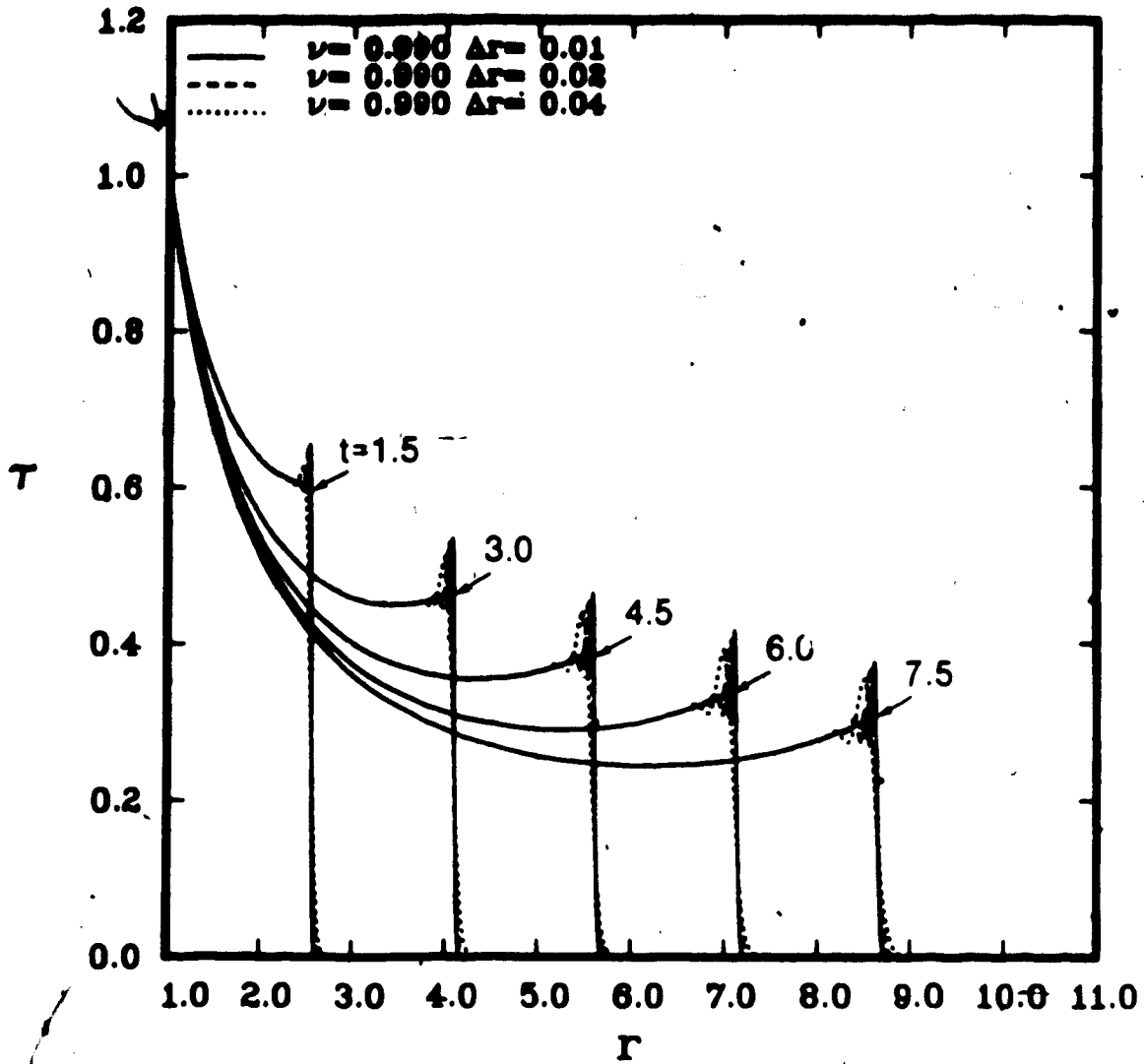


Fig. 4.9 Axial Shear - Effect of grid size on the variation of nondimensional τ with nondimensional r for $\gamma = 0.1$ using the MacCormack scheme with $\nu = 0.99$, for $\tau(1,t) = \tau_0 H(t)$, with $\tau_0 = 1$.

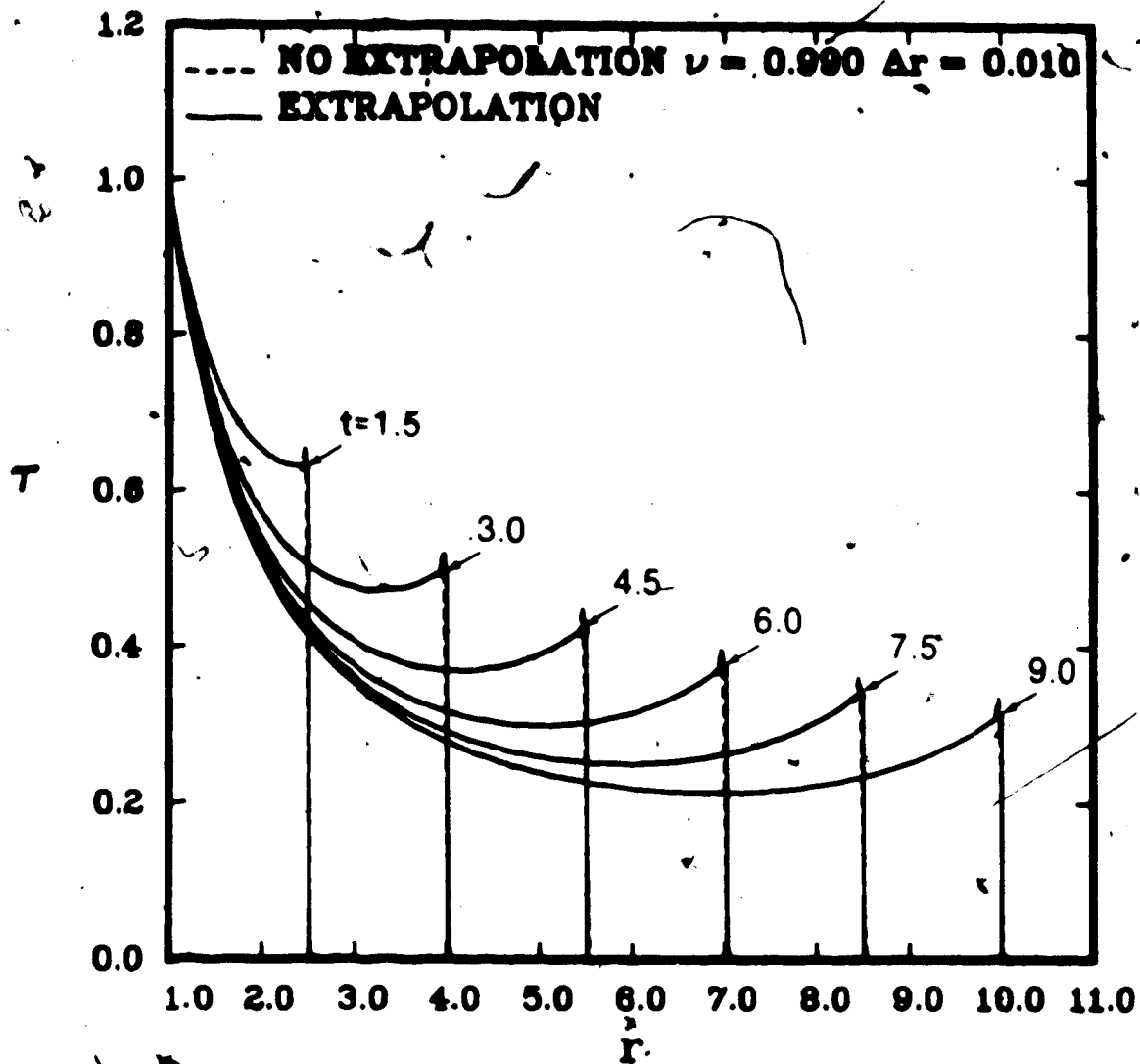


Fig. 4.10 Axial Shear - Variation of nondimensional r with nondimensional r for $\gamma \neq 0$ subject to $r(1,t) = r_0 H(t)$, with $r_0 = 1$ using the MacCormack scheme with and without extrapolation with $\nu = 0.9$.

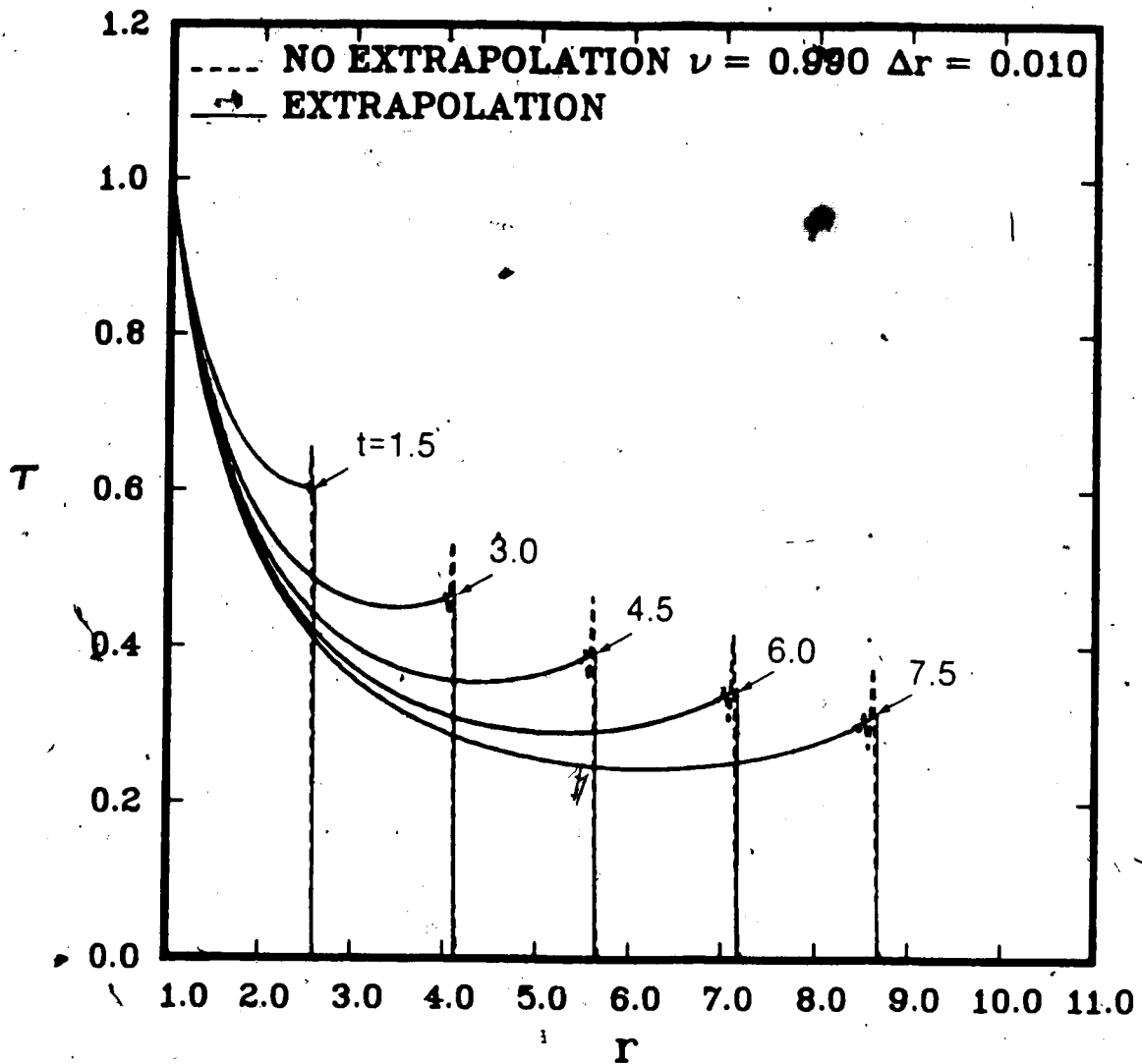


Fig. 4.11 Axial Shear - Variation of nondimensional τ with nondimensional r for $\gamma = 0.1$ subject to $\tau(1,t) = \tau_0 H(t)$, with $\tau_0 = 1$ using the MacCormack scheme with and without extrapolation with $\nu = 0.99$.

calculations corresponding to Figures 4.10 and 4.11 are presented in Tables 4.1 and 4.2 respectively, with and without the extrapolation technique. The numerically evaluated momentum calculations are compared to the exact values found from evaluating equation (4.39) for boundary condition (4.18)₁. There is good agreement with exact values of momentum with and without extrapolation. The extrapolated values are somewhat higher than the values obtained from MacCormack's method without extrapolation, however, the largest difference is approximately 1%.

Figure 4.12 compares the numerical solutions obtained for $\gamma = 0$ and $\gamma = 0.1$ for boundary condition (4.18)₁ with $\tau_0 = 0.01$. Since the amplitude, τ_0 , of the boundary condition is small, the solution for the nonlinear problem, $\gamma = 0.1$, should approach that of the linear problem, $\gamma = 0$. Figure 4.12 shows negligible difference between the two solutions. Momentum calculations corresponding to the two solutions are almost identical.

Figures 4.13 and 4.14 show the variation of w with r for boundary condition (4.18)₁, with $\tau_0 = 1$, for $\gamma = 0$ and $\gamma = 0.1$ respectively. These curves are presented to illustrate that the wavefronts of the velocity profile coincide with the wavefronts of the stress profiles, for both the linear and nonlinear solutions. In addition, the velocity profiles exhibit numerical dispersion similar to the solutions obtained for τ .

Figures 4.15 and 4.16 show the numerical solution for τ for boundary condition (4.18)₂, with $\tau_0 = 1$.

Table 4.1 Nondimensional Momentum Calculations for Axial Shear subject to $\tau(1,t) = \tau_0 H(t)$, with $\tau_0 = 1$, and quiescent unstressed initial conditions for $\gamma = 0$ and $\nu = 0.99$.
(See Figure 4.10)

Nondimensional Time t	Exact Value of Momentum	Numerically Evaluated Momentum	
		No Extrapolation	Extrapolation
1.5	-1.5	-1.500	-1.510
3.0	-3.0	-2.994	-3.018
4.5	-4.5	-4.499	-4.516
6.0	-6.0	-6.004	-6.028
7.5	-7.5	-7.498	-7.520
9.0	-9.0	-9.002	-9.033

Table 4.2 Nondimensional Momentum Calculations for Axial Shear subject to $\tau(1,t) = \tau_0 H(t)$, with $\tau_0 = 1$, and quiescent unstressed initial conditions for $\gamma = 0.1$ and $\nu = 0.99$.
(See Figure 4.11)

Nondimensional Time t	Exact Value of Momentum	Numerically Evaluated Momentum	
		No Extrapolation	Extrapolation
1.5	-1.5	-1.499	-1.526
3.0	-3.0	-3.001	-3.010
4.5	-4.5	-4.496	-4.507
6.0	-6.0	-5.999	-6.040
7.5	-7.5	-7.493	-7.531

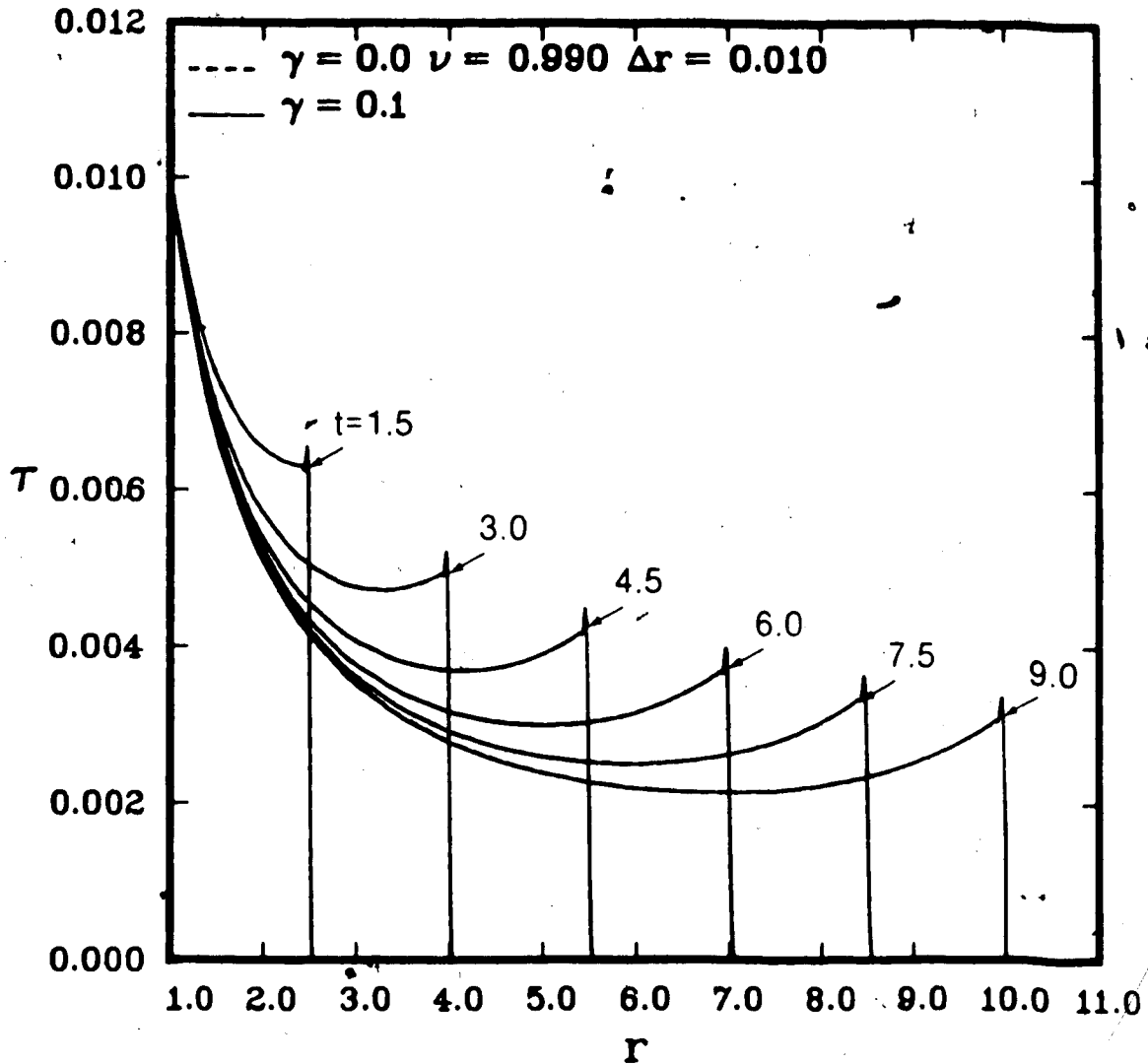


Fig. 4.12 Axial Shear - A comparison of the numerical results obtained for τ vs r with $\gamma = 0$ to those obtained with $\gamma = 0.1$, subject to $\tau(1,t) = \tau_0 H(t)$, with $\tau_0 = 0.01$ using the MacCormack scheme with $\nu = 0.99$.

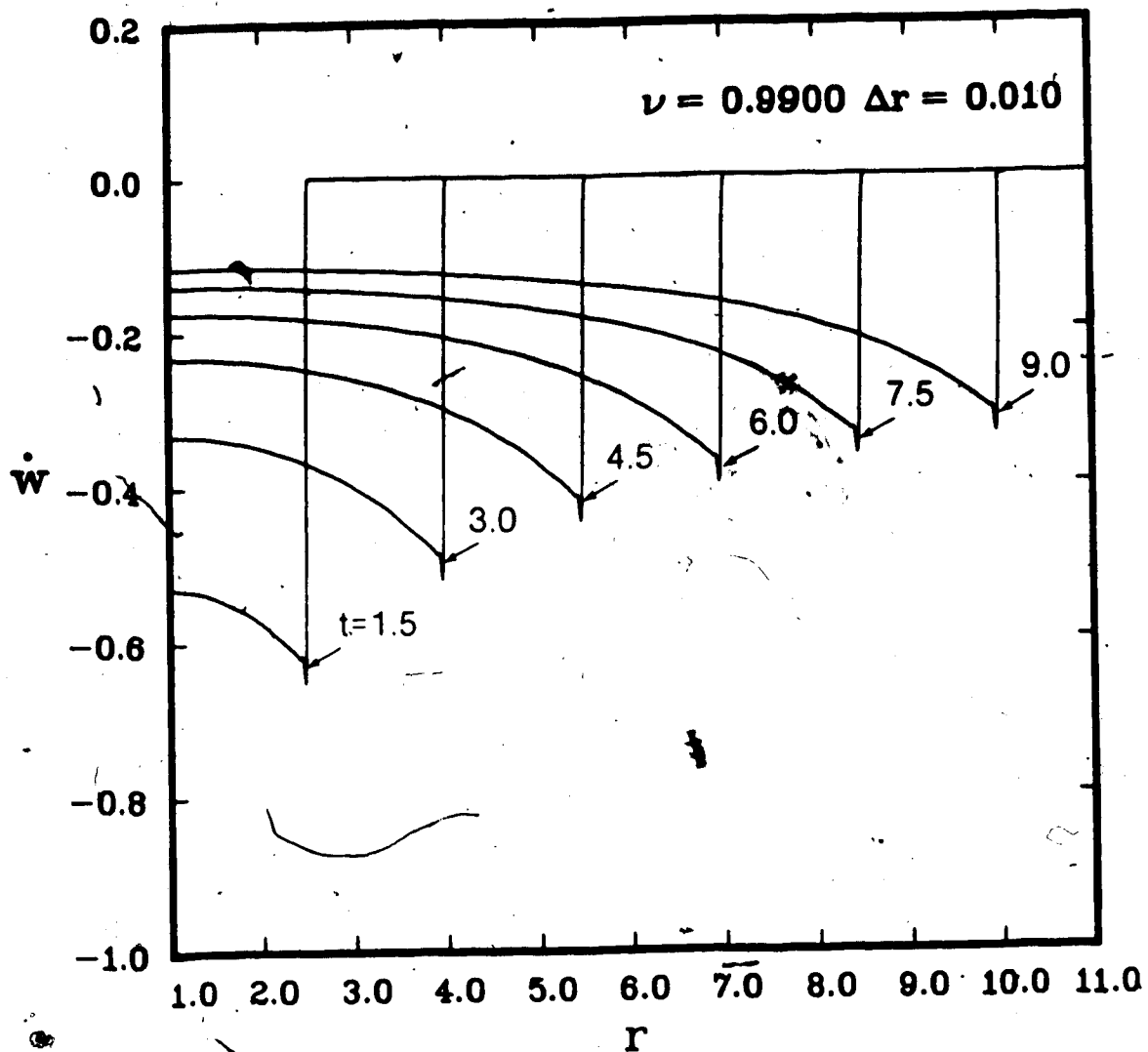


Fig. 4.13 Axial Shear - Variation of nondimensional \dot{w} with nondimensional r for $\gamma = 0$ subject to $r(1,t) = r_0 H(t)$, with $r_0 = 1$ using the MacCormack scheme with $\nu = 0.99$.

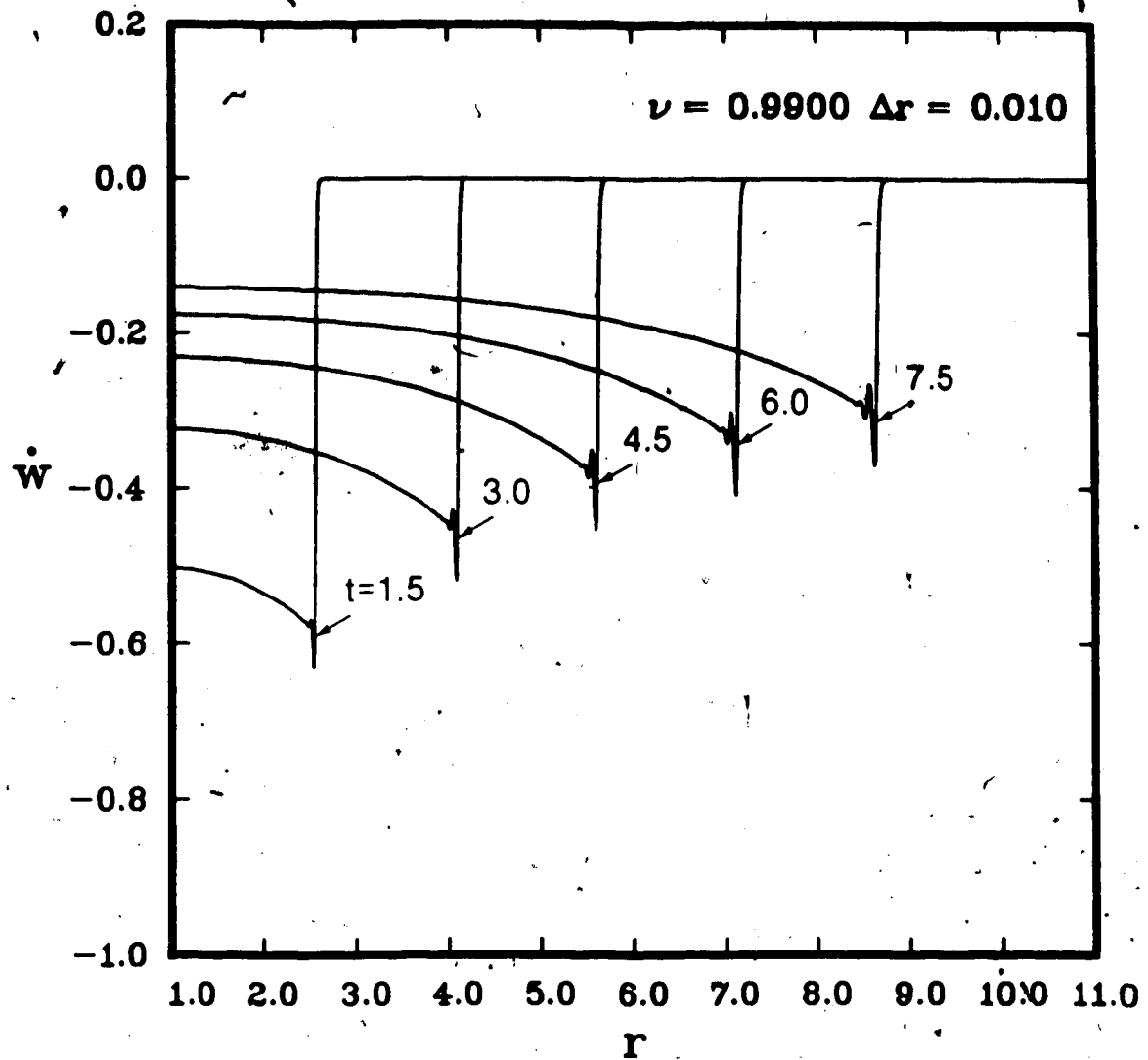


Fig. 4.14 Axial Shear - Variation of nondimensional \dot{w} with nondimensional r for $\gamma = 0.1$ subject to $\tau(1,t) = \tau_0 H(t)$, with $\tau_0 = 1$ using the MacCormack scheme with $\nu = 0.99$.

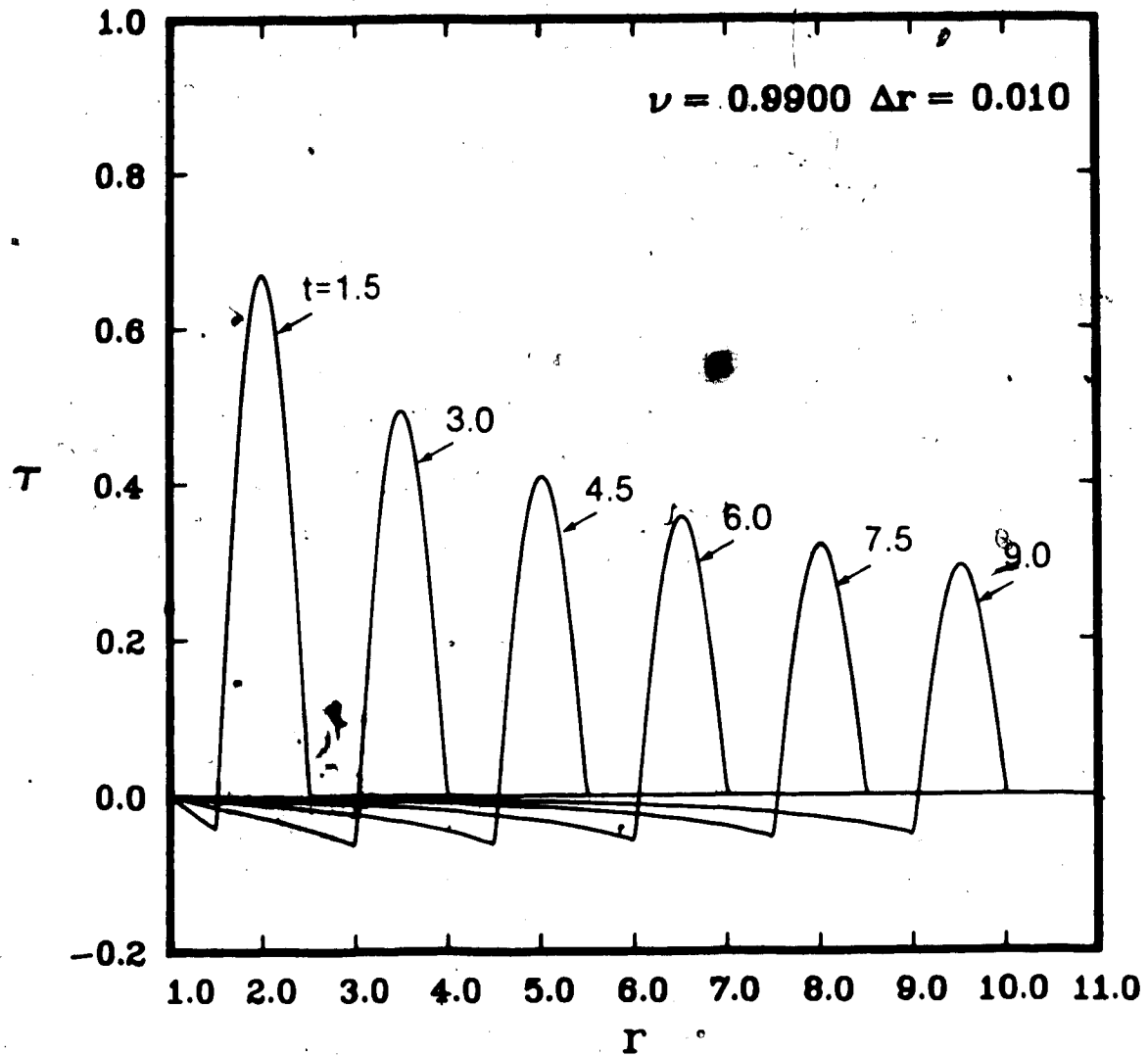


Fig. 4.15 Axial Shear - Variation of nondimensional τ with nondimensional r for $\gamma = 0$ subject to $\tau(1,t) = \tau_0 \sin \pi t H(t) H(1-t)$, with $\tau_0 = 1$ using the MacCormack scheme with $\nu = 0.99$.

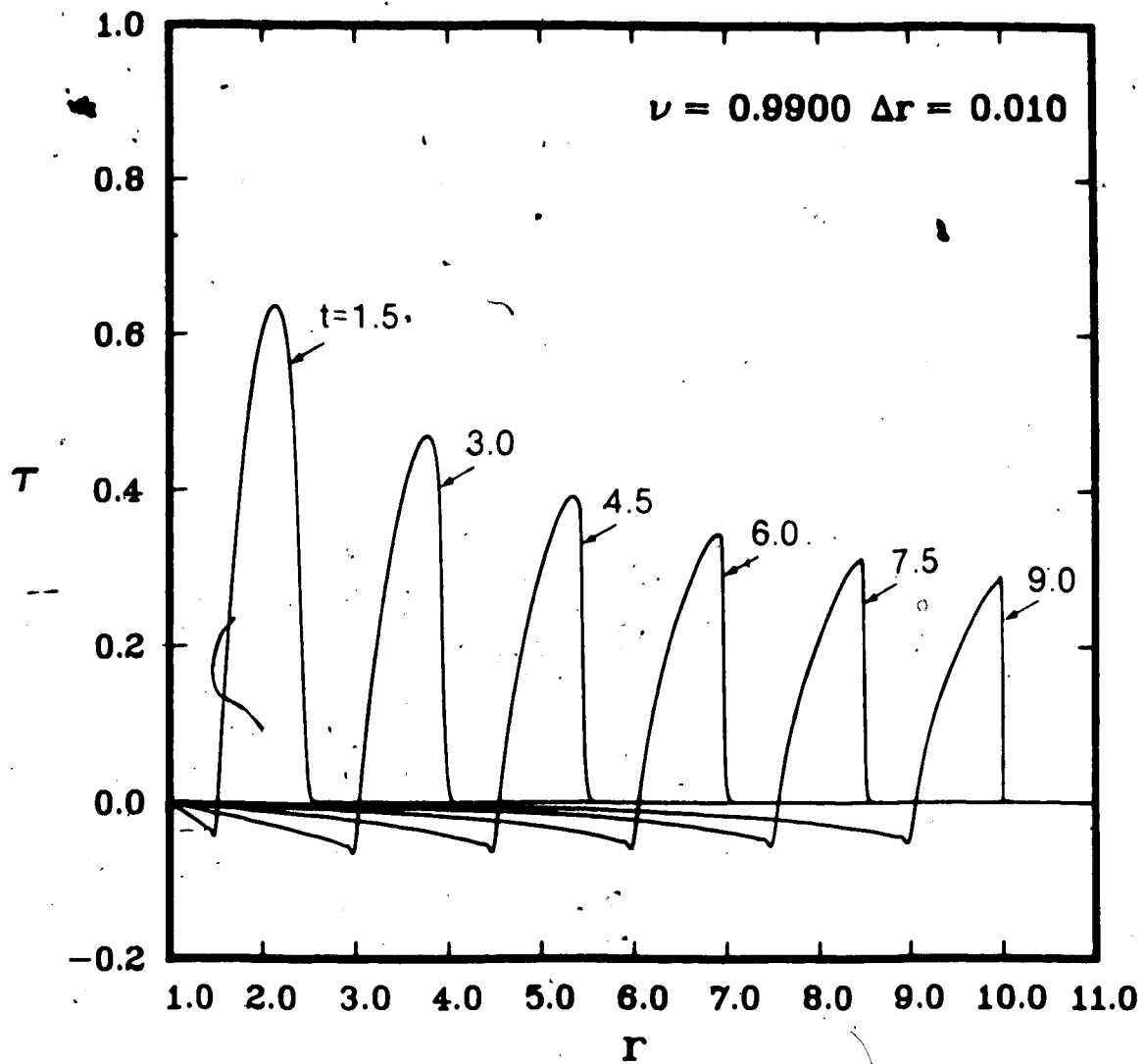


Fig. 4.16 Axial Shear - Variation of nondimensional τ with nondimensional r for $\gamma = 0.1$ subject to $\tau(1,t) = \tau_0 \sin \pi t H(t) H(1-t)$, with $\tau_0 = 1$ using the MacCormack scheme with $\nu = 0.99$.

A value of $t^* = 1$ is used so that

$$r(1,t) = r_0 \sin \pi t H(t) H(1-t) \quad (5.42)$$

for $\gamma = 0$ and $\gamma = 0.1$, respectively. Figure 4.16 indicates shock evolution, since it is visually evident that for $t > 3.0$ the wave has broken. A representation of the shock is obtained using the MacCormack scheme. There is also some numerical dispersion present which can be seen as small oscillations in the solutions shown in Figures 4.15 and 4.16. The extrapolation procedure is not applied to solutions obtained for boundary condition (4.18)₂. Nondimensional momentum and mechanical energy calculations corresponding to Figures 4.15 and 4.16 are presented in Tables 4.3 and 4.4, respectively. Momentum must be conserved. Tables 4.3 and 4.4 compare the exact value obtained from the left hand side of equation (4.39) evaluated for boundary condition (4.18)₂, with results obtained from the numerical evaluation of the right hand side of equation (4.39). Agreement is good. The values obtained for $\gamma = 0.1$ are somewhat higher than the exact values, however, momentum is conserved for the times considered. Mechanical energy calculations using equation (4.40) are also presented in addition to momentum calculations. For the linear problem $\gamma = 0$ (see Table 4.3), energy is conserved. For the nonlinear problem $\gamma = 0.1$, (see Table 4.4) energy decreases significantly between $t = 1.5$ and $t = 9.0$. This is consistent with theoretical expectations, since a shock has evolved between $t = 1.5$ and $t = 9.0$. Although it is difficult to establish the exact time of

Table 4.3 Nondimensional Momentum and Energy Calculations for Axial Shear subject to $\tau(1,t) = \tau_0 \sin t H(t) H(1-t)$, with $\tau_0 = 1$, and quiescent unstressed initial conditions for $\gamma = 0$ and $\nu = 0.99$. (See Figure 4.15)

Nondimensional Time t	Exact Value of Momentum	Numerically Evaluated Momentum	Numerically Eval. Mechanical Energy
1.5	-0.6366	-0.6365	0.8283
3.0	-0.6366	-0.6365	0.8279
4.5	-0.6366	-0.6365	0.8276
6.0	-0.6366	-0.6365	0.8275
7.5	-0.6366	-0.6365	0.8273
9.0	-0.6366	-0.6366	0.8272

Table 4.4 Nondimensional Momentum and Energy Calculations for Axial Shear subject to $\tau(1,t) = \tau_0 \sin t H(t) H(1-t)$, with $\tau_0 = 1$, and quiescent unstressed initial conditions for $\gamma = 0.1$ and $\nu = 0.99$. (See Figure 4.16)

Nondimensional Time t	Exact Value of Momentum	Numerically Evaluated Momentum	Numerically Eval. Mechanical Energy
1.5	-0.6366	-0.6365	0.7829
3.0	-0.6366	-0.6365	0.7818
4.5	-0.6366	-0.6369	0.7776
6.0	-0.6366	-0.6374	0.7681
7.5	-0.6366	-0.6362	0.7574
9.0	-0.6366	-0.6364	0.7468

the formation of the shock from the numerical results, the results presented are in good agreement with analytical considerations and shock formation is indicated.

The importance of conservative versus nonconservative difference schemes is of considerable interest, in regard to the problems considered. Figures 4.17 and 4.18 compare results for $\gamma = 0$ and $\gamma = 0.1$ obtained using the nonconservative difference scheme given by equation (4.33), with those obtained using the conservative version given by equation (4.32), for boundary condition (4.18)₁, with $r_0 = 1$. Agreement is good. The two curves are almost identical. Tables 4.5 and 4.6 compare nondimensional momentum calculations for Figures 4.17 and 4.18, respectively. There is a significant difference between the conservative and nonconservative schemes for the results obtained from the momentum calculations with $\gamma = 0.1$. The numerical results obtained from the nonconservative difference scheme do not conserve momentum as well as the those obtained from the conservative difference scheme. Yet, there is no significant difference in the numerical solutions for nondimensional r . Figures 4.19 and 4.20 show the corresponding velocity solutions for $\gamma = 0$ and $\gamma = 0.1$ respectively. Again, there is not much visual difference between the two solutions.

Figures 4.21 and 4.22 give a comparison of the conservative and nonconservative finite difference solutions for $\gamma = 0$ and $\gamma = 0.1$, respectively, subject to boundary condition (4.18)₂, with $r_0 = 1$. Tables 4.7 and 4.8 give the corresponding momentum calculations. All of the above results indicate that caution must

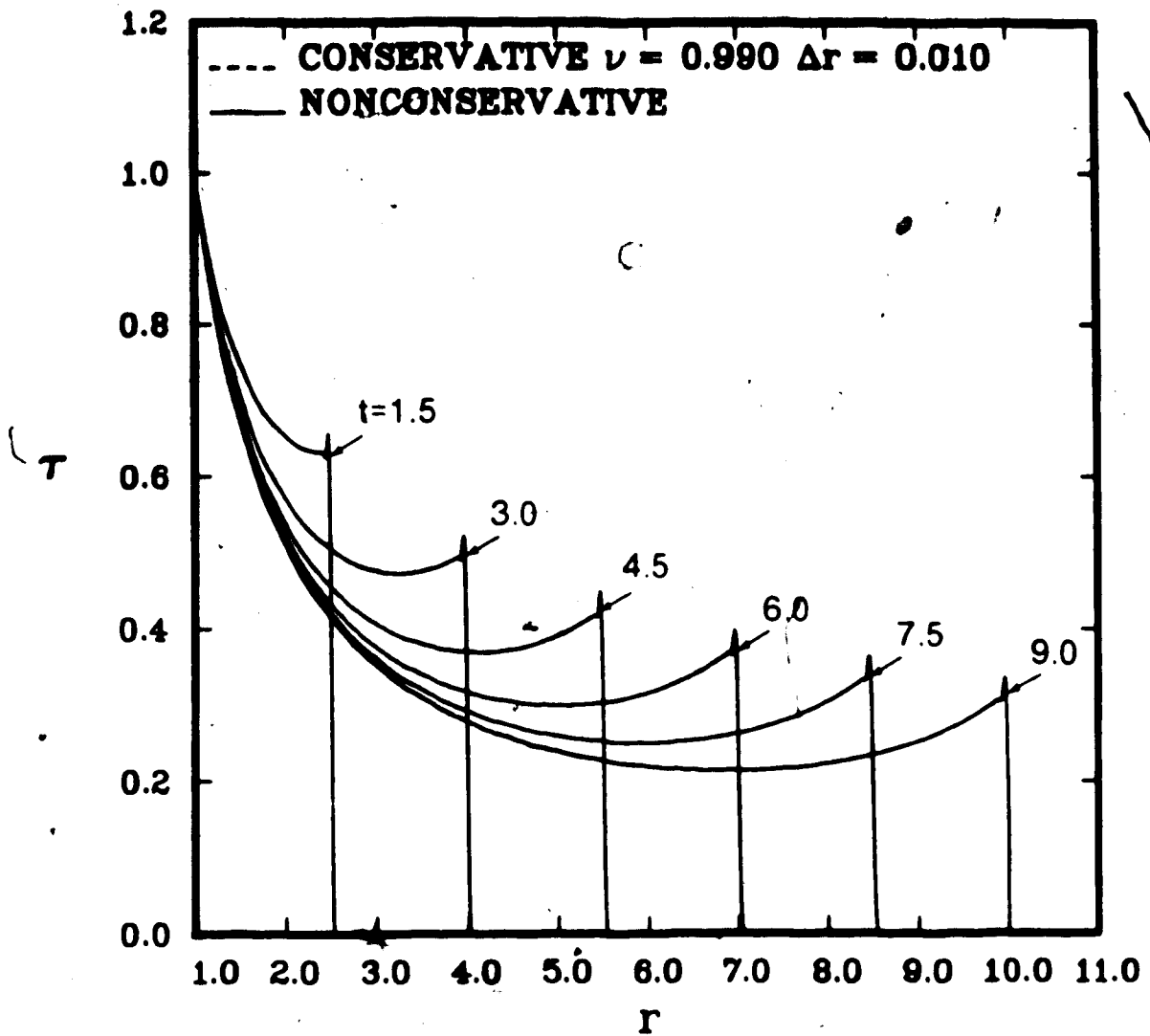


Fig. 4.17 Axial Shear - Variation of nondimensional τ with nondimensional r for $\gamma = 0$ subject to $\tau(1,t) = \tau_0 H(t)$, with $\tau_0 = 1$ using the conservative and nonconservative MacCormack schemes with $\nu = 0.99$.

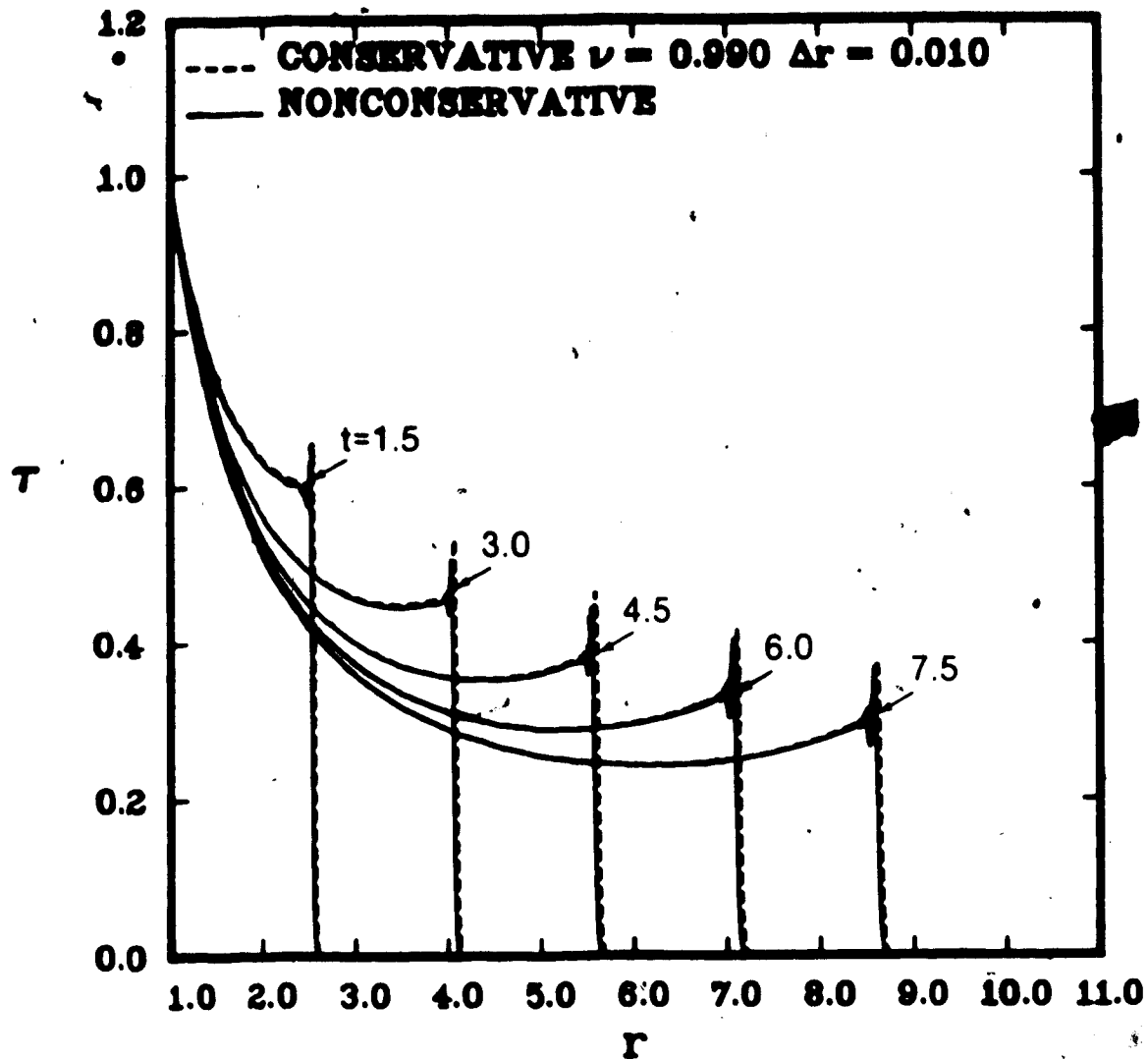


Fig. 4.18 Axial Shear - Variation of nondimensional τ with nondimensional r for $\gamma = 0.1$ subject to $\tau(1,t) = \tau_0 H(t)$, with $\tau_0 = 1$ using the conservative and nonconservative MacCormack schemes with $\nu = 0.99$.

Table 4.5 Nondimensional Momentum Calculations for Axial Shear subject to $\tau(1,t) = \tau_0 H(t)$, with $\tau_0 = 1$, and quiescent unstressed initial conditions for $\gamma = 0$ and $\nu = 0.99$.
(See Figure 4.17)

Nondimensional Time t	Exact Value of Momentum	Numerically Evaluated Momentum	
		Conservative	Nonconservative
1.5	-1.5	-1.500	-1.500
3.0	-3.0	-2.994	-2.994
4.5	-4.5	-4.499	-4.499
6.0	-6.0	-6.004	-6.004
7.5	-7.5	-7.498	-7.498
9.0	-9.0	-9.002	-9.002

Table 4.6 Nondimensional Momentum Calculations for Axial Shear subject to $\tau(1,t) = \tau_0 H(t)$, with $\tau_0 = 1$, and quiescent unstressed initial conditions for $\gamma = 0.1$ and $\nu = 0.99$.
(See Figure 4.18)

Nondimensional Time t	Exact Value of Momentum	Numerically Evaluated Momentum	
		Conservative	Nonconservative
1.5	-1.5	-1.499	-1.450
3.0	-3.0	-3.001	-2.930
4.5	-4.5	-4.496	-4.410
6.0	-6.0	-5.999	-5.902
7.5	-7.5	-7.493	-7.396

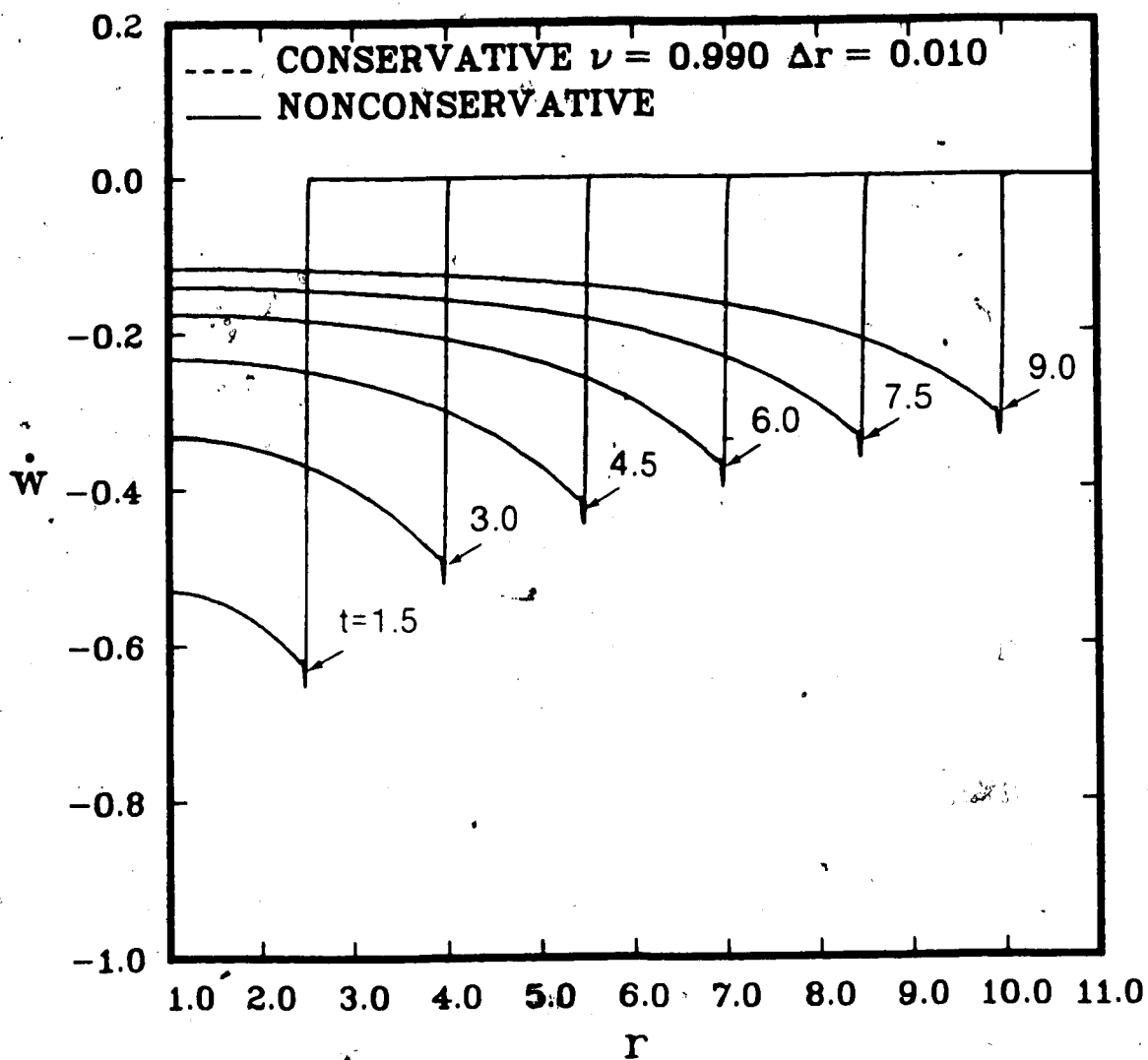


Fig. 4.19 Axial Shear - Variation of nondimensional w with nondimensional r for $\gamma = 0$ subject to $\tau(1,t) = \tau_0 H(t)$, with $\tau_0 = 1$ using the conservative and nonconservative MacCormack schemes with $\nu = 0.99$.

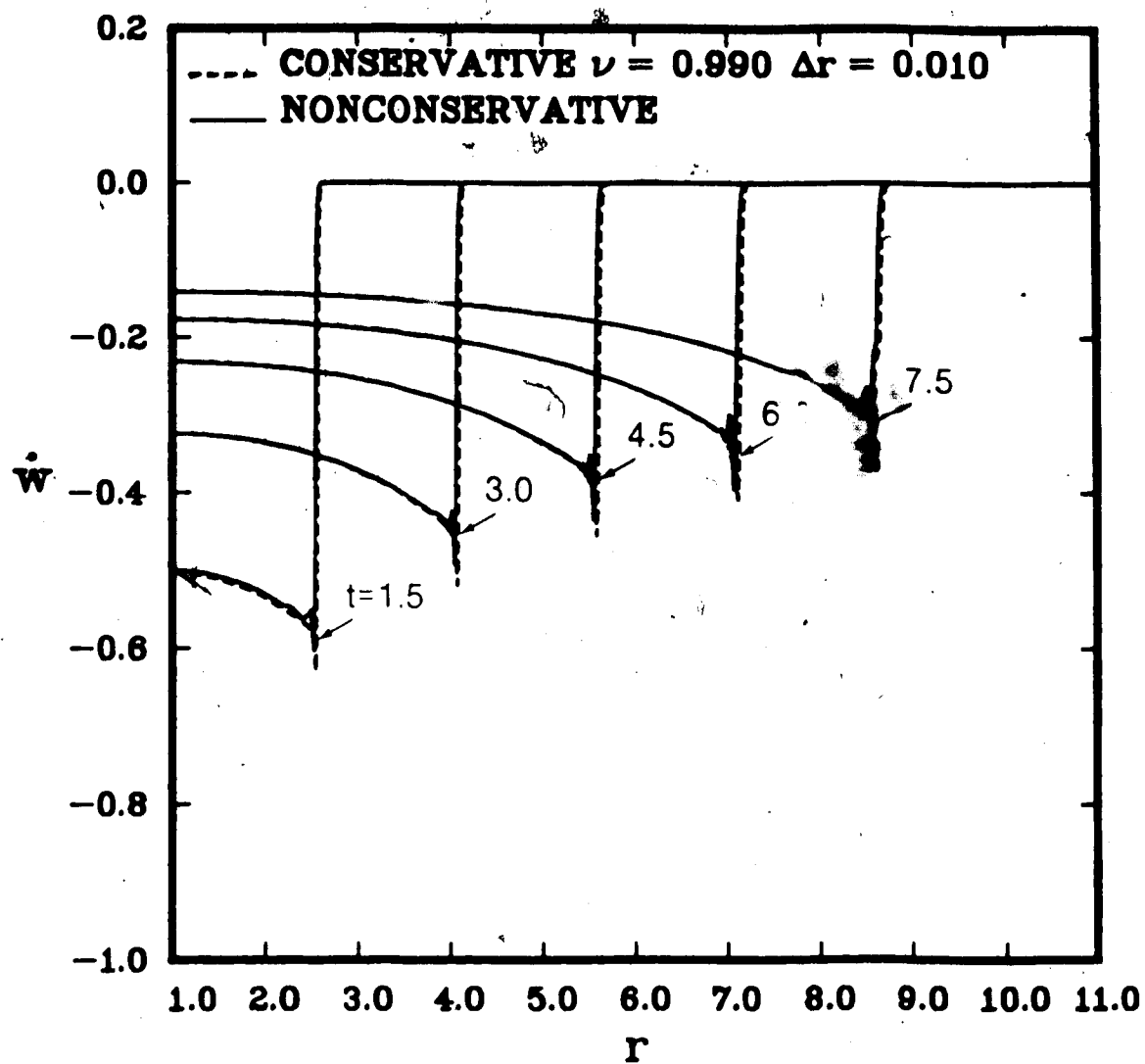


Fig. 4.20 Axial Shear - Variation of nondimensional w with nondimensional r for $\gamma = 0.1$ subject to $\tau(1,t) = \tau_0 H(t)$, with $\tau_0 = 1$ using the conservative and nonconservative MacCormack schemes with $\nu = 0.99$.

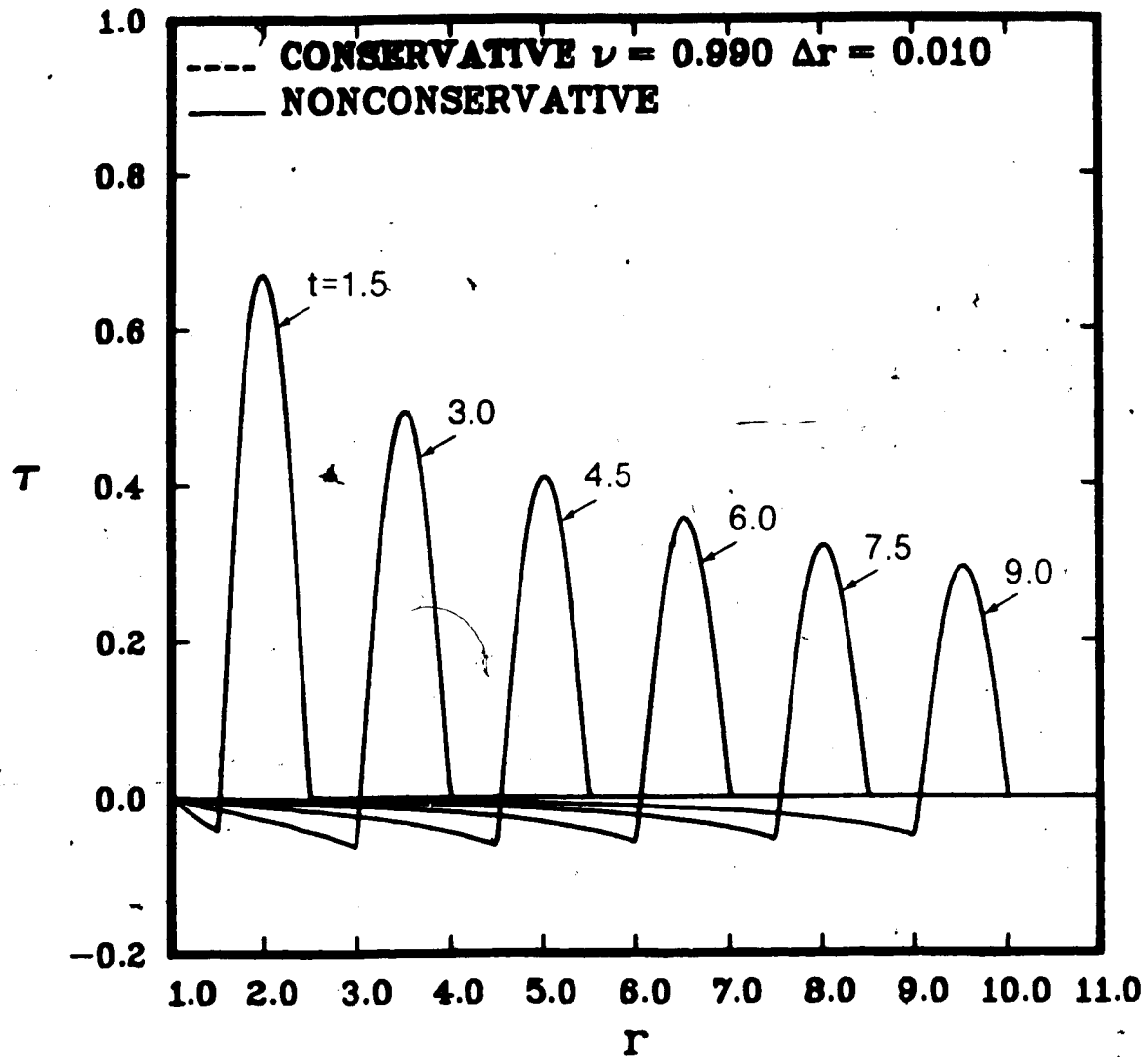


Fig. 4.21 Axial Shear - Variation of nondimensional τ with nondimensional r for $\gamma = 0$ subject to $\tau(1,t) = \tau_0 \sin \pi t H(t) H(1-t)$, with $\tau_0 = 1$ using the conservative and nonconservative MacCormack schemes with $\nu = 0.99$.

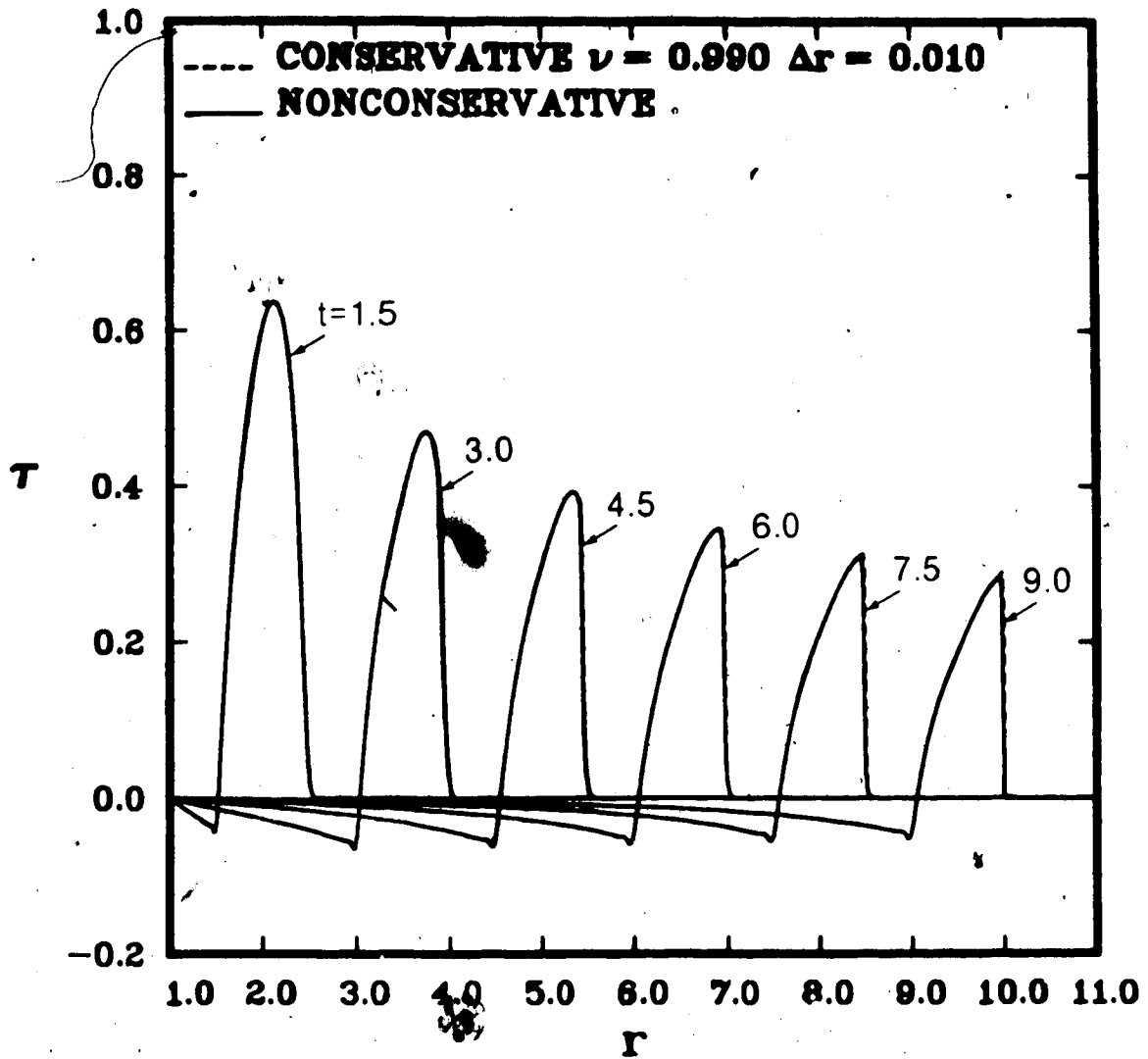


Fig. 4.22 Axial Shear - Variation of nondimensional τ with nondimensional r for $\gamma = 0.1$ subject to $\tau(1,t) = \tau_0 \sin \pi t H(t) H(1-t)$, with $\tau_0 = 1$ using the conservative and nonconservative MacCormack schemes with $\nu = 0.99$.

Table 4.7 Nondimensional Momentum Calculations for Axial Shear subject to $\tau(1,t) = \tau_0 \sin t H(t) H(1-t)$, with $\tau_0 = 1$, and quiescent unstressed initial conditions for $\gamma = 0$ and $\nu = 0.99$. (See Figure 4.21)

Nondimensional Time t	Exact Value of Momentum	Numerically Evaluated Momentum	
		Conservative	Nonconservative
1.5	-0.6366	-0.6365	-0.6365
3.0	-0.6366	-0.6365	-0.6365
4.5	-0.6366	-0.6365	-0.6365
6.0	-0.6366	-0.6365	-0.6365
7.5	-0.6366	-0.6365	-0.6365
9.0	-0.6366	-0.6366	-0.6366

Table 4.8 Nondimensional Momentum Calculations for Axial Shear subject to $\tau(1,t) = \tau_0 \sin t H(t) H(1-t)$, with $\tau_0 = 1$, and quiescent unstressed initial conditions for $\gamma = 0.1$ and $\nu = 0.99$. (See Figure 4.22)

Nondimensional Time t	Exact Value of Momentum	Numerically Evaluated Momentum	
		Conservative	Nonconservative
1.5	-0.6366	-0.6365	-0.6365
3.0	-0.6366	-0.6365	-0.6361
4.5	-0.6366	-0.6369	-0.6267
6.0	-0.6366	-0.6374	-0.6062
7.5	-0.6366	-0.6362	-0.5849
9.0	-0.6366	-0.6364	-0.5658

be taken in interpreting results using nonconservative difference schemes.

In general, the numerical results obtained for axial shear wave propagation using the MacCormack scheme are in good agreement with what is expected theoretically. The presence of the term $B(\underline{U})$ affects the numerical stability of the solutions of the linear system of equations but does not appear to affect the stability of the solutions of the nonlinear system of equations. The numerical results obtained for $\gamma = 0$ have been compared to the method of characteristics. Although none of these results have been included in this analysis, agreement was good.

4.3 Plane Transverse Shear Wave Propagation

4.3.1 Governing Equations

Plane transverse shear wave propagation in an incompressible hyperelastic solid is considered as a test case for the MacCormack scheme, because certain boundary initial value problems can be partially solved using the method of characteristics. The theory for the derivation of the governing equations is similar to that given in Section 4.2 for the axial shear wave problem. The governing equations are derived in reference to previous work done by Haddow (1985).

Transverse shear is defined by the deformation field

$$x_1 = X_1 + \epsilon(t)X_2, \quad x_2 = X_2, \quad x_3 = X_3, \quad (4.43)$$

where (X_1, X_2, X_3) and (x_1, x_2, x_3) are the rectangular Cartesian coordinates of a particle in the undeformed reference and spatial

configurations, respectively, and $\epsilon(t) = \partial u_1 / \partial X_2$ where u_1 is a component of the displacement vector $(u_1, 0, 0)$. The cartesian components of the deformation gradient tensor \underline{F} , where $F_{ik} = \partial x_i / \partial X_k$ and the left Cauchy-Green tensor $\underline{B} = \underline{F}\underline{F}^T$ are

$$\underline{F} = \begin{bmatrix} 1 & \epsilon & 0 \\ 0 & 1 & 0 \\ 0 & 0 & 1 \end{bmatrix} \quad \underline{B} = \begin{bmatrix} 1+\epsilon^2 & \epsilon & 0 \\ \epsilon & 1 & 0 \\ 0 & 0 & 1 \end{bmatrix}$$

and the basic invariants I_1 , I_2 and I_3 are given by

$$I_1 = I_2 = 3 + \epsilon^2, \quad I_3 = 1 \quad (4.45)$$

where $\epsilon = \epsilon(t)$.

The Cauchy stress tensor for an incompressible isotropic hyperelastic material is given in Section 4.2 by equation (4.5). The nonzero components of Cauchy stress for this problem are given by

$$\sigma_x = -p + \frac{2\partial W}{\partial I_1} (1 + \epsilon^2) - \frac{2\partial W}{\partial I_2} \quad (4.46)$$

$$\sigma_y = -p + \frac{2\partial W}{\partial I_1} - \frac{2\partial W}{\partial I_2} (1 + \epsilon^2) \quad (4.47)$$

$$\sigma_z = -p + \frac{2\partial W}{\partial I_1} - \frac{2\partial W}{\partial I_2} \quad (4.48)$$

$$\tau_{yx} = \tau = \frac{2\partial W}{\partial I_1} \epsilon - \frac{2\partial W}{\partial I_2} (-\epsilon) \quad (4.49)$$

with the usual notation for the physical components of Cauchy stress in Cartesian coordinates, and τ is used for the shearing

stress τ_{yx} . The shearing stress $\tau_{yx} = \tau$ can also be regarded as a component of the nominal stress tensor for the simple shear deformation given by equation (4.43). However, the Cauchy shearing stress τ_{xy} is not equal to the corresponding component of the nonsymmetric nominal stress tensor.

The nontrivial equation of motion for plane transverse shear is

$$\frac{\partial \tau}{\partial X} = \rho \ddot{w} \quad (4.50)$$

where, as denoted previously, the superposed dot denotes differentiation with respect to time, and ρ is the constant density and X is used in place of X_2 . In this case, $\dot{w} = \partial u_1 / \partial t$, which is the transverse particle velocity.

The strain energy function which is used for this problem is given by equation (4.16), with $N = 2$. Proceeding in a similar manner to that outlined for the axial shear problem, the strain energy function gives the following nonlinear relation,

$$\tau = \mu (\epsilon + 2\gamma\epsilon^3) \quad (4.51)$$

between τ and ϵ . The form of equation (4.51) to equation (4.17), which gives the axial shear stress in $\gamma = 0$ in equation (4.51), the linear relation of the Mooney-Rivlin material is recovered, and the resulting wave propagation problem is governed by the classical wave equation.

4.3.2 Formulation of the Problem

A homogeneous material half space $X \geq 0$, initially at rest is considered (see Figure 4.3). A spatially uniform shearing stress is applied at the surface of the unbounded half space which is initially unstressed. Two boundary conditions are considered,

$$\tau(0, t) = \tau_0 H(t)$$

or

$$\tau(0, t) = \tau_0 \sin \frac{\pi t}{t^*} H(t) H(t^* - t)$$

(4.52)

and the initial conditions are

$$\tau(X, 0) = 0 \quad \dot{w}(X, 0) = 0$$

(4.53)

where τ_0 and t^* are constants and for the numerical results $t^* = 1$.

It is convenient to introduce

$$\hat{\tau} = \frac{\tau}{\mu}, \quad \hat{w} = \frac{w}{c_0}, \quad \hat{t} = c_0 t, \quad \hat{X} = X$$

(4.54)

which eliminates $c_0 = (\mu/\rho)^{1/2}$ from the governing equations, and the variables given in (4.54) are henceforth referred to as normalized variables.⁶ Henceforth, the normalized variables given by (4.54) are used but the superposed " $\hat{}$ " are omitted.

Substituting equation (4.51) into equation (4.50), and using the normalized variables, gives

⁶ For boundary condition (4.52)2, there is no characteristic length or time so that it is not possible to obtain nondimensional forms for all the variables.

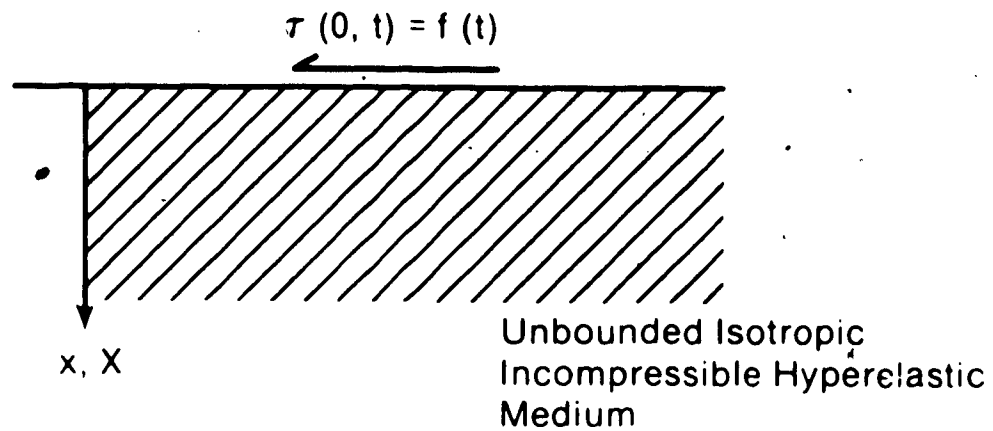


Fig. 4.23 Diagrammatic Representation of Plane Transverse Shear Wave Propagation in an Unbounded Isotropic Incompressible Hyperelastic solid.

$$\frac{\partial \dot{w}}{\partial t} - \frac{\partial (\epsilon + 2\gamma\epsilon^3)}{\partial X} = 0 \quad (4.55)$$

and using the compatibility equation

$$\frac{\partial \epsilon}{\partial t} - \frac{\partial \dot{w}}{\partial X} = 0 \quad (4.56)$$

results in a nonlinear hyperbolic system of partial differential equations of the form

$$\frac{\partial U}{\partial t} + \frac{\partial Q(U)}{\partial X} = 0 \quad (4.57)$$

where

$$\underline{U} = \begin{bmatrix} \dot{w} \\ \epsilon \end{bmatrix} \quad \underline{Q(U)} = \begin{bmatrix} -(\epsilon + 2\gamma\epsilon^3) \\ -\dot{w} \end{bmatrix} \quad (4.58)$$

The conservation form (4.57) can be written in nonconservation form

$$\frac{\partial U}{\partial t} + \underline{A(U)} \frac{\partial U}{\partial X} = 0 \quad (4.59)$$

where the matrix $\underline{A(U)}$ is given as

$$\underline{A(U)} = \begin{bmatrix} 0 & -1 \\ -(1+6\gamma\epsilon^2) & 0 \end{bmatrix} \quad (4.60)$$

and \underline{U} is defined by (4.58)₁.

The eigenvalues of $\underline{A(U)}$ are wave speeds, in this case corresponding to the normalized variables, and are given by

$$c(\epsilon) = \pm (1 + 6\gamma\epsilon^2)^{1/2} \quad (4.61)$$

The slopes of the two families of characteristics in the (X,t) plane are $dx/dt = \pm c$.

The jump conditions for a shock can be found from equations (4.55) and (4.56), and are given by

$$\begin{aligned} [\epsilon + 2\gamma\epsilon^3] - [\tau] &= -V[\dot{w}] \\ [\dot{w}] &= -V[\epsilon] \end{aligned} \quad (4.62)$$

where V is the shock speed, and the square brackets $[\]$ denote the jump. Re-arranging (4.62) gives the shock speed V as

$$V = \left\{ \frac{[\epsilon + 2\gamma\epsilon^3]}{[\epsilon]} \right\}^{1/2} \quad (4.63)$$

Equations (4.63) and (4.31) are of the same form. Equations (4.57) and (4.59) are similar to equations (4.28) and (4.24) except that $\underline{B}(\underline{U}) = 0$. Since $\underline{B}(\underline{U}) = 0$, the system of equations (4.57) or (4.59) can be solved using a simple wave solution until a shock forms (Appendix 2). Therefore, the numerical results obtained using the MacCormack scheme can be compared, for this problem, to the method of characteristics.

4.3.3 Implementation of the MacCormack Scheme

The MacCormack finite difference scheme given by equation (2.6) for the nonconservation form of the equations and by equation (2.7) for the conservation form of equations, is used to solve boundary initial value problems for plane transverse shear in the same manner as that used for axial shear in Section 4.2.3. The numerical scheme is the same as that given in equations

(4.32) and (4.33) except that $\underline{B}(\underline{U}) = \underline{0}$, Δr is replaced by ΔX and $\underline{U}_j = \underline{U}(j\Delta X, n\Delta t)$. The boundary conditions for the conservative and nonconservative schemes are given by (4.34) and (4.35), (4.36), and (4.37) respectively, again, with $\underline{B}(\underline{U}) = \underline{0}$ and Δr replaced by ΔX .

4.3.4 Method of Characteristics

The method of characteristics is used to obtain the solution to boundary initial value problems governed by equations (4.55) and (4.56) with boundary and initial conditions specified by (4.52)₁ or (4.52)₂ and (4.53). Since the term $\underline{B}(\underline{U})$ is not present in equation (4.59) and the wave is propagating into a region of constant state, the solution is a simple wave solution until a shock is formed. The eigenvalues of $\underline{A}(\underline{U})$ have already been derived in equation (4.61); and these give the slopes of the characteristics dX/dt .

For the simple wave solution, the Riemann invariants are given by

$$\bar{w} + g(\epsilon) = \text{constant on } \frac{dX}{dt} = \pm(1 + 6\gamma\epsilon^2)^{1/2}, \quad (4.64)$$

where $g(\epsilon) = (\epsilon + 2\gamma\epsilon^3)$. Since $\bar{w} - \epsilon = 0$ on $t = 0$, due to the initial conditions, $\bar{w} + g(\epsilon) = 0$ on the c^- characteristic so that $\bar{w} = -g(\epsilon)$ in the region where the simple wave solution is valid. It follows (see Figure 4.24) that the characteristics emanating from the t axis are straight lines with the slopes

$$(1 + 6\gamma(\epsilon(0, t_0))^2)^{1/2} = (1 + 6\gamma(f(t_0))^2)^{1/2} = c(f(t_0))$$

where $f(t_0)$ is given by the boundary condition (4.52) solved in

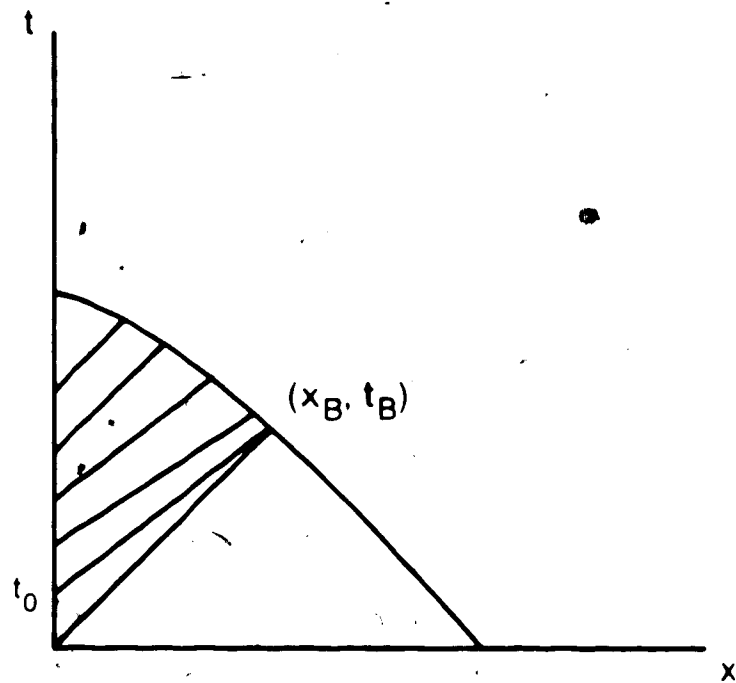


Fig. 4.24 Diagrammatic representation of the method of characteristics applied to the transverse shear problem.

terms of ϵ using equation (4.51). The equations of these c^+ characteristics are

$$t = t_0 + \frac{x}{F(t_0)} \quad (4.65)$$

where $F(t_0) = c(f(t_0))$. The simple wave solution is valid until the c^+ characteristics intersect, then a shock evolves. After intersection, the c^+ characteristics give a multivalued solution which is not physically acceptable. This multivalued solution involves an envelope of the c^+ characteristics which is obtained by eliminating t_0 from equation (4.65) and

$$1 - \frac{x F'(t_0)}{(F(t_0))^2} \quad (4.66)$$

The parametric equations of the envelope, then, become

$$x = \frac{(F(t_0))^2}{F'(t_0)} \quad (4.67)$$

and

$$t = t_0 + \frac{F(t_0)}{F'(t_0)} \quad (4.68)$$

The wave breaks when

$$0 = 2 \frac{F(t_0) F''(t_0)}{(F'(t_0))^2} \quad (4.69)$$

Finding t_0 from equation (4.69) and substituting into equations (4.67) and (4.68) gives (x_B, t_B) where x_B and t_B are the breaking distance and time, respectively. When the boundary condition is (4.52)₁, a shock is initiated at $t = 0$, and there is no simple wave solution. However, when the boundary condition is given by

(4.52)₂, a breaking time t_B can be found, and the simple wave is valid until the wave breaks.

For the boundary condition (4.52)₂, the envelope of characteristics has a cusp at (x_B, t_B) . There is a simple wave solution for the area bounded by the x and t axes and the c^+ characteristic through (x_B, t_B) . Outside this region the c^+ characteristics cross a shock and the Riemann invariant $w + g(\epsilon)$ undergoes a jump across the shock. The argument leading to the characteristics being straight lines is no longer valid, and the simple wave solution breaks down.

Applying this analysis to the problem of plane transverse wave propagation with boundary condition (4.52)₂ and initial conditions (4.53) for $\tau_0 = 1$ and $\gamma = 0.1$ equation (4.69) gives the following breaking conditions

$$\begin{aligned} x_B &= 1.806 \\ t_B &= 1.861 \end{aligned} \quad (4.70)$$

These values were obtained numerically because of the complexity of relation between τ and ϵ given by (4.51), where ϵ must be found in terms of the specified boundary condition for τ .

4.3.5 Momentum and Energy Considerations

Since momentum must be conserved for the problems considered, numerical evaluation of momentum provides a check on the numerical solution. The relation for the momentum, based on the normalized variables (4.54) is

$$\int_0^t \tau(0, \eta) d\eta = \int_0^{X_f(t)} w dX, \quad (4.71)$$

where $X_f(t)$ is the position of the wavefront at time t . The right hand side of equation (4.71) is evaluated numerically using a Simpson's integration scheme. The left hand side is evaluated analytically by substituting the appropriate boundary condition (4.52)₁ or (4.52)₂, and integrating. Tables 4.9 and 4.10 are used to illustrate that the numerical solution satisfies conservation of momentum according to equation (4.71).

Treating the transverse shear problem in a similar manner to the axial shear problem, the mechanical energy is evaluated by considering the sum of the strain and kinetic energies. The mechanical energy in terms of the normalized variables for the problem considered is given by

$$E = \frac{1}{2} \int_0^{X_f(t)} (\epsilon^2 + \gamma \epsilon^4) dX + \frac{1}{2} \int_0^{X_f(t)} (\dot{w})^2 dX \quad (4.72)$$

The same discussion which was given Section 4.2.4 for axial shear, regarding conservation of mechanical energy when $\gamma = 0$ and dissipation of mechanical energy when $\gamma = 0.1$, applies to the plane transverse shear problem.

4.3.6 Numerical Results

The numerical results in this section have been obtained using the conservative version of the MacCormack scheme with $\Delta X = 0.01$, unless otherwise specified. Numerical results are presented for normalized values of τ or w versus normalized X , for normalized times t . Only quiescent unstressed initial conditions (4.53) are considered. In this case τ and w are the normalized transverse shear stress and normalized transverse particle velocity, respectively. Figures 4.25 and 4.26 show the effect of Courant number on the numerical solution τ vs X for boundary condition (4.52)₁, with $\tau_0 = 1$, for $\gamma = 0$, which corresponds to the linear case. There is no instability indicated in either figure, but numerical dispersion is evident in both Figures 4.25 and 4.26, for $\nu = 1.0$ and $\nu = 0.99$, respectively. The numerical dispersion is more severe for $\nu = 0.99$ than for $\nu = 1.0$. Figure 4.27 shows the numerical solution for w which corresponds to the numerical solution for τ given in Figure 4.25, for $\nu = 1.0$. The numerical dispersion evident in the curves in Figure 4.27 for w is similar to that which appears in the curves in Figure 4.25 for τ . The positions of the wavefront are the same in both figures, and are located at $X = t$, which is in complete agreement with theoretical considerations.

Figures 4.28 and 4.29 show the numerical results obtained for boundary condition (4.52)₁, with $\tau_0 = 1$, for $\gamma = 0.1$ and Courant numbers of $\nu = 1.0$ and $\nu = 0.99$, respectively. The oscillations behind the wavefront, which indicate numerical

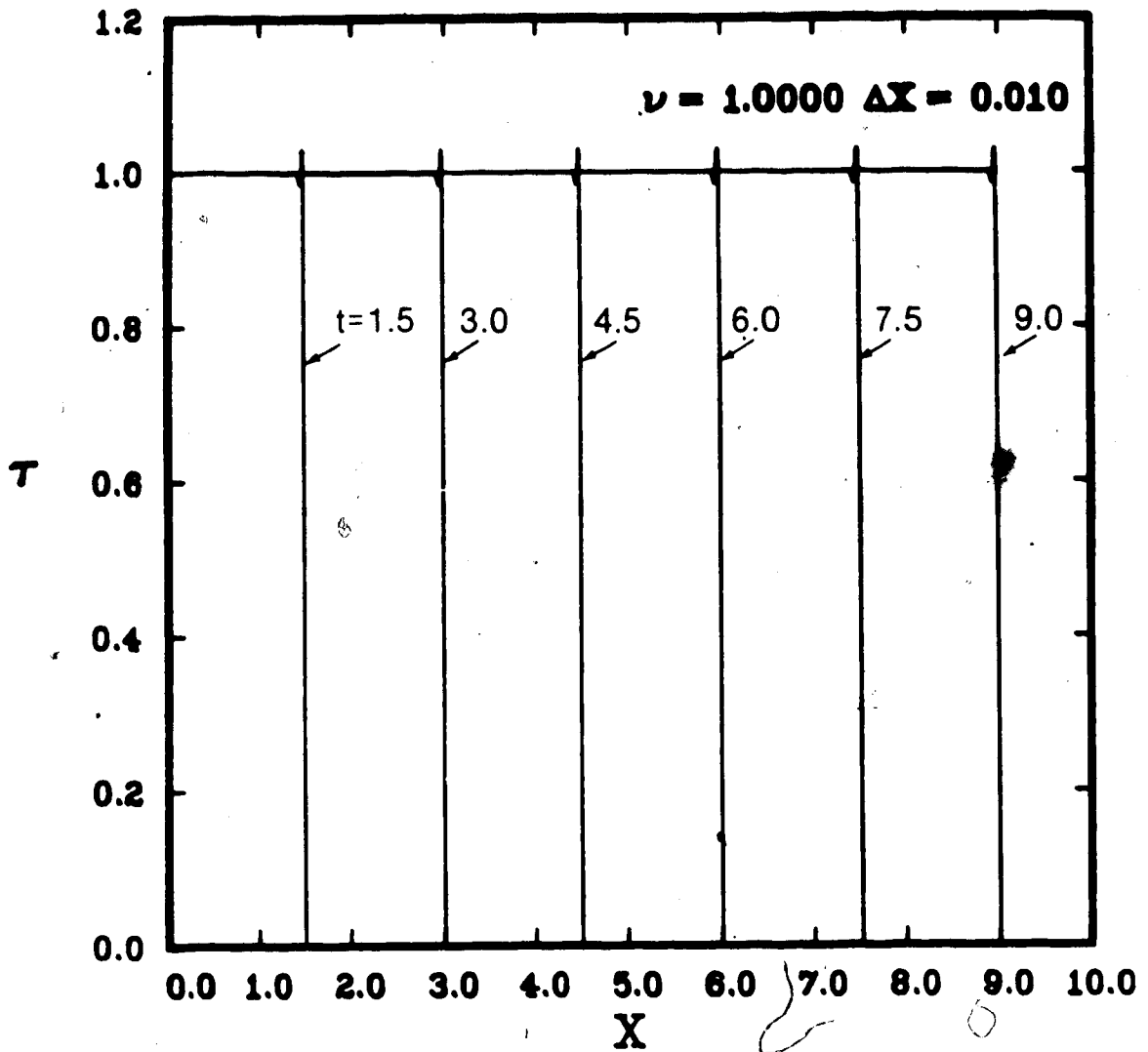


Fig. 4.25 Transverse Shear - Variation of normalized τ with normalized X for $\gamma = 0$ subject to $\tau(0,t) = \tau_0 H(t)$, with $\tau_0 = 1$ using the MacCormack scheme with $\nu = 1.0$.

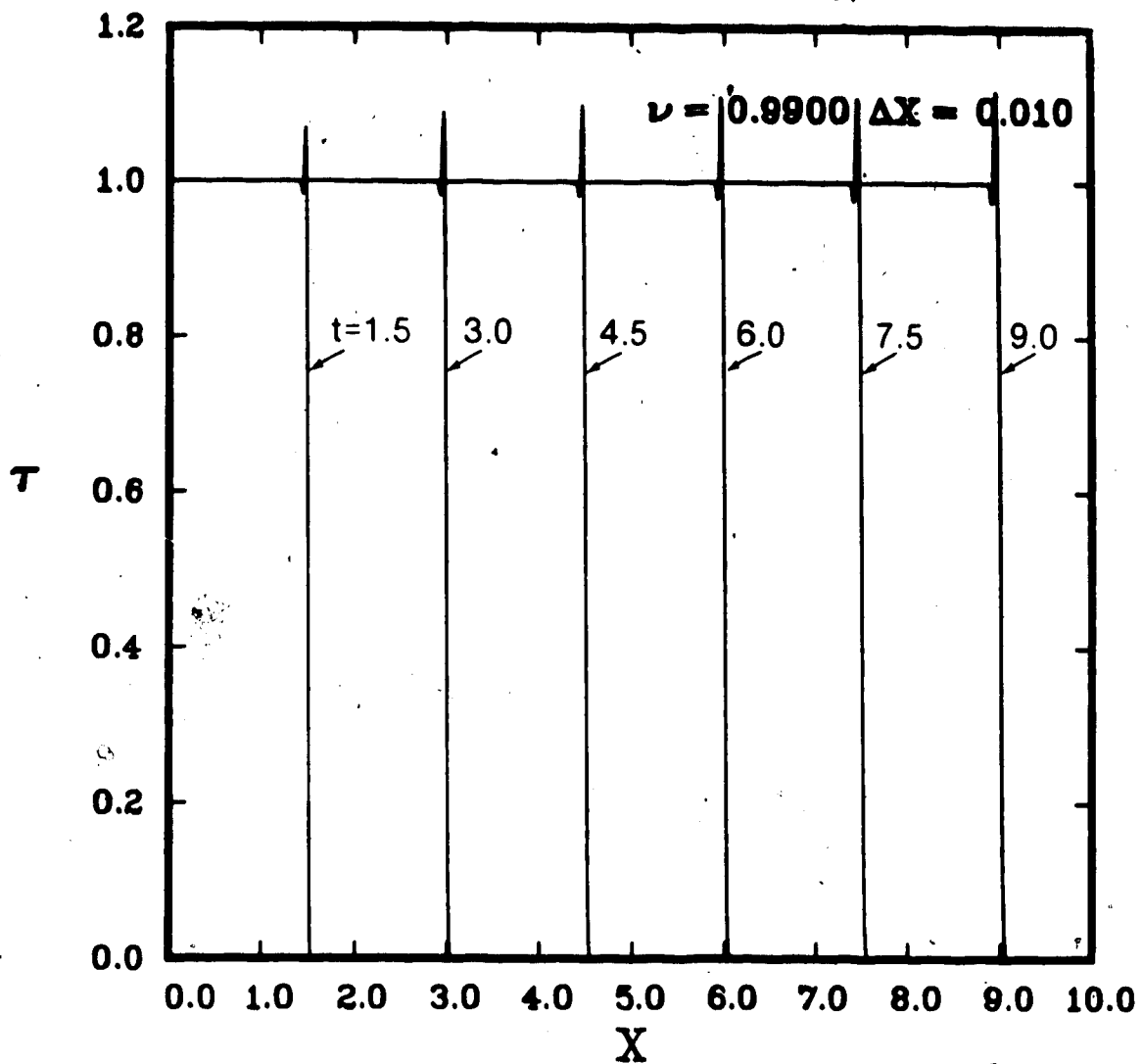


Fig. 4.26 Transverse Shear - Variation of normalized τ with normalized X for $\gamma = 0$ subject to $\tau(0, t) = \tau_0 H(t)$, with $\tau_0 = 1$ using the MacCormack scheme with $\nu = 0.99$.

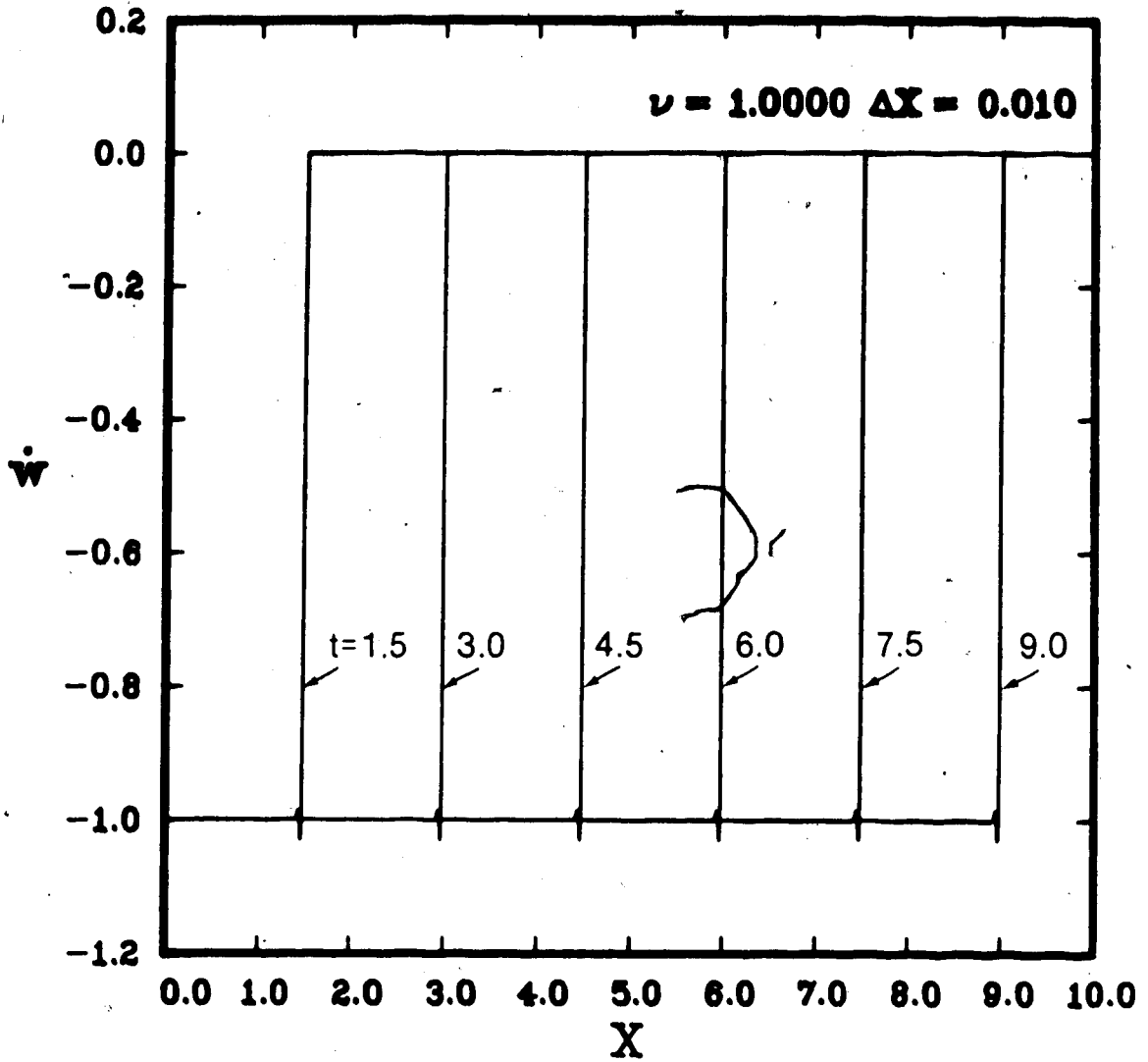


Fig. 4.27 Transverse Shear - Variation of normalized \dot{w} with normalized X for $\gamma = 0$ subject to $\tau(0,t) = \tau_0 H(t)$, with $\tau_0 = 1$ using the MacCormack scheme with $\nu = 1.0$.

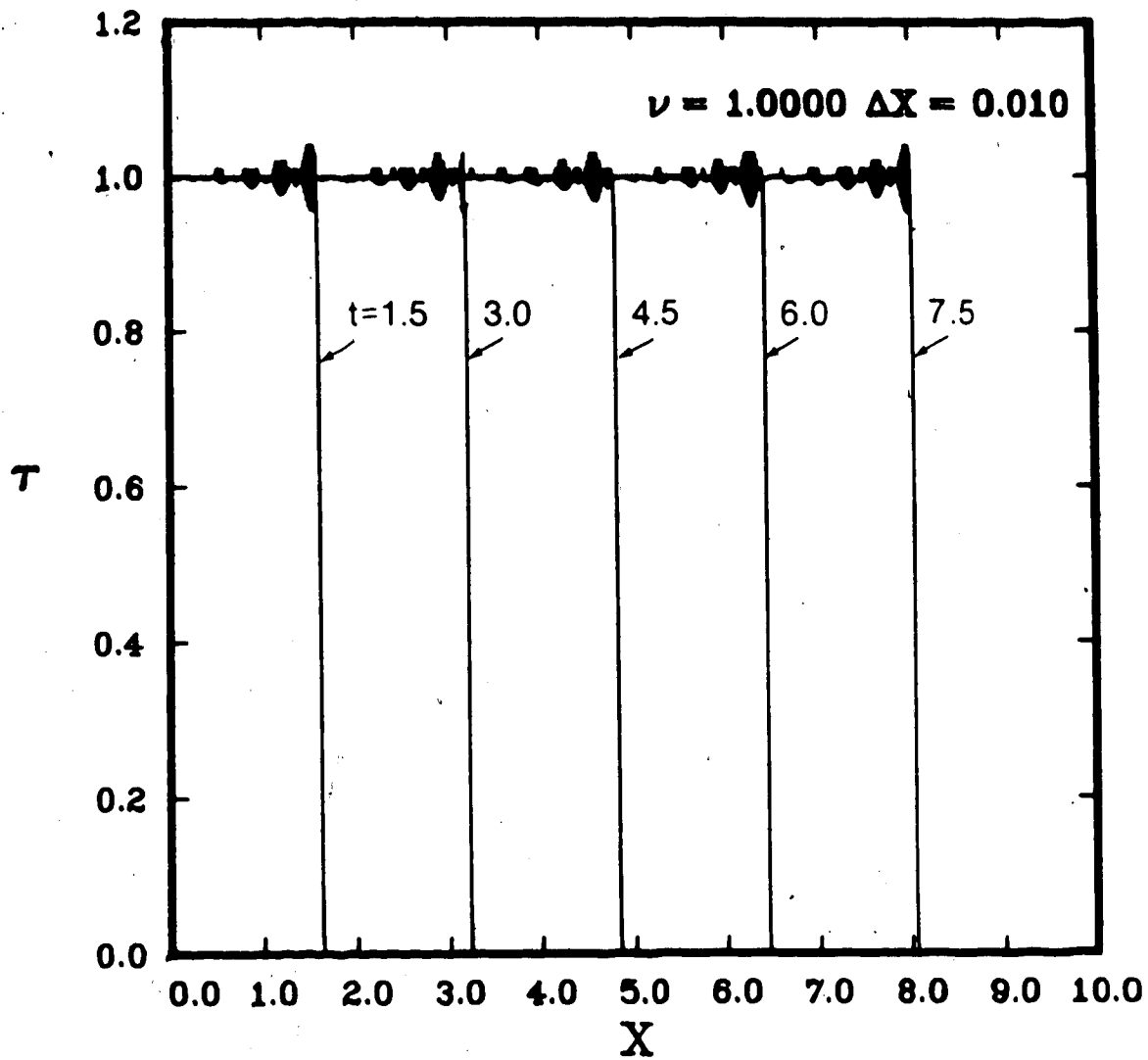


Fig. 4.28 Transverse Shear - Variation of normalized τ with normalized X for $\gamma = 0.1$ subject to $\tau(0,t) = \tau_0 H(t)$, with $\tau_0 = 1$ using the MacCormack scheme with $\nu = 1.0$.

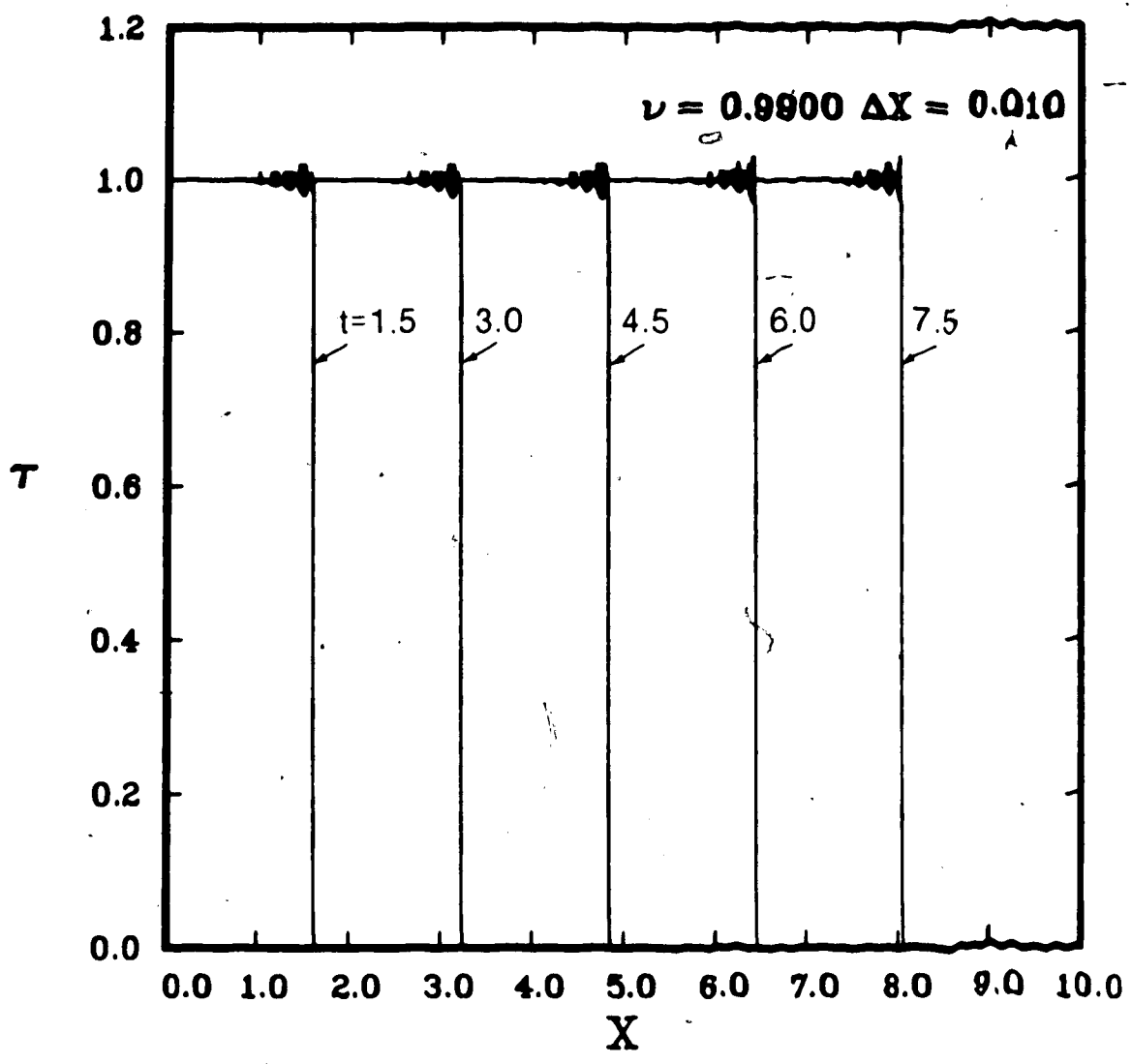


Fig. 4.29 Transverse Shear - Variation of normalized τ with normalized X for $\gamma = 0.1$ subject to $\tau(0,t) = \tau_0 H(t)$, with $\tau_0 = 1$ using the MacCormack scheme with $\nu = 0.99$.

dispersion, are more severe for $\nu = 1.0$ than for $\nu = 0.99$. The oscillations which occur behind the wavefront in the numerical solutions obtained for $\gamma = 0.1$ (Figures 4.28 and 4.29) are qualitatively different from the oscillations which occur behind the wavefront in the numerical solutions obtained for $\gamma = 0$ (Figures 4.25 and 4.26). This could be due to the nonlinearity of the governing system of equations for $\gamma = 0.1$. Figure 4.30 shows the numerical solution for \dot{w} which corresponds to the numerical solution for τ given in Figure 4.28, for $\nu = 1.0$. The oscillations which occur behind the wavefront in the curves presented for \dot{w} are similar to the oscillations which appear in the curves presented for τ in Figure 4.28. The position of the wavefront for a given time t is the same in both figures. In Figures 4.28 - 4.30 the wavefront is not located at $X = t$, but is located ahead of this position. This is consistent with equation (4.63) for the shock speed, which indicates that $V > 1$, for $\gamma = 0.1$.

The variation of τ and \dot{w} with X for boundary condition (4.52)₂, with $\tau_0 = 1$, obtained from the MacCormack scheme with $\nu = 1.0$ is shown in Figures 4.31 and 4.32 for $\gamma = 0$ and in Figures 4.33 and 4.34 for $\gamma = 0.1$. The numerical results presented in Figures 4.31 and 4.32 represent the propagation of a sine pulse for various times t , with no shock formation. The wavefront is located at $X = t$. The numerical results in Figures 4.33 and 4.34 indicate the evolution of a shock, since the wave appears to be broken for $t \geq 3.0$. The representation of a shock given by the MacCormack

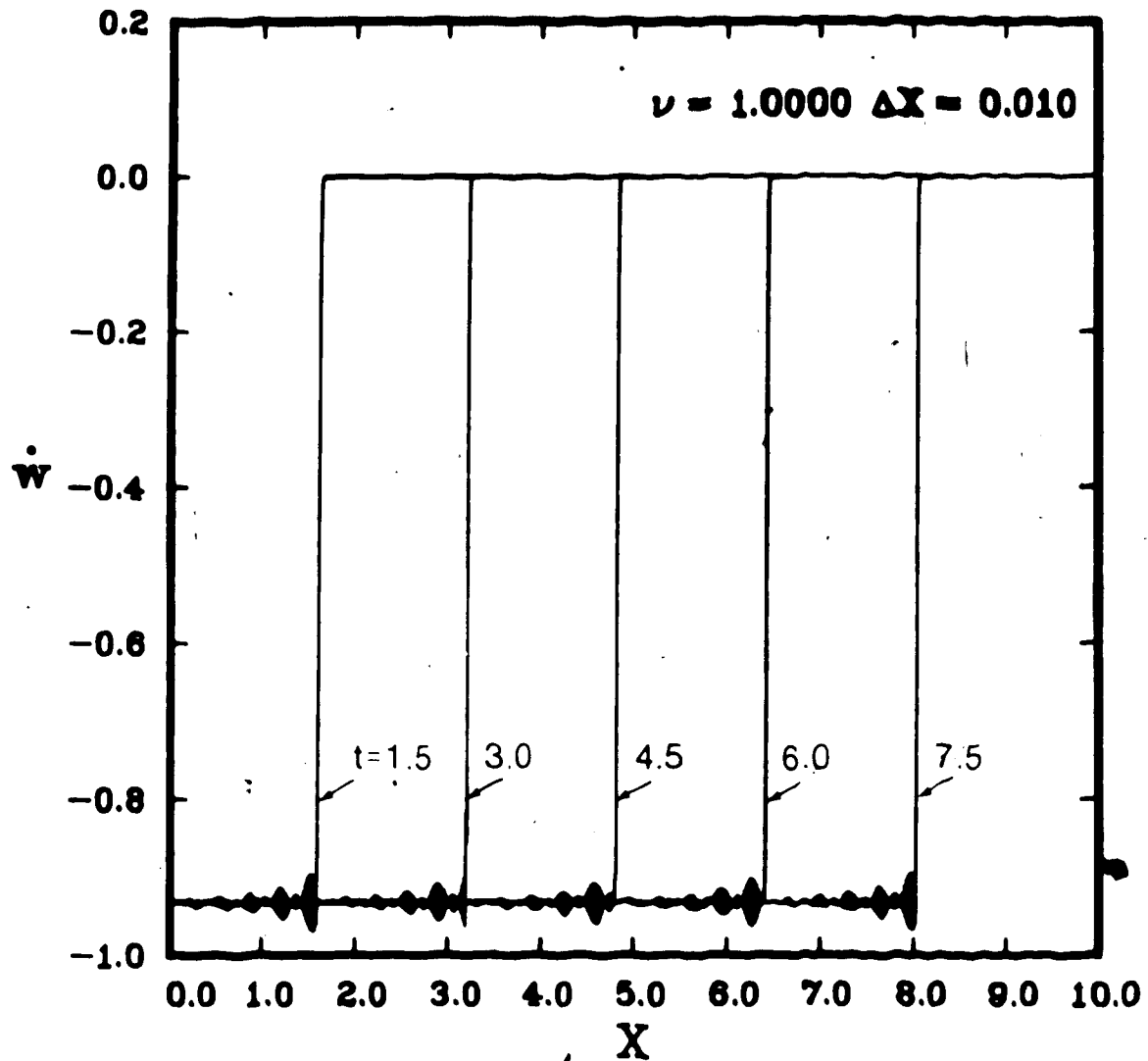


Fig. 4.30 Transverse Shear - Variation of normalized \dot{w} with normalized X for $\gamma = 0.1$ subject to $\tau(0,t) = \tau_0 H(t)$, with $\tau_0 = 1$ using the MacCormack scheme with $\nu = 1.0$.

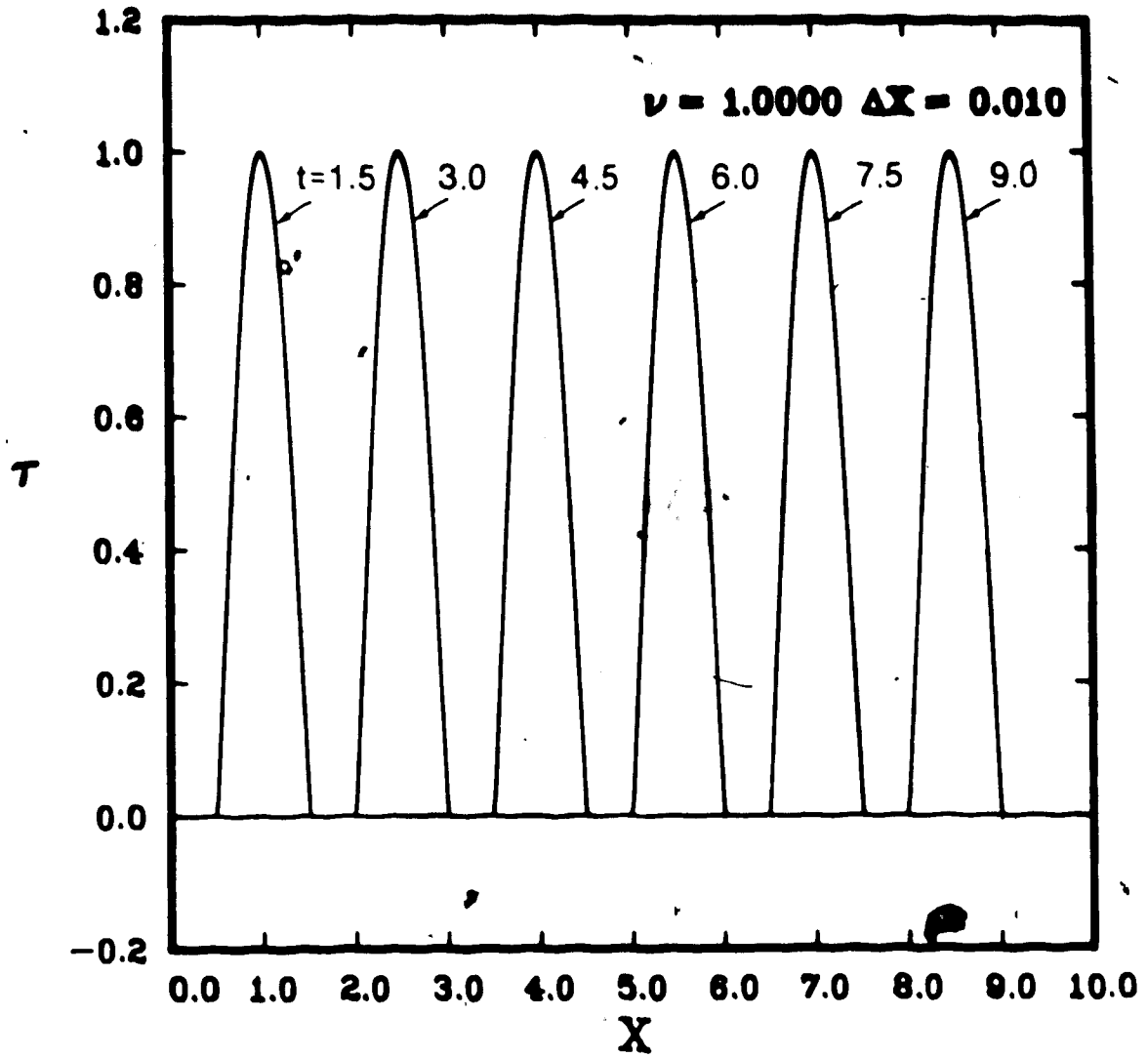


Fig. 4.31 Transverse Shear - Variation of normalized τ with normalized X for $\gamma = 0$ subject to $\tau(0,t) = \tau_0 \sin \pi t H(t) H(1-t)$, with $\tau_0 = 1$ using the MacCormack scheme with $\nu = 1.0$.

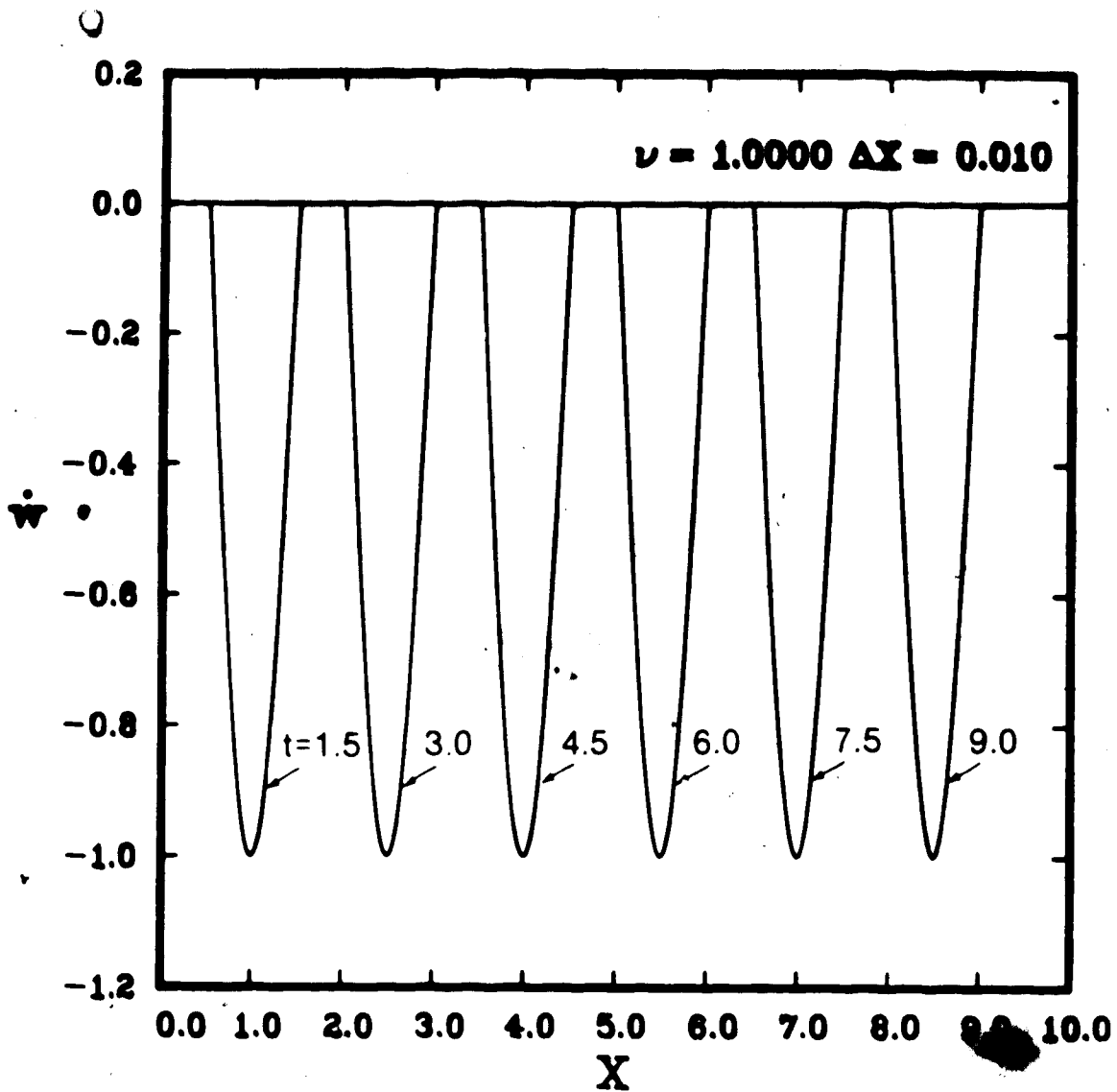


Fig. 4.32 Transverse Shear - Variation of normalized w with normalized X for $\gamma = 0$ subject to $r(0,t) = r_0 \sin \pi t H(t) H(1-t)$, with $r_0 = 1$ using the MacCormack scheme with $\nu = 1.0$.

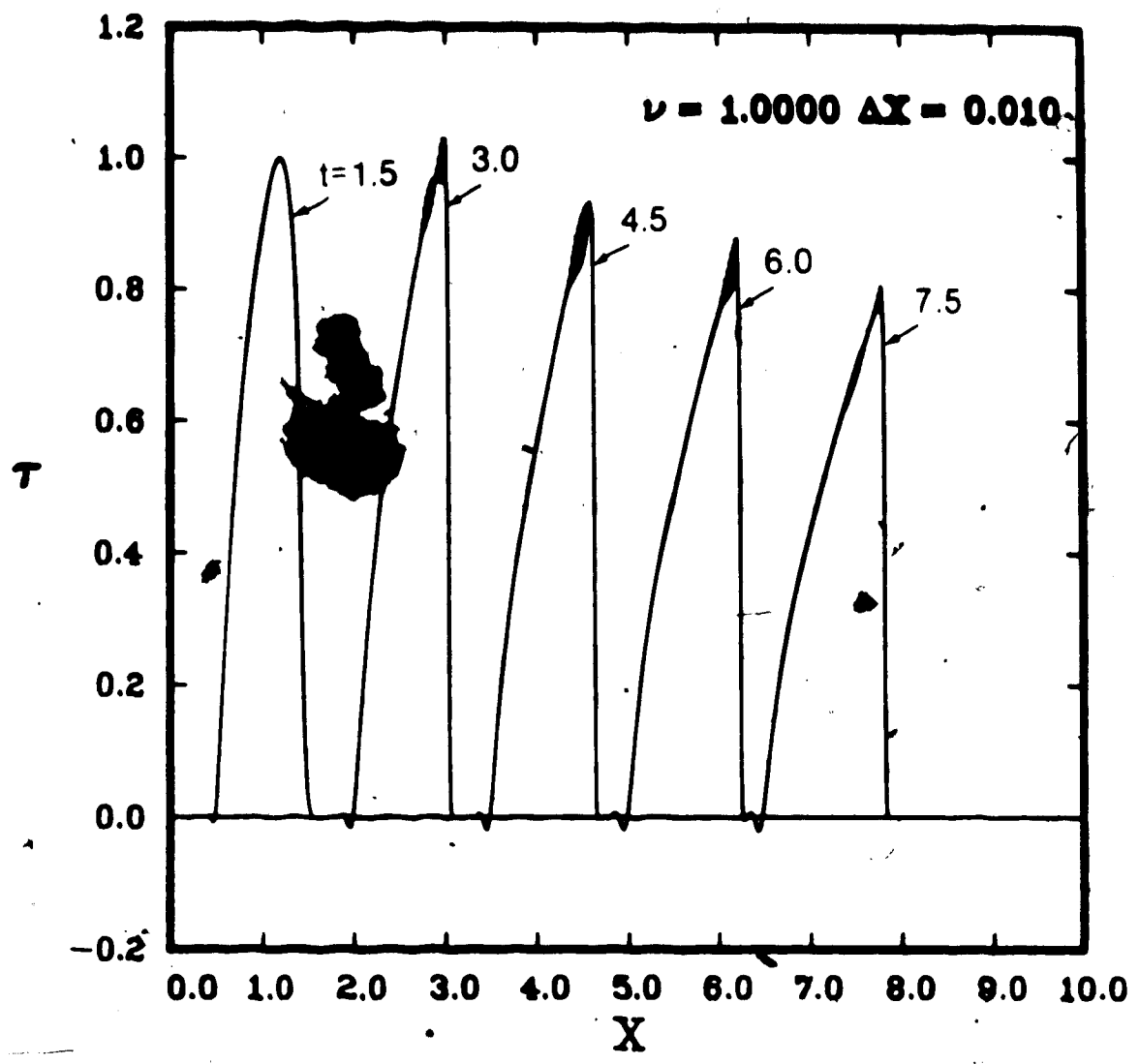


Fig. 4.33 Transverse Shear - Variation of normalized τ with normalized X for $\gamma = 0.1$ subject to $\tau(0,t) = \tau_0 \sin \pi t H(t) H(1-t)$, with $\tau_0 = 1$ using the MacCormack scheme with $\nu = 1.0$.

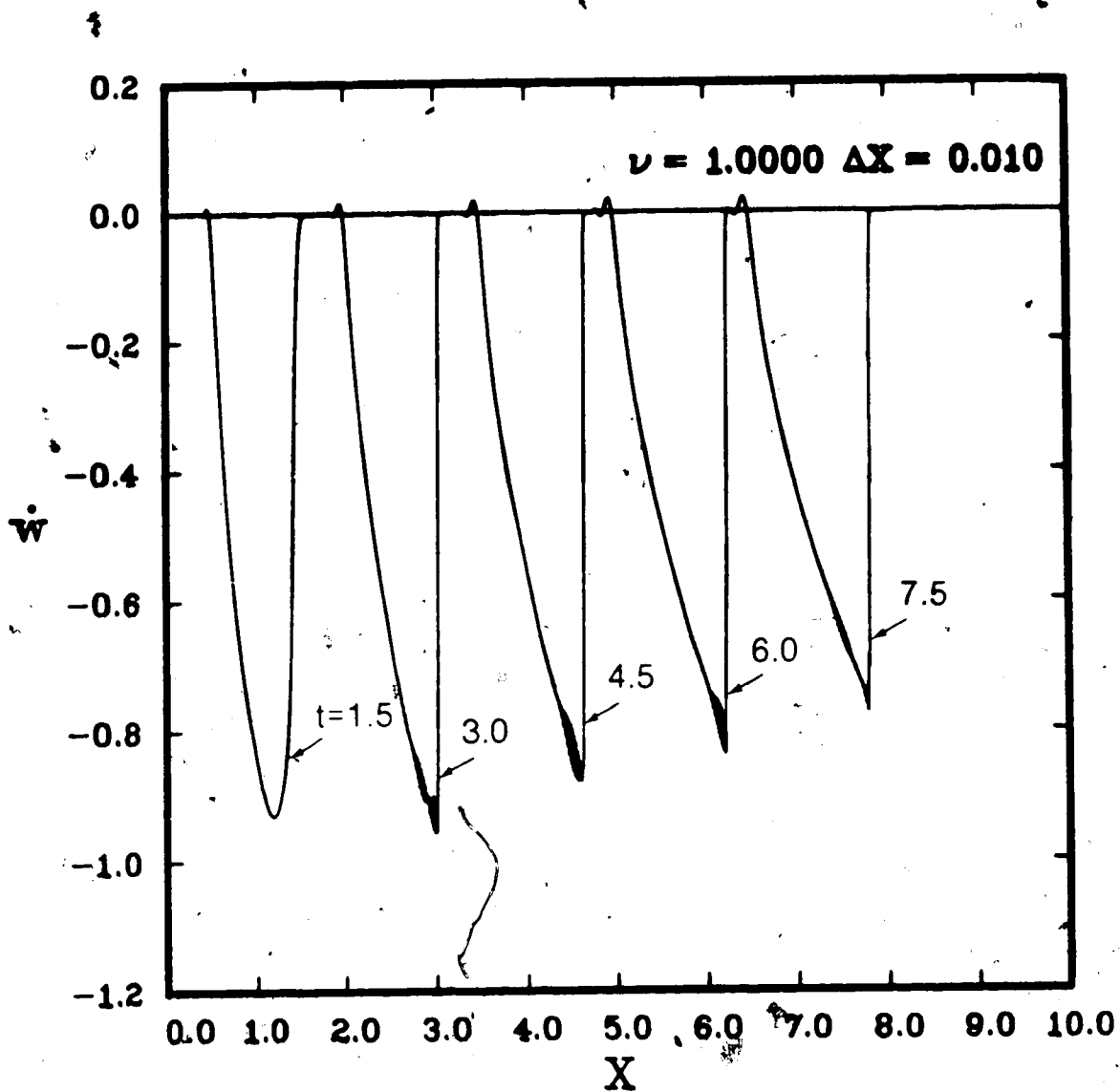


Fig. 4.34 Transverse Shear - Variation of normalized w with normalized X for $\gamma = 0.1$ subject to $\tau(0,t) = \sin \pi t H(t) H(1-t)$, with $\tau_0 = 1$ using the MacCormack scheme with $\nu = 1.0$.

scheme is spread over several mesh intervals. Consequently, an accurate determination of the breaking time is not possible. Figure 4.35 shows the variation of τ with X obtained using the MacCormack scheme for boundary condition (4.52)₂, with $\tau_0 = 1$ and $\nu = 0.99$. The oscillations which appear immediately behind the wavefront for $t > 1.5$, are less severe for $\nu = 0.99$ than for $\nu = 1.0$ (see Figure 4.33). For the times indicated, it appears that the oscillations behind the wavefront appear after the wave breaks. Figure 4.36 gives numerical results for boundary condition (4.52)₂, with $\tau_0 = 1$ and $\nu = 0.99$ which are similar to the results presented in Figure 4.35, except that the time increment between two successive curves is smaller. Figure 4.36 demonstrates that representation of the shock front is not a discontinuity, but is smeared over several mesh intervals. A kink occurs in stress curve, τ vs X , at $t = 1.95$. This could correspond to shock formation. The breaking time calculated using the method of characteristics is $t_B = 1.861$. Although it is difficult to obtain an accurate representation of the shock front using the MacCormack scheme, the numerical results are consistent with theoretical predictions.

Momentum and energy considerations provide a check on the numerical results, since the results are not valid if momentum conservation is violated. Table 4.9 gives normalized values for momentum and mechanical energy calculations according to (4.71) and (4.72), for the numerical results presented in Figure 4.36. Momentum is conserved for the times indicated, and there appears to

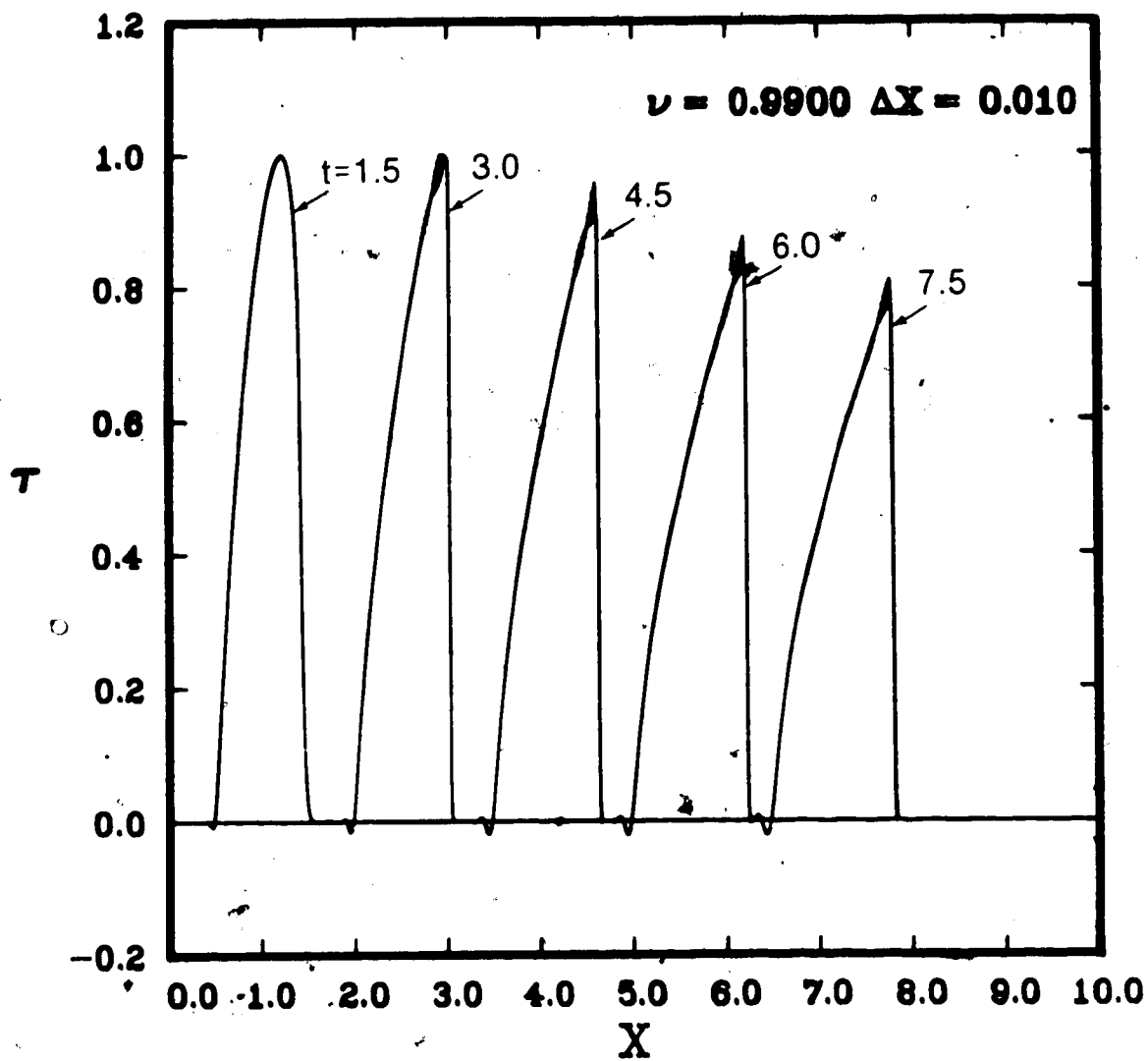


Fig. 4.35 Transverse Shear - Variation of normalized τ with normalized X for $\gamma = 0.1$ subject to $\tau(0, t) = \tau_0 \sin \pi t H(t) H(1-t)$, with $\tau_0 = 1$ using the MacCormack scheme with $\nu = 0.99$.

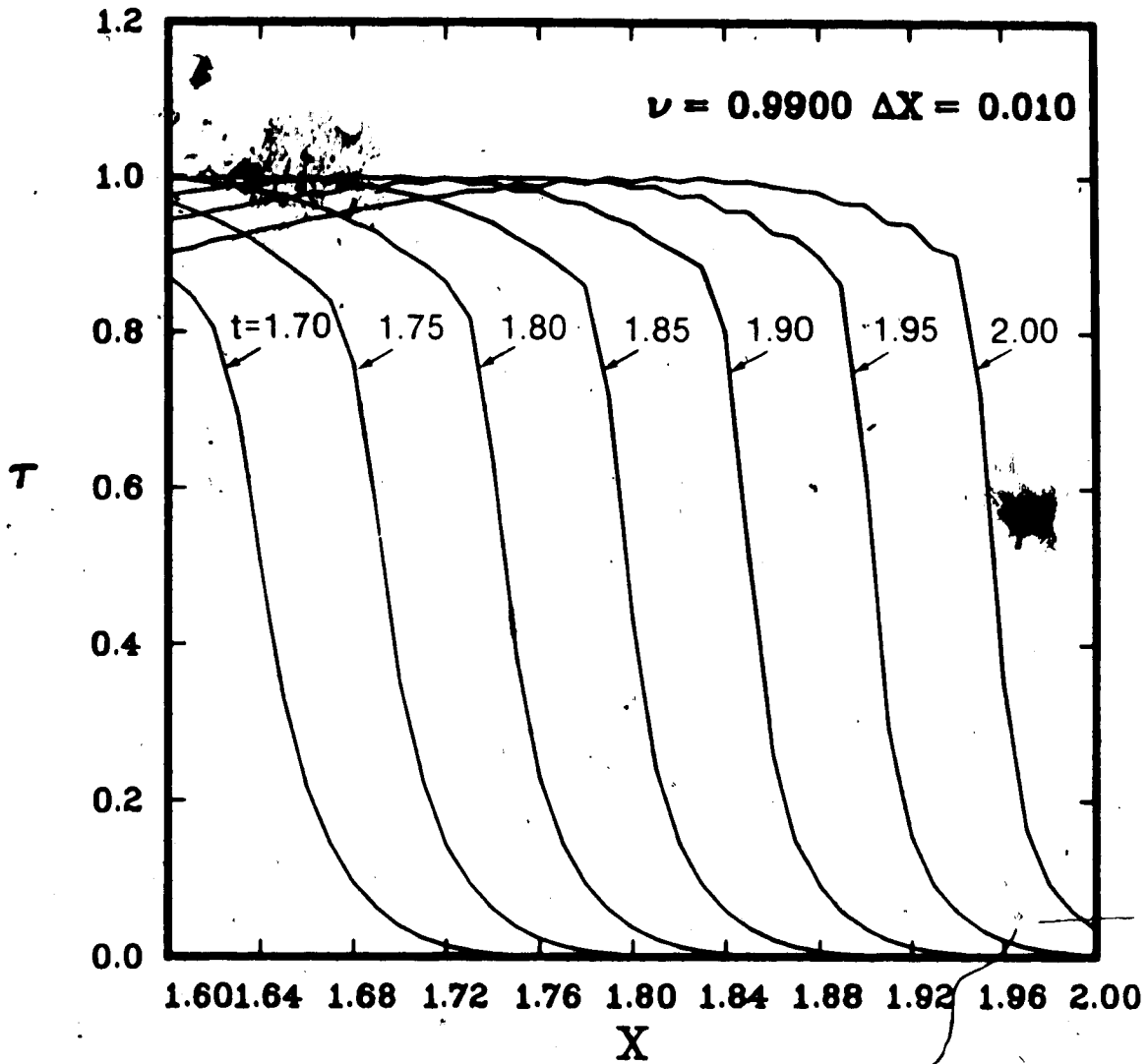


Fig. 4.36 Transverse Shear - Variation of normalized τ with normalized X for $\gamma = 0.1$ subject to $\tau(0,t) = \tau_0 \sin \pi t H(t) H(1-t)$, with $\tau_0 = 1$ using the MacCormack scheme with $\nu = 0.99$.

Table 4.9 Normalized Momentum Calculations and Energy Calculations for Transverse Shear subject to $\tau(1,t) = \tau_0 \sin t H(t) H(1-t)$, with $\tau_0 = 1$, and quiescent unstressed initial conditions for $\gamma = 0.1$ and $\nu = 0.99$.
(See Figure 4.36)

Normalized Time t	Exact Value of Momentum	Numerically Evaluated Momentum	Numerically Eval. Mechanical Energy
1.70	-0.6366	-0.6365	0.4716
1.75	-0.6366	-0.6365	0.4715
1.80	-0.6366	-0.6366	0.4713
1.85	-0.6366	-0.6364	0.4710
1.90	-0.6366	-0.6365	0.4708
1.95	-0.6366	-0.6367	0.4703
2.00	-0.6366	-0.6363	0.4695

Table 4.10 Normalized Momentum Calculations and Energy Calculations for Transverse Shear subject to $\tau(1,t) = \tau_0 \sin t H(t) H(1-t)$, with $\tau_0 = 0.01$, and quiescent unstressed initial conditions and $\nu = 0.99$.
(See Figure 4.37)

Normalized Time t	Exact Value of Momentum	Numerically Eval. Momentum ($\times 10^2$)		Numerically Eval. Mech. Energy ($\times 10^4$)	
		$\gamma = 0$	$\gamma = 0.1$	$\gamma = 0$	$\gamma = 0.1$
1.5	-0.6366	-0.6365	-0.6366	0.4996	0.4997
3.0	-0.6366	-0.6365	-0.6365	0.4996	0.4996
4.5	-0.6366	-0.6365	-0.6365	0.4995	0.4996
6.0	-0.6366	-0.6364	-0.6365	0.4995	0.4995
7.5	-0.6366	-0.6364	-0.6364	0.4994	0.4994
9.0	-0.6366	-0.6364	-0.6364	0.4994	0.4994

be a significant decrease in mechanical energy after $t = 1.95$. When a shock forms, mechanical energy is dissipated, and since the theory presented in this section is based solely on mechanical considerations, the energy should decrease after a shock forms. The numerical results are consistent with conservation of momentum and dissipation of mechanical energy after shock formation.

Figure 4.37 gives a comparison of the numerical results obtained with $\gamma = 0$ to those obtained with $\gamma = 0.1$, for boundary condition $(4.52)_2$, with $r_0 = 0.01$. The curves, for the times considered, are almost identical. This is consistent with theoretical predictions, since the solution of the nonlinear problem ($\gamma = 0.1$) should approach the solution for the linear problem as the amplitude of the wave approaches zero. Table 4.10 contains normalized momentum and energy calculations according to (4.71) and (4.72), which correspond to Figure 4.37. Momentum and mechanical energy are conserved for $\gamma = 0$ and $\gamma = 0.1$. This is consistent with theoretical predictions, since a shock has not yet evolved for $\gamma = 0.1$.

In Figure 4.38 numerical results obtained for $\gamma = 0.1$ using the conservative MacCormack scheme are compared with those obtained using a nonconservative difference scheme for boundary condition $(4.52)_1$, with $r_0 = 1$ and $\nu = 0.99$. The results obtained using the nonconservative difference scheme are significantly different than those obtained using the conservative scheme, and conservation of momentum, evaluated numerically according to equation (4.72), is not satisfied. Figure 4.39 shows similar results for boundary

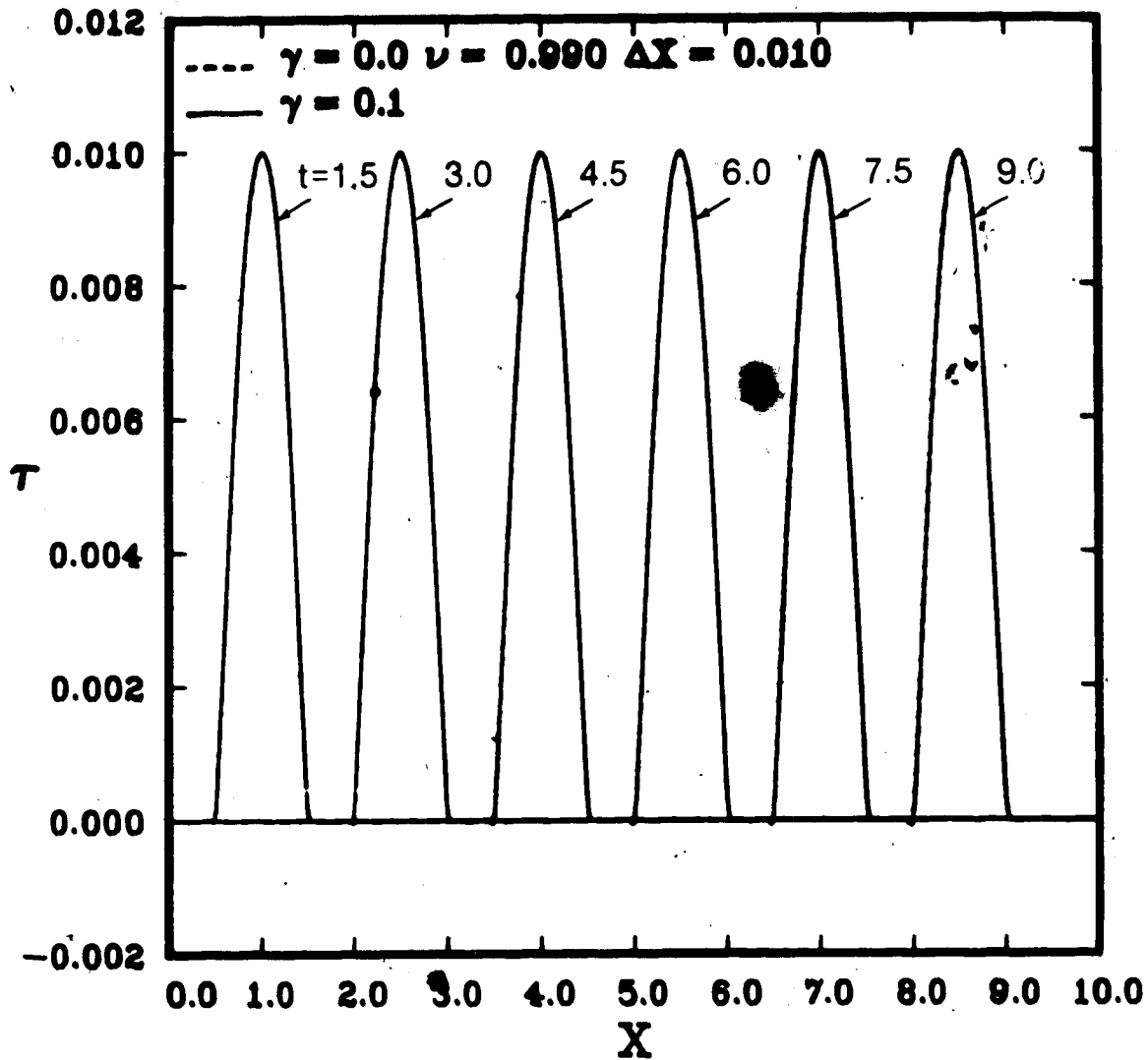


Fig. 4.37 Transverse Shear. A comparison of the numerical results obtained for τ vs X with $\gamma = 0$ to those obtained with $\gamma = 0.1$, subject to $\tau(0,t) = \tau_0 \sin \pi t H(t) H(1-t)$, with $\tau_0 = 0.01$ using the MacCormack scheme with $\nu = 0.99$.

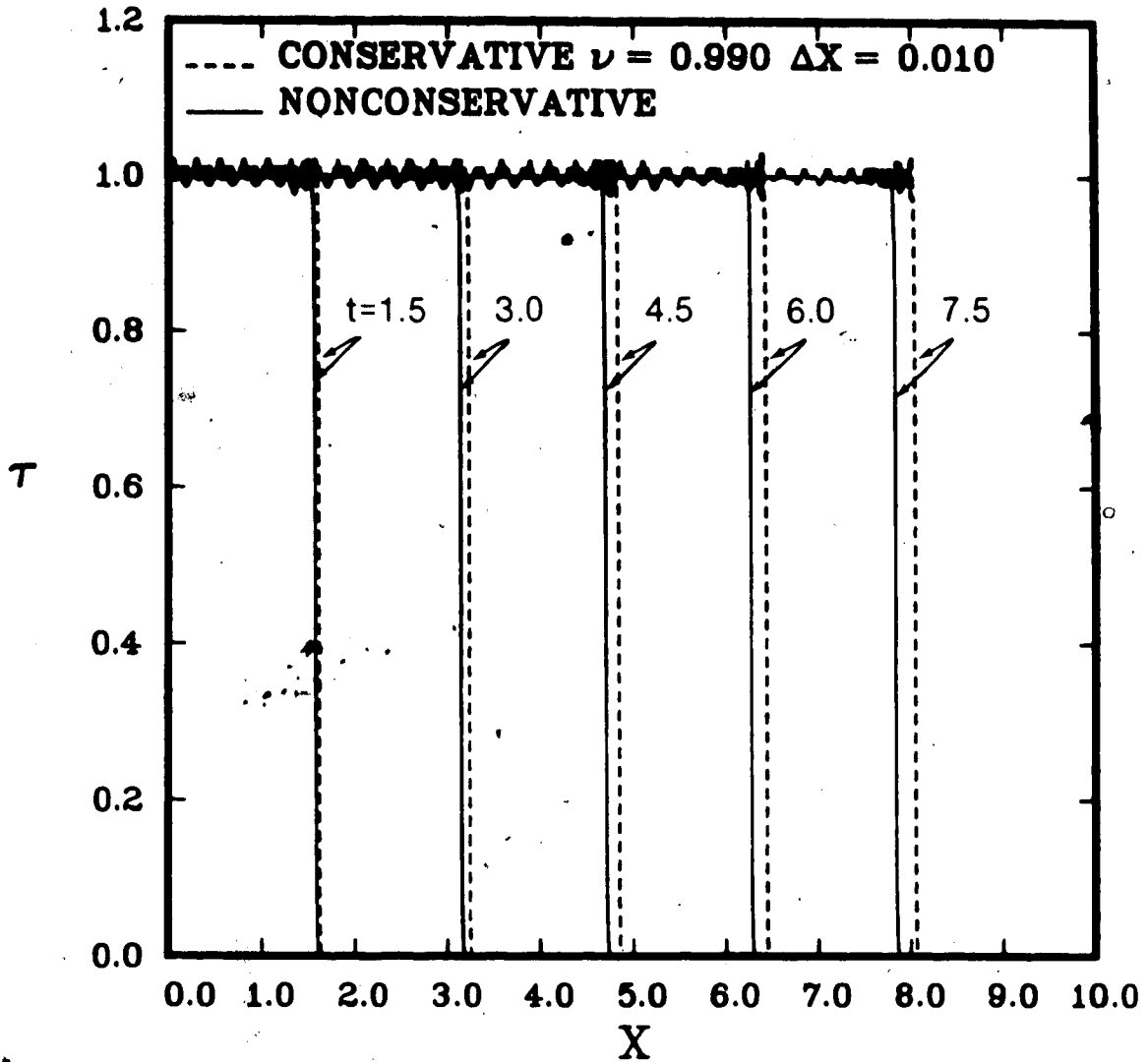


Fig. 4.38 Transverse Shear - Variation of normalized τ with normalized X for $\gamma = 0.1$ subject to $\tau(0,t) = \tau_0 H(t)$, with $\tau_0 = 1$ using the conservative and nonconservative MacCormack schemes with $\nu = 0.99$.

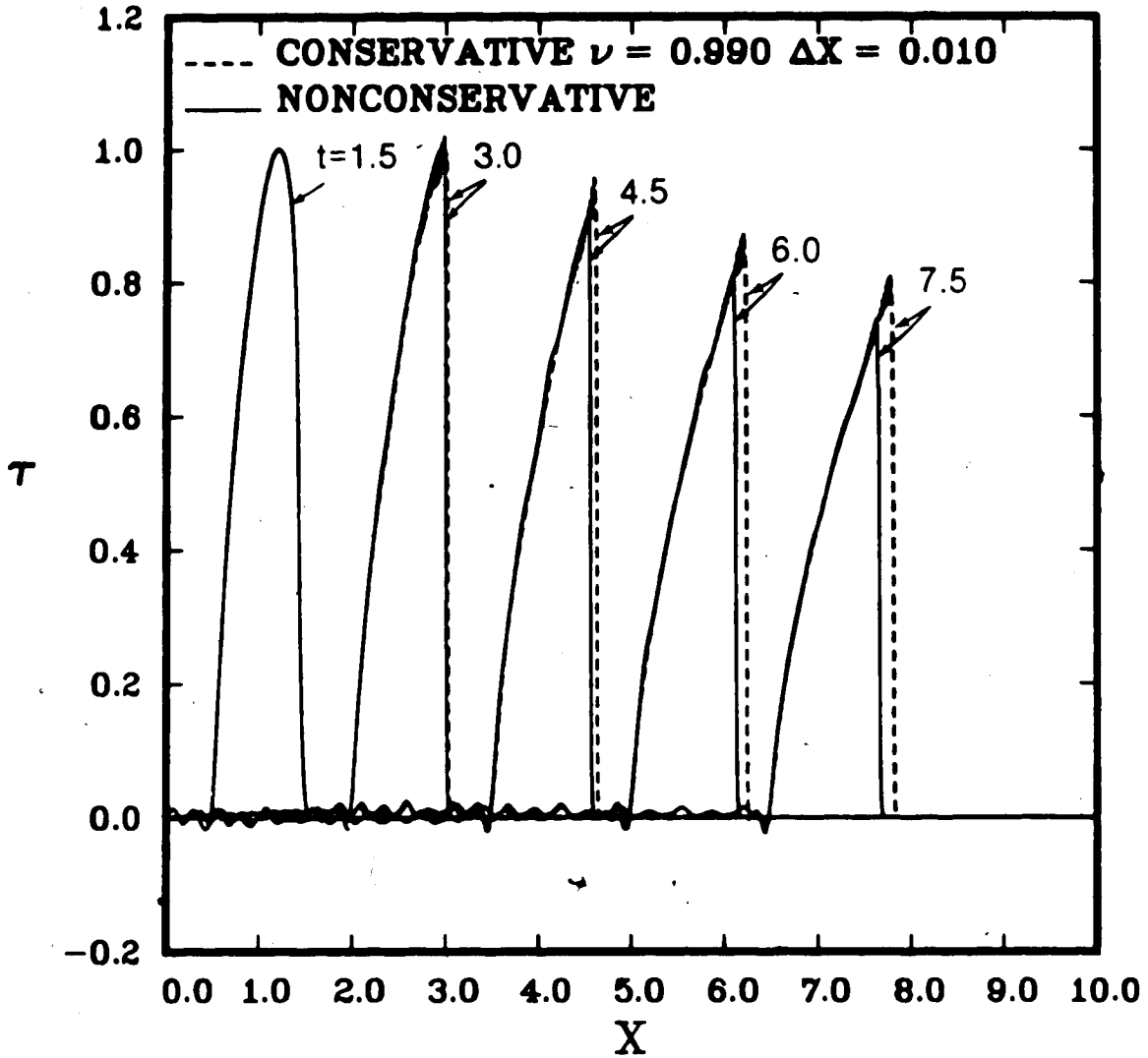


Fig. 4.39 Transverse Shear - Variation of normalized τ with normalized X for $\gamma = 0.1$ subject to $\tau(0,t) = \tau_0 \sin \pi t H(t) H(1-t)$, with $\tau_0 = 1$ using the conservative and nonconservative MacCormack schemes with $\nu = 0.99$.

condition (4.52)₂, with $r_0 = 1$. The jump conditions given by equation (4.62) are not satisfied at $t = 7.5$.

In Figure 4.40 numerical results obtained for $\gamma = 0$ using the conservative MacCormack scheme are compared to those obtained using the nonconservative difference scheme, for boundary condition (4.52)₂, with $r_0 = 1$ and $\nu = 0.99$. Since the governing equations are linear for $\gamma = 0$, there should be no difference. The numerical results are consistent with this expectation. Momentum and energy, evaluated numerically, are conserved.

4.4 Combined Axial and Torsional Shear Wave Propagation

4.4.1 Governing Equations

Combined axial and torsional shear wave propagation in an incompressible isotropic hyperelastic solid is considered. The theory used in the derivation of the governing equations is similar to that given in Sections 4.2 and 4.3 for axial shear and plane transverse shear, respectively. Odgen (1984) and Spencer (1980) provide a more detailed treatment of the finite deformation theory.

Combined axial and torsional shear is defined by the deformation field

$$r = R, \quad \theta = \Theta + \alpha(R, t), \quad z = Z + w(R, t), \quad (4.73)$$

where (R, Θ, Z) and (r, θ, z) are the cylindrical polar coordinates of a particle in the undeformed reference configuration and spatial configuration, respectively, and since quiescent initial conditions

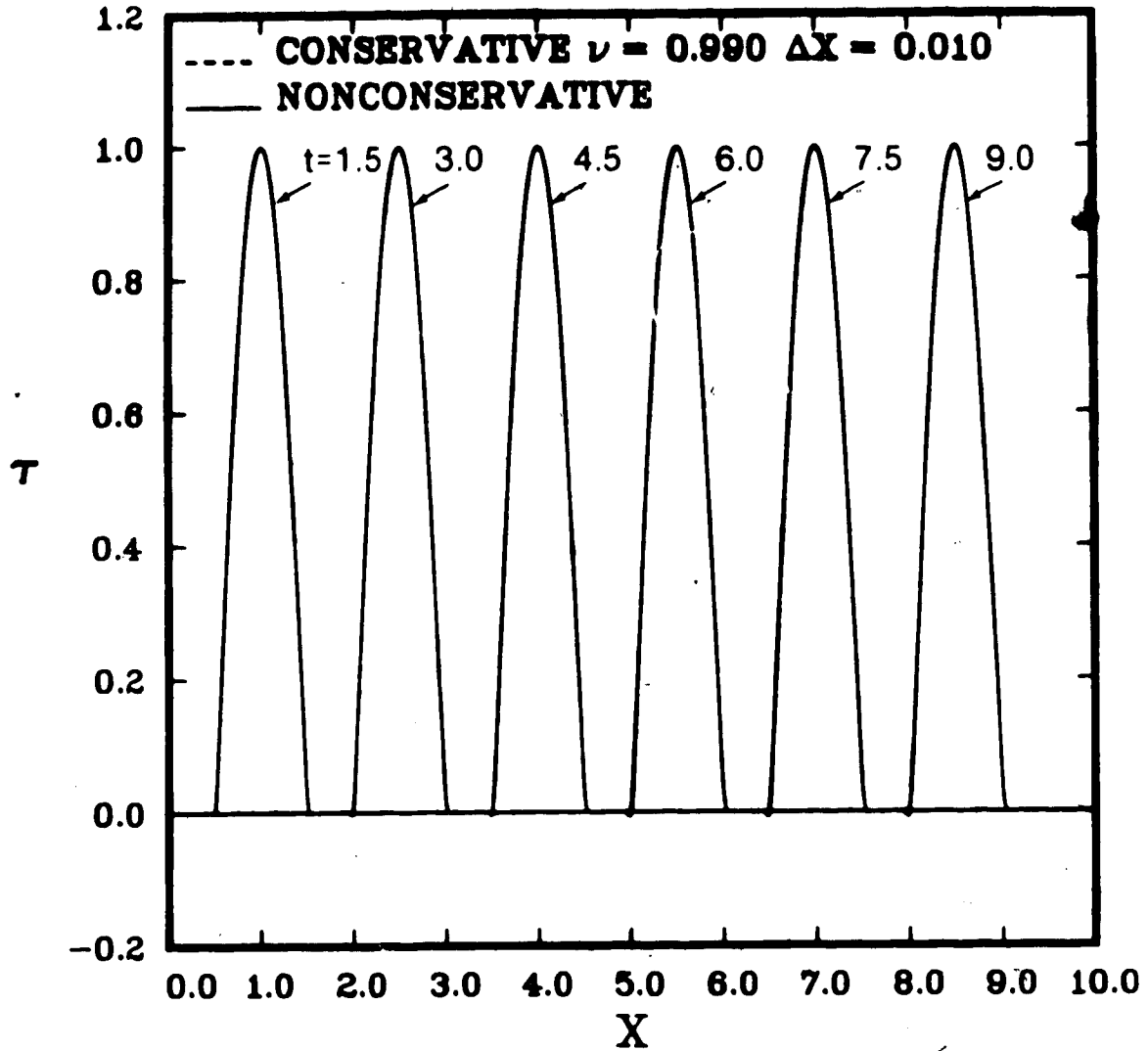


Fig. 4.40 Transverse Shear - Variation of normalized τ with normalized X for $\gamma = 0$ subject to $\tau(0, t) = \tau_0 \sin \pi t H(t) H(1-t)$, with $\tau_0 = 1$ using the conservative and nonconservative MacCormack schemes with $\nu = 0.99$.

are considered, $\dot{w}(R,0) = \dot{\alpha}(R,0) = 0$. The physical components of the deformation gradient tensor \underline{F} , and the left Cauchy-Green tensor \underline{B} , computed from equation (4.73) are

$$\underline{F} = \begin{bmatrix} 1 & 0 & 0 \\ r\alpha_R & 1 & 0 \\ w_R & 0 & 1 \end{bmatrix}, \quad \underline{B} = \begin{bmatrix} 1 & r\alpha_R & w_R \\ r\alpha_R & r^2\alpha_R^2+1 & rw_R\alpha_R \\ w_R & rw_R\alpha_R & w_R^2+1 \end{bmatrix} \quad (4.74)$$

and the basic invariants I_1 , I_2 and I_3 are given by

$$I_1 = I_2 = 3 + r^2\alpha_R^2 + w_R^2, \quad I_3 = 1 \quad (4.75)$$

where $w_R = \partial w / \partial r$, $\alpha_R = \partial \alpha / \partial R$ and from equation (4.72), it follows that $w_R = w_r = \partial w / \partial r$ and $\alpha_R = \alpha_r = \partial \alpha / \partial r$.

The Cauchy stress tensor is given by equation (4.5) in Section 4.2.1, for an incompressible hyperelastic solid. It follows from (4.74), (4.75) and (4.5), and the Rivlin-type strain energy function given by equation (4.12) with $N = 2$, that the nonzero components of Cauchy stress are

$$\sigma_r = -p + \mu(1 + 2\gamma(r^2\alpha_r^2 + w_r^2)) \quad (4.76)$$

$$\sigma_\theta = -p + \mu(1 + 2\gamma(r^2\alpha_r^2 + w_r^2))(r^2\alpha_r^2 + 1) \quad (4.77)$$

$$\sigma_z = -p + \mu(1 + 2\gamma(r^2\alpha_r^2 + w_r^2))(w_r^2 + 1) \quad (4.78)$$

$$\tau_{r\theta} = \mu(1 + 2\gamma(r^2\alpha_r^2 + w_r^2))(r\alpha_r) \quad (4.79)$$

$$\tau_{rz} = \mu(1 + 2\gamma(r^2\alpha_r^2 + w_r^2))(w_r) \quad (4.80)$$

$$\tau_{\theta z} = \mu (1 + 2\gamma(r^2\alpha_r^2 + w_r^2))(r w_r \alpha_r) \quad (4.81)$$

The nontrivial equations of motion for combined axial and torsional shear are

$$\frac{\partial \sigma_r}{\partial r} + \frac{\sigma_r - \sigma_\theta}{r} = -\rho r \ddot{a} \quad (4.82)$$

$$\frac{\partial r_{r\theta}}{\partial r} + \frac{2r_{r\theta}}{r} = \rho r \ddot{a} \quad (4.83)$$

$$\frac{\partial r_{rz}}{\partial r} + \frac{r_{rz}}{r} = \rho \ddot{w} \quad (4.84)$$

where a superposed dot denotes differentiation with respect to time, ρ is the constant density and p , which is not determined by the deformation field is independent of θ and z , w is the axial particle velocity and a is the angular velocity. It follows from equations (4.79) and (4.80), that $r_{r\theta}$ and r_{rz} are functions of both α_r and w_r , consequently equations (4.83) and (4.84) are coupled. By solving equations (4.83) and (4.84) simultaneously, $w(r,t)$ and $\alpha(r,t)$ can be obtained, and the stress components σ_r , σ_θ and σ_z can then be obtained by substituting w_r and α_r in equations (4.76 - 4.78) and solving equation (4.82) to obtain $p(r,t)$. The Cauchy stress $\tau_{\theta z}$ can be found directly from equation (4.81), by substituting w_r and α_r .

4.4.2. Formulation of the Problem

Axial and torsional, spatially uniform time dependent shearing stresses are applied at the surface of a cylindrical

cavity, of radius a , (see Figure 4.41) in an unbounded medium which is initially at rest. The axis of the cavity coincides with the z axis of the cylindrical polar coordinate system. Problems are considered for an unstressed medium and a prestressed medium. Two boundary conditions are considered, applied at the inner surface with radius $r = a$,

$$\begin{bmatrix} \tau_{rz}(a, t) \\ \tau_{r\theta}(a, t) \end{bmatrix} = \begin{bmatrix} T_{11} \\ T_{12} \end{bmatrix} + \begin{bmatrix} T_1 \\ T_2 \end{bmatrix} H(t) \quad (4.85)$$

or

$$\begin{bmatrix} \tau_{rz}(a, t) \\ \tau_{r\theta}(a, t) \end{bmatrix} = \begin{bmatrix} T_1 \\ T_2 \end{bmatrix} \sin \frac{\pi t}{t^*} H(t) H(t^* - t) \quad (4.86)$$

where T_{11} , T_{12} , T_1 and T_2 are all constants, and $t^* = 1$ for the problems considered.

The initial conditions are

$$\tau_{rz}(r, 0) = \frac{T_{11}}{r}, \quad \tau_{r\theta}(r, 0) = \frac{T_{12}}{r^2}, \quad w(r, 0) = 0, \quad \dot{a}(r, 0) = 0, \quad (4.87)$$

where the stresses given by (4.88)₁ and (4.88)₂ satisfy the equilibrium equations. Various combinations of the initial and boundary conditions are used to study the combined wave propagation problem. The combined problem of axial and torsional shear wave propagation can be reduced to the axial problem considered in Section 4.2, by considering $\tau_{r\theta}(a, t) = 0$ with either boundary condition (4.85) or (4.86) for τ_{rz} , and the quiescent initial conditions (4.87). For propagation into an unstressed region

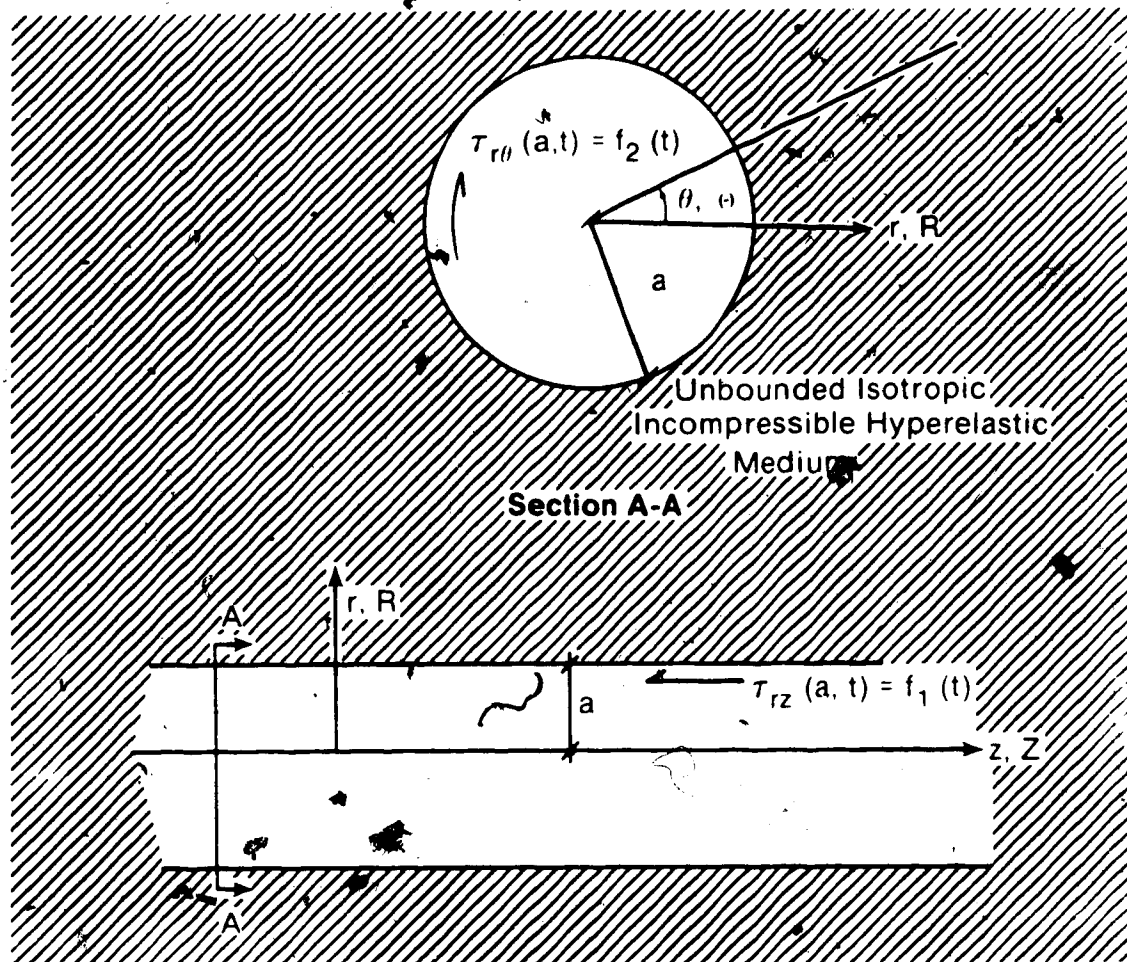


Fig. 4.41 Diagrammatic representation of Combined Axial and Torsional Shear Wave Propagation in an Unbounded Isotropic Incompressible Hyperelastic Solid.

$T_{i1} - T_{i2} = 0$. These results be compared to the previous results, for axial shear wave propagation.

It is convenient to introduce the following nondimensionalization scheme

$$\begin{aligned} (\bar{\tau}_{rz}, \bar{\tau}_{r\theta}) &= \left(\frac{\tau_{rz}, \tau_{r\theta}}{\mu} \right), & (\bar{w}, \bar{r}) &= \left(\frac{w, r}{a} \right), & \bar{t} &= \left[\frac{\mu}{\rho} \right]^{1/2} \frac{t}{a}, \\ \bar{\dot{w}} &= \dot{w} \left[\frac{\rho}{\mu} \right]^{1/2}, & \bar{\alpha} &= \alpha, & \bar{\dot{\alpha}} &= \dot{\alpha} \left[\frac{\rho}{\mu} \right]^{1/2} \frac{1}{a}, \end{aligned} \quad (4.88)$$

Henceforth, nondimensional variables are used but the superposed bars are omitted.

Substituting equations (4.79) and (4.80) into equations (4.83) and (4.84) gives

$$\begin{aligned} [1+6\gamma r^2(\alpha_r)^2+2\gamma(w_r)^2]\alpha_{rr} + 4\gamma w_r w_{rr} \alpha_r + \frac{[3+10\gamma r^2(\alpha_r)^2+6\gamma(w_r)^2]}{r} \alpha_r - \ddot{\alpha} \end{aligned} \quad (4.89)$$

$$\begin{aligned} [1+2\gamma r^2(\alpha_r)^2+6\gamma(w_r)^2]w_{rr} + 4\gamma r^2 w_r \alpha_r \alpha_{rr} + \frac{[1+6\gamma r^2(\alpha_r)^2+2\gamma(w_r)^2]}{r} w_r - \ddot{w} \end{aligned} \quad (4.90)$$

and making the substitution $w_r = \epsilon$ and $\alpha_r = \delta$, equations (4.89) and (4.90) can be replaced by a hyperbolic system of four partial differential equations

$$\frac{\partial \dot{w}}{\partial t} - (1+2\gamma r^2 \delta^2 + 6\gamma \epsilon^2) \frac{\partial \epsilon}{\partial r} - 4\gamma r^2 \epsilon \delta \frac{\partial \delta}{\partial r} - (1+6\gamma r^2 \delta^2 + 2\gamma \epsilon^2) \frac{\epsilon}{r} = 0 \quad (4.91)$$

$$\frac{\partial \epsilon}{\partial t} - \frac{\partial \dot{w}}{\partial r} = 0 \quad (4.92)$$

$$\frac{\partial \dot{\alpha}}{\partial t} - (1+6\gamma r^2 \delta^2 + 2\gamma \epsilon^2) \frac{\partial \delta}{\partial r} - 4\gamma \epsilon \delta \frac{\partial \epsilon}{\partial r} - (3+10\gamma r^2 \delta^2 + 6\gamma \epsilon^2) \frac{\delta}{r} = 0 \quad (4.93)$$

$$\frac{\partial \delta}{\partial t} - \frac{\partial \dot{\alpha}}{\partial r} = 0 \quad (4.94)$$

Equations (4.91 - 4.94) are not in conservation form, but are in the form,

$$\frac{\partial U}{\partial t} + \frac{A(U)}{r} \frac{\partial U}{\partial r} + \frac{B(U)}{r} = 0, \quad (4.95)$$

where

$$\underline{U} = \begin{bmatrix} w \\ \epsilon \\ \alpha \\ \delta \end{bmatrix} \quad \underline{A(U)} = \begin{bmatrix} 0 & -(1+2\gamma r^2 \delta^2 + 6\gamma \epsilon^2) & 0 & -4\gamma r^2 \epsilon \delta \\ -1 & 0 & 0 & 0 \\ 0 & -4\gamma \epsilon \delta & 0 & -(1+6\gamma r^2 \delta^2 + 2\gamma \epsilon^2) \\ 0 & 0 & -1 & 0 \end{bmatrix}$$

(4.96)

$$\underline{B(U)} = \begin{bmatrix} -(1+6\gamma r^2 \delta^2 + 2\gamma \epsilon^2) \epsilon / r \\ 0 \\ -(3+10\gamma r^2 \delta^2 + 6\gamma \epsilon^2) \delta / r \\ 0 \end{bmatrix}$$

The eigenvalues of \underline{A} are the nondimensional wave speeds $\pm c_1$ and $\pm c_2$ where

$$\begin{aligned}
 c_1 &= (1 + 2\gamma r^2 \delta^2 + 2\gamma \epsilon^2)^{1/2} \\
 c_2 &= (1 + 6\gamma r^2 \delta^2 + 6\gamma \epsilon^2)^{1/2}
 \end{aligned}
 \tag{4.97}$$

and the slopes of the four families of characteristics in the (r, t) plane are $dr/dt = \pm c_1, \pm c_2$. Since the method of characteristics is not used in this problem, the relationships along the characteristics are not given.

Because of the complexity of the problem, the numerical procedure is only applied to the conservation form of equations (4.91 - 4.94), given in matrix form as

$$\frac{\partial \underline{U}}{\partial t} + \frac{\partial Q(\underline{U})}{\partial r} + \underline{B}'(\underline{U}) = 0
 \tag{4.98}$$

Equations (4.92) and (4.94) are already in conservation form so that the conservation form of equations (4.91 - 4.94) is given by equation (4.98) where

$$\underline{Q}(\underline{U}) = \begin{bmatrix} -(\epsilon + 2\gamma \epsilon^3 + 2\gamma r^2 \delta^2 \epsilon) \\ -\dot{w} \\ -(\delta + 2\gamma \epsilon^2 \delta + 2\gamma r^2 \delta^3) \\ -\dot{\alpha} \end{bmatrix}, \quad \underline{B}'(\underline{U}) = \begin{bmatrix} -(1+2\gamma \epsilon^2 + 2\gamma r^2 \delta^2) \epsilon / r \\ 0 \\ -(3+6\gamma \epsilon^2 + 6\gamma r^2 \delta^2) \delta / r \\ 0 \end{bmatrix}
 \tag{4.99}$$

and \underline{U} is given by equation (4.96)₁.

If a shock occurs, it follows from equations (4.98) and (4.99) that

$$\begin{aligned}
 V_1[\epsilon] &= -[\dot{\omega}] \\
 V_2[\delta] &= -[\dot{\alpha}] \\
 V_1[\dot{\omega}] &= -[\epsilon + 2\gamma\epsilon^3 + 2\gamma r^2\delta^2\epsilon] \\
 V_2[\dot{\alpha}] &= -[\delta + 2\gamma\epsilon^2\delta + 2\gamma r^2\delta^3]
 \end{aligned}
 \tag{4.100}$$

where V_1 and V_2 are the nondimensional shock speeds, and are given by

$$V_1 = \left\{ \frac{[\epsilon + 2\gamma\epsilon^3 + 2\gamma r^2\delta^2\epsilon]}{[\epsilon]} \right\}^{1/2}
 \tag{4.101}$$

$$V_2 = \left\{ \frac{[\delta + 2\gamma\epsilon^2\delta + 2\gamma r^2\delta^3]}{[\delta]} \right\}^{1/2}
 \tag{4.102}$$

It is interesting to note that there are two shock speeds for the problem considered. If $\delta = 0$, which corresponds to axial shear alone,

$$V_1 = \left\{ \frac{[\epsilon + 2\gamma\epsilon^3]}{[\epsilon]} \right\}^{1/2}
 \tag{4.103}$$

This expression is identical to equation (4.31), the shock speed for axial shear. When $\gamma = 0$, which corresponds to the linear problem, $V_1 = 1$ and $V_2 = 1$, and the governing equations are uncoupled. It should also be noted that for propagation into an undeformed region, $V_1 = V_2$, and the shock speed is identical to the wave speed c_2 given by equation (4.97)₂. Therefore, if shocks are formed in the propagation of axial and torsional finite amplitude waves into an undeformed medium, the shocks should propagate at the same speed.

4.4.3 Implementation of the MacCormack Scheme

The MacCormack finite difference scheme given by equation (2.7) for the conservative system of equations is used to solve the system of equations (4.91 - 4.94) given in matrix form by equation (4.98). Application of the conservative version of the finite difference equations gives the same predictor and corrector equations (4.32) as those for the axial shear problem, where

$$\underline{U}^n = \underline{U}(1 + j\Delta r, n\Delta t)$$

using the same notation for the difference scheme.

The elements $\epsilon(1,t)$ and $\delta(1,t)$ of $\underline{U}(1,t)$ are obtained from the boundary conditions (4.85) or (4.86) and the constitutive equations (4.79) and (4.80), where $\epsilon = w_r$ and $\delta = \alpha_r$ so that ϵ_0^n and δ_0^n are known for all n . In order to apply equations (4.32)₁ and (4.32)₂, \dot{w}_0^n and $\dot{\alpha}_0^n$ are also required for all n , and these are obtained by applying boundary conditions according to Gottlieb (1978), which have been discussed at length in previous sections.

In order to apply the difference equations given by (4.32), \dot{w}_0^n and $\dot{\alpha}_0^n$ are required for all n . Equation (4.32)₁ gives the intermediate values \overline{w}_0^{n+1} and $\overline{\alpha}_0^{n+1}$, and the final values are given by

$$\overline{w}_0^{n+1} = \frac{1}{2} \left\{ \overline{w}_0^{n+1} + \dot{w}_0^n - \frac{\Delta t}{\Delta r} \left((Q_1)_1^{n+1} - (Q_1)_0^{n+1} \right) - \Delta t (B'_1)_{10}^{n+1} \right\}, \quad (4.104)$$

$$\overline{\alpha}_0^{n+1} = \frac{1}{2} \left\{ \overline{\alpha}_0^{n+1} + \dot{\alpha}_0^n - \frac{\Delta t}{\Delta r} \left((Q_3)_1^{n+1} - (Q_3)_0^{n+1} \right) - \Delta t (B'_3)_{10}^{n+1} \right\}$$

where $Q_1 = -(\epsilon + 2\gamma\epsilon^3 + 2\gamma r^2\delta^2\epsilon)$, $B'_1 = -(1 + 2\gamma(\epsilon^2 + r^2\delta^2))\epsilon/r$,

$Q_3 = -(\delta + 2\gamma\epsilon^2 + 2\gamma r^2\delta^3)$ and $B'_3 = -(3 + 6\gamma(\epsilon^2 + r^2\delta^2))\delta/r$.

It should be noted that a numerical procedure is used to find ϵ_0^n and δ_0^n using the nonlinear constitutive relationships, given by equations (4.79) and (4.80), where $\epsilon = w_r$ and $\delta = \alpha_r$.

The stability analysis done in Section 2.4 does not directly apply to the nonlinear system of equations derived in this section. There is no rigorous stability analysis available for boundary initial value problems governed by systems of equations of the form (4.98). However, it has been demonstrated by Hanagud and Abhyankar (1984), that the step size must be varied for nonlinear problems. That is, for a constant Courant number, Δr is held constant and Δt is adjusted at each time step by assuming a constant value of $\nu < 1$, and taking c as the maximum numerical wave speed obtained from the previous time step. This procedure is similar to that used for the axial shear wave problem, except that there are two wave speeds to be considered for the combined problem. A comparison of the wave speeds, c_1 and c_2 , given by (4.97)₁ and (4.97)₂, respectively, for a given ϵ and δ , shows that c_2 is always numerically larger than c_1 . Therefore, $c_2 = (1 + 6\gamma r^2\delta^2 + 6\gamma\epsilon^2)^{1/2}$ is used to adjust the time step Δt . Unsatisfactory results are obtained in some cases, when the time step is not varied.

4.4.4 Numerical Results

The numerical results presented in this section have been obtained using the conservative version of the MacCormack scheme with $\Delta r = 0.01$, unless otherwise specified. Numerical results are presented for nondimensional τ_{rz} and $\tau_{r\theta}$ versus nondimensional r for various nondimensional times t . In this case, τ_{rz} and $\tau_{r\theta}$ are the nondimensional axial and torsional shear stresses, respectively.

Figures 4.42 and 4.43 show the variation of τ_{rz} and $\tau_{r\theta}$, respectively, with r for boundary condition (4.85), with $T_{i1} = T_{i2} = 0$, $T_1 = T_2 = 1$, and $\gamma = 0$, for $\nu = 1.0$ and various times. The numerical solution for τ_{rz} given in Figure 4.42 indicates a slowly growing instability and the numerical solution for $\tau_{r\theta}$ is very unstable for $\nu = 1.0$. Figures 4.44 and 4.45 show the variation of τ_{rz} and $\tau_{r\theta}$, respectively with r for boundary condition (4.85), with $T_{i1} = T_{i2} = 0$ and $T_1 = T_2 = 1$, and $\nu = 0.1$. The numerical solutions in both figures do not appear to be unstable for the times considered, but exhibit some numerical dispersion.

Since some of the numerical results exhibit instability for $\nu = 1.0$, the remainder of the results presented in this section are for $\nu = 0.99$.

Figures 4.46 - 4.49 show the variation of τ_{rz} and $\tau_{r\theta}$ with r for boundary condition (4.85), with $T_{i1} = T_{i2} = 0$, $T_1 = T_2 = 1$, $\gamma = 0$ and $\gamma = 0.1$, respectively, for $\nu = 0.99$. Figures 4.46 and 4.47, for $\gamma = 0$, indicate that the wavefront is located at

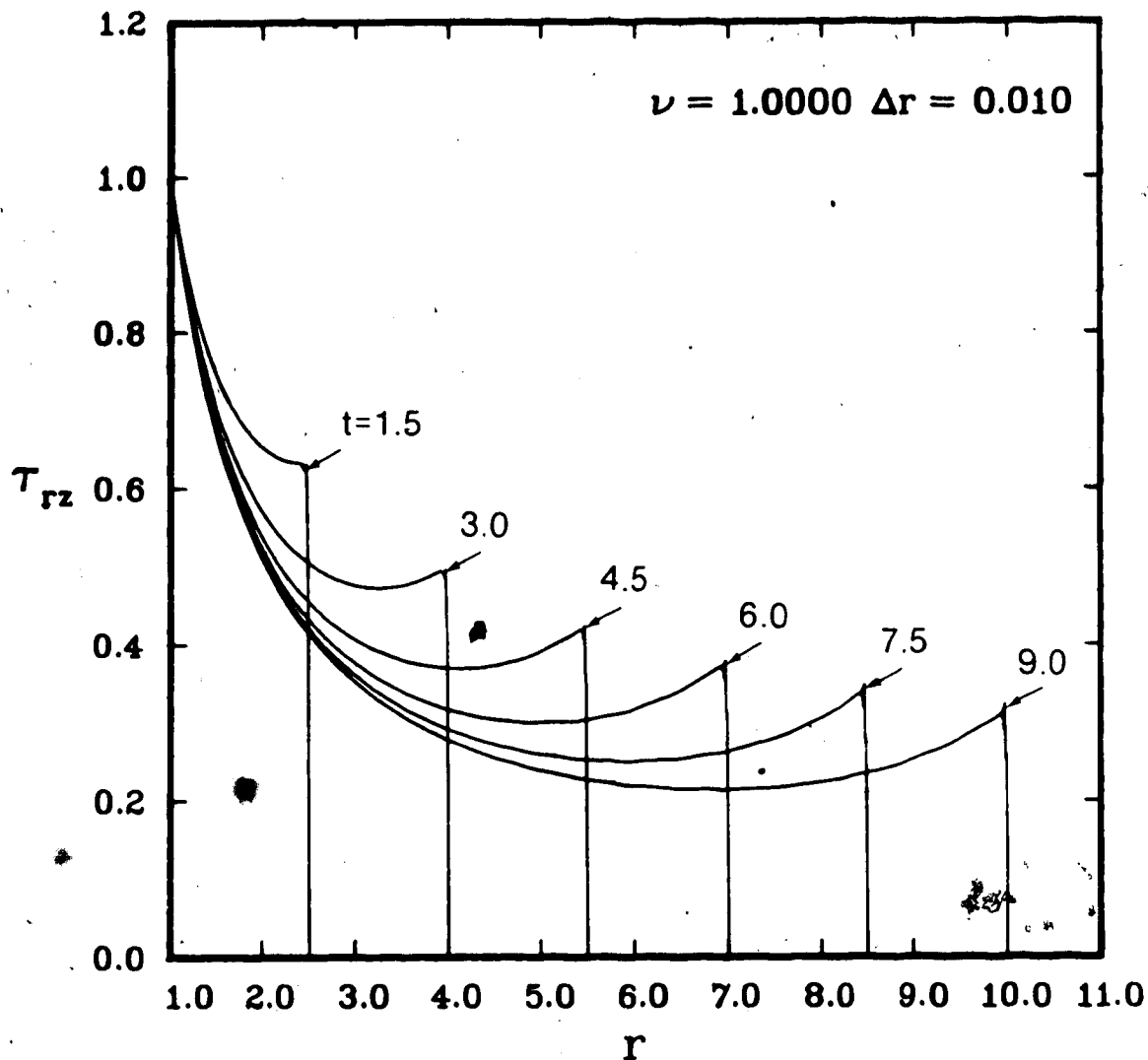


Fig. 4.42 Combined Shear - Variation of nondimensional τ_{rz} with nondimensional r for $\gamma = 0$, for boundary condition (4.85), with $T_{i1} = T_{i2} = 0$ and $T_1 = T_2 = 1$, using the MacCormack scheme with $\nu = 1.0$.

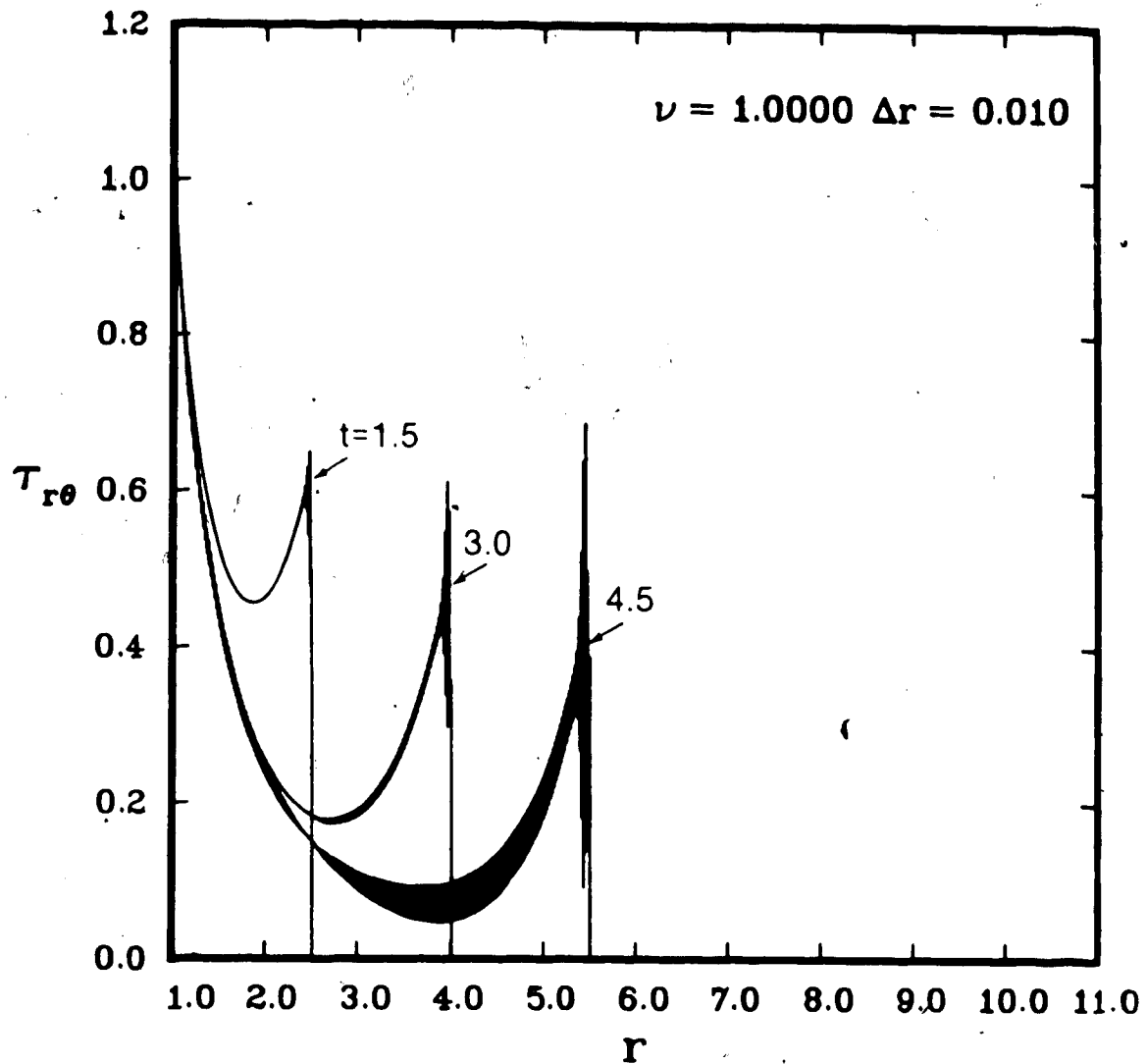


Fig. 4.43 Combined Shear - Variation of nondimensional $\tau_{r\theta}$ with nondimensional r for $\nu = 1.0$ for boundary condition (4.85), with $T_{i1} - T_{i2} = 0$ and $T_1 - T_2 = 1$, using the MacCormack scheme with $\nu = 1.0$.

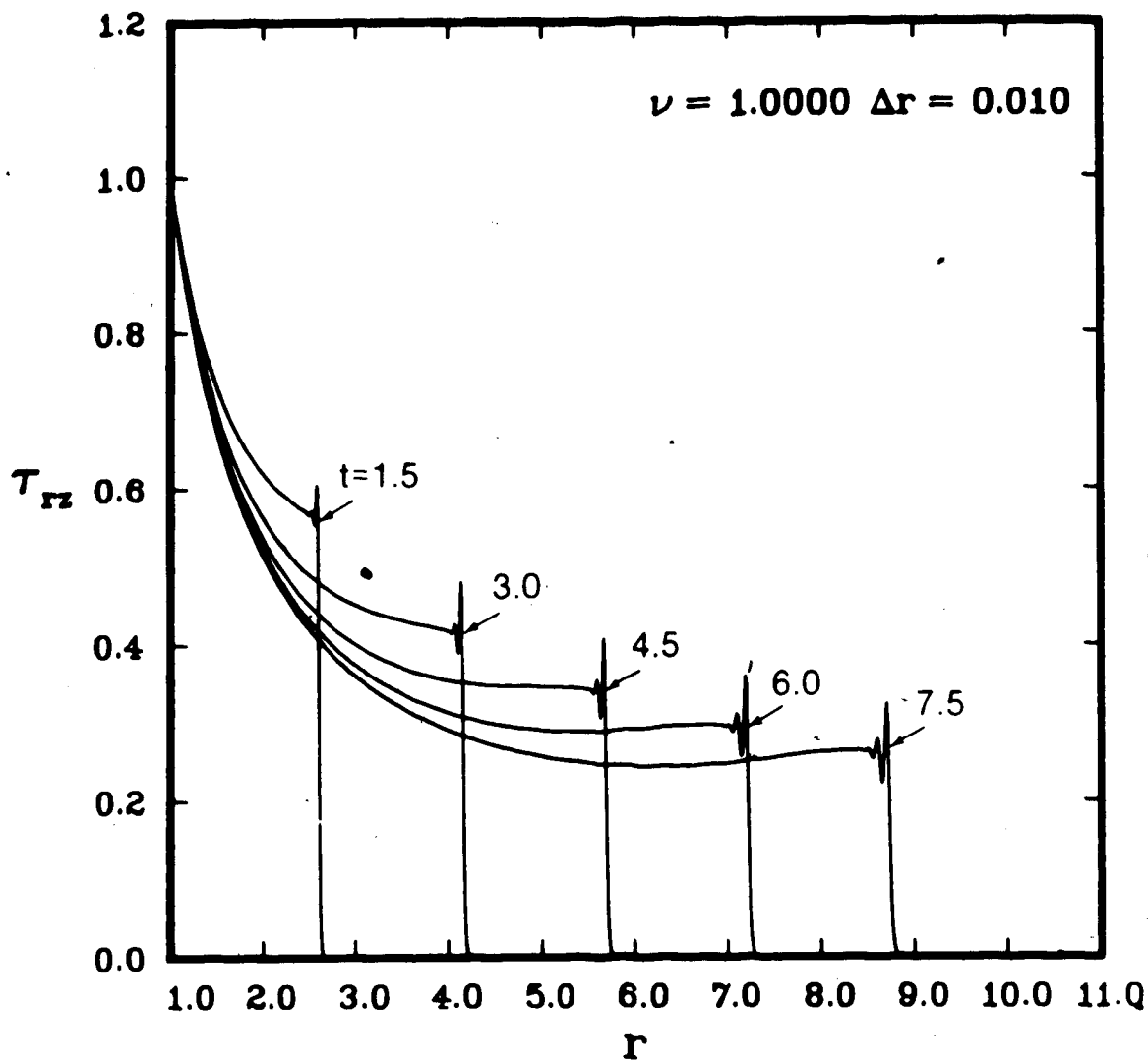


Fig. 4.44 Combined Shear - Variation of nondimensional τ_{rz} with nondimensional r for $\gamma = 0.1$, for boundary condition (4.85), with $T_{i1} = T_{i2} = 0$ and $T_1 = T_2 = 1$, using the MacCormack scheme with $\nu = 1.0$.

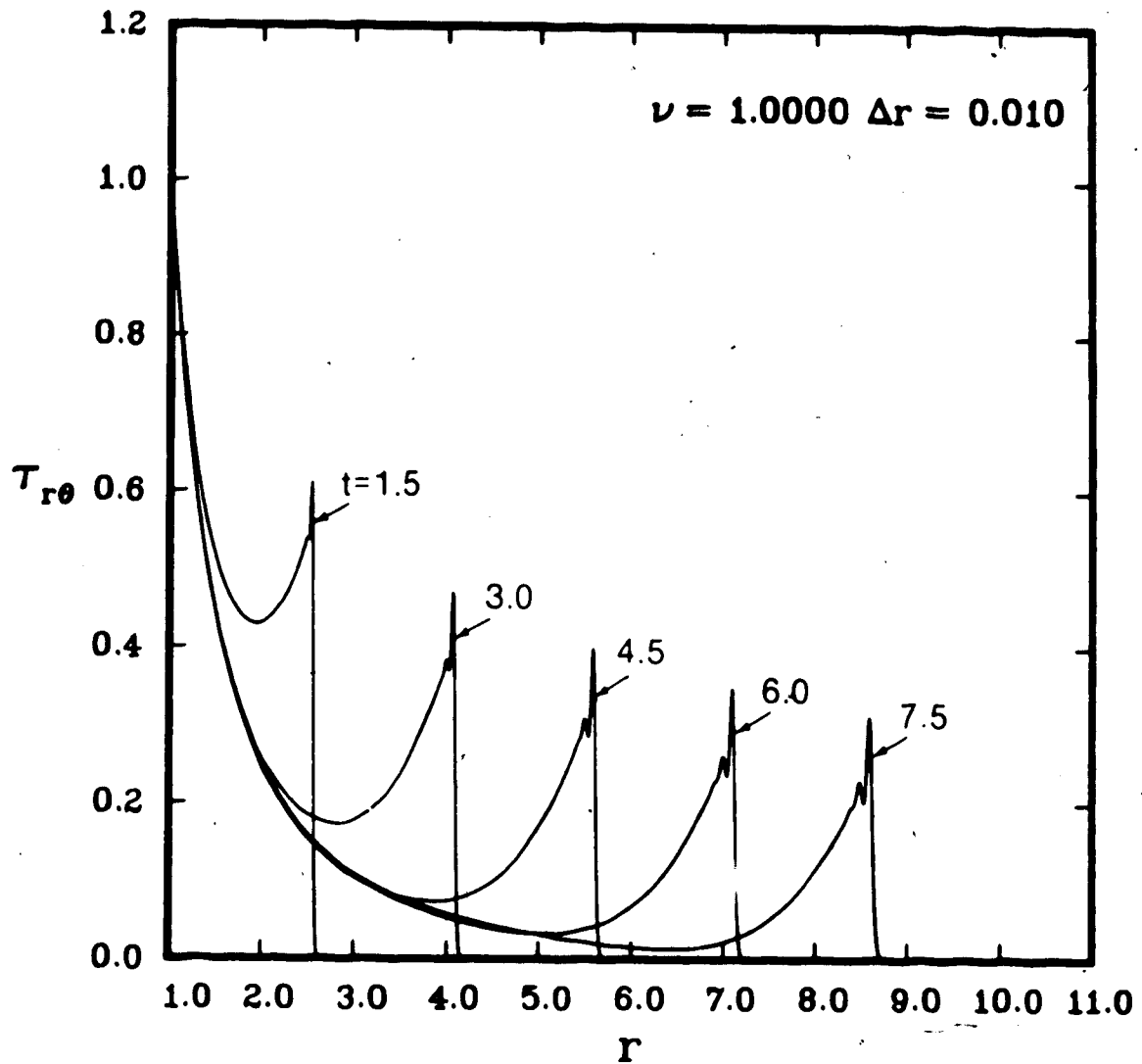


Fig. 4.45 Combined Shear - Variation of nondimensional $\tau_{r\theta}$ with nondimensional r for $\gamma = 0.1$ for boundary condition (4.85), with $T_{i1} = T_{i2} = 0$ and $T_1 = T_2 = 1$, using the MacCormack scheme with $\nu = 1.0$.

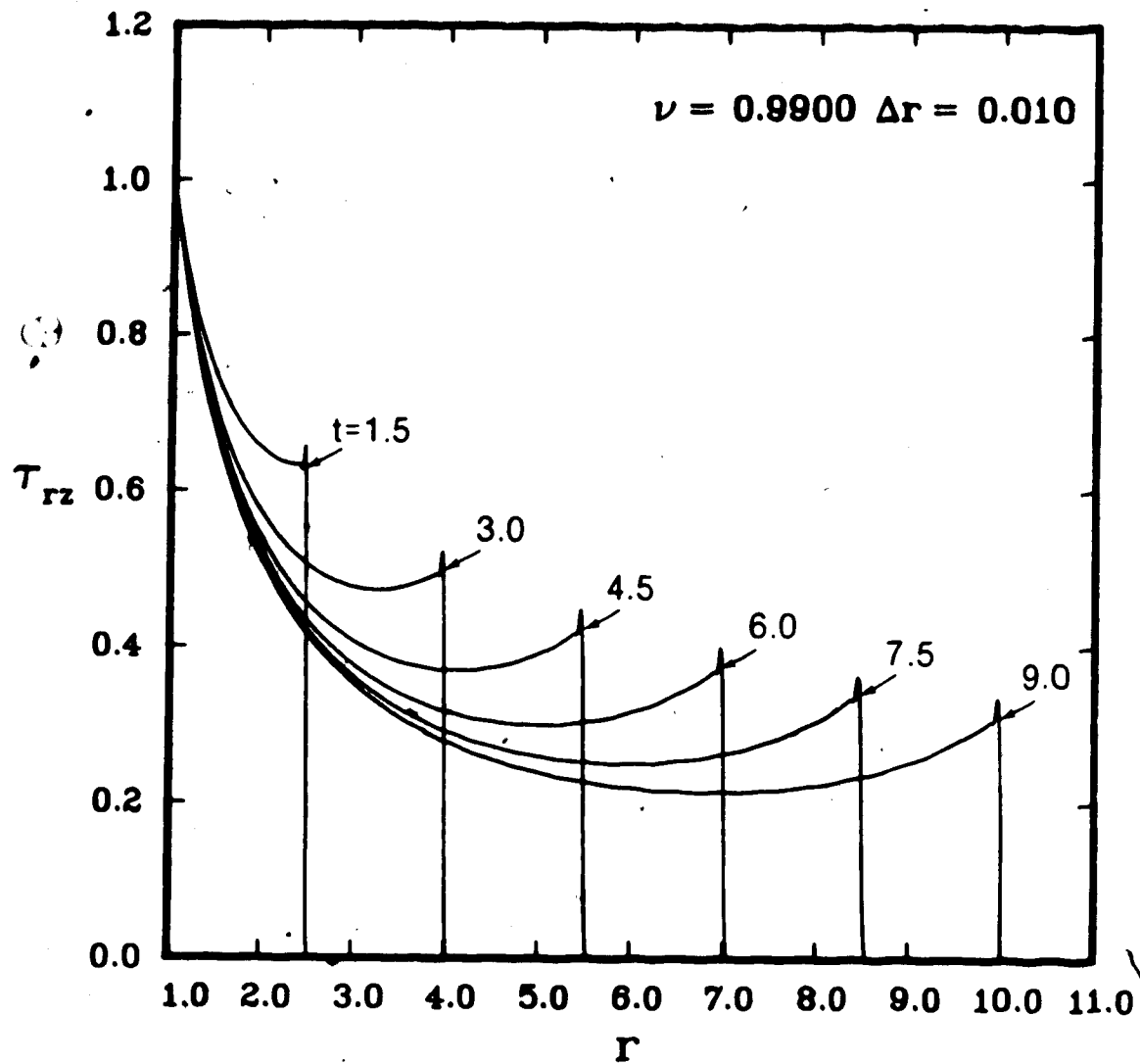


Fig. 4.46 Combined Shear - Variation of nondimensional τ_{rz} with nondimensional r for $\gamma = 0$ for boundary condition (4.85), with $T_{i1} = T_{i2} = 0$ and $T_1 = T_2 = 1$, using the MacCormack scheme with $\nu = 0.99$.

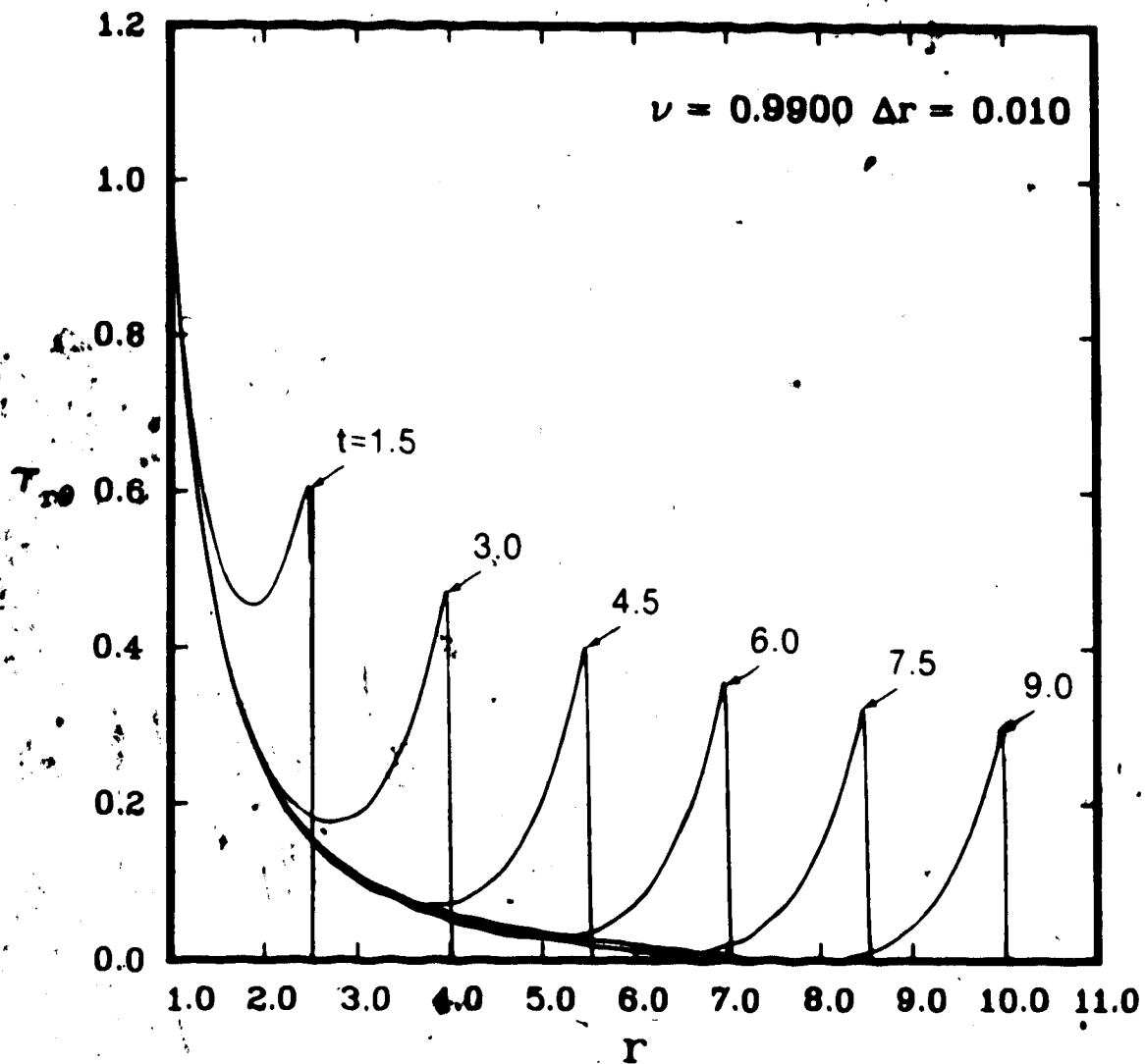


Fig. 4.47 Combined Shear - Variation of nondimensional $\tau_{r\theta}$ with nondimensional r for $\gamma = 0$ for boundary condition (4.85), with $T_{i1} = T_{i2} = 0$ and $T_1 = T_2 = 1$, using the MacCormack scheme with $\nu = 0.99$.

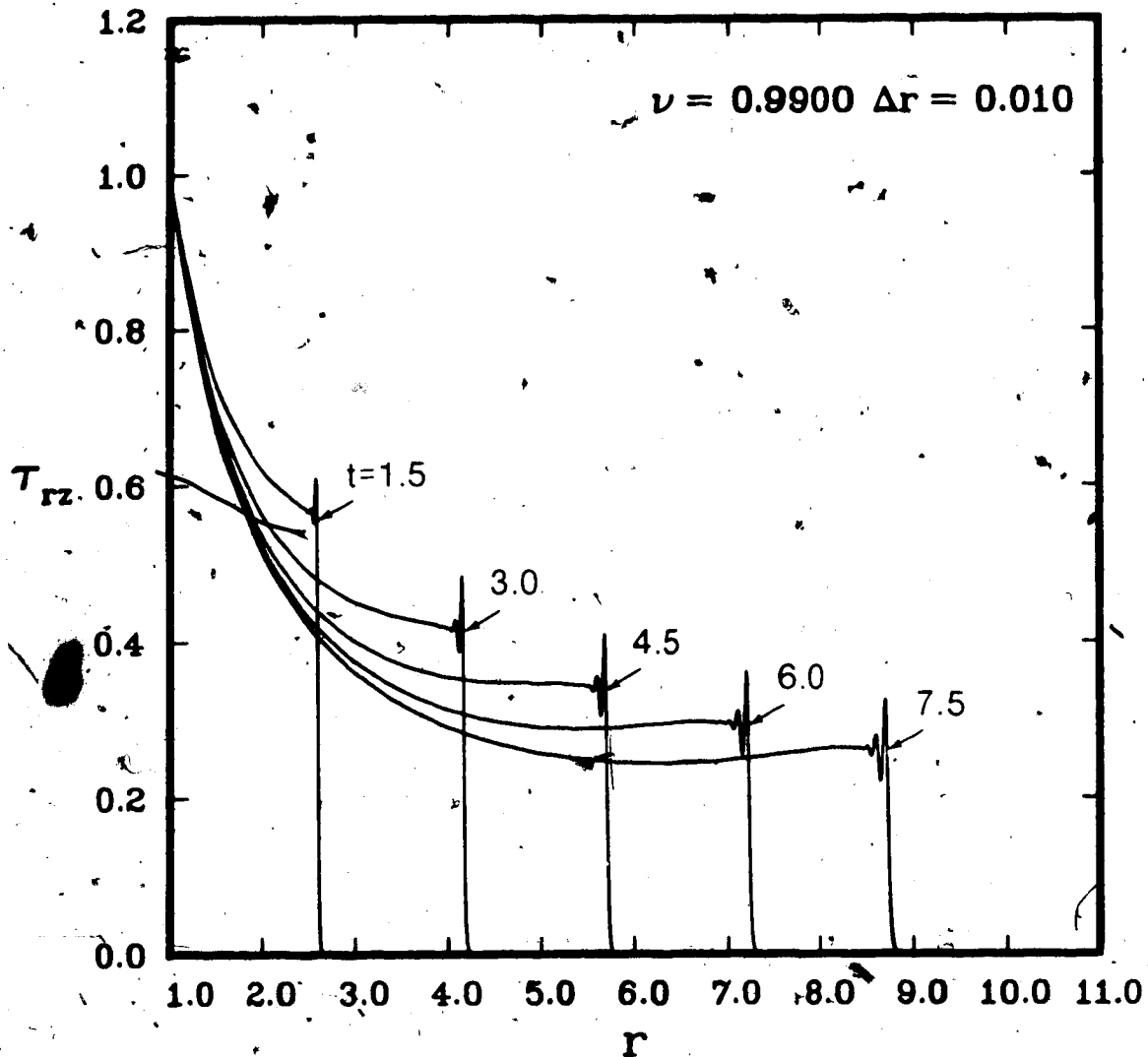


Fig. 4.48 Combined Shear - Variation of nondimensional τ_{rz} with nondimensional r for $\gamma = 0.1$ for boundary condition (4.85), with $T_{i1} = T_{i2} = 0$ and $T_1 = T_2 = 1$, using the MacCormack scheme with $\nu = 0.99$.

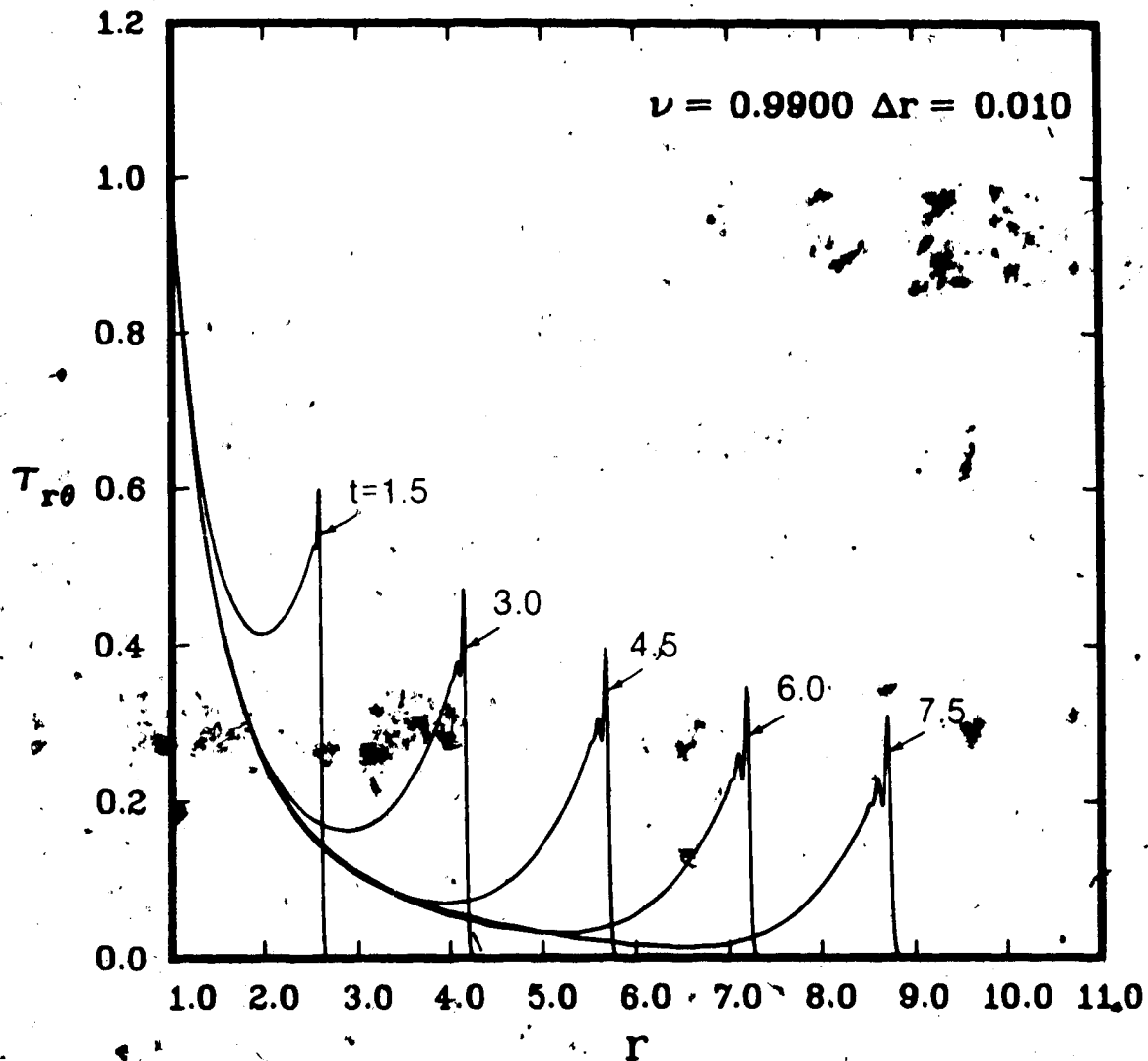


Fig. 4.49 Combined Shear - Variation of nondimensional $T_{r\theta}$ with nondimensional r for $\gamma = 0.1$ for boundary condition (4.85), with $T_{i1} = T_{i2} = 0$ and $T_1 = T_2 = 1$, using the MacCormack scheme with $\nu = 0.99$.

$r = 1+t$, for the times considered, for curves of τ_{rz} and $\tau_{r\theta}$. This is consistent with theoretical predictions, since $\gamma = 0$ corresponds to a linear problem, and both shock speeds $V_1 = V_2 = 1$, and the equations are uncoupled. Figures 4.48 and 4.49, for $\gamma = 0.1$, indicate that the wavefront is located slightly ahead of $r = 1+t$. Again, this is consistent with what is obtained from theoretical considerations. Except for some numerical dispersion behind the wavefront, the curves obtained in Figures 4.46 - 4.49 are good representations of the wave propagation phenomena.

Figures 4.50 - 4.53 compare numerical results obtained with the extrapolation technique to those results obtained using the MacCormack scheme only, for τ_{rz} and $\tau_{r\theta}$ vs r , for boundary condition (4.85), with $T_{i1} = T_{i2} = 0$, $T_1 = T_2 = 1$, $\gamma = 0$ and $\gamma = 0.1$, respectively, for $\nu = 0.99$. The extrapolation technique eliminates numerical dispersion, in each figure, and satisfies the jump conditions given by (4.100). There is significant improvement, with the extrapolation technique, in Figures 4.52 and 4.53 for $\gamma = 0.1$, since the shock fronts obtained without the extrapolation technique are smeared by the numerical dispersion.

Figures 4.54 and 4.55 illustrate the coupling effect on the numerical solutions of the nonlinear governing equations for τ_{rz} and $\tau_{r\theta}$, for boundary condition (4.85). The combined problem is given by $T_{i1} = T_{i2} = 0$, $T_1 = T_2 = 1$, which represents combined axial and torsional shear wave propagation. The pure axial problem is given by $T_{i1} = T_{i2} = 0$, $T_1 = 1$, $T_2 = 0$, and the pure torsional

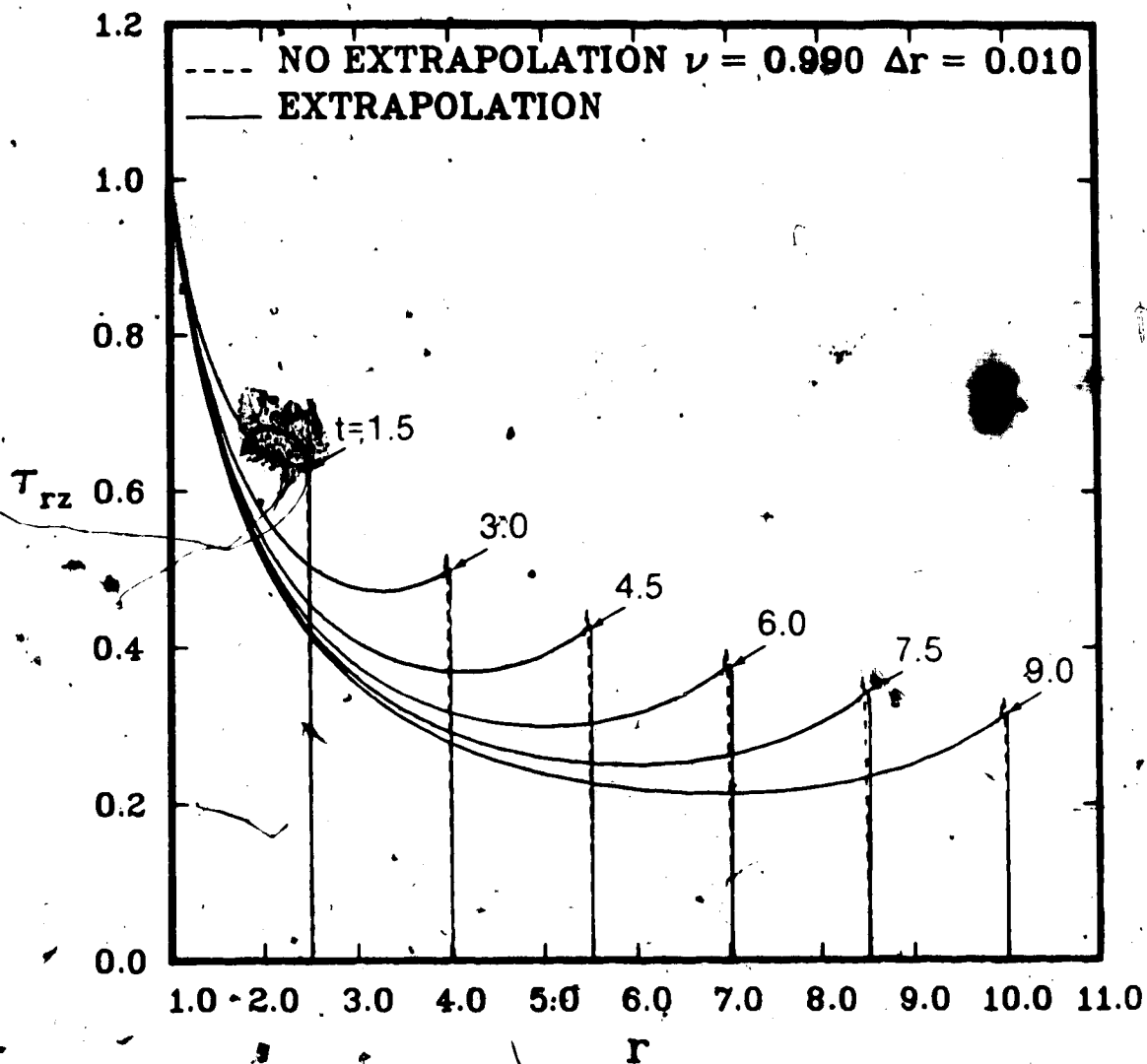


Fig. 4.50 Combined Shear - Variation of nondimensional τ_{rz} with nondimensional r for $\gamma = 0$ for boundary condition (4.85), with $T_{i1} = T_{i2} = 0$ and $T_1 = T_2 = 1$, using the MacCormack scheme with and without extrapolation with $\nu = 0.99$.

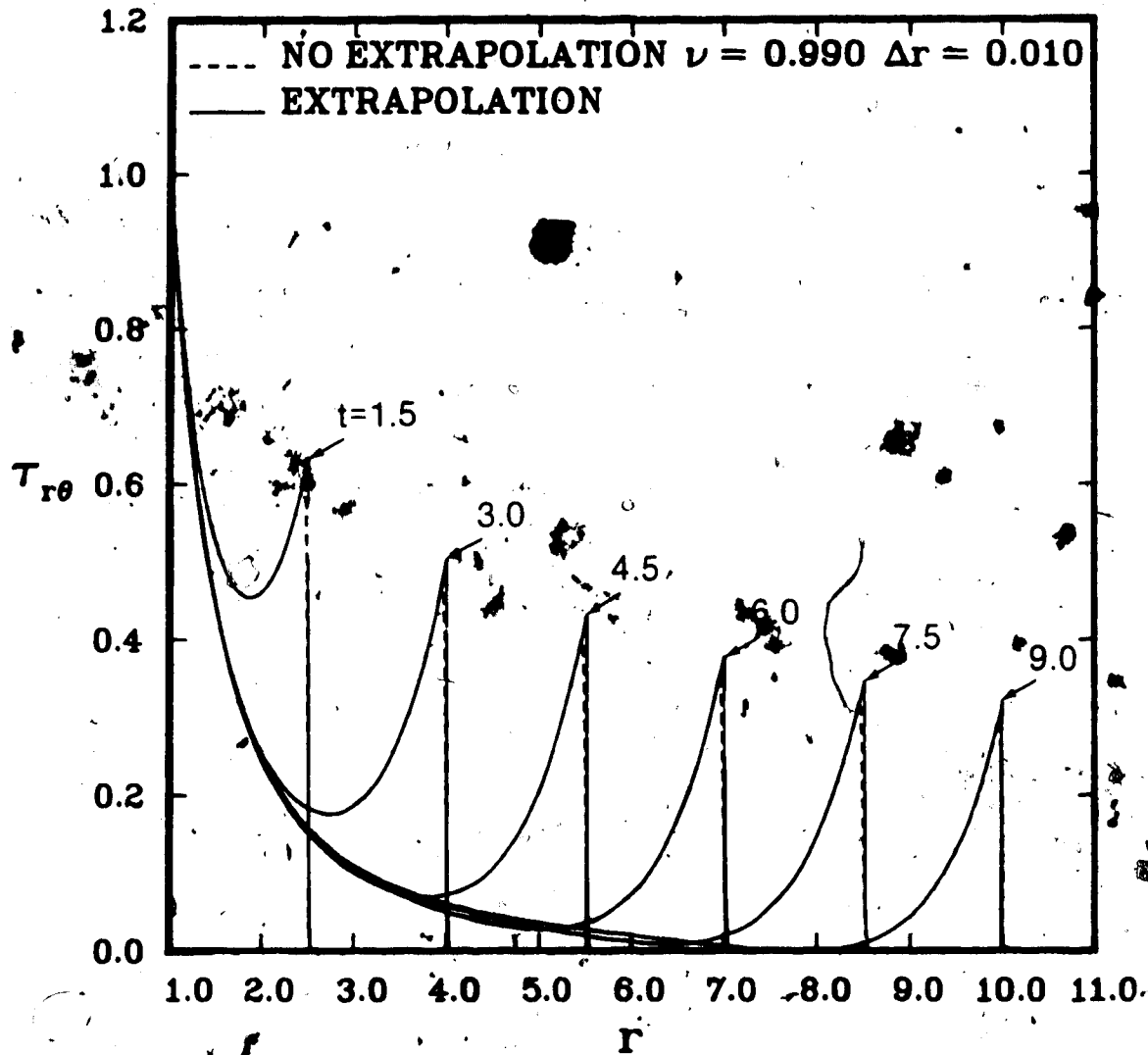


Fig. 4.51 Combined Shear. Variation of nondimensional $T_{r\theta}$ with nondimensional r for $\gamma = 0$ for boundary condition (4.85), with $T_{11} = T_{22} = 0$ and $T_1 = T_2 = 1$, using the MacCormack scheme with and without extrapolation with $\nu = 0.99$.

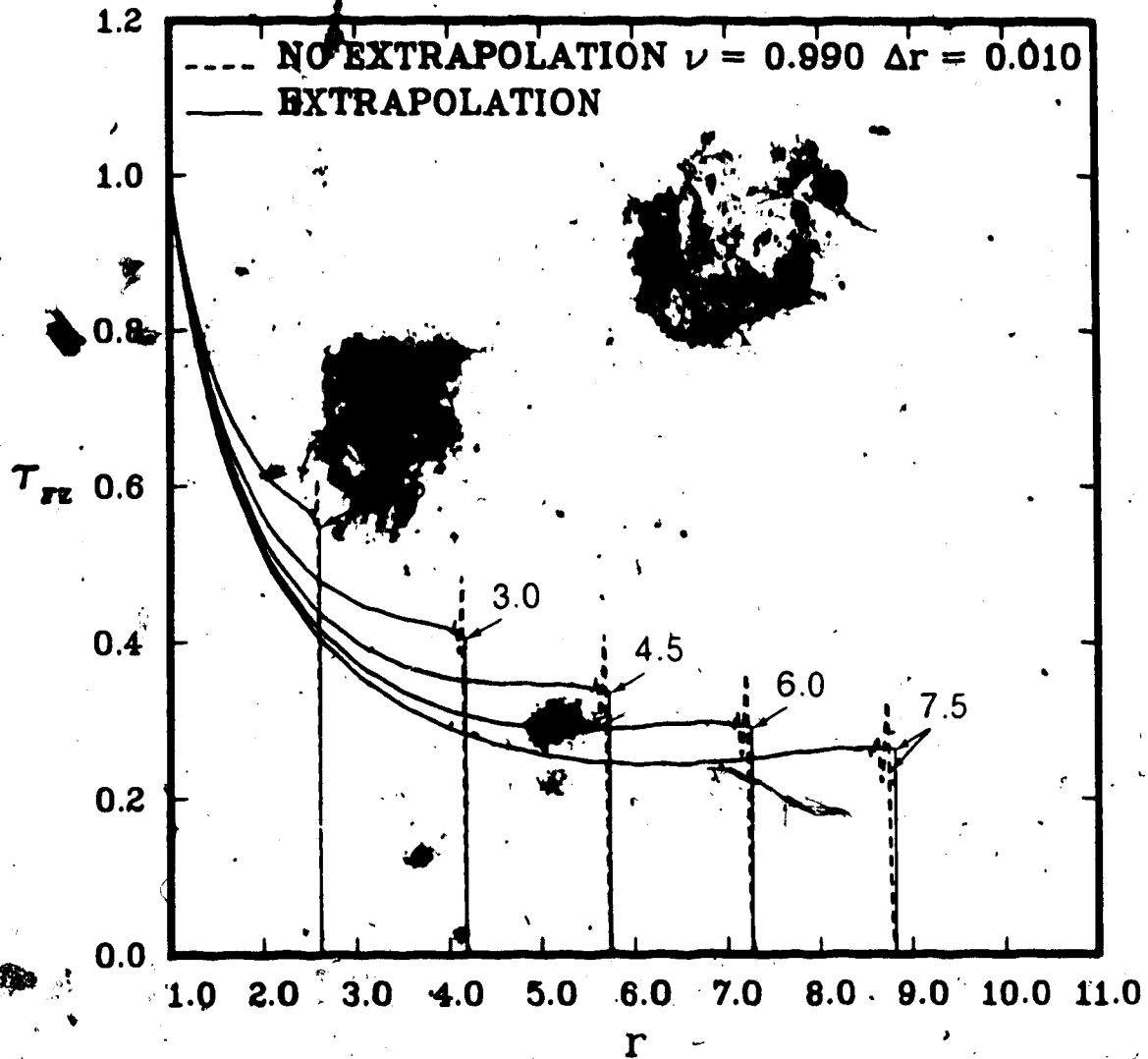


Fig. 4.52. Combined Shear - Variation of nondimensional τ_{rz} with nondimensional r for $\gamma = 0.1$ for boundary condition (4.85), with $T_{i1} = T_{i2} = 0$ and $T_1 = T_2 = 1$, using the MacCormack scheme with and without extrapolation with $\nu = 0.99$.

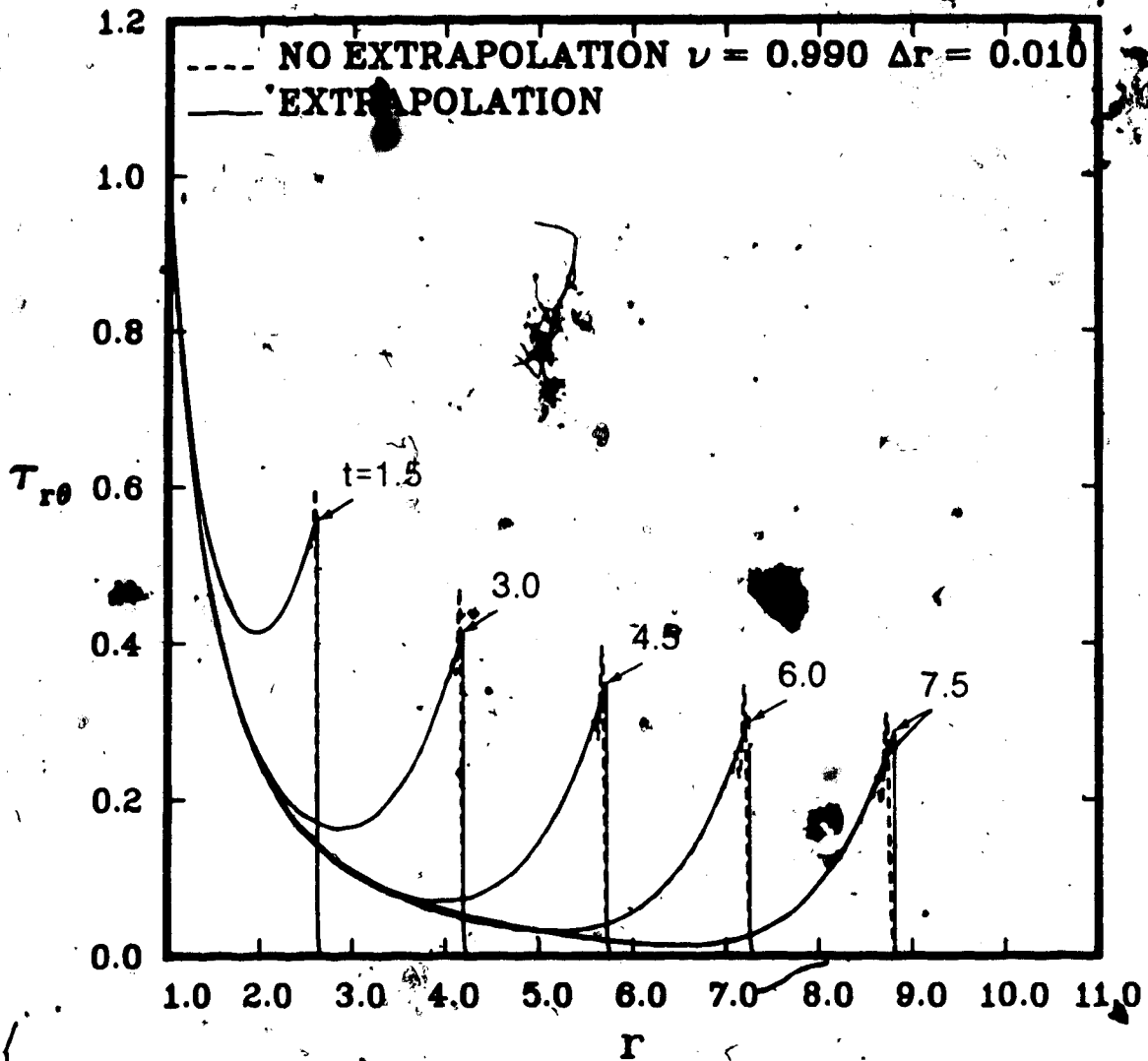


Fig. 4.53 Combined Shear - Variation of nondimensional $T_{r\theta}$ with nondimensional r for $\gamma = 0.1$ for boundary condition (4.85), with $T_{i1} = T_{i2} = 0$ and $T_1, T_2 = 1$, using the MacCormack scheme with and without extrapolation with $\nu = 0.99$.

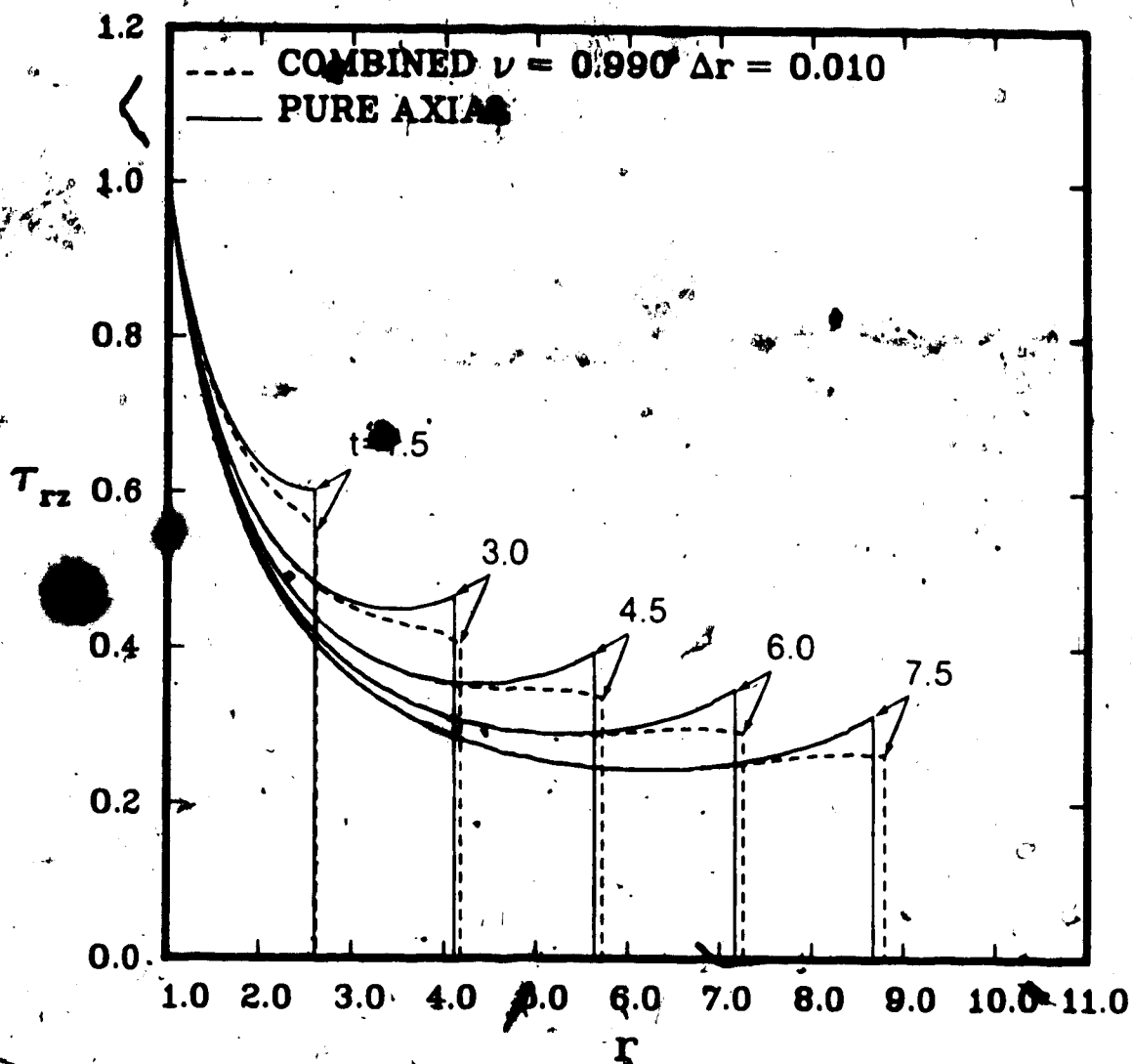


Fig. 4.54 Combined Shear - Variation of nondimensional τ_{rz} with nondimensional r for $\gamma = 0.1$ for boundary condition (4.85), with $T_{11} = T_{12} = 0$ and $T_1 = T_2 = 1$ for combined shear and $T_1 = 1, T_2 = 0$ for axial shear, using the MacCormack scheme with extrapolation with $\nu = 0.99$.

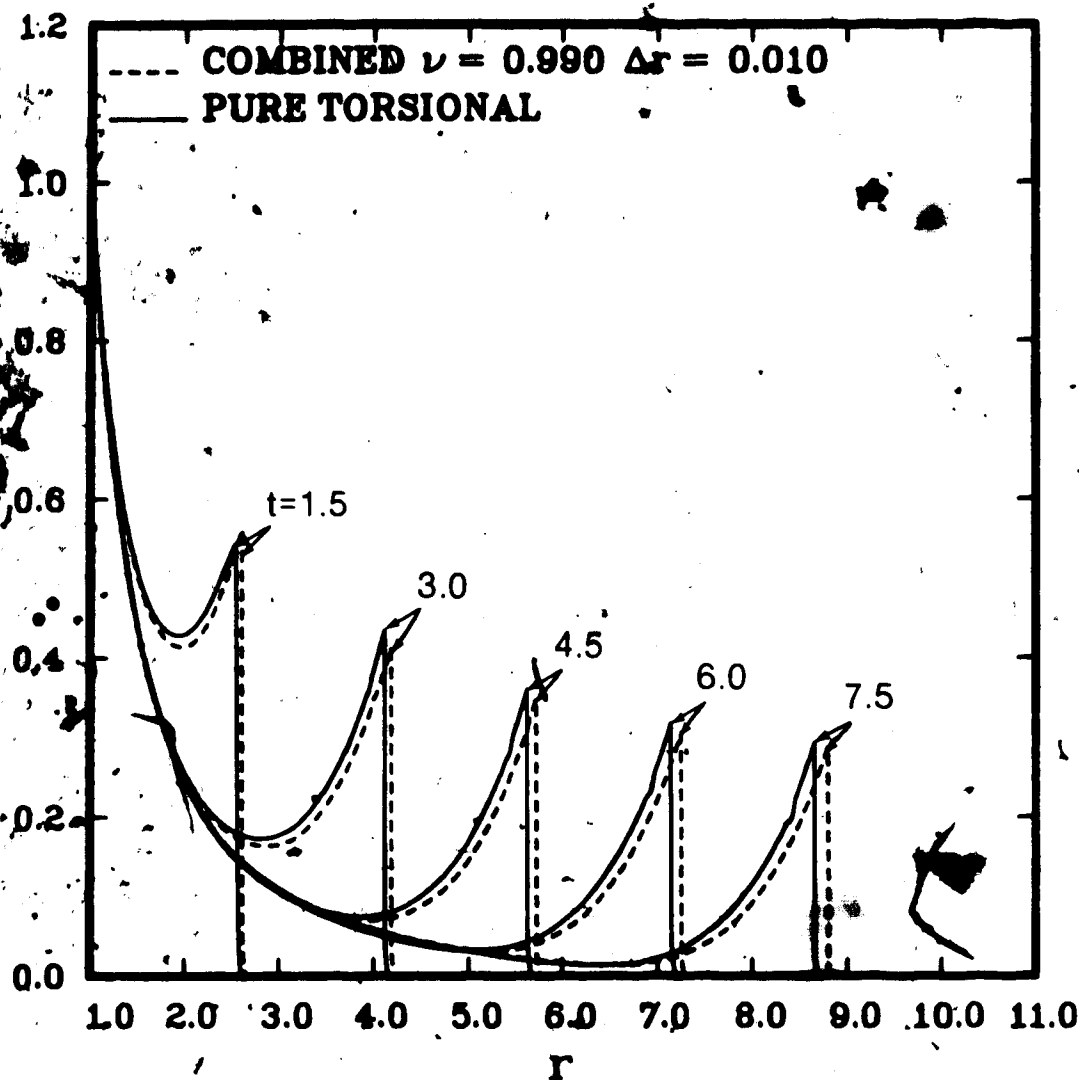


Fig. 4.55 Combined Shear - Variation of nondimensional $r_{r\theta}$ with nondimensional r for $\gamma = 0.1$ for boundary condition (4.85), with $T_{11} = T_{12} = 0$ and $T_1 = T_2 = 1$ for combined shear and $T_1 = 0, T_2 = 1$ for torsional shear, using the MacCormack scheme with extrapolation with $\nu = 0.99$.

problem is given by $T_{11} = T_{12} = 0$, $T_1 = 0$ and $T_2 = 1$. The numerical results presented in Figures 4.54 and 4.55 are smoothed using the extrapolation technique. The numerical results indicate that the shock speeds for the combined wave propagation problem are greater than those for the corresponding uncoupled problems. Again, this is consistent with theoretical considerations.

Figures 4.56 and 4.57 illustrate the coupling effect on the numerical solution of the nonlinear governing equations ($\gamma = 0.1$) for τ_{rz} and $\tau_{r\theta}$ for boundary condition (4.86). The numerical results indicate that the breaking times for the stress pulses for τ_{rz} and $\tau_{r\theta}$ for the combined problem are different than those obtained for axial and torsional shear alone.

Figures 4.58 and 4.59 give numerical results obtained for τ_{rz} and $\tau_{r\theta}$ for boundary condition (4.85), with $T_{11} = T_{12} = 0.5$ and $T_1 = T_2 = 0.5$, which represents combined axial and torsional shear wave propagation into a prestressed quiescent region, for $\gamma = 0.0$ and $\gamma = 0.1$, respectively, with $\nu = 0.99$. The numerical results presented in Figure 4.58 indicate that the shock fronts for τ_{rz} and $\tau_{r\theta}$ coincide. This is consistent with theoretical considerations, since $\gamma = 0$ corresponds to the linear problem. The numerical results presented in Figure 4.59 indicate that the position of the shock fronts for τ_{rz} and $\tau_{r\theta}$ with $\gamma = 0.1$ are not the same, for wave propagation into a prestressed material. Again, this is consistent with theoretical considerations.

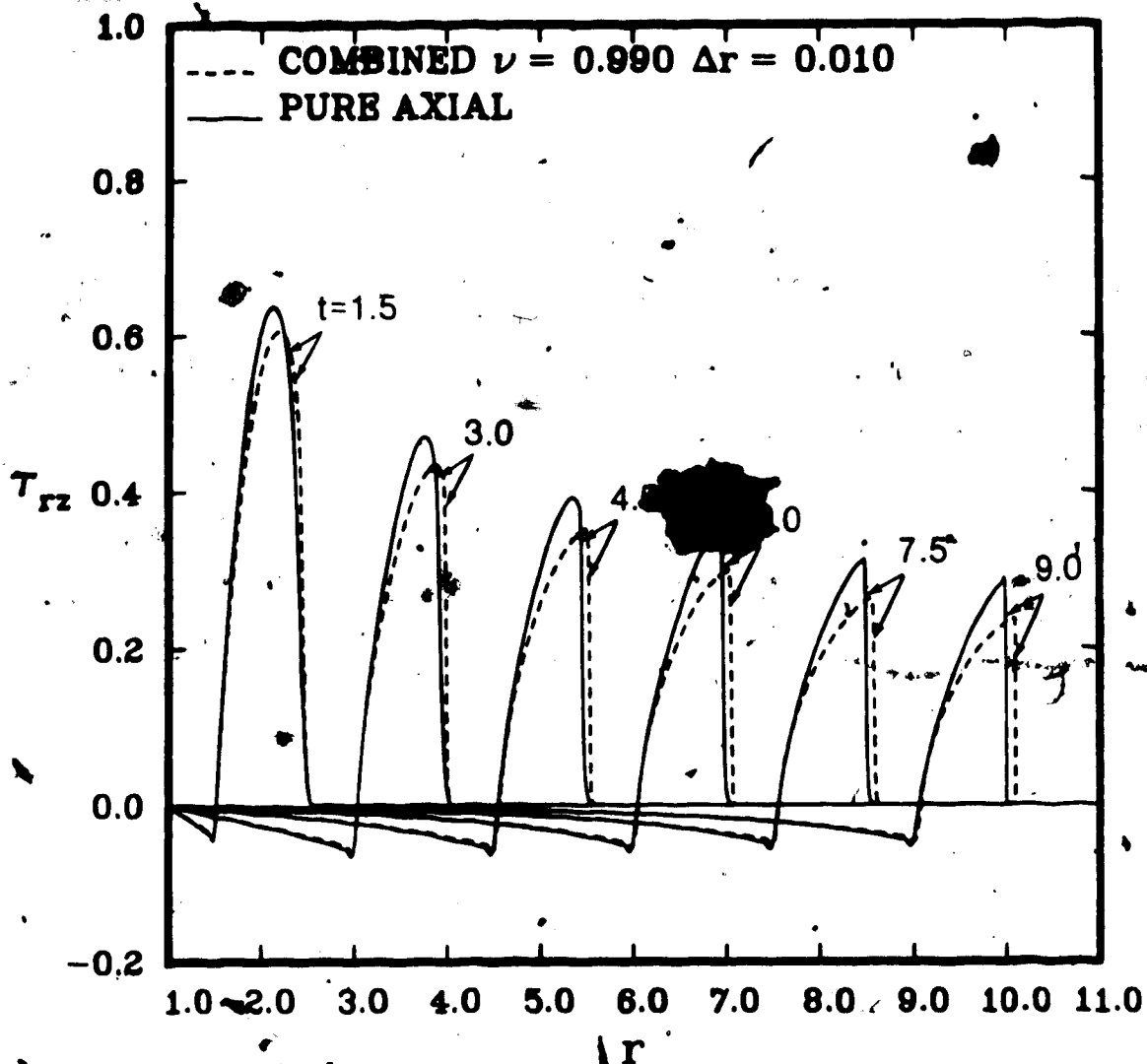


Fig. 4.56 Combined Shear - Variation of nondimensional T_{rz} with nondimensional r for $\gamma = 0.1$ for boundary condition (4.86), with $T_1 = T_2 = 1$ for combined shear and $T_1 = 1, T_2 = 0$ for axial shear, using the MacCormack scheme with $\nu = 0.99$.

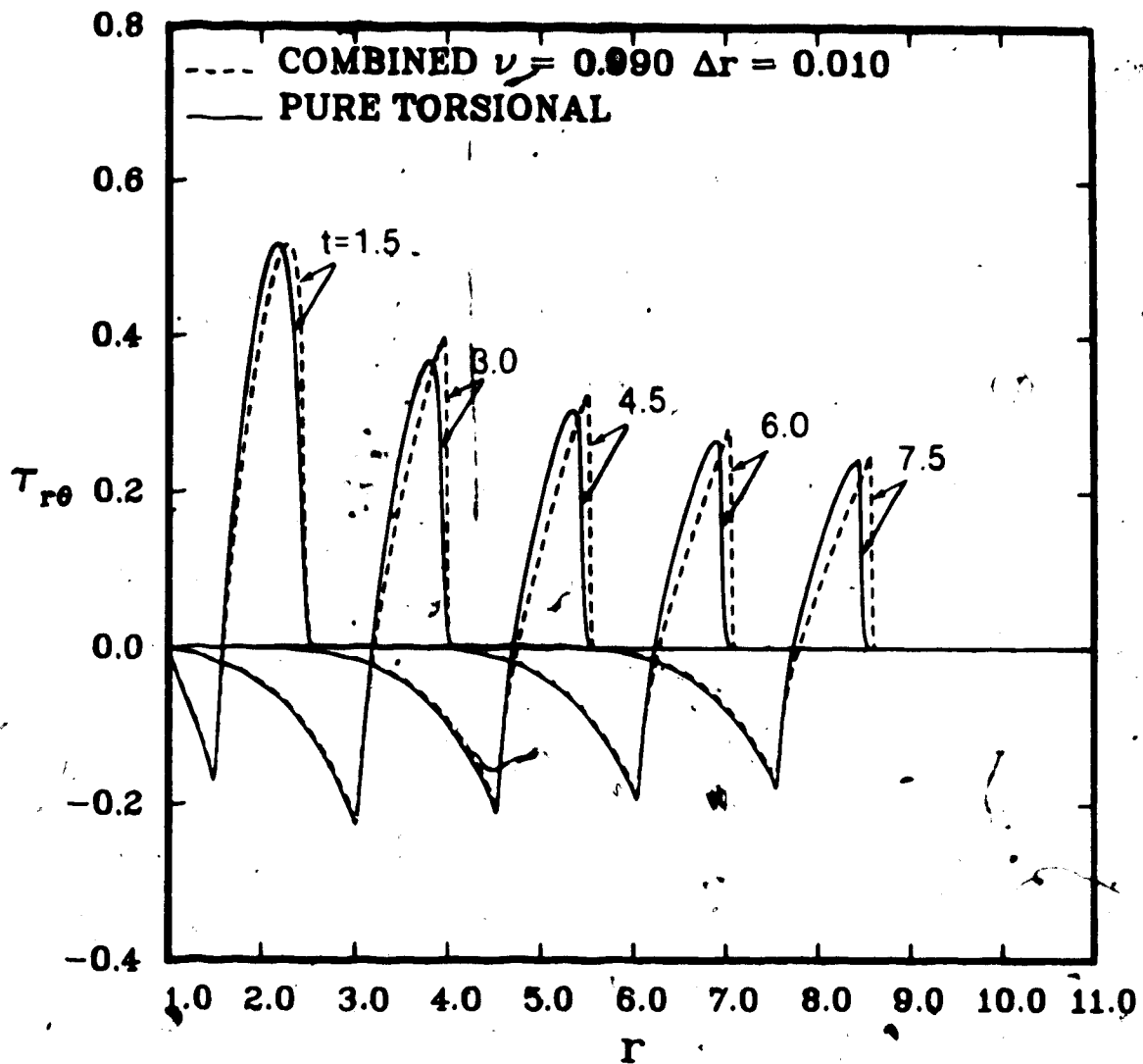


Fig. 4.57 Combined Shear - Variation of nondimensional shear stress $T_{r\theta}$ versus nondimensional r for $\gamma = 0.1$ for boundary condition (4.53) with $T_1 = T_2 = 1$ for combined shear and $T_1 = 0, T_2 = 1$ for torsional shear, using the MacCormack scheme with $\nu = 0.99$.

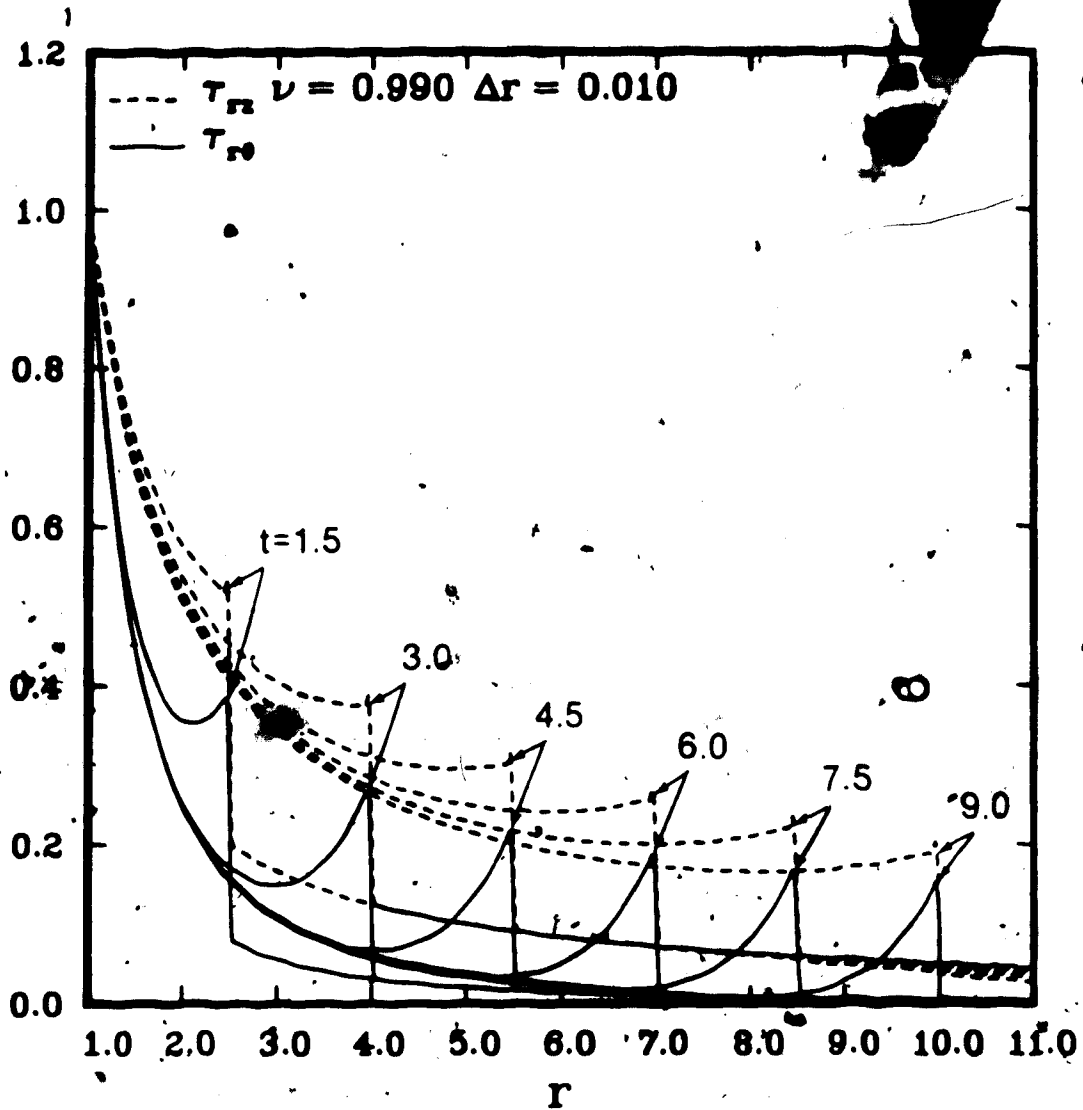


Fig. 4.58 Combined Shear - Variation of nondimensional τ_{rz} and $\tau_{r\theta}$ with nondimensional r for $\gamma = 0$, for boundary condition (4.85), with $T_{11} - T_{12} = 0.5$ and $T_1 - T_2 = 0.5$, using the MacCormack scheme with $\nu = 0.99$.

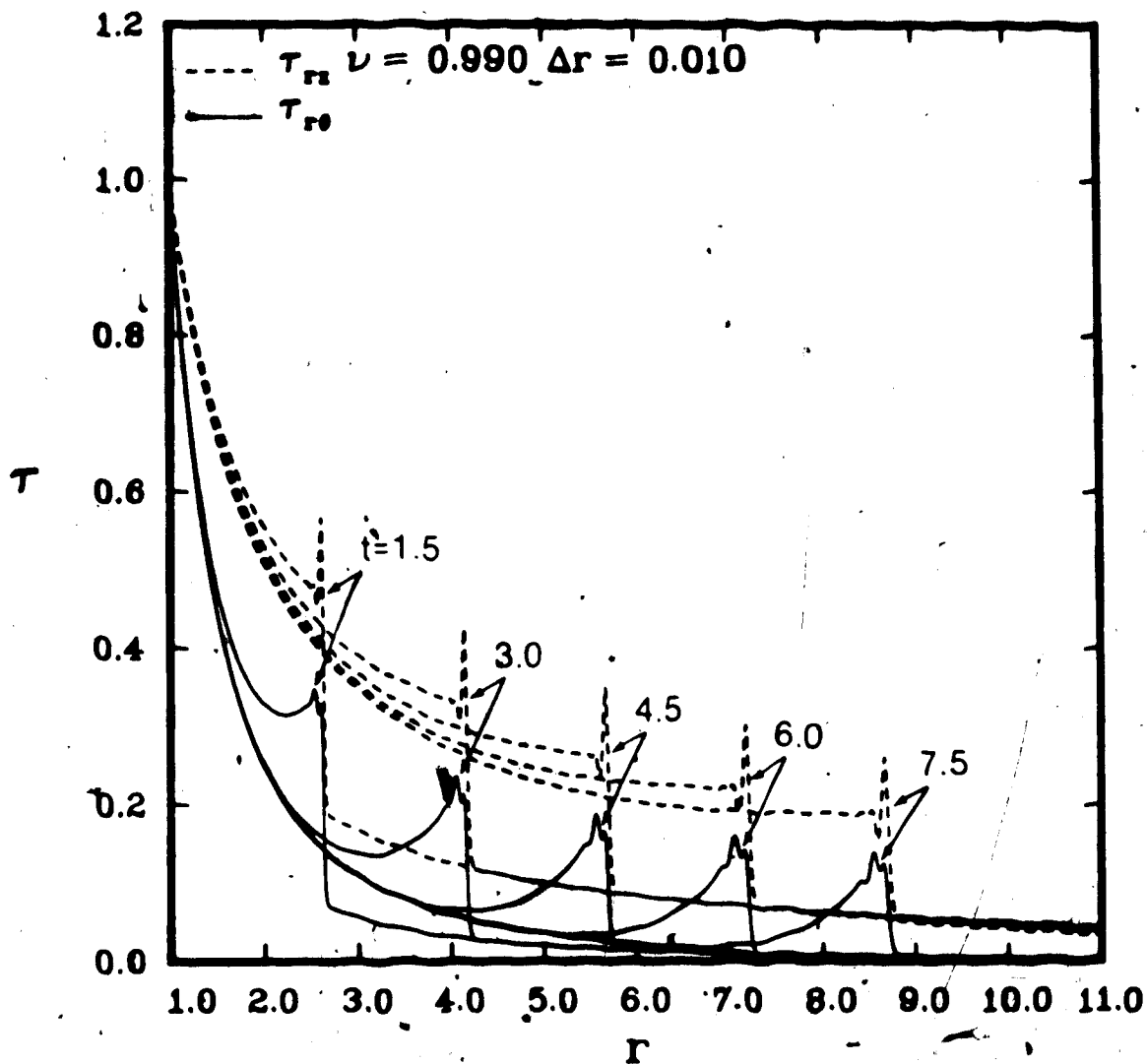


Fig. 4.59 Combined Shear - Variation of nondimensional τ_{rz} and $\tau_{r\theta}$ with nondimensional r for $\gamma = 0.1$, for boundary condition (4.85), with $T_{i1} = T_{i2} = 0.5$ and $T_1 = T_2 = 0.5$, using the MacCormack scheme with $\nu = 0.99$.

4.5 Concluding Remarks

The conservative version of the MacCormack scheme gives results that are in excellent agreement with analytical considerations, for the boundary initial value problems considered, provided the Courant number and Δt are carefully chosen. Numerical solutions are obtained for finite amplitude wave propagation into an initially prestressed quiescent incompressible hyperelastic solid, which would be difficult to obtain using other methods.

CHAPTER 5

FINITE AMPLITUDE WAVE PROPAGATION IN A NONLINEAR VISCOELASTIC SOLID

5.1 Introduction of the Problem

The nonlinear viscoelastic wave propagation problems considered in this chapter are based on a single integral constitutive equation for an isotropic incompressible viscoelastic solid. A class of constitutive equations has been proposed by Tait et al (1984) for finite deformation of viscoelastic solids, and the particular case considered here assumes both the impact and equilibrium responses are neo-Hookean.

Several other classes of single integral constitutive equations have been proposed for finite deformation of isotropic incompressible viscoelastic solids. The class proposed by Tait et al (1984) is a subclass of a more general class proposed by Lockett (1972). This subclass is of the form

$$\underline{\sigma} = -p\underline{I} + \underline{F}(t)[\underline{U}(t)]^{-1} \left[\int_{-\infty}^t G(t-s) \frac{d\psi[\underline{C}(s)]}{ds} ds \right] [\underline{U}(t)]^{-1} \underline{F}(t)^T \quad (5.1)$$

where \underline{I} is the identity matrix, p is not determined by the deformation, $\underline{F}(t)$ is the deformation gradient tensor at time t , $\underline{C}(t)$ is the right Cauchy-Green tensor $\underline{C}(t) = \underline{F}(t)^T \underline{F}(t) = [\underline{U}(t)]^2$ at time t , where superscript T denotes transpose, and $[\underline{U}(t)]^{-1}$ can be written as a function of $\underline{C}(t)$ and the basic invariants of $\underline{C}(t)$. The function $G(t-s)$ is the relaxation function and $\psi[\underline{C}(s)] = \beta_1 \underline{C} + \beta_2 \underline{C}^2$, where β_1 and β_2 are

functions of the first and second invariants of C . A more detailed derivation of the constitutive relationship is given by Tait et al. (1984).

For the problems considered, the relaxation function

$$G(t) = \mu \left\{ m + (1-m)e^{-t/\tau} \right\} \quad (5.2)$$

is assumed, where $0 < m \leq 1$ and τ is the relaxation time, μ is the impact shear modulus along with $\psi(C) = C$ to obtain

$$\underline{\sigma} = -p\underline{I} + \underline{\mu F}(t)[\underline{U}(t)]^{-1} \left[\int_{-\infty}^t [m + (1-m)e^{-(t-s)/\tau}] \frac{dC(s)}{ds} ds \right] [\underline{U}(t)]^{-1} \underline{F}(t)^T \quad (5.3)$$

7 which gives a neo-Hookean relation for both impact and equilibrium responses. This constitutive equation may be a good model for 'slightly' viscoelastic solids for which the impact and equilibrium responses are close. According to Tait et al (1984) a realistic condition for uniaxial stress problems involving compressive shocks, is $[\lambda] < 0.1$ where λ is the axial stretch. Other single integral relations have been proposed by Christensen (1980) and Coleman and Noll (1961). It may be shown that the class (5.1) is very similar but not exactly the same as the class of constitutive equations given by Coleman and Noll (1961). The main purpose of this chapter is to extend the results obtained by Tait et al (1984), using the proposed constitutive relationship and solving the governing equations by implementing the MacCormack scheme for the solution of boundary initial value problems.

5.2 Governing Equations

The nonlinear viscoelastic wave propagation problems considered in this chapter are based on the single integral constitutive equation for a viscoelastic material (Tait et al, 1984). The theory, as it applies to these problems, is summarized. Christensen (1982) and Lockett (1972) give a detailed treatment of the theory of nonlinear viscoelasticity.

The governing equations for the boundary initial value problems considered have been derived by Tait et al (1984) and analytical results presented for $m \rightarrow 1.0$ for an initially quiescent semi-infinite bar for boundary condition $S(0,t) = S_0H(t)$. The derivation of the governing equations, where S is the nominal axial stress, is summarized.

One dimensional wave propagation in a semi-infinite uniform prismatic bar composed of an isotropic incompressible standard viscoelastic solid, with constitutive equation (5.3) is considered. Radial inertia is neglected, the stress is assumed to be uniformly distributed across cross-sections normal to the axis of the bar, and it is assumed that cross-sections remain plane. A one dimensional Cartesian coordinate system is used with the X axis, coinciding with the axis of the bar (see Figure 5.1), where X and x are the coordinates of a particle in the undeformed and spatial configurations, respectively. The axis of the bar occupies the region $0 \leq X < \infty$ in the quiescent undeformed configuration at $t = 0$, where t is the temporal variable.

The deformation gradient tensor for the isochoric deformation due to uniaxial stress is

$$\underline{F} = \text{diag} (\lambda, \lambda^{-1/2}, \lambda^{-1/2}) \quad (5.4)$$

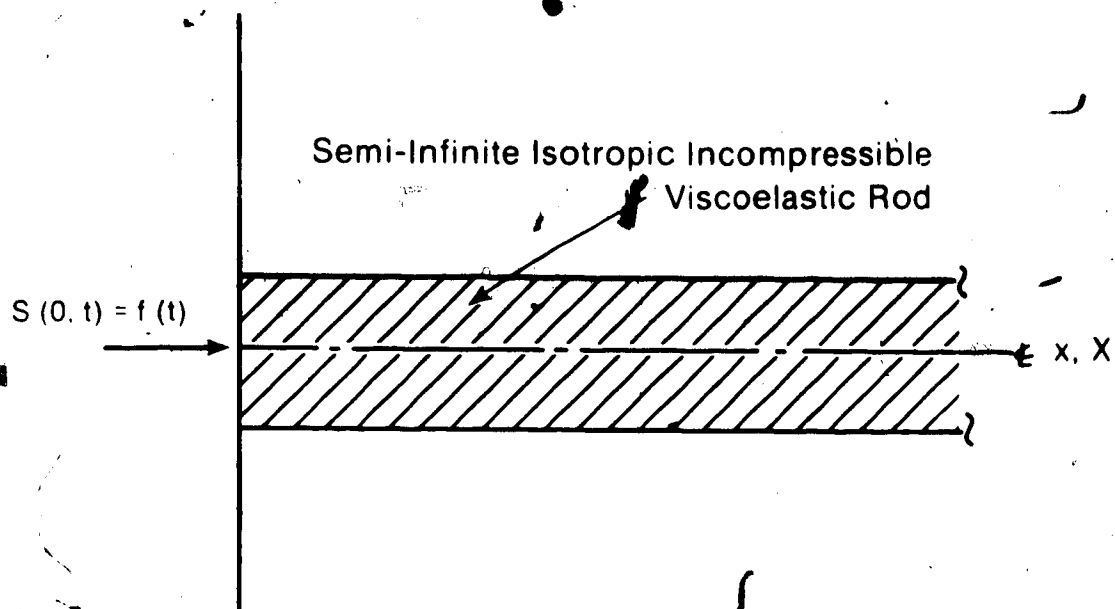


Fig. 5.1 Diagrammatic representation of finite amplitude longitudinal stress wave propagation in semi-infinite incompressible isotropic standard viscoelastic rod.

and the right Cauchy Green tensor $\underline{C} = \underline{F}^T \underline{F}$ is given by

$$\underline{C} = \text{diag} (\lambda^2, \lambda^{-1}, \lambda^{-1}) \quad (5.5)$$

where $\lambda = \partial x / \partial X$ for the uniaxial stress problem considered.

To investigate longitudinal wave propagation in a semi-infinite bar, the constitutive equation for an isotropic incompressible standard viscoelastic solid, as described earlier by equation (5.3), is used.

For the deformation considered, the constitutive relationship (5.3) reduces to

$$\sigma = \int_{-\infty}^t \mu \left\{ m + (1-m)e^{-(t-s)/\tau} \right\} d \left[\frac{\lambda^2 - \lambda^{-1}}{ds} \right] ds, \quad (5.6)$$

where σ is the uniaxial Cauchy stress. Since $\sigma = \lambda S$, where S is the axial nominal stress, the differential form of the constitutive equation is

$$\left\{ \frac{\partial}{\partial t} + \frac{1}{\tau} \right\} \left\{ \lambda S \right\} = \mu \left\{ \frac{\partial}{\partial t} + \frac{m}{\tau} \right\} \left\{ \lambda^2 - \lambda^{-1} \right\}. \quad (5.7)$$

Equation (5.7) along with the equation of motion and compatibility,

$$\frac{\partial S}{\partial X} - \rho \frac{\partial v}{\partial t} = 0 \quad (5.8)$$

$$\frac{\partial v}{\partial X} - \frac{\partial \lambda}{\partial t} = 0 \quad (5.9)$$

where $v = v(X, t)$ is the axial velocity, ρ is the constant density, gives the governing equations.

The governing nonlinear hyperbolic system of equations (5.7 - 5.9) is nondimensionalized, using the nondimensionalization scheme

$$\bar{t} = \frac{t}{\tau}, \quad (\bar{X}, \bar{x}) = \left(\frac{X, x}{c_0 \tau} \right), \quad (\bar{V}, \bar{v}) = \left(\frac{V, v}{c_0} \right), \quad (\bar{S}, \bar{\sigma}) = \left(\frac{S, \sigma}{\mu} \right), \quad (5.10)$$

where $c_0 = (\mu/\rho)^{1/2}$ is a reference velocity, and V is the shock speed.

The governing equations in nondimensional form are

$$\begin{aligned} \frac{\partial S}{\partial X} - \frac{\partial v}{\partial t} &= 0 \\ \frac{\partial v}{\partial X} - \frac{\partial \lambda}{\partial t} &= 0 \end{aligned} \quad (5.11)$$

$$\left\{ \frac{\partial}{\partial t} + 1 \right\} \left\{ \lambda S \right\} - \left\{ \frac{\partial}{\partial t} + m \right\} \left\{ \lambda^2 - \lambda^{-1} \right\}$$

Since equations (5.11)₁ and (5.11)₂ are in conservation form, the following nondimensional discontinuity relations are obtained,

$$\begin{aligned} [S] &= -V[v] \\ [v] &= -V[\lambda] \end{aligned} \quad (5.12)$$

where $[]$ denotes the jump in the quantity and V is the nondimensional shock velocity.

The system of equations (5.11) can be put in the form

$$\frac{\partial U}{\partial t} + \frac{A(U)}{\partial X} \frac{\partial U}{\partial X} + \frac{B(U)}{\partial X} = 0 \quad (5.13)$$

which is the form used for the application of the MacCormack scheme to obtain numerical solutions. Equation (5.11)₃ is not in conservation form. Although it is desirable to apply the MacCormack scheme to

systems of equations in conservation form, a conservation form was not found for equation (5.11)₃.

Equation (5.11) in the form (5.13) gives

$$\underline{U} = \begin{bmatrix} S \\ v \\ \lambda \end{bmatrix} \quad \underline{A}(\underline{U}) = \begin{bmatrix} 0 & ((S/\lambda) - 2 \cdot (1/\lambda^3)) & 0 \\ -1 & 0 & 0 \\ 0 & -1 & 0 \end{bmatrix} \quad \underline{A}(\underline{U}) \underline{U} = \begin{bmatrix} S - m(\lambda - (1/\lambda^2)) \\ 0 \\ 0 \end{bmatrix} \quad (5.14)$$

The matrix $\underline{A}(\underline{U})$ in equation (5.14) has eigenvalues given by $\pm c$, and zero where

$$c = (2 + \lambda^{-3} - \lambda^{-1})^{1/2} \quad (5.15)$$

Consequently the characteristics in the (X,t) plane have slopes

$$\frac{dX}{dt} = \pm c, \quad \frac{dx}{dt} = 0 \quad (5.16)$$

In the undisturbed region ahead of the wavefront $\lambda = 1$, $S = 0$, so that $c(1) = \sqrt{3}$.

5.3 Formulation of the Problem

Longitudinal wave propagation along a semi-infinite uniform prismatic bar (see Figure 5.1) due to a sudden application of an axial force at the free end or a finite duration pulse in the force at the free end is considered. The initial conditions are quiescent and unstressed so that

$$S(X,0) = 0, \quad v(X,0) = 0, \quad \lambda(X,0) = 1 \quad (5.17)$$

The boundary conditions at $X = 0$ are

$$S(0, t) = S_0 H(t) \quad (5.18)$$

or

$$S(0, t) = S_0 \sin \pi t H(t) H(1-t) \quad (5.19)$$

corresponding to the sudden application of axial stress (5.18) or a finite duration stress pulse (5.19). It should be noted that the governing equations are given in terms of the material coordinates. For a compressive axial force, $S_0 < 0$.

5.4 Implementation of the MacCormack Scheme

The MacCormack finite difference scheme given by equation (2.7), for the nonconservation form of the equations is used to solve the system of equations (5.13) and (5.14). Application of the finite difference equations (2.7) gives the following predictor and corrector steps,

$$\overline{U}_{-j}^{n+1} = U_{-j}^n - \frac{\Delta t}{\Delta X} A(U_{-j}^n) (U_{-j+1}^n - U_{-j}^n) - \Delta t B(U_{-j}^n) \quad (5.20)$$

$$U_{-j}^{n+1} = \frac{1}{2} \left\{ U_{-j}^n + \overline{U}_{-j}^{n+1} - \frac{\Delta t}{\Delta X} A(\overline{U}_{-j}^{n+1}) (\overline{U}_{-j}^{n+1} - \overline{U}_{-j-1}^{n+1}) - \Delta t B(\overline{U}_{-j}^{n+1}) \right\}$$

where $U_{-j}^n = U(j\Delta X, n\Delta t)$, $j = 0, 1, 2, \dots$, $n = 0, 1, 2, \dots$,

with the subscript and superscript notation as indicated in Chapter 2.

The element $S(0,t)$ of $U(0,t)$ is obtained from the boundary condition (5.18) or (5.19), so that S_0^n is known for all n . In order to apply equations (5.20), λ_0^n and v_0^n are also required for all n , and this is obtained by applying boundary conditions as discussed in Section 2.3, using forward forward (FF) differencing at the left boundary and backward backward (BB) at the right boundary. For the nonconservative difference scheme, λ_0^{n+1} and v_0^{n+1} can be found directly from the predictor equation (5.20)₁, by substituting $j = 0$, and the corrector equations, then are given by

$$\lambda_0^{n+1} = \frac{1}{2} \left\{ \lambda_0^n + \lambda_0^{n+1} - \frac{\Delta t}{\Delta X} (-v_1^{n+1} + v_0^{n+1}) \right\}$$

and

$$v_0^{n+1} = \frac{1}{2} \left\{ v_0^n + v_0^{n+1} - \frac{\Delta t}{\Delta X} (-S_1^{n+1} + S_0^{n+1}) \right\}$$

according to Gottlieb and Turkel (1978).

For the boundary condition (5.18), a modified treatment of the boundary condition is also used, to compare with the method suggested by Gottlieb and Turkel (1978). Using the constitutive equation (5.7), $\lambda(0,t)$ is found by evaluating the differential equation

$$\left\{ \frac{\partial}{\partial t} + 1 \right\} \left\{ \lambda(0,t) S(0,t) \right\} = \left\{ \frac{\partial}{\partial t} + m \right\} \left\{ (\lambda(0,t))^2 - (\lambda(0,t))^{-1} \right\} \quad (5.22)$$

and for boundary condition (5.18), the equation simplifies to

$$\frac{d\lambda(0,t)}{dt} = \left[m (\lambda(0,t))^2 - S_0 \lambda - \frac{m}{\lambda(0,t)} \right] \left[S_0 - 2\lambda(0,t) - \frac{1}{\lambda^2} \right]^{-1} \quad (5.23)$$

Since S_0 is specified, $\lambda(0,t)$ can be evaluated using a Runge Kutta technique for the solution of the differential equation (5.23).

5.5 Momentum Considerations

Since momentum must be conserved for the problems considered, numerical evaluation of momentum provides a check on the numerical solution. The nondimensional relation

$$\int_0^t S(0,\eta) d\eta = \int_1^{X_f(t)} v(X,t) dX, \quad (5.24)$$

where $X_f(t)$ is the position of the wavefront at time t , follows from conservation of momentum. The right hand side of equation (5.24) is evaluated numerically using a Simpson's integration scheme. The exact values of nondimensional momentum, found by evaluating the left hand side of equation (5.24) are used to compare to those obtained from the numerical results.

The numerical evaluation of momentum for each time step must be equal to the values obtained by integrating the left hand side of (5.24) for the specified boundary conditions. The mechanical energy is not considered, since the governing equations are dissipative.

5.6 Numerical Results

The numerical results in this section have been obtained using the nonconservative version of the MacCormack scheme, and Gottlieb boundary conditions unless otherwise specified. Numerical results are presented

for nondimensional S versus nondimensional X for various nondimensional times t . Only quiescent unstressed initial conditions, given by (5.17), are considered.

The numerical results in Figure 5.2 show the effect of Courant number for boundary condition (5.18), with $S_0 = -1.0$ and $m = 0.1$. The Courant number does not affect the position of the wavefront indicated by the results. However, the numerical solutions at various times obtained using a small Courant number ($\nu = 0.5$) have severe numerical dispersion. There is no apparent instability in the numerical results for this problem, for $\nu = 1.0$, and the maximum nondimensional time considered. The momentum calculations corresponding to each figure, according to equation (5.24), are in agreement with exact values for each of the Courant numbers considered. Figure 5.2 shows results for $S_0 = -1.0$ which is not physically realistic, since the jump in cross-sectional area implied by a shock would have to take place over too long a length for the shock assumption to be valid. A value of $S_0 = -0.16$ gives $|\lambda| = 0.0506$, which is within the recommended limit of $|\lambda| < 0.1$ (Tait et al 1984) and should be considered for practical application. Figure 5.2 is presented as a demonstration of the effect of Courant number on the numerical solution.

Figure 5.3 gives numerical results for a more realistic problem for boundary condition (5.18), since $S_0 = -0.16$. The results presented in Figure 5.3, for $m = 0.9$, are in good agreement with those obtained by Tait et al (1984). The position of the shock front is consistent with the shock speeds given by Tait et al (1984). Nondimensional momentum calculations, based on the numerical results, indicate conservation of

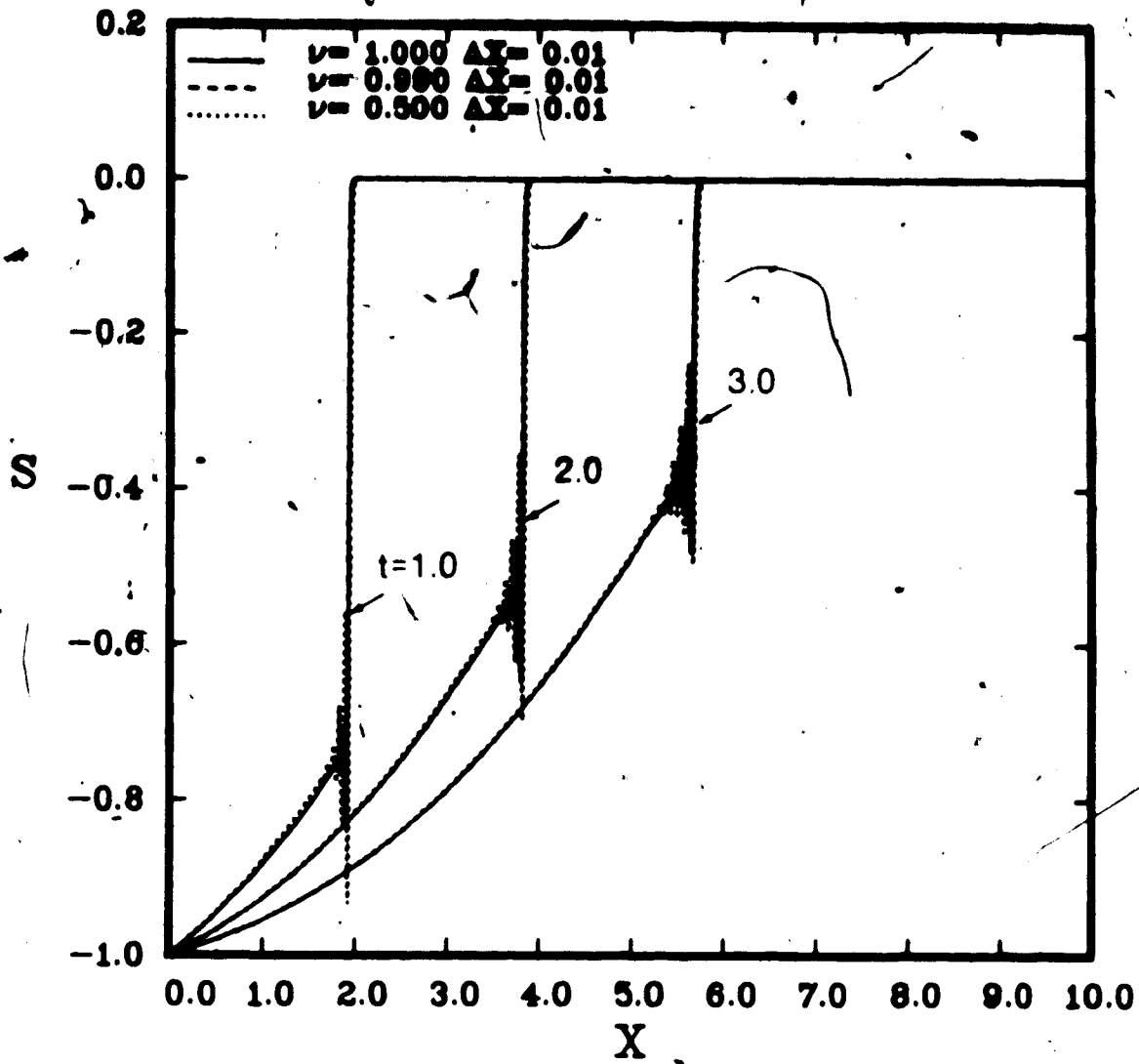


Fig. 5.2 Effect of Courant number on the variation of nondimensional S with nondimensional X for $m = 0.1$ and $S(0, t) = S_0 H(t)$, with $S_0 = -1.0$, using the nonconservative MacCormack scheme with $\nu = 1.0$.

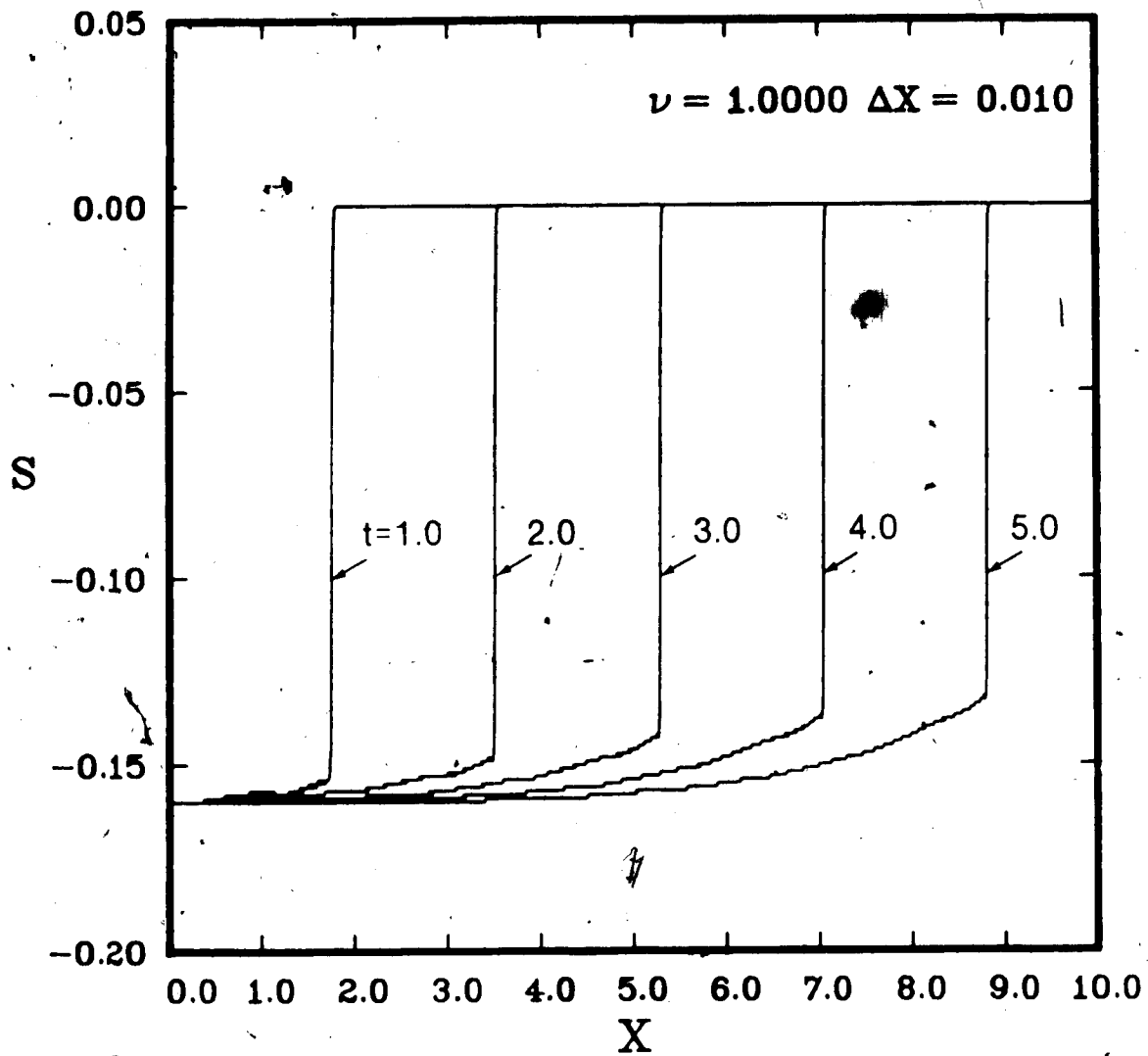


Fig. 5.3 Variation of nondimensional S with nondimensional X for $m = 0.9$ and $S(0,t) = S_0 H(t)$, with $S_0 = -0.16$, using the nonconservative MacCormack scheme with $\nu = 1.0$.

momentum for the times considered, and the jump conditions given by (5.12) are satisfied. Even though the nonconservative version of the MacCormack scheme is used, there does not appear to be any violation of momentum conservation or jump conditions at the shock front. The MacCormack scheme for this problem is in complete agreement with the results obtained by Tait et al (1984), for $m \rightarrow 1.0$.

Figures 5.4 and 5.5 show the variation of S with X at various times for boundary condition (5.18), with $S_0 = -0.16$, for $m = 0.1$ and $m = 1.0$, respectively, where $m = 0.1$ corresponds to a very viscoelastic solid and $m = 1.0$ corresponds to a neo-Hookean solid. The numerical results presented in Figure 5.5 are consistent with theoretical considerations for boundary condition (5.18), which indicate that a compressive step discontinuity in stress should propagate unchanged in shape in an elastic solid. There is numerical dispersion evident in both Figures 5.4 and 5.5, but no instability.

Figures 5.6 - 5.8 show the variation of S with X at various times for boundary condition (5.19), with $S_0 = -0.16$, for $m = 0.1$, $m = 0.9$ and $m = 1.0$, respectively. There is a slight steepening of the wavefront for increasing time in each of Figures 5.6 - 5.8. The numerical results indicate the possibility of shock evolution for each of the problems represented.

Figures 5.9 - 5.11 show the variation of S with X at various times for boundary condition (5.18), with $S_0 = 0.16$, for $m = 0.1$, $m = 0.9$ and $m = 1.0$, respectively. Since $S_0 > 0$, these results are for sudden application of tensile stress at $X = 0$. The numerical results in Figure 5.11 correspond to wave propagation in a neo-Hookean solid, since

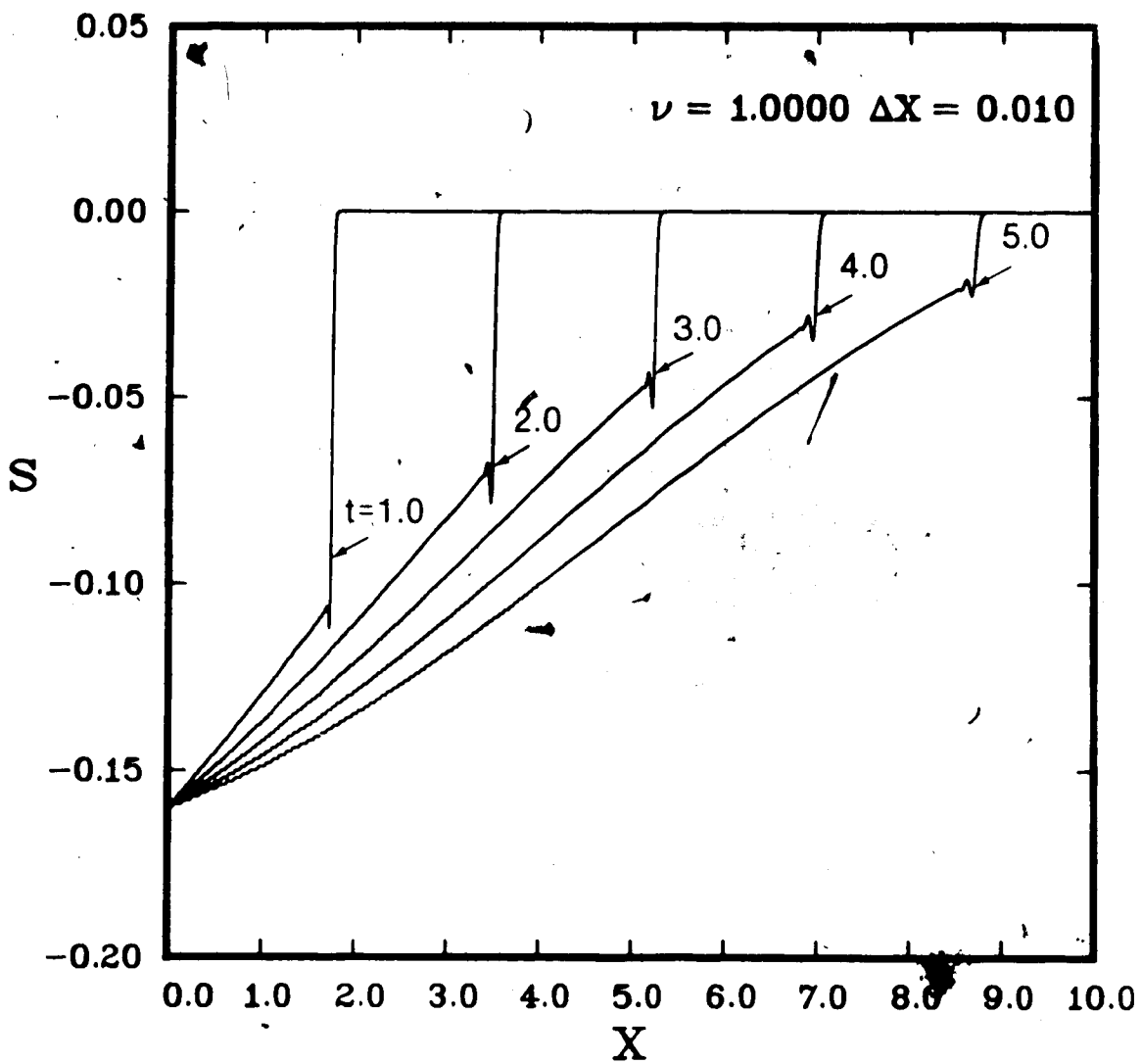


Fig. 5.4 Variation of nondimensional S with nondimensional X for $m = 0.1$ and $S(0,t) = S_0 H(t)$, with $S_0 = -0.16$, using the nonconservative MacCormack scheme with $\nu = 1.0$.

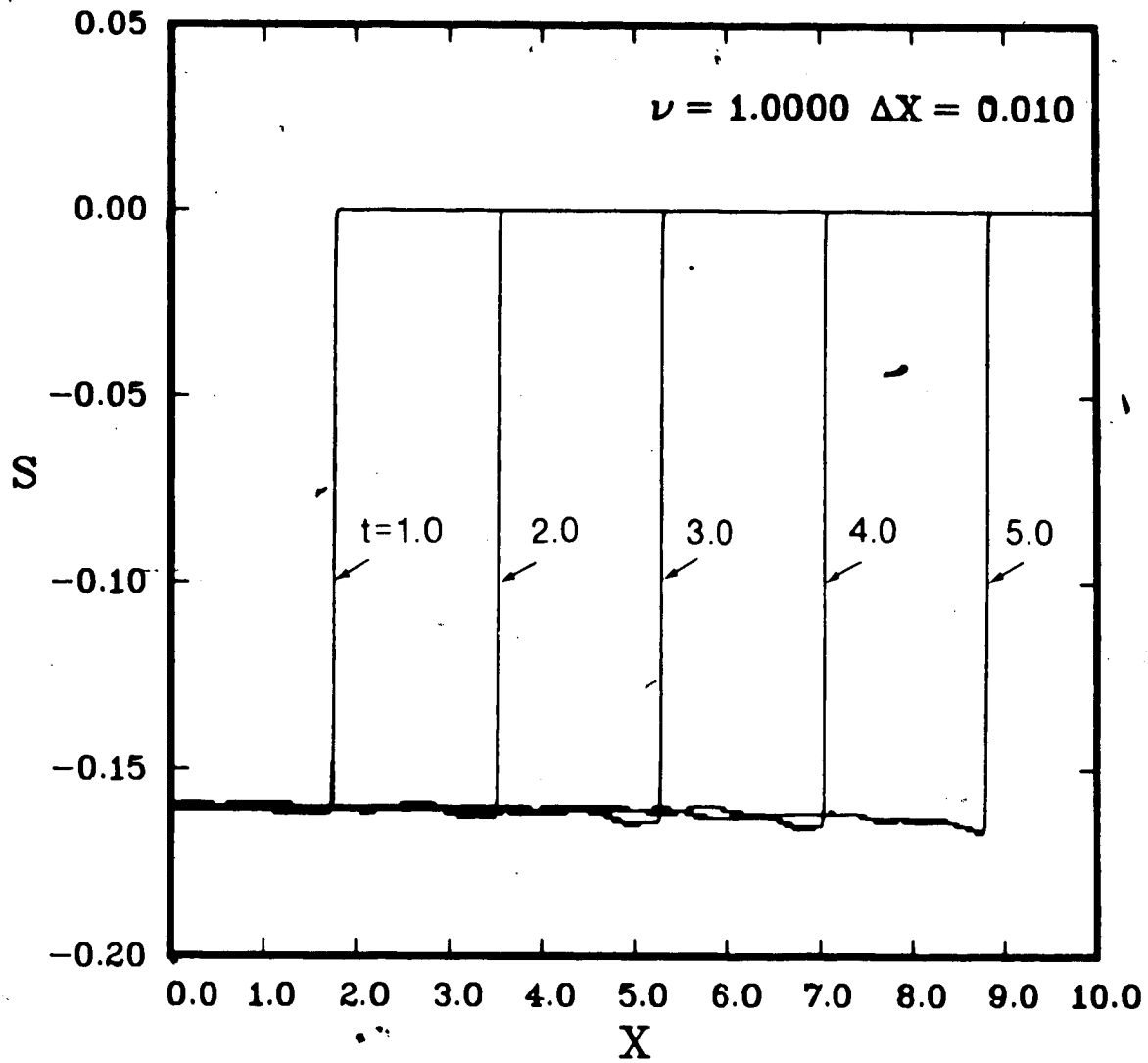


Fig. 5.5 Variation of nondimensional S with nondimensional X for $m = 1.0$ and $S(0,t) = S_0 H(t)$, with $S_0 = -0.16$, using the nonconservative MacCormack scheme with $\nu = 1.0$.

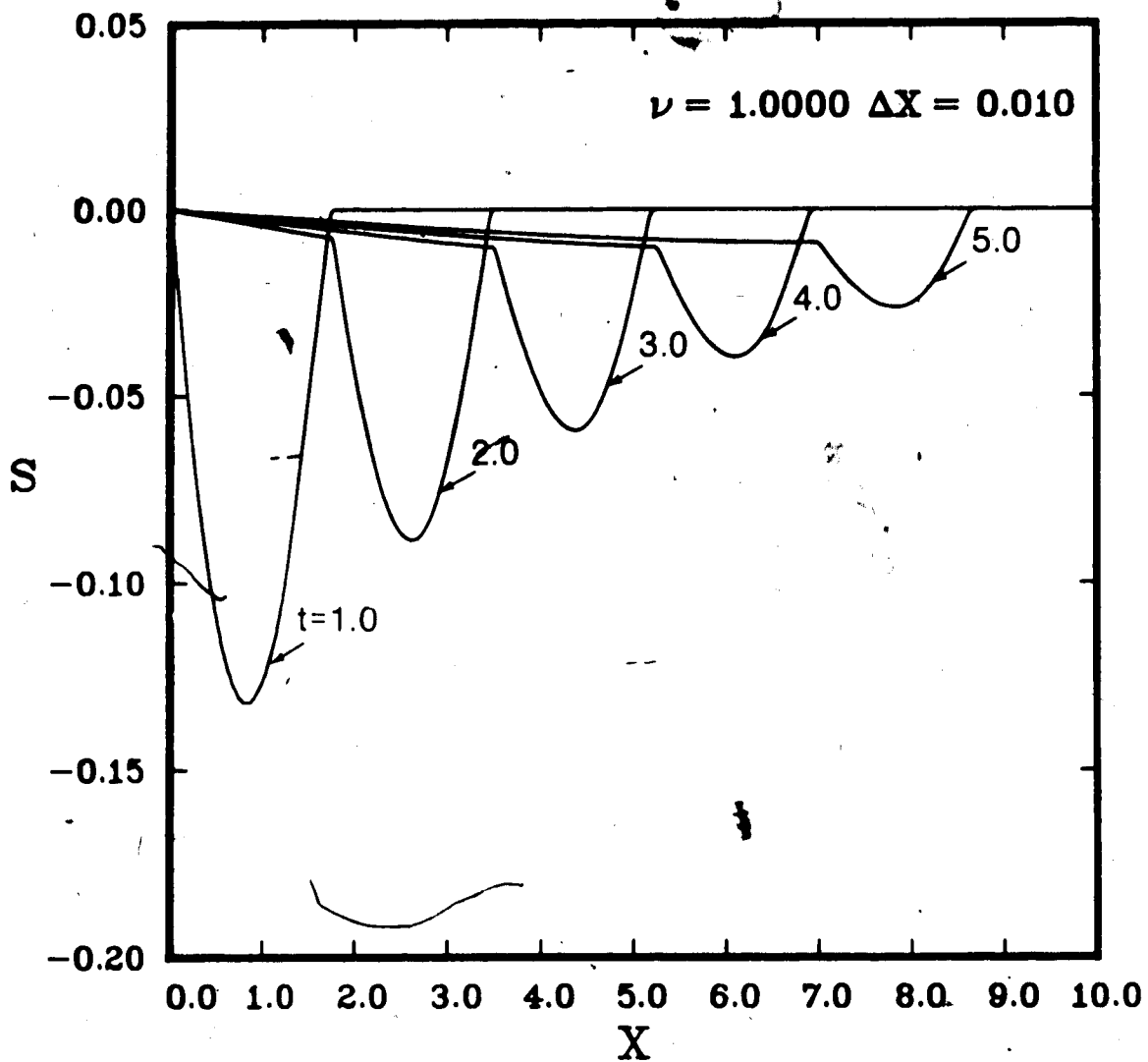


Fig. 5.6 Variation of nondimensional S with nondimensional X for $m = 0.1$ and $S(0,t) = S_0 \sin \pi t H(t) H(1-t)$, with $S_0 = -0.16$, using the nonconservative MacCormack scheme with $\nu = 1.0$.

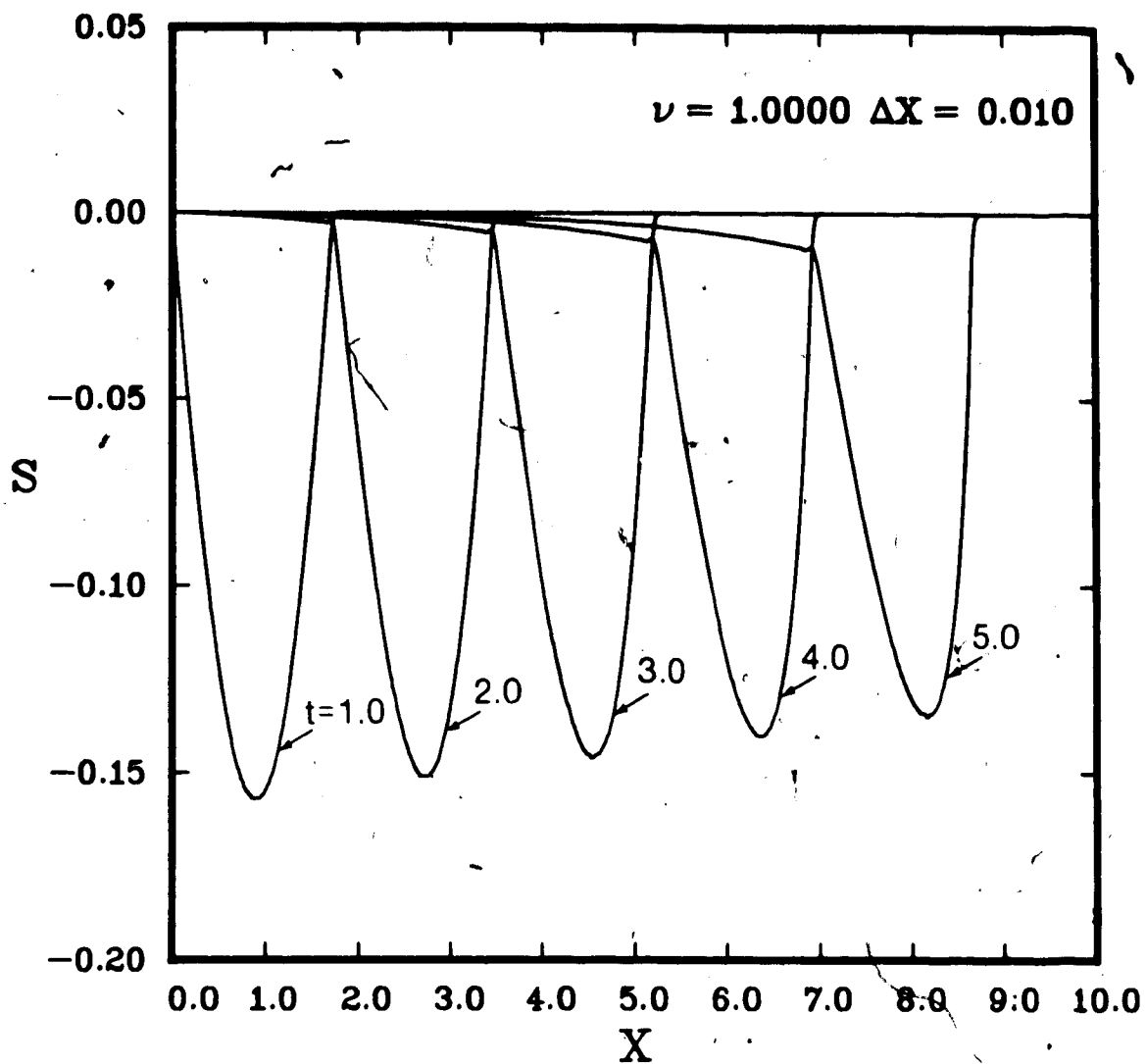


Fig. 5.7 Variation of nondimensional S with nondimensional X for $m = 0.9$ and $S(0,t) = S_0 \sin \pi t H(t) H(1-t)$, with $S_0 = -0.16$, using the nonconservative MacCormack scheme with $\nu = 1.0$.

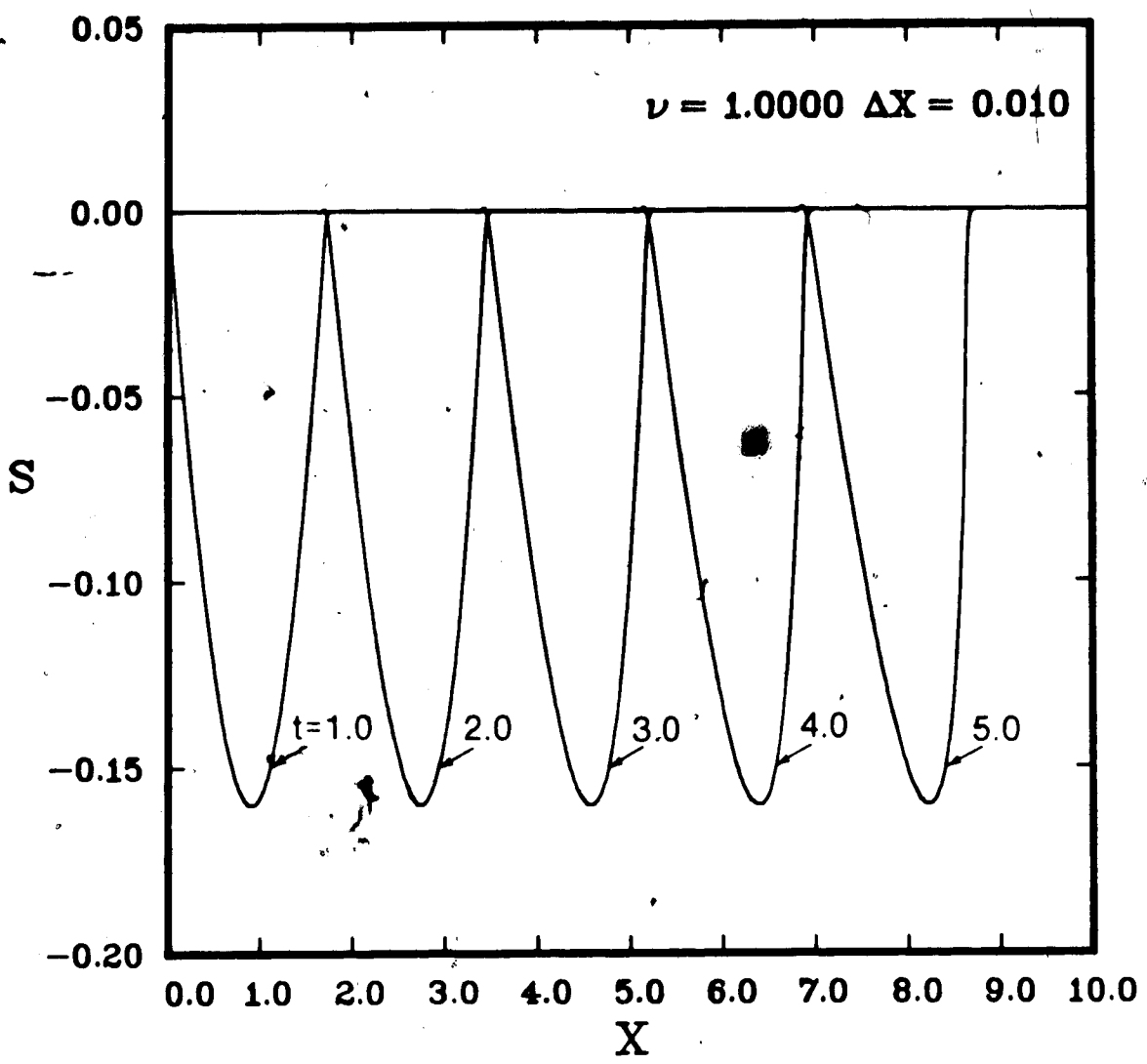


Fig. 5/8 Variation of nondimensional S with nondimensional X for $m = 1.0$ and $S(0,t) = S_0 \sin \pi t H(t) H(1-t)$, with $S_0 = -0.16$, using the nonconservative MacCormack scheme with $\nu = 1.0$.

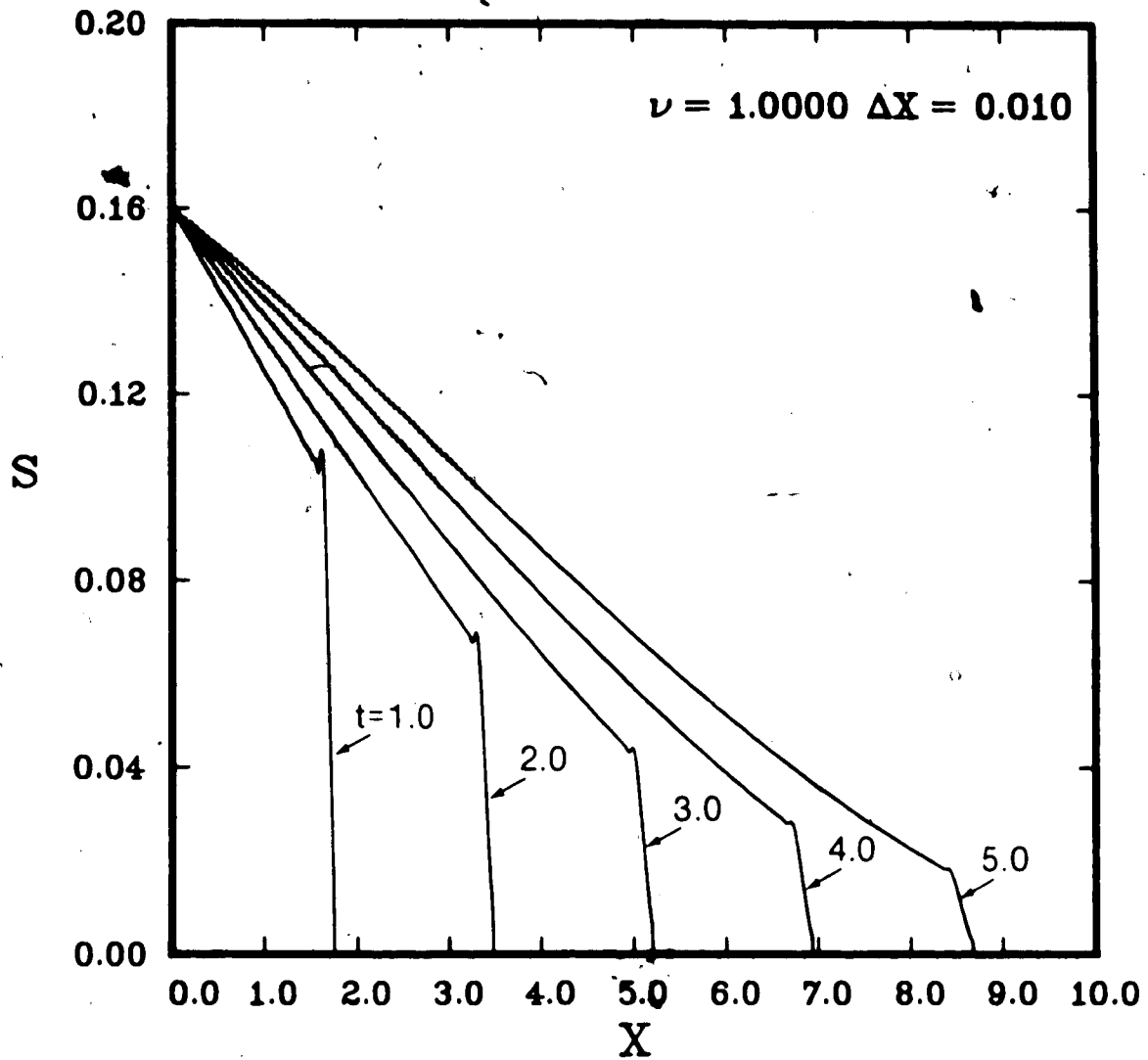


Fig. 5.9 Variation of nondimensional S with nondimensional X for $m = 0.1$ and $S(0,t) = S_0 H(t)$, with $S_0 = 0.16$, using the nonconservative MacCormack scheme with $\nu = 1.0$.

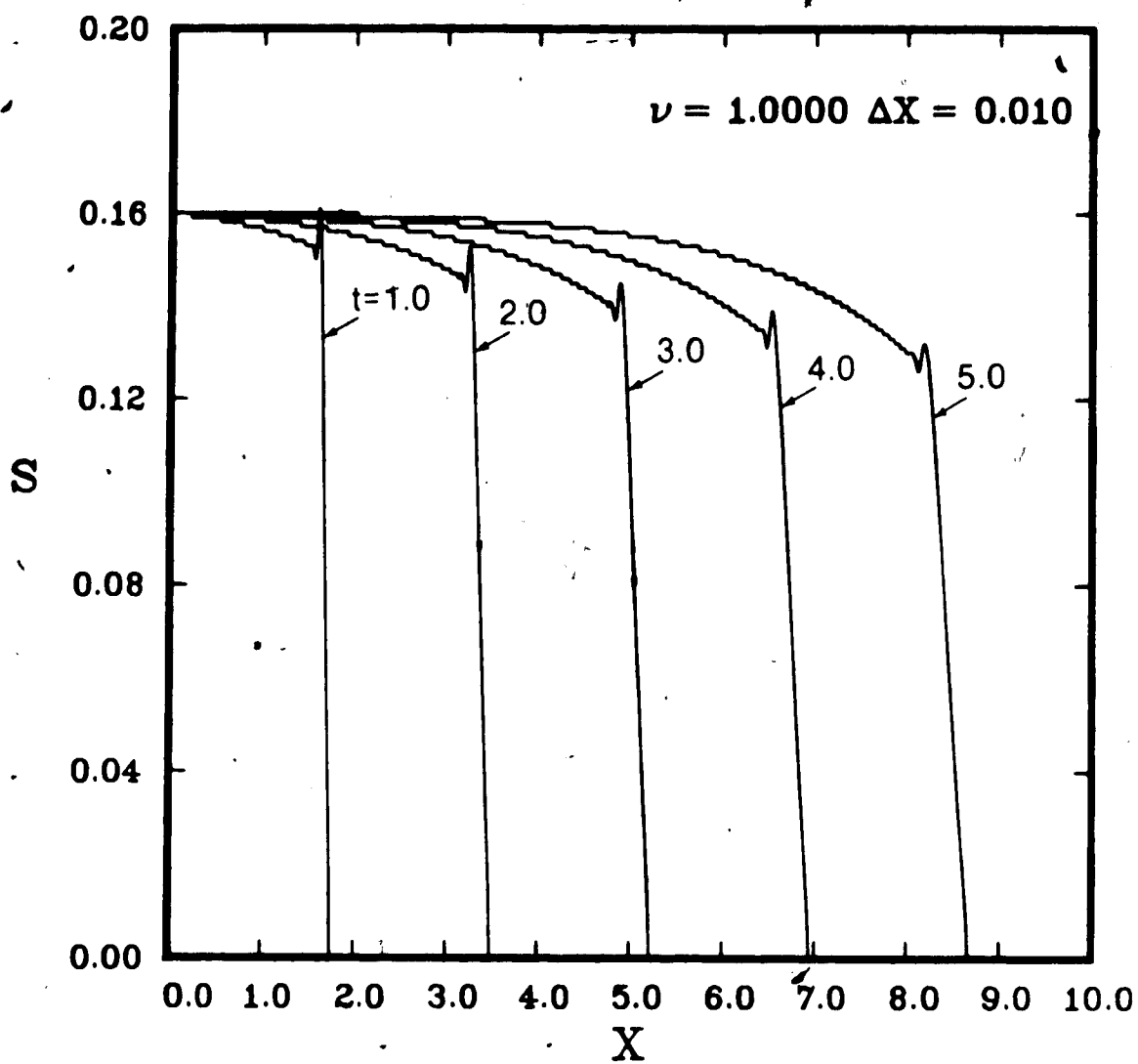


Fig. 5.10 Variation of nondimensional S with nondimensional X for $m = 0.9$ and $S(0,t) = S_0 H(t)$, with $S_0 = 0.16$, using the nonconservative MacCormack scheme with $\nu = 1.0$.

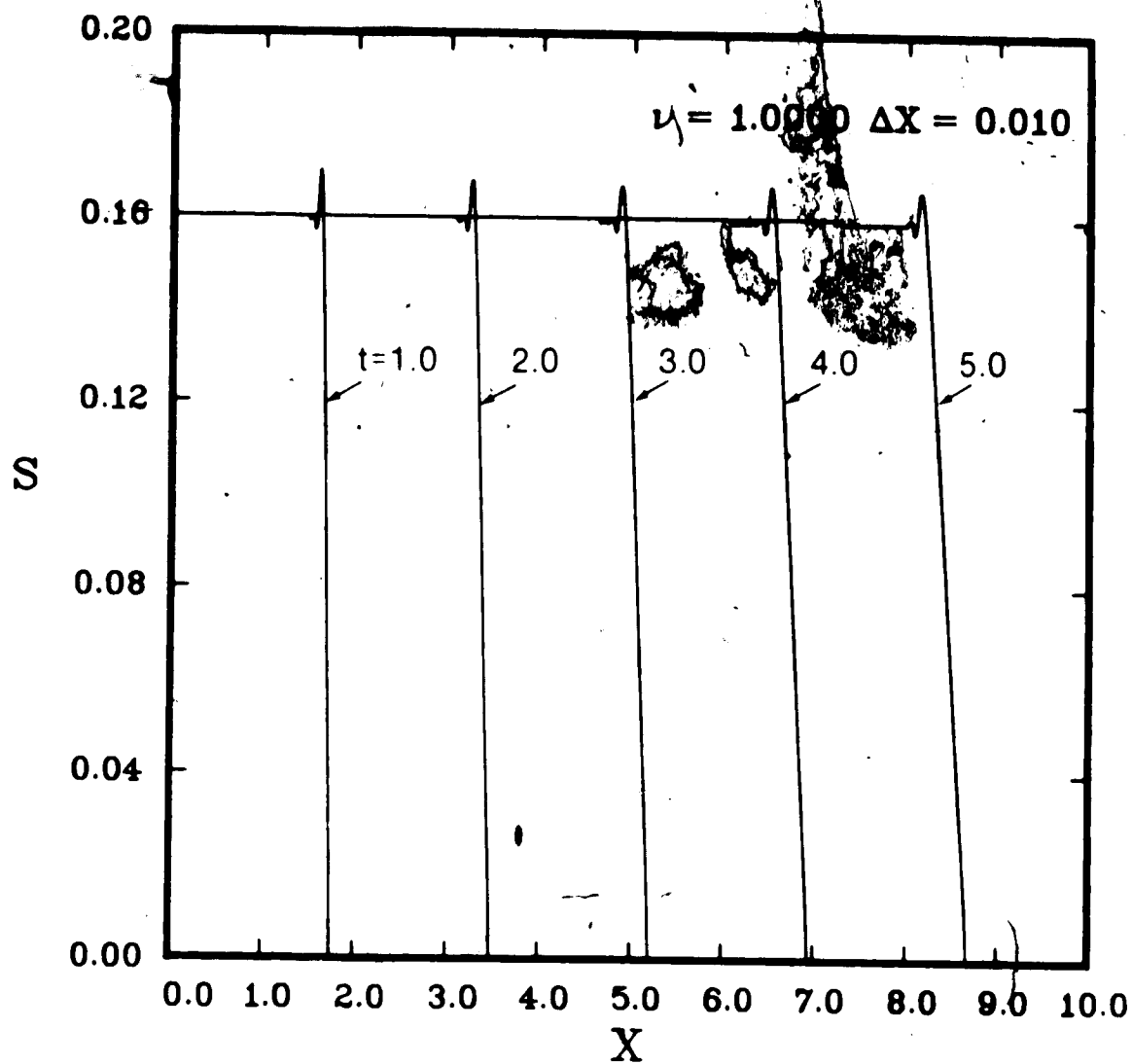


Fig. 5.11 Variation of nondimensional S with nondimensional X for $m = 1.0$ and $S(0,t) = S_0 H(t)$, with $S_0 = 0.16$, using the nonconservative MacCormack scheme with $\nu = 1.0$.

$m = 1.0$. The numerical results in Figure 5.11 are in complete agreement with results obtained by the method of characteristics except for numerical dispersion. There is numerical dispersion evident in Figures 5.9 - 5.11. The amount of numerical dispersion in Figure 5.9 for $m = 0.1$ decreases with increasing time.

Figures 5.12 - 5.14 show the variation of S with X at various times for boundary condition (5.19), with $S_0 = 0.16$, for $m = 0.1$, $m = 0.9$ and $m = 1.0$, respectively. Since $S_0 > 0$, these results correspond to a tensile axial stress pulse at $X = 0$. There appears to be some steepening of the unloading portion of the sine pulse, which indicates the evolution of an unloading shock, in each of Figures 5.12 - 5.14. There appears to be very little numerical dispersion, in any of these figures.

Although the boundary condition (5.19) with $|S_0| = 1$ does not give a physically realistic problem, some interesting results were obtained. Figures 5.15 - 5.17 show the variation of S with X at various times for boundary condition (5.19), with $S_0 = -1.0$, for $m = 0.1$, $m = 0.9$ and $m = 1.0$, respectively. Figures 5.15 - 5.17 indicate that the wave, propagating into the material, breaks. The wave breaks at different times, for different values of m . In Figure 5.15, the wave breaks at $t \approx 3.0$ for $m = 0.1$. In Figure 5.16, the wave breaks at $t \approx 2.0$, for $m = 0.9$. In Figure 5.17, the wave breaks, again for $t \approx 2.0$, for $m = 1.0$. There are very unusual oscillations appearing in the numerical results given in Figures 5.16 and 5.17, which appear after the wave breaks. These oscillations are not apparent in Figure 5.15.

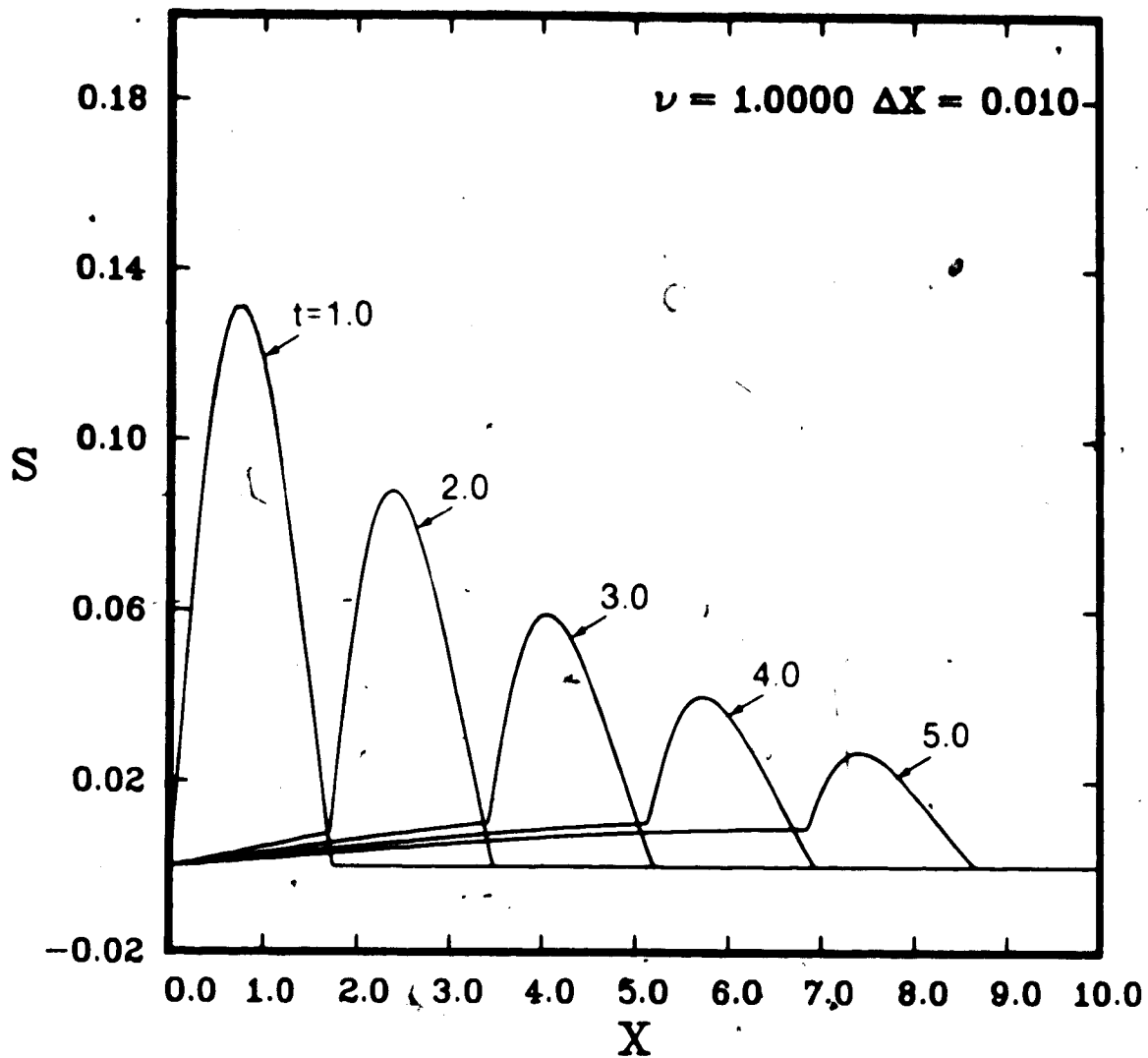


Fig. 5.12 Variation of nondimensional S with nondimensional X for $m = 0.1$ and $S(0,t) = S_0 \sin \pi t H(t) H(1-t)$, with $S_0 = 0.16$, using the nonconservative MacCormack scheme with $\nu = 1.0$.

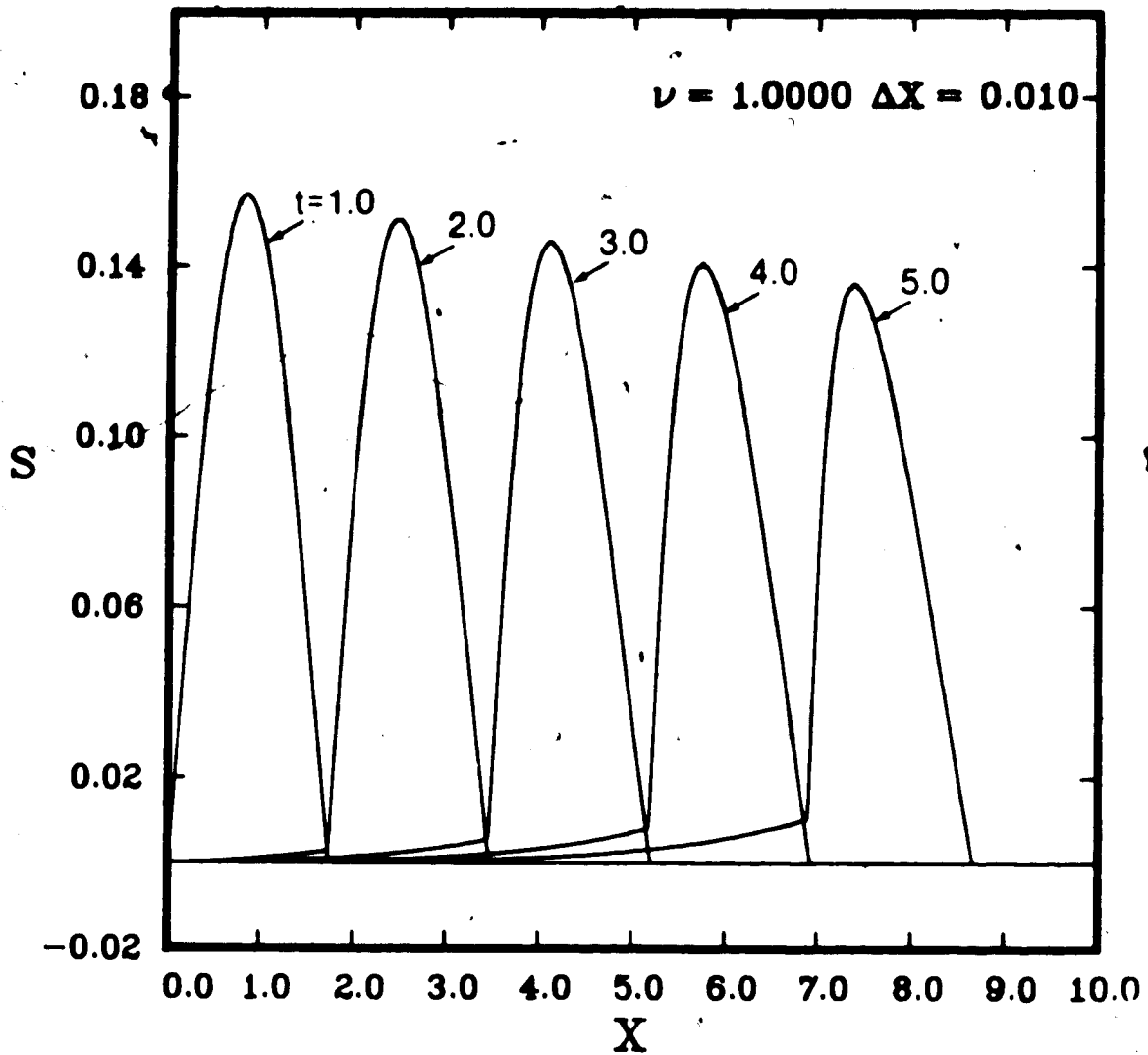


Fig. 5.13 Variation of nondimensional S with nondimensional X for $\nu = 0.9$ and $S(0,t) = S_0 \sin \pi t H(t) H(1-t)$, with $S_0 = 0.16$, using the nonconservative MacCormack scheme with $\nu = 1.0$.

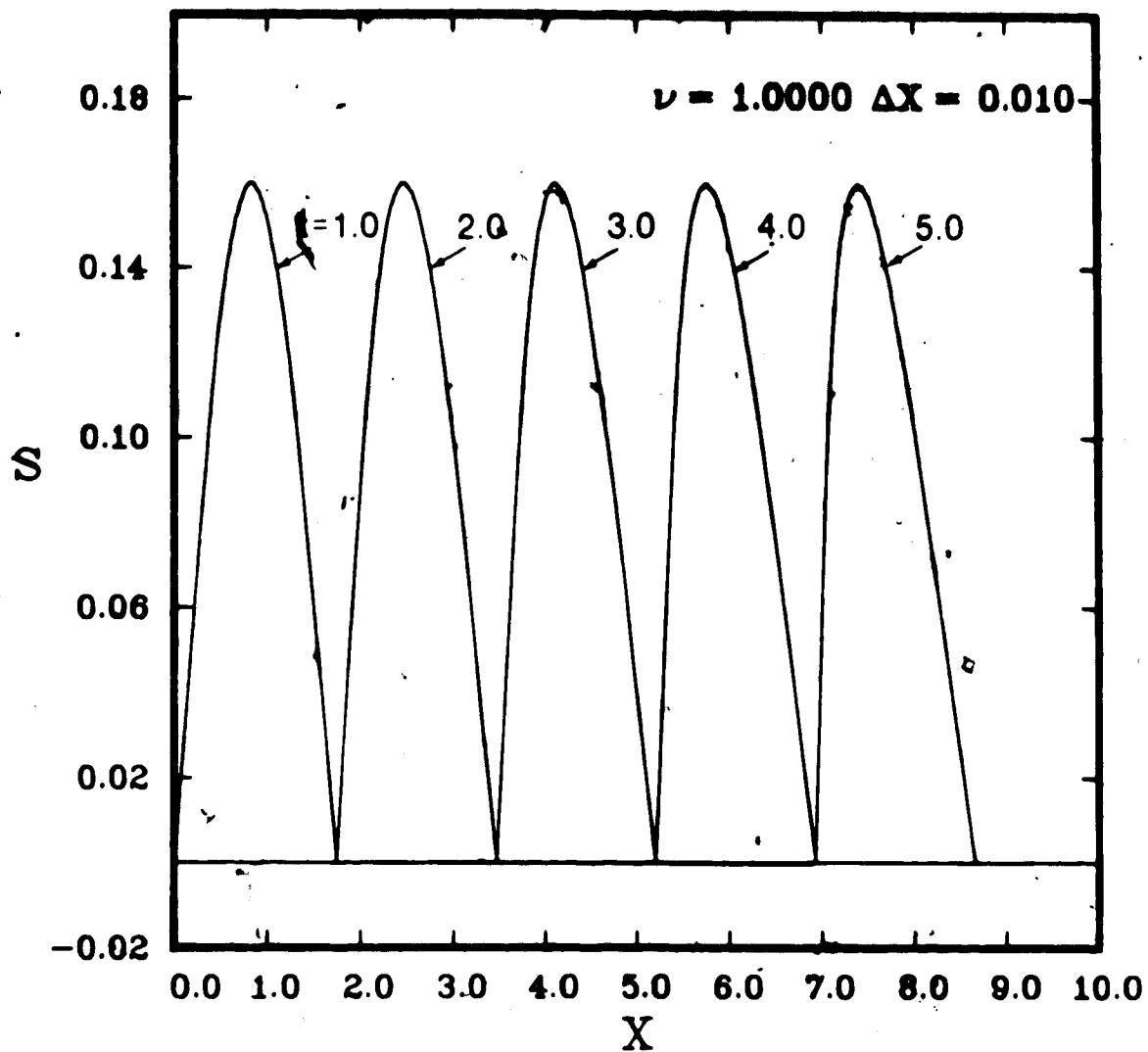


Fig. 5.14 Variation of nondimensional S with nondimensional X for $m = 1.0$ and $S(0, t) = S_0 \sin \pi t H(t) H(1-t)$, with $S_0 = 0.16$, using the nonconservative MacCormack scheme with $\nu = 1.0$.

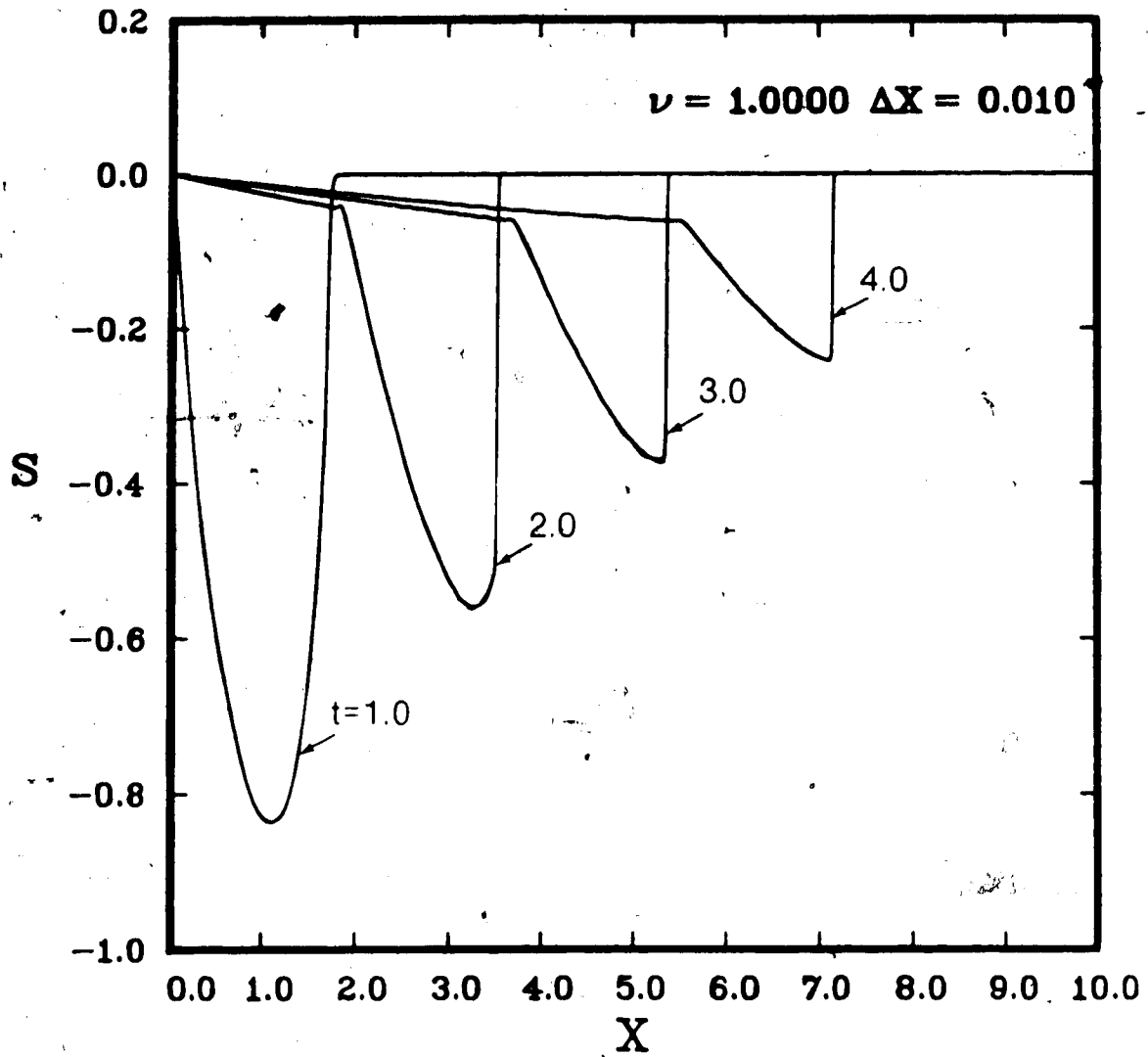


Fig. 5.15 Variation of nondimensional S with nondimensional X for $m = 0.1$ and $S(0,t) = S_0 \sin \pi t H(t) H(1-t)$, with $S_0 = -1.0$, using the nonconservative MacCormack scheme with $\nu = 1.0$.

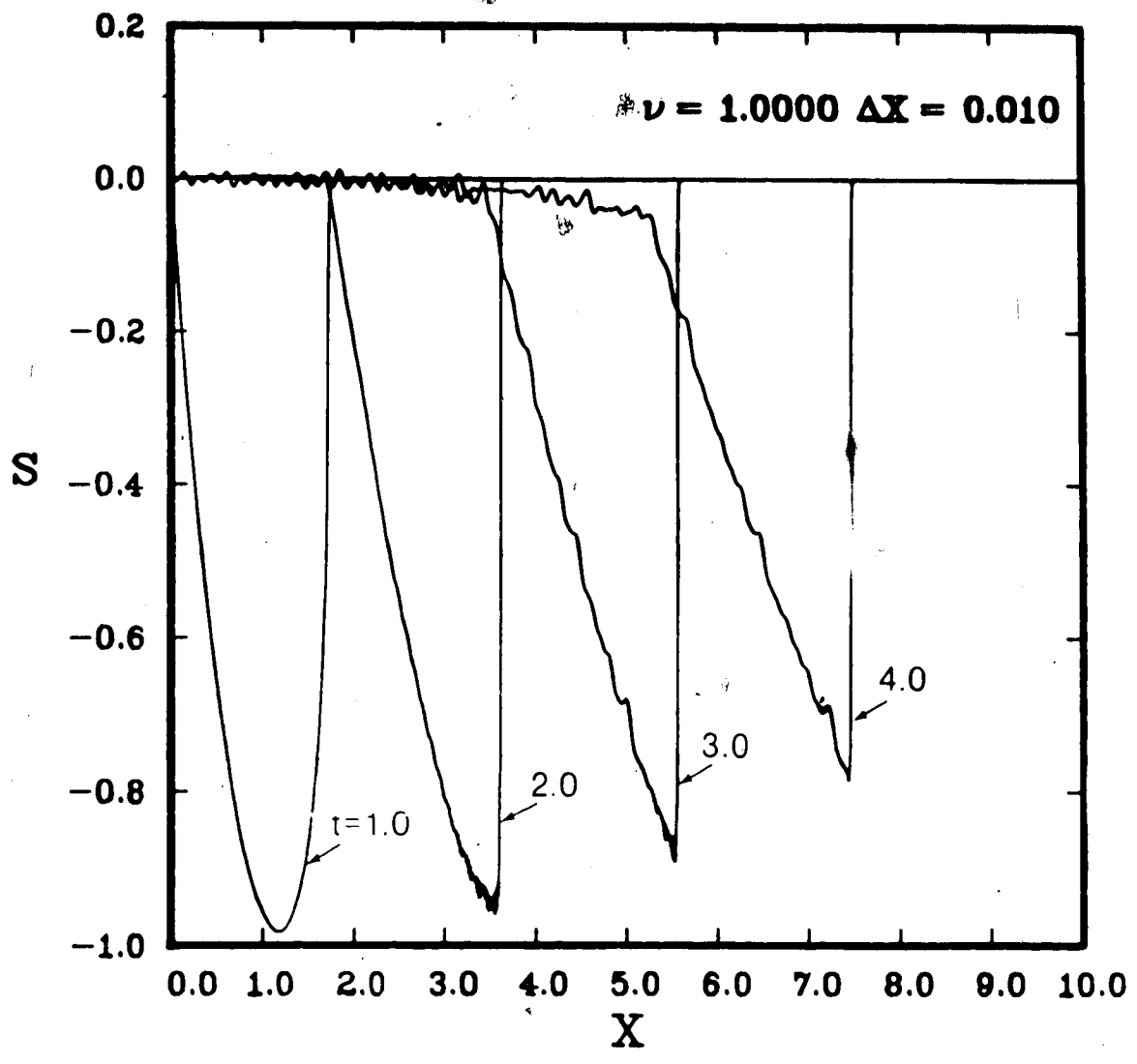


Fig. 5.16 Variation of nondimensional S with nondimensional X for $m = 0.9$ and $S(0,t) = S_0 \sin \pi t H(t) H(1-t)$, with $S_0 = -1.0$, using the nonconservative MacCormack scheme with $\nu = 1.0$.

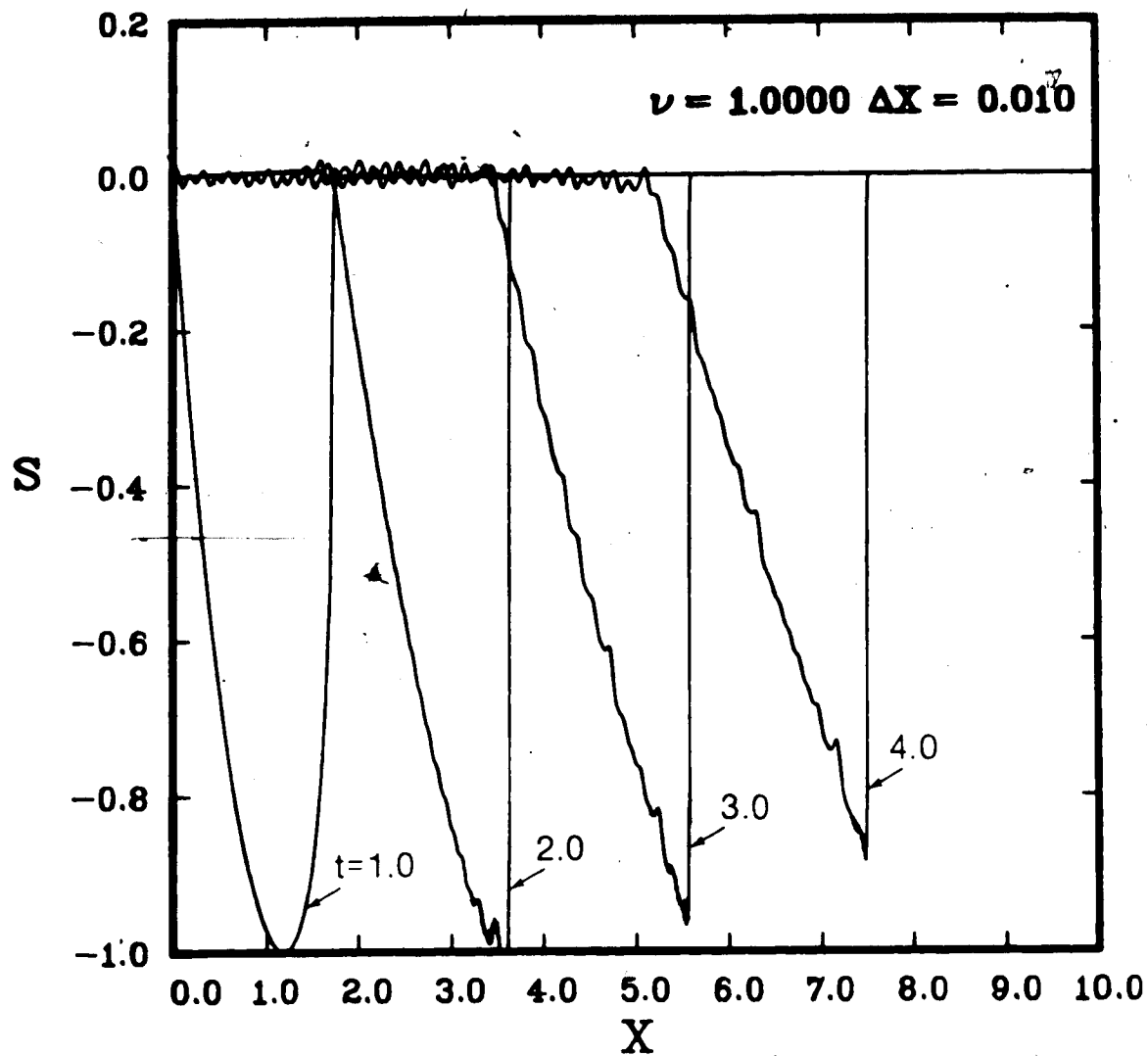


Fig. 5.17 Variation of nondimensional S with nondimensional X for $m = 1.0$ and $S(0,t) = S_0 \sin \pi t H(t) H(1-t)$, with $S_0 = -1.0$, using the nonconservative MacCormack scheme with $\nu = 1.0$.

Figures 5.18 - 5.20 show nonphysical numerical results for the variation of S with X at various times for boundary condition (5.19), with $S_0 = 1.0$, for $m = 0.1$, $m = 0.9$ and $m = 1.0$, respectively. In Figures 5.18 - 5.20 the numerical results indicate that the wave breaks on the unloading portion of the tensile stress pulse. Again, there are severe oscillations behind the shock representation in Figures 5.19 and 5.20, after the wave breaks. These oscillations are not apparent in the results presented in Figure 5.18. Although the numerical results presented for $|S_0| = 1.0$ are not physical, they demonstrate some interesting numerical phenomena and possibly some observations which could apply for smaller S_0 .

The numerical results for boundary condition (5.19), with $S_0 = -1.0$, do indicate shock evolution in the viscoelastic solid modelled by the constitutive relationship given by Tait et al (1984). This suggests, that even though shock evolution is not evident for $|S_0| = 0.16$, for the times considered, that shocks could evolve for larger times.

All of the results presented in this section, satisfy conservation of momentum according to equation (5.24). This is a necessary condition that the numerical results must satisfy. The presence of severe oscillations or numerical dispersion do not cause momentum conservation to be violated. When shocks evolve, jump conditions are satisfied according to equation (5.12). In general, the results are consistent with theoretical considerations except, for numerical dispersion. The modified boundary condition for $\lambda(0,t)$ given by equation (5.23) did not improve the numerical results. The Gottlieb

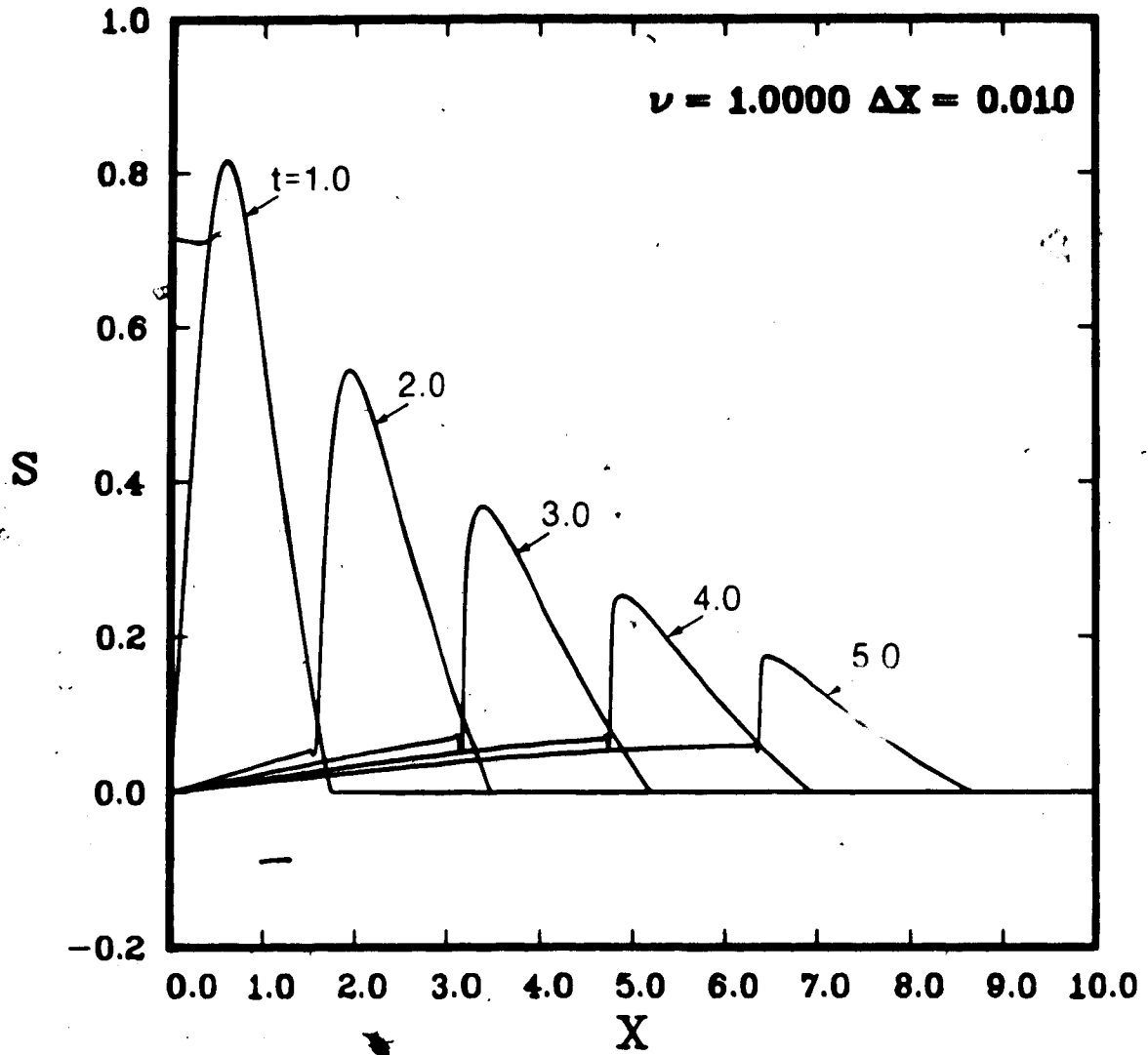


Fig. 5.18 Variation of nondimensional S with nondimensional X for $m = 0.1$ and $S(0,t) = S_0 \sin \pi t H(t) H(1-t)$, with $S_0 = 1.0$, using the nonconservative MacCormack scheme with $\nu = 1.0$.

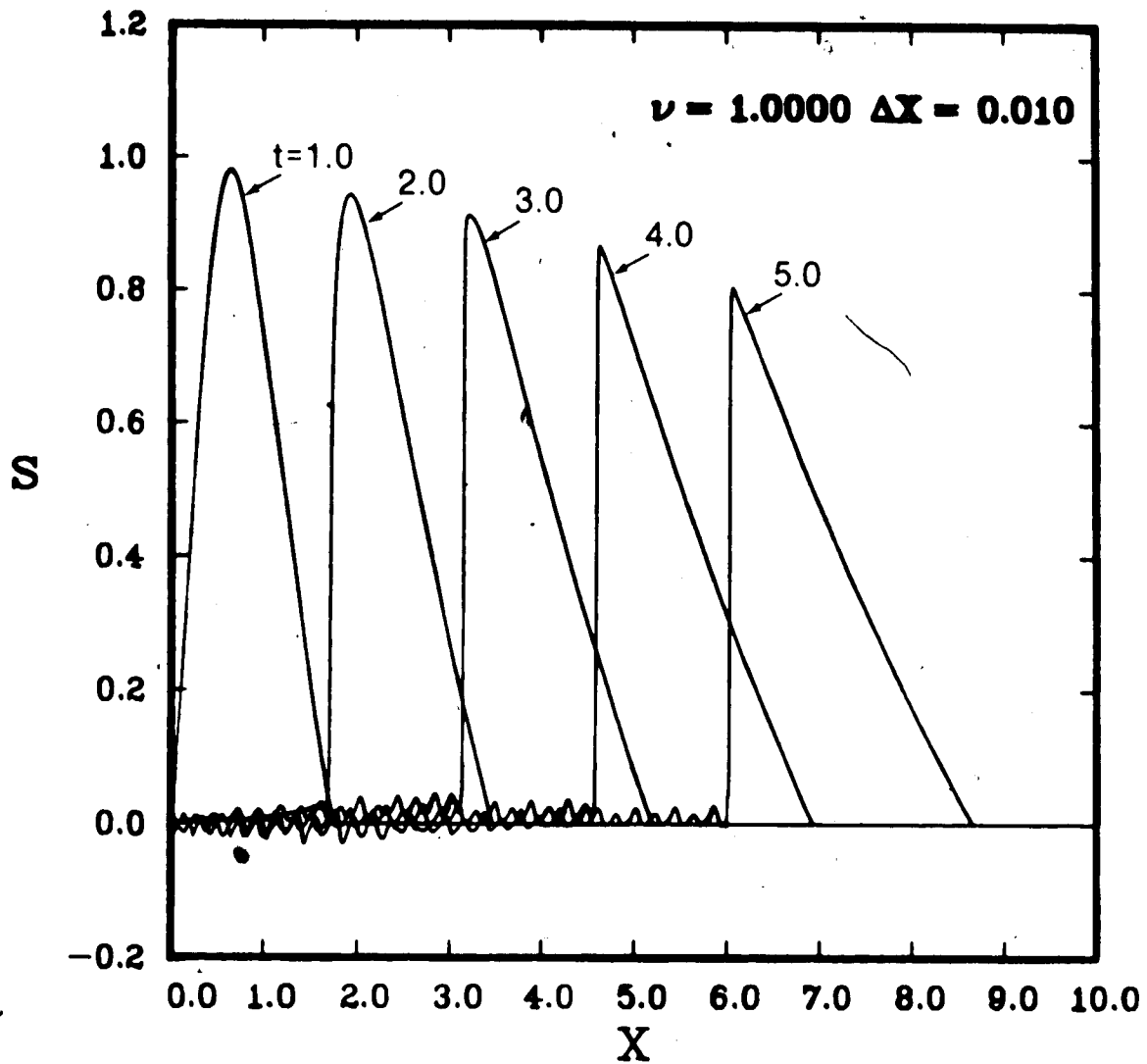


Fig. 5.19 Variation of nondimensional S with nondimensional X for $m = 0.9$ and $S(0,t) = S_0 \sin \pi t H(t) H(1-t)$, with $S_0 = 1.0$, using the nonconservative MacCormack scheme with $\nu = 1.0$.

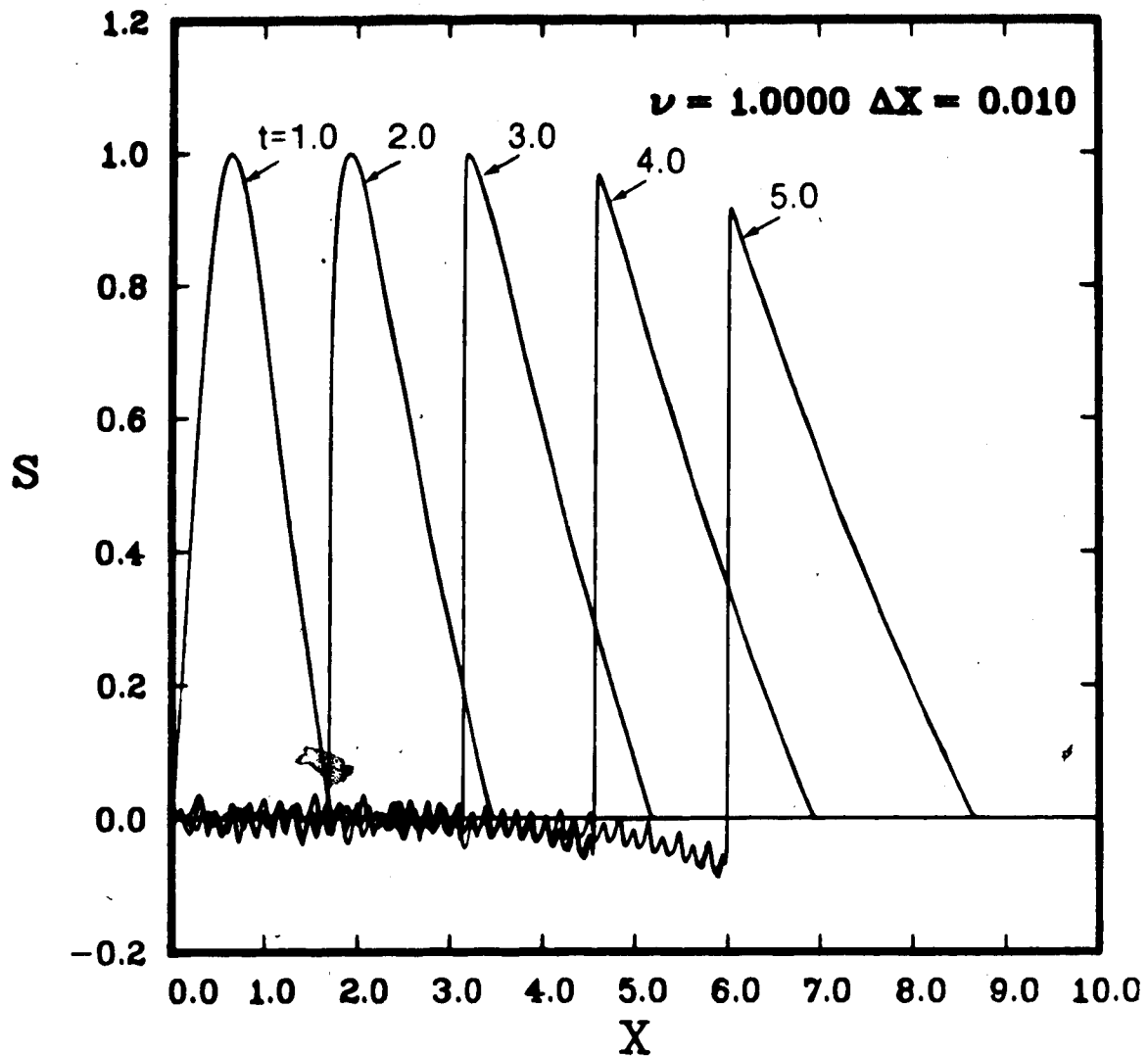


Fig. 5.20 Variation of nondimensional S with nondimensional X for $m = 1.0$ and $S(0,t) = S_0 \sin \pi t H(t) H(1-t)$, with $S_0 = 1.0$, using the nonconservative MacCormack scheme with $\nu = 1.0$.

boundary conditions involve less programming effort and give results which are virtually indistinguishable from the modified approach. The nonconservative difference scheme does not seem to introduce errors in momentum conservation.

5.7 Concluding Remarks

Although a nonconservative system of equations is considered, application of the MacCormack scheme gives results which satisfy momentum conservation and the jump relations. These are not satisfied when the scheme is applied to nonconservative systems for other problems such as axial shear and transverse shear wave propagation in an incompressible hyperelastic solid, for which conservative systems could be found easily. The MacCormack scheme would be useful for examining boundary initial value wave propagation problems in viscoelastic solids modelled by other constitutive relationships. In this way, different constitutive relationships for nonlinear viscoelastic solids could be compared.

CHAPTER 6

CONCLUDING REMARKS

The numerical results obtained in this study show that the MacCormack scheme is a suitable numerical technique for the solution of boundary initial value problems governed by hyperbolic systems of partial differential equations of the form

$$\frac{\partial U}{\partial t} + A(U) \frac{\partial U}{\partial x} + B(U) = 0 \quad (6.1)$$

The solutions of the wave propagation problems considered in Chapters 4 and 5, particularly, are of an intrinsic value to the study of elastodynamics, since analytical solutions to the finite amplitude wave propagation problems in nonlinear elastic and viscoelastic materials are not available. The solutions of the linear plane wave propagation problems considered in Chapter 3 are also extremely important in their own right, since analytical solutions of wave propagation problems in linear viscoelastic solids with more than one relaxation time are extremely difficult to obtain using Laplace transforms or the method of characteristics. The numerical results show that there is a significant difference in the wave solutions for a standard material compared with those for viscoelastic solid with two relaxation times (extended model), for the parameters considered. The extended model has more flexibility in modelling real materials.

Although the numerical solutions obtained using the MacCormack scheme are unstable for certain applications to equations of the form

(6.1), if $\underline{B}(\underline{U}) \neq 0$, sometimes the effect of the instability can be minimized if the grid spacing and Courant number are suitably chosen. In addition, the numerical results often exhibit numerical dispersion, which distorts the solution, usually near the wavefront, and smears the wavefront. The numerical results obtained in this study show that, for some problems, numerical instability and numerical dispersion can be eliminated by modifying the difference scheme.

In general, the numerical solutions for the plane wave propagation problems in linear viscoelastic solids, the axial and transverse shear wave propagation problems in an incompressible hyperelastic solid and the finite amplitude wave propagation problems in the nonlinear viscoelastic solid satisfy conservation of momentum, and conservation of mechanical energy before a shock evolves. The numerical solutions give a representation of shock evolution which is consistent with theoretical predictions that are available.

A major thrust of this study was to examine the suitability of the MacCormack scheme for the solution of boundary initial value wave propagation problems in nonlinear viscoelastic solids. The numerical results indicate that this technique is a valuable tool in solving wave propagation problems governed by systems of partial differential equations of the form (6.1). In particular, the MacCormack scheme could be used in further studies to compare wave propagation effects using various nonlinear viscoelastic constitutive relationships.

REFERENCES

- Achenbach, J.D., Wave Propagation in Elastic Solids, North Holland Publishing Company, 1973.
- Achenbach, J.D., Reddy, D.P., "Note on Wave Propagation in Linearly Viscoelastic Media", Z.A.M.P., V.18, p.141-144, 1967.
- Anderson, D.A., Tannehill, J.C., Pletcher, R.H., Computational Fluid Mechanics and Heat Transfer, Series in Computational Methods in Mechanics and Thermal Sciences, McGraw Hill Book Company, 1984.
- Christensen, R.M., "A Nonlinear Theory of Viscoelasticity for Elastomers", Trans. ASME, J. Appl. Mech., v.47, p.762-768, 1980.
- Christensen, R.M., Theory of Viscoelasticity: An Introduction, 2nd Edition, Academic Press, 1982.
- Coleman, B.D., Noll, W., "Foundations of Linear Viscoelasticity", Reviews of Modern Physics, v.33, P.239-249, 1961.
- Coulson, C.A., Jeffrey, A., Waves: A Mathematical Approach to the Common Types of Wave Motion, 2nd Edition, Longman Group Ltd., 1977.
- Courant, R., Friedrichs, K.O., Supersonic Flow and Shock Waves, Applied Mathematical Sciences 21, Springer-Verlag New York, 1948.
- Engelbrecht, J., Nonlinear Wave Processes of Deformation in Solids, Pitman Advanced Publishing Program, 1983.
- Eringen, A.C., Suhubi, E.S., Elastodynamics, v.I and v.II, Academic Press Inc., 1974.
- Flügge, W., Viscoelasticity, 2nd Revised Edition, Springer-Verlag New York, 1974.
- Gottlieb, D., Turkel, E., "Boundary Conditions for Multi-Step Finite Difference Methods for Time Dependent Equations", J. Comp. Physics, v.26 p.181-196, 1978.
- Haddow, J.B., "Thermodynamic Aspects of Transverse Wave Propagation in an Incompressible Hyperelastic Solid", Acta Mechanica, v.54, p.189-200, 1985.
- Haddow, J.B., Mióduchowski, A., "Analysis of Expansion of Spherical Cavity in Unbounded Medium by Method of Characteristic", Acta Mechanica, v.23, p.219-234, 1975.
- Haines, D.W., Wilson, W.D., "Strain Energy Density Function for Rubber-Like Materials", J. Mech. Phys. Solids, Vol. 27, p.345-360, 1979.

Hanagud, S.V., Abhyankar, N.S., "A Numerical Scheme for the Study of Poynting Effect in Wave Propagation Problems with Finite Boundaries", *Int. J. Non-Linear Mechanics*, v.19, p.507-524, 1984.

Kolsky, H., Stress Waves in Solids, Dover Publications Inc., 1963.

Kutler, P., "Computation of Three-Dimensional Inviscid Supersonic Flows", *Progress in Numerical Fluid Dynamics, von Karman Lecture Series # 63*, 1974.

Lee, E.H., Kanter, I., "Wave Propagation in Finite Rods of Viscoelastic Material", *J. Appl. Phys.*, vol.24, p.1115-1122, 1953.

Lee, E.H., Morrison, J.A., "A Comparison of the Propagation of Longitudinal Waves in Rods of Viscoelastic Materials", *J. Polymer Science*, vol.19, p.93-110, 1956.

Lockett, F.J., Nonlinear Viscoelastic Solids, Academic Press, 1972.

MacCormack, R.W., "The Effect of Viscosity in Hypervelocity Impact Cratering", *AIAA Paper No. 69-354*, Cincinnati, Ohio, 1969.

Mitchell, A.R., Private Communication, 1984.

Mitchell, A.R., Griffiths, D.F., The Finite Difference Method in Partial Differential Equations, John Wiley and Sons, 1980.

Ogden, R.W., Nonlinear Elastic Deformations, Ellis Horwood Series Mathematics and Its Applications, Ellis Horwood Ltd., 1984.

Pipkin, A.C., Lectures on Viscoelasticity Theory, Springer-Verlag New York, 1972.

Richtmyer, R.D., Morton, K.W., Difference Methods for Initial Value Problems, Wiley Interscience Publishers, 2nd Edition, 1967.

Roache, P.J., Computational Fluid Dynamics, Hermosa Publishers, 1972.

Sackman, J.L., Kaya, I., "On the Propagation of Transient Pulses in Linearly Viscoelastic Media", *J. Mech. Phys. Solids*, v.16, p.349-356, 1968.

Spencer, A.J.M., Continuum Mechanics, Longman Group Ltd., 1980.

Tait, R.J., Haddow, J.B., Moodie, T.B., "A Simplified Viscoelastic Constitutive Equation Applied to a Dynamic Finite Deformation Problem", *Int. J. Non-Linear Mechanics*, v.19, p.11-18, 1984.

Timoshenko, S.P., Goodier, J.N., Theory of Elasticity, 3rd Edition, McGraw Hill Book Company, 1951.

Treloar, L.R.G., The Physics of Rubber Elasticity, Oxford University Press, 1958.

Warming, R.F., Hyett, B.J., "The Modified Equation Approach to the Stability and Accuracy Analysis of Finite Difference Methods", *J. Comp. Physics*, v.14, p.156-179, 1974.

Whitham, G.B., Linear and Nonlinear Waves, Pure and Applied Mathematics: A Wiley Interscience Series of Texts, Monographs & Tracts, John Wiley and Sons Ltd., 1974.

APPENDIX 1

1. Modification of the MacCormack Scheme

In this appendix it is shown that for linear hyperbolic systems of equations of the form

$$\frac{\partial \underline{U}}{\partial t} + \underline{A} \frac{\partial \underline{U}}{\partial x} + \underline{B} \underline{U} = \underline{0} \quad (\text{A1.1})$$

where \underline{A} and \underline{B} are constant matrices, the proposed modification of the MacCormack scheme is equivalent to the Lax-Wendroff scheme.

The Lax-Wendroff method is obtained from a Taylor series expansion,

$$\underline{U}(t + \Delta t) = \underline{U}(t) + \Delta t \frac{\partial \underline{U}}{\partial t} + \frac{(\Delta t)^2}{2} \frac{\partial^2 \underline{U}}{\partial t^2} + O((\Delta t)^3) \quad (\text{A1.2})$$

Substituting

$$\frac{\partial \underline{U}}{\partial t} = \left[\underline{A} \frac{\partial \underline{U}}{\partial x} + \underline{B} \underline{U} \right] \quad (\text{A1.3})$$

and

$$\frac{\partial^2 \underline{U}}{\partial t^2} = \underline{A}^2 \frac{\partial^2 \underline{U}}{\partial x^2} + (\underline{A}\underline{B} + \underline{B}\underline{A}) \frac{\partial \underline{U}}{\partial x} + \underline{B}^2 \underline{U}$$

into equation (A1.2), gives

$$\begin{aligned} \underline{U}(t + \Delta t) = \underline{U}(t) + \Delta t \left[\underline{A} \frac{\partial \underline{U}}{\partial x} + \underline{B} \underline{U} \right] + \frac{(\Delta t)^2}{2} \left\{ \underline{A}^2 \frac{\partial^2 \underline{U}}{\partial x^2} + (\underline{A}\underline{B} + \underline{B}\underline{A}) \frac{\partial \underline{U}}{\partial x} \right. \\ \left. + \underline{B}^2 \underline{U} \right\} + O((\Delta t)^3) \quad (\text{A1.4}) \end{aligned}$$

By replacing the terms $\partial^2 U / \partial x^2$, $\partial U / \partial x$, U with the appropriate difference expressions and truncating the terms $O((\Delta t)^3)$, the solution for the $(n+1)^{\text{th}}$ time step is given by

$$\begin{aligned} \bar{U}_{-j}^{n+1} = & \left\{ \left[\bar{I} - \Delta t \hat{B} + \frac{(\Delta t)^2}{2} \hat{B}^2 \right] \bar{U}_{-j}^n + \left[\frac{(\Delta t)^2}{2} (\hat{A}\hat{B} + \hat{B}\hat{A}) - \Delta t \hat{A} \right] \left[\frac{U_{-j+1}^n - U_{-j-1}^n}{2\Delta x} \right] \right. \\ & \left. + \frac{(\Delta t)^2}{2} \hat{A}^2 \left[\frac{U_{-j+1} - 2U_{-j} + U_{-j-1}}{(\Delta x)^2} \right] \right\} \quad (A1.5) \end{aligned}$$

where \bar{I} is the unit matrix, and $U_{-j}^n = U(j\Delta x, n\Delta t)$. When $\hat{B} = 0$, equation (A1.5) reduces to the familiar version of the Lax-Wendroff scheme (Anderson et al, 1984). The finite difference scheme represented by equation (A1.5) is considered to be "second order" accurate, because the terms $O((\Delta t)^2)$ have been retained.

A slight modification of the MacCormack scheme for systems of equations of the form (A1.1), with $\hat{B} \neq 0$ is

$$\begin{aligned} \bar{U}_{-j}^{n+1} = & \bar{U}_{-j}^n - \frac{\Delta t}{\Delta x} \hat{A} (U_{-j+1}^n - U_{-j}^n) - \Delta t \hat{B} U_{-j}^n \\ \bar{U}_{-j}^{n+1} = & \frac{1}{2} \left\{ \bar{U}_{-j}^n + \bar{U}_{-j}^{n+1} - \frac{\Delta t}{\Delta x} \hat{A} (U_{-j}^{n+1} - U_{-j-1}^{n+1}) - \Delta t \hat{B} U_{-j}^{n+1} \right\} \quad (A1.6) \end{aligned}$$

This is a forward backward modified version of the MacCormack scheme (MacCormack, 1969). Elimination of U_{-j}^{n+1} (predictor step) from equations (A1.6)₁, and (A1.6)₂ gives

$$\begin{aligned}
 \hat{u}_{-j}^{n+1} = & \left\{ \left[\hat{I} - \frac{\Delta t \hat{B}}{2} + \frac{(\Delta t)^2 \hat{B}^2}{2\Delta x} + \frac{(\Delta t)^2 (\hat{A}\hat{B} - \hat{B}\hat{A})}{2\Delta x} \right] \hat{u}_{-j}^n + \frac{(\Delta t)^2 \hat{A}^2}{2} \left[\frac{\hat{u}_{-j+1}^n - 2\hat{u}_{-j}^n + \hat{u}_{-j-1}^n}{(\Delta x)^2} \right] \right. \\
 & \left. - \frac{\Delta t}{2} \hat{A} \left[\frac{\hat{u}_{-j+1}^n - \hat{u}_{-j-1}^n}{\Delta x} \right] + \frac{(\Delta t)^2}{2} \left[\frac{\hat{B}\hat{A}\hat{u}_{-j+1}^n - \hat{A}\hat{B}\hat{u}_{-j-1}^n}{\Delta x} \right] \right\} \quad (A1.7)
 \end{aligned}$$

A comparison of equations (A1.5) and (A1.7) shows that the Lax-Wendroff scheme and the MacCormack scheme are equivalent if $\hat{A}\hat{B} = \hat{B}\hat{A}$, in particular, for the scalar equation

$$\frac{\partial u}{\partial t} + c \frac{\partial u}{\partial x} + au = 0 \quad (A1.8)$$

Also, when $\hat{B} = 0$, the two numerical schemes are equivalent for the linear system of equations.

It should also be noted that the analysis provided in this section is much more difficult for the nonlinear version of equation (A1.1). For nonlinear systems of equations, the two schemes are not always equivalent and would not necessarily have the same stability criteria.

The justification for using the modification of the MacCormack scheme given in (A1.6), is based on a comparison with the Lax-Wendroff scheme for linear equations. Since the method reduces to the Lax-Wendroff scheme, in certain cases, and is a two step method suitable for boundary applications, the method is used for the solution of wave propagation problems in solids.

2. Stability Analysis of a Finite Difference Scheme

In order to examine the stability of the modified difference schemes, the von Neumann method (Mitchell & Griffiths, 1980) is used, which assumes a Fourier series representation for the errors ϵ_j^0 , $j = 0, 1, 2, \dots, N$, at time $t = 0$. The error distribution at the grid points for $t = 0$ is then assumed to be given by

$$\epsilon(x, 0) = \sum_{m=0}^N B_m e^{ik_m x} \quad (A1.9)$$

or

$$\epsilon_j^0 = \epsilon(j\Delta x, 0) = \sum_{m=0}^N B_m e^{ik_m(j\Delta x)} \quad (A1.10)$$

for an interval $0 \leq x \leq L$ where $\Delta x = L/N$, so that the number of harmonics $(N + 1)$ is equal to the number of grid points at $t = 0$. In equation (A1.9), the B_m are constant column matrices, which can be determined by the ϵ_j^0 , and $k_m = m\pi/L$. The real part of the series (A1.9) is a half range cosine series for the interval $0 \leq x \leq L$.

The errors satisfy the finite difference equations and a solution of these equations, which reduces to (A1.10) when $t = 0$ is

$$\epsilon_j^n = \sum_{m=0}^N e^{a_n \Delta t} B_m e^{ik_m(j\Delta x)} \quad (A1.11)$$

where a_n may be complex. Since superposition is valid, the stability condition is obtained by substituting a single harmonic in the finite difference equations (A1.5) or (A1.7) to obtain

$$\underline{c}_j^{n+1} = \underline{G}(\Delta t, k) \underline{c}_j^n \quad (A1.12)$$

where \underline{G} is defined as the amplification matrix of the finite difference scheme. A necessary condition for stability is $|e^{a\Delta t}| \leq 1$, and this is satisfied if $\lambda \leq 1$, where λ is the spectral radius of \underline{G} . The spectral radius of \underline{G} is the largest modulus of the eigenvalues of the matrix \underline{G} . If \underline{G} is a normal matrix, then $\lambda \leq 1$ is a necessary and sufficient condition for stability for initial value problems (Richtmyer and Morton, 1967). For the special case of single scalar equation, the amplification matrix degenerates to a scalar factor G .

Application of the von Neumann method to equations (A1.5) and (A1.7), gives the following complex amplification matrices,

$$\underline{G}(\Delta t, k) = \left\{ \left[\underline{I} - \Delta t \underline{\hat{B}} + \frac{(\Delta t)^2}{2} \underline{\hat{B}}^2 + \underline{A}^2 \left[\frac{\Delta t}{\Delta x} \right]^2 (\cos \beta - 1) \right] + i \left[\frac{\Delta t}{\Delta x} \left\{ \Delta t \left[\frac{\underline{\hat{A}}\underline{\hat{B}} + \underline{\hat{B}}\underline{\hat{A}}}{2} \right] - \underline{A} \right\} \right] \sin \beta \right\} \quad (A1.13)$$

for the Lax-Wendroff scheme, and

$$\underline{G}(\Delta t, k) = \left\{ \left[\underline{I} - \Delta t \underline{\hat{B}} + \frac{(\Delta t)^2}{2} \underline{\hat{B}}^2 + \underline{A}^2 \left[\frac{\Delta t}{\Delta x} \right]^2 (\cos \beta - 1) \right] + \frac{(\Delta t)^2}{2\Delta x} (\underline{\hat{B}}\underline{\hat{A}} - \underline{\hat{A}}\underline{\hat{B}})(\cos \beta - 1) + i \left[\frac{\Delta t}{\Delta x} \left\{ \Delta t \left[\frac{\underline{\hat{A}}\underline{\hat{B}} + \underline{\hat{B}}\underline{\hat{A}}}{2} \right] - \underline{A} \right\} \right] \sin \beta \right\} \quad (A1.14)$$

for the modified MacCormack scheme, respectively, where $\beta = k\Delta x$. The spectral radii of (A1.13) and (A1.14), and, hence the stability criteria

are examined by evaluating λ as a function of β . Instability of the difference scheme is indicated, if λ exceeds 1 for some β . However, $\lambda < 1$, does not always imply stability, since the von Neumann method is a necessary condition for stability, but not sufficient unless G is a normal matrix. Also, this analysis does not include the effects of boundary conditions.

This appendix provides an analysis of the effect of the term $\hat{B}U$ in equation (A1.1), as it affects the stability of the MacCormack finite difference scheme. Also, the stability analysis of the linear systems of equations, provides some insight into the application to nonlinear systems.

APPENDIX 2

1. Theory of Hyperbolic Equations and the Method of Characteristics

The wave propagation problems considered in this study are governed by systems of quasi-linear hyperbolic partial differential equations of the form

$$\frac{\partial \underline{U}}{\partial t} + \underline{A}(\underline{U}) \frac{\partial \underline{U}}{\partial x} + \underline{B}(\underline{U}) = \underline{0} \quad (\text{A2.1})$$

where \underline{U} is a vector of the dependent variables, $\underline{A}(\underline{U})$ is a matrix function of \underline{U} , $\underline{B}(\underline{U})$ is a vector function of \underline{U} , and possibly x , and x and t are the independent variables representing space and time respectively. Some of the simpler problems considered, one dimensional infinitesimal wave propagation in linear viscoelastic media, are governed by equation (A2.1), where $\underline{A}(\underline{U})$ is a constant matrix \underline{A} and $\underline{B}(\underline{U})$ is a linear function of \underline{U} .

There is extensive literature on the theory of hyperbolic equations (Whitham, 1974, Jeffrey, 1977), particularly on the method of characteristics. It is interesting to note, however, that linear problems or nonlinear problems with $\underline{B}(\underline{U}) = \underline{0}$ are most frequently considered. Whitham (1974) provides an analytical treatment of the theory of hyperbolic equations and Mitchell (1980) provides a numerical treatment of hyperbolic equations. This appendix summarizes the major concepts of hyperbolic systems of partial differential equations.

Equation (A2.1) represents a quasi-linear system of first order equations, since the equations are linear in the first derivatives of

the dependent variables \underline{U} . The matrix $\underline{A}(\underline{U})$ and the vector $\underline{B}(\underline{U})$ may be functions of x and t as well as \underline{U} . However, in this study $\underline{A}(\underline{U})$ and $\underline{B}(\underline{U})$ are not functions of t . By definition, equation (A2.1) is an n th order hyperbolic system of equations if there are n linearly independent left eigenvectors \underline{l}^n which correspond to n different real roots c^n , given by

$$\det | \underline{A}(\underline{U}) - c\underline{I} | = 0 \quad , \quad (\text{A2.2})$$

where \underline{I} is the identity matrix and $\det | |$ denotes the determinant of the matrix given by $[\underline{A}(\underline{U}) - c\underline{I}]$. The characteristic curves are given by

$$\frac{dx}{dt} = c \quad , \quad (\text{A2.3})$$

and the relationships along the characteristics are

$$\underline{l}^T \frac{d\underline{U}}{dt} + \underline{l}^T \underline{B}(\underline{U}) = 0 \quad , \quad (\text{A2.4})$$

provided that

$$\underline{l}^T \underline{A} = \underline{l}^T c \quad , \quad (\text{A2.5})$$

Equation (A2.1) written in conservation form is

$$\frac{\partial \underline{U}}{\partial t} + \frac{\partial \underline{Q}(\underline{U})}{\partial x} + \underline{B}(\underline{U}) = 0 \quad (\text{A2.6})$$

The conservation form is useful in determining the jump conditions if a shock is formed (Whitham, 1974). A shock exists when the field variables \underline{U} are discontinuous. A shock may exist due to the boundary condition (i.e., in both linear and nonlinear problems), or a shock may evolve from a smooth boundary condition (nonlinear problem). When the

wave breaks and a shock is formed, the jump relationship can be written as

$$-V [U] + [Q(U)] = 0 \quad (A2.7)$$

where V is the velocity of propagation of the discontinuity (shock speed) and the square brackets $[]$ denote the jump in the quantities within the brackets. The jump relationships are useful in determining the magnitude of the discontinuity in the field variables at the shock front. The breaking time for a given problem can be obtained by determining where the characteristics intersect (Whitham, 1974). Whitham primarily considers initial value problems, but the theory is quite easily extended to boundary initial value problems.

Simple wave solutions to equation (A2.6) for boundary initial value problems do not, in general, exist. A simple wave solution for a given problem exists, if one of the Riemann invariants is identically constant, which implies that:

- (i) Riemann invariants exist for the problem; and
- (ii) the wave is propagating into a region of constant state.

Riemann invariants exist if $\underline{B(U)} = 0$. In most of the problems considered in this study, $\underline{B(U)} \neq 0$, and therefore even though the waves propagate into a region of constant state (undeformed and quiescent), the simple wave solution is not possible. Achenbach (1973) has considered simple wave solutions for finite amplitude wave propagation in a hyperelastic medium where the governing equation is of the form (A2.1) with $\underline{B(U)} = 0$. Simple wave solutions are valid until a shock forms.

2. The Method of Characteristics Applied to Scalar Equations

Analytical solutions for some of the boundary initial value problems considered in Section 2.5.1, obtained using the method of characteristics, are presented in this appendix.

The solution of

$$\frac{\partial u}{\partial t} + \frac{\partial u}{\partial x} = 0 \quad (\text{A2.8})$$

for initial condition $u(x,0) = 0$ and boundary condition $u(0,t) = f(t)H(t)$, is easily obtained from the method of characteristics, or otherwise, and is

$$\underline{u(x,t) = f(t-x)H(t-x)} \quad (\text{A2.9})$$

The solution of

$$\frac{\partial u}{\partial t} + \frac{\partial u}{\partial x} + u = 0 \quad (\text{A2.10})$$

for initial condition $u(x,0) = 0$ and boundary condition $u(0,t) = f(t)H(t)$, is obtained from the method of characteristics. It follows from the method of characteristics that

$$\frac{du}{dt} + u = 0 \quad \text{on} \quad \frac{dx}{dt} = u \quad (\text{A2.11})$$

Integrating equation (A2.11), and using the initial condition, gives

$$u = c(t_0)e^{-(x+t_0)} H(t_0) \quad \text{on} \quad t = t_0 + x \quad (\text{A2.12})$$

use of the boundary condition, then, gives

$$c(t_0) = f(t_0)e^{t_0} \quad (A2.13)$$

so that

$$\underline{u(x,t) = f(t-x)e^{-x}H(t-x)} \quad (A2.14)$$

The solution of

$$\frac{\partial u}{\partial t} + u \frac{\partial u}{\partial x} \quad (A2.15)$$

with initial condition $u(x,0) = 0$ and boundary condition $u(0,t) = U_0H(t)$, easily obtained from the method of characteristics, is

$$\underline{u(x,t) = U_0 H\left(t - \frac{2x}{U_0}\right)} \quad (A2.16)$$

satisfies equation (A2.15), the boundary condition and initial conditions, and the jump condition

$$V[u] = [(1/2)u^2] \quad (A2.17)$$

where V is the shock speed. The jump relations (A2.17) come from considering the conservation form of equation (A2.15).

The solution which satisfies

$$\frac{\partial u}{\partial t} + u \frac{\partial u}{\partial x} + u = 0 \quad (A2.18)$$

for initial condition $u(x,0) = 0$ and boundary condition $u(0,t) = U_0H(t)$, follows from the method of characteristics, which implies that

$$\frac{du}{dt} + u = 0 \quad \text{on} \quad \frac{dx}{dt} = u \quad (A2.19)$$

Integration of (A2.19) gives

$$u = ce^{-t} \quad \text{on } \frac{dx}{dt} = u \quad (\text{A2.20})$$

The characteristic emanating from t_0 , where $t_0 > 0$, has the slope

$$\frac{dx}{dt} = c(t_0)e^{-t} \quad (\text{A2.21})$$

Consequently, the equation of the characteristic is

$$x = c(t_0)(e^{-t_0} - e^{-t}) \quad (\text{A2.22})$$

since $x = 0$, when $t = t_0$. Use of the boundary condition, then, gives

$$c(t_0) = U_0 e^{t_0} \quad (\text{A2.23})$$

Therefore, the characteristic emanating from t_0 has the form

$$x = U_0(1 - e^{-(t_0 - t)}) \quad (\text{A2.24})$$

Eliminating t_0 between (A2.24) and (A2.20) gives

$$u(x,t) = \left(1 - \frac{x}{U_0}\right) \quad (\text{A2.25})$$

The position of the wavefront is found by considering the shock speed $V = 1/2[u]$, for the quiescent initial condition. It follows from (A2.25) and the relation for the shock speed that

$$V = \frac{dx^*}{dt} = \frac{1}{2} \left[\frac{1 - x^*}{U_0} \right] \quad (\text{A2.26})$$

where x^* is the position of the wavefront. Therefore,

$$dt = \frac{dx^*}{V} = \frac{2dx^*}{(1 - \frac{x^*}{U_0})} \quad (A2.27)$$

Integration of (A2.27) gives the time required to reach x^* , as

$$t = \int_0^{x^*} \frac{2 dx^*}{(1 - \frac{x^*}{U_0})} = -2 U_0 \ln \left(1 - \frac{x^*}{U_0} \right) \Big|_0^{x^*} \quad (A2.28)$$

and

$$t = -2U_0 \ln \left(1 - \frac{x^*}{U_0} \right) \quad (A2.29)$$

Therefore, for $U_0 = 1$,

$$x^* = 1 - e^{(-t/2)} \quad (A2.30)$$

The wavefront positions x^* for various times are given as

t	x^*
1.5	0.5276
3.0	0.7769
4.5	0.8955
6.0	0.9502
7.5	0.9765

As $t \rightarrow \infty$, $x^* \rightarrow 1.0$

Combining (A2.25) and (A2.30) gives

$$u(x, t) = \left(1 - \frac{x}{U_0} \right) H \left(1 - e^{(-t/2)} - x \right) \quad (A2.31)$$

APPENDIX 3

The wavefront expansion contained in this appendix is similar to that obtained by Christensen (1982), except that the expansion is given in terms of the creep function rather than the relaxation function.

Consider the wave front expansion for the boundary condition,

$$\sigma(0,t) = \sigma_0 H(t) \quad (A3.1)$$

It follows from the equation of motion for an initially quiescent semi-infinite rod, with the end at $x = 0$, that

$$\sigma(x,s) = \frac{\sigma_0}{s} \exp(-\Omega(s)x) \quad (A3.2)$$

where

$$\Omega(s) = \left[\frac{\rho s}{\bar{E}(s)} \right]^{1/2} = \{\rho s^3 \bar{J}(s)\}^{1/2} \quad (A3.3)$$

Expanding $J(t)$ as a Taylor series gives

$$J(t) = J(0) + tJ'(0) + \frac{t^2}{2!} J''(0) + \dots \quad (A3.4)$$

and taking the Laplace transform of (A3.4) gives

$$\bar{J}(s) = \frac{J(0)}{s} + \frac{J'(0)}{s^2} + \frac{J''(0)}{s^3} + \dots \quad (A3.5)$$

Substituting (A3.5) into (A3.3) results in the following expression

$$\Omega(s) = \left\{ \rho s^3 \left[\frac{J(0)}{s} + \frac{J'(0)}{s^2} + \frac{J''(0)}{s^3} + \dots \right] \right\}^{1/2} \quad (A3.6)$$

and simplifying gives

$$- \left\{ \rho \left[s^2 J(0) + s J'(0) + \frac{J''(0)}{s} + \dots \right] \right\}^{1/2} \quad (\text{A3.7})$$

Making the substitution for $c = \left[\frac{1}{\rho J(0)} \right]^{1/2}$ (A3.8)

into (A3.7) and rearranging gives

$$\Omega(s) = \frac{s}{c} \left\{ 1 + \frac{J'(0)}{s J(0)} + \frac{J''(0)}{s^2 J(0)} + \dots \right\}^{1/2} \quad (\text{A3.9})$$

Using the Binomial expansion theorem gives

$$\Omega(s) = \frac{s}{c} \left\{ 1 + \frac{1}{2} \frac{J'(0)}{s J(0)} + \frac{1}{2} \frac{J''(0)}{s^2 J(0)} - \frac{1}{2} \left[\frac{J'(0)}{2s J(0)} \right]^2 + \dots \right\} \quad (\text{A3.10})$$

Substitution of (A3.10) into (A3.2) gives

$$\bar{\sigma}(x, s) = \frac{\sigma_0}{s} \exp \left[-\frac{xs}{c} \right] \exp \left\{ -\frac{J'(0)}{2J(0)} \frac{x}{c} - \frac{J''(0)}{2sJ(0)} \frac{x}{c} + \frac{1}{2s} \left[\frac{J'(0)}{2J(0)} \right]^2 \frac{x}{c} + \dots \right\} \quad (\text{A3.11})$$

Expanding the second exponential gives,

$$\bar{\sigma}(x, s) = \frac{\sigma_0}{s} \exp \left[-\frac{xs}{c} \right] \exp \left[-\frac{J'(0)}{2J(0)} \frac{x}{c} \right] \left\{ 1 - \frac{J''(0)}{2sJ(0)} \frac{x}{c} + \frac{1}{2s} \left[\frac{J'(0)}{2J(0)} \right]^2 + \dots \right\} \quad (\text{A3.12})$$

and rearranging gives,

$$\bar{\sigma}(x, s) = \sigma_0 \exp \left[-\frac{xs}{c} \right] \exp \left[-\frac{J'(0)}{2J(0)} \frac{x}{c} \right] \left\{ \frac{1}{s} - \left[\frac{J''(0)}{2J(0)} \right] \frac{1}{s^2} \frac{x}{c} + \left[\frac{J'(0)}{2J(0)} \right]^2 \frac{1}{2s^2} \frac{x}{c} + \dots \right\} \quad (\text{A3.13})$$

Taking the Laplace transform inversion of the expression within the brackets () in (A3.13) gives

$$\bar{\sigma}(x, s) = \sigma_0 \exp\left[-\frac{xs}{c}\right] \exp\left[-\frac{J'(0)x}{2J(0)c}\right] \left\{ 1 - \frac{J''(0)}{2J(0)} \frac{tx}{c} + \left[\frac{J'(0)}{2J(0)}\right]^2 \frac{tx}{2c} + \dots \right\} \quad (\text{A3.14})$$

The shifting theorem is applied to give

$$\sigma(x, t) = \sigma_0 \exp\left[-\frac{J'(0)x}{2J(0)c}\right] \left\{ 1 - \left[\frac{J''(0)}{2J(0)}\right] \left[\frac{t-x}{c}\right] \frac{x}{c} + \left[\frac{J'(0)}{2J(0)}\right]^2 \left[\frac{t-x}{2c}\right] \frac{x}{c} + \dots \right\} H\left[\frac{t-x}{c}\right] \quad (\text{A3.15})$$

Using the nondimensionalization scheme given by (3.13) in Chapter 3 gives the wavefront expansion, where the superposed bars indicate nondimensional variables, as follows

$$\bar{\sigma}(\bar{x}, \bar{t}) = \bar{\sigma}_0 \exp\left[\frac{-\bar{J}'(0)\bar{x}}{2\bar{J}(0)}\right] \left\{ 1 - \left[\frac{\bar{J}''(0)}{2\bar{J}(0)}\right] (\bar{t}-\bar{x})\bar{x} + \left[\frac{\bar{J}'(0)}{2\bar{J}(0)}\right]^2 \frac{(\bar{t}-\bar{x})\bar{x}}{2} + \dots \right\} H(\bar{t}-\bar{x}) \quad (\text{A3.16})$$

Differentiating with respect to \bar{t} gives

$$\frac{\partial \bar{\sigma}}{\partial \bar{t}} = \bar{\sigma}_0 \exp\left[\frac{-\bar{J}'(0)\bar{x}}{2\bar{J}(0)}\right] \left\{ 1 - \left[\frac{\bar{J}''(0)}{2\bar{J}(0)}\right] \bar{x} + \frac{1}{2} \left[\frac{\bar{J}'(0)}{2\bar{J}(0)}\right]^2 \bar{x} + \dots \right\} H(\bar{t}-\bar{x}) \quad (\text{A3.17})$$

The expression for $\partial \bar{\sigma} / \partial \bar{t}$ at the wavefront is given by

$$\frac{\partial \bar{\sigma}}{\partial \bar{t}} \Big|_{\bar{t}=\bar{x}} = \bar{\sigma}_0 \exp\left[\frac{-\bar{J}'(0)\bar{x}}{2\bar{J}(0)}\right] \left\{ 1 - \left[\frac{\bar{J}''(0)}{2\bar{J}(0)}\right] \bar{x} + \frac{1}{2} \left[\frac{\bar{J}'(0)}{2\bar{J}(0)}\right]^2 \bar{x} \right\} \quad (\text{A3.18})$$

Differentiating with respect to x gives

$$\begin{aligned} \frac{\partial \bar{\sigma}}{\partial \bar{x}} &= \frac{-\bar{J}'(0)}{2\bar{J}(0)} \bar{\sigma}_0 \exp \left[\frac{-\bar{J}'(0)\bar{x}}{2\bar{J}(0)} \right] \left\{ 1 - \left[\frac{\bar{J}''(0)}{2\bar{J}(0)} \right] (\bar{t}-\bar{x})\bar{x} + \left[\frac{\bar{J}'(0)}{2\bar{J}(0)} \right]^2 (\bar{t}-\bar{x})\bar{x} + \dots \right\} \\ &+ \bar{\sigma}_0 \exp \left[\frac{-\bar{J}'(0)\bar{x}}{2\bar{J}(0)} \right] \left\{ + \left[\frac{\bar{J}''(0)}{2\bar{J}(0)} \right] \bar{x} - \left[\frac{\bar{J}''(0)}{2\bar{J}(0)} \right] (\bar{t}-\bar{x}) - \left[\frac{\bar{J}'(0)}{2\bar{J}(0)} \right]^2 \frac{\bar{x}}{2} \right. \\ &+ \left. \left[\frac{\bar{J}'(0)}{2\bar{J}(0)} \right]^2 \frac{(\bar{t}-\bar{x})}{2} + \dots \right\} \end{aligned} \quad (\text{A3.19})$$

and the expression for $\partial \bar{\sigma} / \partial \bar{x}$ at the wavefront is given by

$$\left. \frac{\partial \bar{\sigma}}{\partial \bar{x}} \right|_{\bar{t}=\bar{x}} = \bar{\sigma}_0 \exp \left[\frac{-\bar{J}'(0)\bar{x}}{2\bar{J}(0)} \right] \left\{ \frac{\bar{J}''(0)}{2\bar{J}(0)} + \frac{\bar{J}''(0)\bar{x}}{2\bar{J}(0)} - \left[\frac{\bar{J}'(0)}{2\bar{J}(0)} \right]^2 \frac{\bar{x}}{2} \right\} \quad (\text{A3.20})$$